UNIVERSITY OF CALIFORNIA, SAN DIEGO

# Low-Valent Iron and Cobalt Isocyanide Complexes: Platforms for Small Molecule Activation, Coordination Chemistry and Novel Electronic Structure Motifs.

A dissertation submitted in partial satisfaction of the requirements for the degree of Doctor of Philosophy

in

Chemistry

by

Charles Cameron Mokhtarzadeh

Committee in Charge:

Professor Joshua S. Figueroa, Chair
Professor Guy Bertrand
Professor Shirley Meng
Professor Joseph M. O'Connor
Professor Arnold L. Rheingold

2017

The Dissertation of Charles Cameron Mokhtarzadeh is approved and it is accepted in quality and form for publication on microfilm and electronically.

_____

_____

_____

_____

_____

Chair

University of California, San Diego

2017

# DEDICATION

*For my grandparents, Don and Joan.*

EPIGRAPH

*Two roads diverged in a yellow wood,*
*And sorry I could not travel both*
*And be one traveler, long I stood*
*And looked down one as far as I could*
*To where it bent in the undergrowth;*

*Then took the other, as just as fair,*
*And having perhaps the better claim,*
*Because it was grassy and wanted wear;*
*Though as for that the passing there*
*Had worn them really about the same,*

*And both that morning equally lay*
*In leaves no step had trodden black.*
*Oh, I kept the first for another day!*
*Yet knowing how way leads on to way,*
*I doubted if I should ever come back.*

*I shall be telling this with a sigh*
*Somewhere ages and ages hence:*
*Two roads diverged in a wood, and I–*
*I took the one less traveled by,*
*And that has made all the difference.*

Robert Frost
*The Road Not Taken*

TABLE OF CONTENTS

LIST OF ABBREVIATIONS

The following list details common abbreviations used throughout this dissertation.

| Abbreviation | Definition |
|---|---|
| 2D | Two-dimensional |
| *a, b, c* | Unit cell lattice constants (Å) |
| acac | Acetylacetonate |
| Anal. | Combustion analysis (elemental) |
| Ar | Aryl |
| $Ar^{Clips}$ | 2,6-(2,6-$Cl_2C_6H_3$)$_2C_6H_3$ |
| $Ar^{DArF2}$ | 2,6-(3,5-$(CF_3)_2C_6H_3$)$_2C_6H_3$ |
| $Ar^{Dipp2}$ | 2,6-(2,6-(*i*-Pr)$_2C_6H_3$)$_2C_6H_3$ |
| $Ar^{Mes2}$ | 2,6-(2,4,6-$Me_3C_6H_3$)$_2C_6H_3$ |
| $Ar^{Tripp2}$ | 2,6-(2,4,6-(*i*-Pr)$_3C_6H_3$)$_2C_6H_3$ |
| atm | Atmosphere (unit of pressure) |
| BArF | $[(3,5\text{-}(CF_3)_2C_6H_3)_4]^-$ |
| bp | boiling point |
| ˚C | degrees Celsius |
| $^{13}C\{^1H\}$ | $^{13}C$ NMR with proton decoupling |
| cal | calories |
| calcd. | calculated |
| $C_{ipso}$ | Carbon at ipso position of aryl ring |
| $C_{iso}$ | Isocyanide carbon atom |
| $cm^{-1}$ | Wavenumbers (IR Spectroscopy) |
| CNR | organoisocyanide |
| CO | carbon monoxide, carbonyl |
| Cp | cyclopentadienyl (*i.e.*, $[C_5H_5]^-$) |
| Cp* | pentamethylcyclopentadienyl (*i.e.*, $[Me_5C_5]^-$) |
| CSD | Cambridge Strucutral Database |
| d | doublet (NMR Spectroscopy) |

| | |
|---|---|
| dd | doublet of doublets (NMR Spectroscopy) |
| D | deuterium |
| DFT | density functional theory |
| DME | dimethoxyethane |
| Dipp | 2,6-(*i*-Pr)$_2$C$_6$H$_3$ |
| equiv | Equivalents |
| ESI | electrospray ionization |
| Et | ethyl (*e.g.*, $C_2H_5$) |
| $Et_2O$ | Diethyl ether |
| EtOAc | ethyl acetate |
| ETOH | ethanol |
| ROESY | Nuclear magnetic resonance exchange spectroscopy |
| NOSEY | Nuclear magnetic resonance exchange spectroscopy |
| $F_0$ | observed structure factor |
| FTIR | Fourier transform infrared spectroscopy |
| g | grams |
| GC | gas chromatography |
| GOF | Goodness of fit |
| h | hour |
| HC(O)OH | formic acid |
| HOMO | highest occupied molecular orbital |
| HRMS | high-resolution mass spectroscopy |
| Hz | hertz ($s^{-1}$, cycles per second) |
| *I* | Nuclear angular momentum quantum number (spin) |
| *i*-Pr | isopropyl |
| IR | infrared |
| *J* | coupling constant through bonds |
| k | kilo- ($10^3$) |
| K | degrees Kelvin |
| L | charge neutral ligand (*e.g.*, carbonyl, phosphine, isocyanide |

| | |
|---|---|
| LUMO | lowest unoccupied molecular orbital |
| *m* | *Meta* |
| m | mili- ($10^{-3}$) |
| M | metal |
| Me | Methyl (*e.g.*, $CH_3$) |
| MeCN | acetonitrile |
| *mer* | meridional |
| Mes | mesityl (*i.e.*, 2,4,6-$Me_3C_6H_2$) |
| MHz | megahertz |
| min | minutes |
| MO | molecular orbital |
| mol | moles |
| MS | mass spectroscopy |
| *n* | integer number |
| NaK | sodium –potassium alloy |
| NM | non-metal |
| NMR | nuclear magnetic resonance |
| *o* | ortho |
| OTf | triflate, trifluromethylsulfonate ($[OSO_2CF_3]^-$) |
| *p* | para |
| ph | phenyl (*i.e.*, $C_6H_5$) |
| $PMe_3$ | trimethylphosphine |
| $PPh_3$ | triphenylphosphine |
| ppm | parts per million |
| PPN | Bis(triphenylphosphine)iminium (*i.e.*, $[Ph_3{=}N{=}PPh_3]^+$) |
| q | quartet (NMR spectroscopy) |
| $r_{cov}$ | covalent radii |
| $r_{vdW}$ | van Der Waals radii |
| R | organic moiety, alkyl group |
| $R_1$ | residual value, calculated from $F_0$–data |

| | |
|---|---|
| $wR_2$ | weighted residual, calculated from $F_0^2$–data |
| RT | room temperature |
| s | Singlet (NMR spectroscopy) |
| | seconds |
| *S* | electronic spin |
| sept | Septet (NMR spectroscopy) |
| t | triplet (NMR spectroscopy) |
| tt | triplet of triplets (NMR spectroscopy) |
| *t*-Bu | *tertiary*-butyl |
| Temp | temperature |
| Theo | theoretical |
| THF | tetrahydrofuran |
| TM | transition metal |
| TMS | tetramethylsilane (*i.e.*, $SiMe_4$) |
| | trimethylsilyl (*i.e.*, $–SiMe_3$) |
| $TMS_2O$ | bistrimethylsilyl ether |
| TMSCl | trimethylsilylchloride |
| TMSOTf | trimethylsilyltriflate |
| TOFMS | time of flight mass spectrometry |
| torr | unit of pressure (1/760 of a standard atmosphere) |
| *V* | unit cell volume |
| VT | variable temperature |
| X | one electron ligand (*e.g.*, hydride, aryl, alkyl, halide) |
| *Z* | number of formula units per unit cell |
| ∠ | angle |
| Å | Angstrom ($10^{-10}$ m) |
| α,β,γ | unit cell angles (degrees) |
| δ | NMR chemical shift relative to a standard (*e.g.*, TMS) |
| Δ | change (*i.e.*, difference) |
| | heat |

| | |
|---|---|
| $\eta^n$ | hapticity of a coordinated ligand with *n* contiguous atoms coordinated to a metal center |
| $\theta_{max}$ | Maximum diffraction angle in degrees |
| $\kappa^n$ | hapticity of a ligand with *n* non-contiguous atoms coordinated to a metal center |
| $\lambda$ | X-ray wavelength (Å) |
| $\mu$ | absorption coefficient (X-ray crystallography) |
| $\nu$ | infrared stretch |
| $\rho$ | calculated crystal density ($g/cm^3$) |
| $\sigma$ | standard deviation |
| $\sigma_p$ | paramagnetic shielding tensor |
| $\Sigma$ | sum |
| $\tau_4$ | structure index for four-coordinate complexes |
| $\tau_5$ | structure index for five coordinate complexes |

LIST OF FIGURES

LIST OF SCHEMES

LIST OF TABLES

ACKNOWLEDGMENTS

This dissertation would not have been possible without a number of individuals who have, over the years, been essential to my personal and intellectual growth as a scientist. In no way does an acknowledgment even begin to convey the gratitude that I have for everyone who has been involved in this saga, but for now it will have to suffice.

First I must thank my advisor Prof. Joshua S. Figueroa. As I write this I harken back to my fist practice talk for an ACS meeting, where upon beginning my presentation I was immediately stopped and made aware of its quality (for those of you reading this that were not there, it was bad). I was then met with the question "do you want to go pro?" at which point the only response I could muster was "yes, I want to go pro." Josh, you have built a laboratory that really is unlike anything else within the chemistry department at UCSD. Your creativity, and enthusiasm coupled with an unrelenting drive to understand the chemical space that we explore is a wonder to behold, and so much more to actually be a part of. More times than I can count you have provided me with the creative freedom to follow the chemical leads I thought important, and this freedom has led to some borderline ridiculous molecules. Simultaneously, you have pushed me in more ways than one to understand these systems, to scrutinize every aspect of the science, and develop into a true scientist. For your constant support, mentorship, and pushing me to the limit and beyond, that has led to this moment I cannot say thank you enough.

I would like to also thank my committee, Prof. Arnold L. Rheingold, Prof. Joseph M. O'Connor, Prof. Guy Bertrand, and Prof. Shirley Meng. Thank you for continually being available for me to ask questions, and probe you collective chemical knowledge.

Many of your suggestions have pushed my research to the next level, and your involvement in my development as a scientist is so very much appreciated, thank you. I would also like to thank Prof.'s William Trogler, Clifford Kubiak, Seth Cohen, and Carlos Guerrero, Jeffrey Reinhart for your willingness to engage in discussions regarding my work.

To the rest of the Figueroa Lab a huge debt of gratitude is owed to all of you. Dr.'s Lizzel Labios although our overlapping time was short you were a roll model in how to get it done. Dr. Matthew Millard the words "pentane bro" still resonate with me as well as "strike three Charlie," and for good measure if I could reach strike four I would go for it. Dr. Steven P. George, thank you for introducing me to the beast that is computational chemistry. Dr. Treffly Ditri although there are many differences between our two paths there seem to be many corollaries as well, you have been a mentor and a friend, and your constant support and willingness to listen to me is so very much appreciated. Much of groundwork that has made the research presented herein was made possible by the first generation of Figueroa group members, thank your for all your help.

To the boys in the trenches with me, Dr.'s Alex E. Carpenter, Brandon R. Barnett, and soon to be Dr. Douglas W. Agnew it's been real. There is no shortage of shenanigans that we got into, which has made this one hell of a ride. I could not have asked for a harder-working, intellectual group of lunatics to work with. Your collective drive to push the boundaries of what was possible has only ever pushed me to do the same. Alex, many of the compounds presented within this dissertation would not have been possible without your tutelage and mastery of the air and $N_2$ free ways. Brandon, of

all the people that I met at the start of this endeavor I had no idea that you and I would proceed to spend the better part of 5 years together, its been a privilege. Doug the times have been good, just like the rest of ABCD you have constantly pushed me and for that thank you.

To the "young" member of the lab, Kyle Mandla, your growth as a scientist, enthusiasm about your chemistry, and your intensity is reminiscent of the early lab days and has been so appreciated during these many late nights of sciencing. Joanne "Catwoman" Chan you were brave to sit between Alex and I, but it turned out for the best. I have probably learned as much from you, as you from me. The same goes for Myles Drance. Our discussions have forced me to "level up" how I approach so many things, and for that thank you. Mike Neville and Alejandra Arroyave, the force is strong with both of you; keep up the enthusiasm, work hard, make *all* the things and I look forward to seeing what you two accomplish. And to the army of undergrads Andrew "McNasty" McNeece, Donald Ripatti, Patrick Smith, Isabel Wen, Wesley "Battle-axe" Swords, Ryo Kamezawa, Irena Havrylyuk, Enrique Flores, and Irene Zhu working with all of you has forced me to hone my skills so that I could help all of you hone yours. And with all of your collective help so many things have been accomplished, thank you.

In addition to the members of the Figueroa lab, there are a number of people within the department whom I wish to thank. From the Bertrand lab, Dr. Mohand Melaimi, thank you for all the help with the electrochemistry presented in Chapter 4. And Cory Weinstein, hopefully we will have many for science conversations to come. From the O'Connor lab, I owe a deep debt of gratitude to Dr.'s Stephen Cope, Marisa Aubrey and Ryan Holland, who were always willing to discuss the science at hand. From

the Kubiak group, Prof. Kyle Grice, Prof. Charles Machan, Dr. Matthew Sampson more often then not I stumbled over to your lab with questions, and I thank you for always being willing to indulge my ludicrous ideas. I would also like to thank Dr. Matthew Del Bell who has been my go to guy when trying to make anything organic.

To the UCSD Crystallography Laboratory, Prof. Arnold L. Rheingold, Dr. Curtis E. Moore, and Dr. Millan Gembicky a deep, deep, deep thank you is needed. Your constant tutelage, and willingness to teach crystallography has not fallen by the wayside. Much of the data in this dissertation has been acquired with your assistance. If it is not apparent how *vital* the crystallography facility and all of your efforts were, then I have done a gross disservice to the art that is crystallography, and I have deeply misrepresented my use of your facilities and teachings. Thank you, thank you, thank you for all of your help and hard work.

Dr. Anthony Mrse for the countless experiments and crazy things I have tried to detect by NMR, thank you for all your help. You were right the VX was a paradigm shift in my research and I will be sad to not have that machine at my fingertips in the future. I must also thank Dr. Yongxuan Su for putting up with me when trying to acquire HRMS of some really rowdy molecules, thank you.

All this work would not have been possible if it was not for the generous funding sources. I would like to thank the National Science Foundation (NSF) for a Graduate Research Fellowship that provided funding for three years of research, and UCSD and the Department of Education for a GAANN fellowship in my second year of graduate school.

I must also thank my undergraduate advisor Prof. Trevor Hayton for giving me the opportunity to work in his lab. If it were not for that experience I would not be where

I am to day. It was his lab that I was seduced by the lure of the glovebox and why I made the glovebox my home for the past 5 ½ years. I must also thank Prof. Skye Fortier, and Prof. Jessie Brown who were my mentors in the Hayton lab. Jessie thank you for letting me go rogue, and Skye thank you for suggesting UCSD, and showing me the way.

Of all the people I have had the pleasure of knowing while at UCSD, one person stands out above all, Prof. Angela Blum. You are by far the kindest and most loving person I have ever met. You have been my rock, and have kept me grounded through all of this. There really are not enough words to describe how thankful I am to have you in my life. Your constant support, and love, coupled with Olive and Cyrano have been one of the highlights of my life. Thank your for everything.

To my family, thank you for putting up with me. In the most literal way I would not be here today if it wasn't for all of you. To my mom, you are one of the strongest, and loving people I have ever known, and you continuously inspire me with all that you do. It is impossible to put into words the thanks I owe you, and I would probably ruin it if I tried so I will leave it at this, thank you so very much for everything. James, and Tara again I don't really know what to say because there is too much to say. I most definitely would not be here without you two. Needless to say having you two as brother and sister has only pushed me to be a better person, and I thank you for that.

I would like to say thank you one last time and to everyone. For those that I have forgotten I am sorry, but a I extend a deep thank you. Again this would not have been possible without so many people, and for all the help and support that I have received I am eternally grateful to everyone, thank you.

**Chapter 2**: This chapter is adapted with permission from **C. C. Mokhtarzadeh**; G.W. Marguileux, A.E. Carpenter, N. Weidemann, C. E. Moore, A.L. Rheingold, J. S. Figueroa. "Synthesis and Protonation of an Encumbered Iron Tetraisocyanide Dianion." *Inorgic Chemistry* **2015**, *54*, 7710-7120. Copyright 2015, American Chemical Society, The dissertation author is the first author on this paper.

Material presented in **Chapter 3** will appear as a component in an upcoming publication by Mokhtarzadeh, C. C., Moore, C. E., Rheingold, A. L., Figueroa, J. S. The dissertation author is the primary author of this manuscript.

**Chapter 4** is adapted in part from the manuscript recently submitted by **C. C. Mokhtarzadeh**; A.E. Carpenter; D. Spence; M. Melaimi; D. Agnew; N. Weidemann, C. E. Moore, A.L. Rheingold, J. S. Figueroa. "Geometric and Electronic Strucure Analysis of the Three Membered Electron Transfer Series $[(\mu\text{-CNR})_2[CpCo]_2]^n$ ($n$ = 0, 1–, 2–) and its Relavance to the Classical Bridging-Carbonyl System." The dissertation author is the primary author of this manuscript. Dr. Brandon R. Barnett, Kyle A. Mandla, Prof. Jeffery Rinehart are thanked for helpful discussions.

**Chapter 5.** Chapter 5 is adapted in part from **C. C. Mokhtarzadeh**; A. L. Rheingold; J. S. Figueroa. *Dalton Tras.* **2016**, *45*, 14561. Copyright 2016 The Royal Society of Chemistry. The dissertation author is the primary author on this publication. The synthesis of $CNAr^{Tripp2}$ is adapted in part from A. E. Carpenter; **C. C. Mokhtarzdeh**; D. S. Ripatti; I. Havrylyuk; R. Kamezawa; C. E. Moore; A. L. Rheingold; and J. S.

Figueroa. *Inorg. Chem.* **2105**, *54*, 2936-2944. Copyright 2015, American Chemical Society. The dissertation author is the second author of this pubilication. Permission to include published material in this dissertation has been obtained from all coauthors. Additional unpublished results are reported here in, and are to currently in preparation as manuscript by **C. C. Mokhtarzadeh**; C. E. Moore; M. Gembicky; A. L. Rheingold; J. S. Figueroa. The dissertation author is the primary author of this manuscript.

**Chapter 6** is currently in preparation as a manuscript by **C. C. Mokhtarzadeh**, C. E. Moore; M. Gembicky; A. L. Rheingold; J. S Figueroa. The dissertation author is the primary author of this manuscript. Prof. Adah Almutairi, and Dr. Amy Moore are thanked for generous access to their *in-situ* React-IR spectrometer. Dr. Anthony Mrse is thanked for assistance with hetero-nuclear NMR experiments.

**Chapter 7** is currently in preparation as a manuscript by **C. C. Mokhtarzadeh**; C. E. Moore; A. L. Rheingold; J. S. Figueroa. The dissertation author is the primary author of this manuscript. Dr. Brandon R. Barnett, Douglas W. Agnew, Kyle A. Mandla are thanked for helpful discussions.

# VITA

2017 Ph.D. in Chemistry, University of California, San Diego

2013 M.S. in Chemistry, University of California, San Diego

2010 B.S. in Chemistry, University of California, Santa Barbara

## PUBLICATIONS

**C. C. Mokhtarzadeh**, A. E. Carpenter, D. Spence, M. Melaimi, D. Agnew, N. Weidemann, C. E. Moore, A. L. Rheingold, J. S. Figueroa. "Geometric and Electronic Strucure Analysis of the Three Membered Electron Transfer Series $[(\mu\text{-CNR})_2[\text{CpCo}]_2]^n$ ($n$ = 0, 1–, 2–) and its Relavance to the Classical Bridging-Carbonyl System." *Submitted.*

**C. C. Mokhtarzadeh**, A. L. Rheingold, J. S. Figueroa. "Dinitrogen Binding, $P_4$-Activation and Aza-Büchner Ring Expansions Mediated by an Isocyano Analogue of the CpCo(CO) Fragment." *Dalton. Trans.* **2016**, 14561-14569.

A. J. McNeece, **C. C. Mokhtarzadeh**, C. C. Moore, A. L. Rheingold, J. S. Figueroa. "Nickel bis-*m*-terphenylisocyanide dihalide complexes formed from 1,2-alkyldihalides: probing for isolable β-haloalkyl complexes of square planar nickel." *J. Coord. Chem.* **2016**, *69,* 2059-20698. (*Invited Contribution).*

**C. C. Mokhtarzadeh**, G.W. Marguileux, A.E. Carpenter, N. Weidemann, C. E. Moore, A.L. Rheingold, J.S. Figueroa. "Synthesis and Protonation of an Encumbered Iron Tetraisocyanide Dianion." *Inorg. Chem.* **2015**, *54*, 7710-7120.

A. E. Carpenter, **C. C. Mokhtarzadeh**, D. S. Ripatti, I. Havrylyuk, R. Kamezawa, C.E. Moore, A. L. Rheingold, J. S. Figueroa. "Comparative Measure of the Electronic Influence of Highly Substituted Aryl Isocyanides." *Inorg. Chem.* **2015**, *54*, 2936-2944.

A. E. Carpenter, A. J. McNeece, B. R. Barnett, A. L. Estrada, **C. C. Mokhtarzadeh**, C. E. Moore, A. L. Rheingold, J. S. Figueroa. "Direct Observation of β-Chloride Elimination from an Isolable β-Chloroalkyl Complex of Square Planar Nickel." *J. Am. Chem. Soc.* **2014**, *136, 15481-15484.*

J. L. Brown, **C. C. Mokhtarzadeh**, J. M. Lever, G. Wu, T. W. Hayton. "Facile Reduction of Uranyl (VI) β-Ketoiminate Complex to U(IV) Upon Oxo Silation." *Inorg. Chem.* **2011**, *50,* 5105-5112.

ABSTRACT OF THE DISSERTATION

**Low-Valent Iron and Cobalt Isocyanide Complexes: Platforms for Small Molecule Activation, Coordination Chemistry and Novel Electronic Structure Motifs.**

by

Charles Cameron Mokhtarzadeh

Doctor of Philosophy in Chemistry

University of California, San Diego, 2017

Professor Joshua S. Figueroa, Chair

This dissertation describes the targeted attempts at the generation of transition metal species that function as precise electronic structure mimics to the well known spin triplet ($S$ =1) metal carbonyls fragments $Fe(CO)_4$ and CpCo(CO). These unsaturated fragments have been shown to display a wide range reactivity, and competency towards important reaction chemistry such as alkane and $N_2$ binding, and E–H bond activation due to a unique interplay of a strong ligand field, formal $d^n$ count, and orbital symmetry, rendering these fragments primed for bond activation. Accordingly, ligand architectures

that can accurately mimic the ligand field provided by CO to kinetically stabilize these fragments could provide new inroads to novel small molecule activation pathways. To this end, sterically encumbering *m*-terphenyl isocyanides serve as isolobal ligand surrogates for carbon monoxide (CO). Additionally isocyanides have the added benefit of providing kinetic stabilization by virtue of readily tunable isocyano–*R* (CN–*R*) group.

The first section of this dissertation describes the synthesis and protonation of an encumbered tetra-isocyanide iron dianion, $Na_2[Fe(CNAr^{Mes2})_4]$ ($Ar^{Mes2}$ = 2,6-(2,4,6 – $Me_3C_6H_2)_2C_6H_3$), which serves as a platform for targeting species of the formulation $Fe(CNAr^{Mes2})_4$. It is shown that the reactivity of the electronically unsaturated $Fe(CNR)_4$ fragment upon protonation of $Na_2[Fe(CNAr^{Mes2})_4]$ and subsequent alkylation of $Na[HFe(CNAr^{Mes2})_4]$, yields the dinitrogen stabilized species $Fe(N_2)(CNAr^{Mes2})_4$. $Fe(N_2)(CNAr^{Mes2})_4$ is shown to readily undergo intramolecular C–H activation of the ligand scaffold upon liberation $N_2$ under ambient conditions purportedly through and insipient $[Fe(CNAr^{Mes2})_4]$ fragment. Further more, ability of $Na_2[Fe(CNAr^{Mes2})_4]$ to facilitate the reductive disproportionation of $CO_2$, in addition to $CO_2$ capture with electrophilic silyl sources is presented culminating in a rare class of low valent Fe-aminocarbyne complexes.

The second vignette of this dissertation focuses on the generation of species that mimic the formulation CpCo(L). It is shown that with less encumbering *m*-terphenyl isocyanides that aggregation akin to the unsaturated carbonyl congeners is realized. Use of encumbering *m*-terphenyl isocyanides provides access to the three memebered electron transfer series $[(\mu^2\text{-}CNAr^{Mes2})_2[CpCo]_2]^n$ (n = 0,–1, –2). Notably, this series is the first of its kind to span all three ostensible electronic states (*e.g.* $d^8$-$d^8$, $d^8$-$d^9$, and $d^9$-$d^9$),

previously unavailable with other π-acidic ligand frameworks. Additionally this allows for a systematic reassessment of the metal-metal bonding within this class of dimeric species. Evidence is put forth in favor of no M–M bonding interactions occur within these systems and the integrity of the dimeric framework is in fact mitigated through a unique interplay of the metal *d*-manifold and the isocyanide π*–system.

Modulation of the steric profile of the *m*-terphenyl isocyanide and the Cp unit to Cp* so as to increase the steric pressure provides access to the first reported mono-nuclear Cp*Co($N_2$)L fragments. It is shown that these species function as viable sources of Cp*Co(CNR) for a number of bond activation processes including Si–H, H–H, and P–P bond scission. Moreover, the reactivity of these species culminates with the isolation of the second example of a structurally authenticated transition metal nitrous oxide ($N_2O$) adduct, which exhibits an unprecedented $\eta^2$–(N,N) coordination mode to Co. Finally, the reduction of the encumbered Cp*Co($CNAr^{Tripp2}$) ($CNAr^{Tripp2}$ 2,6-(2,4,6-(*i*-Pr)$_3C_6H_3$)$_2C_6H_3$) fragment provide access to the unique dianion $K_2$[Cp*Co≡$CNAr^{Tripp2}$]. It is shown that the dianion $K_2$[Cp*Co≡$CNAr^{Tripp2}$] exhibits 3-fold bonding between Co and the isocyanide –$C_{iso}$ through an extreme case of M→(CN) π*-back donation and gives rise to the first example of a Co-carbyne complex. The reactivity and electronic structure are presented for $K_2$[Cp*Co≡$CNAr^{Tripp2}$] and it is concluded that this reactive dianion behaves as a potent metal based nucleophile and source of $[Cp^*Co(CNR)]^{2-}$ for a number of bond activation process.

# *Chapter 1*

# *Unsaturated Transition Metal Carbonyls*

## 1.1 Introduction

From the initial postulation and later observation of the unsaturated transition metal carbonyls, namely $Mo(CO)_4$, $Ni(CO)_3$, $Pd(CO)_2$, interest in their reaction chemistry and electronic structure has maintained an area of intense research interest. Observation of these unsaturated transition metal carbonyls are primarily limited to cryogenic infrared matrix isolation studies, where generation via photo-dissociation of a carbonyl ligand (CO) in an "inert" matrix (*e.g.* $N_2$, Ar, $CH_4$) provides a method for their observation.[1-3] Of particular interest are those that possess high spin electronic ground states (S = 1), namely $Fe(CO)_4$ and CpCo(CO), due to their high competency for bond activation processes, and unusual geometric and electronic structures.[4] However, due to their inherent reactivity and instability, proper structural analysis has been precluded. Over the past ten years, our group has taken interest in the generation of precise electronic structure mimics of these unsaturated transition metal carbonyls by utilizing sterically encumbering *m*-terphenyl isocyanides as isolobal surrogates for carbon monoxide. The analogous ligand field coupled with the added kinetic stabilization afforded by the isocyanide –*R* group makes *m*-terphenyl isocyanides attractive ligand architectures for the generation of coordinativley unsaturated metal centers that mimic the geometric and electronic structure of unsaturated metal carbonyls. This dissertation focuses on the attempted generation of isocyano-analogues of the high spin organometallics $Fe(CO)_4$ and CpCo(CO), the trapping of these fragments as

dinitrogen adducts, the ability of the resulting species to provide access to unusual coordination complexes, and their reaction chemistry toward the activation of small molecules.

## 1.2 Unsaturated Transition Metal Carbonyls that Exhibit High-Spin Ground States.

From the initial observation of *cis*-$PtCl_2(CO)_2$ by Schützenberger in 1868,[5] and $Ni(CO)_4$ by Mond and co-workers in 1890,[6] the field of transition-metal carbonyl chemistry has seen untiring interest amongst the organometallic community. Surprisingly the generation of the binary transition-metal carbonyls via the direct reaction of CO with bulk metal precursors has been limited to $Ni(CO)_4$ and later $Fe(CO)_5$ initially described by Mond.[7] Since its discovery the industrial utility of $Fe(CO)_5$ has been utilized in the hydrogenation, isomerization and hydrosilyation of alkenes.[8-12] Additionally, the reaction chemistry of $Fe(CO)_5$ has also been thoroughly studied.[16] Reduction results in carbonyl dissociation and generation of the tetrahedral $d^{10}$ metallate tetra-carbonyl ferrate, $[Fe(CO)_4]^{2-}$, which functions as a potent organometallic nucleophile for the conversion of alkyl halides to aldehydes.[13] Moreover, simple substitution reactions under photolytic conditions which are typified by the ejection of one or two equivalents of CO to generate the unsaturated fragments $Fe(CO)_4$ and $Fe(CO)_3$,[14] respectively. These unsaturated species can then be trapped by incoming L-donor ligands.[15,16] Interestingly, the first report of $Fe(CO)_5$ was in fact misidentified as its unsaturated fragment $Fe(CO)_4$– providing what would be the first report of an unsaturated transition-metal carbonyl complex.[7] It is these unsaturated species that facilitate the broad reactivity profile of $Fe(CO)_5$. In an effort to understand these reactivity profiles tremendous effort in their

generation, observation and isolation, have been ongoing challenges over the past 100 years for organometallic chemists.

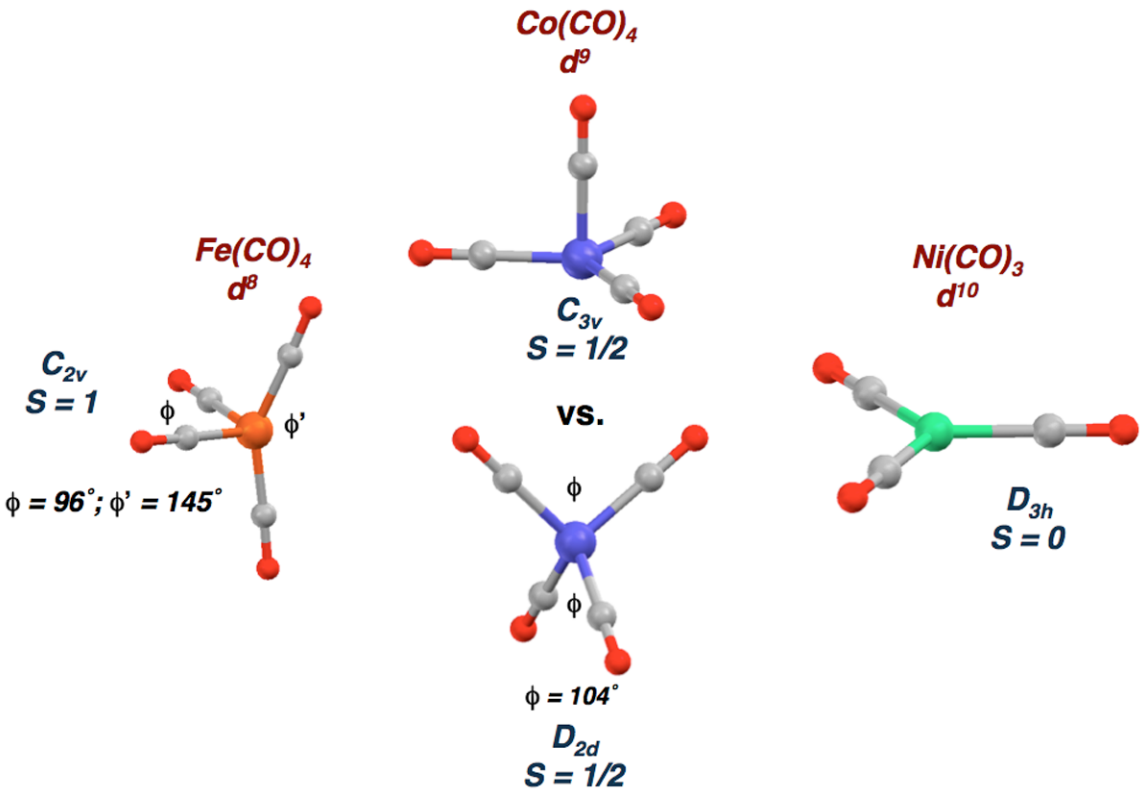


**Figure 1.1** Predicited geometries of late transition-metal unsaturated binary carbonyls $Fe(CO)_4$ (left), $Co(CO)_4$ (center), and $Ni(CO)_3$ (right) with corresponding geometries and electronic states denoted.

The most effective method for the generation of unsaturated transition-metal carbonyl species has typically been through photo-dissociation of CO to generate the corresponding unsaturated fragments.[11,17,18] However the extremely short lifetimes of these fragments coupled with their extreme reactivity profiles have made their observation challenging in the condensed phase. To circumvent the difficulties of observing unsaturated carbonyl fragments the use of cryogenic infrared (IR) matrices[19,20] to immobilize the resultant species, gas phase measurements,[1,2,18,21-24] and ultrafast solution IR spectroscopy[4,25] have been implemented so as to elucidate their electronic and

geometric structural features. This is made possible due to the strong IR active modes characteristic of CO when coordinated to a metal, which can be used to directly access electronic state, coordination number, and importantly geometric structure.

Of particular interest are unsaturated carbonyl species that display high-spin electronic states (S > ½). Previous attention in our lab has focused on late transition-metal unsaturated fragments that feature filled or nearly filled d orbital manifolds (*e.g* $Ni(CO)_3$, $Pd(CO)_2$, $Pt(CO)_2$, $Co(CO)_4$)[26-28] that favor low-spin (S = 0, 1/2) electronic states. This dissertation focuses on two prominent unsaturated transition-metal carbonyl complexes. The first is $Fe(CO)_4$ which due to a unique interplay of $d^n$ count, orbital symmetry, and geometric structure provides a high-spin (S = 1) system despite the strong ligand field. [4,29-32] $Fe(CO)_4$ displays Jahn-Teller instability due to its $d^8$ electronic configuration in a tetrahedral ligand field resulting in a geometric distortion from tetrahedral to $C_{2v}$ or "saw-horse".[33,34] This distortion results in the two highest filled molecular orbitals (*i.e.* $a_1(z^2)$, and $b_2(yz)$) remaining close in energy yet non-degenerate yielding an S = 1 ground state.[33] The second high spin species is $CpCo(CO)$[31,35-39] which has found particular use in the [2+2+2] cyclo-additions of alkynes from the photolysis of $CpCo(CO)_2$.[40-43] Like $Fe(CO)_4$, CpCo(CO) adopts a distorted "bent" structure rather than a linear coordination mode to circumvent the population of a strongly Co–Cp anti-bonding orbitals.[44] Moreover this results in two close in energy yet non-degenerate closely spaced orbitals a"(xz), a"(yz) affording its high-spin electronic state.[44] Furthermore, these two species have shown unusually high reactivity with solution lifetimes on the pico-second time scale depending on the solvent used in their generation.[4,25] And lastly, both $Fe(CO)_4$ and CpCo(CO) have been shown to undergo important bond

activation processes including alkane[25,45] and $N_2$ coordination,[30,46] in addition to E–H bond activation.[8,47-49] Due to their fleeting nature, and proficiency at bond activation, structural authentication in the condensed phase of these species has been precluded. Accordingly, the development of systems that can function as precise electronic structure mimics could provide further insight into the structure and bonding unavailable with current spectroscopic methods, in addition to potentially providing novel methods for small molecule activation previously not observed with carbonyl systems.

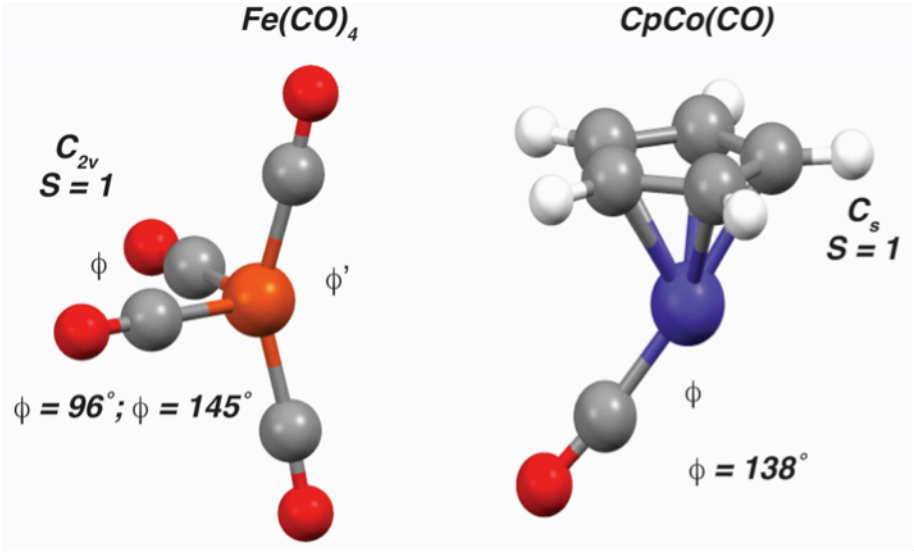


**Figure 1.2** Predicted geometries of $Fe(CO)_4$ and CpCo(CO), both are high spin complexes that exhibit S = 1 ground states.

## 1.3 Transition Metal Isocyanides

Like carbon monoxide, organo-isocyanides (CNR) have a rich history in organometallic chemistry, and despite displaying a stronger σ-donor/π-acidity ratio have been extensively employed as surrogates for carbon monoxide in the generation of neutral and anionic transition metal species.[50-55] Unlike other π-acidic ligands such as phosphites,[56] cyclic alkyl amino carbenes (CAAC's),[57] and $PF_3$,[58,59] isocyanides and CO share an isolobal relationship, Figure 1.3. Isocyanides can coordinate to metal centers via

a direct σ-bonding interaction from the lone pair on carbon, in addition to providing two orthogonal π*-orbitals to engage in π-backdonation analogous to CO, and thus allowing isocyanides to provide a similar ligand field when coordinated to a metal. Isocyanides also have the added benefit of the modulation of the N-bound organic (CN–*R*) substituent, which can be tuned to specific steric and electronic profiles. Indeed, isocyano analogues to the binary transition-metal carbonyls have been synthesized, however, despite the increased steric profile of isocyanides when compared to CO, these transition-metal isocyanides have been met with coordinative saturation.[60-65] Specifically with regards to Fe, penta-coordinate isocyanide complexes have been generated (*e.g.* $Fe(CN\textit{t}–Bu)_5$) and have been shown to mimic the coordination geometry and electronic structure of $Fe(CO)_5$.[66] Additionally, $Fe(CN\textit{t}–Bu)_5$ has been shown to undergo ligand substitution reactions presumably through the ejection of and isocyanide ligand to generate a fleeting four-coordinate fragment $Fe(CNR)_4$ which is rapidly intercepted by incoming L-donnor ligands, thus precluding its observation in the condensed phase.[66]

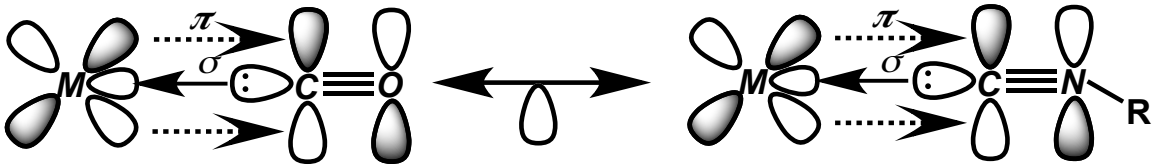


**Figure 1.3** Qualitative molecular orbital representation for transition metal carbonyl and isocyanide bonding interactions.

In addition to $Fe(CO)_4$ which is an iconic high-spin organometallic within a strong ligand field, CpCo(CO) serves as a heteroleptic and isoelectronic fragment. Isocyano-analogues of the CpCo(CO) fragment could potentially provide a route to an increased understanding of the electronic structure and reaction chemistry, however unlike homoleptic iron isocyanides the development of CpCo systems featuring isocyanides as

ligand auxiliaries is surprisingly underdeveloped.[67-69] To date, the only structurally characterized $CpCo(CNR)_2$ species predating our work features acyl isocyanides ligands.[70] Moreover, utilization of isocyanides as isolobal surrogates for the CpCo(CO) fragment are unknown, and thus provide an impetus for the development of these systems. Interesting still are the aggregation processes that plauge CpCo(CO) fragments upon photolysis of $CpCo(CO)_2$ to generate $[\mu^2\text{-}CO]_2[CpCo]_2$.[37] These dimeric species have also found wide study within the literature and their electronic structure to date is still of interest due to the implication of late transition metal, metal-metal bonding.[71-74] It is within these contexts that isocyanide for CO substitution could provide new in-roads in the understanding of the electronic structure of these iconic species that have perplexed organometallic chemists since their initial observation. To bridge these voids, it has proven to be a worthwhile endeavor to generate isocyanide architectures capable of preventing aggregation processes, so as to kinetically stabilize these fleeting $FeL_4$ and CpCoL fragments, and provide detailed insight into their electronic structure and potent reaction chemistry within the condensed phase.

### 1.4 Transition Metal Complexes Supported by *m*-Terphenyl Isocyanides

In an effort to target unsaturated transition metal complexes that mimic the unsaturated carbonyls our group has employed isocyanide ligands that feature the sterically encumbering *m*-terphenyl units. [55,75-77] The *m*-terphenyl framework has shown a wide array of use as a ligand scaffold to transition metals as purely σ-aryls,[78,79] amidos, [80,81] imidos,[80,82] thiolates,[83] and carboxylates[84,85] to name a few. The ability to readily modulate the steric profile of the *m*-terphenyl unit allows for ligand platforms that can be tailored to enforce specific coordination numbers and geometries. Although *m*-terphenyl

isocyanides have been utilized prior to our efforts,[86-88] their use in generating analogues to the unsaturated transition-metal carbonyls has only been recently explored by us. To this end our group has developed a variety of *m*-terphenyl isocyanides with varying steric and electronic profiles tailored to this endeavor Figure 1.4.

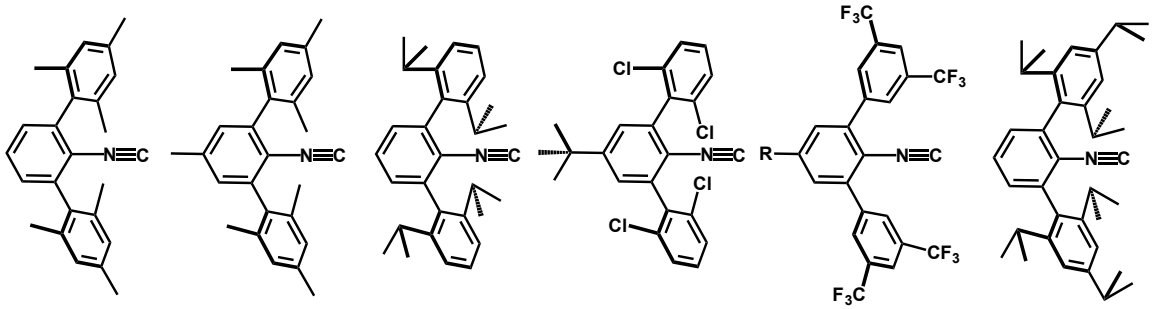


**Figure 1.4** Prototypical *m*-terphenyl isocyanide ligands with varying electronic and steric profiles. (Left to right) $CNAr^{Mes2}$, *p*-Me-$CNAr^{Mes}$, $CNAr^{Dipp2}$, $CNAr^{Clipps2}$, *p*-R-$CNAr^{DArF2}$, $CNAr^{Tripp2}$.

Initial attempts at generating coordinatively unsaturated transition-metal complexes incorporated the *m*-terphenyl isocyanides $CNAr^{Mes2}$ ($Ar^{Mes2}$ = 2,6-(2,4,6-$Me_3C_6H_3)_2C_6H_3$ ) and $CNAr^{Dipp2}$ ($Ar^{Dipp2}$ = 2,6-(2,6-(*i*-$Pr)_2C_6H_3)_2C_6H_3$).[89,90] Efforts at generating unsaturated Ni complexes initially utilized the isocyanide ligand $CNAr^{Mes2}$. Addition of TlOTf to the bis-isocyanide precursor $Ni(COD)(CNAr^{Mes2})_2$ as a coordination site protecting group followed by addition of a third equivalent of $CNAr^{Mes2}$ in the presence of KI afforded the three coordinate species $Ni(CNAr^{Mes2})_3$, an isocyano analogue the unsaturated binary carbonyl species $Ni(CO)_3$.[90] Indeed, increasing the steric profile of the ligand framework to a more encumbering *m*-terphenyl frameworks (*e.g.* $CNAr^{Dipp2}$) allowed for facile generation of analogous three coordinate Ni species. Simple reduction of the diiodide precursor $NiI_2(CNAr^{Dipp2})_2$ with $Mg^0$ in the presence of an equivalent of $CNAr^{Dipp2}$ readily affords an analogous unsaturated Ni species

$Ni(CNar^{Dipp2})_3$ which no longer necessitates a coordination site protecting group strategy.[91]

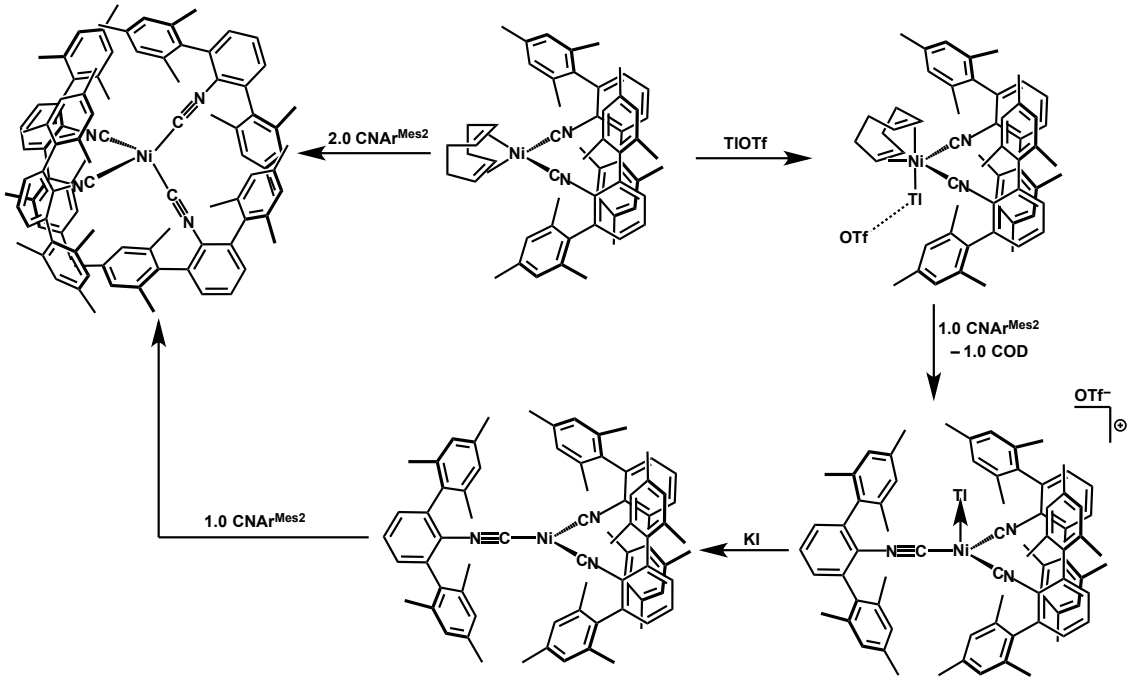


**Scheme 1.1** Synthetic procedure of $Ni(CNAr^{Mes2})_3$ utilizing Tl(I) as a coordination site protecting group strategy.

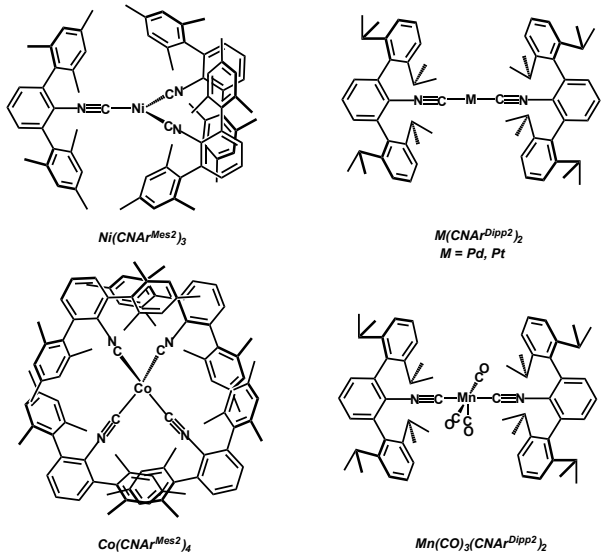


**Figure 1.5** Structurally authenticated unsaturated metal complexes featuring *m*-terphenyl isocyanides and mixed isocyanide/carbonyl ligand fields that mimic the geometric and electronic structures of the binary unsaturated transition-metal carbonyls congeners.

Importantly, use of sterically encumbering *m*-terphenyl isocyanides has been successfully extended to both Pd and Pt in the generation of the di-coordinate species $Pd(CNAr^{Dipp2})_2$ and $Pt(CNAr^{Dipp2})_2$ both of which are isocyano analogues to their carbonyl congeners $Pd(CO)_2$ and $Pt(CO)_2$ respectively.[89,92] Additionally *m*-terphenyl isocyanides have been competent ligand platforms for the generation of unsaturated Co systems, namely with the generation of the three membered electron transfer series $[Co(CNAr^{Mes2})_4]^n$ ($n$ = +1, 0, –1).[93] And lastly the prowess of *m*-terphenyl isocyanides have also been shown to act in conjunction with CO in a mixed ligand field to stabilize the first mono-nuclear five coordinate Mn metallo radical $Mn(CO)_3(CNAr^{Dipp2})_2$, a mixed carbonyl/isocyanide congener of the elusive unsaturated Mn species $Mn(CO)_5$.[94] It is under these pretexts that this dissertation details the attempts to extend these molecular design principles to systems that exhibit high-spin electronic ground states within a strong ligand field that could potentially serve as precise electronic structure mimics of the fleeting unsaturated transition-metal carbonyl fragments $Fe(CO)_4$ and CpCo(CO).

## 1.5. References


(1) Zhou, M.; Andrews, L.; Bauschlicher, C. W. *Chem. Rev.* **2001**, *101*, 1931.

(2) Weitz, E. *J. Phys. Chem.* **1987**, *91*, 3945.

(3) Lippard, S. J. *Progress in Inorganic Chemistry, Vol. 19*; John Wiley & Sons, **2009**, 105.

(4) Lomont, J. P.; Nguyen, S. C.; Harris, C. B. *Acc. Chem. Res.* **2014**, *47*, 1634.

(5) Schützenberger, P. *Bull. Soc. Societe Chim. Fr.* **1868**, *10*, 188.

(6) Mond, L.; Langer, C.; Quincke, F. *J. Chem. Soc., Trans.* **1890**, *57*, 749.

(7) Mond, L.; Quincke, F. *J. Chem. Soc., Trans.* **1891**, *59*, 604.

(8) Schroeder, M. A.; Wrighton, M. S. *J. Am. Chem. Soc.* **1976**, *98*, 551.

(9) Schroeder, M. A.; S Wrighton, M. *J. Organomet. Chem.* **1977**, *128*, 345.

(10) Whetten, R. L.; Fu, K. J.; Grant, E. R. *J. Am. Chem. Soc.* **1982**, *104*, 4270.

(11) Mitchener, J. C.; Wrighton, M. S. *J. Am. Chem. Soc.* **1981**, *103*, 975.

(12) Hendrix, W. T.; Cowherd, F. G. *Chem. Commun.* **1968**, 97.

(13) Collman, J. P. *Acc. Chem. Res.* **1975**, *8*, 342.

(14) Ouderkirk, A. J.; Wermer, P.; Schultz, N. L.; Weitz, E. *J. Am. Chem. Soc.* **1983**, *105*, 3354.

(15) Wrighton, M. *Chem. Rev.* **1974**, *74*, 401.

(16) Von Gustorf, R. A. K.Pauson, Grevels, F.W., Fischler, I. *The Organic Chemistry of Iron, Vol. 2.* Academic Press, **1981**,1-258.

(17) Tumas, W.; Gitlin, B.; Rosan, A. M.; Yardley, J. T. *J. Am. Chem. Soc.* **1982**, *104*, 55.

(18) Ishikawa, Y.; Brown, C. E.; Hackett, P. A.; Rayner, D. M. *J. Phys. Chem.* **1990**, *94*, 2404.

(19) Perutz, R. N.; Turner, J. J. *Inorg Chem* **1975**, *14*, 262.

(20) Perutz, R. N.; Turner, J. J. *J. Am. Chem. Soc.* **1975**, *97*, 4800.

(21) Fletcher, T. R.; Rosenfeld, R. N. *J. Am. Chem. Soc.* **1985**, *107*, 2203.

(22) Seder, T. A.; Church, S. P.; Weitz, E. *J. Am. Chem. Soc.* **1986**, *108*, 4721.

(23) Andrews, L.; Zhou, M; Gutsev, G. L. *J. Phys. Chem. A.* **2003**, *107*, 990.

(24) Andrews, L.; Zhou, M.; Gutsev, G. L.; Wang, X. *J. Phys. Chem. A.* **2003**, *107*, 561.

(25) Lomont, J. P.; Nguyen, S. C.; Schlegel, J. P.; Zoerb, M. C.; Hill, A. D.; Harris, C. B. *J. Am. Chem. Soc.* **2012**, *134*, 3120.

(26) Hanlan, L. A.; Huber, H.; Kuendig, E. P.; McGarvey, B. R.; Ozin, G. A. *J. Am.*

*Chem. Soc.* **1975**, *97*, 7054.

(27) Basolo, F.; Wojcicki, A. *J. Am. Chem. Soc.* **1961**, *83*, 520.

(28) Zhou, M.; Andrews, L.; Bauschlicher, C. W. *Chem. Rev.* **2001**, *101*, 1931.

(29) Poliakoff, M. *J. Chem. Soc. Dalton Trans.* **1974**, 210.

(30) Poliakoff, M.; Weitz, E. *Acc. Chem. Res.* **1987**, *20*, 408.

(31) Snee, P. T.; Payne, C. K.; Kotz, K. T.; Yang, H.; Harris, C. B. *J. Am. Chem. Soc.* **2001**, *123*, 2255.

(32) Poliakoff, M.; Turner, J. J. *Angew. Chem. Int. Ed.* **2001**, *40*, 2809.

(33) Elian, M.; Hoffmann, R. *Inorg Chem* **1975**, *14*, 1058.

(34) Burdett, J. K. *Inorg Chem* **1975**, *14*, 375.

(35) Vollhardt, K. P. C.; Bercaw, J. E.; Bergman, R. G. *J. Am. Chem. Soc.* **1974**, *96*, 4998.

(36) Peter, K.; Vollhardt, C.; Bercaw, J. E.; Bergman, R. G. *J. Organomet. Chem.* **1975**, *97*, 283.

(37) Lee, W. S.; Brintzinger, H. H. *J. Organomet. Chem.* **1977**, *127*, 87.

(38) Bengali, A. A.; Bergman, R. G.; Moore, C. B. *J. Am. Chem. Soc.* **1995**, *117*, 3879.

(39) Siegbahn, P. E. M. *J. Am. Chem. Soc.* **1996**, *118*, 1487.

(40) Lautens, M.; Klute, W.; Tam, W. *Chem. Rev.* **1996**, *96*, 49.

(41) Field, L. D.; Ward, A. J.; Turner, P. *Aust. J. Chem.* **1999**, *52*, 1085.

(42) Saito, S.; Yamamoto, Y. *Chem. Rev.* **2000**, *100*, 2901.

(43) Heller, B.; Hapke, M. *Chem. Soc. Rev.* **2007**, *36*, 1085.

(44) Hofmann, P.; Padmanabhan, M. *Organometallics* **1983**, *2*, 1273.

(45) Dougherty, T. P.; Heilweil, E. J. *J Chem Phys* **1994**, *100*, 4006.

(46) Crichton, O.; Rest, A. J.; Taylor, D. J. *J. Chem. Soc., Dalton Trans.* **1980**, 167.

(47) Rest, A. J.; Whitwell, I.; Graham, W. A. G.; Hoyano, J. K.; McMaster, A. D. *J. Chem. Soc., Dalton Trans.* **1987**, 1181.

(48) Wasserman, E. P.; Bergman, R. G.; Moore, C. B. *J. Am. Chem. Soc.* **1988**, *110*, 6076.

(49) Musaev, D. G.; Morokuma, K. *J. Am. Chem. Soc.* **1995**, *117*, 799.

(50) Weber, L. *Angew. Chem. Int. Ed.* **1998**, *37*, 1515.

(51) Barybin, M. V.; Young, V. G.; Ellis, J. E. *J. Am. Chem. Soc.* **2000**, *122*, 4678.

(52) Malatesta, L. *Progress In Inorganic Chemistry*. Interscience Publishers, Inc., New York, **1959**, 283-379.

(53) Brennessel, W. W.; Ellis, J. E. *Angew. Chem. Int. Ed. Engl.* **2007**, *46*, 598.

(54) Barybin, M. V.; Brennessel, W. W.; Kucera, B. E.; Minyaev, M. E.; Sussman, V. J.; Young, V. G.; Ellis, J. E. *J. Am. Chem. Soc.* **2007**, *129*, 1141.

(55) Carpenter, A. E.; Mokhtarzadeh, C. C.; Ripatti, D. S.; Havrylyuk, I.; Kamezawa, R.; Moore, C. E.; Rheingold, A. L.; Figueroa, J. S. *Inorg Chem* **2015**, *54*, 2936.

(56) Dias, P. B.; de Piedade, M. E. M.; Simões, J. A. M. *Coordination Chemistry Reviews* **1994**, *135-136*, 737.

(57) Soleilhavoup, M.; Bertrand, G. *Acc. Chem. Res.* **2015**, *48*, 256.

(58) Kruck, T. *Angew. Chem. Int. Ed.* **1966**, *6*, 53.

(59) Xiao, S.; Trogler, W. C.; Ellis, D. E.; Berkovitch-Yellin, Z. *J. Am. Chem. Soc.* **2002**, *105*, 7033.

(60) Mann, K. R.; Cimolino, M.; Geoffroy, G. L.; Hammond, G. S.; Orio, A. A.; Albertin, G.; Gray, H. B. *Inorganica Chimica Acta* **1976**, *16*, 97.

(61) Yamamoto, Y.; Yamazaki, H. *J. Organomet. Chem.* **1977**, *137*, C31.

(62) Yamamoto, Y.; Yamazaki, H. *Inorg Chem* **1978**, *17*, 3111.

(63) Yamamoto, Y. *Coord. Chem. Rev.* **1980**, *32,* 193.

(64) Otsuka, S.; Yoshida, T.; Tatsuno, Y. *J. Am. Chem. Soc.* **2002**, *93,* 6462.

(65) Barker, G. K.; Galas, A. M. R.; Green, M.; Howard, J. A. K.; Stone, F. G. A.; Turney, T. W.; Welch, A. J.; Woodward, P. *J. Chem. Soc., Chem. Commun.* **1977**, 256.

(66) Bassett, J.-M.; Berry, D. E.; Barker, G. K.; Green, M.; Howard, J. A. K.; Stone, F. G. A. *J. Chem. Soc., Dalton Trans.* **1979**, 1003.

(67) Heiser, B.; Werner, H. *Synthesis and Reactivity in Inorganic and Metal-Organic Chemistry* **2006**.

(68) Beaumont, I.; Wright, A. H. *J. Organomet. Chem.* **1992**, *425* (1-2), C11.

(69) Yamamoto, Y.; Mise, T.; Yamazaki H. *Bull. Chem. Soc. Jap.* **1978**, *51*, 2743.

(70) Carter, S. J.; Foxman, B. M.; Stuhl, L. S. *Organometallics* **1986**, *5*, 1918.

(71) Pinhas, A. R.; Hoffmann, R. *Inorg Chem* **1979**, *18*, 654.

(72) Byers, L. R.; Dahl, L. F. *Inorg Chem* **1980**, *19*, 277.

(73) Schugart, K. A.; Fenske, R. F. *J. Am. Chem. Soc.* **1986**, *108,* 5100.

(74) Wang, H.; Xie, Y.; King, R. B.; Schaefer, H. F. *J. Am. Chem. Soc.* **2005**, *127*, 11646.

(75) Fox, B. J.; Sun, Q. Y.; DiPasquale, A. G.; Fox, A. R.; Rheingold, A. L.; Figueroa, J. S. *Inorg Chem* **2008**, *47*, 9010.

(76) Ditri, T. B.; Fox, B. J.; Moore, C. E.; Rheingold, A. L.; Figueroa, J. S. *Inorg Chem* **2009**, *48*, 8362.

(77) Ditri, T. B.; Carpenter, A. E.; Ripatti, D. S.; Moore, C. E.; Rheingold, A. L.; Figueroa, J. S. *Inorg Chem* **2013**, *52*, 13216.

(78) Twamley, B.; Haubrich, S. T.; Power, P. P. In *Advances in Organometallic Chemistry, Vol. 44*. Elsevier, 1999; *44*, 1–65.

(79) Clyburne, J. A. C.; McMullen, N. *Coord. Chem. Rev.* **2000**, *210*, 73.

(80) Gavenonis, J.; Tilley, T. D. *Organometallics* **2002**, *21*, 5549.

(81) Wright, R. J.; Steiner, J.; Beaini, S.; Power, P. P. *Inorg. Chimica Acta* **2006**, *359*, 1939.

(82) Gavenonis, J.; Tilley, T. D. *Organometallics* **2004**, *23*, 31.

(83) Ito, M.; Matsumoto, T.; Tatsumi, K. *Inorg Chem* **2009**, *48*, 2215.

(84) Hagadorn, J. R.; Que, L.; Tolman, W. B. *J. Am. Chem. Soc.* **1999**, *121*, 9760.

(85) Yoon, S.; Lippard, S. J. *J.* Am. Chem. Soc. **2005**, 127*,* 8386.

(86) Tanabiki, M.; Tsuchiya, K.; Kumanomido, Y.; Matsubara, K.; Motoyama, Y.; Nagashima, H. **2004**, *23*, 3976.

(87) Ito, H.; Kato, T.; Sawamura, M. *Chem. Lett.* **2006**, *35*, 1038.

(88) Chomitz, W. A.; Sutton, A. D.; Krinsky, J. L.; Arnold, J. *Organometallics* **2009**, *28*, 3338.

(89) Labios, L. A.; Millard, M. D.; Rheingold, A. L.; Figueroa, J. S. *J. Am. Chem. Soc.* **2009**, *131*, 11318.

(90) Fox, B. J.; Millard, M. D.; DiPasquale, A. G.; Rheingold, A. L.; Figueroa, J. S. *Angew. Chem. Int. Ed. Engl.* **2009**, *48*, 3473.

(91) Emerich, B. M.; Moore, C. E.; Fox, B. J.; Rheingold, A. L.; Figueroa, J. S. *Organometallics* **2011**, *30*, 2598.

(92) Barnett, B. R.; Moore, C. E.; Rheingold, A. L.; Figueroa, J. S. *J. Am. Chem. Soc.* **2014**, *136*, 10262.

(93) Margulieux, G. W.; Weidemann, N.; Lacy, D. C.; Moore, C. E.; Rheingold, A. L.; Figueroa, J. S. *J. Am. Chem. Soc.* **2010**, *132*, 5033.

(94) Agnew, D. W.; Moore, C. E.; Rheingold, A. L.; Figueroa, J. S. *Angew. Chem. Int. Ed.* **2015**, *54*, 12673.

# *Chapter 2*

# *Synthesis and Protonation of an Encumbered Iron Tetraisocyanide Dianion.*

## 2.1. Introduction

Tetracarbonylferrate(2–) ($[Fe(CO)_4]^{2-}$) is one of the most well-known and well-studied organometallic complexes.[1-5] It has been shown to mediate a host of important transformations in organic synthesis including carbonylation, reductive coupling, reduction, and nucleophilic displacement.[2,5] This inherent reactivity of $[Fe(CO)_4]^{2-}$ originates from a high-energy, closed-shell, $d^{10}$ orbital manifold that manifests from a doubly reduced, formally Fe(2–) center. It is well understood that $\pi$-backbonding, interactions to the carbonyl ligands stabilize the excess charge equivalents on the Fe center of this dianion.[4,6] However, the degree of π-backbonding, while significant, does not preclude the Fe center from functioning readily as a nucleophile toward a wide range of electrophilic substrates.[2]

In 2007, Ellis reported the first tetraisocyano analogue of $[Fe(CO)_4]^{2-}$, namely, $[Fe(CNXyl)_4]^{2-}$ (Xyl = 2,6-$Me_2C_6H_3$), and showed that it exhibits structural features and a reactivity profile toward $ClSnPh_3$ similar to that of $[Fe(CO)_4]^{2-}$.[8] This work advanced the long-standing interest in isocyanide variants of the carbonyl metalates,[9-18] which began with Cooper's synthesis of $[Co(CNXyl)_4]^-$ as an analogue of $[Co(CO)_4]^-$.[9] The impetus for generating and studying isocyanide analogues of the carbonyl metalates stems from the fact that isocyanides are excellent $\pi$-acids, but are far stronger $\sigma$-donors than carbon

monoxide.[19-24] Accordingly, efforts have been made to exploit this difference in $\sigma$-donor-strength to provide a class of highly reduced organometallics that display nucleophilic character exceeding that of the homoleptic carbonyl metalates. In recent years, our group has extended the chemistry of isocyano metalates through the use of sterically encumbering *m*-terphenyl isocyanide ligands.[25-35] The goal of these investigations has been to couple the potentially increased nucleophilicity of isocyano metalates with a kinetically stabilizing steric environment. This approach has resulted in the successful synthesis of the tetraisocyano cobalt monoanion, $[Co(CNAr^{Mes2})_4]^-$ ($Ar^{Mes2}$ = 2,6-(2,4,6-$Me_3C_6H_2$)$C_6H_3$),[36] which retains a mononuclear formulation upon oxidation, and a highly reactive synthon for the coordinatively unsaturated trisisocyano cobalt monoanion, $[Co(CNAr^{Mes2})_3]^-$.[37]

In this chapter, we expand our work on *m*-terphenyl isocyanide-supported metalates and present the synthesis and characterization of $[Fe(CNAr^{Mes2})_4]^{2-}$, which is a sterically encumbered variant of Ellis' dianion, $[Fe(CNXyl)_4]^{2-}$. We also demonstrate that $[Fe(CNAr^{Mes2})_4]^{2-}$ is protonated readily, leading to the reactive monohydride isocyanometalate $[HFe(CNAr^{Mes2})_4]^-$. Both $[Fe(CNAr^{Mes2})_4]^{2-}$ and $[HFe(CNAr^{Mes2})_4]^-$ display properties that parallel their well-known carbonyl analogues (i.e., $[Fe(CO)_4]^{2-}$ and $[HFe(CO)_4]^-$),[38] but also display distinct reactivity and decomposition profiles that are emblematic of a sterically encumbered isocyano environment.

## 2.2 Synthesis and Characterization of $Na_2[Fe(CNAr^{Mes2})_4]$ ($Na_2$[**1**]).

Treatment of 2 equivalents of $CNAr^{Mes2}$ with $FeCl_2$ followed by the addition of sodium amalgam provides the disodium tetraisocyanoferrate salt, $Na_2[Fe(CNAr^{Mes2})_4]$ (Na[**1**]), as a dark brick red crystalline solid in 23% isolated yield (Scheme 2.1). While

the yield of $Na_2[Fe(CNAr^{Mes2})_4]$ ($Na_2$[**1**]) by this protocol is modest, the reaction can be carried out at room temperature and does not require a slow addition of reducing agent. Notably, use of a higher equivalency of $CNAr^{Mes2}$ in this reaction does not lead to improved yields. Tetraisocyanoferrate $Na_2[Fe(CNAr^{Mes2})]$ ($Na_2$[**1**]) gives rise to a single, sharp set of $Ar^{Mes2}$ resonances in its $^1H$ NMR spectrum ($C_6D_6$). The $^{13}C\{^1H\}$ NMR spectrum of $Na_2[Fe(CNAr^{Mes2})_4$ ($Na_2$[**1**]) likewise displays a single $Ar^{Mes2}$ environment and additionally features a significantly deshielded resonance at +219.2 ppm assigned to the Fe-bound iscyano carbon atoms. Notably, the large downfield $^{13}C\{^1H\}$ NMR resonance for the Fe-bound carbon atoms in $Na_2[Fe(CNAr^{Mes2})_4]$ ($Na_2$[**1**]) is consistent with those observed from both $K_2[Fe(CNXyl)_4]$ and $K_2[Fe(CO)_4]$ (238.7 and 234.6 ppm, respectively) and can be considered an NMR spectroscopic marker for significant Fe-to ligand $\pi$-back-donation.[15,39,40] The solution IR spectrum ($C_6D_6$) of $Na_2[Fe(CNAr^{Mes2})]$ (Na[**1**]) is also in line with this interpretation and features a broad, prominent band centered at 1682 $cm^{-1}$ assignable to a low-energy isocyanide $\nu$(CN) stretch. In comparison, $K_2[Fe(CNXyl)_4]$ also gives rise to a broad, low-energy $\nu$(CN) band centered at 1670 $cm^{-1}$ (THF).[7]

Single crystals of $Na_2[Fe(CNAr^{Mes2})_4]$ ($Na_2$[**1**]) can be grown from a saturated $Et_2O$ solution stored at –35 ˚C. In the solid-state $Na_2[Fe(CNAr^{Mes2})_4]$ ($Na_2$[**1**]) is found as an unsolvated contact-ion pair[41] with significant interactions between the Na cations and isocyano CN units, as well as between the $\pi$-faces of the $CNAr^{Mes2}$ mesityl rings (Figure 2.1). In this regard, the solid-state structure of $Na_2[Fe(CNAr^{Mes2})_4]$ ($Na_2$[**1**]) resembles that of the cobalt isocyanometalate, $Na[Co(CNAr^{Mes2})_4]$, which likewise exhibited Na/isocyano and Na/$\pi$-arene interactions.[36] Despite this ion pairing, however,

the Fe center in $Na_2[Fe(CNAr^{Mes2})_4]$ ($Na_2$[**1**]) adopts a tetrahedral coordination geometry (Houser $\tau_4$ geometry index[42] = 0.97) as expected for a $d^{10}$, four-coordinate metal center.

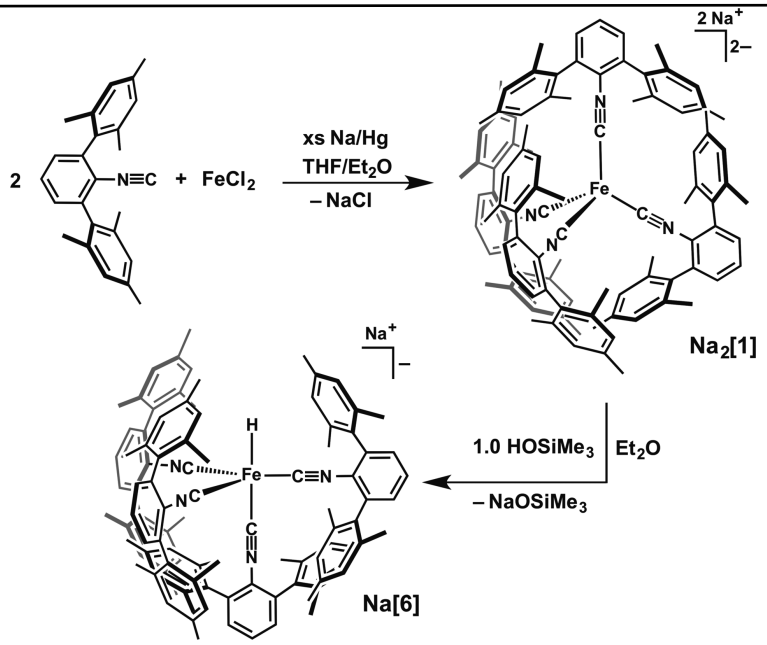


**Scheme 2.1** Synthesis of $Na_2[Fe(CNAr^{Mes2})_4]$ ($Na_2$[**1**]) and subsequent protonation to afford $Na[HFe(CNAr^{Mes2})]$ (Na[**6**]).

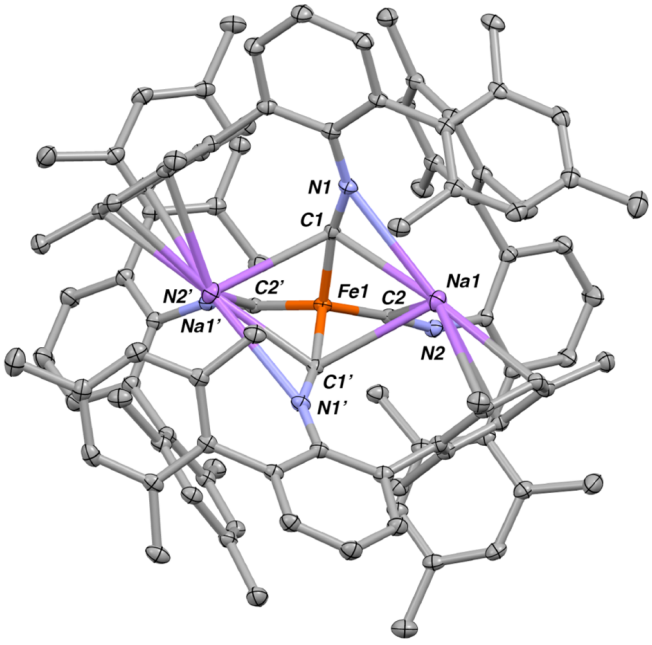


**Figure 2.1** Molecular structure of $Na_2[Fe(CNAr^{Mes2})_4]$ ($Na_2$[**1**]).

The metrical parameters associated with $Na_2[Fe(CNAr^{Mes2})_4]$ ($Na_2$[**1**]) are also consistent with a substantial degree of Fe-to-isocyanide $\pi$-back-donation. As shown in Table 2.1, $Na_2$[**1**] exhibits very short average $Fe–C_{iso}$ bond lengths and significantly elongated average $C_{iso}–N$ bond lengths relative to the formally Fe(0) complexes $Fe(CO)_4(CNAr^{Mes2})$ (**2**) and $Fe(CO)_3(CNAr^{Mes2})_2$ (**3**), and the formally Fe(II) complex *cis,cis,trans*-$FeI_2(CO)_2(CNAr^{Mes2})_2$ (**4**) (Figure 2.2). However, the average $Fe–C_{iso}$ and $C_{iso}–N$ bond lengths in $Na_2$[**1**] are slightly longer and slightly shorter, respectively, than the corresponding parameters found in Ellis' discrete dianion $[Fe(CNXyl)_4]^{2–}$, isolated as its di-[K-[2.2.2]cryptand)]$^+$ salt (Table 2.1).[7] We believe these small differences arise from the steric constraints placed on the $[Fe(CNR)_4]^{2–}$ core by both the *m*-terphenyl groups and the tightly bound sodium cations, rather than an electronic difference between the aryl isocyanides $CNAr^{Mes2}$ and CNXyl. Indeed, we have recently shown that $CNAr^{Mes2}$ and CNXyl exert a nearly identical electronic influence on metal centers, despite the presence of encumbering *ortho*-mesityl substituents in the former.[24]

**Table 2.1** Average $Fe–C_{iso}$ and $C_{iso}–N$ bond distances for tetraisocyano and related iron complexes.

| Compound | $d(Fe–C_{iso})_{av}$ (Å) | $d(C_{iso}–N_{iso})_{av}$ (Å) |
|---|---|---|
| $Na_2[Fe(CNAr^{Mes2})_4]$ ($Na_2$[**1**])[a] | 1.789(18) | 1.219(17) |
| $[K(crypt\text{-}[2.2.2])]_2[Fe(CNXyl)_4]$[b] | 1.765(3) | 1.237(7) |
| $Fe(CO)_4(CNAr^{Mes2})$ (**2**) | 1.869(3) | 1.157(3) |
| $Fe(CO)_3(CNAr^{Mes2})_2$ (**3**)[a] | 1.845(6) | 1.160(5) |
| *cis,cis,trans*-$FeI_2(CO)_2(CNAr^{Mes2})_2$ (**4**) | 1.877(2) | 1.152(2) |
| $Na[HFe(CNAr^{Mes2})_4]$ (Na[**6**]) | 1.801(17) | 1.208(20) |
| $Fe(N_2)(CNAr^{Mes2})_4$ | 1.843(20) | 1.286(8) |

[a] Average of two crystallographically independent molecules. [b] Ref 7.

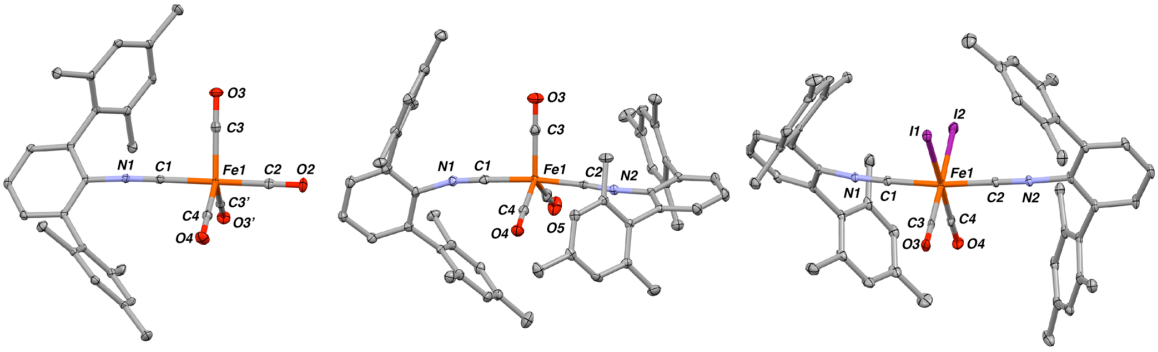


**Figure 2.2** Molecular structures of $Fe(CO)_4(CNAr^{Mes2})$ (**2**, left), $Fe(CO)_3(CNAr^{Mes2})_2$ (**3**, center), and *cis-cis-trans*-$FeI_2(CO)_2(CNAr^{Mes2})_2$ (**4**, right).

## 2.3 Disruption of Alkali cation/$\pi$-Interactions in an Attempt to Isolate a Bare $[Fe(CNAr^{Mes2})_4]^{2-}$ Fragment.

In contrast to $K_2[Fe(CNXyl)_4]^{2-}$,[7] disruption of the cation–anion interactions in $Na_2$[**1**] with cryptands or crown ethers does not provide a discrete example of $[Fe(CNAr^{Mes2})_4]^{2-}$. Several attempts to encapsulate the Na cations in $Na_2$[**1**] with 15-crown-5 or dibenzo-18-crown-6 in THF or $Et_2O$ solution led to intractable mixtures, with free $CNAr^{Mes2}$ being the dominant product. These observations mirror those made for the cobaltate salt $Na[Co(CNAr^{Mes2})_4]$, for which Na-anion interactions can only be disrupted when "non-coordinating" cations are employed.[36,37] In addition, other highly reduced carbonyl metalates are known to decompose upon attempts to separate contact alkali-metal cation/anion pairs.[4] However, when $Na_2$[**1**] was treated with 2.0 equivalents of 18-crown-6 (18-c-6) the bis-isocyanide cycloheptatrienyl product **5** (Figure 2.3) was isolated in very low yield (ca. 2%) as red-brown single crystals. The remainder of the reaction mixture contained free $CNAr^{Mes2}$ and several other decomposition products as assayed by $^1$H NMR spectroscopy. Whereas the low isolated yield prevented full characterization by spectroscopic techniques, it is notable that complex **5** is formally an Fe(I) species

reminiscent of the unstable metalloradical $CpFe(CO)_2$.[43] In addition, it is important to note that the $\eta^5$-cyclopentatrienyl unit in **5** is part of a formally dianionic 1-azabenz[*b*]azulene formed from an apparent aza-Büchner ring expansion for a $CNAr^{Mes2}$ ligand.[44-46] While the mechanistic sequence leading to the formation of complex **5** is presently unknown, Arnold has reported a similar aza-Büchner ring expansion for $CNAr^{Mes2}$ in the presence of a highly reduced, low-coordinate zirconium center.[47] On the basis of this precedent, we presume that removal of a Na cation from $Na_2$[**1**] may mirror that of the tetra-isocyano cobaltate salt $Na[Co(CNAr^{Mes2})_4]$, which has been shown to yield an equivalent of three-coordinate $[Co(CNAr^{Mes2})_3]^-$ via $CNAr^{Mes2}$ dissociation when its cation/anion contacts are disrupted.[36,37]

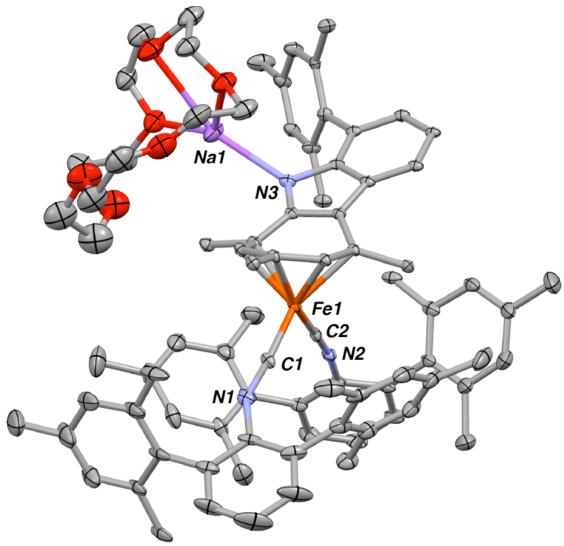


**Figure 2.3** Molecular structure of [Na(18-crown-6)][($\eta^5$-$Me_6$-1-azabenz[*b*]azulene)-Fe($CNAr^{Mes2}$)$_2$] (**5**)

## 2.4 Protonation of $Na_2[Fe(CNAr^{Mes2})_4]$ ($Na_2$[**1**]) and the Generation of $Na[HFe(CNAr^{Mes2})_4]$: an Isocyano Analogue to $[HFe(CO)_4]^-$.

While $Na_2$[**1**] is not well behaved in cation-encapsulation reactions, it does react with certain protic sources to yield an isocyano analogue of $Na[HFe(CO)_4]$. As shown in

Scheme 2.1, treatment of $Na_2$[**1**] with trimethylsilanol ($HOSiMe_3$; $pK_a \approx 11.5$ (DMSO)[48-50]) generates the anionic monohydride complex Na[$HFe(CNAr^{Mes2})_4$] (Na[**6**]) as a red-orange crystalline solid. Notably, treatment of cold (*ca*. ~100 ˚C) $Et_2O$ solutions of $Na_2$[**1**] with 1.0 equivalents of stronger Brønsted acids, such as 3,5-dimethylbenzoic acid, pivalic acid, pyridinium chloride ([Hpy]Cl), and ethylammonium chloride ([$EtNH_3$]Cl),[51] led to complex mixtures containing unreacted starting material, free ligand, and several unidentified products. Although not conclusively observed, we presume these reactions produce the neutral dihydride complex $H_2Fe(CNAr^{Mes2})_4$, which rapidly decomposes under the conditions surveyed. In contrast however, monohydride Na[**6**] does not react with additional equivalents of $HOSiMe_3$ in $Et_2O$ solution. Accordingly, as has been established for the tetracarbonyl monoanion $[HFe(CO)_4]^-$,[38,52] this observation indicates that tetraisocyanide Na[**6**] exhibits only moderate Brønstead basicity in nonpolar media.

Crystallographic characterization of Na[$HFe(CNAr^{Mes2})_4$] (Na[**6**]) revealed an unsolvated contact-ion pair with interactions between the Na cation and both the mesityl (i.e., $\pi$-arene) and CN units of the $CNAr^{Mes2}$ ligands (Figure 2.4). These contacts result in an Fe coordination geometry in the solid state that is intermediate between trigonal bipyramidal and square pyramidal on the basis of the Addison–Reedijk $\tau_5$ geometry index ($\tau_5$ for Na[**6**] = 0.53).[53] Nevertheless, Na[**6**] gives rise to a single set of $Ar^{Mes2}$ resonances in its $^1$H NMR spectrum ($C_6D_6$) at room temperature, thereby indicating that the $[Na]^+/CNAr^{Mes2}$ contacts do not prevent a high degree of fluxionality for the five-coordinate Fe center in solution. The IR spectrum of Na[$HFe(CNAr^{Mes2})_4$] (Na[**6**]) in $C_6D_6$ solution displays several broad and unresolved bands in the $\upsilon$(CN) stretching region, which is consistent with a lowering of the local site symmetry of either an

idealized trigonal bipyramidal ($C_{3v}$) or square pyramidal ($C_s$) center by the Na cation.[54] A similar lowering of idealized site symmetry was observed in the solution IR spectrum of the related cobaltate salt $Na[Co(CNAr^{Mes2})_4]$[36] and is also well-known to occur for alkali-metal salts of $[HFe(CO)_4]^-$ and its monophosphine derivatives (i.e., $[HFe(CO)_3(PR_3)]^-$).[54-56] However the $\upsilon$(CN) bands or Na[**6**] fall within the range 1994-1828 $cm^{-1}$ and are markedly higher in energy that was found for the dianion $Na_2[Fe(CNAr^{Mes2})_4]$ ($Na_2$[**1**]). In addition, the Fe–$C_{iso}$ bond lengths in the solid-state structure of Na[**6**] are elongated relative to $Na_2$[**1**] (Table 1), but are significantly shorter than those found in the formally Fe(0) complexes $Fe(CO)_4(CNAr^{Mes2})$ (**2**) and $Fe(CO)_3(CNAr^{Mes2})_2$ (**3**). These data and comparisons indicate that the Fe center in $Na[HFe(CNAr^{Mes2})]$ (Na[**6**]) remains highly reduced and, as in the case for $[HFe(CO)_4]^-$,[38] may likewise be reactive toward strong electrophiles despite exhibiting only moderate Brønstead basicity.

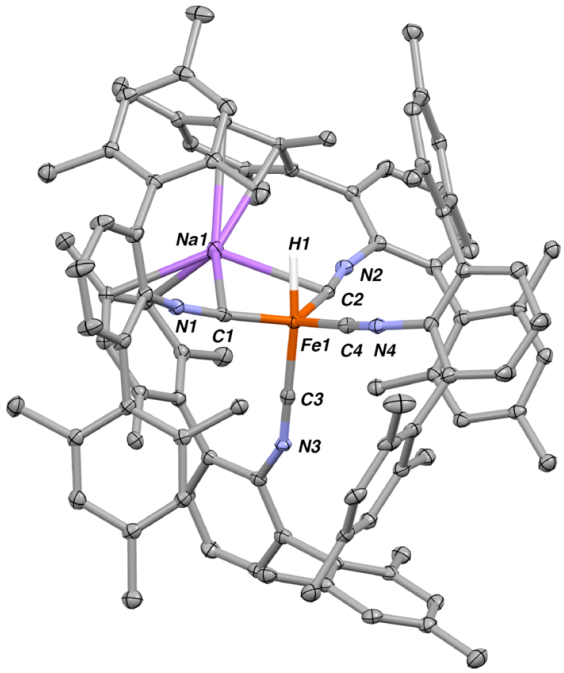


**Figure 2.4** Molecular structure of $Na[HFe(CNAr^{Mes2})_4]$ (Na[**6**]).

## 2.5. Nucleophilic Assessment of Na[HFe(CNAr$^{Mes2}$)$_4$] (Na[6]) with MeOTf and the Generation of Fe(N$_2$)(CNAr$^{Mes2}$)$_4$.

To test this hypothesis, Na[HFe(CNAr$^{Mes2}$)$_4$] (Na[**6**]) was treated with methyl triflate (MeOTF; [OTf]$^-$ = [O$_3$SCF$_3$]$^-$) at –40 ˚C in an Et$_2$O solution. This reaction proceeds readily without the buildup of detectable intermediates to yield methane (CH$_4$) and the zerovalent dinitrogen complex, Fe(N$_2$)(CNAr$^{Mes2}$)$_4$ ) (**7**), as determined by both $^1$H NMR spectroscopy and single-crystal X-ray diffraction (Scheme 2.2, Figure 2.5). In the solid state, dinitrogen complex **7** adopts a near trigonal bipyramidal coordination geometry ($\tau_5$ = 0.86),[53] with the N$_2$ ligand located in the equatorial position. The solution IR spectrum of Fe(N$_2$)(CNAr$^{Mes2}$) (**7**) features a $\nu$(NN) band centered at 2067 cm$^{-1}$, which is reflective of weak N≡N bond activation in the context of mononuclear Fe(0) dinitrogen complexes.[57] Most importantly however, this product outcome from the reaction between Na[**6**] and MeOTf mirrors those established by Whitmire for the reactivity of alkyl iodides with [HFe(CO)$_4$]$^-$.[58] Furthermore, in these latter studies, the unstable paramagnetic (S = 1) tetracarbonyl complex, Fe(CO)$_4$,[59-61] has been proposed as an unobservable intermediate, which then rapidly undergoes ligand redistribution and aggregation reactions. For the reaction between Na[**6**] and MeOTf, the steric encumbrance provided by the CNAr$^{Mes2}$ ligand presumably imparts the analogous tetraisocyanide complex Fe(CNAr$^{Mes2}$) with a lifetime sufficient to be trapped by dinitrogen present within the reaction mixture. Notably, several isoloable zerovalent FeL$_4$ complexes have now been reported.[62-64] However, none to date feature L-type ligands with two orthogonal $\pi$* orbitals akin to CO, which would render such complexes as precise electronic analogues to the high-spin, binary carbonyl Fe(CO)$_4$. In this respect,

complex **7** potentially points to a molecular-design strategy for the isolation of kinetically stabilized $FeL_4$ complexes that more appropriately mimic the electronic features of $Fe(CO)_4$.

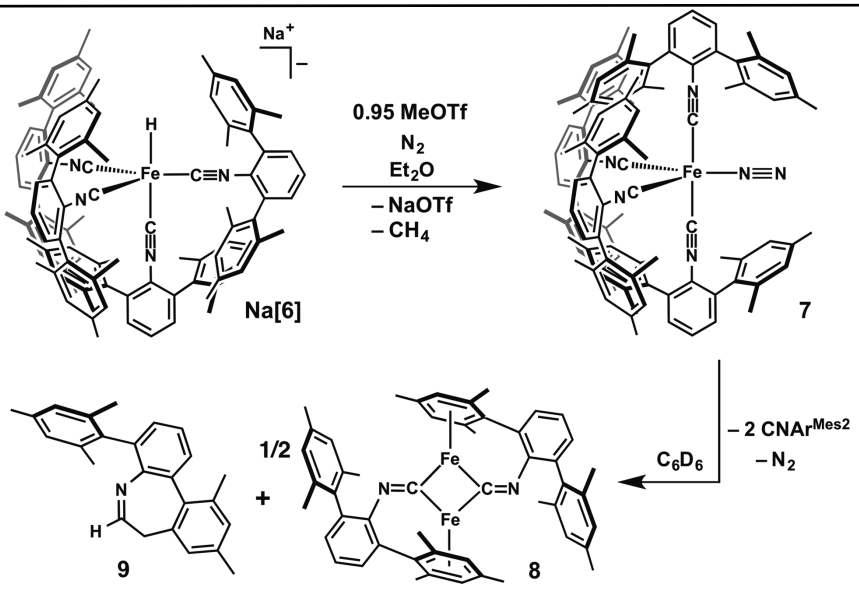


**Scheme 2.2** Synthesis of $Fe(N_2)(CNAr^{Mes2})_4$ (**7**) from the alkylation of $Na[HFe(CNAr^{Mes2})_4]$ (Na[**6**]) with MeOTf, and subsequent decomposition.

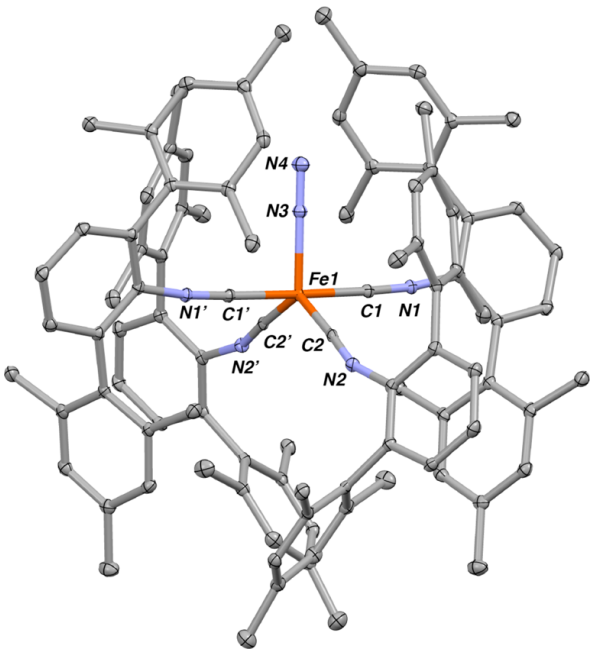


**Figure 2.5** Molecular structure of $Fe(N_2)(CNAr^{Mes2})_4$ (**7**).

## 2.6. Decomposition of $Fe(N_2)(CNAr^{Mes2})_4$ via C–H Activation of the *m*-Terphenyl Isocyanide.

Thus, while the dinitrogen complex $Fe(N_2)(CNAr^{Mes2})$ (**7**) can be viewed as a trapped form of $Fe(CNAr^{Mes2})_4$, it is critical to note that the dissociation of $N_2$ from the Fe center results in a multistep decomposition process. Furthermore, this decomposition sequence highlights the points of incompatibility of the $CNAr^{Mes2}$ ligand for the goal of isolating a kinetically persistent $FeL_4$ species. Accordingly, when crystals of **7** are dissolved in either $C_6D_6$ or $Et_2O$ at room temperature, complete conversion to the diamagnetic, symmetric dimer $[Fe(\eta^6\text{-(Mes)-}\mu^2\text{-C-}CNAr^{Mes2})]_2$ (**8**) is observed over the course of *ca*. 4 hours. Dimer **8** has been crystallographically characterized (Figure 2.6), and its solid-state structure shows that the $CNAr^{Mes2}$ ligands adopt a $\mu^2$-bridging mode, and also provide a $\eta^6$-arene interaction to the Fe centers. In this respect, dimer **8** serves as a valence-isoelectronic analogue to the neutral, bridging carbonyl dimer $[CpCo(\mu^2\text{-CO})]_2$, which has been subject to both extensive experimental and computational studies.[65-69] However, along with dimer **8**, the decomposition of $Fe(N_2)(CNAr^{Mes2})_4$ (**7**) also produces 2 equivalents of free $CNAr^{Mes2}$ and the 7-membered cyclic imine **9** (Scheme 2.2), which was isolated from the reaction mixture and structurally characterized by X-ray diffraction (Figure 2.7).

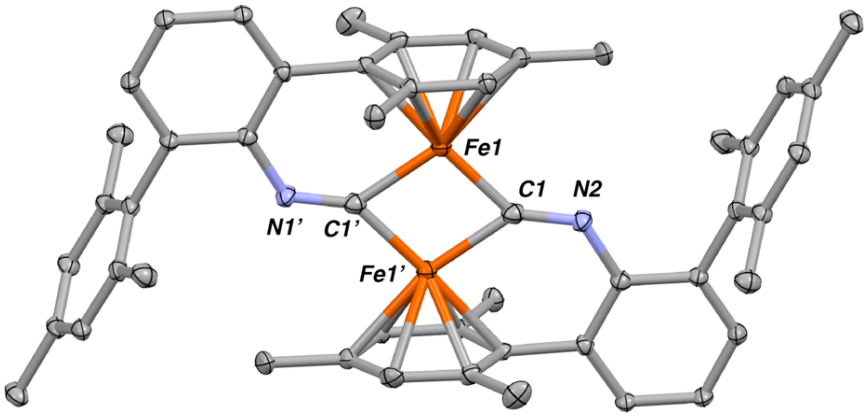


**Figure 2.6** Molecular structure of [Fe($\eta^6$-(Mes)-$\mu^2$-C-CNAr$^{Mes}$)]$_2$ (**8**).

The formation of imine **9** can be rationalized by the mechanistic sequence shown in Scheme 2.3, which proceeds by methyl-group C–H activation by four-coordinate Fe(CNAr$^{Mes2}$)$_4$, followed by alkyl migration to a "tethered" isocyano unit and subsequent C–H bond reductive elimination. Notably, Jones has proposed a similar mechanism for the production of *C*-phenyl aldimines from isocyanides and benzene mediated by the related, and likewise unobservable, four-coordinate Fe species [Fe(PMe$_3$)$_2$(CNXyl)$_2$].[70] In addition, we speculate that the driving force for the production of dimer **8** in this reaction stems from the formation of a strong $\eta^6$-arene interaction as a means to provide a coordinatively saturated Fe center. Formation of flanking-ring $\eta^6$-arene interactions from *m*-terphenyl isocyanides in this fashion is reminiscent of our previous studies on the *in-situ*-generation of three coordinate Co and Mo isocyanide complexes.[35-37] Most importantly however, this reaction indicates that the CNAr$^{Mes2}$ framework, although seemingly able to extend the lifetime of putative Fe(CNAr$^{Mes2}$)$_4$, is not resistant to degradation processes and secondary binding interaction by a low-coordinate Fe(0) center. Therefore, and alternative isocyanide architecture that is not susceptible to C–H

activation or the formation of a strong $\eta^6$-arene interaction is required,[24,35] at minimum, to generate an isolable $Fe(CNR)_4$ complex and complete the series of isocyano analoges to the classic mononuclear iron carbonyls $Fe(CO)_5$,[71] $[Fe(CO)_4]^{2-}$,[7] $[HFe(CO)_4]^-$, and $Fe(CO)_4$.

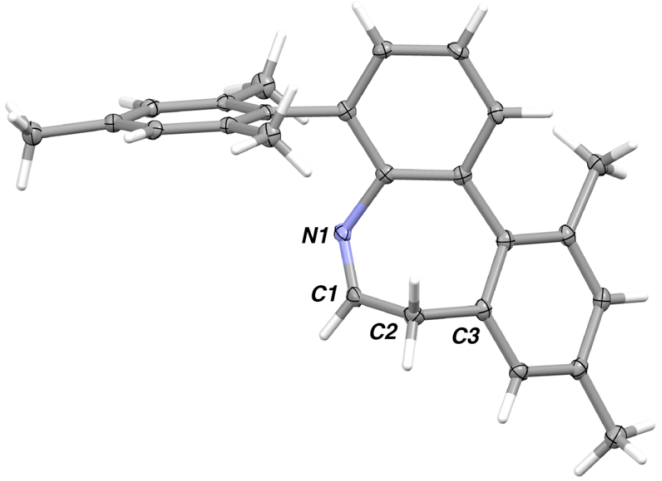


**Figure 2.7** Molecular structure of cyclic imine (**9**).

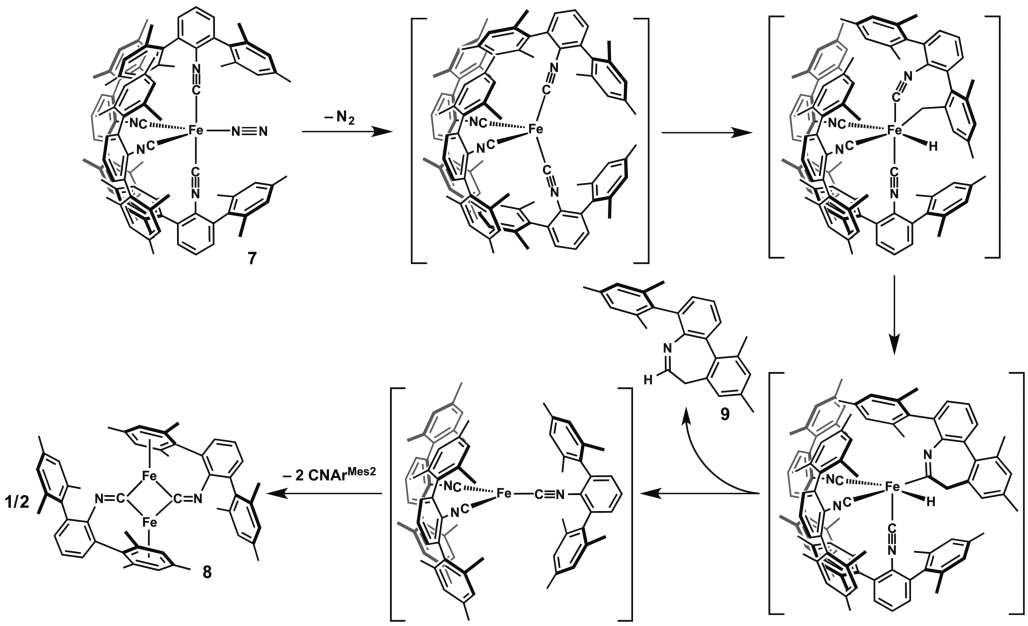


**Scheme 2.3** Proposed mechanism depicting the generation of $[Fe(\eta^6\text{-(Mes)-}\mu^2\text{-C-CNAr}^{Mes})]_2$ (**8**) and cyclic imine (**9**) via the C–H activation of the *m*-terphenyl mesityl methyl group.

## 2.7. Concluding Remarks.

Isocyano analogues of the classic carbonyl metalates remain intriguing synthetic targets to explore the effect of enhanced metal-based nucleophilicity within a strongly $\pi$-acidic ligand field. Coupling this electronic environment with a sterically encumbering ligand topology potentially offers the ability to further control or augment the reactivity of highly reduced metal centers towards substrate molecules in both stoichiometric and catalytic transformations. Here, we show that an encumbering *m*-terphenyl isocyanide variant of $[Fe(CO)_4]^{2-}$, namely $[Fe(CNAr^{Mes2})_4]^{2-}$, can be readily prepared and isolated as a disodium contact-ion pair. The nucleophilic character of $Na_2[Fe(CNAr^{Mes2})_4]$ has been demonstrated by its reaction with $HOSiMe_3$ to produce the monohydride monoanion $[HFe(CNAr^{Mes2})_4]^-$, which serves as a unique isocyanide analogue of $[HFe(CO)_4]^-$. The latter is also shown to react readily with MeOTf at low temperatures to produce methane and the dinitrogen complex $Fe(N_2)(CNAr^{Mes2})_4$, likely via the intermediacy of the four-coordinate Fe(0) species, $[Fe(CNAr^{Mes2})_4]$. Accordingly, this synthetic sequence illustrates reaction chemistry for these isocyanometalates paralleling that of the classic iron carbonylmetalates. We believe the synthetic results presented here will enable further development of small-molecule activation processes at a sterically protected but nucleophilic Fe center. In addition, this work has suggested the minimum requirements necessary for an isocyanide ligand framework capable of stabilizing highly reduced Fe centers with low coordination numbers.

## 2.8 Synthetic Procedures and Characterization Data.

**General Considerations:** All manipulations were carried out under an atmosphere of dry dinitrogen or Argon using standard Schlenk and glove box techniques.

Solvents were dried and degassed according to standard procedures.[72] The isocyanide ligand $CNAr^{Mes2}$ was prepared as previously reported.[25] Unless otherwise stated all materials were obtained from commercial vendors and used as received. Benzene-$d_6$ was dried with Na/K and benzophenone followed by distillation and stored on 4 Å molecular sieves for 3 days prior to use. Celite 405 (Fischer Scientific) was dried under vacuum for 24 hours at a temperature greater then 250 $^{o}$C and stored inside the glove box prior to use.

Solution $^{1}$H, and $^{13}$C{$^{1}$H} NMR spectra were recorded on a Varian Mercury 400 spectrometer, and a Varian XSENS-500 spectrometer. $^{1}$H, and $^{13}$C chemical shifts are reported in ppm relative to $SiMe_4$ ($^{1}$H and $^{13}$C $\delta$ = 0.0 ppm) with reference to residual $C_6D_5H$ or solvent references of 7.16 ppm (1H) and 128.06 ppm ($^{13}$C) for benzene $d_6$ respectively.[73] FTIR spectra were recorded on a Thermo-Nicolet iS10 FTIR spectrometer. Samples were prepared either as KBr pellets or as $C_6D_6$ solutions injected into a Thermo-Fischer solution cell equipped with KBr windows. For solution FTIR spectra, solvent peaks were digitally subtracted from all spectra by comparisons with an authentic spectrum obtained immediately prior to that of the sample. The following abbreviations were used for the intensities and characteristic of important IR absorption bands: vs = very strong, s = strong, m = medium, w = weak, vw = very weak, b = broad, vb = very broad, sh = shoulder. High-resolution mass spectrometry (HRMS) was performed using an Agilent 6230 ESI-TOFMS running in positive or negative ion mode as necessary. Photolysis experiments were performed with a 254 nm model UVGL-25 Hg lamp (UVP, Inc., Upland, CA). Combustion analyses were performed by Robertson Microlit Laboratories of Ledgwood, NJ (USA), and Midwest Microlab of Indianapolis, IN (USA).

**Synthesis of $Na_2[Fe(CNAr^{Mes2})_4]$ ($Na_2$[1]):** To a suspension of anhydrous $FeCl_2$ (0.607 g, 4.79 mmol, 1 equiv) in a 30:70 mixture of THF:$Et_2O$ (100mL) $CNAr^{Mes2}$ (3.08 g, 9.1 mmol, 1.9 equiv) and was added. The resultant suspension was allowed to stir for 5 min, followed by the addition of a 0.9% Na/Hg (Na 1.10 g, 47.9 mmol, 10 equiv; Hg 122 g). The reaction mixture was then shaken vigorously for 20 min where upon a color change to deep red was observed. After shaking, the reaction mixture was allowed to stir for an additional 1 hr. The mixture was then decanted from the Na/Hg and filtered over Celite packed on a medium porosity frit and evaporated to dryness. The resultant red solid was slurried in *n*-pentane (30mL) followed by evaporation to dryness. This was repeated two additional times to desolvate the NaCl by-products. The red solid was then extracted with $C_6H_6$ (40mL) and filtered over Celite packed on a medium porosity frit followed by lyophilization. This process was repeated an additional time to remove any NaCl, and other Iron by-products. The resultant dark red solid was then recrystallized via a layered solution of THF/*n*-pentane (1:6) at -40$^o$C over 2 days, where upon the crystals were washed with *n*-pentane (4 mL) and dried *in vacuo.* The isolated crystals were then dissolved in $C_6H_6$ (10 mL) and filtered over Celite packed on a medium porosity frit to remove any remaining salts and yield a dark red fluffy solid, 1.6 g, 23%. Analytically pure crystals of $Na_2[Fe(CNAr^{Mes2})_4]$ can be grown from a toluene solution layered with *n*–hexane (1:10 mL). $^1$HNMR (499.8 MHz, $C_6D_6$, 20$^o$C) δ = 6.83 (t, 4H, 6Hz, *p*-Ph), 6.78 (d, 8H, 8Hz, *m*-Ph), 6.74 (s, 16H, *m*-Mes), 6.24 (s, 24H, *p*-CH3 Mes), 2.09 (s, 48H, *o*-CH3 Mes) ppm. $^{13}C\{^1H\}$ NMR (125.7 MHz, C6D6, 20$^o$C) δ = 219.2, 140.1, 137.9, 136.8, 135.3, 134.8, 130.3, 128.4, 120.7, 21.6 (*o*-CH3 Mes), 21.4 (*p*-CH3 Mes) ppm. FTIR (solution ($C_6D_6$), KBr windows, 25$^o$C): ($\nu_{CN}$) 1675 (s,b), 1748 (sh), 1889 (m,b) cm$^-$

[1] also 2956 (m), 2920 (m), 2872 (m), 2856 (m), 2038 (m), 2009 (m), 1567 (s), 1484 (w), 1439 (w), 1406 (s) 1377 (m), 1284 (w), 1271 (w), 1252 (w), 1223 (w), 1205 (w), 1095 (w), 1068 (w), 1034 (m), 852 (m), 754 (m), 636 (w), 571 (w) $cm^{-1}$. Anal. Calc.: C, 82.28; H, 6.91; N, 3.84. Found C, 81.89; H, 6.87; N, 3.79.

**Synthesis of $Fe(CO)_4(CNAr^{Mes2})$ (2).** A 100 mL re-sealable ampoule was charged with $C_6H_6$ and $Fe_2(CO)_9$ (0.537 g, 1.47 mmol) then stirred for 5 min. Solid $CNAr^{Mes2}$ (1.00 g, 2.95 mmol, 2 equiv) was then added over course of 5 minutes. The resulting mixture was refluxed for 5 days then concentrated to a solid under reduced pressure. $Fe(CO)_4(CNAr^{Mes2})$ was then extracted with $C_5$ (40 mL) and filtered through a medium porosity fritted funnel packed with Celite. The filtrate was then concentrated to a solid under reduced pressure. The solid residue was then dissolved in minimal amount of pentane filtered and stored at -40 ˚C to afford pale yellow crystals that were collected and dried *in vacuo*. Yield: 0.746 g, 1.47 mmol, 49.8 %. $^1H$ NMR (499.8 MHz, $C_6D_6$, 20 $^oC$): δ = 6.94 (t, 1H, *J* = 8 Hz, *p*-Ph), 6.91 (s, 4H, *m*-Mes), 6.82 (d, 2H, *J* = 8 Hz, *o*-Ph), 2.21 (s, 6H, *p*-Mes), 2.02 (s, 12H, *o*-Mes) ppm. $^{13}C\{^1H\}$ NMR (100.6 MHz, $C_6D_6$, 20 $^oC$): δ = 212.5 (*C*O ), 170.6 (*C*NR), 139.1, 138.4, 135.5 (two peaks), 133.8, 129.5, 129.3, 129.0, 21.2 (*p*-Mes), 20.1 (*o*-Mes) ppm. FTIR ($C_6D_6$; KBr Window): ($\nu_{CN}$) 2164 (s) $cm^{-1}$, ($\nu_{CO}$) 2051 (s), 1994 (vs), 1968 (vs) $cm^{-1}$ also, 3055 (w, sh), 2975 (w), 2948 (w), 2920 (m), 2869 (w), 1614 (m), 1467 (sh), 1454 (m), 1416 (w), 1349 (w), 1330 (w), 1273 (vw), 1029 (vw), 851 (m), 813 (s), 787 (w), 757 (m), 735 (vw), 636 (s) 614 (s) $cm^{-1}$. Anal. Calcd. For $C_{29}H_{25}FeNO_4$: C, 68.65; H, 4.97; N, 2.76, Found: C, 68.80, H, 4.75; N, 2.77.

**Synthesis of $Fe(CO)_3(CNAr^{Mes2})_2$ (3).** To a 100 mL ampule equiped with a side arm gas inlet was charged $CNAr^{Mes2}$ in THF (0.801 g, 2.36 mmol, 2 equiv, 40mL), and $FeCO_5$ (0.231 g, 1.18 mmol, 1 equiv). The ampule was sealed and subject to UV photolysis for 30 min, followed by a Freeze-Pump-Thaw cycles (40 mtorr) to de-gas the head-space of the reaction mixture. This process was repeated 3 times, followed by UV-photolysis for 12 hours or until the reaction showed complete consumption of $CNAr^{Mes2}$ by $^1$HNMR. The reaction mixture was then concentrated to a solid under reduced pressure and washed with *n*-pentane (3x10mL) followed by subsequent evaporation to dryness. The resulting solid was then transferred to a medium porosity frit where it was washed with *n*-pentane (25 mL), followed by extraction with $Et_2O$ (30 mL) and collected, followed by concentration to a solid and washed with *n*-pentane to yield $Fe(CO)_3(CNAr^{Mes2})_2$, 0.332 g, 34.4%. Crystals suitable for X-ray diffraction were obtained from saturated layered solution of THF/*n*-Hexane (1:10) at room temperature over the course of 1 week. $^1$HNMR (399.9 MHz, $C_6D_6$, 20$^o$C) δ = 6.91 (t, 2H, 8 Hz, *p*-Ph), 6.87 (s, 8H, *m*-Mes), 6.80 (d, 4H, 8 Hz *m*-Ph), 2.22 (s, 12H, *p*-$CH_3$ Mes), 2.00 (s, 24H, *O*-$CH_3$ Mes) ppm. $^{13}C\{^1H\}$ NMR (125.7 MHz, C6D6, 20$^o$C) δ = 212.6 (CO), 178.5 (CN), 138.6, 137.8, 135.5, 134.3, 129.2, 128.9, 128.3, 128.2, 21.2, 20.2 ppm. FTIR (solution ($C_6D_6$), KBr windows, 25$^o$C): ($\nu_{CN}$) = 2097 (s), ($\nu_{CO}$) = 1936 (s), also, 3030 (w), 2958 (w), 2920 (w), 2869 (w), 1416 (w), 1356 (w), 851 (w), 755 (w), 640 (w), 606 (m), 596 (w) cm$^{-1}$. Anal. Calc.: C, 77.74; H, 6.16; N, 3.42. Found C, 77.51; H, 5.88; N, 3.51.

**Synthesis of *cis,cis,trans*-$FeI_2(CO)_2(CNAr^{Mes2})_2$ (4).** To a thawing THF solution of $Fe(CO)_3(CNAr^{Mes2})_2$ (0.243 g, 0.3081 mmol, 1 equiv, 13mL) was added an equally cold solution of $I_2$ in THF (0.0782 g, 0.0308 mmol, 1 equiv, 2 mL). The resulting mixture was allowed to slowly warm to room temperature over the course of 45 min, where upon it was concentrated to a solid *in vacuo*. The red/brown solid was then washed with *n*-pentane (3 X 5mL) and decanted. The resulting solid was then recrystallized from a statured layered solution of THF/*n*-Hexane (1:10) over the course of 5 days at room temperature, yielding *cis-cis-trans*-$FeI_2(CO)_2(CNAr^{Mes2})_2$, as large red/brown crystals 0.109g, 34%. $^1$HNMR (399.9 MHz, $C_6D_6$, 20°C) δ = 6.90 (m, 10H, 6, *p*-Ph/*m*-Mes), 6.75 (d, 4H, 7Hz, *m*-Ph), 2.24 (s, 12H, *p*-$CH_3$ Mes), 2.09 (s, 24H, *p*-$CH_3$ Mes) ppm. $^{13}C\{^1H\}$ NMR (125.7 MHz, C6D6, 20°C) δ = 211.4 (CO), 157.1 (CN), 140.6, 138.2, 135.6, 134.8, 133.7, 130.2, 129.3, 129.2 (2 peaks overlayed), 21.3 (*p*-CH3 Mes), 20.5 (*o*-CH3 Mes) ppm. FTIR (solution ($C_6D_6$), KBr windows, 25°C): ($\nu_{CN}$) 2168 (s), 2140 (w, sh), ($\nu_{CO}$) 2058 (s), 2020 (m), also 3005 (w), 2974 (w), 2940 (w), 2919 (w), 2868 (w), 2854 (w), 1466 (w), 1416 (w), 1378 (w), 850 (w), 756 (w), 605 (w), 591 $cm^{-1}$ Anal. Calc.: C, 59.79; H, 4.82; N, 2.68. Found C, 59.62; H, 4.91; N, 2.67.

**Isolation of [Na(18-crown-6)][($\eta^5$-$Me_6$-1-azabenz[*b*]azulene)-$Fe(CNAr^{Mes2})_2$] (5).** To a thawing $Et_2O$ solution of **(1)** (0.078 g, 0.0539 mmol, 1 equiv) (15 mL), an equally cold solution of 18-Crown-6 (0.0284 g, 0.108 mmol, 2 equivs) (2 mL) was slowly added over the course of 2 minutes. The reaction mixture was allowed to stir and warm to room temperature over the course of one hour where upon a color change from deep red to purple was observed. All volatile materials were then removed under reduced

pressure, and the resulting purple-brown residue was washed with *n*-pentane (3 X 5 mL) and dried *in vacuo*. Crystalization from a layered solution of toluene and *n*-hexane (1:7) at –40 ˚C over the course of 10 days produced a small quantity of complex **5** as red-brown X-ray diffraction quality crystals. Analysis of an aliquot of the crystallization mixture by $^{1}$H NMR spectroscopy indicated the presence of several unidentifiable products. Several attempts to reproduce the synthesis and isolation of **5** were unsuccessful.

**Synthesis of Na[HFe(CNAr$^{Mes2}$)$_4$] (Na[6]).** To a thawing $Et_2O$ solution $Na_2$[Fe(CNAr$^{Mes2}$)$_4$] (0.213 g, 0.146 mmol, 1 equiv, 15 mL) was added TMSOH (0.013 g, 0.146 mmol, 1 equiv) as a neat solution via micro-syringe. The reaction mixture was allowed to slowly warm to room temperature over the course of 3 hours where upon evaporated to dryness. The resulting red-orange solid was subjected to 3 (5mL) washes of *n*-pentane followed by evaporation to dryness to desolvate NaOTMS, after which the red-orange solid was slurried in thawing *n*-pentane (4 mL) and filtered over 4 cm of Celite packed on fiberglass to yield a red solid. The resulting solid was extracted with $C_6H_6$ (10 mL) followed by lyophilization to yield a fluffy red-orange solid, 0.114 g, 54 %. Analytically pure Na[HFe(CNAr$^{Mes2}$)$_4$] was obtained via a saturated solution of *n*-pentane (1mL) at -40$^{o}$C over 1 week, or a saturated solution of MeCN/$Et_2O$ (3:1) over the course of 2 days. $^{1}$HNMR (499.8 MHz, $C_6D_6$, 20$^{o}$C) δ = 6.85 (s, 28H*, o/p*-Ph, *m*-Mes), 2.25 (s, 24H, *p*-CH3 Mes), 2.04 (s, 48H, *o*-CH3 Mes), -10.9 (s, 1H, Fe-H) ppm. $^{13}$C{$^{1}$H} NMR (125.7 MHz, C6D6, 20$^{o}$C) δ = 206.1 (*C*N), 137.8, 137.6, 136.2, 135.7, 134.4, 130.6, 128.8, 123.0, 21.5 (*p*-CH3 Mes), 21.3 (*o*-CH3 Mes) ppm. FTIR (solution (*$C_6D_6$*),

KBr windows, 25oC): ($\nu_{CN}$) 1896 (s), 1846 (s), 1826 (s), 1726 (sh) $cm^{-1}$ also 3036 (w), 2955 (w), 2920 (m), 2856 (w), 2026 (w) (Fe-H), 1997 (w) (Fe-H), 1613 (w), 1575 (m), 1484 (w), 1460 (w), 1448 (w), 1407 (m), 1371 (w), 1272 (m), 1252 (m), 852 (w), 812 (w), 755 (w), 679 (w), 633 (w), 569(w) cm-1. Analysis is consistent with the inclusion of one equivalent of MeCN. Anal. Calc.: C, 82.84; H, 7.09; N, 4.74. Found C, 83.95; H, 6.83; N, 4.80.

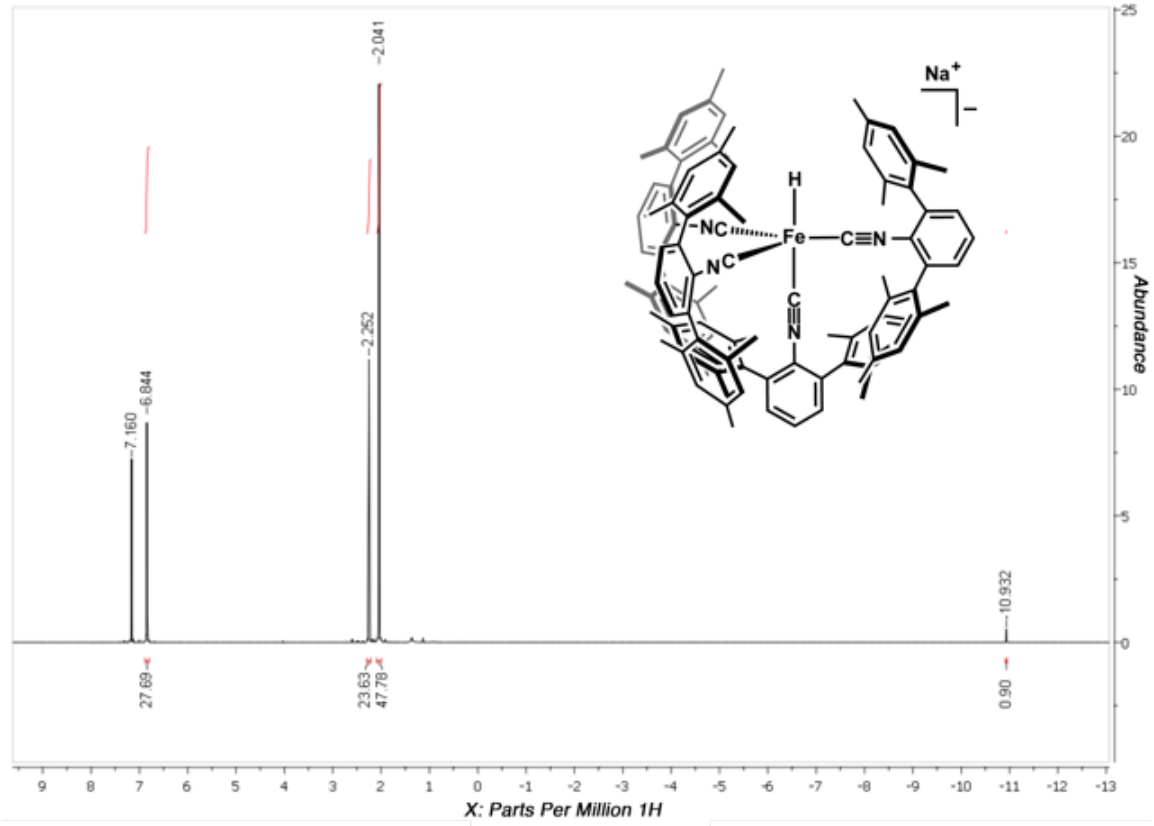


**Figure 2.8** $^{1}$H NMR spectrum (499.8 MHz, $C_6D_6$, 20 ˚C) of Na[HFe(CNAr$^{Mes2}$)], Na[**6**].

**Synthesis of Fe($N_2$)(CNAr$^{Mes2}$)$_4$ (7).** To a frozen solution of Na[HFe(CNAr$^{Mes2}$)$_4$] (0.043 g, 0.0302 mmol, 1 equiv) in $Et_2O$, a thawing solution of MeOTf (0.00520 g, 0.0317 mmol, 1.05 equivs) in $Et_2O$ (1 mL) was layered and allowed to freeze in the cold well. Upon freezing the reaction was allowed to warm to -40$^{o}$C in

the freezer, thaw and react for a ca. 45 minuets where upon the observation of a deep red precipitate was observed. The resulting suspension was then filtered over fiberglass packed with Celite (2 cm) to isolate the suspended solid. The solid was then washed with 1 X 2mL thawing $Et_2O$, followed by 1 X 1 mL *n*-pentane. The solid was then extracted with benzene and lyophilized. Recrystallization from a saturated $Et_2O$/toluene solution at -40°C for 1 day yielded $Fe(N_2)(CNAr^{Mes2})_4$ as deep red crystals, 2 mg, 4.6%. Low yields are due to a complex mixture of products upon formation of $Fe(N_2)(CNAr^{Mes2})_4$, details of the mixture are discussed below. $^1$HNMR (499.8 MHz, $C_6D_6$, 20°C) δ = 6.91 (s, 16H, *m*-Mes), 2.30 (s, 24H, *p*-CH3 Mes), 2.05 (s, 48H, *o*-CH3 Mes) ppm. $^{13}C\{^1H\}$ NMR (125.7 MHz, C6D6, 20°C) δ = 139.2, 137.7, 136.9, 136,3, 131.7, 130.6, 128.8, 125.1, 21.5 (*p*-Mes), 20.8 (*o*-Mes) ppm; prolonged scanning did not reveal the isocyanide carbon. FTIR (solution ($C_6D_6$), KBr windows, 25oC): ($\nu_{CN}$) 1967 (s), 1951 (s), 2017 (m, sh), (s), ($\nu_{NN}$) 2067 (m), also 2970 (w), 2945 (w), 2920 (w), 2848 (w), 1542 (w), 1453 (m), 1416 (w), 1377 (w), 1324 (w), 851 (w), 804 (w), 756 (w), 668 (w), 631 (w) $cm^{-1}$. Due to the thermal instability and loss of $N_2$ even at -40° C suitable analysis was not obtained.

**Isolation of $[Fe(\eta^6\text{-(Mes)-}\mu^2\text{-C-CNAr}^{Mes})]_2$ (8) from the decomposition of $Fe(N_2)(CNAr^{Mes2})_4$:** Upon generation of $Fe(N_2)(CNAr^{Mes2})_4$ from $Na[HFe(CNAr^{Mes2})_4]$ (0.0256 g, 0.01782 mmol, 1 equiv), and MeOTf (0.0034 g, 0.02072 mmol, 1.1 equiv) as described above, a mixture of **(7)**, **(8)**, and **(9)** is generated. If allowed to warm to room temperature and stir for a ca. 2.5 hours conversion to **(8)**, is observed via $^1$HNMR. Filtration of a thawing $Et_2O$ solution of the reaction mixture over fiberglass affords a dark

grey solid, that when extracted into benzene followed by evaporation to dryness afforded $Fe_2(\mu^2\text{–}CNAr^{Mes2})_2$ as a blue green solid, 0.0036 g, 28.2 % yield. $^1$HNMR (499.8 MHz, $C_6D_6$, 20°C) δ = 7.40 (q of d, 4H, 7 Hz, *m*-Ph), 7.26 (s, 4H, *m*-Mes), 7.21 (t, 2H, 7 Hz, *p*-Ph), 4.04 (s, 4H, $\eta^6$-*m*-Mes), 2.59 (s, 12H, $\eta^6$-Mes-*o*-$CH_3$), 2.50 (s, 6H, $\eta^6$-Mes-*p*-$CH_3$), 2.47 (s, 6H, Mes-*p*-$CH_3$), 1.13 (s, 12H, Mes-*o*-$CH_3$) ppm. $^{13}C\{^1H\}$ NMR (125.7 MHz, C6D6, 20°C) δ = 153.5 (*C*N), 140.3, 136.9, 136.8, 136.1, 135.7, 130.9, 126.8, 124.7, 124.0, 114.5, 108.3, 88.5, 87.7, 30.3, 21.6, 20.0, 17.7 ppm. FTIR (solution ($C_6D_6$), KBr windows, 25ºC): ($\nu_{CN}$) 1707 (s), also 2919 (w), 1542 (s), 1003 (m) $cm^{-1}$. Multiple attempts at producing analytically pure material proved unsuccessful in addition to attempts at observation via HRMS.

**Isolation of $Ph^{Me2}CH_2C(H)NAr^{Mes}$ from the decomposition of $Fe(N_2)(CNAr^{Mes2})_4$:** Upon generation of $Fe(N_2)(CNAr^{Mes2})_4$ from $Na[HFe(CNAr^{Mes2})_4]$ (0.0463 g, 0.03223 mmol, 1 equiv), and MeOTf (0.0056 g, 0.0338 mmol, 1.05 equiv) as described above, a mixture of **(7)**, **(8)**, and **(9)** is generated.as described above, a mixture of **(7)**, **(8)**, and **(9)** is generated. If allowed to warm to room temperature and stir for a ca. 2.5 hours appreciable conversion to **(8)**, and **(9)** is observed via $^1$HNMR. Filtration of a thawing $Et_2O$ solution over fiber glass followed by evaporation to dryness of the resulting red filtrate yielded a red film. A serial extraction of MeCN and *n*–pentane 3 X (5mL:5mL) collecting the MeCN fraction followed by evaporation to dryness afforded $Ph^{Me2}CH_2C(H)NAr^{Mes}$ as an off white solid, 0.0021 mg, 72 % yield. $^1$HNMR (499.8 MHz, $C_6D_6$, 20°C) δ = 7.46 (d of d, $1H_a$, 7 Hz, *m*–Ph), 7.41 (t, $1H_b$, 5 Hz, N=C*(H)*), 7.12 (d of d, $1H_c$, 5 Hz, *m*–Ph), 7.05 (t, $1H_d$, 7 Hz, *p*-Ph), 6.96 (s, $1H_e$, *m*–Mes), 6.95 (s, $1H_f$,

*m*–Mes), 6.85 (s, 1$H_g$, *m*–Mes), 6.52 (s, 1$H_h$, *m*–Mes), 2.71 (d of q, 2$H_i$, 28 Hz, 5Hz, C$H_2$), 2.36 (s, 3$H_j$, C$H_3$), 2.30 (s, 3$H_k$, C$H_3$), 2.25 (s, 3$H_l$, C$H_3$), 2.14 (s, 3$H_m$, C$H_3$), 2.00 (s, 3$H_n$, C$H_3$ ppm. $^{13}C\{^1H\}$ NMR (125.7 MHz, $C_6D_6$, 20°C) δ = 159.0 (*C*N), 145.8, 139.2, 138.0, 137.1, 136.6, 136.5, 136.4, 136.3, 135.9, 133.5, 131.1, 130.7, 130.4, 129.1, 128.6, 127.5, 125.7, 123.0, 37.4, 22.1, 21.2, 21.1, 20.9, 20.6 ppm. FTIR (solution ($C_6D_6$), KBr windows, 25ºC): ($\nu_{CN}$) 1613 (m) , also 2022 (w), 2957 (w), 2919 (w) $cm^{-1}$. HRMS (ESITOF): m/z calc'd for C25H25N [M]+H : 340.2060 Found: 340.2054.

## 2.9 Details of Crystallographic Structure Determinations.

Single-crystal X-ray structure determinations were carried out using Bruker Platform or Kappa X-ray Diffractometers equipped with Mo or Cu radiation sources (sealed tube or rotating anode), low-temperature cryostats, and CCD detectors (Bruker APEX or Bruker APEX II). All structures were solved by direct methods using SHElXS[74] and refined by full matrix least-squares procedures utilizing SHELXL[74] within the Olex2 small-molecule solution, refinement and analysis software package.[75] Crystallographic data collection and refinement information are listed below in Table 2.2.

The solid-state structure of *cis,cis,trans*-$FeI_2(CO)_2(CNAr^{Mes2})_2$ (**4**) was found to be compositionally disordered with a small amount its isomer *trans,trans,trans*-$FeI_2(CO)_2(CNAr^{Mes2})_2$. Satisfactory refinement of the data set was achieved using a 10% compositional disorder model. $^1H$ NMR spectroscopy indicated only trace amounts of *trans,trans,trans*-$FeI_2(CO)_2(CNAr^{Mes2})_2$ in bulk samples of *cis,cis,trans*$FeI_2(CO)_2(CNAr^{Mes2})_2$ (**4**).

The solid-state structure of [Na(18-crown-6)][($Me_6$-1-azabenz[*b*]azulene)Fe($CNAr^{Mes2}$)$_2$] (**5**) was found to possess significant positional disorder of the [Na(18-crown-6)] unit. The electron-density difference map was modeled, using restraints, as a two-site positional disorder containing a major (80%, shown in text) and minor (20%) orientation of the [Na(18-crown-6)] unit. The chemical significance of both orientations is identical.

**Table 2.2.** Crystallographic data collection and refinement information.

| Name | $Na_2[Fe(CNAr^{Mes2})_4]$ [$Na_2$(**1**)] | $Fe(CO)_4(CNAr^{Mes2})$ (**2**) | $Fe(CO)_3(CNAr^{Mes2})_2$ (**3**) |
|---|---|---|---|
| Formula | $C_{100}H_{100}FeN_4Na_2$ | $C_{29}H_{25}NO_4Fe$ | $C_{53}H_{50}N_2O_3Fe$ |
| Crystal System | Monoclinic | Monoclinic | Monoclinic |
| Space Group | $P2_1/c$ | $P2_1/m$ | $P2_1/n$ |
| $a$, Å | 27.1109(10) | 8.2857(3) | 26.7165(11) |
| $b$, Å | 11.8497(4) | 18.0545(7) | 13.6599(5) |
| $c$, Å | 27.5348(10) | 8.6241(3) | 27.7314(11) |
| α, deg | 90 | 90 | 90 |
| β, deg | 115.721(2) | 96.625(2) | 117.941(3) |
| γ, deg | 90 | 90 | 90 |
| V, Å$^3$ | 7969.3(5) | 1281.50(8) | 8940.7(6) |
| $Z$ | 4 | 2 | 8 |
| Radiation (λ, Å) | Cu-Kα, 1.54178 | Mo-Kα, 0.71073 | Mo-Kα, 0.71073 |
| ρ (calcd.), g/cm$^3$ | 1.217 | 1.315 | 1.217 |
| μ, mm$^{-1}$ | 2.009 | 0.623 | 0.382 |
| Temp, K | 100 | 100 | 100 |
| θ max, deg | 69.669 | 25.351 | 26.393 |
| data/parameters | 14070/0/989 | 2407/0/175 | 26325/0/1091 |
| $R_1$ | 0.0629 | 0.0313 | 0.0593 |
| $wR_2$ | 0.1637 | 0.0722 | 0.1055 |
| GOF | 1.072 | 1.073 | 1.041 |

**Table 2.3**. Crystallographic data collection and refinement information.

| Name | $FeI_2(CO)_2(CNAr^{Mes2})$ (**4**) | [Na(18-c-6)][Fe($\eta^5$-(1-azabenz[*b*]azulene)($CNAr^{Mes2}$)$_2$]•0.5($Et_2O$) (**5**) | Na[$HFe(CNAr^{Mes2})_4$]•($C_5H_{12}$) (Na[**6**]) |
|---|---|---|---|
| Formula | $C_{152}H_{50}FeN_2O_2I_2$ | $C_{89}H_{104}FeN_3NaO_{6.5}$ | $C_{105}H_{113}FeN_4Na$ |
| Crystal System | Triclinic | Triclinic | Triclinic |
| Space Group | *P*–1 | *P*–1 | $P2_1/n$ |
| *a*, Å | 13.5946(5) | 16.260(2) | 13.4873(10) |
| *b*, Å | 14.6648(5) | 16.648(3) | 27.8985(17) |
| *c*, Å | 15.0797(5) | 18.225(3) | 22.7298(14) |
| α, deg | 64.878(2) | 64.902(5) | 90 |
| β, deg | 64.999(2) | 89.753(6) | 90.479(5) |
| γ, deg | 64.8240(10) | 62.66(5) | 90 |
| V, Å$^3$ | 2353.46(1) | 3855.1(10) | 8552.4(10) |
| *Z* | 2 | 2 | 4 |
| Radiation (λ, Å) | Mo-Kα, 0.71073 | Mo-Kα, 0.71073 | Cu-Kα, 1.54178 |
| ρ (calcd.), g/cm$^3$ | 1.474 | 1.205 | 1.173 |
| μ, mm$^{-1}$ | 1.673 | 0.258 | 1.840 |
| Temp, K | 100 | 100 | 100 |
| θ max, deg | 29.147 | 22.000 | 57.708 |
| data/parameters | 12639/58/568 | 9092/980/1166 | 10905/49/1048 |
| $R_1$ | 0.0412 | 0.1170 | 0.0556 |
| $wR_2$ | 0.0953 | 0.2913 | 0.1222 |
| GOF | 1.056 | 1.050 | 1.007 |

**Table 2.4.** Crystallographic data collection and refinement information.

| Name | $Fe(N_2)(CNAr^{Mes2})_4$ (**7**) | $Fe_2(\mu^2\text{-}CNAr^{Mes}\eta^6\text{-}Mes)_2$ (**8**) | $^{Mes}ArNC(H_2)CH_2Ar^{Mes}$ (**8**) |
|---|---|---|---|
| Formula | $C_{100}H_{100}FeN_6$ | $C_{50}H_{50}Fe_2N_2$ | $C_{25}H_{25}N$ |
| Crystal System | Monoclinic | Monoclinic | Monoclinic |
| Space Group | *C*2/*c* | $P2_1/c$ | $P2_1/n$ |
| *a*, Å | 16.195(2) | 7.8487(9) | 13.7638(11) |
| *b*, Å | 23.161(3) | 21.294(3) | 7.2450(5) |
| *c*, Å | 21.453(3) | 11.8949(14) | 18.9715(15) |
| α, deg | 90 | 90 | 90 |
| β, deg | 97.426(6) | 95.471(2) | 96.205(3) |
| γ, deg | 90 | 90 | 90 |
| V, $Å^3$ | 7979(2) | 1979.0(4) | 1880.7(2) |
| *Z* | 4 | 2 | 4 |
| Radiation (λ, Å) | Mo-Kα, 0.71073 | Mo-Kα, 0.71073 | Mo-Kα, 0.71073 |
| ρ (calcd.), $g/cm^3$ | 1.200 | 1.327 | 1.199 |
| μ, $mm^{-1}$ | 0.242 | 0.771 | 0.069 |
| Temp, K | 100 | 100 | 100 |
| θ max, deg | 25.354 | 25.347 | 25.382 |
| data/parameters | 7270/0/496 | 3628/0/250 | 3451/0/240 |
| $R_1$ | 0.0441 | 0.0609 | 0.0492 |
| $wR_2$ | 0.0935 | 0.1689 | 0.1026 |
| GOF | 1.016 | 1.043 | 1.024 |

## 2.10. Acknowledgements

Chapter 2 is adapted in part from Mokhtarzadeh, C. C.; Margulieux, G. W.; Carpenter, A. E.; Weidemann, N.; Moore, C. E.; Rheingold, A. L; Figueroa, J. S. *Inorg. Chem.* **2015**, *54*, 5579-5587. Copyright 2015, American Chemical Society. Permission to include published material in this dissertation has been obtained from all coauthors. The dissertation author is the first author of this paper.

## 2.11. References

(1) Krumholz, P.; Stettiner, H. M. A. *J. Am. Chem. Soc.* **1949**, *71*, 3035.

(2) Collman, J. P. *Acc. Chem. Res.* **2006**, *45*, 3167.

(3) Ellis, J. E. *Inorg. Chem.* **2006**, *45*, 3167.

(4) Ellis, J. E. *Organometallics* **2003**, *22*, 3322.

(5) Pike, R. D. In *Encyclopedia of Reagents for Organic Synthesis*; John Wiley Sons, Ltd.: New York, 2001.

(6) Ellis, J. E. *Adv. Organomet. Chem.* **1990**, *31*, 1.

(7) Brennessel, W> W.; Ellis, J. E. *Angew. Chem., Int. Ed.* **2007**, *46*, 598.

(8) In addition to $[Fe(CNXyl)_4]^{2-}$, Ellis' 2007 communication (ref 7) also disclosed the synthesis of $[Fe(CN\text{-}t\text{-}Bu)_4]^{2-}$, which was too thermally unstable to characterize by crystallographic or spectroscopic means. However, *in-situ*-generated $[Fe(CN\text{-}t\text{-}Bu)_4]^{2-}$ reacted with $ClSnPh_3$ at –78 ˚C to provide *trans*-$Fe(SnPh_3)_2(CN\text{-}t\text{-}Bu)_4$, thus providing reasonable evidence for its existence.

(9) Warnock, G. F.; Cooper, N. J. *Organometallics* **1989**, *8*, 1826.

(10) Leach, P. A.; Geib, S. J.; Corella, J. A.; Warnock, G. F.; Cooper, N. J. *J. Am. Chem. Soc.* **1994**, *116*, 8566.

(11) Corella, J. A.; Thompson, R. L.; Cooper, N. J. *Angew. Chem., Int. Ed.* **1992**, *31*, 83.

(12) Utz, T. L.; Leach, P. A.; Geib, S. J.; Cooper, N. J. *Chem. Commun.* **1997**, 847.

(13) Utz, T. L.; Leach, P. A.; Geib, S. J.; Cooper, N. J. *Organometallics* **1997**, *16*, 4109.

(14) Weber, L. *Angew. Chem., Int. Ed.* **1988**, *37,* 1515.

(15) Barybin, M. V.; Brennessel, W. W.; Kucera, B. E.; Minyaev, M. E.; Sussman, V. J.; Young, V. G.; Ellis, J. E. *J. Am. Chem. Soc.* **2007**, *129*, 1141.

(16) Barybin, M. V.; Young, V. G.; Ellis, J. E. *J. Am. Chem. Soc.* **1998**, *120*, 429.

(17) Barybin, M. V.; Young, V. G.; Ellis, J. E. *J. Am. Chem. Soc.* **2000**, *122*, 4678.

(18) Barybin, M. V.; Young, V. G.; Ellis, J. E. *J. Am. Chem. Soc.* **1999**, *121*, 9237.

(19) Yamamoto, Y. *Coord. Chem. Rev.* **1980**, *32*, 193.

(20) Sarapu, A. C.; Fenske, R. F. *Inorg. Chem.* **1974**, *14*, 247.

(21) King, R. B.; Saran, M. S. *Inorg. Chem.* **1974**, *13*, 74.

(22) Sarapu, A. C.; Fenske, R. F. *Inorg. Chem.* **1972**, *11*, 3021.

(23) Cotton, F. A.; Zingales, F. *J. Am. Chem. Soc.* **1961**, *83*, 351.

(24) Carpenter, A. E.; Mokhtarzadeh, C. C.; Ripatti, D.S.; Havrylyuk, I.; Kamezawa, R.; Moore, C. E.; Rheingold, A. L.; Figueroa, J. S. *Inorg. Chem.* **2015**, *54*, 2936.

(25) Fox. B. J.; Sun, Q. Y.; DiPasquale, A. G.; Fox, A. R.; Rheingold, A. L.; Figueroa, J. S. *Inorg. Chem.* **2008**, *47*, 9010.

(26) Ditri, T. B.; Fox. B. J.; Moore, C. E.; Rheingold, A. L.; Figueroa, J. S. *Inorg. Chem.* **2009**, *48*, 8362.

(27) Fox, B. J.; Mullard, M. D.; Dipasquale, A. G.; Rheingold, A. L.; Figueroa, J. S. *Angew. Chem., Int. Ed.* **2009**, *48*, 3473.

(28) Labios, L. A.; Millard, M. D.; Rheingold, A. L.; Figueroa, J. S. *J. Am. Chem. Soc.* **2009**, *131*, 11318.

(29) Weidemann, N,; Margulieux, G. W.; Moore, C. E.; Rheingold, A. L.; Figueroa, J. S. *Inorg. Chim. Acta.* **2010**, *364*, 238.

(30) Ditri, T. B.; Moore, C. E.; Rheingold, A. L.; Figueroa, J. S. *Inorg. Chem.* **2011**, *50*, 10448.

(31) Emerich, B. M.; Moore, C. E.; Rheingold, A. L.; Figueroa, J. S. *Organometllics* **2011**, *30,* 2598.

(32) Stewart, M. A.; Moore, C. E.; Ditri, T. B.; Labios, L. A.; Rheingold, A. L.; Figueroa, J. S. *Chem. Commun.* **2011**, *47,* 406.

(33) Tomson, N. C.; Labios, L. A; Weyhermuller, T.; Figueroa, J. S.; Wieghardt, K. *Inorg. Chem.* **2011**, *50*, 5763.

(34) Carpenter, A. E.; Wen, I.; Moore, C. E.; Rheingold, A. L.; Figueroa, J. S. *Chem. –Eur. J.* **2013**, *19*, 10452.

(35) Ditri, T. B.; Carpenter, A. E.; Ripatti, D. S.; Moore, C. E.; Rheingold, A. L.; Figueroa, J. S. *Inorg. Chem.* **2013**, *52,*13216.

(36) Margulieux, G. W.; Weidemann, N.; Lacy, D. C.; Moore, C. E.; Rheingold, A. L.; Figueroa, J. S. *J. Am. Chem. Soc.* **2010**, *132*, 5033.

(37) Carpenter, A. E.; Margulieux, G. W.; Millard, M. D.; Moore, C. E.; Rheingold, A. L.; Figueroa, J. S. *Angew. Chem., Int. Ed.* **2012**, *51*, 9412.

(38) Brunet, J. J. *Chem. Rev.* **1990**, *90*, 1041.

(39) Cronin, D. L.; Wilkinson, J. R.; Todd, L. J. *J. Magn. Reson.* **1975**, *17*, 353.

(40) Todd, L. J.; Wilkinson, J. R. *J. Organomet. Chem.* **1974**, *77*, 1.

(41) (a) Darensbourg, M. Y. *Prog. Inorg. Chem.* **1985**, *33*, 221. (b) Macchioni, A. *Chem. Rev.* **20005**, *105*, 2039.

(42) Yang, L.; Powell, D. R.; Houser, R. P. *Dalton Trans.* **2007**, 955.

(43) Bitterwolf, T. E. *Cord. Chem. Rev.* **2000**, *206-207*, 419.

(44) Buchner, E.; Curtius, T. *Ber. Dtsch, Chem. Ges.* **1885**, *18*, 2371.

(45) Li, J. *Name Reactions for Carbocyclic Ring Formations*; John Wiley & Sons, Inc.: New York, **2010**, p 423.

(46) Boyer, J. H.; De Jong, J. *J. Am. Chem. Soc.* **1969**, *91*, 5929.

(47) Chomitz, W. A.; Suton, A. D.; Krinsky, J. L.; Arnold, J. *Organometallics* **2009**, *28*, 3338.

(49) Kagiya, T.; Sumida, Y; Tachi, T. *Bul. Chem. Soc. Jpn.* **1970**, *43*, 3716.

(50) Blaschette, A.; Bressel, B. *Inorg, Nucl. Chem. Lett.* **1968**, *4*, 175.

(51) Bordwell, F. G.; *Acc. Chem. Res.* **1988**, *21*, 456.

(52) Krumholz, P.; Galembeck, F. *J. Am. Chem. Soc.* **1971**, *93*, 1909.

(53) Addison, A. W.; Rao, T. M.; Reedijk, J.; van Rijn, J.; Verschoor, G. C. *J. Chem. Soc., Dalton Trans.* **1984**, 1349.

(54) Ash, C. E.; Delord, T.; Simmons, D.; Darensbourg, M. Y. *Organometallics* **1986**, *5*, 17.

(55) Darensbourg, M. Y.; Darensbourg, D. J.; Barros, H. L. C.; *Inorg. Chem.* **1987**, *17*, 297.

(56) Ash, C. E.; Darensbourg, M. Y.; Hall, M. B. *J. Am. Chem. Soc.* **1987**, *109*, 4173.

(57) Hazari, N. *Chem. Soc. Rev.* **2010**, *39*, 4044.

(58) Whitmire, K. H.; Lee, T. R.; Lewis, E.S. *Organometallics* **1896**, *5*, 987.

(59) Zhou, M,; Andrews, L,; Bauschlicher, C. W. *Chem. Rev.* **2001**, *101*, 1931.

(60) Poliakoff, M.; Turner, J. J. *Angew. Chem., Int. Ed.* **2001**, *40*, 2809.

(61) Poliakoff, M.; Turner, J. J. *J. Chem. Soc., Dalton Trans.* **1973**, 1351.

(62) Zhang, H,; Ouyang, Z.; Liu, Y.; Zhang, Q.; Wang, L.; Deng, L. *Angew. Chem., Int. Ed.* **2014**, *54,* 268.

(63) Lavallo, V.; El-Batta, A.; Bertrand, G.; Grubbs, R. H. *Angew. Chem., Int. Ed.* **2011**, *50*, 268.

(64) Lavallo, V.; Grubbs, R. H. *Science* **2009,** *326*, 559.

(65) Schore, N. E.; Ilenda, C. S.; Bergman, R. G. *J. Am. Chem. Soc.* **1976**, *99*, 1781.

(67) Pinhas, A. R.; Hoffmann, R. *Inorg. Chem.* **1979**, *18*, 654.

(68) Cirjak, L. M.; Finsburg, R. E.; Dahl, L. F. *Inorg. Chem.* **1982**, *21*, 940.

(69) Wang, H.; Xie, Y.; King, R. B.; Schaefer, H. F. *J. Am. Chem. Soc.* **2005**, *127*, 11646.

(70) Jones, W. D.; Foster, G. P.; Putinas, J. M. *J. Am. Chem. Soc.* **1987***, 109*, 5047.

(71) Bassett, J. M.; Berry, D. E.; Barker, G. K.; Green, M.; Howard, J. A. K.; Stone, F. G. A. *J. Chem. Soc., Dalton Trans.* **1979**, 1003.

(72) Pangborn, A. B.; Giardello, M. A.; Grubbs, R. H.; Rosen, R. K.; Timmers, F. J. *Organometallics* **1996**, *15,* 1518.

(73) Fulmer, G. R.; Miller, A. J. M.; Sherden, N. H.; Gottlieb, H. E.; Nudelman, A.; Stoltz, B. M.; Bercaw, J. E.; Goldberg, K. I. *Organometallics* **2010**, *29*, 2176.

(74) Sheldrick, G. *Acta Crystallogr., Sect. A*. **2008**, *64*, 112.

(75) Dolomanov, O.V.; Bourhis, L. J.; Gildea, R. J.; Howard, J. A. K.; Puschmann H. *J. Appl. Crystallogr.* **2009**, *42*, 339.

# *Chapter 3*

# *$CO_2$ Reduction With A Tetraisocyanide Iron Dianion: Reductive Disproportionation and $CO_2$ Capture With Electrophilic Silyl Sources to Facilitate Fe-C Multiple Bonding.*

## 3.1 Introduction

The development of transition-metal systems that can affect the chemical, photolytic, and electrochemical reduction of $CO_2$ to value added chemical commodities (*e.g* CO, HCOOH, $CH_3OH$) have seen untiring interest within the chemical community.[1-5] This impetus for the development and understanding of systems that can facilitate the reduction of $CO_2$ has been sustained by the large increases in atmospheric $CO_2$ from anthropogenic sources and its impact on climate chagne,[6-9] in addition to its potential use as an abundant $C_1$ feedstock. Indeed, the coordination chemistry of transition metal–$CO_2$ complexes have been documented with a number of structurally authenticated $CO_2$ adducts.[10-12] However, the observation of $\kappa^1$–*C*-metalo-carboxylate intermediates generated from the reduction of $CO_2$ are limited,[13] despite their implication in a number of instances.[14-18] The difficulties in isolating $\kappa^1$–*C*-metalo-carboxylates stems from their propensity to reductively disproportionate to CO and $CO_3^{2-}$ with a second equivalent of $CO_2$.[15,16,19] To circumvent unwanted decomposition, $\kappa^1$–*C*-metalo-carboxylate have been generated and isolated from the hydroxylation of CO (*i.e.* addition of $HO^-$ to a carbonyl

containing metal complex), and have been shown to serve as reactive motifs for the generation of value added $C_1$ synthons.[12,20] Accordingly, transition-metal platforms capable of accomplishing $CO_2$ capture, and its reduction to energy rich carbon containing species still remains a worthwhile endeavor.

Our interest stem from classical examples of stoichiometric reductive disproportionation of $CO_{2-,}$ in which homoleptic carbonyl metallates (*e.g.* $[M(CO)_n]^{2-}$ (M = Fe, Ru, Os, Cr, Mo, W; n = 4, 5)) have been employed.[19,21,22] Addition of $CO_2$ to these dianionic metallates results in the formation of CO which is rapidly intercepted by the resultant neutral $M(CO)_4$ fragment to yield an equivalent of $M(CO)_5/M(CO)_6$ and an equivalent of $CO_3^{2-}$. The generation of systems that can mimic the coordination modes, electronic structure, and importantly the reactivity of these carbonyl metallates could provide mechanistic insight and synthetic strategies for $CO_2$ capture and potentially redirecting the reductive disproportionation of $CO_2$ to more exotic carbon containing materials.

To this end, our group has shown the success of utilizing sterically encumbering *m*-terphenyl isocyanides as isolobal surrogates for CO to kinetically stabilize a number of homoleptic and mixed carbonyl/isocyanide systems that mimic many of the geometric and electronic structures of the classical binary carbonyl metallates,[23-26] and their unsaturated neutral partners.[27-29] From a molecular design strategy when compared to CO, isocyanides (CNR) exhibit a higher σ-donnor/π–acceptor ratio,[30] thus providing the added benefit of rendering a metal center more electron rich, culminating in a substantially more nucleophilic site for the activation of electrophilic substrates. Recently we reported the synthesis of the tetraisocyano Ferrate (2–) complex,

$Na_2[Fe(CNAr^{Mes2})_4$, $Na_2$[**1**], as an encumbered isocyano analogue to the well studied Collman's reagent, $[Fe(CO)_4]^{2-}$.[25] In this report it was found that based on the homoleptic isocyanide ligand field the Fe center in this system displayed increased metal-based nucleophilicity most notably shown upon protonation $Na_2$[**1**] to afford $Na[HFe(CNAr^{Mes2})_4]$ which upon alkylation proceeds to give $Fe(N_2)(CNAr^{Mes2})_4$.[25] Herein we report the reactivity of $Na_2$[**1**] with $CO_2$, and its ability to facilitate the facile reductive disproportionation of $CO_2$ to afford $Fe(CO)(CNAr^{Mes2})_4$ (**2**) and $CO_3^{2-}$. It is shown that the resultant $Fe(CO)(CNAr^{Mes2})_4$ (**2**) is kinetically destabilized due to the large steric pressure about Fe and displays a mechanistically distinct decomposition pathway when compared to the isostructural dinitrogen complex $Fe(N_2)(CNAr^{Mes2})_4$ via the intermolecular activation of aromatic $sp^2$ C–H bonds and subsequent isocyanide insertion. Additionally we report our targeted attempts at trapping the proposed $\kappa^1$–*C*-metalo-carboxylate intermediate with reactive silyl triflates ($SiR_3OTf$), resulting in the formal electrophilic functionalization of the isocyanide–*N* to yield a series of novel $CO_2$ derived iron aminocarbyne complexes. It is postulated that formation of the resultant aminocarbyne species is mechanistically divergent from typical electrophilic functionalization of isocyanides, and that $CO_2$ capture is reversible upon addition of 2.0 equivalents of $NaHBEt_3$ resulting in the regeneration of $Na_2[Fe(CNAr^{Mes2})_4]$.

### 3.2 Reductive Disproportionation of $CO_2$ With $Na_2[Fe(CNAr^{Mes2})_4]$, $Na_2$[1].

Treatment of $Na_2[Fe(CNAr^{Mes2})_4]$, $Na_2$[**1**], with an atmosphere of $CO_2$ results in an immediate color change from a deep red to a bright red-orange, and clean conversion to a new diamagnetic species assayed by $^1$H NMR, and determined by single crystal X-Ray diffraction to be $Fe(CO)(CNAr^{Mes2})_4$ (**2**), Scheme 3.1. The solid state structure of

complex (**2**) is depicted in Figure 3.1 and adopts a near trigonal bi–pyramidal structure (Addison-Reedijk parameter $\tau^5$ = 0.90)[31] with the CO ligand occupying an equatorial coordination site. Fe(CO)(CNAr$^{Mes2}$)$_4$ (**2**) exhibits bond lengths of ~1.8466(15) Å for the CNR and 1.796(2) Å for the CO respectively, which agree well with other established zero valent mixed carbonyl isocyanides species.[25] Additionally, solution phase FTIR spectrum of (**2**) exhibits a low energy CO stretch at 1931 cm$^{-1}$, in addition to two blue shifted isocyanide stretches at 2004, and 1996 cm$^{-1}$ consistent with local $C_{2v}$ site symmetry..

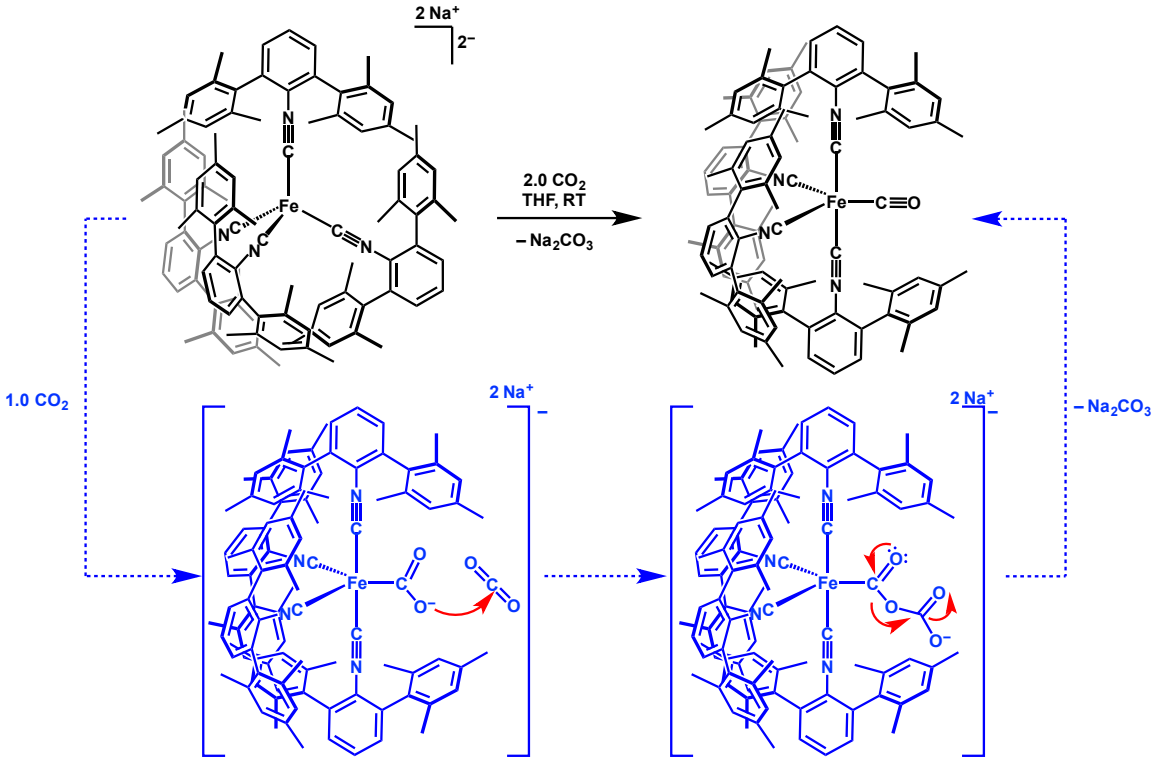


**Scheme 3.1** Reaction scheme depicting the formation of Fe(CO)(CNAr$^{Mes2}$)$_4$ from the reductive disproportionation of $CO_2$.

Addition of one equivalent of $CO_2$ to $Na_2$[Fe(CNAr$^{Mes2}$)] leads to a 50:50 mixture of $Na_2$[Fe(CNAr$^{Mes2}$)$_4$] and Fe(CO)(CNAr$^{Mes2}$)$_4$, with no indication of observable intermediates as assayed by $^1$H NMR, mimicking the reactivity of other dianionic

carbonyl metallates with $CO_2$.[19] To determine the fate of the oxygen atom, treatment of $Na_2$[**1**] with isotopically enriched $^{13}CO_2$ indicates an intense $^{13}C$ resonance at 212 ppm corresponding to the coordinate CO in $Fe(CO)(CNAr^{Mes2})_4$. Importantly after addition of $^{13}CO_2$ and dissolution of the reaction mixture in alkaline $D_2O$, the presence of isotopically enriched $CO_3^{2-}$ by $^{13}C\{^1H\}$ NMR at 168 ppm was observed, Figure 3.2. Accordingly, $Na_2$[**1**] undergoes nucleophilic attack at the $CO_2$–carbon to generate a short-lived $\kappa^1$–*C*-metalo-carboxylate.[19] Upon immediate generation, subsequent nucleophilic attack originating at the reactive carboxylate fragment toward a second equivalent of $CO_2$ yields the final products $Fe(CO)(CNAr^{Mes2})_4$ and $CO_3^{2-}$, Scheme 3.1.

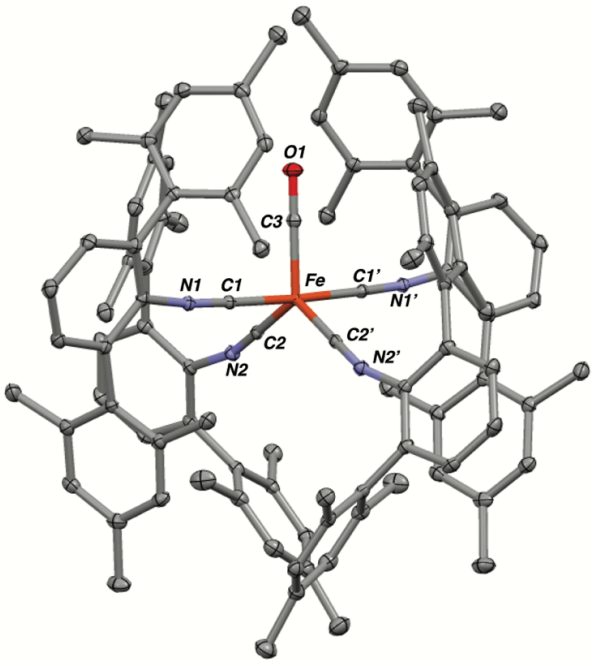


**Figure 3.1** Solid state structure of $Fe(CO)(CNAr^{Mes2})_4$. Hydrogen atoms omitted for clarity. Selected bond distances (Å): Fe-$C_1$ = 1.8465(14), Fe-$C_2$ = 1.8467(15), Fe-$C_3$ = 1.796(2). Selected bond angles (˚): $C_1$-Fe-$C_{1'}$ = 177.20(9), $C_2$-Fe-$C_{2'}$ = 123.43(9), $C_1$-Fe-$C_3$ = 88.60(5), $C_2$-Fe-$C_3$ = 118.29(5).

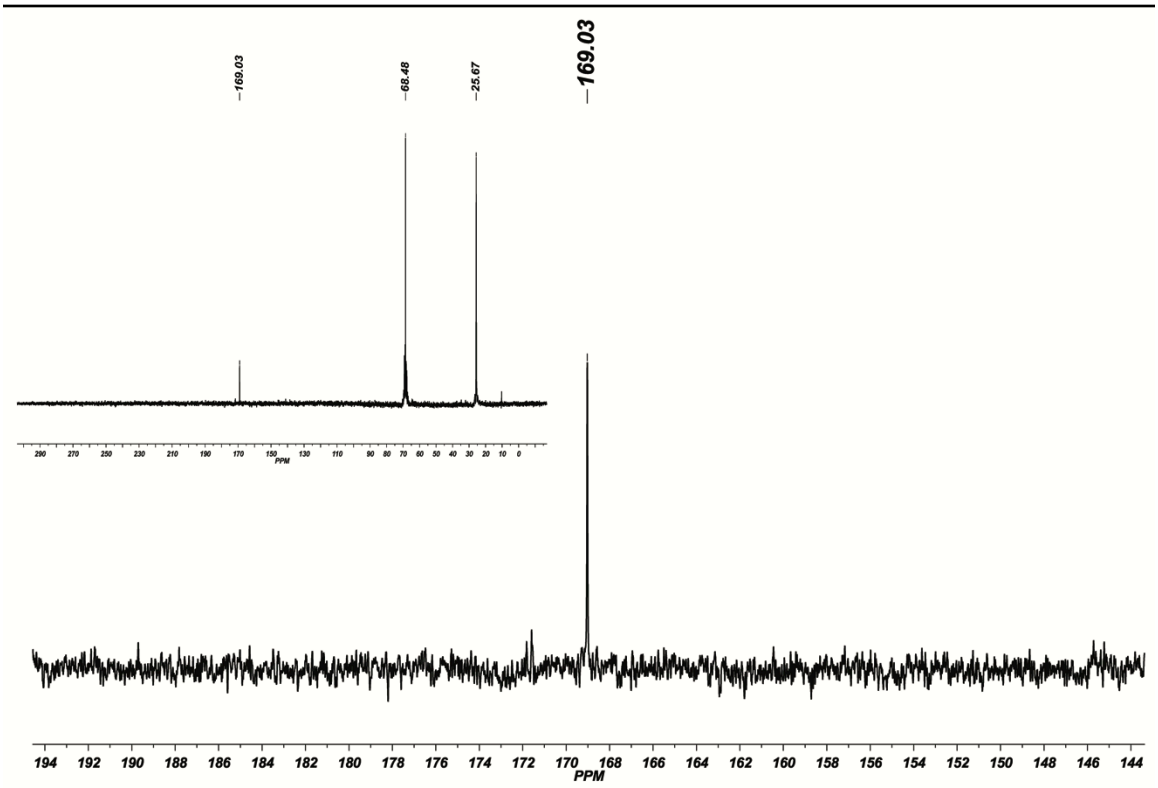


**Figure 3.2** Room temperature $^{13}C\{^{1}H\}$ NMR spectrum (125.7 MHz, $C_6D_6$) of the crude reaction mixture from the reaction of $Na_2$[**1**] with $^{13}CO_2$ in order to verify $^{13}CO_3^{2-}$ formation. Inset depicts the full $^{13}C\{^{1}H\}$ with THF for reference.

### 3.3 Decomposition of Fe(CO)(CNAr$^{Mes2}$)$_4$ via C-H activation of $C_6H_6$.

Fe(CO)(CNAr$^{Mes2}$) (**2**) displays instability in aromatic solvents when exposed to ambient light. Photolysis of Fe(CO)(CNAr$^{Mes2}$)$_4$ (**2**) over 2 hours with a mercury lamp UV source or exposure to ambient light over 24 hours leads to a color change from deep red to green and the observation of a new diamagnetic species as assayed by $^{1}H$ NMR spectroscopy. Following irradiation solution FTIR spectroscopy ($C_6D_6$) indicated conversion to a new species with a significantly red shifted C–N stretch at 1638 cm$^{-1}$ which was identified by X–ray diffraction to be the aldimine, PhC(H)NAr$^{Mes2}$ (**3**), Figure 3.3. Jones, and co–workers have previously reported the zero valent species Fe(PMe$_3$)$_2$(CN-*t*Bu)$_3$ which was effective at catalyzing the insertion of isocyanides into

aromatic $sp^2$ C–H bonds under photolytic conditions via the fleeting four coordinate fragment [Fe(PMe$_3$)$_2$(CN-*t*Bu)$_2$].[32] Since Jones' seminal finding's the insertion of isocyanides into aromatic $sp^2$ bonds has been thoroughly examined experimentally and represents an additional transformation to afford highly functionalized aldimines.[33-35]

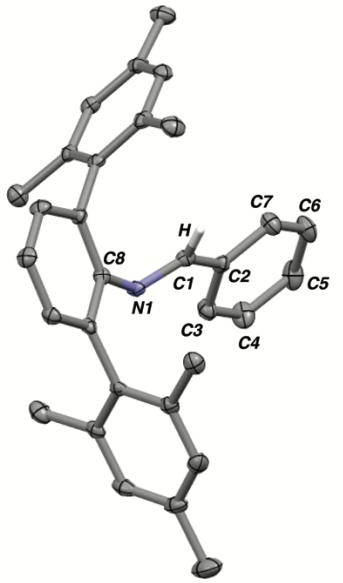


**Figure 3.3** Solid state structure of PhC(H)CNAr$^{Mes2}$, (**3**). Hydrogen atoms omitted for clarity. Selected bond distances (Å): $C_1$-$N_1$ = 1.2710(19), $C_1$-$C_2$ = 1.465(2), $N_1$-$C_8$ = 1.4226(19). Selected bond angles (˚): $C_1$-$N_1$-$C_{8'}$ = 118.91(13), $N_1$-$C_1$-$C_{2'}$ = 122.91(14).

Recently we reported the isolation of Fe(N$_2$)(CNAr$^{Mes2}$)$_4$ which readily releases N$_2$ at room temperatures and subsequently falls victim to $sp^3$ C–H activation of the *m*-terphenyl framework, presumably through generation of the fleeting [Fe(CNAr$^{Mes2}$)$_4$] fragment (Chapter 2.4-5).[25] Interestingly, there is no evidence of the generation of Fe(N$_2$)(CNAr$^{Mes2}$)$_4$ or the C-H activated aldimine[25] at different reaction time points upon irradiation of (**2**) via $^1$H NMR spectroscopy. Consequently, this indicates a divergence in reactivity for five coordinate tetra-isocyanide ligated Fe(0) species when the fifth ligand is varied from N$_2$ to CO. As a result of the increase in π-accepor capabilities of CO vs. N$_2$[36] we believe that the insipient [FeL$_4$] species within these two systems differ in the

specific ligand that is ejected. Jones reported similar reactivity to the decomposition of $Fe(CO)(CNAr^{Mes2})_4$ (**2**) resultant of CNR dissociation,[32] and as such we contend that similar isocyanide ligand ejection leads to the transitory species $[Fe(CO)(CNR)_3]$.

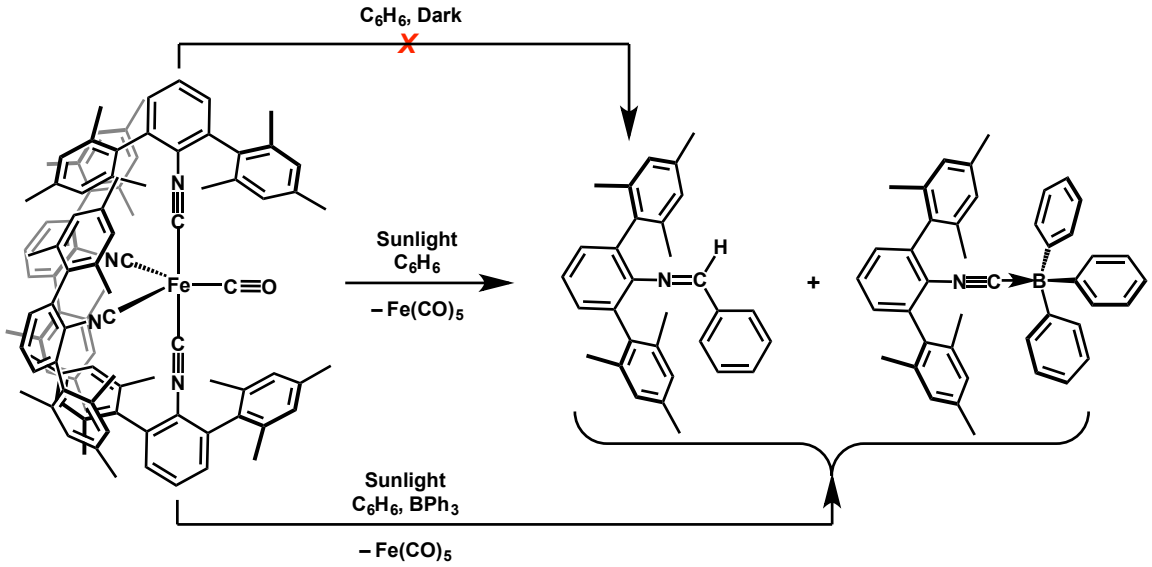


**Scheme 3.2** Reactivity of $Fe(CO)(CNAr^{Mes2})_4$ (**2**) with $C_6H_6$ under various conditions. The top reaction indicates no reaction in the absence of light. The middle reaction results in the formation of imine (**3**). And the bottom reaction depicts the formation of both imine (**3**), and the isocyanide-borane Lewis acid-base adduct upon exposure of (**2**) to light in the presence of $BPh_3$.

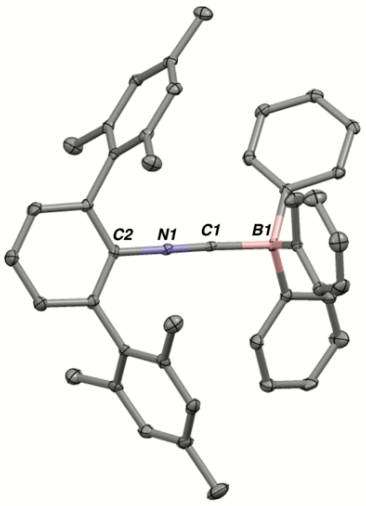


**Figure 3.4** Solid state molecular structure of $Ph_3B–CNAr^{Mes2}$, (**4**). Hydrogen atoms omitted for clarity. Selected bond distances (Å): $C_1$-$N_1$ = 1.151(4), $C_1$-$B_1$ = 1.625(4). Selected bond angles (˚): $C_2$-$N_1$-$C_{1'}$ = 177.9(3), $N_1$-$C_1$-$B_{2'}$ = 174.8(3).

In an effort to provide mechanistic insight the decomposition pathway was probed via the photolysis of $Fe(CO)(CNAr^{Mes2})_4$ (**2**) in the presence of boranes. Treatment of $CNAr^{Mes2}$ with $BPh_3$ results in the immediate formation of the corresponding Lewis acid-base adduct, [37] Scheme 3.2, Figure 3.4. It stands that the impetus for the formation of such Lewis-acid/base adducts between triarylboranes and isocyanides could potentially function as an isocyanide scavenger to provide evidence for isocyanide dissociation. Indeed, treatment of isotopically enriched $Fe(^{13}CO)(CNAr^{Mes2})_4$ with $BPh_3$ in the absence of light led to no perceived reaction as assayed by $^1H$ NMR spectroscopy. However, subsequent irradiation in $C_6D_6$ followed by analysis by $^1H$ NMR spectroscopy does indeed indicate the formation of the isocyanide-borane Lewis acid-base adduct (**4**), in addition to aldimine (**3**). Moreover, no indication of liberated $^{13}CO$ is observed via $^{13}C$ NMR, upon photolysis in a sealed J-Young NMR tube. Importantly further photolysis under Ar(g) purge maintains the incorporation of $^{13}CO$ as indicated by the formation of $Fe(^{13}CO)_5$ as assayed by $^{13}C\{^1H\}$ NMR spectroscopy. It is with this observation that we favor a mechanism that proceeds via isocyanide dissociation to generate a reactive four coordinate $[Fe(CO)(CNAr^{Mes2})_3]$ which then mediates activation of $C_6H_6$ to yield the corresponding aldimine (**4**), Scheme 3.3. Mechanistically, this suggests that the insertion of $CNAr^{Mes2}$ into $C_6H_6$ could be catalytic with added equivalent of isocyanide. Indeed, addition of *ca.* 20 equivalents of $CNAr^{Mes2}$ to $Fe(CO)(CNAr^{Mes2})_4$ (**2**) and photolyisis leads to complete consumption of isocyanide and exclusive formation of imine (**4**) as the only *m*-terphenly containing species as assayed by $^1H$ NMR spectroscopy of the crude material. Moreover, this observation servers as a stark contrast to the generation of $[Fe(N_2)(CNAr^{Mes2})_4]$ such that the incorporation of CO results in attenuated

nucleophilicity, and isocyanide ejection rather than CO and preferential intermolecular C–H activation of $sp^2$ C–H bonds rather than intramolecular aliphatic C–H activation of the ligand framework.

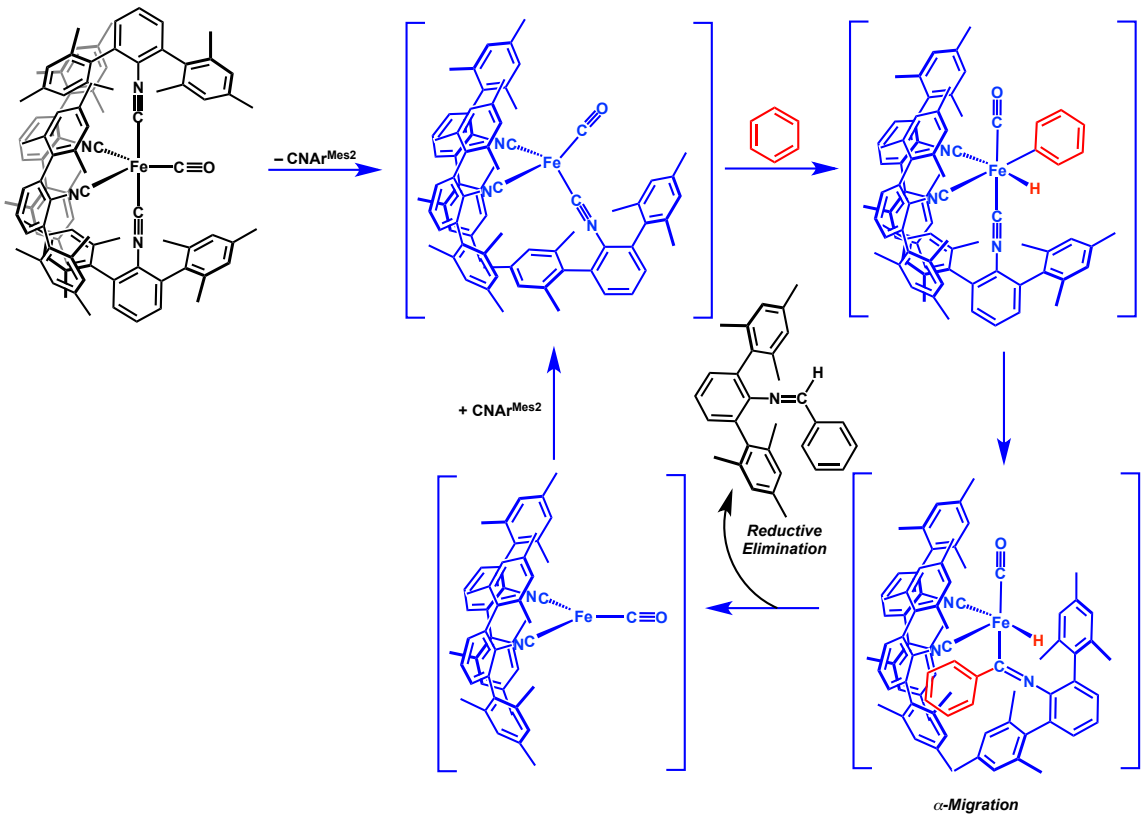


**Scheme 3.3** Proposed mechanism for the C-H activation of benzene and subsequent formation of imine (**3**).

### 3.4 Trapping of $CO_2$ Reduction Intermediates.

In an effort to implicate reduced intermediates upon the reductive disproportionation pathway of $CO_2$ by Na[**1**] a number of trapping agents were surveyed so as to append the $CO_2$–derived $\kappa^1$–*C*-metalo-carboxylate to the metal center. However, use of tri-aryl boranes ($BPh_3$, $B(C_6F_5)_3$),[38] in an attempt to take advantage of the oxophilicity of boron and to generate a Lewis acid-base adduct were unsuccessful. Moreover, attempts at employing trimethyltin chloride ($ClSnMe_3$), which has been shown

previously to stabilize metallo-carboxylates,[39] electrophilic alkyl sources (MeI, MeOTf) so as to generate a metalloester,[40,41] and halogenated silyl sources ($XSiMe_3$; X = Cl, Br, I) also all proved unsuccessful at functionalizing carbon dioxide at Fe.[41]

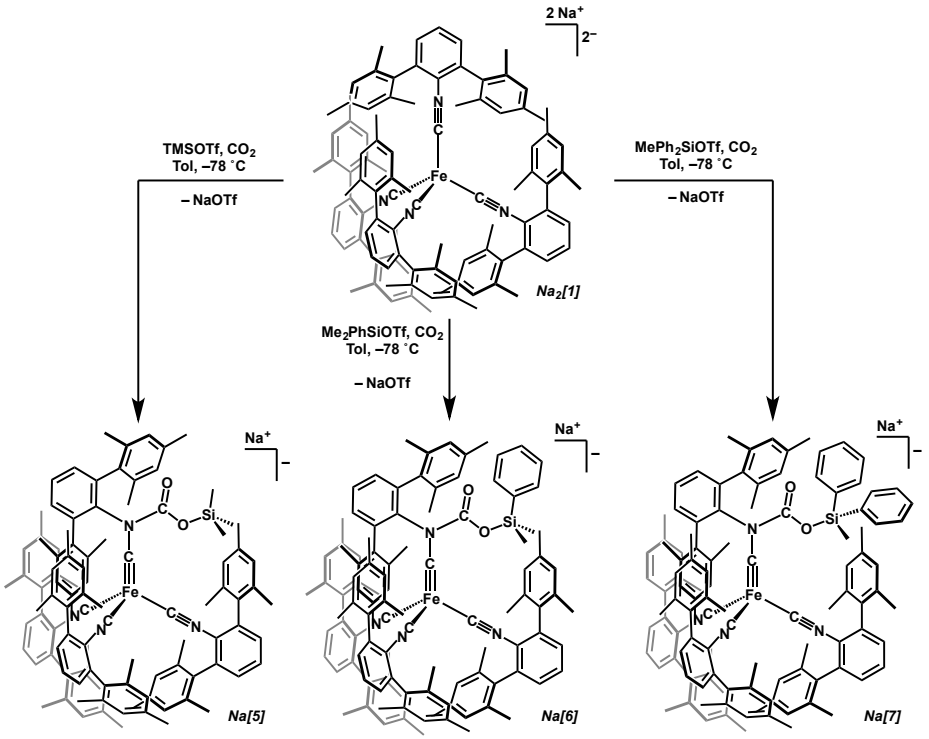


**Scheme 3.4** Synthetic route depicting the reactivity of $Na_2[Fe(CNAr^{Mes2})_4]$, $Na_2$[**2**], with $CO_2$ in the presence of $R_3SiOTf$ yielding Na[**5**], Na[**6**], and Na[**7**].

Although the uses of silyl-halide species were unable to trap the ephemeral $\kappa^1$–*C*-metalo-carboxylate, favorable Si–O bond formation was still an attractive synthetic strategy for trapping $CO_2$.[42] Accordingly the utilization of silyl-triflates were attempted due to the increased rate of silaytion that TMSOTf with respect to TMSCl (*c.a.* $10^9$) has shown.[43] Indeed, treatment of $Na_2$[**1**] with TMSOTf followed by introduction of an atmosphere of $CO_2$ at –78˚ C results in a color change from deep brown-red to a bright red–orange. Analysis of the crude reaction mixture via $^1$H NMR spectroscopy indicated a new diamagnetic species that displayed complete desymmetrization of the *m*-terphenyl

units, Figure 3.10. Crystallization from a saturated *n*-hexane/benzene solution afforded X-ray diffraction quality crystals which were unambiguously determined to be the $CO_2$ trapped complex Na[Fe(CNAr$^{Mes2}$)$_3$(CN(Ar$^{Mes2}$)(COOTMS))] Na[**4**]. The solid state structure of complex Na[**4**] is shown in Figure 3.5 and adopts a squashed tetrahedral geometry (Houser $\tau_4$ geometry index = 0.49)[44] with the apical $C_1$–carbon exhibiting an extremely short Fe–$C_{CNR}$ bond at 1.655(9) Å, with concomitant elongation of the $C_{apical}$-N linkage to 1.436(12) Å. A search of the Cambridge crystallographic database[64] shows that the Fe-$C_1$ bond length of Na[**5**] is amongst the shortest characterized to date for carbon bound ligands with a single –R group, and can most appropriately be described as a rare example of an Iron aminocarbyne.[45,46] Additionally, due to the reduced nature of Na[**5**] a substantial degree of π–back donation is still operable and manifests in the remaining isocyanide Fe–C bonds with an average Fe–C bond length of 1.823(6) Å indicative of the electron releasing ability of Fe from π-back donation into the isocyanide π*-manifold.

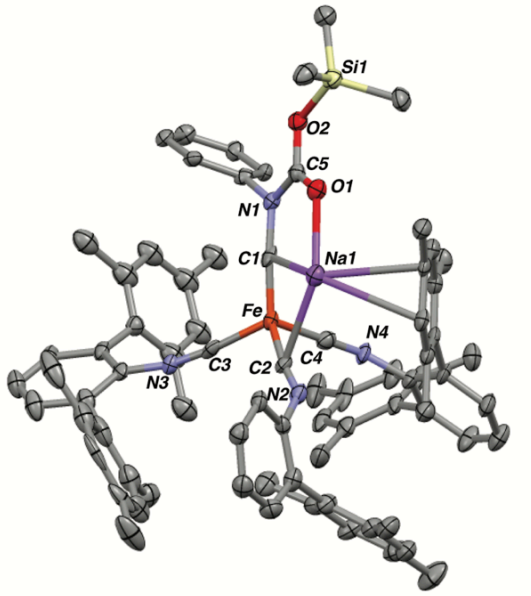


**Figure 3.5** Solid state structure of Na[Fe(CNAr$^{Mes2}$)$_3$(CN(Ar$^{Mes2}$)(C(O)OTMS)], Na[**5**]. Hydrogen atoms, and flanking mesityl rings omitted for clarity. Selected bond distances (Å): Fe-$C_1$ = 1.655(9), Fe-$C_2$ = 1.790(9), Fe-$C_3$ = 1.836(10), Fe-$C_4$ = 1.843(9), $C_1$-$N_1$ = 1.436(12), $C_2$-$N_2$ = 1.221(12), $C_3$-$N_3$ = 1.192(10), $C_4$-$N_4$ = 1.173(10), $N_1$-$C_5$ = 1.377(11), $C_5$-$O_1$ = 1.200(10), $C_5$-$O_2$ = 1.361(11), $O_2$-$Si_1$ = 1.707(6). Selected bond angles (˚): Fe-$C_1$-$N_1$ = 170.7(7), Fe-$C_2$-$N_2$ = 172.4(7), Fe-$C_3$-$N_3$ = 174.1(6), Fe-$C_4$-$N_4$ = 175.4(8), $C_1$-$N_1$-$C_9$ = 119.7(6), $C_2$-$N_2$-$C_{33}$ = 144.5(7), $C_3$-$N_3$-$C_{57}$ = 168.4(7), $C_4$-$N_4$-$C_{81}$ = 147.8(9).

Carbyne Na[**5**] exhibits local $C_2$ symmetry about Fe which is manifested in the $^1$H NMR spectrum. Further, isotopic enrichment with $^{13}$CNAr$^{Mes2}$ displays three resonances in the $^{13}$C{$^1$H} NMR that are carbyne and isocyanide in parentage (Figure 3.11). The furthest downfield shifted resonance is a triplet at 225.9 ppm corresponding to the carbyne carbon which exhibits splitting presumably due to coupling to the three other isotopically enriched isocyanide carbons (peak to peak separation *ca.* 5 Hz) coordinated to Fe seen at 214.8 and 201.0 ppm. This distribution of isocyanide–C resonances reflects the local $C_2$ site symmetry of Na[**5**]. Further analysis by solution FTIR spectroscopy corroborates the break down of local site symmetry with red shifted isocyanide stretches characteristic of a low-valent Fe center at 2019, 1988, and 1883 cm$^{-1}$, in addition to a

carbonyl shift at 1761 $cm^{-1}$ which was independently identified from the use of isotopically enriched $^{13}CO_2$ to generate Na[$^{13}$**5**].

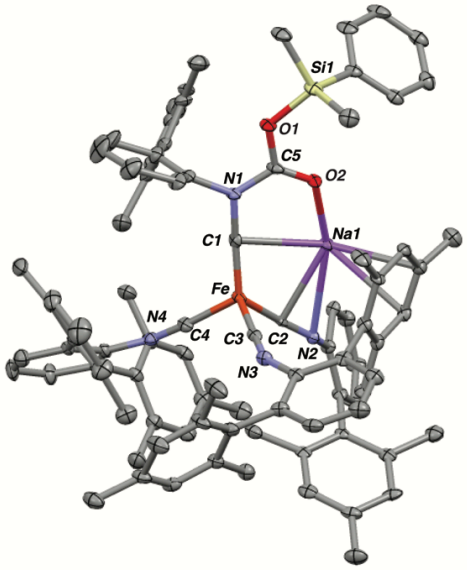


**Figure 3.6** Solid state structure of Na[Fe(CNAr$^{Mes2}$)$_3$(CN(Ar$^{Mes2}$)(C(O)OSiMe$_2$Ph)], Na[**6**]. Hydrogen atoms, and flanking mesityl rings omitted for clarity. Selected bond distances (Å): Fe-$C_1$ = 1.680(5), Fe-$C_2$ = 1.790(5), Fe-$C_3$ = 1.801(6), Fe-$C_4$ = 1.840(6), $C_1$-$N_1$ = 1.430(6), $C_2$-$N_2$ = 1.212(6), $C_3$-$N_3$ = 1.210(6), $C_4$-$N_4$ = 1.185(6), $N_1$-$C_5$ = 1.371(7), $C_5$-$O_1$ = 1.354(6), $C_5$-$O_2$ = 1.205(6), $O_1$-$Si_1$ = 1.700(4). Selected bond angles (˚): Fe-$C_1$-$N_1$ = 171.9(4), Fe-$C_2$-$N_2$ = 174.3(4), Fe-$C_3$-$N_3$ = 176.8(4), Fe-$C_4$-$N_4$ = 174.0(5), $C_1$-$N_1$-$C_{14}$ = 118.8(4), $C_2$-$N_2$-$C_{38}$ = 147.4(5), $C_3$-$N_3$-$C_{57}$ = 153.4(5), $C_4$-$N_4$-$C_{81}$ = 164.7(5).

Indeed the isolation of $\kappa^1$–*C*-metalo-carboxylates from the reduction of $CO_2$ still *remains* a challenging task. It is with this observation that complex Na[**5**] plays an important role at delineating the role of the $\kappa^1$–*C*-metalo-carboxylate upon $CO_2$ coordination to Na[**1**]. To this end it must be noted that the electrophilic functionalization of the isocyanides via activation at the CNR–*N,* although uncommon to alternative isocyanide activation routes, [47-49] has been well documented.[50] Typical activation of the isocyanide–*N* toward electrophilic functionalization is resultant of increased electron density deposited onto the isocyanide π*-manifold from an electron rich metal center.[50,51] The resulting π-back donation results in a substantial degree of

bending within the isocyanide linkage and charge localization on the N-atom rendering it nucleophilic and thus susceptible toward electrophilic attack.[51,52] However we believe the electrophilic functionalization of the $CNAr^{Mes2}$ ligand is mechanistically distinct from previous examples of isocyanide–N functionalization due to the metal-based nucleophilicity of $Na_2[Fe(CNAr^{Mes2})_4]$ $Na_2$[**1**] toward electrophiles which has previously been assessed.[25] Moreover, it is generally considered that reactivity of the dianionic carbonyl metallates of group 6 and 8 (*eg.* $[M_A(CO)_5]2^-$ ($M_A$ = Cr, Mo, W) and $[M_B(CO)_4]2^-$ ($M_B$ = Fe, Ru, Os)) proceeds via metal attack at $CO_2$.[19] It is with this precedence that we offer mechanistic insight into the formation of Na[**5**] which is atypical to traditional forms of electrophilic functionalization of isocyanides. Accordingly, nucleophilic attack at the $CO_2$–*C* by $Na_2$[**1**] to generate the short-lived $\kappa^1$–*C*-metalo-carboxylate occurs, which then undergoes rapid nucleophilic attack on $Me_3SiOTf$ to generate a fleeting $\kappa^1$–*C*-metalo-silylester. Subsequent rearrangement via a metallocyclobutene intermediate stemming from attack of the nucleophilic isocyanide–*N*, followed by collapse of the metalocycle yields the resulting aminocarbnye, Scheme 3.5.

It must be acknowledged that a more conventional activation pathway is possible, (in line with the electrophilic activation of isocyanides *vida supra*), in that the extreme bending in the isocyanide ligands bound to Fe in $Na_2[Fe(CNAr^{Mes2})_4]$, $Na_2$[**1**], (*ca.* 154.1(1)˚)[25] renders the CNR –*N* nucleophilic. Indeed, Kubiak and co–workers previously reported the isoelectronic $d^{10}$ nickel tetraisocyanide, $Ni(CNXylyl)_4$, and its reactivity toward $CO_2$ which was found to proceed via a metathesis route initiated by electrophilic attack the isocyanide–*N*.[53] In this report it was also found that

$Ni(CO)(CNXylyl)_3$ and OCNXylyl were the major constituents of the resulting reaction mixture.[53]

To address this reaction pathway it is important to note that the isocyanide linkage bound to a metal can be interrogated via the ν(CN) stretching frequency by FTIR, which in turn provides a direct measure of the electron richness of the coordinated metal.[30,54] Correspondingly, due to the increased π-bacisity of $d^{10}$ Fe centers when compared to less π-basic $d^{10}$ Ni centers it can be reasoned that the activation of the C*N*–R ligand would be greater for $Na_2$[**1**] then for $Ni(CNXylyl)_4$.[54] Indeed this is the case such that $Na_2[Fe(CNAr^{Mes2})_4]$ $Na_2$[**1**] exhibits and extremely red shifted ν(CN) stretch at 1682 $cm^{-1}$ where compared to $Ni(CNXylyl)_4$ which exhibits a ν(CN) stretching frequency 2028 and 1994 $cm^{-1}$ consistent with the diminished π-bacisty of $d^{10}$ metals.[53] As such this would potentially bias $Na_2$[**1**] toward a metathesis resulting in the formation of isocyanate (OCNR). Despite this assessment and the activation CNC linkages in $Na_2$[**1**], we observe no formation of $OCNAr^{Mes2}$ by $^1$HNMR or solution FTIR and thus favor a mechanism featuring generation of a $\kappa^1$–*C*-metalo-carboxylate followed by subsequent rearrangement depicted in scheme 3.5.

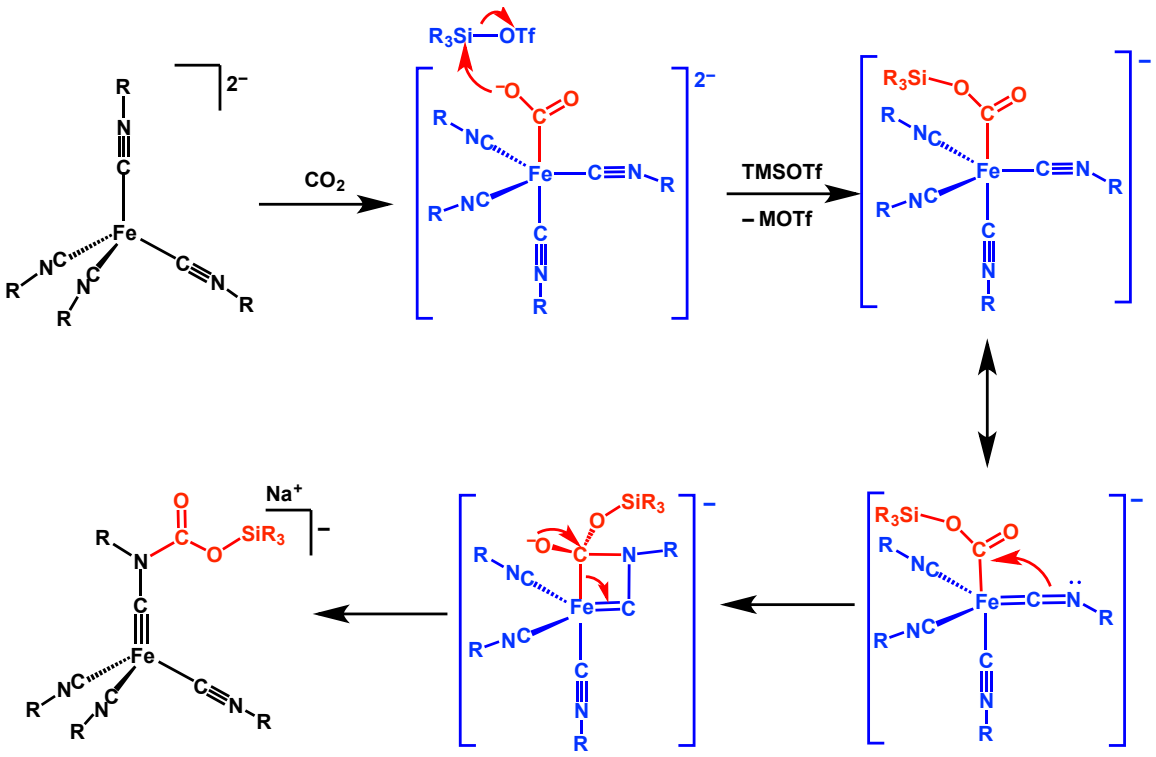

**Scheme 3.5** Proposed mechanism for the conversion of dianion Na[**1**] to to carbyne Na[**5**].

Further attempts to arrest the $\kappa^1$–*C*-metalo-carboxylate at the metal center by modulating the steric profile of the silyl–triflates in hopes to mitigate migration into the isocyanide nitrogen proved unsuccessful. Use of both $PhMe_2SiOTf$, and $Ph_2MeSiOTf$ resulted in an analogous reactivity profile affording aminocarbynes Na[**6**] and Na[**7**]. Notably use of $Ph_2MeSiOTf$ affords primarily $Fe(CO)(CNAr^{Mes2})_4$ (**2**) with Na[**7**] only as a minor product upon addition of $CO_2$ presumably due to the increased steric profile of the $^+SiR_3$ fragment. Attempts to increase yields of Na[**7**] with excess $Ph_2MeSiOTf$ and lessen the formation of $Fe(CO)(CNAr^{Mes2})_4$, (**4**) were unsuccessful. Moreover, use of $Ph_3SiOTf$ in generating the corresponding aminocarbyne species was unproductive affording exclusively $Fe(CO)(CNAr^{Mes2})_4$ (**4**) as the only Fe containing product as assayed by both $^1H$ NMR and solution FTIR spectroscopy. This is notable in the context

that the trapping of $CO_2$ requires silyl triflates that have moderate steric profiles so as to come within proximity of the fleeting $\kappa^1$–*C*-metallo-carboxylate within an encumbered ligand field in order to out compete a second equivalent of $CO_2$.

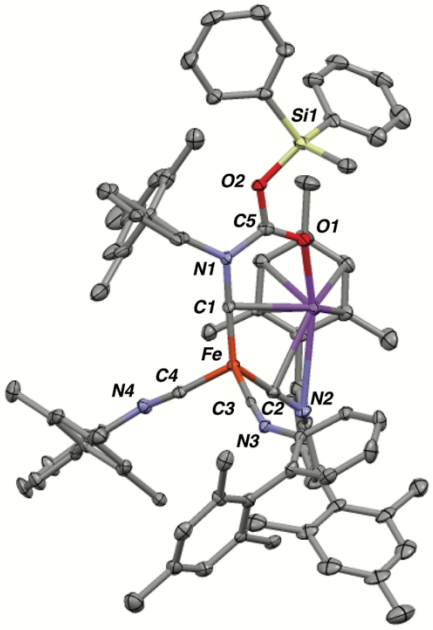


**Figure 3.7** Solid state structure of Na[Fe(CNAr$^{Mes2}$)$_3$(CN(Ar$^{Mes2}$)(C(O)OSiMePh$_2$)], Na[**7**]. Hydrogen atoms, and flanking mesityl rings omitted for clarity. Selected bond distances are an average of two independent molecules within the unit cell (Å): Fe-$C_1$ = 1.687(15), Fe-$C_2$ = 1.780(7), Fe-$C_3$ = 1.810(25), Fe-$C_4$ = 1.838(2), $C_1$-$N_1$ = 1.420(75), $C_2$-$N_2$ = 1.225(2), $C_3$-$N_3$ = 1.204(76) $C_4$-$N_4$ = 1.196(85), $N_1$-$C_5$ = 1.380(25), $C_5$-$O_2$ = 1.341(7), $C_5$-$O_1$ = 1.221(2), $O_1$-$Si_1$ = 1.694(45). Selected bond angles are an average of two independent molecules within the unit cell (˚): Fe-$C_1$-$N_1$, = 173.5(5), Fe-$C_2$-$N_2$ = 175.8(1), Fe-$C_3$-$N_3$ = 176.5(6), Fe-$C_4$-$N_4$ = 173.47(7), $C_1$-$N_1$-$C_{20}$ = 120.7(8), $C_2$-$N_2$-$C_{44}$ = 140.6(1), $C_3$-$N_3$-$C_{68}$ = 151.0(2), $C_4$-$N_4$-$C_{92}$ = 162.9(2).

### 3.5. Electronic Structure Analysis.

Due to the paucity of low-valent iron carbyne complexes, Na[**5**-**7**] provide an opportunity to explore the electronic structure of carbyne ligands bound to $ML_3$ fragments. Therfore, geometry optimized structures of the model complex Na[Fe(CNXyly)$_3$(CN(Xylyl)(C(O)OSiMe$_3$)]$^-$ (Xylyl = 2,6-$Me_2$-$C_6H_3$) reproduced experimental bond metrics consistent with experimental data, Table 3.1. The five highest

in energy molecular orbitals consisting primarily of Fe and isocyanide π* orbitals are shown in Figure 3.8. Indeed, the observation of two Fe–isocyanide π-bonds are readily apparent upon inspection of HOMO-3/4 for the isocyanide ligand featuring β-functionalization. Additionally, the remaining Fe-*d* orbitals show large amounts of Fe-CNR π* back donation to the remaining three ligands.

**Table 3.1** Experimental and computed bond distances and angles for $CO_2$–aminocarbyne complexes.

| | $Fe_1–C_1$ (Å) | $C_1–N_1$ (Å) | $C_1–N_1–C_{ipso}$ (°) | $Fe–C_2$ (Å) | $Fe–C_3$ (Å) | $Fe–C_4$ (Å) |
|---|---|---|---|---|---|---|
| Na[**5**] | 1.655(9) | 1.4369(12) | 119.7(2) | 1.790(9) | 1.836(10) | 1.843(9) |
| Na[**6**] | 1.680(5) | 1.430(6) | 118.8(4) | 1.790(5) | 1.801(6) | 1.840(6) |
| Na[**7**] | 1.687(15) | 1.420(75) | 120.7(8) | 1.780(7) | 1.810(25) | 1.838(2) |
| [**m**]$^{-1*}$ | 1.66979 | 1.37472 | 115.847 | 1.77107 | 1.78162 | 1.77008 |

* = The model comples $[Fe(CNXylyl)_3CN(ArXylyl)(C(O)OTMS)]^{-1}$; BP86 Def2-TZVP/J.

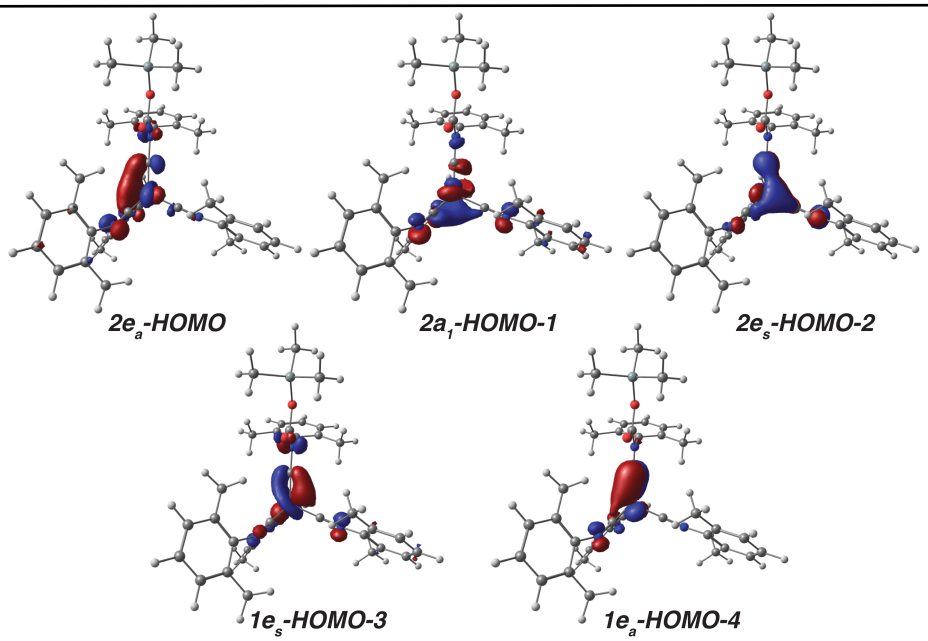


**Figure 3.8** Frontier bonding molecular orbitals for $Na[Fe(CNXyly)_3(CN(Xylyl)(C(O)OSiMe_3)]^-$. HOMO-3/-4 represents Fe–C π-bonding. BP86/def2-TZVP, iso-surface value = 0.05184.

This provides sufficient information to develop a qualitative molecular orbital picture of the bonding scheme operative in these iron carbyne species (Figure 3. 9). A molecular fragment based approach was used to develop the corresponding bonding

interaction within these carbynes,[63] such that an $FeL_3$ fragment functions as one fragment that interacts with a Fischer-type carbyne ligand. Na[**5-7**] represent examples of Fischer carbynes[45,55-57] (electron rich late transition metals that can engage in π-back donation), and it is well known that amoinocarbynes function as 3-electron LX donor ligands.[58] However, it has been shown that treatment of Fischer carbyne ligands as $[CR]^+$ in an analogues fashion to Fischer carbenes $[CR_2]$, [58,59] provides a method of deconvoluting the resultant complications as a 3-electron donor ligand. Accordingly it can be shown that the carbyne engages in sigma interaction with $1a_1$ orbital of the $FeL_3$ fragment, which drops low in energy away from the frontier orbital interactions. Further interaction between the *1e* set of the $FeL_3$ fragment with the orthogonal carbyne-*C p*-orbitals provide the additional two bonding interactions between Fe and C. Moreover, the resulting *2e* sets remain close in energy yet split with the $2a_1$ orbital dropping in energy based on favorable interactions with the isocyanide π*-manifolds. For electron counting purposes this would provide a $16e^-$ species and so addition of the remaining 2 electrons, one from the carbyne ligand and one due to the overall anionic state of the complex, yielding an electronically saturated metal-center consistent with the overall diamagnetism observed for these carbyne species.

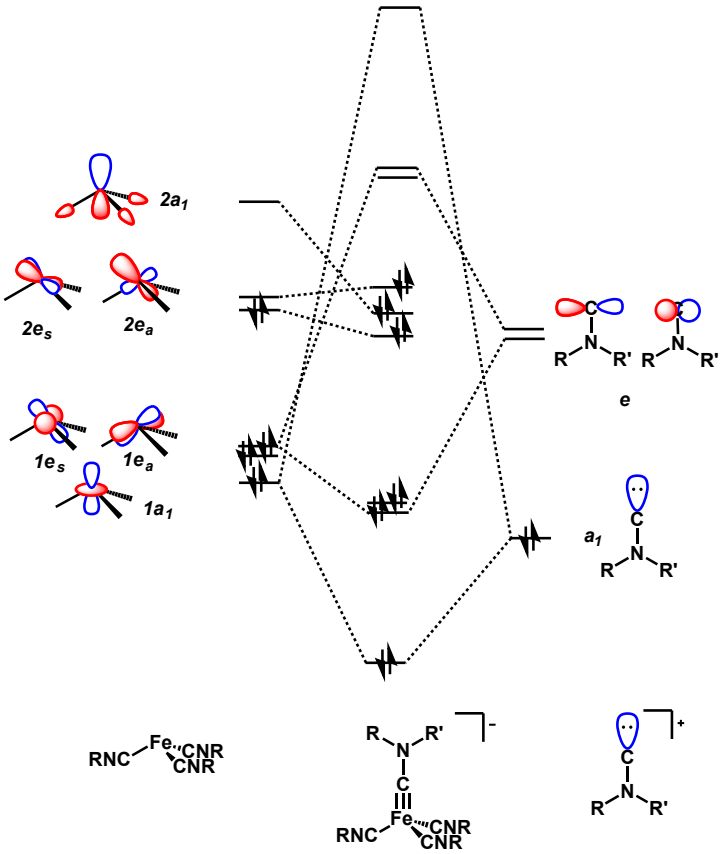


**Figure 3.9** Qualitative molecular orbital diagram depicting the frontier molecular orbital interactions of $[L_3Fe{\equiv}CR]^-$. **Note:** Treatment of the carbyne ligand as $[CR]^+$ provides a method to deconvolute electron counting. Upon construction of the final electronic structure 2 additional electrons are incorporated due to the carbyne ligand and overall anionic state of $[L_3Fe{\equiv}CR]^-$.

### 3.6. Reactivity of Iron Carbynes with Na[HBEt$_3$].

In attempts to redirect the reduction of $CO_2$ we examined the reactivity with $H^-$ sources. Accordingly treatment of Na[**5**] with 1 equivalent of Na[HBEt$_3$] at room temperature in a $C_6D_6$ solution afforded a 50:50 mixture of $Na_2$[**1**] and Na[**5**] as assayed by $^1$H NMR spectroscopy. Treatment of Na[**5**] with 2 equivalents of Na[HBEt$_3$] led to the smooth conversion of Na[**5**] to $Na_2$[**1**]. Inspection of the crude reaction mixture by $^1$H NMR ($C_6D_6$) spectroscopy indicated the formation of small amounts of $HSiMe_3$ with the appearance of a small broad peak at 4.17 ppm. Interestingly, the formation of $Na_2$[**1**]

shows that the capture of $CO_2$ with $R_3SiOTf$ reagents is reversible upon addition of H–. Additionally analysis of the reaction mixture by $^{11}B\{^1H\}$ NMR indicated the presence of $BEt_3$ with a broad peak at 85.7 ppm. Consequently a reaction mechanism involving hydride attack at the Si-O bond resulting in release of $HSiMe_3$, and $Na_2$[**1**] can be rationalized. The subsequent loss of $CO_2$ can then go on to react with the second equivalent of $Na[HBEt_3]$. Indeed the capabilities of borohydride reductants to facilitate $CO_2$ reduction have been to formate, ([HC(O)O–]), have been realized. [60-62]

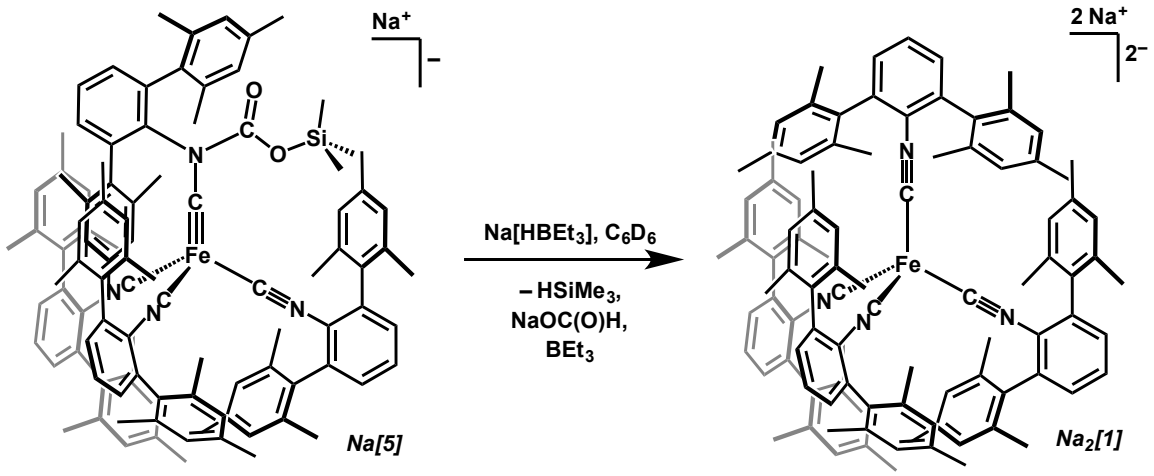


**Scheme 3.6** Reaction scheme depicting the regeneration of $Na_2$[**1**] from the treatment of Na[**5**] with $Na[HBEt_3]$.

To verify this mechanism and to track the extrusion of $CO_2$ from Na[**5**], $^{13}C$ enrichment at the $^{13}C$=O moiety was undertaken. In an analogous method for the generation of Na[**5**], addition of $^{13}CO_2$ to $Na_2$[**1**] in the presences of TMSOTf yielded Na[$^{13}$**5**]. Treatment of Na[$^{13}$**5**] with $Na[HBEt_3]$ followed by analysis via $^{13}C\{^1H\}$ NMR spectroscopy indicated no apparent peaks consistent with a $^{13}C$ enriched species. Concentration of the resulting mixture to a solid, and dissolution in $D_2O$ followed by analysis via $^{13}C\{^1H\}$ NMR spectroscopy indicated the formation of Na[HC(O)O].

Additionally analysis of this mixture by $^{11}B$ NMR indicate the presence of $B(OH)_3$. This suggests the proposed follow up reactivity with boro-hydride upon release of $CO_2$ as the exclusive generation of $BEt_3$ would indicate no boron containing species post work-up. This observation also explains the need for two equivalents of $Na[HBEt_3]$ to reconvert Na[**5**] back to $Na_2$[**1**] with no subsequent observation of follow up reactivity between $Na_2$[**1**] and $CO_2$ to yield $Fe(CO)(CNAr^{Mes2})_4$ (**2**).

### 3.7. Concluding Remarks.

Herein we present the reactivity of $Na_2[Fe(CNAr^{Mes2})]$ $Na_2$[**1**] with $CO_2$ and the subsequent reduction via reductive disproportionation to yield an equivalent of CO which is intercepted by the incipient $[Fe(CNAr^{Mes2})_4]$ fragment to yield $Fe(CO)(CNAr^{Mes2})_4$ (**2**) and $CO_3^{2-}$. Complex (**2**) is shown to display instability in aromatic solvents due to the steric pressure engendered from the tetra-isocyanide ligand field. Due to the steric pressure resultant of tetra-isocyanide coordination to Fe, decomposition of the $CO_2$ reduction product (**2**) is shown via scavenging of liberated isocyanide with $BPh_3$ upon photolysis to mediate the C–H activation and subsequent isocyanide insertion into the $sp^2$ C–H bonds of benzene ($C_6H_6$). Furthermore, attempts towards implication $\kappa^1$-*C*-metalocarboxylate intermediates results in the formation of the aminocarbyne products Na[**5-7**]. Formation of these novel carbynes exhibits formal electrophilic functionalization of the isocyanide –*N*. However, due to the reactivity profile of $Na_2$[**2**] it is proposed that generation of these unique late transition metal aminocarbynes is mechanistically distinct and results in reorganization from a $\kappa^1$-*C*-metalocarboxylate and subsequent migration into the isocyanide ligand versus direct electrophilic

functionalization. Finally it is reported that $CO_2$ capture at a $d^{10}$-Fe center with silyl triflates is reversible upon treatment of $Na[HBEt_3]$ and results in the reconversion to $Na_2$[**1**], and subsequent loss of $CO_2$ that is intercepted by a second equivalent of $Na[HBEt_3]$ to subsequently afford conversion to formate.

### 3.8. Synthetic Procedures and Characterization Data.

**General Considerations:** All manipulations were carried out under an atmosphere of dry dinitrogen or Argon using standard schlenk, and glove box techniques. Solvents were dried and degassed according to standard procedures.[65] Unless otherwise stated all materials were obtained from commercial vendors and used as received.[66] Benzene-$d_6$ was dried with Na/K and Benzophenone followed by distillation and stored on 4 A molecular sieves for 3 days prior to use. Celite 405 (Fischer Scientific) was dried under vacuum for 24 hours at a temperature greater then 250$^o$C and stored inside the glove box prior to use. $Na_2[Fe(CNAr^{Mes2})_4]$,[25] $Me_2PhSiOTf$, $MePh_2SiOTf$, and $Ph_3SiOTf$ was prepared via reported methods.[67] $^{13}CO_2$ was obtained from Sigma Aldrich 99.9% isotopic enrichment.

Solution $^1H$, $^{13}C\{^1H\}$ NMR spectra were recorded on a Varian Mercury 400 spectrometer, and a Varian XSENS-500 spectrometer. $^1H$, and $^{13}C$ chemical shifts are reported in ppm relative to $SiMe_4$ ($^1H$ and $^{13}C$ $\delta$ = 0.0 ppm) with reference to residual solvent references of 7.16 ppm ($^1H$) and 128.06 ppm ($^{13}C$) for benzene–$d_6$;[68] $B^{11}$ chemical shifts were referenced externally to a solution of phenylboronic acid in acetone-$d_6$ ($\delta$ = 29 ppm vs. $BF_3$•$Et_2O$ ($\delta$ = 0.0 ppm)). FTIR spectra were recorded on a Thermo-Nicolet iS10 FTIR spectrometer. Samples were prepared either as KBr pellets or as $C_6D_6$ solutions

injected into a Thermo-Fischer solution cell equipped with KBr windows. For solution FTIR spectra, solvent peaks were digitally subtracted from all spectra by comparisons with an authentic spectrum obtained immediately prior to that of the sample. The following abbreviations were used for the intensities and characteristic of important IR absorption bands: vs = very strong, s = strong, m = medium, w = weak, vw = very weak, b = broad, vb = very broad, sh = shoulder. High-resolution mass spectrometry (HRMS) was performed using an Agilent 6230 ESI-TOFMS running in positive or negative ion mode as necessary. Combustion analyses were preformed by and Midwest Microlab of Indianapolis, IN (USA).

**Synthesis of Fe(CO)(CNAr$^{Mes2}$)$_4$ (2):** $Na_2[Fe(CNAr^{Mes2})_4]$, $Na_2$[**1**] (0.173 g, 0.119 mmol, 1 equiv) was dissolved in THF (6 mL) and transferred to a 50 mL resalable ampule equipped with 14/20 side-arm adapter. The reaction mixture was subjected to 3 freeze pump thaw cycles (40 mtorr). After warming to room temperature the reaction mixture was placed under an atmosphere of $CO_2$ where a color change was immediately observed from deep red to deep red-orange. The resulting solution was transferred to the glove box where it was the evaporated to dryness and subjected to 3 X 5 mL washes of *n*-pentane to de-solvate $NaCO_3$. The bright red-orange solid was then extracted with $C_6H_6$ and filtered over 4 cm of Celite packed on fiberglass followed by lyophilization to yield a solid. The resultant solid was then slurried in *n*-pentane (5 mL) and filtered to yield a red-orange solid 0.163 g, 95%. Crystals of Fe(CO)(CNAr$^{Mes2}$)$_4$ were obtained from a saturated $Et_2O$ solution over 1 day at -40$^o$C. **Note: Fe(CO)(CNAr$^{Mes2}$)$_4$ is light sensitive in aromatic solvents, as a precaution work up should be conducted in the dark to**

**avoid appreciable decomposition**. $^{1}$HNMR (399.9 MHz, $C_6D_6$, 20$^{o}$C) δ = 6.88 (s, 16H, *m*-Mes), 6.85-6.78 (m, 12H, *m/o*-Ph), 2.46 (s, 24H, *p*-CH3 Mes), 1.97 (s, 48H, *o*-CH3 Mes) ppm. $^{13}$C{$^{1}$H} NMR (125.7 MHz, C6D6, 20$^{o}$C) δ = 212.1 (*C*O), 194.1 (*C*N), 138.2, 136.4, 136.3, 136.0, 130.9, 130.7, 129.0, 125.8, 21.8(*p*-CH3 Mes), 21.1(*o*-CH3 Mes) ppm. FTIR (solution ($C_6D_6$), KBr windows, 25˚C): ($\nu_{CN}$) 2024 (s), 1996 (s), ($\nu_{CO}$) 1931 (s) cm$^{-1}$ also 2957, 2921, 2871, 2848, 1729, 1412, 1376, 1273, 1252, 850, 756, 628, 584 cm-1. Anal. Calc.: C, 84.14; H, 6.99; N, 3.89. Found C, 81.77; H, 6.56; N, 3.63.

**Isolation of $(C_6H_5)C(H)NAr^{Mes2}$, (3), from the decomposition of $Fe(CO)(CNAr^{Mes2})_4$:** In the dark $Fe(CO)(CNAr^{Mes2})_4$ (0.009 g, 0.00603 mmol, 1 equiv), was dissolved in $C_6H_6$ (2 mL) and transferred to a 25 mL resealable glass ampule. To the ampule $CNAr^{Mes2}$ ( 0.046 g, 12.07 mmol, 20 equiv) was added in a $C_6H_6$ solution. The ampule was sealed and brought out of the glove box and was irradiated for 2 hours at room temperature using a mercury arc lamp (Oriel Corporation, model 66023, 1000W). Following the reaction mixture was brought back into the glove box and filtered over neutral alumina packed on fiberglass (2 cm) and concentrated to a solid. The resulting solid was then taken up in *n*-pentane (4 mL) and filtered alumina packed on fiberglass (2 cm) to remove remaining metal species (this process was repeated one additional time). The resulting solution was then concentrated to a colorless/off-white solid to yield $C_6H_5C(H)NAr^{Mes2}$ 0.021 g, 0.053 mole, 32% yield. Analytically pure X-ray diffraction quality crystals can be grown from a saturated $Et_2O$ solution at –40 ˚C over 1 week. $^{1}$HNMR (499.9 MHz, $C_6D_6$, 20$^{o}$C) δ = 7.09 (s, 1H, C(H)), 7.29 (dd, 2H, 6Hz, *m*-$C_6H_5$), 7.09 (s, 3H, *o/p*- $C_6H_5$), 6.82-6.72 (mult., 7H, *o/p*-Ph/*m*-Mes), 2.25 (s, 6H *o*-C$H_3$), 2.08 (s. 3H, *p*-C$H_3$) ppm.

$^{13}C\{^{1}H\}$ NMR (125.7 MHz, C6D6, 20°C) δ = (C=N) 149.0, 160.4, 137.2, 136.6, 136.4, 136.0, 133.0, 130.9, 129.8, 128.5, 127.7, 125.0, 21.1, 21.08. FTIR (solution ($C_6D_6$), KBr windows, 25˚C): ($\nu_{CN}$) 1638 (m), 3029 (w), 2998 (w), 2979 (m), 2956 (m), 2914 (s), 2848 (m), 1740 (w), 1716 (w), 1581 (w), 1559 (w), 1489 )w), 1454 (w), 1436 (w), 1420 (w), 1376 (w), 1190 (w), 1172 (w), 1076 ( m), 1025 (w), 970 (w), 914 (w), 880 (w), 850 (m), 759 (m), 747 (w), 739 9w), 722 (w), 649 (w), 672 (w) $cm^{-1}$. HRMS (ESI-APCI-TOF, pos. ion; MeCN) *m/z* calcd for $[C_{37}H_{50}NOH]^{+}$: 418.2529. Found for $[C_{37}H_{50}NOH]^{+}$: 418.2530, δ = 0.2.

**Synthesis $Ph_3B–CNAr^{Mes2}$, (4):** To a $C_6H_6$ solution of $CNAr^{Mes2}$ (0.032 g, 0.095 moles, 1 equiv., 1 mL) a benzene solution of $BPh_3$ (0.023 g, 0.095 moles, 1 equiv., 1 mL) was added drop wise over the course of 2 minutes. The reaction mixture was allowed to react for 1hour. There after the reaction mixture was concentrated to a white solid. Recrystallization from $Et_2O$ (1 mL) at –40 ˚C yielded $Ph_3B–CNAr^{Mes2}$ as colorless blocks after 1 day suitable for X-ray diffraction, 0.044 g, 0.075 mmole, 80%. $^{1}$HNMR (499.8 MHz, $C_6D_6$, 20°C) δ = 7.16 (mult., 9H, B*Ph*), 7.03 (mult., 6H, B*Ph*), 6.87 (t, 1H, 7Hz, *p*-PH), 6.75 (s, 4H, *m*-mes), 6.68 (d, 2H, 7Hz, *m*-Ph), 2.19 (s, 6H, *p*-C$H_3$ Mes), 1.81 (s, 12H, *o*-C$H_3$ Mes) ppm. $^{13}C\{^{1}H\}$ NMR (125.7 MHz, C6D6, 20°C) δ = 143.7(*C*N), 149.4, 140.6, 138.9, 135.4, 134.9, 132.7, 131.6, 129.8, 129.3, 129.1, 128.9 125.5, 21.3, 20.1 ppm. $^{11}B\{^{1}H\}$ NMR (160.5 MHz, $C_6D_6$, 20°C) δ = 43.2 ppm. FTIR (solution ($C_6D_6$), KBr windows, 25oC): ($\nu_{CN}$) = 2236 (s), also 3087 (w), 3066 (w), 3045 (w), 2999 (w), 2977 (w), 2947 (w), 29 18 (w), 1487 (w), 1468 (w), 1431 (m), 1378 (w), 1274 (w), 1248

(s), 1186 (m), 1150 (w), 1032 (m), 851 (m), 756 (w), 743 (m), 728 (w), 703 (s), 680 (w) $cm^{-1}$. Anal. Calc.: C, 88.80; H, 6.93; N, 2.41. Found 88.57; H, 6.84; N, 2.32.

**Synthesis of Na[Fe(CNAr$^{Mes2}$)$_3$(CN(Ar$^{Mes2}$)(COOTMS))]; Na[5]:** In the glove box $Na_2[Fe(CNAr^{Mes2})_4]$ (0.183 g, 0.152 mmole, 1 equivs) was dissolved in 5 mL of Toluene and transferred to a 25 mL resealable glass ampule. TMSOTf (23.8 μL, 0.131 mmole, 1.05 equivs) was added to the $Na_2[Fe(CNAr^{Mes2})_4]$ mixture and sealed. The reaction mixture was connected to the schlenk line and subject to 3 freeze pump thaw cycles (40 mtorr). There after the thawing reaction mixture was exposed to an atmosphere of $CO_2$ (g) where upon an immediate color change from deep red to red/orange was observed. The reaction mixture was allowed to react for a *ca.* 10 minuets where upon all volatiles were removed under vacuum to yield a red orange film. The reaction mixture was transferred back into the glove box where the red solid was slurried in *n*–pentane (5 mL) and evaporated to a solid to desolvate NaOTf. The resulting solid was extracted into benzene (4 mL) and filtered over Celite packed on fiberglass to remove NaOTf, followed by removal of all volatiles under reduced pressure. Analytically pure crystals suitable for X-ray diffraction were grown from a saturated solution of *n*–hexane (2 mL) spiked with a *ca.* 5 drops of $C_6H_6$ at –40º C over 3 weeks to yield large red blocks of Na[Fe(CNAr$^{Mes2}$)$_3$(CN(Ar$^{Mes2}$)(COOTMS))], 0.096 g, 39 %. $^1$HNMR (399.9 MHz, $C_6D_6$, 20$^o$C) δ = 7.14 (s, 2H, *m*-Mes), 7.04–6.96 (m, 8H,), 6.89 (t, 3H, 8 Hz, *p*–Ph), 6.83–6.80 (m, 4H, Ph), 6.70 (s, 3H, *m*–Mes), 6.74 (s, 1H, *m*–Mes), 6.70 (d, 2H, 7Hz, *m*–Ph), 6.59 (s, 3H, *m*–Mes), 6.40 (s, 2H, *m*–Mes), 2.59 (s, 6H, $CH_3$–Mes), 2.30 (s, 6H, $CH_3$–Mes), 2.28 (s, 6H, $CH_3$–Mes), 2.23 (s, 12H, $CH_3$–Mes), 2.22 (s, 18H, CH3–Mes), 2.05 (s, 6H, $CH_3$–

Mes), 1.98 (s, 6H, $CH_3$–Mes), 1.86 (s, 6H, $CH_3$–Mes), 1.74 (s, 6H, $CH_3$–Mes), 0.210 (s, 9H, $CH_3$–TMS) ppm. $^{13}C\{^1H\}$ NMR (125.7 MHz, C6D6, 20°C) δ = 225.9 (Fe≡*C*), 214.9 (*C*N), 214.8 (*C*N), 200.9 (*C*N), 153.3 (*C*O), 140.7, 140.6, 140.3, 139.2, 138.3, 137.8, 137.6, 137.4, 137.3, 137.2, 137.1, 137.0, 136.2, 136.1, 135.8, 135.6, 135.4, 134.7, 133.5, 131.4, 131.3, 131.2, 129.4, 127.3, 126.3, 124.1, 123.1, 30.2, 22.7, 22.5, 22.1, 22.0, 21.6, 21.4, 21.3, 21.2, 20.9, 1.48 (*C*$H_3$–TMS) ppm. FTIR (solution (*$C_6D_6$*), KBr windows, 25˚C): ($\nu_{CN}$) 2019 (m), ($\nu_{CN}$) 1988 (m), ($\nu_{CN}$) 1883 (s), ($\nu_{CO}$) 1769 (s), $cm^{-1}$ also 2956 (w), 2920 (w), 2871 (w), 2852 (w), 1640 (m), 1593 (sh), 1574 (m), 1408 (m), 1378 (w), 1300 (m), 1033 (w), 1019 (w), 900 (w), 851 (m), 754 (w) $cm^{-1}$. Anal. Calc. $FeC_{104}H_{109}N_4SiO_2Na$: C, 80.19; H, 6.93; N, 3.70. Found C, 81.04; H, 7.40; N, 3.77.

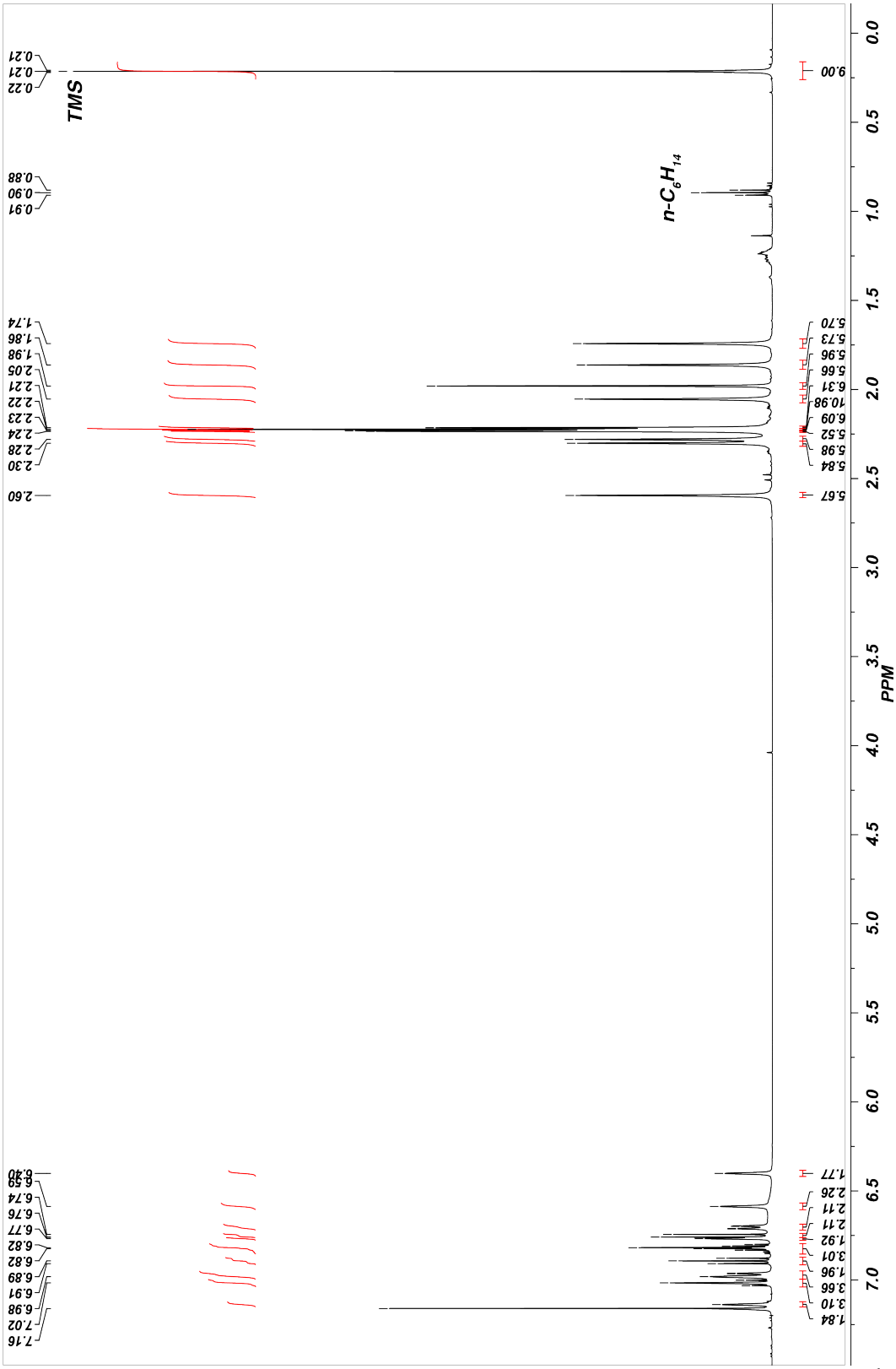


**Figure 3.10** Room temperature $^{1}$H NMR spectrum (499.9 MHz, $C_6D_6$) of Na[Fe(CNAr$^{Mes2}$)$_3$(CN(Ar$^{Mes2}$)(COOTMS))], Na[**4**] .

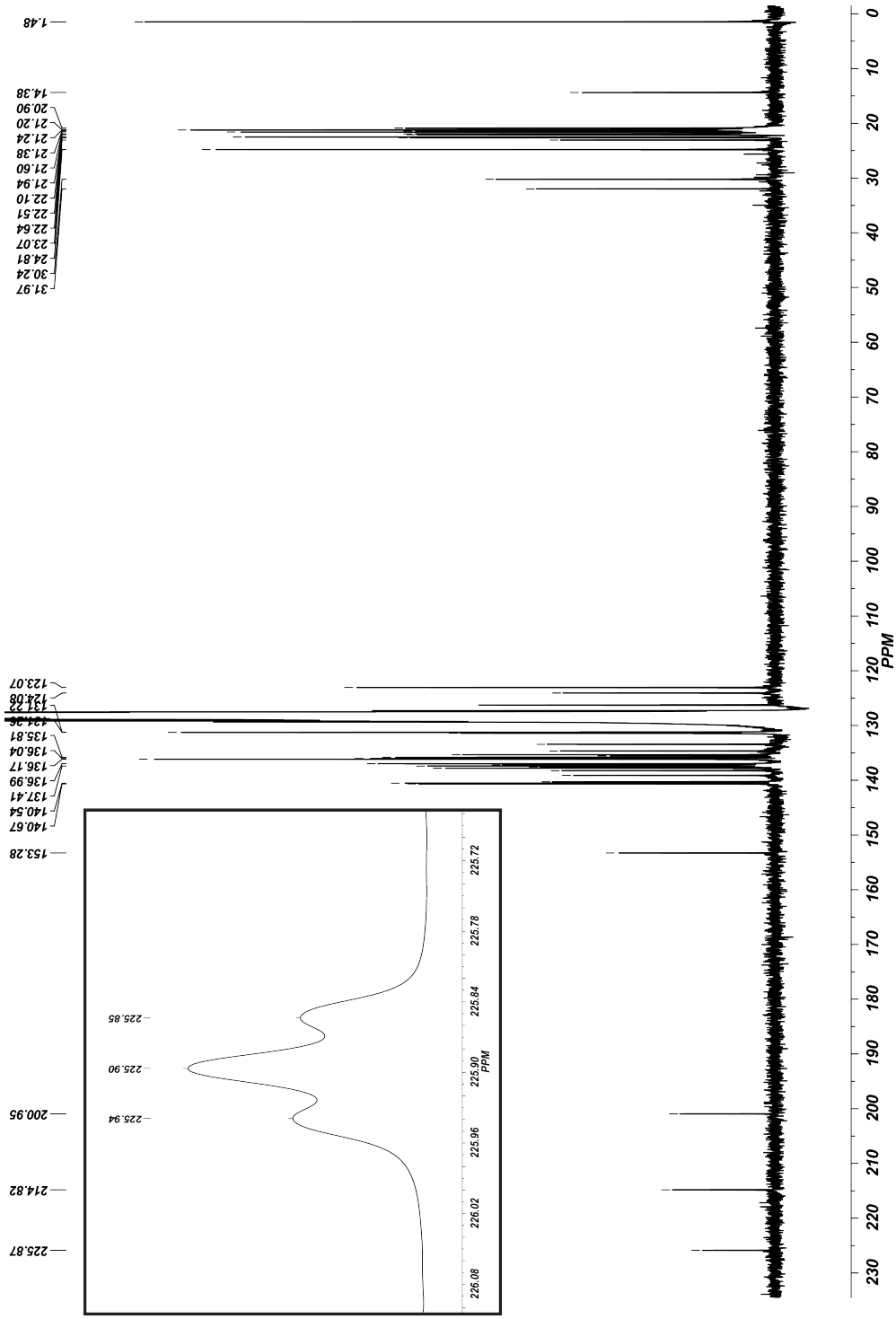


**Figure 3.11** Room temperature $^{13}C\{^{1}H\}$ NMR spectrum (125.7 MHz, $C_6D_6$) of $Na[Fe(CNAr^{Mes2})_3(CN(Ar^{Mes2})(COOTMS))]$, Na[**4**]. Inset depicts the $^{13}C$ resonance for the Fe≡*C* resonance utilizing isotopic ally enriched $Na[Fe(^{13}CNAr^{Mes2})_3(^{13}CN(Ar^{Mes2})(COOTMS))]$. Note that coupling to all three $^{13}CNAr^{Mes2}$ units are detected indicating two different isocyanide ligand environments; coupling = 5 Hz.

**Synthesis of Na[Fe(CNAr$^{Mes2}$)$_3$(CN(Ar$^{Mes2}$)(COOSiMe$_2$Ph)], Na[6]:** An analogous procedure to **Na[6]** was utilized for the generation of Na[Fe(CNAr$^{Mes2}$)$_3$(CN(Ar$^{Mes2}$)(COOSiMe$_2$Ph)]. PhMe$_2$SiOTf (0.027 g, 0.0621 mmol, 1 equivs) was added to a solution of Na$_2$[Fe(CNAr$^{Mes2}$)$_4$] (0.0906 mg, 0.0621 mmol, 1 equivs) in toluene (3 mL) in a resalable ampule. The reaction mixture was connected to a schlenk line and subject to 3 freeze pump thaw cycles (40 mtorr) where upon thawing the reaction mixture was exposed to an atmosphere of $CO_2$ (g) where upon an immediate color change from deep red to red/orange was observed. The reaction mixture was allowed to react for a *ca.* 10 minuets where upon all volatiles were removed under vacuum to yield a red orange film. The reaction mixture was transferred back into the glove box where the red solid was slurried in *n*–pentane (5 mL) and evaporated to a solid. Following the solid was extracted into benzene (4 mL) and filtered over Celite packed on fiberglass to remove NaOTf, followed by removal of all volatiles under reduced pressure. Analytically pure crystals suitable for X-ray diffraction were grown from a saturated solution of *n*–hexane (2 mL) spiked with a *ca.* 5 drops of $C_6H_6$ at –40º C over 5 days to yield large red blocks of **Na[7],** 0.042 g, 41 %. $^1$HNMR (499.8 MHz, $C_6D_6$, 20$^o$C) δ = 7.86 (2, 2H*,* 8Hz, Ph–TMS), 7.26 (t, 2H, 7Hz, Ph–TMS), 7.20 (t, 1H, 7 Hz, *Ph*–TMS), 7.12 (s, 2H, *m*–Mes), 7.02 (m, 3H, *m*–Mes/*p*–Ph), 6.97–6.94 (broad multiplet, 4H), 6.88 (t, 3H, 7Hz, *p*–Ph), 6.82–6.76 (m, 8H), 6.67–6.66 (broad multiplet, 4H), 6.55 (s, 2 H, *m*–Mes), 6.03 (s, 2H, *m*–Mes), 3.32 (s, 6H, *CH$_3$*–Mes), 2.57 (s, 6H, *CH$_3$*–Mes), 2.28 (broad singlet, 12H, *CH$_3$*–Mes), 2.26 (s, 6H, *CH$_3$*–Mes), 2.24 (s, 6H, *CH$_3$*–Mes), 2.23 (s, 6H, *CH$_3$*–Mes), 2.20 (s, 12H, *CH$_3$*–Mes), 2.03 (s, 6H, *CH$_3$*–Mes), 1.86 (s, 6H, *CH$_3$*–Mes), 1.78 (s, 6H, *CH$_3$*–Mes), 1.73 (s, 6H, *CH$_3$*–Mes) ppm. $^{13}$C{$^1$H} NMR (125.7 MHz, C6D6,

20°C) δ = 225.5 (Fe≡*C*), 214.7 (*C*N, 2 overlapped peaks), 201.4 (*C*N), 153.3 (*C*O), 140.7, 140.5, 140.3, 139.0, 138.4, 137.9, 137.6, 137.2, 137.0, 136.9, 136.2, 136.1, 136.0, 135.6, 135.2, 134.8, 134.7, 133.4, 131.5, 131.4, 131.2, 131.2, 130.4, 126.3, 124.1, 123.1, 27.2, 24.9, 23.0, 22.8, 22.6, 22.1, 21.8, 21.6, 21.3, 21.2, 20.9, –0.272 (*C*$H_3$–TMS) ppm FTIR (solution ($C_6D_6$), KBr windows, 25°C): ($\nu_{CN}$) 2017 (m), ($\nu_{CN}$) 1985 (m), ($\nu_{CN}$) 1881 (s), ($\nu_{CO}$) 1770 (s), $cm^{-1}$ also 3090 (w), 3071 (w), 3036 (w), 2956 (w), 2920 (w), 2860 (w), 2852 (w), 1640 (m), 1612 (w), 1574 (m), 1480 (w), 1445 (w), 1409 (m), 1377 (w), 1298 (m), 1210 (m), 1119 (w), 1097 (w), 1034 (w), 1016 (w), 897 (w), 851 (m), 754 (w), 739 (w), 705 (w), 680 (w), 609 (w) $cm^{-1}$. Anal. Calc. $FeC_{109}H_{111}N_4SiO_2Na$: C, 81.29; H, 6.82; N, 3.42. Found C, 82.24; H, 7.08; N, 3.42.

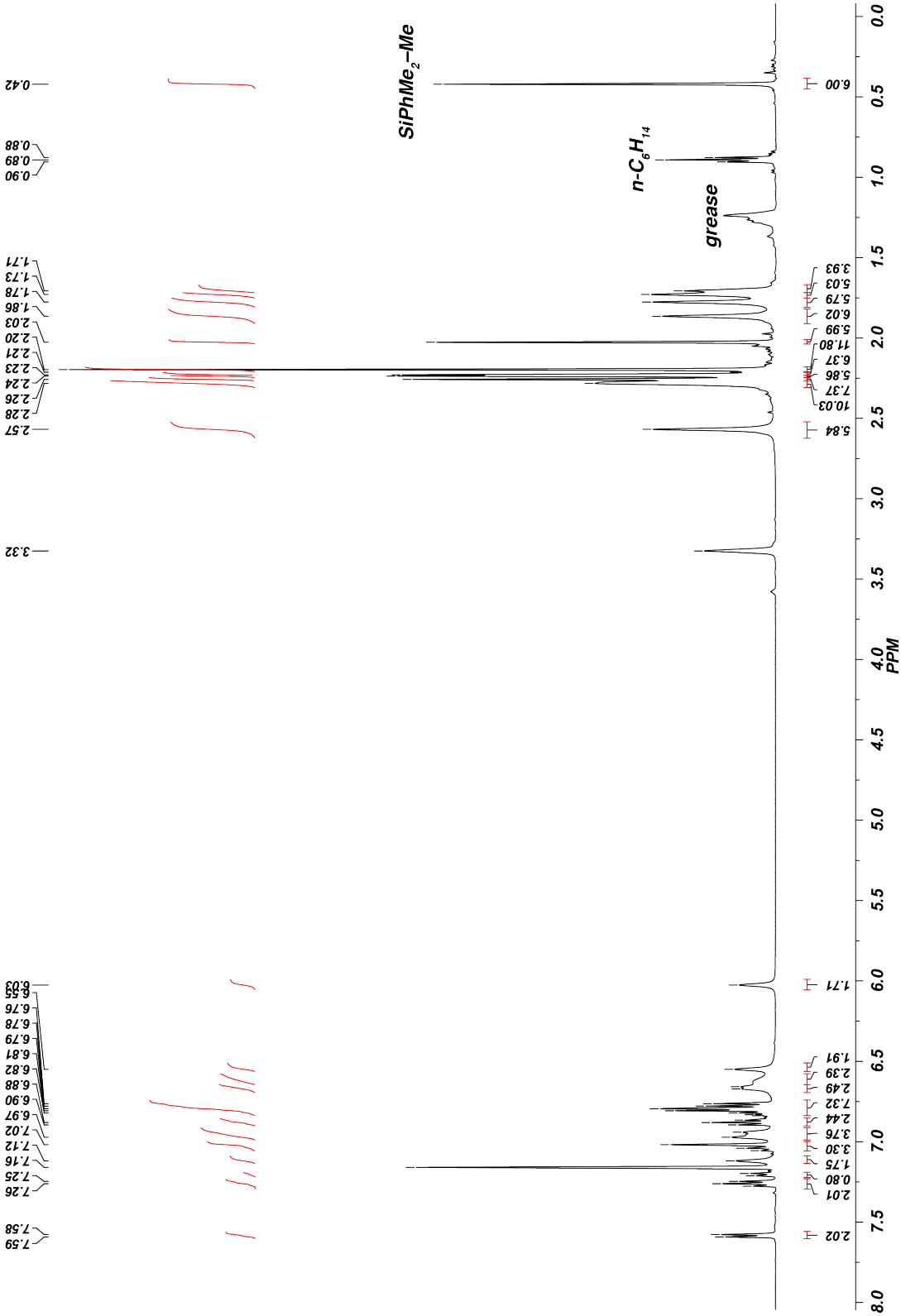


**Figure 3.12**. Room temperature $^{1}$H NMR spectrum (499.9 MHz, $C_6D_6$) of Na[Fe(CNAr$^{Mes2}$)$_3$(CN(Ar$^{Mes2}$)(COOSiMe$_2$Ph))], Na[**5**].

**Synthesis of Na[Fe(CNAr$^{Mes2}$)$_3$(CN(Ar$^{Mes2}$)(COOSiMePh$_2$)], Na[7]:** In the glove box $Na_2[Fe(CNAr^{Mes2})_4]$ (0.044 g, 0.0299 mmol, 1 equivs) was dissolved in 2 mL of $C_7H_8$ and transferred to a 25 mL resealable glass ampule. $Ph_2MeSiOTf$ (0.010 g, 0.0299 mmol, 1 equivs) was added to the $Na_2[Fe(CNAr^{Mes2})_4]$ mixture and sealed. The reaction mixture was connected to a schlenk line and subject to 3 freeze pump thaw cycles (40 mtorr) where upon thawing the reaction mixture was exposed to an atmosphere of $CO_2$ (g) where upon an immediate color change from deep red/black to red/orange was observed. The reaction mixture was allowed to react for a *ca.* 10 minuets where upon all volatiles were removed under vacuum to yield a red orange film. The reaction mixture was transferred back into the glove box where the red solid was extracted into benzene (4 mL) and filtered over Celite packed on fiberglass to remove NaOTf, followed by removal of all volatiles under reduced pressure. Analysis of the crude $^1$H NMR spectrum indicated the formation of Fe(CO)(CNAr$^{Mes2}$)$_4$ (*ca.* 75%) as the primary component of the reaction mixture in addition to [Fe($\eta^6$-(Mes)-$\mu^2$-C-CNAr$^{Mes}$)]$_2$. Crystallization of the resulting reaction mixture from a saturated solution of *n*–hexane (2 mL) spiked with a *ca.* 5 drops of $C_6H_6$ at –40º C over 3 weeks afforded a small amount of deep red-orange crystals (*ca.* < 5 mg, < 10%) of Na[Fe(CNAr$^{Mes2}$)$_3$(CN(Ar$^{Mes2}$)(COOSiMePh$_2$)], Na[**7**] suitable for X-ray diffraction. Due to the extremely low conversion to Na[Fe(CNAr$^{Mes2}$)$_3$(CN(Ar$^{Mes2}$)(COOSiMePh$_2$)], Na[**7**], its isolation has been limited to mixtures of products, however its $^1$H NMR spectrum and solution FTIR can be assigned. $^1$HNMR (499.8 MHz, $C_6D_6$, 20$^o$C) δ = 7.47 (t, 4H, 8Hz), 7.05-6.85 (broad overlapping multiplets, 20H), 6.77 (t, 4 H, 7 Hz), 6.70-6.50 (broad overlapping multiplets, 9H), 5.91

(broad singlet, 2H), 2.54 (s, 6H, C$H_3$), 2.27 (s, 18H, C$H_3$) 2.23 (s, 18H, C$H_3$), 2.18 (s, 12H, C$H_3$), 1.93 (s, 6H, C$H_3$) 1.86 (broad singlet, 6H, C$H_3$), 1.75 (broad singlet, 6H, C$H_3$), *0.*77 (s, 3H, TMS-*H)* ppm. FTIR (solution ($C_6D_6$), KBr windows, 25oC): ($\nu_{CN}$) 1875 (s, br), 1984 (m, br), 2017 (w, sh), ($\nu_{C0}$) 1776 (br., s), also 3071 (w), 3047 (w), 2999( w), 2957 (w), 2918 (w), 2852 (w), 1634 (m), 1611 (w), 1574 (m), 14440 (w), 1408 (m), 1378 (w), 1297 (m), 1264 (m, sh), 1208 (m), 1110 (w), 1037 (w), 1012 (w), 891 (w), 852 (w), 800 (w), 775 (m), 755 (w), 741 (w), 633 (w), 851 (w), 657 (w) $cm^{-1}$. Suitable combustion analysis was not obtained due to the inability to sufficiently remove Fe(CO)($CNAr^{Mes2}$) from the reaction mixture.

**S1-9: Treatment of Na[Fe($CNAr^{Mes2}$)$_3$($CN(Ar^{Mes2})$(C(O)OTMS))] with Na[$HBEt_3$]:** A 20 mL sintilation vial was charged with with Na[**5**] (0.076 g, 0.00489 mmol, 1 equiv) and dissolved in $C_6D_6$ (0.75 mL). To this mixture 2,4,6-*t*-$Bu_3$-$C_6H_2$ (0.001 g, 0.00489 mmol, 1 equiv) was added and transferred to a resealable J-Young's NMR tube. Then an initial $^1$H NMR was acquired on a Varian 400 Spectrometer so as to ascertain the concentration of Na[**5**] in solution. Following Na[$HBEt_3$] as a toluene solution that was titrated immediately prior to addition was added, (1.89 µL, 2.65M, 1 equiv) was added via micro-syringe and immediately sealed. Analysis of the reaction mixture via $^1$H NMR spectroscopy indicated *ca.* 50 % conversion to $Na_2$[**1**]. An addition 1.89 µL of Na[$HBEt_3$] was added and analysis via $^1$H NMR spectroscopy indicated complete consumption of Na[**5**] and $Na_2$[**1**] as the singular *m*-terphenyl containing product.

### 3.8 Results of Computational Studies.

**Computational Details:** Density Functional Theory (DFT) calculations were carried out on $[Fe(CNXylyl)_3(CN(Xylyl)(C(O)OTMS))]^{-1}$, which is a truncated model of the structurally characterized complex $Na[Fe(CNAr^{Mes2})_3(CN(Ar^{Mes2})(C(O)OTMS))]$, Na[**2**]. Calculations were carried out using the ORCA program package.[69] Geometry optimizations and single-point calculations were performed using the pure functional BP86.[70-72] The all-electron Ahlrichs triple-zeta basis sets def2-TZVP (standard)[73] and def2-TZVP/J (auxiliary)[74] were used in all calculations. The resolution of identity (RI) approximation was employed.[75] Relativistic effects were included by use of the zerothorder regular approximation (ZORA).[76-78] Crystallographic atomic coordinates were used as input for geometry optimizations where appropriate. Viewing of optimized structures and rendering of molecular orbitals was performed using the program Chemcraft.[79] After each geometry optimization, the optimized coordinates were reorientated so as to make the Fe-C bond along the z axis. These coordinates were then used to run a single point calculation to deconvolute orbital contributions. This research was supported in part by the W. M. Keck Foundation through computing resources at the W. M. Keck Laboratory for Intergrated Biology II.

**Input for the geometry optimization of $[Fe(CNXylyl)_3(CN(Xylyl)(C(O)OTMS))]^{-1}$ Utilizing BP86.**

```
#RKS OPT of  ironcarbyne BP86
#
%pal nprocs 8 end
! RKS BP86 ZORA def2-TZVP def2-TZVP/J RIJCOSX OPT NormalPrint NumFreq VerySlowConv
KDIIS XYZFile
%SCF
```

```
 MaxIter 1000
end

%output
Print[ P_Basis ] 2
Print[ P_MOs ] 1
end

* xyz -1 1
Fe     -11.210040000    -11.767018000     -6.099663000
Si     -16.547644000     -8.065848000     -7.350965000
O      -14.947330000    -10.426435000     -6.737407000
N       -8.707213000    -12.182241000     -7.745622000
N      -12.921422000     -9.443805000     -7.180254000
O      -14.867506000     -8.322046000     -7.510128000
C       -7.766406000    -12.186438000     -8.733380000
C      -12.180331000    -10.600101000     -6.760184000
N      -10.628668000    -11.034067000     -3.234636000
C      -12.041905000    -15.929339000     -5.633358000
C      -12.907982000    -16.298234000     -6.687217000
C       -6.582636000    -13.350280000    -10.499131000
H       -6.424268000    -14.144874000    -10.995124000
C       -9.839122000    -11.669108000      0.253315000
H       -9.108248000    -11.576788000      0.853144000
C      -14.296351000     -9.494506000     -7.120472000
N      -11.944081000    -14.568171000     -5.300483000
C      -11.618281000    -13.465715000     -5.710552000
C      -12.891994000    -17.637520000     -7.092694000
H      -13.444530000    -17.898716000     -7.820044000
C       -9.656027000    -12.043898000     -7.038276000
C      -11.335575000    -16.912866000     -4.882777000
C      -10.766545000     -6.322921000     -9.048796000
H      -10.240552000     -5.654480000     -9.471913000
C      -11.385549000     -7.305679000     -9.803605000
H      -11.313466000     -7.283589000    -10.750628000
C      -11.642544000     -7.327322000     -7.037276000
C      -10.919636000     -6.322473000     -7.680066000
H      -10.526777000     -5.626990000     -7.165797000
C      -12.103152000     -8.313172000     -9.201686000
C      -12.121476000    -18.579284000     -6.492048000
H      -12.087700000    -19.464756000     -6.834514000
C      -12.052066000    -12.444222000     -0.171802000
H      -12.836137000    -12.876906000      0.145206000
C       -7.016927000    -11.022148000     -9.054934000
C      -11.380821000    -18.228251000     -5.365813000
H      -10.890278000    -18.902187000     -4.910099000
C      -12.228828000     -8.336624000     -7.812315000
C      -12.022300000    -11.971858000     -1.460473000
C      -10.967049000    -12.305286000      0.677023000
H      -11.009213000    -12.655246000      1.559172000
C      -17.003566000     -8.244128000     -5.564801000
H      -17.161723000     -9.189529000     -5.360812000
```

| | | | |
|---|---|---|---|
| H | -17.817713000 | -7.729985000 | -5.382588000 |
| H | -16.272495000 | -7.907208000 | -5.005843000 |
| C | -10.814817000 | -11.282495000 | -4.366235000 |
| C | -6.125110000 | -11.069341000 | -10.121750000 |
| H | -5.657605000 | -10.279152000 | -10.365745000 |
| C | -7.508032000 | -13.378137000 | -9.452091000 |
| C | -9.727604000 | -11.151040000 | -1.032583000 |
| C | -17.474772000 | -9.186229000 | -8.445331000 |
| H | -17.032107000 | -9.230266000 | -9.318524000 |
| H | -18.388304000 | -8.850110000 | -8.558759000 |
| H | -17.503116000 | -10.081585000 | -8.047900000 |
| C | -10.796057000 | -11.402785000 | -1.913913000 |
| C | -16.817066000 | -6.332293000 | -7.904513000 |
| H | -16.289679000 | -5.724917000 | -7.344691000 |
| H | -17.767639000 | -6.107797000 | -7.824408000 |
| H | -16.537399000 | -6.240646000 | -8.839261000 |
| C | -5.900174000 | -12.217083000 | -10.830233000 |
| H | -5.275062000 | -12.224917000 | -11.545535000 |
| C | -13.258262783 | -12.052985207 | -2.375576477 |
| H | -12.970766392 | -12.082900215 | -3.432723284 |
| H | -13.849540596 | -12.952275360 | -2.168754545 |
| H | -13.915209723 | -11.186840174 | -2.236572263 |
| C | -8.493889065 | -10.340507437 | -1.471427418 |
| H | -7.827738579 | -10.138068795 | -0.625040639 |
| H | -7.911726746 | -10.878314765 | -2.228367215 |
| H | -8.783221326 | -9.375101466 | -1.901993121 |
| C | -8.235358364 | -14.685265221 | -9.086014265 |
| H | -8.875944558 | -15.028656712 | -9.906282554 |
| H | -7.524099306 | -15.488968296 | -8.864024487 |
| H | -8.871391269 | -14.554216169 | -8.203179649 |
| C | -7.189322598 | -9.729554363 | -8.235738391 |
| H | -8.234344858 | -9.399480131 | -8.226361251 |
| H | -6.879055354 | -9.872726761 | -7.194420262 |
| H | -6.588572521 | -8.911707509 | -8.649664158 |
| C | -11.793445822 | -7.327412759 | -5.504687134 |
| H | -12.848325019 | -7.336343276 | -5.207603679 |
| H | -11.316973118 | -8.206927274 | -5.056875206 |
| H | -11.332337081 | -6.439037277 | -5.058283279 |
| C | -12.764512725 | -9.409735130 | -10.057110628 |
| H | -12.124496583 | -9.700112734 | -10.898043823 |
| H | -12.962682466 | -10.311371285 | -9.466442751 |
| H | -13.720442984 | -9.070092006 | -10.471777434 |
| C | -10.560056822 | -16.548873797 | -3.603057799 |
| H | -11.230940472 | -16.463216627 | -2.740685239 |
| H | -9.808327571 | -17.309133414 | -3.362192715 |
| H | -10.038083203 | -15.591334983 | -3.711554954 |
| C | -13.832233297 | -15.267909681 | -7.362340202 |
| H | -13.474466587 | -15.007568539 | -8.365003618 |
| H | -14.852441806 | -15.654608166 | -7.466005155 |
| H | -13.888222293 | -14.340668459 | -6.780792594 |

*

**Optimized coordinates for Utilizing $[Fe(CNXylyl)_3(CN(Xylyl)(C(O)OTMS))]^{-1}$ BP86.**

| | | | |
|---|---|---|---|
| Fe | -10.95173177853953 | -11.83108234858133 | -6.10851068077514 |
| Si | -16.72476424691802 | -8.70630397064629 | -7.21850802328611 |
| O | -14.90499045012888 | -10.85318922766389 | -6.37302160720681 |
| N | -8.37826029792822 | -12.05218127495429 | -7.61463263315328 |
| N | -12.97472676675772 | -9.75552518959400 | -7.05312445145372 |
| O | -15.02392388371939 | -8.78939869771838 | -7.34221297317161 |
| C | -7.26382505774838 | -12.06958613239789 | -8.39060388653373 |
| C | -12.07759090987843 | -10.72279517906157 | -6.64920384608585 |
| N | -10.06848026289748 | -11.28833859184286 | -3.30554632780908 |
| C | -12.56623199234565 | -15.78063019760442 | -6.31720698430389 |
| C | -13.67183127616745 | -15.65406692360791 | -7.20443508311722 |
| C | -5.55106184006167 | -13.30656713756417 | -9.57867276730630 |
| H | -5.11647878365906 | -14.26239044346922 | -9.88241631143257 |
| C | -9.26206107983387 | -10.75480003829766 | 0.23162340375050 |
| H | -8.39490998748079 | -10.49167072627913 | 0.84337789524409 |
| C | -14.34873448525194 | -9.88860727026862 | -6.87743459150080 |
| N | -11.79076532189100 | -14.69733147700129 | -6.00430423717540 |
| C | -11.44627896111452 | -13.53151163652264 | -6.08269221620033 |
| C | -14.42850279978099 | -16.79559642995750 | -7.48673538901091 |
| H | -15.27895636156365 | -16.70223258804596 | -8.16797660857043 |
| C | -9.40708481242054 | -11.97836824509251 | -6.98404085619341 |
| C | -12.24634749172403 | -17.03684066445171 | -5.73619753961449 |
| C | -11.23407393127877 | -6.38644245756312 | -8.92989214850574 |
| H | -10.77588970273414 | -5.52106734304639 | -9.41342658248894 |
| C | -11.66530851356842 | -7.46915116076480 | -9.69793611214025 |
| H | -11.53797756549332 | -7.45570375078352 | -10.78342946629872 |
| C | -11.95349803898047 | -7.52036116042811 | -6.89943729906939 |
| C | -11.37471516201117 | -6.41796409048523 | -7.54151519073169 |
| H | -11.02000991670570 | -5.57932884098025 | -6.93742478564821 |
| C | -12.24973560404858 | -8.59169501699861 | -9.09682290703767 |
| C | -14.12212996663136 | -18.03812110899779 | -6.92357357304035 |
| H | -14.72736850229548 | -18.91480321803856 | -7.16168264371253 |
| C | -11.60233070333255 | -11.31572367901323 | 0.04437988502017 |
| H | -12.57405405512837 | -11.49624513049906 | 0.51208966017385 |
| C | -6.66585448743321 | -10.84339661879907 | -8.79660056088276 |
| C | -13.03326918472154 | -18.14678976603857 | -6.05435012912995 |
| H | -12.78597087272293 | -19.11290518119999 | -5.60676809177346 |
| C | -12.39997432215550 | -8.58911031127595 | -7.69793373661098 |
| C | -11.49710636549527 | -11.43476309524128 | -1.34481228593148 |
| C | -10.50181915620588 | -10.97737837036192 | 0.83736293459454 |
| H | -10.61068211172651 | -10.88825602106526 | 1.92014458688155 |
| C | -17.26259129342430 | -8.74892998018873 | -5.42045594339463 |
| H | -16.98960206454072 | -9.70960570598402 | -4.96350237217254 |
| H | -18.35314538560028 | -8.61853215592644 | -5.33767462473843 |
| H | -16.78049410239155 | -7.94571615898878 | -4.84458661995114 |
| C | -10.45733438110510 | -11.53363648367233 | -4.43510685280353 |
| C | -5.51768092899681 | -10.89249979166943 | -9.59081356222053 |

| | | | |
|---|---|---|---|
| H | -5.05583878008234 | -9.95202075613278 | -9.90222881813989 |
| C | -6.70116807935592 | -13.31497811100919 | -8.78565240700038 |
| C | -9.10342713079469 | -10.85949119310777 | -1.15268339218011 |
| C | -17.53455442609584 | -10.07025254115415 | -8.22275393457804 |
| H | -17.18798935459758 | -10.05055684607497 | -9.26646347664398 |
| H | -18.62978883311189 | -9.95091954117830 | -8.22890112715834 |
| H | -17.29152044835360 | -11.05398218451004 | -7.79973364566270 |
| C | -10.23002449444855 | -11.19921664434898 | -1.94873608305124 |
| C | -17.08809488643630 | -7.02454829334223 | -7.97882405725871 |
| H | -16.58575641812215 | -6.22249562689228 | -7.41938767932714 |
| H | -18.16943553205192 | -6.81734392295774 | -7.97671531338715 |
| H | -16.73569593272322 | -6.97713208616903 | -9.01942353110417 |
| C | -4.95379399235292 | -12.10970427023802 | -9.98513780922506 |
| H | -4.05446513430463 | -12.12545108847103 | -10.60336233230723 |
| C | -12.68002174741274 | -11.80537768579774 | -2.19339244110566 |
| H | -12.49344680478754 | -12.72646222563271 | -2.76647319472505 |
| H | -13.57425559220864 | -11.95387996329808 | -1.57253579979716 |
| H | -12.89815529414817 | -11.03546769648283 | -2.94883910660708 |
| C | -7.77263401895368 | -10.62319756869214 | -1.81360254650491 |
| H | -7.00597164185268 | -10.36365952828032 | -1.07035659005910 |
| H | -7.43745015187969 | -11.51430251787216 | -2.36709511980772 |
| H | -7.83406505001304 | -9.81188675917613 | -2.55582478624508 |
| C | -7.35079254449413 | -14.59745001625772 | -8.34576872972946 |
| H | -8.40221676615010 | -14.64520956907462 | -8.66685221670919 |
| H | -6.81903864191099 | -15.46598627483026 | -8.75736599452558 |
| H | -7.36618488415292 | -14.68305626365201 | -7.24786943741711 |
| C | -7.27367790018868 | -9.53937781232092 | -8.36108853399068 |
| H | -8.32674142344207 | -9.46014597509413 | -8.67036634176590 |
| H | -7.27712734019348 | -9.44629025064478 | -7.26365199177082 |
| H | -6.71943906474089 | -8.69016832071894 | -8.78294023789255 |
| C | -12.07414876965186 | -7.57884225477060 | -5.40114586233339 |
| H | -13.12784613863543 | -7.61720316979030 | -5.08385219981649 |
| H | -11.58848604596936 | -8.48644797071100 | -5.01187517614899 |
| H | -11.60809223654251 | -6.69935941938735 | -4.93695466258753 |
| C | -12.68407897529760 | -9.77728509866738 | -9.91585400999577 |
| H | -12.38995121323521 | -9.65191732215157 | -10.96675755046948 |
| H | -12.23091513906159 | -10.70166029541568 | -9.52866239235044 |
| H | -13.77617954502697 | -9.91424753641159 | -9.87951596787279 |
| C | -11.07696643981530 | -17.14336485954275 | -4.79560480980345 |
| H | -11.20584155803187 | -16.48529613098401 | -3.92223702981339 |
| H | -10.95260888534470 | -18.17547311907811 | -4.44022040193050 |
| H | -10.14192947856623 | -16.82337061630059 | -5.28068229616535 |
| C | -13.99869659289191 | -14.32201709173803 | -7.81634003429932 |
| H | -13.15002551668830 | -13.93172132960086 | -8.39910937852142 |
| H | -14.87220597693943 | -14.40229088328440 | -8.47817317437347 |
| H | -14.20414789940151 | -13.55531536812017 | -7.05312843032185 |

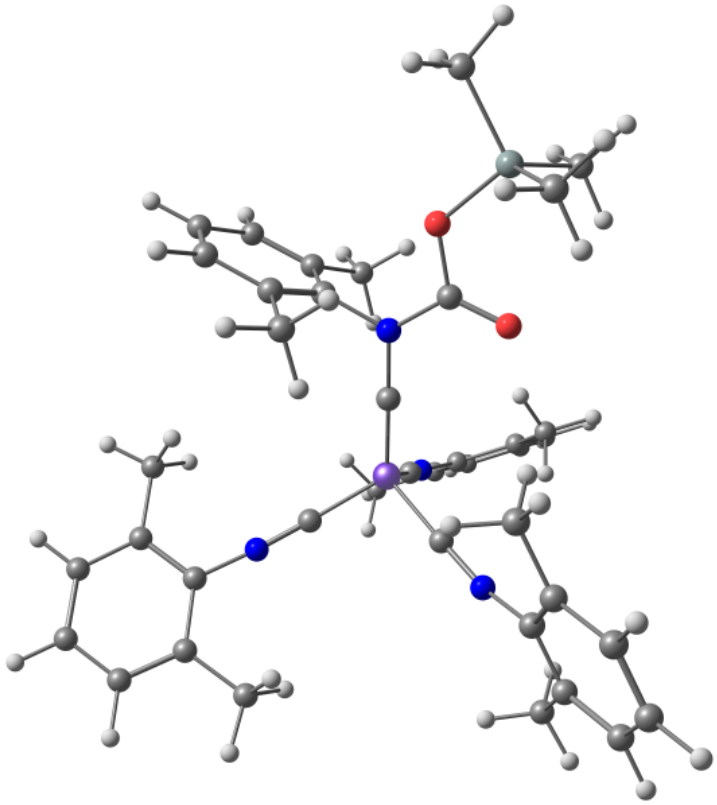

**Figure 3.13** Geometry optimized structure of $[Fe(CNXylyl)_3(CN(Xylyl)(C(O)OTMS))]^{-1}$ utilizing the BP86 functional.

### 3.10 Structure Search Criteria for the Cambridge Structural Database.

**CSD Version Details.** Molecular structures were performed using the Cambridge Structural Database version 5.37. [64] The database was queried using ConQuest Version 1.18.[82]

The Search resulted in 298 unique compounds that contained an Fe bound to a carbon atom containing one additional constituent. All structures were manually analyzed for their relevance and then exported to Mercury: visualization and analysis of crystal structures packages [83] for statistical analysis.

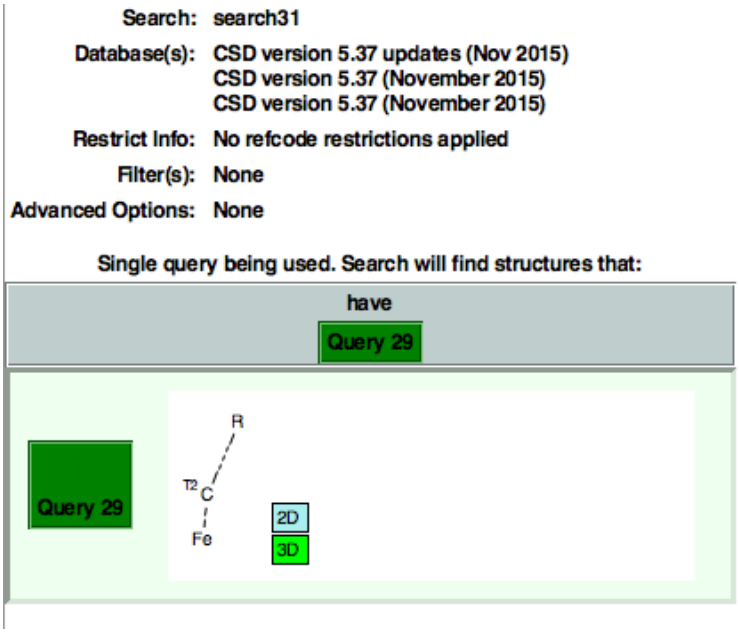


**Figure 3.14** Search criteria to quantify the number of iron complexe containing a carbon bound ligand with only one additional bound substituent. An analysis of the Fe-C distance was also conducted.

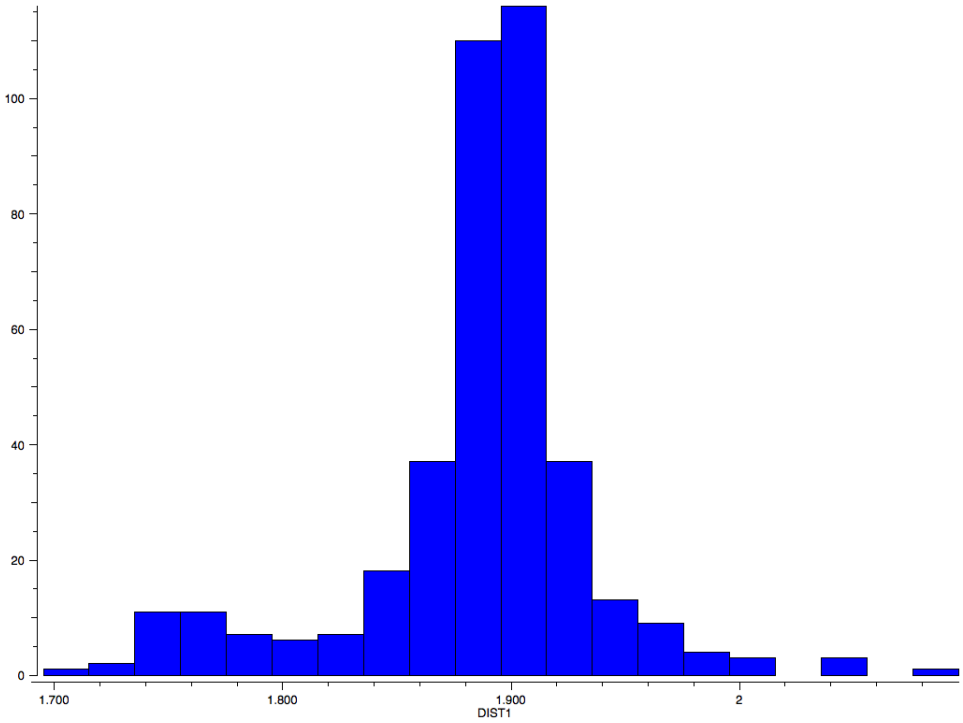


**Figure 3.15** Histogram of 298 unique complexes containing a Fe-carbon bound ligand with only one additional constituent bound to carbon analyzed by Fe-C bond length. X-access reflected Fe-C distance where the Y-axis represents the number of unique molecules with a specie Fe-C distance. It is noted that complexes Na[**5-7**] fall amongst the shortest Fe-C bond lengths with respect to the give search criteria.

### 3.11 Details of Crystallographic Structure Determinations.

**General Information.** Single crystal X-ray structure determinations were carried out at low temperature on Bruker Kappa diffractometers equipped with a Mo sealed tube or rotating anode or Cu rotating anode radiation source and a Bruker APEX-II, APEX-I, or Proteum Pt135 detector. All structures were solved via direct methods with SHELXS[80] and refined by full-matrix least squares procedures using SHELXL[80] within the Olex2 small-molecule solution, refinement and analysis software package.[81] Crystallographic data collection and refinement information are listed in Table 3.2-3.3.

The following molecules contained positionally disordered components that were modeled and refined anisotropically. They are listed along with their respective disordered components:

**$Na[Fe(CNAr^{Mes2})_3(CN(Ar^{Mes2})(COOTMS))]$; Na[5]** was found to co-crystalize with 2 molecules of $C_6H_6$ and one molecule of $C_6H_{14}$ that were disordered. The Platon routine SQUEEZE was used to account for this disordered molecule as a diffuse contribution to the overall scattering pattern without specific atom positions.

**$Na[Fe(CNAr^{Mes2})_3(CN(Ar^{Mes2})(COOSiMe_2Ph)]$, Na[6]** was found to contain two molecules of $C_6H_6$ which were disordered. The Platon routine SQUEEZE was used to account for this disordered molecule as a diffuse contribution to the overall scattering pattern without specific atom positions.

**Na[Fe(CNAr$^{Mes2}$)$_3$(CN(Ar$^{Mes2}$)(COOSiMePh$_2$)], Na[7]** was found to contain a disordered molecule of $C_6H_{14}$. The Platon routine SQUEEZE was used to account for this disordered molecule as a diffuse contribution to the overall scattering pattern without specific atom positions. Additionally a global RIGU command was used on Na[**7**] to account for low resolution data (*ca.* 0.95 Å) and the resultant effects on thermal movement within the crystal structure.

**Table 3.2** Crystallographic data collection and refinement information.

| Name | $Fe(CO)(CNAr^{Mes2})_4$ (**2**): | $(C_6H_5)C(H)NAr^{Mes2}\bullet(Et_2O)_{1/2}$ | $Ph_3B–CNAr^{Mes2}$ (**4**): |
|---|---|---|---|
| Formula | $C_{101}H_{100}FeN_4O$ | $C_{33}H_{36}NO_{0.5}$ | $C_{43}H_{40}BN$ |
| Crystal System | Monoclinic | Monoclinic | Tetragonal |
| Space Group | *C2/c* | $P2_1/C$ | $P\text{-}42_1c$ |
| *a*, Å | 15.1572(4) | 10.2814(3) | 19.8812(7) |
| *b*, Å | 23.1053(7) | 22.0451(9) | 19.8812(7) |
| *c*, Å | 21.3767(5) | 23.9574(9) | 16.8405(9) |
| α, deg | 90 | 90 | 90 |
| β, deg | 97.335(2) | 91.4384(14) | 90 |
| γ, deg | 90 | 90 | 90 |
| V, $Å^3$ | 7915.0(4) | 5428.3(3) | 6654.4(6) |
| *Z* | 4 | 8 | 8 |
| Radiation (λ, Å) | Mo-Kα, 0.71073 | Mo-Kα, 0.71073 | Mo-Kα, 0.71073 |
| ρ (calcd.), $g/cm^3$ | 1.210 | 1.113 | 1.161 |
| μ (Mo Ka), $mm^{-1}$ | 0.244 | 0.065 | 0.066 |
| Temp, K | 100 | 100 | 100 |
| θ max, deg | 29.170 | 27.107 | 25.370 |
| data/parameters | 10673/496 | 11951/636 | 6103/412 |
| $R_1$ | 0.0432 | 0.0436 | 0.0461 |
| $wR_2$ | 0.1089 | 0.0804 | 0.0909 |
| GOF | 1.034 | 0.865 | 1.060 |

**Table 3.3** Crystallographic data collection and refinement information.

| Name | $Na[Fe(CNAr^{Mes2})_3(CN(Ar^{Mes2})(COOTMS))]$ Na[**5**] | $Na[Fe(CNAr^{Mes2})_3(CN(Ar^{Mes2})(COOSiMe_2Ph))]$ Na[**6**] | $Na[Fe(CNAr^{Mes2})_3(CN(Ar^{Mes2})(COOSiMePh_2))]$ Na[**6**] |
|---|---|---|---|
| Formula | $C_{104}H_{109}FeN_4NaO_2Si$ | $C_{109}H_{111}FeN_4NaO_2Si$ | $C_{114}H_{113}FeN_4NaO_2Si$ |
| Crystal System | Orthorhombic | Triclinic | Triclinic |
| Space Group | $P2_12_12_1$ | $P\text{–}1$ | $P\text{–}1$ |
| $a$, Å | 45.411(6) | 15.7619(15) | 15.7192(7) |
| $b$, Å | 14.0836(17) | 17.5031(18) | 24.9235(12) |
| $c$, Å | 16.022(3) | 19.218(2) | 25.0422(13) |
| α, deg | 90 | 92.100(4) | 85.509(3) |
| β, deg | 90 | 90.693(4) | 79.262(3) |
| γ, deg | 90 | 107.858(3) | 78.684(3) |
| V, $Å^3$ | 10247(2) | 5041.6(9) | 9442.9(8) |
| $Z$ | 4 | 2 | 4 |
| Radiation (λ, Å) | Cu-Kα, 1.54178 | Mo-Kα, 0.71073 | Mo-Kα, 0.71073 |
| ρ (calcd.), $g/cm^3$ | 1.007 | 1.064 | 1.180 |
| μ (Mo Ka), $mm^{-1}$ | 1.672 | 0.214 | 0.230 |
| Temp, K | 100 | 100 | 100 |
| θ max, deg | 54.238 | 20.875 | 22.026 |
| data/parameters | 11465/1045 | 10596/1089 | 22973/2181 |
| $R_1$ | 0.0614 | 0.0589 | 0.0809 |
| $wR_2$ | 0.1361 | 0.1323 | 0.1807 |
| GOF | 0.887 | 1.015 | 1.026 |

**3.12 Acknowledgments.**

Material presented in Chapter 3 will appear as a component in an upcoming publication by Mokhtarzadeh, C. C., Moore, C. E., Rheingold, A. L., Figueroa, J. S. The dissertation author is the primary author of this manuscript.

**3.13 References**

(1) Wang, W.-H.; Himeda, Y.; Muckerman, J. T.; Manbeck, G. F.; Fujita, E. *Chem. Rev.* **2015**, *115*, 12936.

(2) Takeda, H.; Cometto, C.; Ishitani, O.; Robert, M. *ACS Catal.* **2017**, *7*, 70.

(3) Grice, K. A.; Kubiak, C. P. *Advances in Inorganic Chemistry*; Elsevier, 2014; Vol. 66, pp 163–188.

(4) Kumar, B.; Llorente, M.; Froehlich, J.; Dang, T.; Sathrum, A.; Kubiak, C. P. *Annu. Rev. Phys. Chem.* **2012**, *63*, 541.

(5) Rakowski Dubois, M.; DuBois, D. L. *Acc. Chem. Res.* **2009**, *42*, 1974.

(6) Solomon, S.; Plattner, G.-K.; Knutti, R.; Friedlingstein, P. *PNAS* **2009**, *106*, 1704.

(7) Le Quéré, C.; Raupach, M. R.; Canadell, J. G.; Marland et al, G.; Le Quéré et al, C.; Le Quéré et al, C.; Raupach, M. R.; Canadell, J. G.; Marland, G.; Bopp, L.; Ciais, P.; Conway, T. J.; Doney, S. C.; Feely, R. A.; Foster, P.; Friedlingstein, P.; Gurney, K.; Houghton, R. A.; House, J. I.; Huntingford, C.; Levy, P. E.; Lomas, M. R.; Majkut, J.; Metzl, N.; Ometto, J. P.; Peters, G. P.; Prentice, I. C.; Randerson, J. T.; Running, S. W.; Sarmiento, J. L.; Schuster, U.; Sitch, S.; Takahashi, T.; Viovy, N.; van der Werf, G. R.; Woodward, F. I. *Nature Geosci* **2009**, *2*, 831.

(8) Raupach, M. R.; Marland, G.; Ciais, P.; Le Quere, C.; Canadell, J. G.; Klepper, G.; Field, C. B. *PNAS* **2007**, *104*, 10288.

(9) Davis, S. J.; Caldeira, K. *PNAS* **2010**, *107*, 5687.

(10) Calabrese, J. C.; Herskovitz, T.; Kinney, J. B. *J. Am. Chem. Soc.* **1983**, *105*, 5914.

(11) Fachinetti, G.; Floriani, C.; Zanazzi, P. F. *J. Am. Chem. Soc.* **1978**, *100*, 7405.

(12) Gibson, D. H. *Chem. Rev.* **1996**, *96*, 2063.

(13) Gambarotta, S.; Arena, F.; Floriani, C.; Zanazzi, P. F. *J. Am. Chem. Soc.* **1982**, *104*, 5082.

(14) Pinkes, J. R.; Steffey, B. D.; Vites, J. C.; Cutler, A. R. *Organometallics* **1994**, *13*, 21.

(15) Lee, G. R.; Cooper, N. J. *Organometallics* **1985**, *4*, 794.

(16) Forschner, T.; Menard, K.; Cutler, A. *J. Chem. Soc., Chem. Commun.* **1984**, *2*, 121.

(17) Giuseppetti, M. E.; Cutler, A. R. *Organometallics* **1987**, *6*, 970.

(18) Bodnar, T.; Coman, E.; Menard, K.; Cutler, A. *Inorg Chem* **1982**, *21*, 1275.

(19) Lee, G. R.; Maher, J. M.; Cooper, N. J. *J. Am. Chem. Soc.* **1987**, 109, 2956.

(20) Fan, T.; Chen, X.; Lin, Z. *Chem. Commun.* **2012**, *48*, 10808.

(21) Lee, G. R.; Cooper, N. J. *Organometallics* **1989**, *8*, 1538.

(22) Ellis, J. E. *Organometallics* **2003**, *22*, 3322.

(23) Margulieux, G. W.; Weidemann, N.; Lacy, D. C.; Moore, C. E.; Rheingold, A. L.; Figueroa, J. S. *J. Am. Chem. Soc.* **2010**, *132*, 5033.

(24) Carpenter, A. E.; Margulieux, G. W.; Millard, M. D.; Moore, C. E.; Weidemann, N.; Rheingold, A. L.; Figueroa, J. S. *Angew. Chem. Int. Ed. Engl.* **2012**, *51*, 9412.

(25) Mokhtarzadeh, C. C.; Margulieux, G. W.; Carpenter, A. E.; Weidemann, N.; Moore, C. E.; Rheingold, A. L.; Figueroa, J. S. *Inorg Chem* **2015**, *54*, 5579.

(26) Stewart, M. A.; Moore, C. E.; Ditri, T. B.; Labios, L. A.; Rheingold, A. L.; Figueroa, J. S. *Chem. Commun.* **2011**, *47*, 406.

(27) Labios, L. A.; Millard, M. D.; Rheingold, A. L.; Figueroa, J. S. *J. Am. Chem. Soc.* **2009**, *131*, 11318.

(28) Fox, B. J.; Millard, M. D.; DiPasquale, A. G.; Rheingold, A. L.; Figueroa, J. S. *Angew. Chem. Int. Ed. Engl.* **2009**, *48*, 3473.

(29) Emerich, B. M.; Moore, C. E.; Fox, B. J.; Rheingold, A. L.; Figueroa, J. S.

*Organometallics* **2011**, *30*, 2598.

(30) Carpenter, A. E.; Mokhtarzadeh, C. C.; Ripatti, D. S.; Havrylyuk, I.; Kamezawa, R.; Moore, C. E.; Rheingold, A. L.; Figueroa, J. S. *Inorg Chem* **2015**, *54*, 2936.

(31) Addison, A. W.; Rao, T. N.; Reedijk, J.; van Rijn, J.; Verschoor, G. C. *J. Chem. Soc., Dalton Trans.* **1984**, *7*, 1349.

(32) Jones, W. D.; Foster, G. P.; Putinas, J. M. *J. Am. Chem. Soc.* **1987**, *109*, 5047.
(33) Song, B.; Xu, B. *Chem Soc Rev* **2017**, Advanced Article, 10.1039/C6CS00384B.

(34) Li, B.-J.; Shi, Z.-J. In *Homogeneous Catalysis for Unreactive Bond Activation*; Shi/Homogeneous Catalysis for Unreactive Bond Activation; John Wiley & Sons, Inc.: Hoboken, NJ, USA, 2014; pp 441–573.

(35) Jones, W. D.; Hessell, E. T. *Organometallics* **1990**, *9,* 718.

(36) Wong, M. W.; Nobes, R. H.; Bouma, W. J.; Radom, L. *J Chem Phys* **1989**, *91*, 2971.

(37) Agnew, D. W.; Moore, C. E.; Rheingold, A. L.; Figueroa, J. S. *Organometallics* **2017**, *36*, 363.

(38) Kim, Y.-E.; Kim, J.; Lee, Y. *Chem. Commun.* **2014**, *50*, 11458.

(39) Senn, D. R.; Emerson, K.; Larsen, R. D. *Inorg Chem* **1987,** *26*, 2738.

(40) Hirano, M.; Akita, M.; Tani, K.; Kumagai, K.; Kasuga, N. C.; Fukuoka, A.; Komiya, S. *Organometallics* **1997**, *16*, 4206.

(41) Cutler, A. R.; Hanna, P. K.; Vites, J. C. *Chem. Rev.* **1988**, *88*, 1363.

(42) Silvia, J. S.; Cummins, C. C. *Chemical Science* **2011**, *2*, 1474.

(43) Sweeney, J.; Perkins, G.; Aguilar, E.; Fernández-Rodríguez, M. A. *Trimethylsilyl Trifluoromethanesulfonate*; John Wiley & Sons, Ltd: Chichester, UK, 2001.

(44) Yang, L.; Powell, D. R.; Houser, R. P. *Dalton Trans.* **2007**, 955.

(45) Fischer, E. O.; Schneider, J.; Neugebauer, D. *Angew. Chem. Int. Ed. Engl.* **1984**, *23*, 820.

(46) Lee, Y.; Peters, J. C. *J. Am. Chem. Soc.* **2011**, *133*, 4438.

(47) Qiu, G.; Ding, Q.; Wu, J. *Chem Soc Rev* **2013**, *42*, 5257.

(48) Dömling, A. *Chem. Rev.* **2006**, *106*, 17.

(49) Boyarskiy, V. P.; Bokach, N. A.; Luzyanin, K. V.; Kukushkin, V. Y. *Chem. Rev.* **2015**, *115*, 2698.

(50) Pombeiro, A.; da Silva, M.; Michelin, R. A. *Coordination Chemistry Reviews* **2001**, *218*, 43.

(51) Pombeiro, A. J. L.; Richards, R. L. *Coordination Chemistry Reviews* **1990**, *104*, 13.

(52) Pombeiro, A. J. L. *Polyhedron* **1989**, *8* (13-14), 1595.

(53) Kim, W. Y.; Chang, J.-S.; Park, S.-E.; Ferrence, G.; Kubiak, C. P. *Chem. Lett.* **1998**, *27*, 1063.

(54) Cotton, F. A.; Zingales, F. *J. Am. Chem. Soc.* **1961**, *83*, 351.

(55) Chatt, J.; Pombeiro, A.; Richards, R. L. *J. Chem. Soc.Chem. Commun.* **1975**, 708.

(56) Bronk, B. S.; Protasiewicz, J. D.; Pence, L. E.; Lippard, S. J. *Organometallics* **1995**, *14*, 2177.

(57) Helmut, F., Motsch, A., Schubert, U., Neugebauer, D. *Angew. Chem. Int. Ed.* **1981**, *20*, 463.

(58) Vyboishchikov, S. F.; Frenking, G. *Chemistry* **1998**, *4*, 1439.

(59) Vyboishchikov, S. F.; Frenking, G. *Chemistry* **1998**, *4*, 1428.

(60) Miller, A. J. M.; Labinger, J. A.; Bercaw, J. E. *Organometallics* **2011**, *30*, 4308.

(61) Knopf, I.; Cummins, C. C. *Organometallics* **2015**, *34*, 1601.

(62) Shintani, R.; Nozaki, K. *Organometallics* **2013**, *32*, 2459.

(63) Albright, T. A., BUrdett, J. K., Whangbo, M.-H. *Orbital Interactions in Chemistry*, John Wiley & Sons, 2013, pp. 570-615.

(64) The Cambridge structural database (CSD v 5.37, Nov 2015) contains 298 unique transition metal complexes featruing an Fe bound to a carbon atom containing only one other bound R-group.

(65) Pangborn, A. P.; Giardello, M. A.; Grubbs, R. H.; Rosen, R. K.; Timmers, F. J. *Organometallics.* **1996**, *15*, 1518.

(66) Armarego, W. L. F.; Chai, C. L. L. *Purification of Laboratory Chemicals,* 5thEd.; Elsevier, 2003.

(67) Weicker, S. A., Stephan, D. W. *Chem. Eur. J.* **2015**, *21*, 13027.

(68) Fulmer, G. R., Miller, A. J. M., Sherden, N. H., Gottlieb, H. E., Nudelman, A., Stoltz, B. M., Bercaw, J. E., Goldberg, K. I. *Organometallics* **2010**, *29*, 2176.

(69) Neese, F. *Wiley Interdiscip. Rev.: Comput. Mol. Sci.* 2012, 2, 73.

(70) Becke, A. D. *J. Chem. Phys.* **1986**, *84*, 4524.

(71) Becke, A. D. *J. Chem. Phys.* **1993**, *98*, 5648.

(72) Lee, C. T.; Yang, W. T.; Parr, R. G. *Phys. Rev. B.* **1988**, *37*, 785

(73) Schaefer, A.; Horn, H.; Ahlrichs, R. *J. Chem. Phys.* **1992**, *97*, 2571.

(74) Weigend, F.; Ahlrichs, R. *Phys. Chem. Chem. Phys.* **2005**, *7*, 3297.

(75) Werner, H.J.; Manby, F. R.; Knowles, P. J. *J. Chem. Phys.* **2003**, *118*, 8149.

(76) van Lenthe, E.; Baerends, E. J.; Snijders, J. G. *J. Chem. Phys.* **1993**, *99*, 4597.

(77) van Lenthe, E.; Snijders, J. G.; Baerends, E. J. *J. Chem. Phys.* **1996**, *105*, 6505.

(78) Pantazis, D. A.; Chen, X. Y.; Landis, C. L.; Neese, F. *J. Chem. Theory Comput.* **2008**, *4*, 908.

(79) ChemCraft. Zhurko, G. A.; Zhurko, D. A. 2014, www.chemcraftprog.com.

(80) Sheldrick, G. M. *Acta Crystallogr. A.*, **2008**, *64*, 112.

(81) Dolomanov, O. V.; Bourhis, L. J.; Gildea, R. J.; Howard, J. A. K.; Puschmann, H. *J. Appl. Cryst.* **2009**, *42*, 339.

(82) I.J. Bruno, J.C. Cole, P.R. Edgington, M. Kessler, C.F. Macrae, P McCabe, J. Pearson, R. Taylor, *Acta Cryst.* (2002), B58, 389.

(83) C.F. Macrae, P.R. Edgington, P McCabe, E. Pidcock, G.P. Shields, R. Taylor, M. Towler, J. van de Streek, *J. Appl. Cryst.* (2006), 39-3, 453.

# *Chapter 4*

# *Geometric and Electronic Structure Analysis of the Three-Membered Electron-Transfer Series $[(\mu^2\text{-}CNR)_2[CpCo]_2]^n$ (n = 0, –1, –2) and its Relevance to the Classical Bridging-Carbonyl System. Reassessment of the Metal-Metal Bonding Interactions in $[(\mu^2\text{-}CE)_2[CpCo]_2]^n$ Dimers (E = O, NR).*

## 4.1 Introduction.

The dimeric cyclopentadienyl complexes $[(\mu\text{-}EO)_2[CpM]_2]^n$ (E = C, N; M = Fe, Co, Ni; $n$ = 0, 1–) are well-known species that provided early tests for metal-metal multiple bonding and mixed valency in organometallic systems.[1-8] However, the degree of M-M bond multiplicity in these dimers, in addition to the fundamental question as to whether M-M bonds are present at all, has remained contentious.[9-24] The central issue in this debate has stemmed from the discrepancy between classical electron-counting formalisms and the crystallographic and/or theoretically determined structural features of the $(\mu\text{-}EO)_2M_2$ core.[11, 21] These structural features (Scheme 4.1), which include the M-M separation (d), $(\mu\text{-}EO)_2M_2$ core puckering ($\theta$) and Cp-ring slippage (s), do not track in a straight forward manner with the ostensible, formal $d^n$ combination for the two metal centers (i.e. $d^8$–$d^8$, $d^9$–$d^8$, $d^9$–$d^9$). In addition, the well recognized and substantial

contribution that the bridging ligands make to the electronic structure also compounded the difficulty in determining the extent of M-M bonding interactions of these dimers.[14, 21]

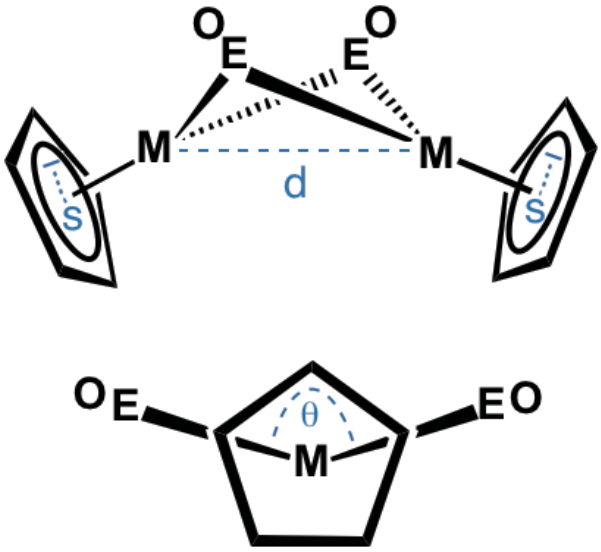


**Scheme 4.1** Topological features of $[(\mu\text{-EO})_2[\text{CpM}]_2]^n$ dimers.

While significant synthetic, spectroscopic and theoretical attention has been given to $[(\mu\text{-EO})_2[\text{CpM}]_2]^n$ dimers,[1-24] it has been noted previously that synthetic access to a homologous series of $d^8$–$d^8$, $d^8$–$d^9$ and $d^9$–$d^9$ partners has been the main limitation of a full, systematic investigation into this class of complexes.[11,13] For example, the neutral bridging carbonyl complex $(\mu\text{-CO})_2[\text{CpCo}]_2$ and its radical anion $[(\mu\text{-CO})_2[\text{CpCo}]_2]^-$, which function as $d^8$–$d^8$, $d^8$–$d^9$, pairs respectively, have been long known and well studied.[9-22] However, the corresponding dianion $[(\mu\text{-CO})_2[\text{CpCo}]_2]^{2-}$, which represents the $d^9$–$d^9$ combination, has remained elusive toward isolation.[13,25] To combat this synthetic limitation, the neutral dinitrosyl dimer $[(\mu\text{-NO})_2[\text{CpCo}]_2]$, has served as a surrogate for the $d^9$–$d^9$ system.[1,11,14,21,26] However, the differing orbital energies attendant

between CO and NO can dramatically affect the energetics of the d-orbital manifold,[27-28] thus rendering this comparison imprecise for the goal of elucidating M-M bond multiplicity.[11,17,21]

Given the recent attention being paid to M-M multiple bonding in the first transition series,[29-46] and new, detailed suggestions for understanding M-M bond multiplicity when bridging ligands are present,[47-48] electronic/geometric structure correlations of classic $[(\mu\text{-EO})_2[\text{CpM}]_2]^n$ dimers and related complexes continue to be of interest. Accordingly, here we present the synthesis and structures of a homologous series of bridging isocyanide (CNR) dimers of the [CpCo] fragment spanning the full series of canonical $d^8$–$d^8$, $d^8$–$d^9$, $d^9$–$d^9$ configurations. Based on the less disparate orbital energetics between isocyanides and CO[49-50] relative to CO and NO,[11, 21, 27-28, 51] this series represents the most electronically accurate model of the bridging carbonyl complexes, $[(\mu\text{-CO})_2[\text{CpCo}]_2]^n$, reported to date. To this end, it is shown that a bridging isocyanide dianion, which serves as an isolable analogue of the proposed $d^9$–$d^9$ carbonyl dianion $[(\mu\text{-CO})_2[\text{CpCo}]_2]^{2-}$, can be stabilized toward isolation by favorable cation/π-arene interactions when an encumbering aryl isocyanide is employed. As a compliment to this Cp-based system, a new series of isoelectronic $\eta^6$-arene/bridging-isocyanide dimers is also reported and shown to provide additional insight into the structural variation accessible to the $(\mu^2\text{-CNR})_2\text{M}_2$ core. Density Functional Theory (DFT) calculations of these bridging-isocyanide dimers are also presented and suggests that, like their carbonyl and nitrosyl counterparts,[14, 21] Co-Co bonds are not present for any $d^n$–$d^n$ combination.

## 4.2 Synthesis and Characterization of $[(\mu^2\text{-CNR})_2[CpCo]_2]^n$ Dimers ($n$ = 0, 1–, 2–).

Synthetic routes to the bridging isocyanide dimers $[(\mu\text{-CNAr}^{Mes2})_2[CpCo]_2]^n$ ($Ar^{Mes2}$ = 2,6-(2,4,6-$Me_3C_6H_2)_2C_6H_3$;[50, 52-53] $n$ = 0, 1–, 2– ) are shown in Scheme 4.2. Treatment of $CpCoI_2(CO)$ with 1.0 equiv. of the *m*-terphenyl isocyanide $CNAr^{Mes2}$ in a benzene solution provides the mono-isocyanide complex, $CpCoI_2(CNAr^{Mes2})$ (**1**) in 94% yield as a purple solid. Reduction of **1** with 2.0 equiv. of $KC_8$ in a 1:2 DME/$Et_2O$ mixture afforded the neutral, bridging isocyanide dimer $[(\mu\text{-CNAr}^{Mes2})_2[CpCo]_2]$ (**2**) as determined by X-ray diffraction (Figure 4.2). Dimer **2** was isolated in 87% yield as a green crystalline solid by this synthetic route. $^1H$ NMR analysis in $C_6D_6$ solution indicated that **2** is diamagnetic and possesses a single $Ar^{Mes2}$ environment, which is consistent with a symmetric dimeric structure found in the solid state. In addition, the solution IR spectrum of **2** gives rise to a low energy ν(CN) stretch at 1837 $cm^{-1}$, which is consistent with the presence of bridging isocyanide units (Figure 4.18).

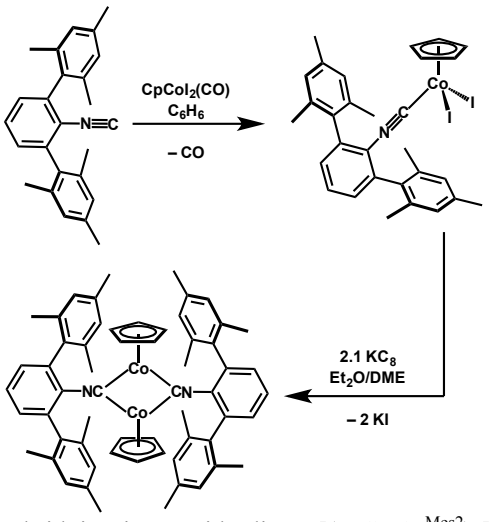


**Scheme 4.2.** Synthetic route to bridging isocyanide dimer $[(\mu\text{-CNAr}^{Mes2})_2[CpCo]_2]$ (**2**) via generation of $CpCoI_2(CNAr^{Mes2})$ (**1**) and reduction with $KC_8$.

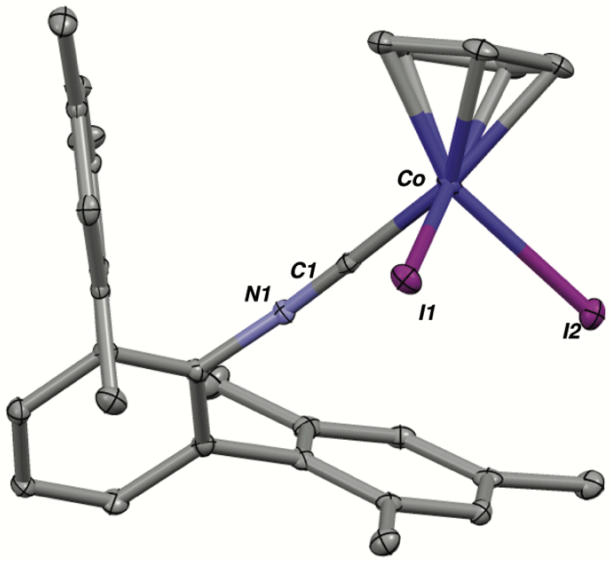


**Figure 4.1.** Molecular Structure of $CpCoI_2(CNAr^{Mes2})$ **(1)**; Hydrogen atoms omitted for clarity. Selected bond distances (Å) and angles (˚): Co-C1 = 1.832(3); Co-I1 = 2.5727(5); Co-I2 = 2.5752(5); C1-N1 = 1.153(4); C1-N1-C7 = 178.1(3).

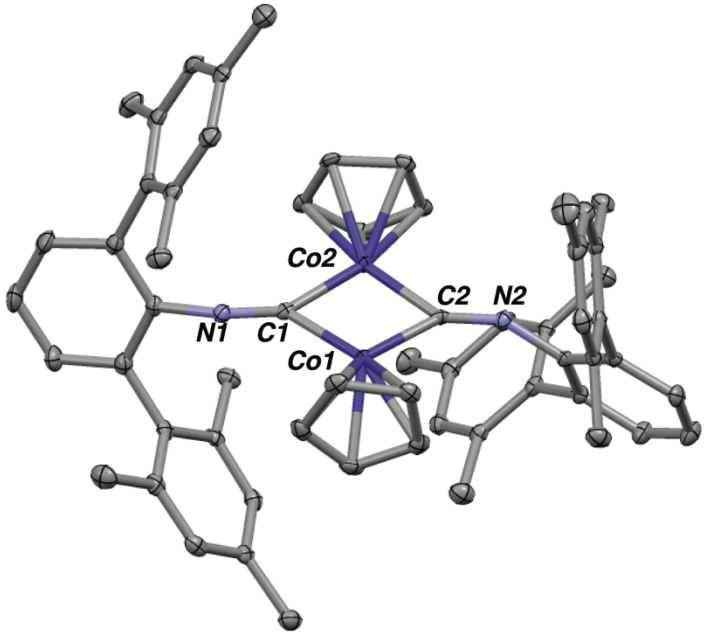


**Figure 4.2.** Molecular Structure of (μ-$CNAr^{Mes2}$) $[CpCo]_2$•($Et_2O$) (**2**); Hydrogen atoms and one $Et_2O$ molecule of solvation omitted for clarity. Selected bond distances (Å) and angles (˚): Co1-Co2 = 2.3484(6); Co1-C1 = 1.891(4); Co1-C2 = 1.876(4); Co2-C1 = 1.887(4); Co2-C2 = 1.886(4); C1-N1 = 1.205(5); C2-N2 = 1.207(5); N1-C13 = 1.376(5); N2-C37 = 1.382(5); C1-N1-C3 = 158.8(4)˚; C2-N2-C37 = 150.3(4)˚; C1-Co1-C2-Co2 = 174.3(2)˚.

With respect to the formation of dimer **2**, analysis of the reduction mixture by $^{1}$H NMR spectroscopy at short reaction times did not conclusively reveal the presence of intermediate species. It is plausible that rapid 2e$^{-}$ reduction of diiodide **1** results in the direct formation of the 16e$^{-}$ mono-isocyanide species [CpCo(CNAr$^{Mes2}$)],[54] which dimerizes under the reaction conditions employed. However, treatment of diiodide **1** with 1.0 equiv of $KC_8$ allows for the isolation of the monoiodide complex CpCoI(CNAr$^{Mes2}$) (**3**), which can be further transformed into the bridging iodide cation [(μ-I)[CpCo(CNAr$^{Mes2}$)]$_2$]OTf (**4**) via treatment with 0.5 equiv. of AgOTf (Scheme 4.3; Figure 4.3-4). Accordingly, reduced dimeric species related to **4** may also potentially serve as intermediates along the reduction pathway to **2**.[55]

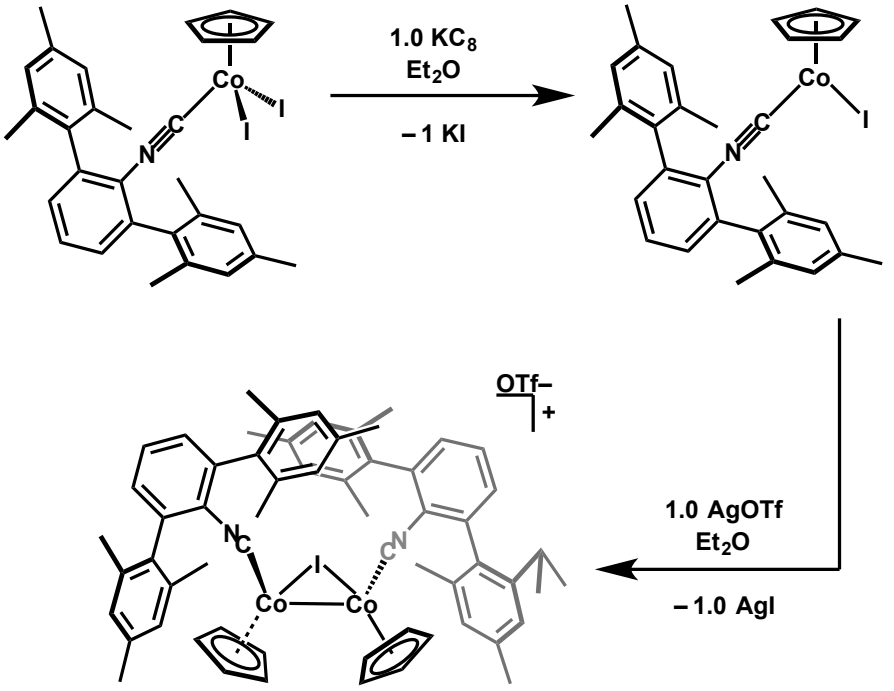


**Scheme 4.3** Reduction of CpCoI$_2$(CNAr$^{Mes2}$) (**1**) with $KC_8$ to afford CpCoI(CNAr$^{Mes2}$) (**3**) and subsequent halogen abstraction to yield [(μ-I)[CpCo(CNAr$^{Mes2}$)]$_2$]OTf (**4**).

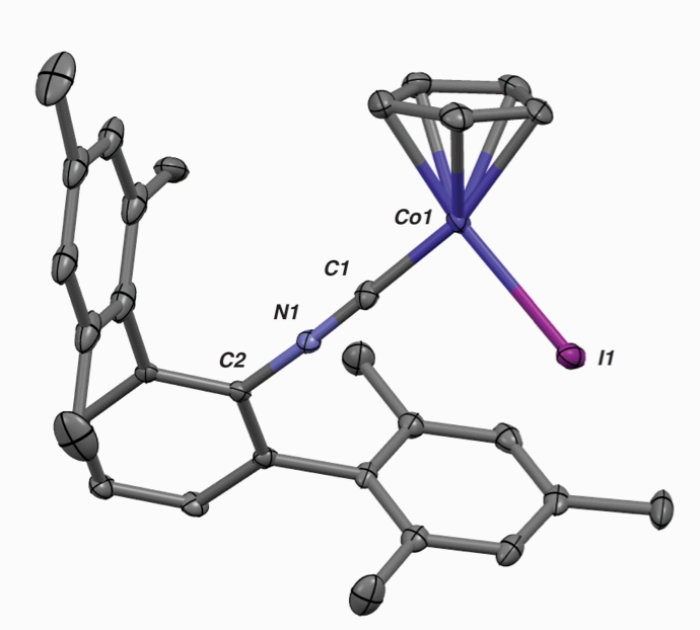


**Figure 4.3** Molecular Structure of CpCoI(CNAr$^{Mes2}$) (**3**); Hydrogen atoms, and disordered methyl group omitted for clarity. Selected bond distances (Å) and angles (˚): Co–C1 = 1.818(4); Co–I1 = 2.4945(6); C1–N1 = 1.158(5); C1–N1–C2 = 174.9(4)˚.

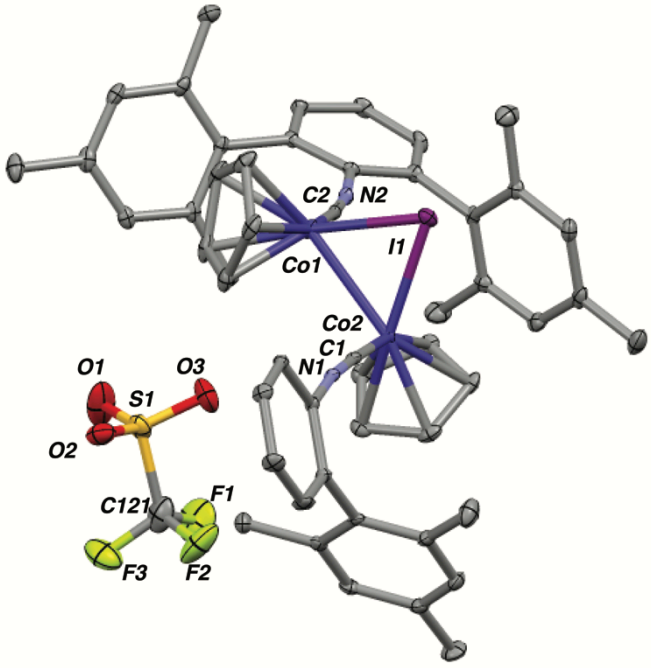


**Figure 4.4.** Molecular Structure of [(μ–I)Cp$_2$Co$_2$(CNAr$^{Mes2}$)$_2$]OTf•(Et$_2$O),[**4**]OTf; Hydrogen atoms and two Et$_2$O molecules of solvation omitted for clarity. Selected bond distances (Å) and angles (˚): Co1-Co2 = 2.6129(5); Co1-I1 = 2.5115(5); Co2-I1 = 2.5176(4); Co2-C1 = 1.826(3); Co1-C2 = 1.827(3); C1-N1 = 1.166(4); C2-N2 = 1.162(4); Co1-I1-Co2 = 62.61(2)˚; C1-N1-C3 = 169.8(3)˚; C2-N2-C27 = 171.6(3)˚.

The monoanion of dimer **2** can also be obtained by adding an additional reducing equivalent to the synthesis mixture. For example, treatment of diiodide **1** with 3.1 equiv. of $KC_8$ be provides the red-orange mono-potassium salt, $K[(\mu\text{-}CNAr^{Mes2})_2[CpCo]_2]$ ($K[\mathbf{2}]$), as determined by X-ray diffraction (Scheme 4.4, Figure 4.5). In the solid state, $K[\mathbf{2}]$ is found as a tight ion pair[56-57] with significant π-arene interactions between the $CNAr^{Mes2}$ mesityl groups and the potassium cation.[58-61] The solution IR spectrum of $K[\mathbf{2}]$ in $C_6D_6$ features a prominent ν(CN) stretch centered at 1664 $cm^{-1}$, which reflects significant increase in Co→(CN)π* back-donation relative to **2**. $^1H$ NMR analysis of $K[\mathbf{2}]$ in $C_6D_6$ solution revealed broad, shifted resonances consistent with a paramagnetic complex. Evans method magnetic moment determination ($C_6D_6$, 20 ˚C) provided a $\mu_{eff}$ value of 1.74(3) μB, which corroborates the presence of an S = ½ species. In addition, EPR analysis of $K[\mathbf{2}]$ in $Et_2O$ solution at room temperature revealed a near-isotropic 15-line pattern consistent with spin-delocalization of a single unpaired electron over two I = 7/2 Co centers (Figure 4.6; $g_{iso}$ = 2.079, $A_{iso}(^{59}Co)$ = 46.2 G). Most importantly, the isolable "$d^8$-$d^9$" bridging-carbonyl radical anion, $[(\mu\text{-}CO)_2[CpCo]_2]^-$, gives rise to a similar EPR spectrum, and has likewise been postulated to feature symmetrical delocalization of the unpaired spin over both Co centers.[4,9,12]

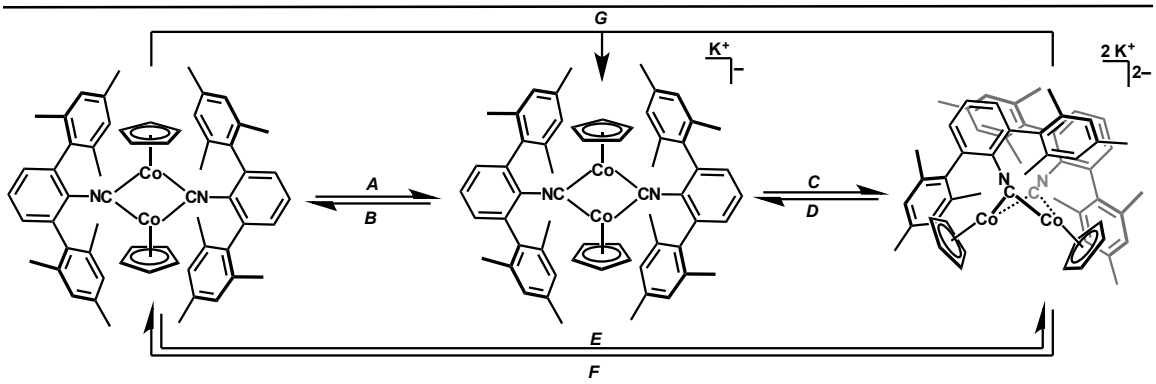


**Scheme 4.4** Chemical Reduction/Oxidation pathways available to $[(\mu\text{-CNAr}^{Mes2})_2[CpCo]_2]^n$ (n = 0 1–, 2–) dimers. A) Reduction of (2) to K[2] with 1 equivalent of $KC_8$; B) Oxidation of K[2] to (2) with 1 equivalent of FcOTF; C) Reduction of K[2] to $K_2$[2] with 1 equivalent of $KC_8$; D) Oxidation of $K_2$[2] to K[2] with 1 equivalent of TlOTf; E) Reduction of (2) to $K_2$[2] with 2 equivalents of $KC_8$; F) Oxidation of $K_2$[2] to (2) with 2 equivalents of FcOTF; G) Comproportionation of $K_2$[2] with (2) to yield K[2].

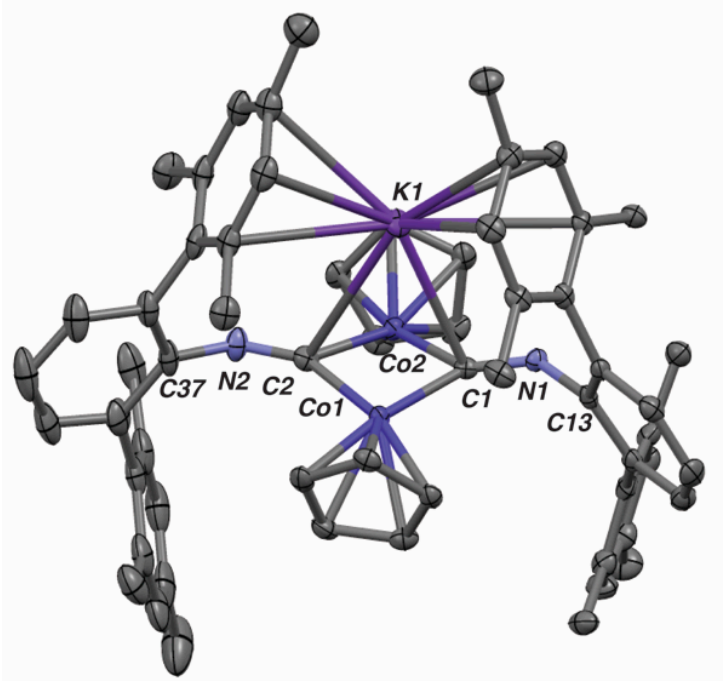


**Figure 4.5.** Molecular structure of $K[(\mu\text{-CNAr}^{Mes2})_2[CpCo]_2]\bullet(Et_2O)$ K[(**2**)]; Hydrogen atoms, one $Et_2O$ molecule of solvation and positional disorder of the flanking mesityl ring omitted for clarity. Selected bond distances (Å) and angles (˚): Co1-Co2 = 2.3513(5); Co1-C1 = 1.844(3); Co1-C2 = 1.852(3); Co2-C1 = 1.859(3); Co2-C2 = 1.854(3); C1-N1 = 1.250(3); C2-N2 = 1.248(4); N1-C13 = 1.403(3); N2-C37 = 1.395(4); C1-K1 = 3.185(3); C2-K1 = 3.380(3); C1-N1-C13 = 132.1(2)˚; C2-N2-C37 = 141.0(3); C1-Co1-C2-Co2 = 165.6(1)˚.

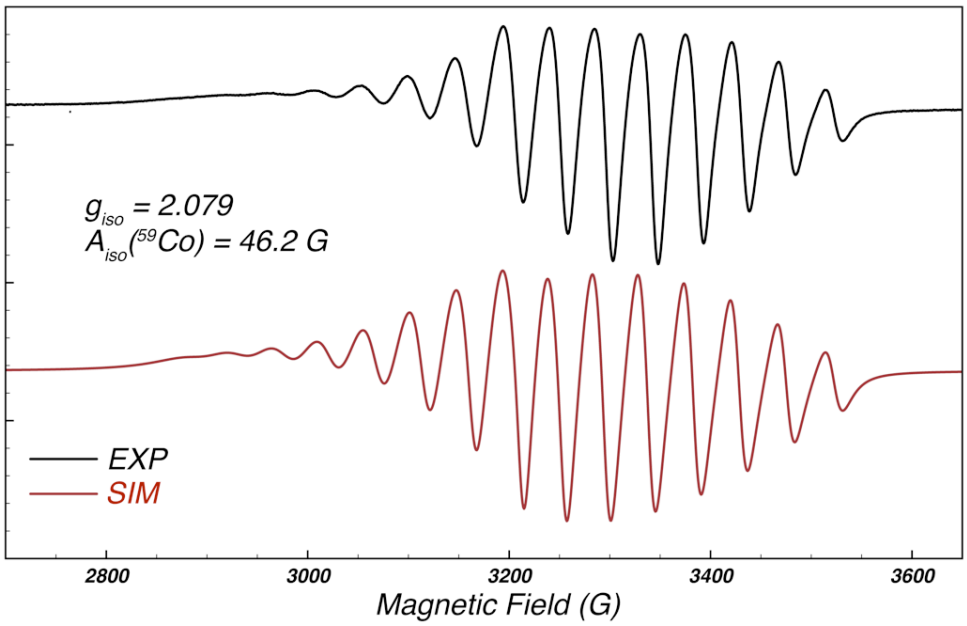


**Figure 4.6** Experimental EPR spectrum of K[(μ-CNAr$^{Mes2}$)$_2$[CpCo]$_2$] K[**2**], in $Et_2O$ at 295 K, (0.05mM) (Experimental, black/top); (simulated spectrum, red/bottom). Simulation of the spectrum yielded $\mu_{eff}$ = 1.800(8) $\mu$B. The slight anisotropy in the simulated spectrum arises from rotational tumbling below the diffusion limit. For other examples of small molecule EPR spectra within the fast, but not isotropic, motion regime.[89-91]

Whereas the neutral and monoanionic dimers **2** and [**2**]$^-$ can be readily generated, the corresponding dianion is also available via simple reduction of the diiodide precursor. Accordingly, treatment of **1** with an excess (10 equiv.) of $KC_8$ produces the di-potassium salt of the dianionic dimer [(μ-CNAr$^{Mes2}$)$_2$[CpCo]$_2$]$^{2-}$ ([**2**]$^{2-}$) as a brown-black solid in 91% isolated yield. The solid state structure of $K_2(Et_2O)$[(μ-CNAr$^{Mes2}$)$_2$[CpCo]$_2$] ($K_2$[**2**]·$Et_2O$) was determined by X-ray diffraction (Figure 4.7) and also revealed a tight ion pair with significant π-arene/K+ interactions. In addition, the potassium centers in $K_2$[**2**]·$Et_2O$ also make close contacts with the CN π-bonds of the bridging CNAr$^{Mes2}$ ligands.[58-59] $^1$H NMR spectroscopy indicated that $K_2$[**2**] is diamagnetic in solution ($C_6D_6$),

while $^{13}C\{^1H\}$ NMR spectroscopy revealed a markedly downfield isocyano $^{13}C\{^1H\}$ chemical shift of 268 ppm ($C_6D_6$), which is consistent with other highly reduced isocyanometallates.[58-60, 62-64] In addition, relative to **2** and the mono potassium salt K[**2**], $K_2$[**2**] exhibits a significantly red-shifted isocyanide ν(CN) band of 1510 $cm^{-1}$, which is indicative of progressively increased Co→(CN)π* back donation.

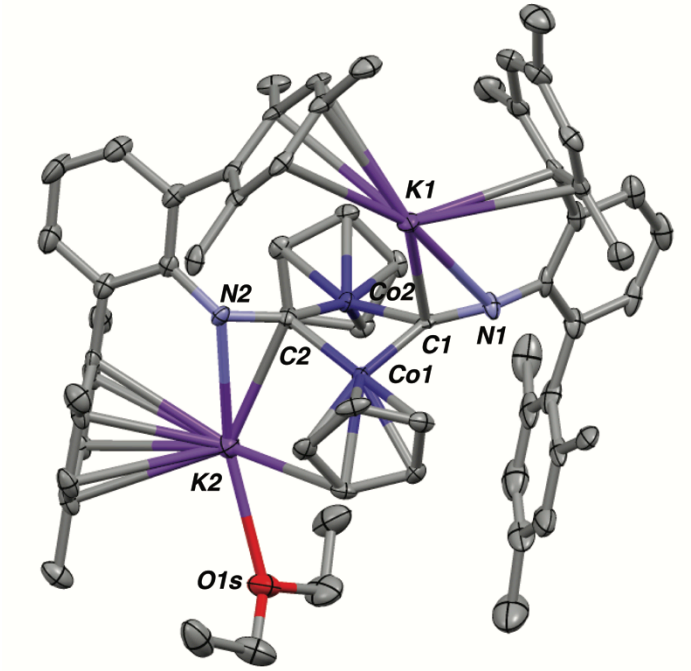


**Figure 4.7** Molecular Structure of $K_2$[(μ-$CNAr^{Mes2}$) $[CpCo]_2$]•$(Et_2O)_2$; $K_2(Et_2O)_2$[**2**]; Hydrogen atoms and one $Et_2O$ molecule of solvation omitted for clarity. Selected bond distances (Å) and angles (˚): Co1-Co2 = 2.4120(10); Co1-C1 = 1.846(5); Co1-C2 = 1.858(5); Co2-C1 = 1.857(5); Co2-C2 = 1.830(5); C1-N1 = 1.279(6)); C2-N2 = 1.286(6); N1-C13 = 1.391(6); N2-C37 = 1.388(6); C1-K1 = 2.883(5); N1-K1 = 3.013(4); C2-K2 = 2.915(5); N2-K2 = 2.867(4); K2-O1s = 2.751(4); C1-N1-C13 = 136.3(5)˚; C2-N2-C37 = 132.3(4)˚; C1-Co1-C2-Co2 = 159.49(2)˚.

Most importantly, K2[2] represents an isolable isocyano analogue of the elusive dimeric dicarbonyl dianion, $[(\mu^2\text{-}CO)_2[CpCo]_2]^{2-}$. This observation is particularly significant, given the fact that isocyanide ligands are well known to decrease reduction potentials relative to CO,[65-67] and are also considerably less effective π-acids.[49-50] Accordingly, we believe that the ability of the $CNAr^{Mes2}$ ligands to encapsulate alkali-

metal cations with π-arene interactions[68] provides an effective pathway for the stabilization of this class of highly reduced dianions. While the presence of alkali-metal cations in solution have long been known to effect positive shifts in reduction potentials of substrates, the specific formation of π-arene/alkali-metal-cation interactions by m-terphenyl groups has been proposed to significantly contribute to the stability of highly reduced main-group element compounds.[69-72] In this respect, it is important to note that attempts to disrupt the π-arene/$K^+$ interactions in $K_2$[**2**] with sequestering agents such as 18–crown–6, dibenzo–18–crown–6, as well as traditionally non-coordinating cations such as $[Ph_3P{=}N{=}PPh_3]^+$,[64] resulted rapidly in intractable mixtures. However, comproportionation $K_2$[**2**] with [**2**], or treatment of $K_2$[**2**] with TlOTf, leads cleanly to the mono-potassium salt K[**2**]. These observations indicate that cation removal concomitant with an oxidation event (i.e. cation-coupled electron transfer; CCET)[73] allows the structural integrity of this dimeric system to be maintained and points to the fact that tight association of the $K^+$ counterion is a critical stabilizing feature for the doubly-reduced dimer $[\mathbf{2}]^2-$.

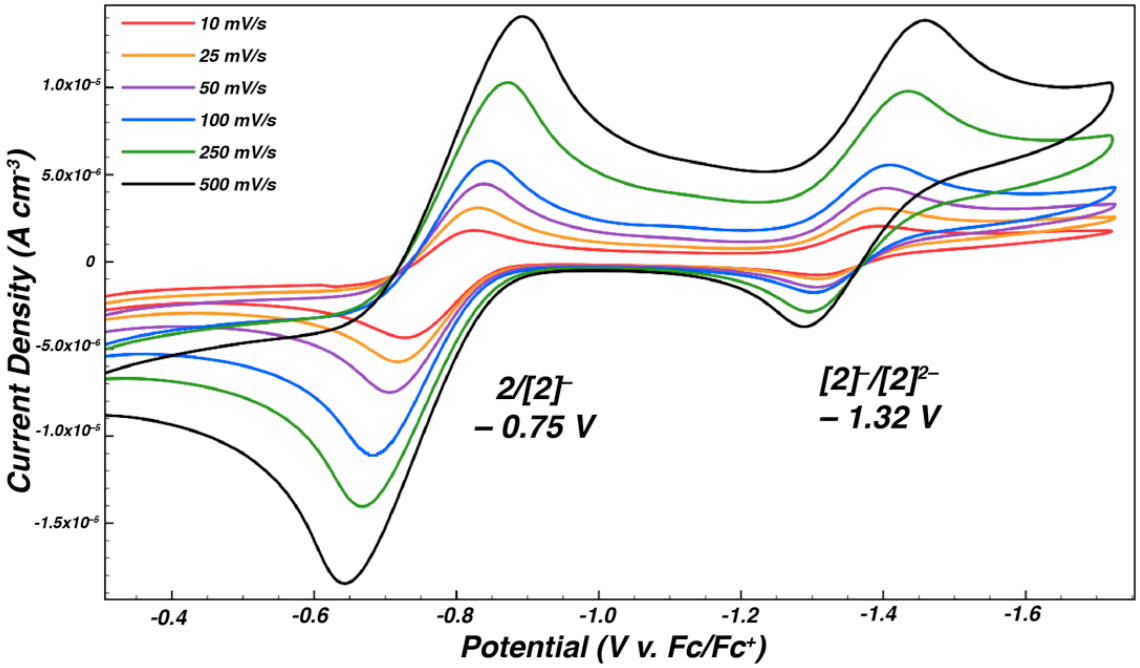


**Figure 4.8** Variable-Scan-Rate cyclic voltammetry (CV) of ($\mu^2$-CNAr$^{Mes2}$)$_2$[CpCo]$_2$ (**2**) in THF under an Ar atmosphere using 0.1 M Na[BAr$^F{}_4$] as a supporting electrolyte.

To further interrogate the redox events of dimer **2**, cyclic voltammagrams were recorded. Cyclic voltammetry in a THF solution featuring [NBu$_4$]PF$_6$ as a supporting electrolyte under an argon atmosphere indicated a reversible redox event at –1.8 V vs. Fc/Fc$^+$ corresponding to a one electron reduction ($\Delta E_p$ = 100 mV) attributable to the **2**/[**2**] redox couple (Figure 4.26). However, sweeping to more negative potentials did not reveal a second redox event prior to the onset of solvent reduction. Accordingly, to more thoroughly probe for the electrochemical generation of dianionic [2]$^{2–}$, CV scans of dimer **2** in THF using Na[BAr$^F{}_4$] (Ar$^F$ = 3,5-(CF$_3$)$_2$C$_6$H$_3$) as a supporting electrolyte were conducted. This salt is well known to foster more positive reduction potentials[74] but it can also potentially deliver Na$^+$ cations to reduced organometallic species during cathodic scans. Similar to the CV scans using [NBu$_4$]PF$_6$, scans using Na[BAr$^F{}_4$] as an

electrolyte result in a reversible $1e^-$ reduction event centered at –0.75 V corresponding to the **2**/[**2**]$^-$ couple (Figure 4.8). However, an additional quasi-reversible redox proves now becomes observable at –1.32 V, which we attribute to the reduction of [**2**]$^-$/[**2**]$^{2-}$ (Figure 4.8).

Notably, this –1.32 V redox process proceeds with roughly 1/3 the current amplitude of the –0.75 V feature at a scan rate of 100 mV/s, but becomes increasingly more reversible with increased scan rate (Figure 4.8). This difference in current amplitude was corroborated by differential pulsed voltammetry (DPV) measurements (Figure 4.27) and we tentatively interpret these combined observations as indicative of the binding of $Na^+$ ions by [**2**]$^-$ on the CV time scale at slow scan rates. Indeed, CV measurements in THF using [$NBu_4$][$BAr^F{}_4$] as an electrolyte, which gives rise to operating potentials intermediate between those of [$NBu_4$]$PF_6$ and Na[$BAr^F{}_4$],[74] the event ascribable to the [**2**]$^-$ to [**2**]$^{2-}$ reduction again becomes unobservable (Figure 4.28). Accordingly, we contend that this electrochemical data reasonably suggest that the formation of cation/π-arene interactions play a critical role in the ability to generate and isolate dianion [**2**]$^{2-}$ on a preparative scale. Given that we have previously shown that the flanking rings of *m*-terphenyl isocyanides can readily form π-arene interactions with both $Na^+$ and $K^+$ ions,[58-61] this system offers a platform for the stabilization of highly reduced organometallics, despite the fact that the isocyanide donor group itself creates a more electron-rich coordination environment relative to CO.

## 4.3 Synthesis and Characterization of ($\eta^6$-arene)Co and CpNi Analogues of [($\mu^2$-$CNAr^{Mes2}$)$_2$[CpCo]$_2$]$^{2-}$ ([2]$^{2-}$).

As noted above, the neutral bridging dinitrosyl dimer, ($\mu^2$-NO)$_2$[CpCo]$_2$ has been studied as an isoelectronic surrogate to the elusive carbonyl dianion, [($\mu^2$-CO)$_2$[CpCo]$_2$]$^{2-}$.[11,21] However, the disparate π* orbital energies between NO and CO render this isoelectronic substitution quantitatively imprecise.[11,21] An alternative valence-isoelectronic mimic of [(μ-CO)$_2$[CpCo]$_2$]$^{2-}$ is a neutral $\eta^6$-arene containing dimer that retains the (μ-CO)$_2$Co$_2$ core (*i.e.* (μ-CO)$_2$[($\eta^6$–arene)Co]$_2$). Such dimers have not been reported for the bridging CO system, but they are synthetically accessible for the bridging isocyanide complexes considered here. Accordingly, as shown in Scheme 4.5, exhaustive thermal decarbonylation of Co$_2$(CO)$_8$ in the presence of 2.0 equiv[75] of $CNAr^{Mes2}$ provides the $\eta^6$-arene dimer, Co$_2$(($\eta^6$-Mes)(μ-$CNAr^{Mes}$))$_2$ (**5**), as determined by X-ray diffraction (Figure 4.9). In dimer **5**, the $\eta^6$-arene interactions are supplied by flanking mesityl groups of the $CNAr^{Mes2}$ ligands. This binding mode for $CNAr^{Mes2}$ has been observed previously in monomeric Mo complexes.[76] Notably, dimer **5** gives rise to a low energy $\nu_{CN}$ stretch at 1609 cm$^{-1}$, which is only *ca.* 100 cm$^{-1}$ higher in energy to that of dianionic dimer [**2**]$^{2-}$ despite its charge neutrality. However, it must be noted that the tethered nature of the isocyano group in **5** results in geometric constraints that may significantly affect the energy of the ν(CN) band. Nevertheless, **5** exhibits a downfield $^{13}C\{^1H\}$ resonance of δ = 253 ppm reflective of significant π-backbonding interactions to the bridging isocyanide carbon.[62-63]

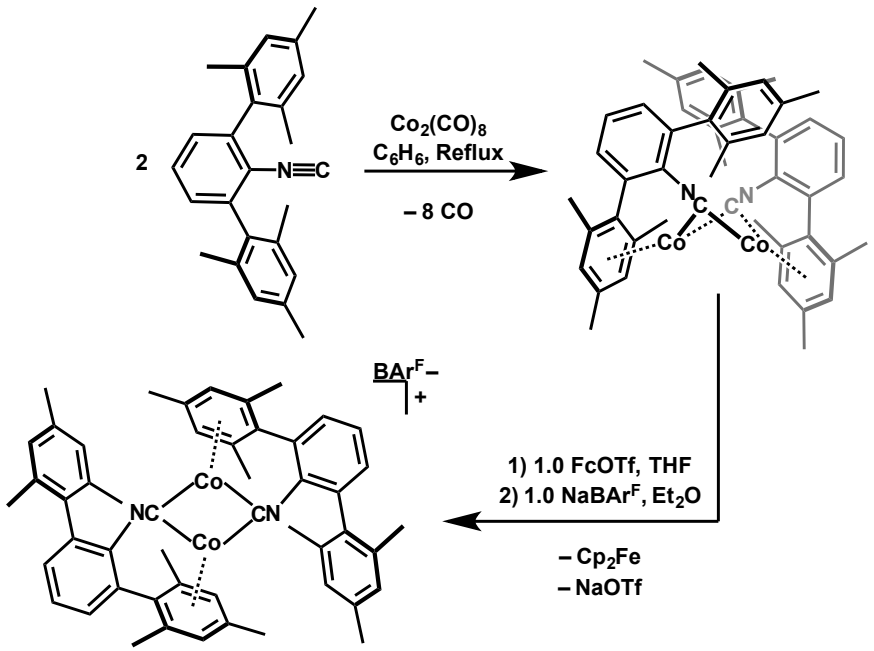


**Scheme 4.5** Synthetic scheme depicting the generation of $Co_2((\eta^6\text{-Mes})(\mu^2\text{-CNAr}^{Mes}))_2$ (**5**) and $[Co_2((\eta^6\text{-Mes})(\mu^2\text{-CNAr}^{Mes}))_2]BAr^F{}_4$ ([**5**]$BAr^F{}_4$).

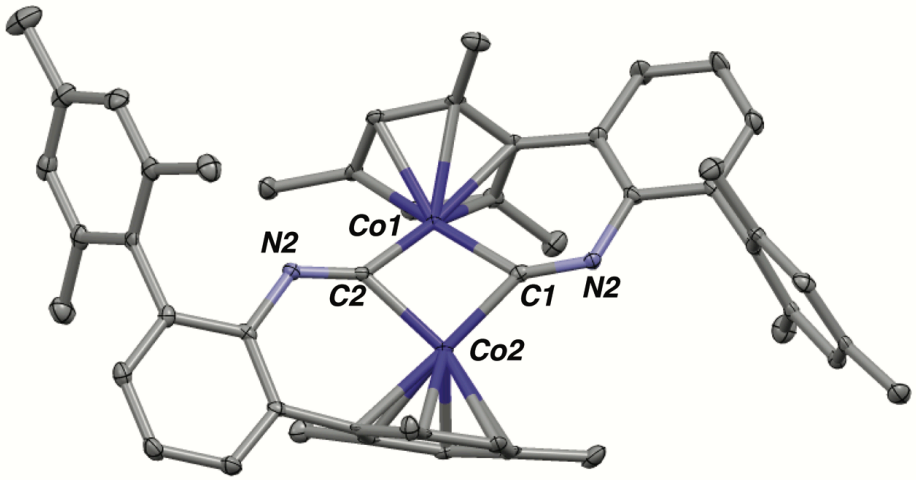


**Figure 4.9** Molecular structure of $Co_2((\eta^6\text{-Mes})(\mu^2\text{-CNAr}^{Mes}))_2$; (**5**). Selected bond distances (Å) and angles (˚): Co1-Co2 = 2.3894(7); Co1-C1 = 1.894(3); Co1-C2 = 1.832(3); Co2-C1 = 1.814(3); Co2-C2 = 1.890(3); C1-N1 = 1.247(4); C2-N2 = 1.251(4); N1-C3 = 1.397(4); N2-C27 = 1.396(4); C1-N1-C3 = 126.6(3); C2-N2-C27 = 126.7(3); C1-Co1-C2-Co2 = 151.6(1).

To further compare these $\eta^5$-cyclopentadienyl and $\eta^6$-arene bridging isocyanide dimers, the behavior of dimer **5** toward oxidants was probed. As shown in Scheme 4.5,

sequential treatment of **5** with 1.0 equiv of ferrocenium triflate (FcOTf; OTf = $[CF_3SO_3]^-$) and $NaBAr^F{}_4$ ($Ar^F{}_4$ = 3,5-$(CF_3)_2C_6H_3$) provided the radical cation $[Co_2((\eta^6\text{-Mes})(\mu^2\text{-}CNAr^{Mes}))_2]BAr^F{}_4$ ([**5**]$BAr^F{}_4$) as a light orange solid.[75] Solution magnetic moment determination on [**5**]$BAr^F{}_4$ resulted in a $\mu_{eff}$ value of 1.79 (±0.2) $\mu_B$, which is consistent with a monoradical formulation. In addition, the room-temperature EPR spectrum of [**5**]$BAr^F{}_4$ in $Et_2O$ (Figure 4.25) is largely similar to that observed for K[**2**] and features a 15-line pattern ($g_{iso}$ = 2.113, $A_{iso}(Co^{59})$ = 43.1 G) indicative of symmetric delocalization of the unpaired spin across the two Co centers. Dimer [**5**]$BAr^F{}_4$ also displays an ν(CN) band at 1700 $cm^{-1}$ in its solution IR spectrum ($C_6D_6$), which reflects a decrease in π-backdonation to the bridging isocyanide groups relative to the neutral dimer **5**. Attempts to further oxidize [**5** ]$BAr^F{}_4$ were unsuccessful and resulted in intractable mixtures.

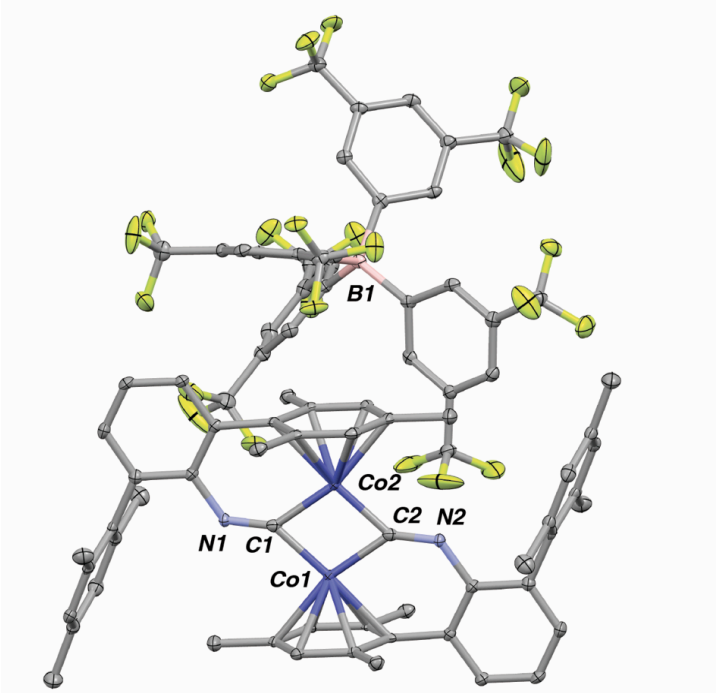


**Figure 4.10** Molecular Structure $[Co_2((\eta^6\text{-Mes})(\mu^2\text{-}CNAr^{Mes}))_2]BAr^F{}_4$; [**5**]$BAr^F{}_4$. Selected bond distances (Å) and angles (°): Co1-Co2 = 2.4044(7); Co1-C1 = 1.889(4); Co1-C2 = 1.830(4); Co2-C1 = 1.839(3); Co2-C2 = 1.903(3); C1-N1 = 1.233(4); C2-N2 = 1.230(4); N1-C27 = 1.406(4); N2-C3 = 1.403(4); C1-N1-C27 = 129.5(3)°; C2-N2-C3 = 130.8(3)°; C1-Co1-C2-Co2 = 177.1(2)°.

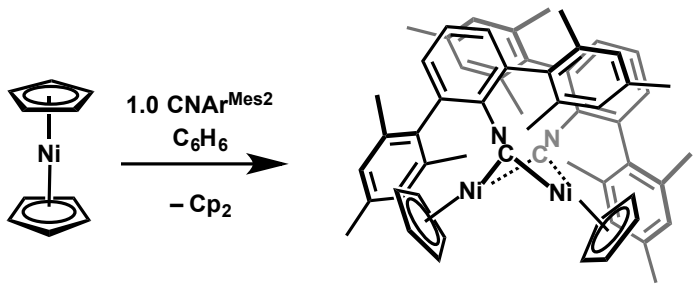


**Scheme 4.6** Synthetic routes to *m*-terphenyl isocyanide–Ni dimers ($\mu^2$-$CNAr^{Mes2}$)$_2$[CpNi]$_2$ (**7**).

As a final point of comparison to dianion [**2**]$^{2-}$, we targeted the neutral nickel dimer ($\mu^2$-$CNAr^{Mes2}$)$_2$[CpNi]$_2$, as this species represents an isoelectronic analogue where both the Cp and bridging, unthethered, $CNAr^{Mes2}$ ligands are retained. Neutral $Ni_2$ dimers of the formulation ($\mu^2$-CO)$_2$[CpNi]$_2$ and ($\mu^2$-CNMe)$_2$[CpNi]$_2$ have been prepared previously[8, 78] and, as shown in Scheme 4.6, the *m*-terphenyl isocyanide derivative ($\mu$-$CNAr^{Mes2}$)$_2$[CpNi]$_2$ (**6**) is readily accessible by treatment of nickelocene ($Cp_2Ni$) with 1.0 equiv. of $CNAr^{Mes2}$. Cyclopentadiene dimer (*i.e.* $Cp_2$) is generated as a byproduct in this reaction, thereby indicating that neutral **6** is likely formed by a coordinatively-induced Cp-radical ejection process. In the solid state (Figure 4.11), **6** possesses gross topological features similar to the neutral cobalt dimer **2**, with the exception that it possesses increased puckering of the ($\mu$-CNR)$_2$Ni$_2$ core. A similarly puckered core has been observed for the bridging methyl isocyanide derivative, ($\mu$-CNMe)$_2$[CpNi]$_2$.[78] Most notably however, single crystals of dimer **6** gives rise to a $\nu$(CN) stretch of 1914 cm$^{-1}$ in the solid state, which is preserved in $C_6D_6$ solution (Figures 4.22), and is significantly higher in energy than the corresponding band of both $K_2$[**2**] and **5**. In addition, the $^{13}C\{^1H\}$ chemical shift of the bridging CN units of **6** is $\delta$ = 171 ppm, which is

substantially up-field of those of $K_2$[**2**] and **5**, and reflects an electronic environment where π-backbonding interactions are significantly diminished.

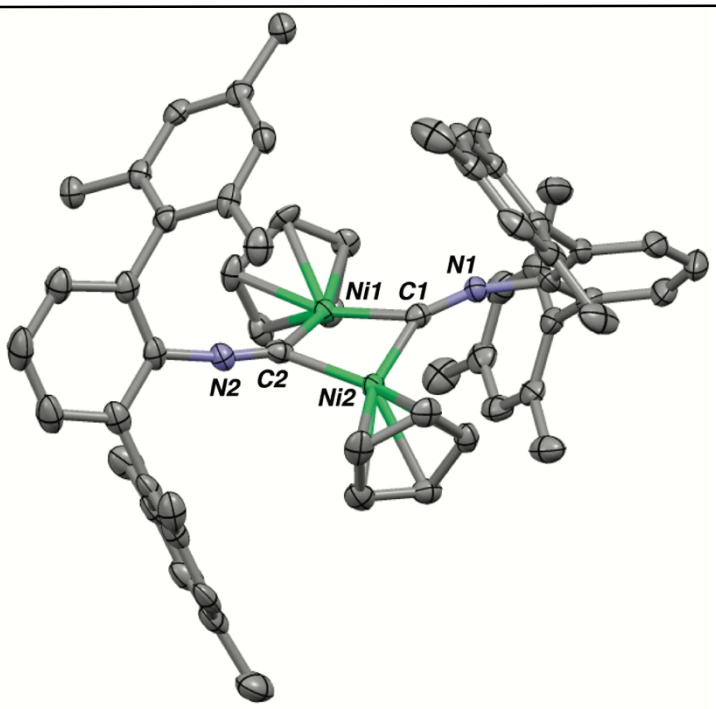


**Figure 4.11.** Molecular Structure of ($\mu^2$–$CN^{ArMes}$)[CpNi]$_2$, (**7**); one molecule form the asymmetric unit depicted, hydrogen atoms, and two $C_5H_{14}$ molecules of solvation omitted for clarity**.** Selected bond distances (Å) and angles (˚): Ni1-Ni2 = 2.3797(10); Ni1-C1 = 1.867(6); Ni1-C2 = 1.891(6); Ni2-C1 = 1.870(6); Ni2-C2 = 1.887(6); C1-N1 = 1.211(7); C2-N2 = 1.192(7); N1-C13 = 1.377(7); N2-C37 = 1.378(7); C1-N1-C13 = 157.3(6); C2-N2-C37 = 171.8(6); C1-Ni1-C2-Ni2 = 157.3(2)˚.

## 4.4 X-ray Crystallographic Structure Determinations of [($\mu^2$-$CNAr^{Mes2}$)$_2$[CpM]$_2$]$^n$ (M = Co, *n* = 0, 1–, 2–; M = Ni, n =0) and $Co_2$(($\eta^6$-Mes)($\mu^2$-$CNAr^{Mes}$))$_2$ (*n* = 0, 1+) Dimers.

In the prototypical neutral dimer ($\mu^2$-CO)$_2$[CpCo]$_2$, debate over the presence or absence of direct Co-Co bonding has stemmed from the fact that introduction of an additional electron (*i.e.* formation of [($\mu^2$-CO)$_2$[CpCo]$_2$]$^-$) results in only a minor elongation of the Co-Co internuclear separation (*ca.* 2.5%).[9,11-14,21] However, internuclear

separation alone does not support or preclude the existence of M-M bonding interactions.[79] Furthermore, both the multi-centered bonding between the metal centers and the bridging ligands, as well as the geometric response of the ostensible $d^n$–$d^n$ count further complicates an analysis of direct of M-M interactions.[11, 14, 21] However, both the lack of synthetic access to the dianion $[(\mu\text{-CO})_2[\text{CpCo}]_2]^{2-}$, and quantitatively imprecise comparison represented by the bridging nitrosyl complex, $[(\mu\text{-NO})_2[\text{CpCo}]_2]$, has not allowed a full structural interrogation of these features across a homologous $d^n$–$d^n$ series. In addition, more detailed comparison of metrical parameters associated with π-backbonding interactions in these dimers (such as C-O bond distances) have been partially hampered by the low crystallographic resolution reported for the solid-state structures of $(\mu\text{-CO})_2[\text{CpCo}]_2$, $[(\mu\text{-CO})_2[\text{CpCo}]_2]^-$ and $(\mu\text{-NO})_2[\text{CpCo}]_2$.[13] Accordingly access to a full, three-membered series of isocyanide analogues, along with high-resolution crystallographic data, has enabled a more detailed analysis of the structural changes accommodated by the dinuclear core of this class of complexes.

Table 4.1 lists pertinent experimental metrical parameters for the core of dimers $K_n$[**2**], [**5**][$BAr^F{}_4$]$_n$ and **6** ($n$ = 0, 1, 2). Remarkably, comparison of the crystallographic data for neutral dimer **2** relative to K[**2**] reveal that their Co-Co separations are statistically identical ($\Delta_{d(Co\cdots Co)}$ = 0.0029 Å; 0.01%). While the $K^+/\pi$ interactions observed in K[**2**] (Figure 4.5) could potentially draw the Co centers into closer proximity, it is important to note that DFT optimizations (B3LYP/def2-TZVP) on the model complexes $[(\mu\text{-CNPh})_2[\text{CpCo}]_2]^{0/1-}$ (**2m** and [**2m**]$^{1-}$), which lack both $K^+$ counter ions and flanking aryl substituents, also show a negligible difference in Co-Co separation between the neutral and monoanionic dimers (Table 4.1). However, the crystallographic data do

reveal a non-negligible lengthening of the Co-Co separation in $K_2$[**2**] relative to K[**2**] ($\Delta_{d(Co\cdots Co)}$= 0.0607; 2.6%). Contrastingly, a DFT optimization of the dianion [($\mu^2$-CNPh)$_2$[CpCo]$_2$]$^{2-}$ ([**2m**]$^{2-}$) resulted in a Co-Co separation that is again nearly identical to both **2m** and [**2m**]$^{1-}$. Accordingly, for the specific case of $K_2$[**2**], π-arene/cation interactions to two $K^+$ centers may in fact marginally affect the Co-Co separation in the solid state.

While the Co-Co separations in **2**, K[**2**] and $K_2$[**2**] do not provide a conclusive relationship between the geometric and electronic structure, several other metrical parameters provide substantial evidence for a positive correlation between both increased Co→π*(CN) backbonding and population of Co/Cp antibonding orbitals with successive addition of electrons. For example, the isocyanide C-N separations display an elongation upon reduction from neutral dimer **2** to K[**2**] ($\Delta_{d(C\cdots N)Avg}$ = 0.0338 Å; 2.6%). In addition the C-N separation also elongates upon reduction from K[**2**] to $K_2$[**2**] ($\Delta_{d(C\cdots N)Avg}$ = 0.0429 Å; 3.4%), and is supportive of increase in Co→π*(CN) π-backdonation. The geometry optimizations of models [**2m**]$^n$ show an overall C-N bond elongation from **2m** to [**2m**]$^{2-}$ similar to that observed experimentally. In light of the increase in M→π*(CN) π-backdonation it is important to also consider the Co-$C_{iso}$ bond distances, and indeed contractions in the Co- $C_{iso}$ bonds do occur upon reduction of neutral dimer **2** to dianionic dimer $K_2$[**2**] ($\Delta_{d(Co\cdots C)Avg}$ = 0.0354 Å; 1.9%). These Co-$C_{iso}$ contractions are also corroborated by geometry optimized structures of models [**2m**]$^n$ which show an overall contraction of the Co-$C_{iso}$ bond lengths as function of increased charge on the dimeric core.

In addition to changes in bond lengths, prominent structural distortions of the [(μ-CNR)$_2$[CpCo]$_2$] core are observed as the dimers are reduced. Accordingly, while neutral dimer **2** displays a near-planar $Co_2C_2$ core with a torsion angle (θ) of 174.2(2)˚ (Scheme 1), monoanion K[**2**] and dianion $K_2$[**2**] exhibit significantly decreased torsional angles of 165.6(1)˚ and 152.49(2)˚, respectively, resulting in far more puckered geometries. Importantly this progressive puckering is also reflected in the optimized structures of models [**2m**]$^n$ (Table 4.1), despite the decreased steric profile of the CNPh bridging ligand and the absence of $K^+$/arene interactions. It is also noteworthy that neutral dimer **2** exhibits symmetric coordination of the Cp units to both Co centers, with an average M-$C_{Cp}$ bond distance of 2.098(± 0.008) Å (Figure 4.13). However, upon reduction to K[**2**] and $K_2$[**2**], there is a distinct and unsymmetrical lengthening of Co-$C_{Cp}$ bond lengths. Indeed, for $K_2$[**2**] (Figure 4.12) a *ca.* 0.1 Å elongation of two Co-$C_{Cp}$ bond distances is observed relative to **2**. This structural feature is strongly suggestive of Cp ring slippage to an unsymmetric $\eta^3$-allyl/$\eta^2$-olefin form rather a symmetric $\eta^5$-Cp form due to the population of high-lying Co-Cp antibonding orbitals with successive addition of electrons.

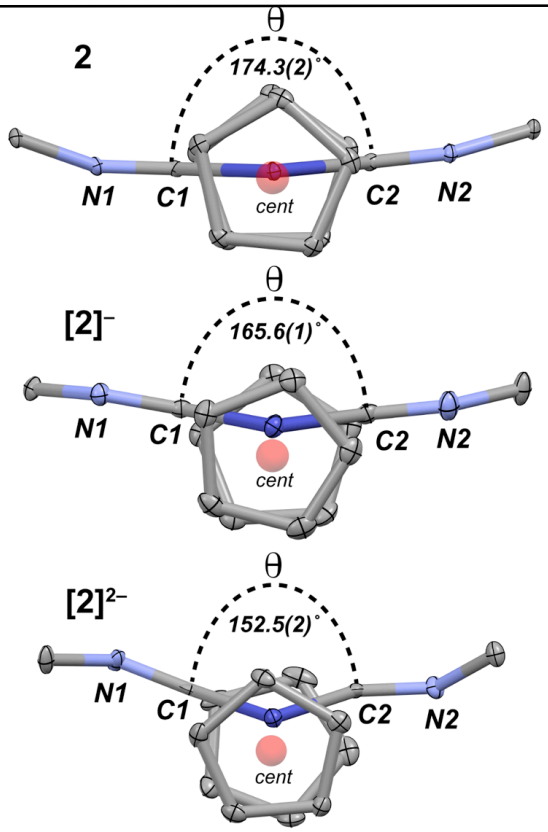


**Figure 4.12** Depiction of the central core of $[(\mu^2\text{–}CN^{ArMes})[CpCo]_2]^n$ (n = 0, –1, –2) dimers bisecting $Co_1$ and $Co_2$ emphasizing the centroid of the Cp–ring (red-dot). It is noted that upon sequential injection of electrons into the core (*e.g* (**2**) → K[**2**] → $K_2$[**2**]) the Cp rings cant below the plane of the core. Flanking *m*-terphenyl substituents, hydrogen atoms omitted for clarity.

Comparison of dimers $[\mathbf{2}]^n$ ($n$ = 0, –1, –2) to the $\eta^6$-arene containing dimers **5** and [**5**]$BAr^F{}_4$ further highlight the pitfalls of evaluating M-M bond multiplicity based on metal-metal separations. As mentioned above, dimers **5** and $[\mathbf{5}]^+$ are valence isoelectronic to the anions $[\mathbf{2}]^{2-}$ and $[\mathbf{2}]^-$, and the 18-electron rule likewise predicts formal Co-Co bond order of 1.0 and 1.5, respectively. However, upon oxidation of **5** to the radical cation [**5**]$BAr^F{}_4$, a small elongation of the Co-Co separation ($\Delta_{d(Co\cdots Co)}$= 0.0113; 0.5%) is observed. Although not as dramatic as a change seen from the oxidation of $K_2$[**2**] to K[**2**], this deviation is *reversed* from the CpCo dimers which exhibit a contraction in Co-

Co separation from reduced to oxidized forms. However, oxidation of **5** to [**5**]$BAr^{F}_{4}$ does result in slight contractions of the C-N bond of the isocyanide ($\Delta_{d(C\cdots N)Avg}$ = 0.017; 1.4%), in addition to an elongation of the Co-$C_{iso}$ bonds ($\Delta_{d(Co\cdots Ciso)Avg}$ = 0.00713; 0.4%) consistent with a decrease in π-backdonation to the bridging isocyanide ligand. Notably however, when comparing the metrical parameters of neutral **6** to dianion [**2**]$^{2-}$, or cation [**6**]$^{+}$ to monoanion [**2**]$^{-}$, a greater degree of Co-to-isocyanide π-backdonation is observed for the Cp derivatives, which is consistent with the FTIR spectroscopic signatures of the complexes.

To further highlight the subtleties of π-backdonation interactions within these dimers, it is important to also compare the structural and spectroscopic properties of $K_2$[**2**] with the valence-isoelectronic nickel dimer, (μ-$CNAr^{Mes2}$)$_2$[CpNi]$_2$ (**6**). While both $K_2$[**2**] and **6** are representatives of the $d^9$-$d^9$ configuration of [(μ-EO)$_2$[CpM]$_2$]$^n$ dimers, the core of the Ni-derivative **6** possesses both a neutral charge and a less π-basic[49] metal relative to $K_2$[**2**] and therefore should exhibit a diminished propensity for π-backdonation. Indeed, as noted above, the nickel dimer **6** exhibits a high energy $\nu_{CN}$ stretch of 1914 $cm^{-1}$ consistent with less π-backdonation from Ni to the isocyanide ligands relative to $K_2$[**2**]. In addition, nickel dimer **6** possesses elongated M–C bond lengths and contracted isocyanide CN bond distances when compared to $K_2$[**2**], which are also fully consistent with diminished M→π*(CN) π-backdonation (Table 4.1).

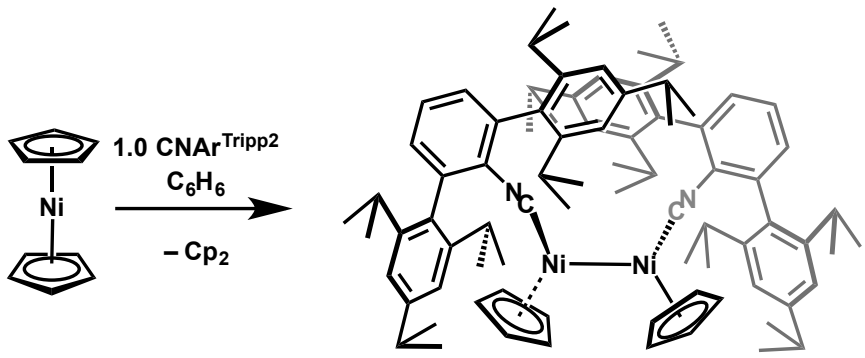


**Scheme 4.7** Synthetic process for the generation of $[CpNi(CNAr^{Tripp2})]_2$ (**8**).

Importantly however, this diminished π-backdonation significantly affects the ability of the isocyanide ligands to bridge the Ni centers in these dimers, such that the CN binding mode can be modulated by steric pressures of the *m*-terphenyl group.[80] For example, treatment of nicklocene with the more encumbering *m*-terphenyl isocyanide $CNAr^{Tripp2}$ ($Ar^{Tripp2}$ = 2,6-(2,4,6-$^{i}Pr_3$-$C_6H_3$)$_2$$C_6H_3$)[50] affords the nickel dimer $[CpNi(CNAr^{Tripp2})]_2$ (**7**, Scheme 4.7) which was determined by X-ray diffraction analysis to contain two terminally bound isocyanide units (Figure 4.13). Notably, dimer **7** is an exceedingly rare example of a dinuclear species possessing an unsupported Ni-Ni bond, with $K_4[Ni_2(CN)_6]$ and $[CpNi(PEt_3)]_2$ serving as the only prior examples.[81-82] Nickel dimer **8** exhibits a Ni-Ni bond length of 2.3797(10) Å, which is slightly elongated when compared to the Ni-Ni separation of the bridging isocyanide $Ni_2$ dimer **7 (**2.3484(19) Å). Importantly, geometry optimization of the unbridged truncated model $[CpNi(CNPh)]_2$ (**7m**) shows good structural correlation to **7** with a Ni-Ni separation of 2.3457 Å (*ca.* 1.5%) despite lacking the increased steric profile found with $CNAr^{Tripp2}$, which could potentially impose a larger Ni-Ni separation due to increased steric pressures (Figure 4.37).

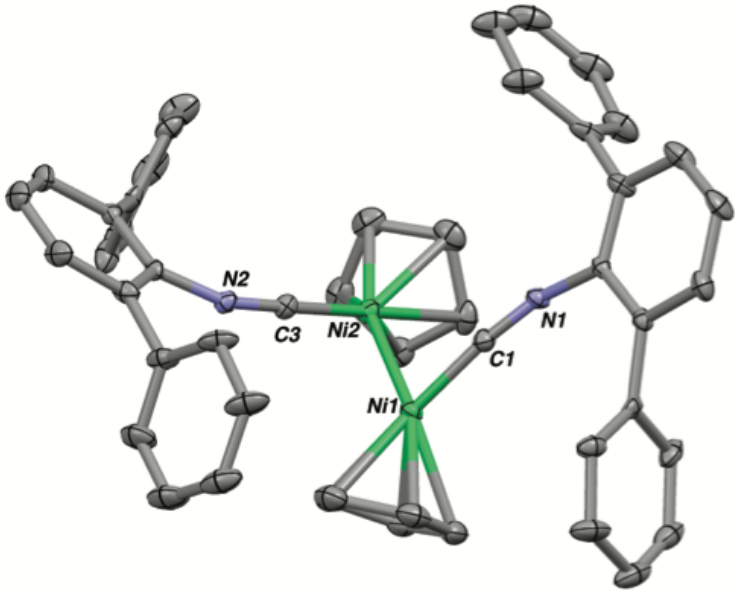


**Figure 4.13** Molecular Structure of ($\mu^2$–$CN^{ArMes}$)$[CpNi]_2$, (**8**); one molecule form the asymmetric unit depicted, hydrogen atoms, and disorderd *i*-Pr groups omitted for clarity**.** One half of complex **6** is symmetry generated and therefor both CpNi($CNAr^{Tripp2}$) fragments are crystallographic ally identical. Selected bond distances (Å) and angles (˚): Ni1-Ni2 = 2.345(1); Ni1-C1 = 1.755(6); C1-N1-C2 = 159.4(6).

Most notably, the unbridged dimer **7** displays a blue shifted isocyanide ν(CN) stretching frequency at 1997 $cm^{-1}$ (Figure 4.23) when compared to dimer **6**, which is consistent with terminally coordinated isocyanide ligands in solution. However, VT-FTIR spectroscopy revealed that upon cooling to –90 ˚C, unbridged **7** can be fully converted to a bridging-isocyanide isomer, as indicated by a red shifted ν(CN) stretch at 1896 $cm^{-1}$ (Figure 4.24). This stretch is comparable to that of the bridged $Ni_2$ dimer **7** (ν(CN) = 1914 $cm^{-1}$) when the more electron-releasing nature of $CNAr^{Tripp2}$ relative to $CNAr^{Mes2}$ is considered.[50] Accordingly, the observed temperature-dependent fluxionality in isocyanide coordination for **7** emphasizes the importance of strong π-backbonding interactions in stabilizing the bridged $(\mu^2\text{-AE})_2M_2$ (A = N, C; E = O, NR) core of these dimeric species. This observation also suggests that unsupported metal-metal bonds in

$[CpM(AE)]_2$ dimers may be accessible when sufficient steric pressures are coupled to a system where π-backbonding interactions to bridging ligands are diminished or inhibited. In fact, Stalk and Roesky have recently reported Co–Co interactions in the dimers $[[\eta^6\text{-arene})Co(cAAC)]_2]^{0/+}$ (cAAC = cyclicalkylaminocarbene) where such a situation begins to materialize for $d^9$-$d^9$ and $d^8$-$d^9$ pairs.[83]

**4.5 Bonding Analysis of $[(\mu^2\text{-}CNAr^{Mes2})_2[CpCo]_2]^n$ Dimers.**

Due to the discrepancy between the M-M separations of $[(\mu\text{-}EO)_2[CpCo]_2]^n$ dimers (E = C, $n$ = 0, 1–; E = N, $n$ = 0) as a function of reduction level and the predicted M-M bond multiplicity based on the 18-electron rule, the electronic structure properties of these species have received considerable attention. Early reports based on qualitative MO considerations influenced by the 18-electron rule argued that Co-Co multiple bonds were indeed present and that the mono-radical mono-anion, $[(\mu\text{-}CO)_2[CpCo]_2]^{1-}$ possessed an unpaired electron in a Co-Co π* orbital (for an overall formal bond order of 1.5).[12-13, 25] However, the consensus arising from later studies using more quantitative computational methods converged on an electronic structure environment where direct metal-metal bonds are not present for any $[(\mu\text{-}EO)_2[CpCo]_2]^n$ dimer, irrespective of charge state or identity of the bridging ligand.[14-15, 17-22,84] Instead, these analyses have concluded that the neutral $d^8$-$d^8$ dimer, $(\mu\text{-}CO)_2[CpCo]_2$ possesses completely filled $(\delta^4)/(\delta)^4$ and $(\sigma)^2/(\sigma)^2$ Co-Co orbital levels, while both the in-plane (relative to the bridging ligands) and out-of-plane Co-Co π-type orbitals are filled.[14,21] However, these π-type orbitals also have significant contributions from the bridging carbonyl ligands in the form of Co→CO π-backdonation interactions. Importantly, it is these multi-centered interactions between the two Co centers and the bridging CO/NO ligands that mitigate

any direct Co-Co bonding.[20-21, 47, 79] Notably, this view is supported experimentally by a series of photoelectron spectroscopic studies on $[(\mu^2\text{-EO})_2[\text{CpM}]_2]^n$ dimers, which did not reveal the presence of ionizations bands arising from a M-M bonding manifold.[14, 18-19, 21]

For the isocyanide system reported here, the DFT-calculated molecular orbitals for the truncated models $[(\mu^2\text{-CNPh})_2[\text{CpCo}]_2]^n$ ($[\mathbf{2m}]^n$; $n$ = 0, 1–, 2–) are also consistent with the absence of direct Co-Co bonding interactions. As shown in Figure 4.14A, the neutral dimer **2m** possesses filled $(\delta^4)/(\delta)^4$ (MO pairs = 110/111, 112/113) and $(\sigma)^2/(\sigma)^2$ (MO pair = 100/109) levels comprised from dxy, $dx^2\text{-}y^2$ and $dz^2$ pairs, respectively. The Co-Co π-oriented orbitals (i.e. dxz and dyz pairs) are represented by the filled molecular orbitals 114 and 115 and show clear participation of the CN π* orbitals of the bridging ligands indicative of Co→isocyanide π-backdonation. Notably, the LUMO calculated for **2m (**MO 116) is a π-type ($d_{yz}$ pair) Co-Co antibonding interaction that lacks a contribution from the CN π* orbitals. This is consistent with the $b_g$-symmetric nature (in idealized $C_{2h}$ symmetry) of this MO and agrees with the molecular orbital analysis of $(\mu^2\text{-CO})_2[\text{CpCo}]_2$ by both Green and Lichtenberger informed by PES spectroscopic data.[14, 21]

While the LUMO of **2m** ostensibly represents the site of reduction of neutral dimer **2**, DFT calculations reveal an energetic reordering of the highest-occupied molecular orbitals in monoanion $[\mathbf{2m}]^-$ and dianion $[\mathbf{2m}]^{2-}$ that emphasizes the importance of Co-to-bridging ligand π-backdonation in these dimers. Accordingly, the calculated SOMO for monoanion $[\mathbf{2m}]^-$ (MO 116; Figure 4.14A) is the in-plane Co→(CN)π*-backbonding interaction that corresponds to the HOMO, rather than LUMO, of neutral **2m**. This re-ordering renders the SOMO-1 of $[\mathbf{2m}]^-$ the $b_g$-type symmetric orbital that lacks participation of the bridging isocyanide CN π* orbitals. We

interpret this calculated re-ordering as a manifestation of unpaired-spin delocalization in [**2m**]$^{-}$ over the bridging ligands via π-backdonation, which would be precluded in a $b_g$-type SOMO that lacks bridging-ligand contributions. Notably, the in-plane $a_g$-type SOMO of [**2m**]$^{-}$ has equal participation from both Co centers, which is consistent with the 15-line EPR pattern observed for K[**2**] (Figure 4.6). However, the SOMO of [**2m**]$^{-}$ also suggests that nitrogen hyperfine coupling should also contribute to the EPR spectrum of K[**2**], and we contend that the lack of this hyperfine coupling is due to the relatively broad observed spectral linewidths. It is also important to note that an in-plane SOMO for [**2m**]$^{-}$ (and by extension K[**2**]) contrasts with early electronic structure analyses of the bridging carbonyl monoanion $[(\mu\text{-CO})_2[\text{CpCo}]_2]^{1-}$, which was based most predominantly on an apparent contraction of C-O bond lengths upon oxidation of $[(\mu\text{-CO})_2[\text{CpCo}]_2]^{1-}$ to $[(\mu\text{-CO})_2[\text{CpCo}]_2]$ via low-resolution X-ray crystallographic studies.[13] As mentioned above, the high-resolution X-ray structures of K[**2**] and **2** show an elongation of C-N bond lengths of the bridging isocyanide ligands, which is consistent with a greater degree of Co→(CN)π*-backdonation. As the out-of-plane $b_g$-type orbital does not feature contributions from the bridging isocyanides, the high-resolution structural data are consistent with these calculations and suggest an energetic orbital reordering is operative upon reduction of **2** to K[**2**]. Furthermore, this contention implies that the SOMO of K[**2**] is the in-plane orbital where π-backbonding to the bridging ligands can effectively delocalize the unpaired spin.

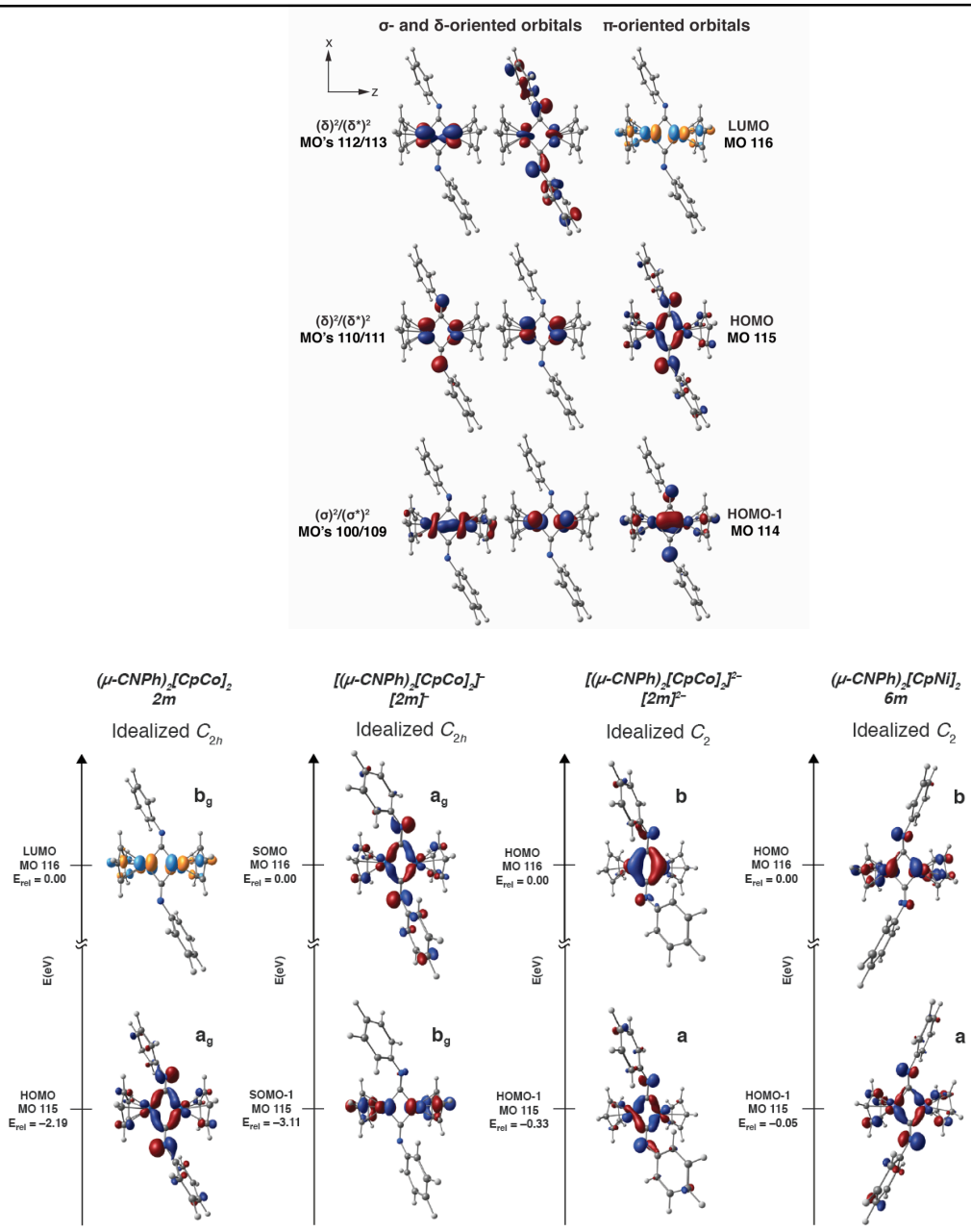


**Figure 4.14** A) Selected orbital interactions for (μ-CNPh)$_2$[CpCo]$_2$ (**2m**) depicting orbital pairs negating Co-Co bonding. B) Calculated SOMO/SOMO-1 and HOMO/HOMO-1 orbital interaction with corresponding energy gaps for [(μ-CNPh)$_2$[CpCo]$_2$]$^{-1/-2}$ (**2m**$^{-1/-2}$) and (μ-CNPh)$_2$[CpNi]$_2$ (**6m**). B3LYP def2-TZVP.

The DFT calculations also suggest that the ordering of the in-plane and out-of-plane π-oriented Co-based orbitals is again reversed upon reduction of monoanion [**2**]$^-$ to dianion [**2**]$^{2-}$, although the relative energetic separation between these highest-lying

occupied orbitals is quite small (~0.33 eV). Figure 4.14b shows that HOMO for the dianion $[\mathbf{2m}]^{2-}$ corresponds to the $b_g$-type LUMO for neutral **2m**. However, there is a distinct symmetry lowering from idealized $C_{2h}$ to $C_{2v}$ that renders the HOMO of $[\mathbf{2m}]^{2-}$ $b_2$-symmetric and allows the out-of-plane CN $\pi^*$ orbitals to contribute substantially to the MO featuring the $d_{yz}$-oriented Co orbitals. In effect, this symmetry breaking, which rationalizes the progressive core-puckering observed in the solid-state structures of **2**, K[**2**] and $K_2$[**2**], results in order to maximize π-backbonding interactions to the bridging ligands as electrons are successively added to the system. This effect is also observed in the calculated SOMO-1 of the monoanion $[\mathbf{2m}]^-$, in which a small contribution of the out-of-plane CN $\pi^*$ orbitals is apparent as the $Co_2C_2$ core distorts to lower symmetry. However, the contribution of these CN $\pi^*$ orbitals is to a far lesser than is present for $[\mathbf{2m}]^{2-}$, where two significant π-backbonding interactions are formed to accommodate the second electron equivalent. In this respect, it is important to note that the calculated HOMO for the neutral, puckered Ni dimer $(\mu^2\text{-CNPh})_2[\text{CpNi}]_2$ (**6m**), which is isoelectronic to $[\mathbf{2m}]^{2-}$, is similarly out-of-plane, $b_2$-symmetric-type in character (Figure 10). However, this orbital shows significantly diminished overlap between the Ni centers and the CN $\pi^*$ orbitals of the bridging ligands. We interpret this result as consistent with both the neutral charge of the dimer and the weaker π-basicity of Ni relative to Co,[49] and contend that this diminished π-backbonding is the origin of the ability of sterics to modulate[81] bridged and un-bridged isomers as observed experimentally for complexes **6** and **7**.

Two additional features of the DFT calculations on models $[\mathbf{2m}]^n$ are worthy of mention. First, whereas the molecular orbitals of $[\mathbf{2m}]^n$ rationalize the structural

perturbations of the $M_2C_2$ core with varying electron occupation, they also point to the origin of the progressive Cp-ring slippage observed upon reduction of **2** to $[\mathbf{2}]^-$ and $[\mathbf{2}]^{2-}$. As shown in Figure 4.14A, both the in-plane and out-of-plane π-oriented Co orbitals are Co/Cp anti-bonding in character,[85] in addition to being either $Co_2/(\pi^*CN)$ non-bonding or π-backbonding. Accordingly, as pointed out in prior electronic structure analyses,[13, 17, 21] population of these MOs should destabilize the Co/Cp bonding interactions and lead readily to an asymmetry in the hapticity of the Cp binding mode. Second, it is instructive to compare the calculated Mayer bond order (MBO)[86-88] for the Co-Co vector in models $[\mathbf{2m}]^n$. As pointed out by Parkin,[79] comparison of Mayer bond orders for a homologous series of complexes provides for particularly useful self-consistent comparisons when evaluating M-M bond multiplicities. Notably, the neutral dimer **2m** gives rise to a computed MBO of 0.713. While this value does not preclude the existence of direct Co-Co bonding, it is clearly far lower than MBO values of other complexes possessing M-M double bonds.[79, 88] In addition, the computed MBO values for $[\mathbf{2m}]^-$ and $[\mathbf{2m}]^{2-}$ are 0.702 and 0.518, respectively. These MBO changes, which range from negligible to small, and are inconsistent with the MBO variation expected for integer changes in formal M-M bond order calculated in other systems.[79, 88] However, such MBO insensitivity for the models $[\mathbf{2m}]^n$ is consistent with the negligible changes in Co-Co bond distances observed experimentally for dimers $[\mathbf{2}]^n$. Accordingly, we believe these small MBO values, their insensitivity to increases in electron occupation and the presence of significant multi-centered interactions to the bridging isocyanide ligands, argue strongly against the presence of direct M-M bonds in any of these dimers.

**4.6 Concluding Remarks**.

Reported here is the synthesis, structural characterization and bonding analysis of the dimeric cyclopentadienyl Co complexes $[(\mu\text{-CNAr}^{Mes2})_2[CpCo]_2]^n$ ($n$ = 0, 1–, 2–). These dimers represent the first example of homologous series spanning the formal $d^8$–$d^8$, $d^8$–$d^9$, $d^9$–$d^9$ triad of $[(\mu\text{-EO})_2[CpCo]_2]^n$–type complexes , and allows for systematic comparison of geometric and electronic structure features upon addition or removal of electrons from the system. Notably $K_2$[**2**] is an analogue to the bridging-carbonyl dianion $[(\mu\text{-CO})_2[CpCo]_2]^{2-}$, which has not been amenable to isolation. Due to the less disparate orbital energies between isocyanides (CNR) and CO, relative to NO and CO, a more accurate comparison to the classic bridging-carbonyl system can be made, especially for the formal $d^9$–$d^9$ configuration. Computational analysis of the orbital interactions in these bridging isocyanide dimers suggests that the electronic and geometric structure within the $(\mu\text{-CNR})_2M_2$ core is dictated by significant π-backbonding interactions with the bridging ligands rather than through direct metal-metal bonds. In addition, these features are modulated as a function of electron occupation of the highest-lying $(\mu\text{-CNR})_2M_2$-based orbitals, which are p-backbonding in nature. These electronic/structure trends can be readily extended to $[(\mu\text{-CNR})_2[(arene)Co]_2]^n$ ($n$ = 0, 1+), which represent formal $d^8$–$d^9$ and $d^9$–$d^9$ pairs, as well as the formal $d^9$–$d^9$ Ni dimer $(\mu\text{-CNR})_2[CpNi]_2$. However, the bridging-isocyanide ligands in $(\mu\text{-CNR})_2[CpNi]_2$ complexes can isomerize to a terminal bridging mode when increased steric pressures are introduced to the system. Given the weaker π-basicity of Ni relative to Co, this observation punctuates the importance of π-backbonding interactions to the bridging ligands as a dominant electronic structure feature of this class of dinuclear complexes.

**Table 1.** Comparative bond metrics for late transition metal dimers supported with π-acidic ligands.

| Compound/ Parameter | $M_1$-$M_2$ Å | $M_1$-$C_1$ Å | $M_1$-$C_2$ Å | $M_2$-$C_1$ Å | $M_2$-$C_2$ Å | $C_1$-$E_1$ Å | $C_2$-$E_2$ Å | ($C_1$-$M_1$-$C_2$-$M_2$) angle (°) |
|---|---|---|---|---|---|---|---|---|
| | | | | | | | | |
| (**2**)[a] | 2.3484(6) | 1.886(4) | 1.887(4) | 1.876(4) | 1.891(4) | 1.207(5) | 1.205(5) | 174.3(2)° |
| ($\mu^2$-CNPh)$_2$[CpCo]$_2$[b] (**2m**) | 2.336 | 1.8513 | 1.8618 | 1.8465 | 1.8572 | 1.2248 | 1.2224 | 178.38° |
| ($\mu^2$-CO)$_2$[CpCo]$_2$[b] | 2.3409 | 1.8436 | 1.8446 | 1.8444 | 1.8456 | 1.753 | 1.753 | 174.34° |
| | | | | | | | | |
| K[**2**][a] | 2.3513(5) | 1.844(3) | 1.852(3) | 1.859(3) | 1.854(3) | 1.250(3) | 1.248(4) | 165.6(1)° |
| [**5**]BAr$^F$[a] | 2.4044(7) | 1.889(4) | 1.830(4) | 1.839(3) | 1.903(3) | 1.233(4) | 1.230(4) | 177.09(14)° |
| PPN[($\mu^2$-CO)$_2$[CpCo]$_2$][a] | 2.3656(2)[c] | 1.80(2)[c] | 1.84(2)[c] | 1.84(2)[c] | 1.80(2)[c] | 1.21(2)[c] | 1.21(2)[c] | 180° |
| [($\mu^2$-CNPh)$_2$[CpCo]$_2$]$^{-}$[b] [**2m**]$^-$ | 2.3333 | 1.85119 | 1.8606 | 1.854 | 1.8503 | 1.2258 | 1.2223 | 168.54° |
| [($\mu^2$-CO)$_2$[CpCo]$_2$]$^{-}$[b] | 2.4042 | 1.835 | 1.8336 | 1.8339 | 1.8347 | 1.1922 | 1.1924 | 179.25° |
| | | | | | | | | |
| K$_2$[**2**] [a] | 2.4120(10) | 1.846(5) | 1.858(5) | 1.857(5) | 1.830(5) | 1.279(6) | 1.286(6) | 152.49(2)° |
| (**5**) [a] | 2.3894(7) | 1.894(3) | 1.832(3) | 1.814(3) | 1.890(3) | 1.246(4) | 1.251(4) | 151.6(1)° |
| (**6**) [a] | 2.3797(10) | 1.867(6) | 1.891(6) | 1.870(6) | 1.887(6) | 1.211(7) | 1.192(7) | 157.3(2)° |
| [($\mu^2$-CNPh)$_2$[CpCo]$_2$]$^{2-}$[b] [**2m**]$^{2-}$ | 2.373 | 1.8428 | 1.8181 | 1.8446 | 1.8152 | 1.2768 | 1.2774 | 133.13° |
| [($\mu^2$-CO)$_2$[CpCo]$_2$]$^{2-}$[b] | 2.4141 | 1.83 | 1.8311 | 1.8314 | 1.8311 | 1.2133 | 1.2133 | 129.32° |
| ($\mu^2$-CO)$_2$[CpNi]$_2$ [a] | 2.3627(9) | 1.856(5) | 1.874(5) | 1.862(6) | 1.853(5) | 1.156(6) | 1.169(6) | 150.9° |
| ($\mu^2$-CNMe)$_2$[CpNi]$_2$ [a] | 2.3217 | 1.9057 | 1.8688 | 1.8577 | 1.8925 | 1.1928 | 1.1957 | 138.67° |
| Co$_2$(CO)$_8$ [a] | 2.526 | 1.93 | 1.93 | 1.95 | 1.95 | 1.18 | 1.19 | 142.81° |

Structural measurements for [a]Complexes are taken from crystallographic structure determinations. Parameters for [b]Complexes are computationally derived from geometry optimized coordinates using the OCRA computational suite utilizing the B3LYP functional with Def2-TZVP/ Def2-TZVPJ basis set/auxiliary basis set (see secion 4.). [C]Compound measurements are the average of 2 crystallographically independent molecules within an asymmetric unit.

**4.7 Synthetic Procedures and Characterization Data.**

**General Considerations:** All manipulations were carried out under an atmosphere of dry dinitrogen or Argon using standard schlenk, and glove box techniques. Solvents were dried and degassed according to standard procedures.[92] Unless otherwise stated all materials were obtained from commercial vendors and used as received or purified by by standard procedures.[93] Benzene-$d_6$ was dried with Na/K and Benzophenone followed by distillation and storage on 4 Å molecular sieves for 3 days prior to use. Celite 405 (Fischer Scientific) was dried under vacuum for 24 hours at a temperature greater then 250° C and stored inside the glove box prior to use. $KC_8$ was prepared according to published procedures.[94] The *m*-terphenyl isocyanide $CNAr^{Mes2}$,[52] $CpCoI_2(CO)$[95] were prepared according to literature procedures. Ferrocenium triflate (FcOTf, OTf = $OSO_2CF_3$) was prepared via the reaction between Ferrocene and AgOTf in $CH_2Cl_2$.

Solution $^1H$, $^{13}C\{^1H\}$ NMR spectra were recorded on a Varian Mercury 300, and 400, Varian XSENS-500, and Joel ECA 500 spectrometers. $^1H$, and $^{13}C$ chemical shifts are reported in ppm relative to $SiMe_4$ ($^1H$ and $^{13}C$ $\delta = 0.0$ ppm) with reference to residual $C_6D_5H$ or solvent references of 7.16 ppm (1H) and 128.06 ppm ($^{13}C$) for benzene–$d_6$.[96] FTIR spectra were recorded on a Thermo-Nicolet iS10 FTIR spectrometer. Samples were prepared either as KBr pellets, $C_6D_6$ solutions injected into a Thermo Fischer solution cell equipped with KBr windows, or prepared as a Nujul Mull on KBr plates. For solution FTIR spectra, solvent peaks were digitally subtracted from all spectra by comparisons with an authentic spectrum obtained immediately prior to that of the sample. The following abbreviations were used for the intensities and characteristic of important

IR absorption bands: vs = very strong, s = strong, m = medium, w = weak, vw = very weak, b = broad, vb = very broad, sh = shoulder. Combustion analyses were performed by Midwest Microlab LLC, Indianapolis, IN

**Synthesis of ($\eta^5$-*Cp*)$CoI_2$($CNAr^{Mes2}$) (1):** Additional care was taken to remove excess Iodine from $CpCoI_2(CO)$: $CpCoI_2(CO)$ was taken up in 50 mL of $CH_2Cl_2$ where it was then subject to an aqueous work up followed by washing 3x200 mL 1M $Na_2S_2O_3$ to quench excess Iodine. The organics were then dried over $Na_2SO_4$ followed by filtration over a medium porosity glass sintered frit and concentration via rotary evaporation to a purple microcrystalline solid. Upon isolation of crystalline $CpCo(CO)I_2$ (1.0409g, 2.565 mmol, 1 equiv.) was dissolved in 50 mL of Benzene ($C_6H_6$), where $CNAr^{Mes2}$ (0.8701 g, 2.565 mmol, 1.0 equiv.) was added as a solid. The reaction mixture was allowed to react for 12 hours at room temperature, where upon all volatiles were removed in *vacuo*. The resulting purple solid was then isolated and transferred to a medium porosity glass sintered frit where it was then washed with *n*-pentane (3x20mL) to remove impurities, yielding $CpCoI_2(CNAr^{Mes2})$ as a purple solid 1.74 g, 2.43 mmol, 94.6%. X-ray quality crystals were grown from a saturated $Et_2O$ solution at -40$^o$C over the course of 3 days. $^1$HNMR (500MHz, $C_6D_6$, 20$^\circ$ C) δ = 6.97 (*t*, 1H, $J_{H-H}$ = 8 Hz, *o*-Ph), 6.89 (*s*, 4H, *m*-Mes), 6.85 (*d*, 2H, $J_{H-H}$ = 8Hz, *m*-Ph), 4.38 (*s,* 5H, *Cp*-H), 2.17 (s, 18H, *o,p*-C$H_3$ Mes). It is noted that appearance of one singlet results in coalescence of the C$H_3$ resonances of the mesityl ligands. $^{13}C\{^1H\}$ NMR (500MHz, $C_6D_6$, 20$^\circ$ C) δ = 150.68 (*C*NR), 140.17, 138.23, 136.11, 134.1, 129.96, 129.4, 129.01, 128.59, 128.35, 86.73 (*Cp-C*), 21.18 (*p-C*$H_3$ Mes), 20.85 (*o-C*$H_3$ Mes) ppm. FTIR solution ($C_6D_6$) $\nu_{CN}$: 2168 (s), also 1611 (w),

1331 (w), 1024 (w), 835 (w) 680 (m). Analytically pure crystals can be grown from a saturated $CH_2Cl_2$ layered with hexanes over 3 days. Anal. Calc. $CoC_{30}H_{30}NI_2$: C, 56.96; H, 6.15; N, 1.58. Found: C, 57.01; H, 6.30; N, 1.60.

**Synthesis of $K_2[(\mu\text{-}CNAr^{Mes2})_2[CpCo]_2]$, $K_2$[2], from the reduction of $CpCo(CNAr^{Mes2})I_2$ with $KC_8$:** This synthesis is best done on a scale uses less then 150 mg of $(\eta^5\text{-Cp})Co(CNAr^{Mes2})I_2$ and then combined with additional reactions to yield the desired product. A typical synthesis: (**1**) (98.7mg, 0.1376 mmol, 1 equiv) was dissolved in a 2:1 mixture of $Et_2O$/DME (9mL total) and frozen in the Coldwell. Upon thawing $KC_8$ was added (186.0 mg, 1.376 mmol, 10 equivalents) and the solution and allowed to stir for 15 minuets, where it was refrozen in the cold well in 3 minuet intervals for 1 minuet. The resulting reaction mixtures were filtered over 3 cm of Celite packed on a medium porosity frit to remove KI, and excess $KC_8$. The solution was concentrated in *vacuo* to 3 mL where upon 20 mL of cold *n*-pentane was rapidly added to precipitate out the desired product followed by evaporation to dryness to yield a dark brown solid 0.066 g, 0.059 mmol, 91%. X-ray diffraction quality crystals can be grown from a saturated solution of $Et_2O$ at -40° C for 2 days to give $K_2(Et_2O)_2[(\mu^2\text{-}CNAr^{Mes2})\ [CpCo]_2]$, $K_2(Et_2O)_2$[**2**]. $^1$HNMR (400MHz, $C_6D_6$, 20°C) δ = 6.88 ( 6H, *m,o*-Ph), 6.73 (*s*, 8H, *m*-Mes), 4.46 (*s,* 10H, *Cp*-H), 2.46 (s, 24H, *p*-C*H*$_3$ Mes), 2.15 (s, 12H, *o*-C*H*$_3$ Mes). $^{13}C\{^1H\}$ NMR (500MHz, $C_6D_6$, 20°C) δ = 265.07 (*C*NAr$^{Mes2}$), 142.97, 141.67, 138.30, 135.33, 130.89, 129.16, 127.54, 116.75, 82.23 (*Cp-C*), 21.58 (*o,p-C*H$_3$ Mes) ppm. FTIR solution ($C_6D_6$): 2984 (w), 2947 (w), 2919 (w), 2816 (w), $\nu_{CN}$: 1510 (vs), 1818 (sh) also 1480 (sh), 1397 (m), 1377 (sh), 1108 (w), 857 (w). Fractional recrystallization from *n*–

hexane layered atop THF (10:1) yields analytically pure crystals of $K_2(THF)_2[(\mu^2\text{-}CNAr^{Mes2})\ [CpCo]_2]$, $K_2(THF)_2$[**2**], Anal. Calc. $K_2Co_2C_{68}H_{76}N_2$: C, 71.06; H, 6.66; N, 2.44. Found: C, 70.33; H, 6.54; N, 2.43.

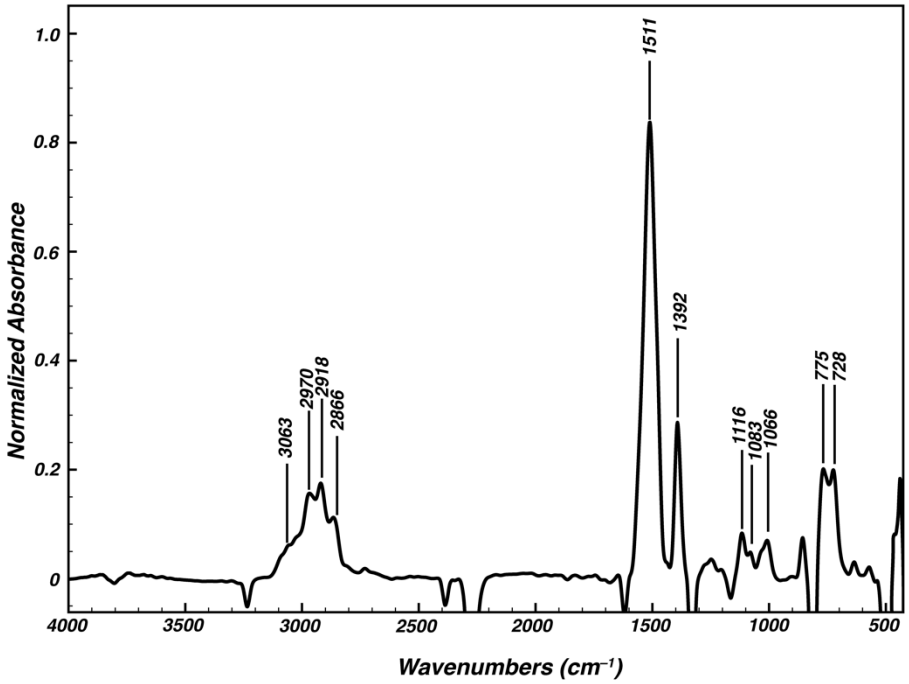


**Figure 4.15** Room–temperature solution–state FTIR spectrum ($C_6D_6$) of $K_2[(\mu\text{-}CNAr^{Mes2})_2[CpCo]_2]$; ($K_2$[**2**]).

**Synthesis of $K[(\mu\text{-}CNAr^{Mes2})_2[CpCo]_2]$, K[2], from the oxidation of $K_2[(\mu\text{-}CNAr^{Mes2})_2[CpCo]_2]$, $K_2$[2] with TlOTf:** To a thawing solution of $K_2$[**2**] (100.3 mg, 0.08461 mmol, 1 equiv) in DME (4mL) an equally cold solution of TlOTf (32.9 mg, 0.0931 mmol, 1.1 equiv) in DME (1mL) was added drop wise over the course of 2 minuets. The reaction mixture was allowed to stir for 10 minuets with intermittent cooling in the cold well, where upon a color change from dark brown to deep red-orange was observed. The resulting solution was then filtered over 3 cm of Celite packed on a fiberglass filter pad. Following filtration the solution was concentrated to a solid where it

was then subject 2x3 mL slurries in *n*-pentane followed by evaporation to dryness to de-solvate any remaining KOTf. The resulting solid was then slurried in 3 mL of *n*-pentane and filtered of fiberglass to yield a red brown solid. Dissolution of the solid in $C_6H_6$, followed by removal of all volatiles under reduced pressure to yield a red-brown solid 0.064 g, 0 066 mmol, 78.3%. X-ray quality crystals were grown from a saturated $Et_2O$ solution at –40° C over the course of 3. $\mu_{eff}$ (Evans Method; $C_6D_6$ with $(Me_3Si)_2O$ reference, 500.2 MHz, 20 °c, 5 runs) = 1.74 (±0.05) $\mu_B$. FTIR solution ($C_6D_6$): 3035 (w), 2950 (w) 2919 (w) 2854 (w), $\nu_{CN}$: 1664 (vs) 1611 (sh), 1571 (s) 1399 (m). Fractional recrystallization from *n*–hexane layered atop THF (10:1) yields analytically pure crystals of $K(THF)[(\eta^5\text{-}Cp)_2Co_2(\mu^2\text{-}CNAr^{Mes2})]_2$ Anal. Calc. $Co_2C_{64}H_{68}N_2K$: C, 74.04; H, 6.60; N, 2.70. Found: C, 73.36; H, 6.82; N, 2.74.

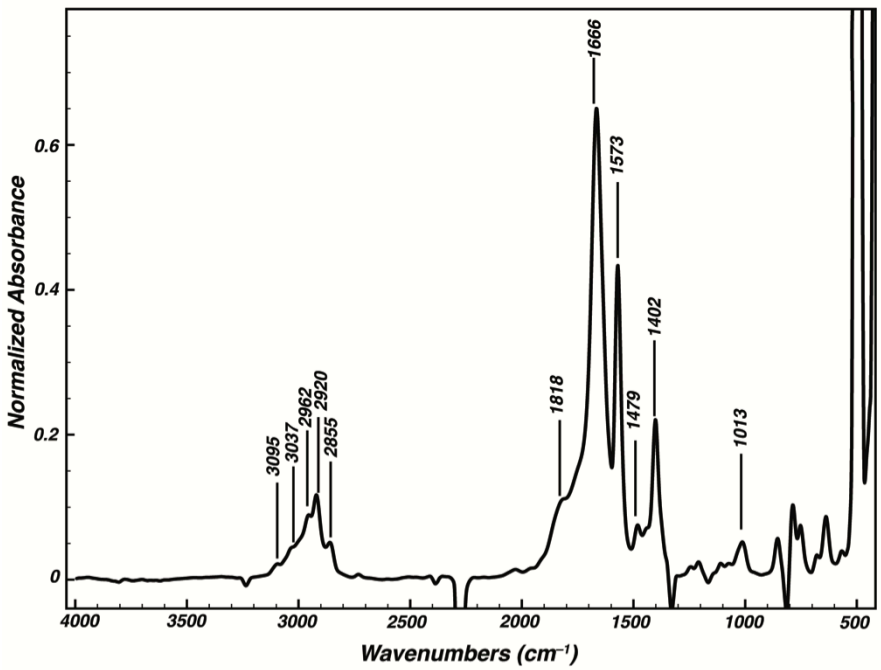


**Figure 4.16** Room–temperature solution–state FTIR spectrum ($C_6D_6$) of $K[(\mu^2\text{-}CNAr^{Mes2})_2[CpCo]_2]$; (**K[2]**).

**Synthesis of K[($\mu^2$-CNAr$^{Mes2}$)$_2$[CpCo]$_2$], K[2], from the reduction of ($\eta^5$-Cp)CoI$_2$(CNAr$^{Mes2}$), (1), with $KC_8$:** To a thawing solution of (**1**) (236.1 mg, 0.3292 mmol, 1 equiv) in a 2:1 $Et_2O$/DME (9 mL) $KC_8$ (137.9 mg, 1.0210 mmol, 3.1 equiv) was added. The reaction mixture was allowed to stir for 10 minuets, where upon a color change from dark purple to green to deep red-orange to was observed. The resulting solution was then filtered over 3cm of Celite packed on a fiberglass filter pad. Following filtration the solution was concentrated to a solid where it was then subject 2 x 3 mL slurries in *n*-pentane followed by evaporation to dryness to de-solvate any remaining salts. The resulting solid was then slurried in 3 mL of *n*-pentane and filtered of fiberglass to yield a red brown solid followed by dissolution in $C_6H_6$, followed by removal of all volatiles under reduced pressure to yield a red-brown solid. The resulting solid was recrystallized from a 3:1 $Et_2O$/DME solution at –40$^{\circ}$ C over 2 days to yield red crystals, 0.124 g, 0.129 mmol, 78.3 %.

**Synthesis of K[($\mu^2$-CNAr$^{Mes2}$)$_2$[CpCo]$_2$], K[2], from the comporportinaiton of K$_2$[($\eta^5$-Cp)$_2$Co$_2$($\mu^2$-CNAr$^{Mes2}$)$_2$], K$_2$[2] and ($\eta^5$-Cp)$_2$Co$_2$($\mu^2$-CNAr$^{Mes2}$)$_2$, (2):** A solution of K$_2$[**2**] (14.3 mg, 0.0142 mmol, 1 equiv) in DME (3mL) was frozen in the cold-well. Separately a solution of ($\mu^2$-CNAr$^{Mes2}$) [CpCo]$_2$ (13.2 mg, 0.0142 mmol, 1 equiv) in DME (2mL) was also frozen in the cold-well. Upon thawing the solution of (**2**) was added drop wise to the stirring solution of K$_2$[**2**]. The reaction mixture was allowed to stir for 30 minuets and warm to room temperature, where a color change to red-orange was observed, at which point all volatiles were removed *in vacuo* to yield a red-orange solid which was washed with 3 X 2mL *n*-pentane and dried under reduced pressure,

0.025 g, 0.026 mmol, 92%. A solution phase FTIR in $C_6D_6$ exhibited the characteristic IR spectra of K[($\mu^2$-CNAr$^{Mes2}$) [CpCo]$_2$] as described above with no trace of either $K_2$[**2**] or (**2**), characteristic *v*(CN) stretches at 1510, and 1834 cm$^{-1}$ respectively.

**Synthesis of ($\mu^2$-CNAr$^{Mes2}$)$_2$[CpCo]$_2$, (2), from the reduction of ($\eta^5$-*Cp*)CoI$_2$CNAr$^{Mes2}$, (1), with KC$_8$:** ($\eta^5$-*Cp*)CoI$_2$(CNAr$^{Mes2}$) (0.225 g, 0.314 mmol, 1 equiv) was dissolved in a 2:1 $Et_2O$/DME mixture and frozen in the cold well. Upon thawing $KC_8$ (0.0848 g, 0.627 mmol, 2 equivs) was added and allowed to stir for 15 minutes with intermittent cooling in the cold well every 5 minuets (2 X 2 minutes). Upon observation of a color change from purple to green the reaction mixture was filtered over Celite packed on a medium porosity glass sintered frit followed by evaporation to dryness. The green residue was taken up in *n*–pentane (15 mL) and stirred for 15 minutes followed by evaporation to dryness to desolvate any residual KI. This procedure was repeated 2 additional times. Following, the green residue was taken up in *n*–pentane and filtered over Celite packed on a medium porosity glass sintered frit and evaporated to dryness. The resulting green solid was recrystallized from a minimal amount of $Et_2O$ (1 mL) at –40˚ C to yield green X–ray diffraction quality crystals after 48 hours, 0.127 g, 0.137 mmol, 87.6 % yield. $^1$HNMR (500MHz, $C_6D_6$, 20˚ C) δ = 7.24 (*d*, 4H, $J_{H\text{-}H}$ = 8 Hz, *m*-Ph), 6.93 (*t*, 2H, $J_{H\text{-}H}$ = 8 Hz, *p*-Ph), 6.71 (*s,* 8H, *m*-Mes), 3.88 (*s,* 10H, *Cp-H*), 2.34 (*s*, 24H, *o*-C*H*$_3$ Mes), 2.06 (*s*, 12H, *p*-C*H*$_3$ Mes) ppm. $^{13}$C{$^1$H} NMR (500MHz, $C_6D_6$, 20˚ C) δ = 208.86 ($\mu^2$-*C*NAr$^{Mes2}$), 137.18, 136.91, 136.25, 134.61, 133.61, 128.7, 128.59, 128.04, 82.99 ($\eta^5$-*Cp*), 21.09 (*o*-*C*H$_3$ Mes), 21.03 (*p*-*C*H$_3$ Mes) ppm. FTIR solution (*$C_6D_6$*) $\nu_{CN}$: 1854 (sh), 1834 (vs), also 3036 (w), 2949 (w), 2918 (w), 2853 (w), 1576 (m), 1485 (w), 1403 (m),

1376 (w), 1210 (m), 1112 (w), 1032 (w), 1005 (w) 853 (w), 803 (w), 781 (w), 752 (w), 681 (w), 632 (w), 566 (w) $cm^{-1}$. Anal. Calc. $Co_2C_{60}H_{60}N_2$: C, 77.74; H, 6.52; N, 3.02; Found: C, 74.10; H, 6.10; N, 3.02. Repeated attempts to obtain a more satisfactory elemental analysis were unsuccessful and we believe this is due to a thermal degradation process available to neutral dimer **2**. A $^1H$ NMR spectrum of **2** to establish purity is shown in Figure 4.17.

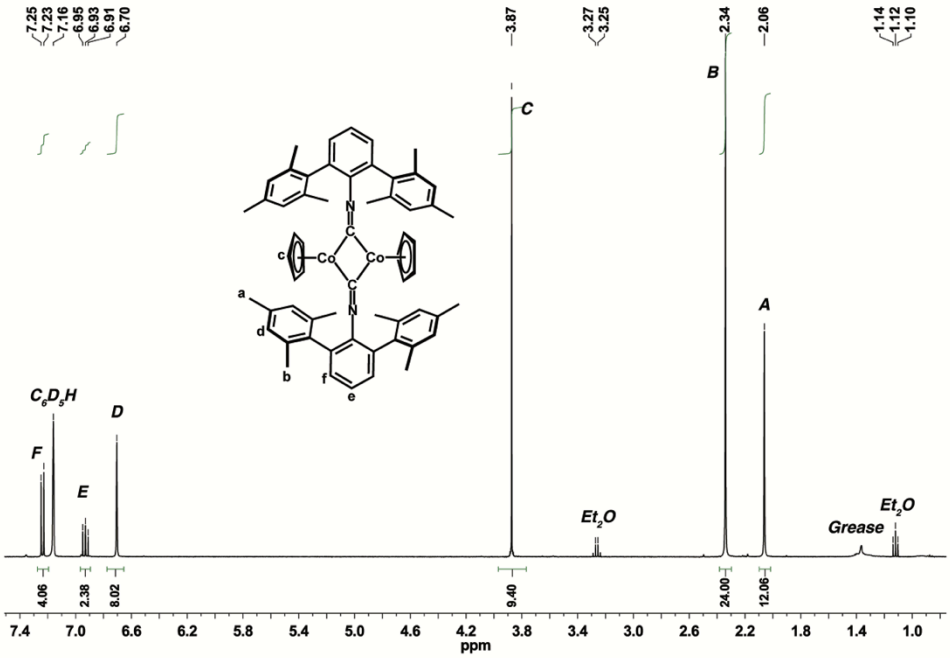


**Figure 4.17** Room temperature $^1H$ NMR spectrum of $(\mu^2\text{-}CNAr^{Mes2})_2[CpCo]_2$, (**2**) ($C_6D_6$).

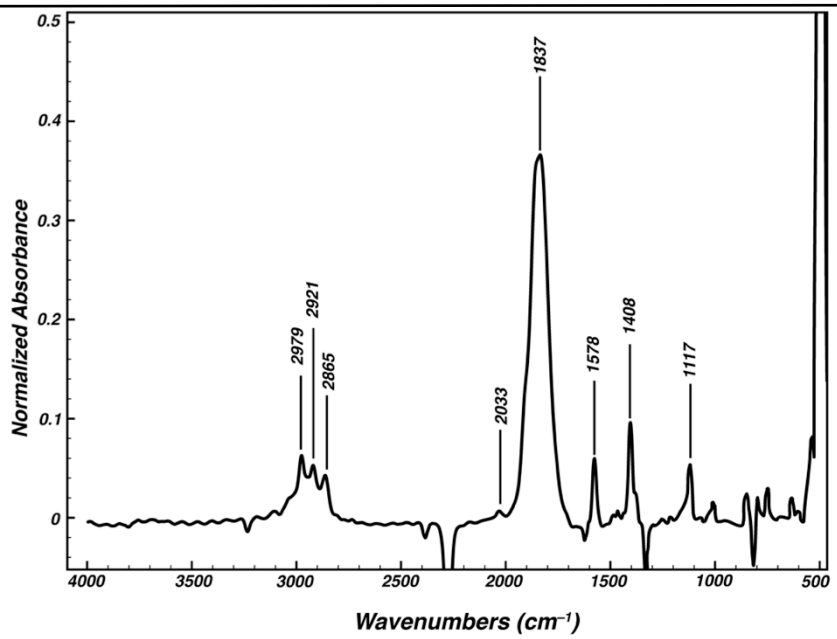


**Figure 4.18** Room–temperature solution–state FTIR spectrum ($C_6D_6$) of $(\mu^2\text{-CNAr}^{Mes2})_2[CpCo]_2$; **(2)**.

**Synthesis of $(\mu\text{-CNAr}^{Mes2})_2[CpCo]_2$, (2), from the oxidation $K_2[(\mu\text{-CNAr}^{Mes2})_2[CpCo]_2]$, $K_2$[2], with TlOTf:** To a thawing solution of $K_2$[**2**] (0.0510 g, 0.0507 mmol, 1 equiv) in a 4:1 mixture of $Et_2O$/ DME (4 mL) an equally cold slurry of FcOTf (0.0340 g, 0.102 mmol, 2 equiv) in $Et_2O$ (2mL) was added drop wise over the course of 1 minute. The reaction mixture was allowed to warm to room temperature over the course of 30 minutes were a color change from brown to red–orange was observed followed by an additional color change from red orange to dark green. Upon completion the reaction mixture was concentrated to a solid where the resulting green/orange residue was washed slurried in 5 mL of *n*-pentane followed by evaporation to dryness to desolvate KOTf. This process was repeated two additional times. The resultant solid was then extracted into $Et_2O$ (4 mL) and filtered over Celite (2 cm) packed on a fiberglass pad followed by concentration to *ca.* 0.75 mL and placed in the freezer for

recrystallization. 24 hours at –40˚ C yielded dark green plates of (**2**), 0.0121 g, 0.0130, 26 %, which was judged pure by $^1$H NMR.

**Synthesis of ($\mu^2$-CNAr$^{Mes2}$)$_2$[CpCo]$_2$, (2), from the oxidation K[($\mu^2$-CNAr$^{Mes2}$)$_2$[CpCo]$_2$], K[2], with FcOTf:** To a thawing solution of K[**2**] (0.0313 g, 0.0324 mmol, 1 equivs) in a 4:1 $Et_2O$/DME FcOTf (0.0108 g, 0.0324 mmol, 1 equiv) was added. The reaction mixture was allowed to warm to room temperature and stir for 30 minutes whereupon a color change from red–orange to green was observed. Thereafter the reaction mixture was concentrated to a solid under reduced pressure. The orange green solid was then slurried in 5 mL of *n*–pentane and stirred for 10 minutes followed by evaporation to dryness. This process was repeated two additional times to desolvate KOTf. Following evaporation to dryness the solid was extracted into $Et_2O$ (3 mL) and filtered over Celite (2cm) packed on fiberglass and concentrated to *ca.* 0.75 mL whereupon the mixture was placed in the freezer for recrystallization at –40˚ C. After 24 hours deep green plates of (**2**) were isolated 0.0113 g, 0.0122 mmol, 38 % yield, and judged pure by $^1$H NMR.

**Synthesis of CpCoI(CNAr$^{Mes2}$), (3) from the reduction of CpCoI$_2$(CNAr$^{Mes2}$), (1), with $KC_8$ :** To a solution of (**1**) (0.358 g, 0.499 mmol, 1 equiv) dissolved in 75 mL of $Et_2O$ and frozen in the cold well. Upon thawing $KC_8$ (0.0742 g, 0.599 mmol, 1.1 equiv) was added, and allowed to stir for 20 minutes and warm to room temperature. The reaction mixture was filtered over Celite packed on a glass-sintered frit to remove $C_8$ and KI. The solution was then concentrated to a *ca*. 2 mL and allowed to stand until

precipitation of an orange solid was observed. The purple orange slurry was then filtered over a medium glass sintered frit yielding an orange solid that was washed with a *n*-pentane (20 mL) yielding an CpCoI($CNAr^{Mes2}$), (**3**) as an orange solid 0.144 g, 0.244 mmol, 49%. $^1$HNMR (500MHz, $C_6D_6$, 20°C) δ = 9.07 (*s*, 2H, J, *m*-Ph), 6.65 (*s*, 4H, *m*-Mes), 4.29 (*s,* 5H, *Cp*-H), 2.93 (s, 12H, *p*-C*H*$_3$ Mes), 1.70 (s, 6H, *o*-C*H*$_3$ Mes). $\mu_{eff}$ (Evans Method; $C_6D_6$ with $(Me_3Si)_2O$ reference, 500.2 MHz, 20 ˚C, 5 runs) = 1.9 (±0.08) $\mu_B$. FTIR ($C_6D_6$; KBr Window; 20 ˚C): $\nu_{CNR}$ =: 2126 (s), also 3036 (w), 2970 (w), 2951 (w), 2914 (w), 2848 (w), 1419 (w), 1374 (w), 1008 (w), 849 (w), 758 (w), 678 (w). Anal. Calc. $CoC_{30}H_{30}NI$: C, 61.03; H, 5.12; N, 2.37. Found: C, 60.74; H, 4.98; N, 2.21.

**Synthesis of [$Cp_2Co_2(\mu$-I)($CNAr^{Mes2}$)$_2$]OTf, [4]OTf:** To a stirring solution of (**3**) (0.091 g, 0.173 mmol, 1 equivs) in $Et_2O/C_6H_6$ (3:1; 6 mL) a solution of AgOTf (0.022 g, 0.087 mmol, 0.5 equivs) in $Et_2O$ (1 mL) was added dropwise over the course of 1 minute. Immediate, precipitation of AgI was observed. The reaction mixture was allowed to stir at room temperature for 20 mins, where upon filtration over Celite (2 cm) packed on fiberglass afforded a deep red-orange solution. The resulting solution was concentrated to a solid where upon it was subject to stirring in *n*–pentane (5 mL) followed by evaporation to dryness to desolvate any residual AgI. Then the resulting red–orange solid was taken up in THF (1.0 mL) and filtered over fiberglass, followed by layering with *n*-pentane (5 mL). After 24 hours the mother liquor was decanted and the resulting dark brown powder was dried under vacuum to yield [$Cp_2Co_2(\mu$-I)($CNAr^{Mes2}$)$_2$]OTf, [**3**]OTf, 0.041 g, 0.038 mmol, 45 % yield. X-ray diffraction quality crystals were grown from a saturated $CH_2Cl_2$ solution layered with $Et_2O$ over 1 week at room temperature. $\mu_{eff}$

(Evans Method; $C_6D_6$ with $(Me_3Si)_2O$ references, 500.2 MHz, 20 ˚C, 3 runs) = 1.83 (±0.12) $\mu_B$. FTIR ($C_6D_6$; KBr Window; 20 ˚C): $\nu_{CN}$ = 2130 (vs), 2162 (m), 1953 (m), also 2974 (w), 2920 (w), 2853 (w), 1290 (w), 1272 (w), 1236 (m), 1220 (w), 1151 (m), 1068 (m), 1025 (m), 852 (m), 756 (m), 637 (m). Anal. Calc. $Co_2C_{61}H_{60}N_2IF_3SO_3$: C, 60.09; H, 5.03; N, 2.33. Found: C, 62.92; H, 5.01; N, 3.26. Repeated attempts to obtain a more satisfactory elemental analysis were unsuccessful. We believe this is do to a small amount of unreacted CpCoI($CNAr^{Mes2}$) present in crystalline samples of **4**.

**Preparation of $Co_2((\eta^6\text{-Mes})(\mu^2\text{-}CNAr^{Mes}))_2$, (5):** A re-sealable ampoule with magnetic stir bar, was charged with $Co_2(CO)_8$ (0.502 g, 1.48 mmol) and $C_6H_6$ (30 mL). To this solution, $CNAr^{Mes2}$ (1.00 g, 2.96, 2 equiv) was added as a powder over 10 min. Effervescence of CO was observed. The reaction mixture was then connected to a reflux condenser and nitrogen bubbler and heated for 2 weeks at 80˚C. The reaction mixture was concentrated to a brown solid under reduced pressure. This residue was suspended in pentane (100 mL) and filtered through a medium porosity fritted funnel. The brown precipitate was dissolved in $C_6H_6$ (50 mL) and filtered through two through medium porosity fritted funnels packed with Celite. The resulting filtrate was concentrated to a solid under reduced pressure, suspended in pentane (100 mL) and filtered. The black/brown precipitate was then washed with additional pentane (3 x 50 mL) to afford powdered $Co_2((\eta^6\text{-Mes})(\mu^2\text{-}CNAr^{Mes}))_2$, (**4**). Yield: 0.581 g, 0.73 mmol, 49.3 %. *Note*: Single crystals of (**4**) were obtained by layering pentane atop a concentrated THF solution of (**4**) followed by storage at -35 ˚C. $^1$H NMR (500.2 MHz, $C_6D_6$, 20 ˚C): δ = 7.12 (dd, 2H, *J* = 7 Hz, *J* = 2 Hz, *m*-Ph), 7.05 (dd, 2H, *J* = 7 Hz, *J* = 2 Hz, *m*-Ph), 7.03 (s, 4H, *m*-

Mes), 7.00 (t, 2H, $J$ = 7 Hz, *p*-Ph), 5.35 (s, 4H, *m*-$\eta^6$-Mes), 2.34 (s, 6H, *p*-Mes), 2.22 (s, 12H, *o*-Mes), 1.79 (s, 6H, *p*-$\eta^6$-Mes), 1.59 (s, 12H, *o*-$\eta^6$-Mes) ppm. $^{13}C\{^1H\}$ NMR (125.8 MHz, $C_6D_6$, 20 ˚C): δ = 253.3 (μ-*C*NR), 148.4, 139.8, 136.1, 135.8, 135.6, 130.4, 128.6, 128.3, 126.6, 124.6, 122.8, 110.7, 100.3, 99.4, 21.5 (*p*-Mes), 21.3 (*o*-Mes), 20.1 (*o*-Mes), 18.7 (*p*-Mes) ppm. FTIR ($C_6D_6$; KBr Window; 20 ˚C): $\nu_{CN}$ = 1557 (vs) $cm^{-1}$ also, 3067 (w), 2964 (w), 2916 (m), 2856 (w), 1609 (s) 1404 (w), 792 (w), 740 (m) $cm^{-1}$. Anal. Calcd. For $C_{50}H_{50}Co_2N_2$: C, 75.37; H, 6.32; N, 3.52. Found: C, 74.31; H, 6.28; N, 3.45.

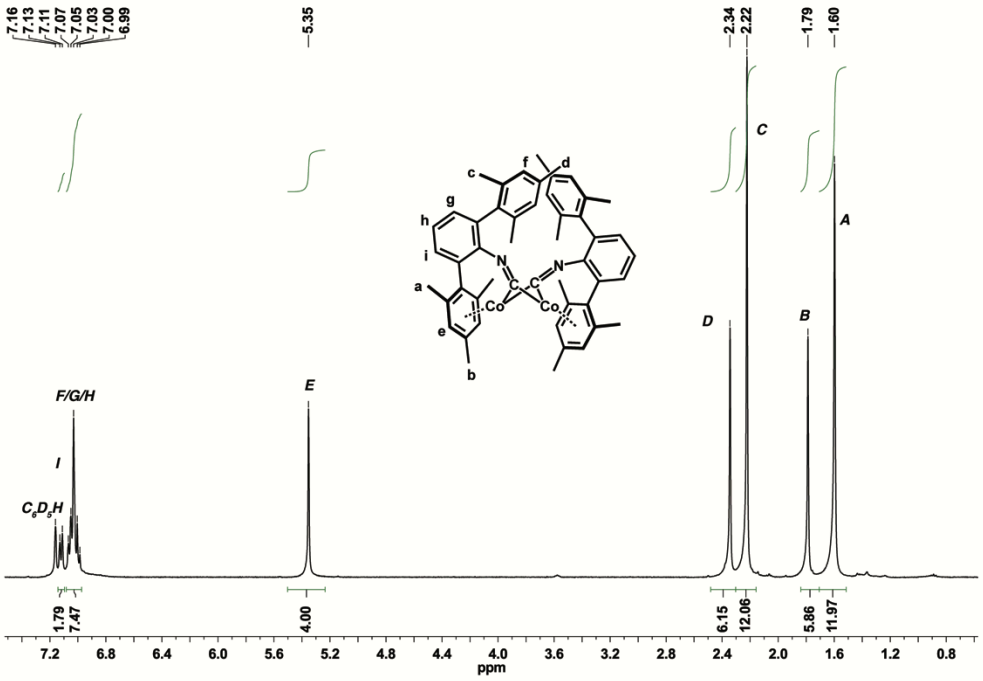


**Figure 4.19** Room temperature $^1H$ NMR spectrum of $Co_2((\eta^6\text{-Mes})(\mu^2\text{-CNAr}^{Mes}))_2$, (**5**) in $C_6D_6$.

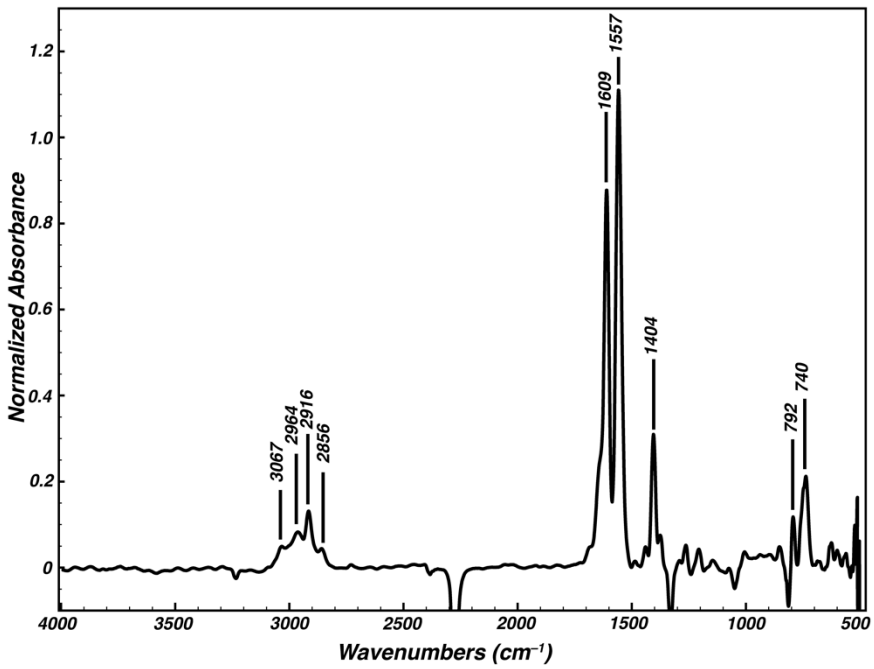


**Figure 4.20** Room–temperature solution–state FTIR spectrum ($C_6D_6$) of $Co_2((\eta^6\text{–Mes})(\mu^2\text{-CNAr}^{Mes}))_2$; (**6**).

**Synthesis of $[Co_2((\eta^6\text{-Mes})(\mu^2\text{-CNAr}^{Mes}))_2]BAr^F{}_4$, [5]$BAr^F{}_4$:** To a solution of (**5**) (0.026 g, 0.0325 mmol, 1 equiv) in THF (3 mL) at –40˚C an equally cold THF solution of FcOTf (0.011 mg, 0.0325 mmol, 1 equivs) was added (2 mL). Upon addition there was an instant color change and the precipitation of a yellow orange solid. The mixture was allowed to warm to room temperature and react for 30 minutes, where upon it was concentrated to a solid. The yellow orange solid was suspended in *n*–pentane (10mL) and filtered over a fiberglass filter pad to remove Ferrocene. The resulting solid with slurried in 5 mL of $Et_2O$ where a solution of $NaBAr^F{}_4$ in $Et_2O$ (0.0287 g, 0.0325 mmol, 1 equiv) was added drop wise. The resulting mixture was allowed to react for 30 mins where upon the slurry became a homogenous red–orange solution which was filtered over Celite packed on fiberglass (2 cm) to remove NaOTf, followed by evaporation to dryness to yield $[Co_2((\eta^6\text{-Mes})(\mu^2\text{-CNAr}^{Mes}))_2]BAr^F{}_4$, [**5**]$BAr^F{}_4$ as a yellow–orange solid 0.049 g,

0.021 mmol, 96.4 %. X–ray diffraction quality crystals were grown from a saturated $Et_2O$ (*ca.* 0.75 mL) solution at –40˚ C over 1 week. . $\mu_{eff}$ (Evans Method; $C_6D_6$ with $(Me_3Si)_2O$ references, 500.2 MHz, 20 ˚C, 5 runs) = 1.79 (±0.2) $\mu_B$. FTIR ($C_6D_6$; KBr Window; 20 ˚C): $\nu_{CN}$ = 1700 (s), also 3023 (w), 2979 (w), 2922 (w), 1578 (w), 1355 (m), 1276 (w), 1172 (sh), $\nu_{CF}$ = 1133 (s), 890 (w), 751 (w), 713 (w), 677 (w). Anal. Calcd. For $C_{82}H_{62}Co_2N_2BF_{24}$: C, 59.33; H, 3.76; N, 1.69. Found: C, 57.99; H, 3.9; N, 1.94. Repeated attempts to obtain a more satisfactory elemental analysis were unsuccessful. We believe this is du due to a small amount of unreacted $Na[BAr^F{}_4]$ that accompanies the bulk crystallization of [**5**]$BAr^F{}_4$.

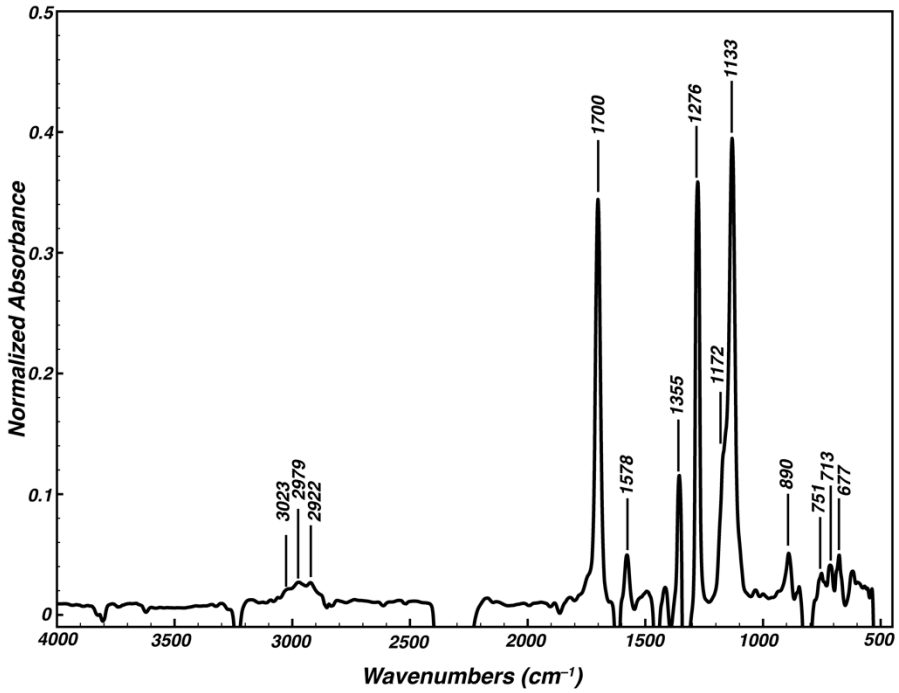


**Figure 4.21** Room–temperature solution–state FTIR spectrum ($C_6D_6$) of $[Co_2((\eta^6\text{–Mes})(\mu^2\text{-}CNAr^{Mes}))_2]Bar^F{}_4$; ([**5**]$BAr^F{}_4$).

**Synthesis of ($\mu$-$CNAr^{Mes2}$)$_2$[CpNi]$_2$, (6):** To a forest green $C_6H_6$ solution (5 mL) of $Cp_2Ni$ (0.166 g, 0.879 mmol, 1 equiv) was added a $C_6H_6$ of $CNAr^{Mes2}$ (0.298 g, 0.879

mmol, 1 equiv, 5 mL). Upon addition a color change from forest green to red-orange was observed. The reaction was allowed to react at room temperature for 12 hours where upon an additional color change to deep red was observed. The resultant mixture was frozen and all volatiles were removed via lyophilization. The resultant dark red powder was recrystallized from a 2:1 *n*-pentane/$Et_2O$ mixture at -40˚ C over night to yield ($\mu$-$CNAr^{Mes2}$)$_2$[CpNi]$_2$ as red needles, 0.230 g, 0.248 mmol, 56%. $^1$H NMR (400.1 MHz, $C_6D_6$, 20 ˚C): $\delta$ = 6.97 (s, 8H, *m*-Mes), 6.86 (m, 3H, *J* = 4 Hz *m/p*-Ph), 4.76 (s, 10H, H-*Cp*), 2.28 (s, 12H, *p*-$CH_3$), 2.18 (s, 24H, *p*-$CH_3$) ppm. $^{13}$C{$^1$H} NMR (125.8 MHz, $C_6D_6$, 20 ˚C): $\delta$ = 171.2 ($\mu^2$-*C*NR), 136.9, 136.4, 136.2, 133.6, 131.8, 130.4, 128.9, 124.4, 93.1, 21.2 (*p*-Mes), 20.8 (*o*-Mes ppm. FTIR ($C_6D_6$; KBr Window; 20 ˚C): $\nu_{C=NR}$ = 1914 (vs), 1964 (sh) also, 2956 (w), 2871 (w), 2026 (w), 1564 (w), 1516 (w), 1406 (w), 1250 (m), 1180 (w), 1148 (w), 1039 (w), 779 (w), 750 (w), 643 (w), 584 (w) cm$^{-1}$. Anal. Calcd. For $C_{60}H_{60}Ni_2N_2$: C, 77.78; H, 6.53; N, 3.02. Found: C, 77.69; H, 7.04; N, 2.81.

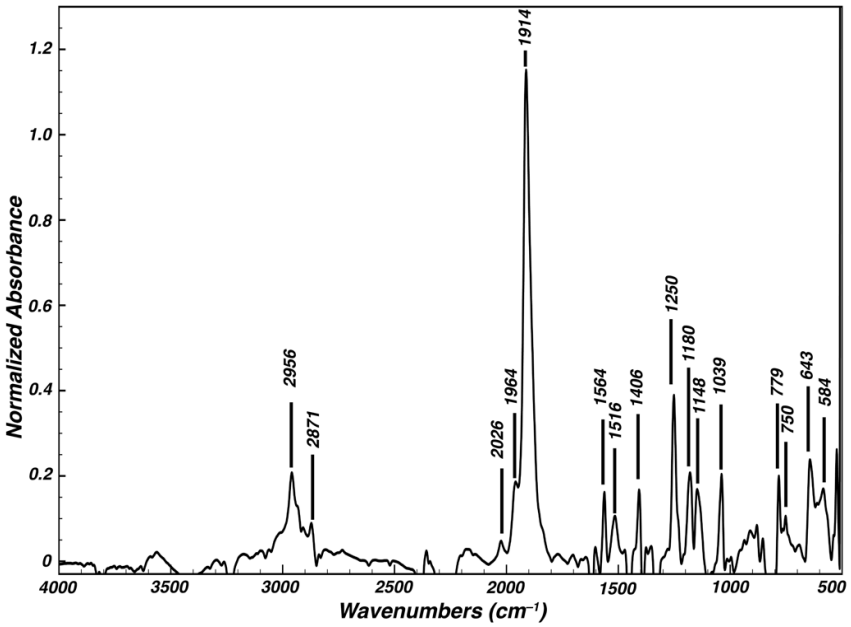


**Figure 4.22** Room–temperature solution–state FTIR ($C_6D_6$) of ($\mu^2$-$CNAr^{Mes2}$)$_2$[CpNi]$_2$, (**6**).

**Synthesis of [CpNi(CNAr$^{Tripp2}$)]$_2$, (7):** To a forest green $C_6H_6$ solution (5 mL) of $Cp_2Ni$ (0.150 g, 0.794 mmol, 1 equiv) was added a $C_6H_6$ of $CNAr^{Tripp2}$ (0.403 g, 0.794 mmol, 1 equiv, 5 mL). Upon addition a color change from forest green to red-orange was observed. The reaction was allowed to react at room temperature for 12 hours where upon an additional color change to deep red was observed. The resultant mixture was frozen and all volatiles were removed via lyophilization. The resultant dark red powder was recrystallized from a 6:1 *n*-pentane/$C_7H_8$ mixture at -40˚ C over night to yield [CpNi(CNAr$^{Tripp2}$)]$_2$ as dark red crystals, 0.155 g, 0.123 mmol, 31%. $^1$H NMR (400.1 MHz, $C_6D_6$, 20 ˚C): δ = 6.97 (s, 8H, *m*-Mes), 6.86 (m, 3H, *J* = 4 Hz *m/p*-Ph), 4.76 (s, 10H, H-*Cp*), 2.28 (s, 12H, *p*-$CH_3$), 2.18 (s, 24H, *p*-$CH_3$) ppm. $^{13}C\{^1H\}$ NMR (125.8 MHz, $C_6D_6$, 20 ˚C): δ = 171.2 ($\mu^2$-*C*NR), 136.9, 136.4, 136.2, 133.6, 131.8, 130.4, 128.9, 124.4, 93.1, 21.2 (*p*-Mes), 20.8 (*o*-Mes ppm. FTIR ($C_6D_6$; KBr Window; 20 ˚C): $\nu_{C=NR}$ = 1914 (vs), 1964 (sh) also, 2956 (w), 2871 (w), 2026 (w), 1564 (w), 1516 (w), 1406 (w), 1250 (m), 1180 (w), 1148 (w), 1039 (w), 779 (w), 750 (w), 643 (w), 584 (w) cm$^{-1}$. Anal. Calcd. For $C_{84}H_{108}Ni_2N_2$: C, 79.87; H, 8.61; N, 2.21. Found: C, 79.86; H, 8.54; N, 2.19.

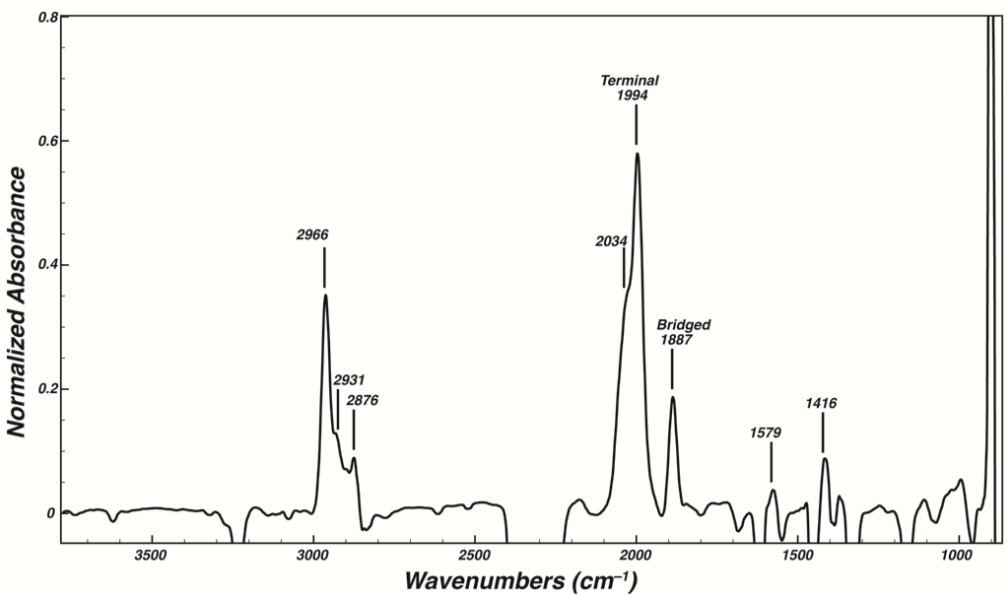


**Figure 4.23** Room–temperature solution–state FTIR ($C_6D_6$) of $[CpNi(CNAr^{Tripp2})]_2$, (**7**), depicting both bridged and terminal conformations.

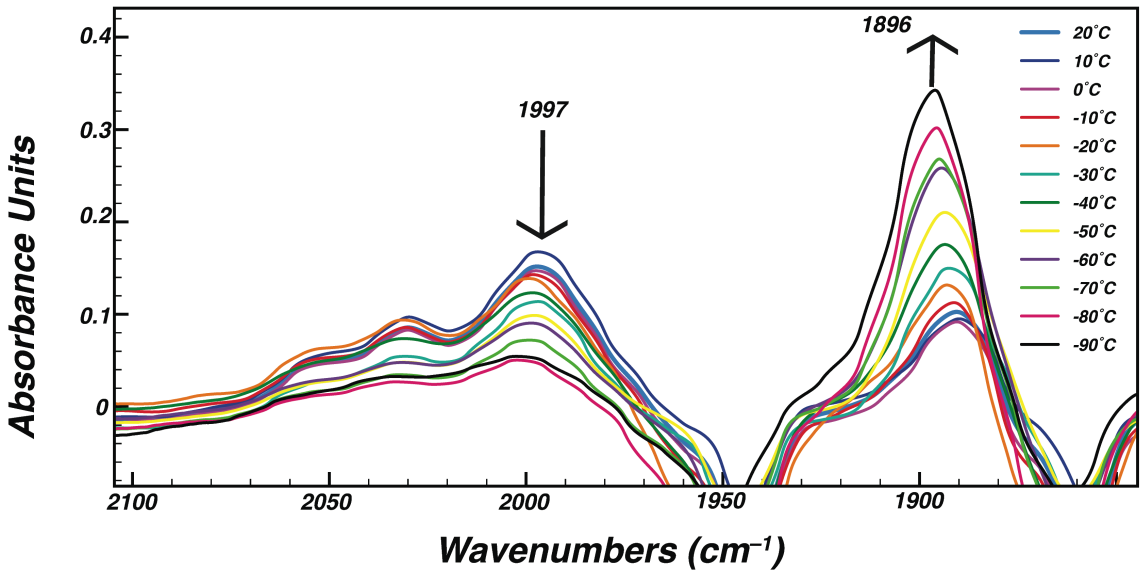


**Figure 4.24** Variable temperature solution–state FTIR (Toluene) of $[CpNi(CNAr^{Tripp2})]_2$, (**7**). Upon cooling from room-temperature to –90 ˚C the resononance at 1997 $cm^{-1}$ decreases and the resonance at 1896 becomes the prominent vibrational feature.

**Results of EPR Measurements and Simulations:**

X-Band continuous wave (CW) EPR spectra were measured on a Bruker E500 spectrometer equipped with a Bruker ER 041 X Microwave Bridge and a liquid nitrogen

cooling system. Spectra were recorded in 4 mm quartz tubes, and the magnetic field was calibrated with DPPH. Samples were prepared in a dinitrogen-filled glvoebox from analytical-grade crystals in concentration ranging between 0.2-0.5 mM. Complex K[**2**], and [**3**]$BAr^F_4$ were prepared in dry/deoxygenated $Et_2O$. To ensure no decomposition products were formed during spectral acquisition, all samples were verified by $^1H$ NMR and IR spectroscopy immediately after EPR data acquisition. EPR data was acquired at 295 K, and repeated on two independent samples that were shown to have identical spectroscopic behavior. Simulations for complex K[**2**], and [**3**]$BAr^F_4$ were performed using the program *EasySpin*.[7]

**Spectrometer Conditions**

**$K(Et_2O)[(\eta^5\text{-}Cp)_2Co_2(\mu^2\text{-}CNAr^{Mes2})_2]$:** X-band (9.3769 GHz): centerfield/sweep-width = 3300 G/1500 G; microwave power = 2.017 mW; modulation amplitude = 1.00 G; modulation frequency = 100.0 KHz; time constant = 10.24 ms; scans = 32.

**Simulated spectrum spin system:**

g = [2.0875, 2.0588, 2.0869]
$g_{corrected}$ = [2.0892, 2.0605, 2.0886]
$\mu_{eff}$ = 1.800(8)
$A_{Co(1)}$ (MHz) = [145.8054, 131.1572, 119.8835]; (G) [50.098, 45.065, 41.192]
$A_{Co(2)}$ (MHz) = [142.2820, 128.5033, 138.8099]; (G) [48.888, 44.153, 47.695]
Line broadening, Gaussian = 0.0961
Correlation time: $10^{-8.2434}$ s

**Spectrometer Conditions**

**$[Co_2((\eta^6\text{–}Mes)(\mu^2\text{-}CNAr^{Mes}))_2]Bar^F_4$**, [**3**]$BAr^F_4$**:** X-band (9.3809 GHz): centerfield/sweep-width = 3201 G/1219.4 G; microwave power = 1.266 mW; modulation amplitude = 3.00 G; modulation frequency = 100.0 KHz; time constant = 20.97 ms; scans = 20.

**Simulated spectrum spin system:**

g = [2.1347, 2.1047, 2.1095]
$g_{corrected}$ = [2.1302, 2.1047, 2.1050]
$\mu_{eff}$ = 1.533(8)
$A_{Co(1)}$ (MHz) = [124.5467, 119.7437, 115.1086]; (G) [42.108, 40.483, 38.917]
$A_{Co(2)}$ (MHz) = [136.4042, 132.5534, 137.1897]; (G) [46.116, 44.814, 46.382]
Line broadening, Gaussian = 0.0941
Correlation time: $10^{-8.10}$ s.

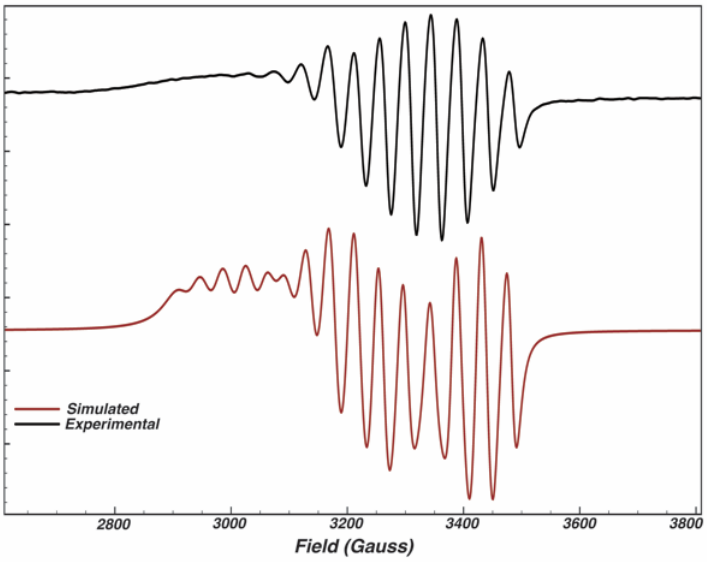


**Figure 4.25** Experimental room temperature EPR spectrum of of $[Co_2((\eta^6\text{–Mes})(\mu^2\text{-CNAr}^{Mes}))_2]Bar^F{}_4$, [**3**]$BAr^F{}_4$ in $Et_2O$ (black/top); simulated spectrum (red/bottom). Simulation of the spectrum yielded $\mu_{eff}$ = 1.533(8) $\mu$B.

**Electrochemical Experimental Conditions**

Cyclic voltammetry (CV) and differential pulse voltammetry (DPV) measurements were performed at room temperature under Argon in THF with and EG&G potentiostat (PAR-model 263A) and an electrochemical cell for sensitive compounds. A general electrochemical cell featured a freshly polished Pt disk working electrode, Pt wire counter electrode, and Ag as a (pseudo) reference electrode, with [*n*-$Bu_4N$][$PF_6$] or

$NaBAr^{F}_{4}$ (0.1 M) as an electrolyte. Potentials were calibrated against the $Fc/Fc^{+}$ redox couple (internal standard).

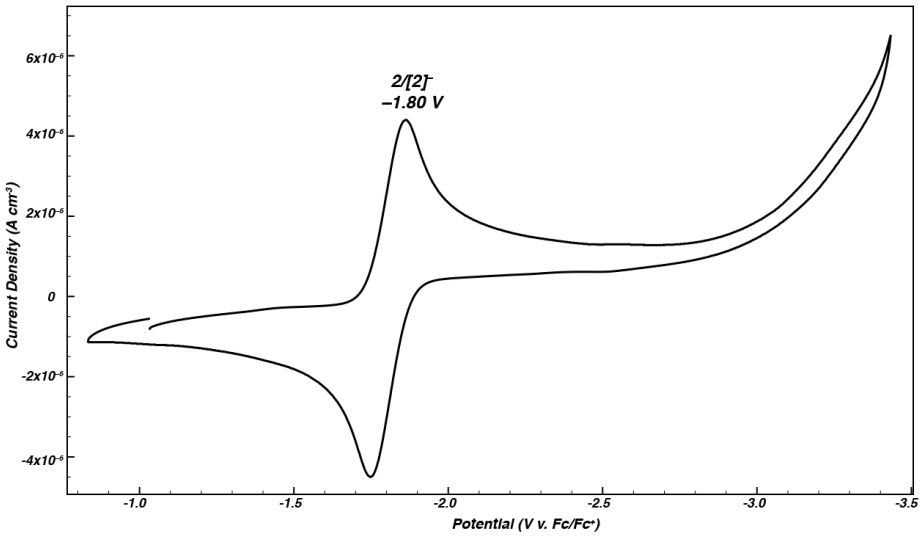


**Figure 4.26** CV of $(\mu\text{-}CNAr^{Mes2})_2[CpCo]_2$ (**2**) in THF under an Ar atmosphere with 0.1 M[*n*-$Bu_4N$][$PF_6$].

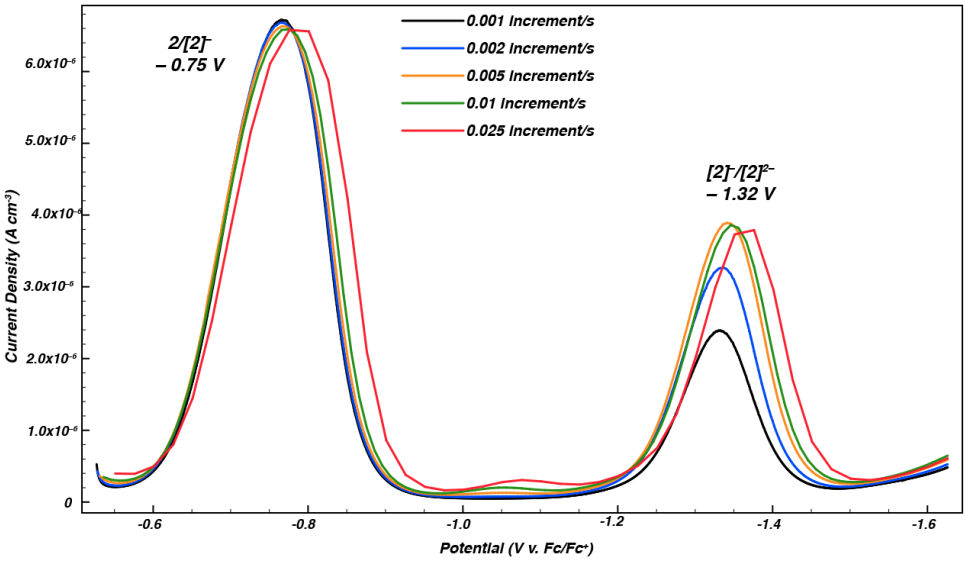


**Figure 4.27** Variable-Scan-Rate Differential Pulsed Voltammetry of $(\mu\text{-}CNAr^{Mes2})_2[CpCo]_2$ (**2**) in THF under an Ar atmosphere with 0.1 M $Na[BAr^{F}_{4}]$ as the supporting electrolyte. The –1.32 V feature, ascribed to $[\mathbf{2}]^{-}/[\mathbf{2}]^{-2}$ couple, increases in current amplitude with increasing scan rate, while the –0.75 V feature ascribed to the $\mathbf{2}/[\mathbf{2}]^{-}$ couple is invariant Note, at 0.005 increments/s (corresponding to a scan rate of 100 mV/s), the $[\mathbf{2}]^{-}/[\mathbf{2}]^{-2}$ couple reaches a maximum current amplitude of ca. 1/3 that of the $\mathbf{2}/[\mathbf{2}]^{-}$ couple.

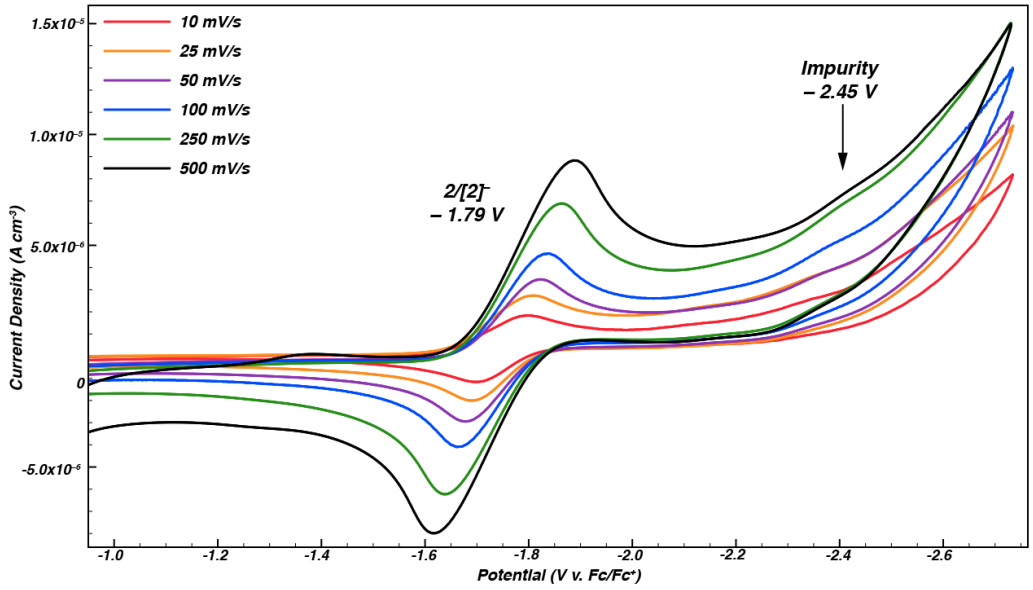


**Figure 4.28** Variable-Scan-Rate cyclic voltammetry of (μ-$CNAr^{Mes2}$)$_2$[CpCo]$_2$ (**2**) in THF under an Ar atmosphere with 0.1 M [*n*-$Bu_4N$][$BAr^F{}_4$] as the supporting electrolyte. A second redox feature ascribed to the [**2**]$^-$/[**2**]$^{-2}$ is not observed. Note, The redox feature centered at –2.45 V is due to an impurity associated with the [*n*-$Bu_4N$][$BAr^F{}_4$] electrolyte (See Figure 4.29 below).

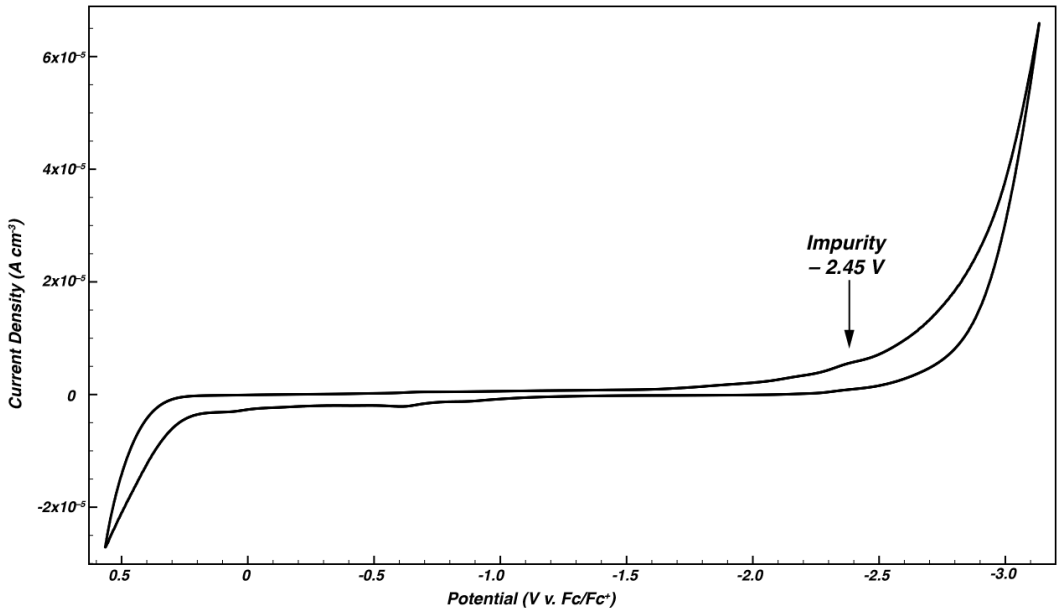


**Figure 4.29** Background CV of [*n*-$Bu_4N$][$BAr^F{}_4$] electrolyte in THF under an Ar atmosphere (100 mV/s). The small feature at –2.45 V is an impurity in the electrolyte that is also present when measuring the CV of **2** under these conditions (see Figure 4.28).

### 4.8 Crystallographic Structure Determinations

**General Information.** Single crystal X-ray structure determinations were carried out using a Burker Platfom of Kappa X-ray Diffractometers equipped with Mo or Cu radiation sources (sealed tube or ratating anode), low temperature cryostats, and CCD detectors (Bruker APEX or Bruker APEX II). All structures were solved by Direct Methods using SHELXS.[97] All structures were refined by full matrix least squares procedures utilizing SHELXL[97] within Olex 2 small-molecule solution, refinement and analysis software package.[98] Crystallographic data-collection and refinement information are listed in Table S5.1.

**Information on Crystallographic Disorder:** The following molecules contain positionally disordered components that were modeled and refined anisotropically. They are listed along with their respective disordered components.

Complex K[**2**] displays positional disorder in one of the flanking mesityl rings located at $C_{38}$, in addition to one $Et_2O$ molecule of solvation. The disordered mesityl ring was fully refined to 77 % and 23 % occupancy (part 1 and part 2 respectively) and the disordered $Et_2O$ molecule was fully refined to 79% and 21% occupancy (part 1 and part 2 respectively).

Complex **7** exhibits positional disorder of multiple *i*-Pr groups. Each *i*-Pr was split and linked with via a free variable and refined anisotropically. The Platon routine SQUEEZE was used to account for residual solvent accessible voids.

Complex **6** exhibits positional disorder over two positions of one methyl group at C20. This methyl group was split and linked via a free variable and refined anisotropically.

Complex [**4**]OTf contains one $Et_2O$ molecule of solvation that contains position disorder of the oxygen atom over two position. Each oxygen atom is modeled at 68% and 32% occupancy for part 1 and part 2 respectively, and refined anisotropically. Complex [**4**]OTf also displays pseudo symmetry. However use of the Platon Suit *Add Sym* displayed no space group consistent with higher symmetry, and based on the low R-factor and only 95% confidence in higher symmetry we are confident that the current symmetry and space group are acceptable for the model presented.

**Table 4.2** Crystallographic Data Collection and Refinement Information.

| Name | ($\eta^5$–*Cp*)$CoI_2(CNAr^{Mes2})$ **(1)** | $K_2[(\mu\text{-}CNAr^{Mes2})$ $[CpCo]_2]\cdot(Et_2O)_2$ **$K_2$[2]** | $K[(\mu\text{-}CNAr^{Mes2})$ $[CpCo]_2]\cdot(Et_2O)$ **K[2]** |
|---|---|---|---|
| Formula | $C_{30}H_{30}CoNI_2$ | $C_{68}H_{80}Co_2N_2O_2$ | $C_{64}H_{70}Co_2N_2O$ |
| Crystal System | Triclinic | Monoclinic | Monoclinic |
| Space Group | *P*–1 | *P*21/n | $P2_1/C$ |
| *a*, Å | 7.6313(6) | 13.5246(8) | 13.4964(9) |
| *b*, Å | 10.8515(7) | 30.165(2) | 26.8113(15) |
| *c*, Å | 17.6245(11) | 15.2884(9) | 15.3703(10) |
| α, deg | 85.012(4) | 90 | 90 |
| β, deg | 84.215(4) | 110.741(2) | 103.6250(19) |
| γ, deg | 73.885(4) | 90 | 90 |
| V, $Å^3$ | 1392.36(17) | 5833.0(6) | 5405.3(6) |
| *Z* | 2 | 4 | 4 |
| Radiation (λ, Å) | Mo-$K_\alpha$, 0.71073 | Mo-$K_\alpha$, 0.71073 | Mo-$K_\alpha$, 0.71073 |
| ρ (calcd.), $g/cm^3$ | 1.711 | 1.313 | 1.278 |
| μ (Mo Ka), $mm^{-1}$ | 2.852 | 0.758 | 0.734 |
| Temp, K | 100 | 100 | 100 |
| θ max, deg | 25.452 | 25.027 | 25.357 |
| data/parameters | 5202/313 | 10297/701 | 9885/742 |
| $R_1$ | 0.0259 | 0.0635 | 0.0456 |
| $wR_2$ | 0.0259 | 0.1257 | 0.0839 |
| GOF | 1.023 | 1.014 | 1.009 |

**Table 4.3.** Crystallographic Data Collection and Refinement Information.

| Name | ($\mu$-$CNAr^{Mes2}$) $[CpCo]_2$ $\cdot(Et_2O)$ **(2)** | $CpCoI(CNAr^{Mes2})$ **(3)** | $[(\mu\text{–}I)$ $Cp_2Co_2(CNAr^{Mes2})_2]OTf$ $\bullet(Et_2O)$ **[4]OTf** |
|---|---|---|---|
| Formula | $C_{64}H_{70}Co_2N_2O$ | $C_{30}H_{30}CoNI$ | $C_{65}H_{70}Co_2F_3IN_2O_4S$ |
| Crystal System | Monoclinic | Monoclinic | Triclinic |
| Space Group | *Pn* | *P*21/c1 | *P*-1 |
| *a*, Å | 14.2277(5) | 10.1608(8) | 13.7410(5) |
| *b*, Å | 12.8689(5) | 16.3598(14) | 21.2368(8) |
| *c*, Å | 15.2248(6) | 16.3005(15) | 22.5173(9) |
| $\alpha$, deg | 90 | 90 | 68.060(2) |
| $\beta$, deg | 109.215(2) | 106.344(3) | 82.156(2) |
| $\gamma$, deg | 90 | 90 | 80.347(2) |
| V, $Å^3$ | 2632.29(18) | 2600.1(4) | 5989.1(4) |
| *Z* | 2 | 4 | 4 |
| Radiation ($\lambda$, Å) | Mo-$K_\alpha$, 0.71073 | Mo-$K_\alpha$, 0.71073 | Mo-$K_\alpha$, 0.71073 |
| $\rho$ (calcd.), $g/cm^3$ | 1.263 | 1.508 | 1.416 |
| $\mu$ (Mo Ka), $mm^{-1}$ | 0.674 | 1.865 | 1.162 |
| Temp, K | 100 | 100 | 100 |
| $\theta$ max, deg | 33.142 | 26.731 | 27.103 |
| data/parameters | 19001/636 | 5512/309 | 26323/1443 |
| $R_1$ | 0.0303 | 0.0308 | 0.0364 |
| $wR_2$ | 0.0647 | 0.0648 | 0.0812 |
| GOF | 1.006 | 1.014 | 1.024 |

**Table 4.4.** Crystallographic Data Collection and Refinement Information.

| Name | $Co_2((\eta^6$–Mes)(μ–$CNAr^{Mes}))_2$ **(5)** | $[Co_2((\eta^6$–Mes)(μ–CNArMes))$_2]BAr^F$·$(Et_2O)$ **[5]BAr$^F_4$** | (μ-$CNAr^{Mes2}$)$[CpNi]_2$ •$(C_5H_{14})$ **(7)** |
|---|---|---|---|
| Formula | $C_{50}H_{50}Co_2N_2$ | $C_{68}H_{72}Co_2N_2O_2$ | $C_{65}H_{72}N_2Ni_2$ |
| Crystal System | Monoclinic | Triclinic | Monoclinic |
| Space Group | *P*121/n1 | *P*–1 | *P*121/n1 |
| *a*, Å | 15.0030(16) | 14.8790(5) | 17.4359(8) |
| *b*, Å | 18.630(2) | 17.7111(6) | 25.3986(11) |
| *c*, Å | 15.2981(14) | 18.2157(6) | 25.6346(11) |
| α, deg | 90 | 96.464(2) | 90 |
| β, deg | 109.314(5) | 109.136(2) | 105.452(2) |
| γ, deg | 90 | 114.0260 | 90 |
| V, Å$^3$ | 4035.2(7) | 3970.1(2) | 10941.9(8) |
| *Z* | 4 | 2 | 8 |
| Radiation (λ, Å) | Mo-$K_\alpha$, 0.71073 | Mo-$K_\alpha$, 0.71073 | Mo-$K_\alpha$, 0.71073 |
| ρ (calcd.), g/cm$^3$ | 1.312 | 1.451 | 1.212 |
| μ (Mo Ka), mm$^{-1}$ | 0.859 | 0.522 | 0.729 |
| Temp, K | 100 | 100 | 100 |
| θ max, deg | 26.37 | 25.365 | 25.388 |
| data/parameters | 7451/499 | 14134/1059 | 39006/1272 |
| $R_1$ | 0.0479 | 0.0592 | 0.00654 |
| $wR_2$ | 0.0899 | 0.1198 | 0.1138 |
| GOF | 1.007 | 1.008 | 1.017 |

**Table 4.5.** Crystallographic Data Collection and Refinement Information.

| Name | $Cp_2Ni_2(CNAr^{Tripp2})_2$ (**8**) |
|---|---|
| Formula | $C_{84}H_{108}N_2Ni_2$ |
| Crystal System | Orthorhombic |
| Space Group | *Pbcn* |
| *a*, Å | 15.7052(14) |
| *b*, Å | 17.1228(15) |
| *c*, Å | 29.167(3) |
| α, deg | 90 |
| β, deg | 90 |
| γ, deg | 90 |
| V, Å$^3$ | 784.6(12) |
| *Z* | 4 |
| Radiation (λ, Å) | Mo-$K_\alpha$, 0.71073 |
| ρ (calcd.), g/cm$^3$ | 1.070 |
| μ (Mo Ka), mm$^{-1}$ | 0.521 |
| Temp, K | 100 |
| θ max, deg | 25.026 |
| data/parameters | 6937/515 |
| $R_1$ | 0.1087 |
| $wR_2$ | 0.2711 |
| GOF | 1.150 |

**4. 9 Results of Computational Studies.**

**Computational Details.** Density Functional Theory calculations on the model compounds $[(\mu\text{-CNPh})_2[CpCo]_2]^n$ (n = 0, -1,-2; [**2m**]$^n$), and $[(\mu\text{-CO})_2[CpCo]_2]^n$, (n = 0, -1,-2), $[(\mu\text{-CNPh})_2[CpNi]_2]$ (**7m**), and [CpNi(CNPh)]$_2$] (**8m**) were preformed with the ORCA computational suite 3.0.0.[99] $[(\mu\text{-CNPh})_2[CpCo]_2]^n$, (n = 0, -1,-2; [**2m**]$^n$), and $[(\mu\text{-CNPh})_2[CpNi]_2]$ (**6m**), and [CpNi(CNPh)]$_2$] (**7m**) are truncated versions of the structurally characterized complexes (**2**), K[**2**], $K_2$[**2**], (**6**), and (**7**), with original coordinates taken from crystallographic structure determinations. $[(\mu\text{-CNPh})_2[CpCo]_2]^n$, (n = 0, -1) were originally optimized using the BP86 pure functional where upon optimized structural coordinates were re-optimized using the B3LYP/G hybrid functional.[100-102] $[(\mu\text{-CNPh})_2[CpCo]_2]^{2-}$ [**2m**]$^{2-}$ was originally optimized using the B3LYP/G hybrid functional as $[(\mu\text{-CNMe})_2[CpCo]_2]^{2-}$ which is a truncated version of the structurally characterized $K_2$[**2**], and followed by re-optimization with the inclusion of CNPh as the bridging ligand using optimized coordinates from the B3LYP/G hybrid functional.[100-102] Lastly after all geometry optimizations all optimized structures were orientated such that the M-M vector was orientated along the Cartesian Z-axis. The all-electron Ahlrichs triple-zeta basis sets def2-TZVP (standard)[103-105] and def2-TZVP/J (auxiliary)[106-111] were used in all calculations. The resolution of identity (RI) approximation was employed.[16] Relativistic effects were included by use of the zeroth-order regular approximation (ZORA).[105,109-112] Viewing of optimized structures and rendering of molecular orbitals was performed using the program Chemcraft.[113] This research was supported in part by the W. M. Keck Foundation through computing resources at the W. M. Keck Laboratory for Integrated Biology II.

**Hardware Specifics.** DFT calculations were performed on a dual Intel Xenon E5640 2.66GHz quad-core processors featuring; 24GB DDR 1333 RAM; 120 GB SATA2 Intel 520 Cherryville SSD; 2TB 6Gb/s HDD; GTX620 1GB DDR3 GPU; GTX680 4 GB DDR5 GPU.

**Input and Results.**

**Input for geometry optimization of $(\mu\text{–}CO)_2[CpCo]_2$.**

```
#UKS OPT of carbonylneutral

%pal nprocs 8 end

! UKS B3LYP/G ZORA def2-TZVP def2-TZVP/J Opt SlowConv XYZFile
%SCF
 MaxIter 300
end

* xyz 0 1
Co      3.09199502      4.83589372      6.88810445
Co      3.82436783      3.03732743      8.20859645
O       5.48637947      3.45151688      5.85897779
O       1.65117077      4.64224566      9.39211615
C       4.56238560      3.68366739      6.59670623
C       2.47425760      4.30199523      8.57720568
C       2.41353998      5.31602174      4.96760621
H       2.32126872      4.69639870      4.25436433
C       3.56932510      6.07707033      5.27366674
H       4.38986012      6.05366667      4.79620691
C       3.29551842      6.87576064      6.40585524
H       3.89748972      7.48046142      6.82613109
C       1.95951444      6.61061052      6.80313869
H       1.50649353      7.01077874      7.53523453
C       1.42229717      5.65196379      5.92130951
H       0.54482223      5.29203533      5.96134846
C       4.00095449      0.95732523      8.23909444
H       3.78013662      0.39016999      7.50982079
C       5.26854298      1.53740326      8.48462699
H       6.04689714      1.42136785      7.95272214
C       5.17362806      2.31264028      9.65081545
H       5.87581003      2.81878643     10.04297975
C       3.85157714      2.21257472     10.13969701
H       3.50931921      2.63663380     10.91830217
C       3.12135791      1.36374474      9.26315600
```

H 2.20713205 1.11741398 9.35134761
*

**Optimized coordinates for ($\mu^2$–CO)$_2$[CpCo]$_2$.**

| | | | |
|---|---|---|---|
| Co | 3.079708 | 4.809338 | 6.864277 |
| Co | 3.785738 | 3.014572 | 8.190943 |
| O | 5.256977 | 3.330102 | 5.766567 |
| O | 1.565713 | 4.452065 | 9.255035 |
| C | 4.436732 | 3.594611 | 6.565683 |
| C | 2.412161 | 4.212317 | 8.475693 |
| C | 2.429390 | 5.383871 | 4.953619 |
| H | 2.313921 | 4.693956 | 4.133676 |
| C | 3.608143 | 6.101656 | 5.278250 |
| H | 4.549491 | 6.039176 | 4.757894 |
| C | 3.350965 | 6.852660 | 6.457753 |
| H | 4.061132 | 7.473513 | 6.979550 |
| C | 2.001047 | 6.624129 | 6.844244 |
| H | 1.513262 | 7.028623 | 7.715619 |
| C | 1.434072 | 5.708246 | 5.922568 |
| H | 0.434951 | 5.306161 | 5.963181 |
| C | 4.050299 | 0.933849 | 8.284191 |
| H | 3.811655 | 0.266432 | 7.471883 |
| C | 5.299307 | 1.570858 | 8.498785 |
| H | 6.168980 | 1.485988 | 7.868559 |
| C | 5.172699 | 2.403018 | 9.643440 |
| H | 5.937925 | 3.048117 | 10.043925 |
| C | 3.852971 | 2.255612 | 10.156069 |
| H | 3.438868 | 2.777760 | 11.002482 |
| C | 3.156413 | 1.354565 | 9.312687 |
| H | 2.123524 | 1.064277 | 9.412556 |

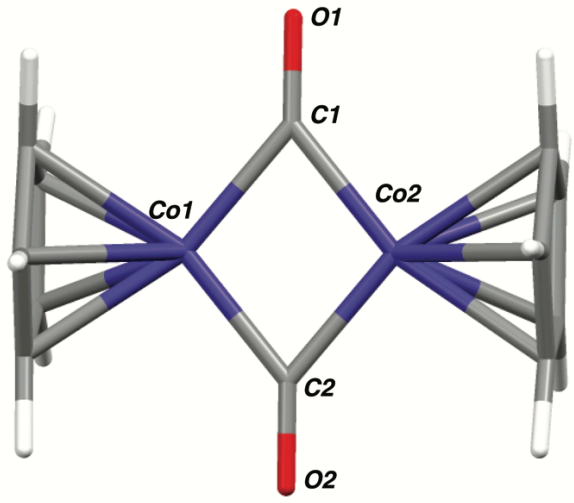


**Figure 4.30** Optimized molecular structure of (μ–CO)$_2$[CpCo]$_2$.

## Input for geometry optimization of $[(\mu\text{–}CO)_2[CpCo]_2]^-$.

```
#UKS OPT of  carbonylanion

%pal nprocs 8 end

! UKS B3LYP/G ZORA def2-TZVP def2-TZVP/J Opt SlowConv XYZFile
%SCF
 MaxIter 300
end

* xyz -1 2
Co     4.797423    16.911492     3.363739
Co     5.007917    14.640820     2.635660
C      4.121142    13.056548     1.509699
H      3.166915    13.186426     1.003747
C      5.690039    12.688993     3.163439
H      6.155150    12.475232     4.123425
C      4.294352    12.629184     2.867454
H      3.500059    12.348956     3.556101
C      6.163628    15.692599     3.620953
C      6.377635    13.138475     1.983706
H      7.446909    13.324213     1.908685
C      5.408587    13.353377     0.956617
H      5.605542    13.715741    -0.050198
C      3.623816    15.847328     2.411896
C      3.545999    18.335092     4.350449
H      2.562183    18.084955     4.741947
C      5.239701    18.968509     2.889308
H      5.770501    19.283184     1.993224
C      4.786945    18.231621     5.048891
H      4.924981    17.891122     6.072963
C      5.832699    18.610267     4.140875
H      6.898425    18.576512     4.356525
C      3.828203    18.781944     3.014300
H      3.092470    18.906113     2.222605
O      2.527259    15.909976     1.912205
O      7.242927    15.617474     4.155197
*
```

## Optimized coordinates for $[(\mu\text{–}CO)_2[CpCo]_2]^-$.

```
 Co     4.798024   16.915980    3.366690
 Co     5.008355   14.635136    2.636138
 C      4.130168   13.026086    1.505466
 H      3.185198   13.146409    1.000246
 C      5.687798   12.655330    3.145960
 H      6.148817   12.432025    4.094728
 C      4.303708   12.596601    2.851266
 H      3.516859   12.317949    3.533667
 C      6.146358   15.696921    3.607507
```

| | | | |
|---|---|---|---|
| C | 6.370971 | 13.101967 | 1.974851 |
| H | 7.432266 | 13.277279 | 1.897160 |
| C | 5.409490 | 13.313911 | 0.956201 |
| H | 5.605644 | 13.674278 | -0.040891 |
| C | 3.649536 | 15.846806 | 2.415388 |
| C | 3.550423 | 18.370223 | 4.360205 |
| H | 2.575751 | 18.126157 | 4.751198 |
| C | 5.229090 | 19.000443 | 2.910234 |
| H | 5.754207 | 19.312924 | 2.021804 |
| C | 4.781692 | 18.270477 | 5.052422 |
| H | 4.917939 | 17.939176 | 6.069398 |
| C | 5.820281 | 18.642671 | 4.150374 |
| H | 6.876396 | 18.620259 | 4.366565 |
| C | 3.829011 | 18.810085 | 3.032328 |
| H | 3.098605 | 18.941137 | 2.249891 |
| O | 2.569264 | 15.911976 | 1.914839 |
| O | 7.215557 | 15.623947 | 4.129776 |

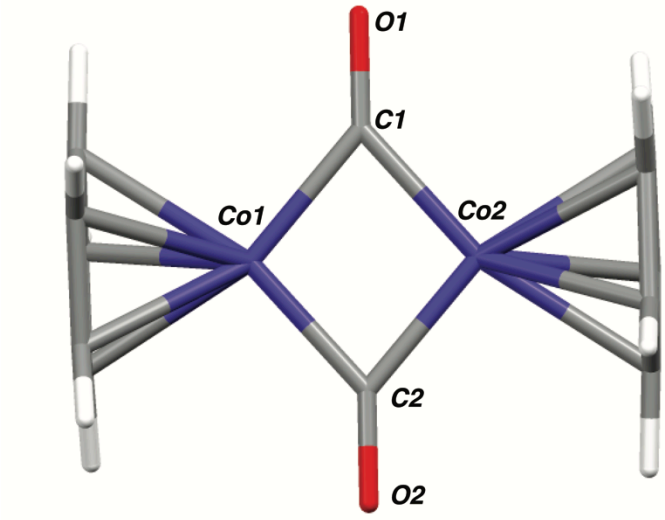


**Figure 4.31** Optimized molecular structure of $[(\mu\text{–}CO)_2[CpCo]_2]^-$ .

## Input for geometry optimization of $[(\mu\text{–}CO)_2[CpCo]_2]^{2-}$.

```
#UKS OPT of  carbonyldianion

%pal nprocs 8 end

! UKS B3LYP/G ZORA def2-TZVP def2-TZVP/J Opt SlowConv XYZFile
%SCF
 MaxIter 300
end
```

```
* xyz -2 1
 Co    -0.034720     2.557163    12.863020
 Co    -0.620864     3.175918    10.588753
 C     -0.259552     3.852799     8.629791
 H      0.725707     3.754299     8.173535
 C     -2.420849     3.420914     9.350851
 H     -3.344298     2.890388     9.584602
 C     -2.072831     4.733850     9.792237
 H     -2.684404     5.382261    10.420388
 C      0.217832     1.274303    14.511240
 H      0.357873     0.201305    14.378199
 C      0.609114     3.552758    14.720914
 H      1.112204     4.519888    14.701935
 C      0.957804     3.355617    11.529440
 C     -0.737878     4.998352     9.360268
 H     -0.150129     5.884307     9.601782
 C     -0.795740     3.341045    14.861743
 H     -1.553798     4.117850    14.965953
 C     -1.305590     2.872570     8.622987
 H     -1.270319     1.887529     8.157107
 C     -1.041517     1.941883    14.719179
 H     -2.021150     1.463781    14.696504
 C     -0.935488     1.630337    11.546003
 C      1.243339     2.276520    14.509821
 H      2.311835     2.111154    14.369587
 O     -1.525237     0.564385    11.408196
 O      2.070564     3.846136    11.373140
*
```

**Optimized coordinates for $[(\mu\text{–}CO)_2[CpCo]_2]^{2-}$.**

```
 Co    -0.010576    2.531143   12.842620
 Co    -0.589115    3.145205   10.580688
 C     -0.294778    3.883108    8.616737
 H      0.671915    3.795586    8.143140
 C     -2.429858    3.438056    9.353241
 H     -3.348709    2.915451    9.575905
 C     -2.081437    4.737056    9.798038
 H     -2.681725    5.371490   10.434272
 C      0.199105    1.295621   14.552961
 H      0.335692    0.230259   14.438466
 C      0.597465    3.556812   14.730685
 H      1.102055    4.512011   14.722249
 C      0.988875    3.273051   11.500769
 C     -0.761175    5.008628    9.362135
 H     -0.184991    5.892964    9.592513
 C     -0.798654    3.352668   14.858050
 H     -1.547194    4.127039   14.945163
 C     -1.331065    2.908066    8.610618
```

| | | | |
|---|---|---|---|
| H | -1.300070 | 1.940934 | 8.131041 |
| C | -1.050293 | 1.964188 | 14.731916 |
| H | -2.022432 | 1.493104 | 14.723250 |
| C | -0.842933 | 1.589566 | 11.510486 |
| C | 1.221735 | 2.284793 | 14.550622 |
| H | 2.281299 | 2.112122 | 14.431329 |
| O | -1.392408 | 0.518257 | 11.360669 |
| O | 2.101181 | 3.730133 | 11.339613 |

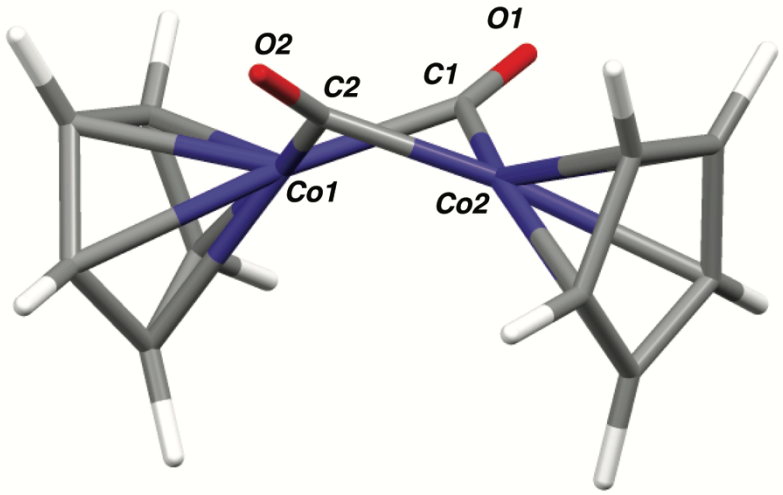


**Figure 4.32** Optimized molecular structure of $[(\mu\text{–}CO)_2[CpCo]_2]^{2-}$.

## Input for geometry optimization of $(\mu\text{–}CNPh)_2[CpCo]_2$ (2m).

```
#UKS OPT of  phenylneutral

%pal nprocs 8 end

! UKS B3LYP/G ZORA def2-TZVP def2-TZVP/J Opt RIJCOSX VerySlowConv KDIIS XYZFile
%SCF
 MaxIter 300

end

* xyz 0 1

 Co    3.209772   4.655301   6.689691
 Co    4.325481   4.251170   8.688136
 N     5.295928   2.563646   6.544591
 N     2.302497   6.407015   8.806833
 C     4.600574   3.464158   7.028681
```

| | | | |
|---|---|---|---|
| C | 3.017379 | 5.522705 | 8.320035 |
| C | 2.091684 | 3.677612 | 5.213188 |
| H | 1.920409 | 2.605146 | 5.198855 |
| C | 3.178391 | 4.361134 | 4.592156 |
| H | 3.976980 | 3.900348 | 4.018574 |
| C | 3.061087 | 5.754720 | 4.903836 |
| H | 3.754188 | 6.535680 | 4.604450 |
| C | 1.884039 | 5.933669 | 5.692055 |
| H | 1.541977 | 6.867766 | 6.126029 |
| C | 1.289759 | 4.651006 | 5.896998 |
| H | 0.404572 | 4.446110 | 6.491306 |
| C | 4.635642 | 2.730863 | 10.072345 |
| H | 4.235236 | 1.728279 | 9.953885 |
| C | 5.897352 | 3.194002 | 9.588237 |
| H | 6.608625 | 2.609954 | 9.012761 |
| C | 6.009808 | 4.582331 | 9.901015 |
| H | 6.838328 | 5.232003 | 9.633577 |
| C | 4.827198 | 4.973475 | 10.609616 |
| H | 4.601874 | 5.969200 | 10.977055 |
| C | 3.975670 | 3.833903 | 10.709936 |
| H | 2.987233 | 3.812772 | 11.159190 |
| C | 5.817600 | 2.110627 | 5.351078 |
| C | 5.708944 | 0.747390 | 5.008181 |
| C | 6.270524 | 0.273543 | 3.823910 |
| H | 6.168246 | -0.782914 | 3.569046 |
| C | 6.963121 | 1.135671 | 2.966878 |
| H | 7.405362 | 0.758196 | 2.044635 |
| C | 7.090622 | 2.485461 | 3.311571 |
| H | 7.637018 | 3.166655 | 2.656138 |
| C | 6.527536 | 2.975943 | 4.488827 |
| H | 2.063022 | 10.043716 | 12.638728 |
| C | 1.035771 | 8.437034 | 11.612179 |
| C | 2.264947 | 7.333574 | 9.827562 |
| C | 3.351796 | 8.204683 | 10.065778 |
| C | 1.098445 | 7.473976 | 10.607085 |
| C | 3.272922 | 9.166597 | 11.071640 |
| H | 4.121699 | 9.831694 | 11.243397 |
| C | 2.119813 | 9.287970 | 11.854434 |
| H | 5.176405 | 0.076876 | 5.683814 |
| H | 6.637728 | 4.024489 | 4.767769 |
| H | 0.127165 | 8.527045 | 12.210535 |
| H | 4.242750 | 8.117262 | 9.441902 |
| H | 0.252242 | 6.814738 | 10.409320 |

*

**Optimized coordinates for (μ–CNPh)$_2$[CpCo]$_2$ (2m).**

| | | | |
|---|---|---|---|
| Co | 3.45488028515046 | 4.86690590441269 | 6.59667499371069 |
| Co | 4.51026372049536 | 4.46361585665043 | 8.64124533817452 |

| | | | |
|---|---|---|---|
| N | 5.31805296044956 | 2.60285231933177 | 6.60352201103087 |
| N | 2.71707224396341 | 6.79920643772775 | 8.59621070309575 |
| C | 4.70390071699171 | 3.56567460973940 | 7.03944406328306 |
| C | 3.29688058624088 | 5.80083337734472 | 8.18735698076860 |
| C | 2.50297573493256 | 3.94073609022777 | 4.94786908091744 |
| H | 2.39155909391103 | 2.87507913002763 | 4.83343779107829 |
| C | 3.59454927765306 | 4.71847269563056 | 4.48288356421257 |
| H | 4.45796203092010 | 4.34651710920459 | 3.95753323831350 |
| C | 3.36246186214209 | 6.06929385071531 | 4.86500378408818 |
| H | 4.02328546031314 | 6.90070638037198 | 4.68210911322868 |
| C | 2.12207767511958 | 6.12613320050434 | 5.55206469959201 |
| H | 1.69009781201724 | 7.00065875377592 | 6.00795689631971 |
| C | 1.59467983017482 | 4.81123800119096 | 5.61383950505100 |
| H | 0.68113760978707 | 4.51576978996692 | 6.10375910990957 |
| C | 5.01737347946537 | 2.94426840153845 | 9.98957625182301 |
| H | 4.75495842817627 | 1.91373004313904 | 9.81597140322394 |
| C | 6.20137562754634 | 3.59106767320096 | 9.54618256872685 |
| H | 6.98931256044374 | 3.13666171075382 | 8.96951592612602 |
| C | 6.12459115405973 | 4.95585082199220 | 9.93173073742710 |
| H | 6.85506366849038 | 5.71766187637852 | 9.71297058457862 |
| C | 4.90161564158360 | 5.15199844666327 | 10.62451419984552 |
| H | 4.54801351359282 | 6.08270214051226 | 11.03313845120559 |
| C | 4.21208667497686 | 3.91069904360108 | 10.65419091878847 |
| H | 3.24261107551593 | 3.73323984741056 | 11.08933372461645 |
| C | 5.64748310739285 | 1.97057336237800 | 5.42084337942634 |
| C | 4.97122098404538 | 0.81068862085385 | 5.02175670914529 |
| C | 5.33347512805012 | 0.16198051172054 | 3.84927972611529 |
| H | 4.79761072647513 | -0.72819952143863 | 3.54470478149661 |
| C | 6.38185742708320 | 0.64094523071520 | 3.06956102853357 |
| H | 6.66884639013587 | 0.12640039282371 | 2.16219805289571 |
| C | 7.06304132120876 | 1.78609122954770 | 3.46987162420602 |
| H | 7.87968973471656 | 2.16917569707345 | 2.87043702034022 |
| C | 6.70843598412224 | 2.44603073722171 | 4.63757306495764 |
| H | 1.40217289460683 | 9.35972396607134 | 13.00652526978899 |
| C | 1.29770380363410 | 7.50253851696391 | 11.92696908141834 |
| C | 2.39259247533642 | 7.45157984193267 | 9.76999477480797 |
| C | 2.75997772461424 | 8.79200936553318 | 9.94713240815042 |
| C | 1.64533336957170 | 6.81633784667356 | 10.77170992104760 |
| C | 2.41551699638905 | 9.46453091692061 | 11.11100106268628 |
| H | 2.72115511350567 | 10.49532457622512 | 11.24053413431218 |
| C | 1.68058645909171 | 8.82786056678983 | 12.10629730429423 |
| H | 4.16730229404889 | 0.43250922824607 | 5.63990078891676 |
| H | 7.24065493354587 | 3.33178579128631 | 4.95839533681094 |
| H | 0.72175993439915 | 6.99719617350805 | 12.69247547061278 |
| H | 3.32068765802797 | 9.28829599526013 | 9.16600836783220 |
| H | 1.33941781588517 | 5.78924144168079 | 10.62623305306858 |

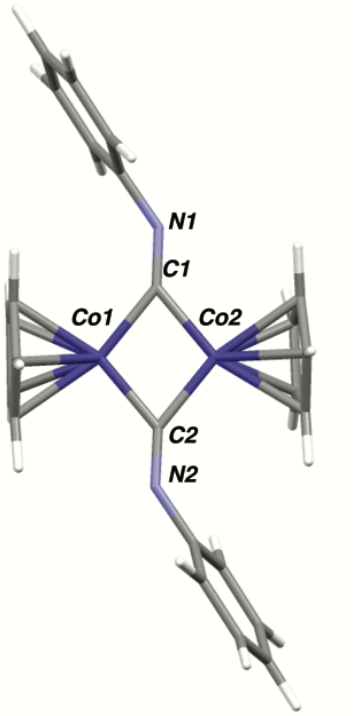


**Figure 4.33** Optimized molecular structure of $(\mu\text{–CNPh})_2[CpCo]_2$ (**2m**).

## Input for geometry optimization of $[(\mu\text{–CNPh})_2[CpCo]_2]^-$ [2m]$^-$.

```
#UKS OPT of  phenylanion5

%pal nprocs 8 end

! UKS B3LYP/G ZORA def2-TZVP def2-TZVP/J Opt RIJCOSX VerySlowConv KDIIS XYZFile
%SCF
 MaxIter 1000

end

* xyz -1 2

  Co     3.209772    4.655301    6.689691
  Co     4.325481    4.251170    8.688136
  N      5.295928    2.563646    6.544591
  N      2.302497    6.407015    8.806833
  C      4.600574    3.464158    7.028681
  C      3.017379    5.522705    8.320035
  C      2.091684    3.677612    5.213188
  H      1.920409    2.605146    5.198855
  C      3.178391    4.361134    4.592156
  H      3.976980    3.900348    4.018574
```

| | | | |
|---|---|---|---|
| C | 3.061087 | 5.754720 | 4.903836 |
| H | 3.754188 | 6.535680 | 4.604450 |
| C | 1.884039 | 5.933669 | 5.692055 |
| H | 1.541977 | 6.867766 | 6.126029 |
| C | 1.289759 | 4.651006 | 5.896998 |
| H | 0.404572 | 4.446110 | 6.491306 |
| C | 4.635642 | 2.730863 | 10.072345 |
| H | 4.235236 | 1.728279 | 9.953885 |
| C | 5.897352 | 3.194002 | 9.588237 |
| H | 6.608625 | 2.609954 | 9.012761 |
| C | 6.009808 | 4.582331 | 9.901015 |
| H | 6.838328 | 5.232003 | 9.633577 |
| C | 4.827198 | 4.973475 | 10.609616 |
| H | 4.601874 | 5.969200 | 10.977055 |
| C | 3.975670 | 3.833903 | 10.709936 |
| H | 2.987233 | 3.812772 | 11.159190 |
| C | 5.817600 | 2.110627 | 5.351078 |
| C | 5.708944 | 0.747390 | 5.008181 |
| C | 6.270524 | 0.273543 | 3.823910 |
| H | 6.168246 | -0.782914 | 3.569046 |
| C | 6.963121 | 1.135671 | 2.966878 |
| H | 7.405362 | 0.758196 | 2.044635 |
| C | 7.090622 | 2.485461 | 3.311571 |
| H | 7.637018 | 3.166655 | 2.656138 |
| C | 6.527536 | 2.975943 | 4.488827 |
| H | 2.063022 | 10.043716 | 12.638728 |
| C | 1.035771 | 8.437034 | 11.612179 |
| C | 2.264947 | 7.333574 | 9.827562 |
| C | 3.351796 | 8.204683 | 10.065778 |
| C | 1.098445 | 7.473976 | 10.607085 |
| C | 3.272922 | 9.166597 | 11.071640 |
| H | 4.121699 | 9.831694 | 11.243397 |
| C | 2.119813 | 9.287970 | 11.854434 |
| H | 5.176405 | 0.076876 | 5.683814 |
| H | 6.637728 | 4.024489 | 4.767769 |
| H | 0.127165 | 8.527045 | 12.210535 |
| H | 4.242750 | 8.117262 | 9.441902 |
| H | 0.252242 | 6.814738 | 10.409320 |

*

**Optimized coordinates for $[(\mu\text{–}CNPh)_2[CpCo]_2]^-$ [2m]$^-$.**

| | | | |
|---|---|---|---|
| Co | 2.82619771754695 | 4.38809068171552 | 6.70946810422786 |
| Co | 4.00217280451923 | 4.02271562184644 | 8.75331563153862 |
| N | 4.96068124565684 | 2.39404585816819 | 6.59315290736306 |
| N | 2.27998752004551 | 6.40639892936302 | 8.66703684327956 |
| C | 4.23220587339682 | 3.28472051333790 | 7.08908806628252 |
| C | 2.86419985800752 | 5.37517791890850 | 8.25693394747391 |
| C | 1.65579074779540 | 3.25489367016507 | 5.26487971583341 |

| | | | |
|---|---|---|---|
| H | 1.62531371975737 | 2.17688125813149 | 5.25576728438328 |
| C | 2.61316870110710 | 4.06350318709309 | 4.58362630400936 |
| H | 3.41345920326814 | 3.69678112153344 | 3.96160240003690 |
| C | 2.33239658224309 | 5.42317051631065 | 4.87416965876099 |
| H | 2.87912447391657 | 6.27794825377996 | 4.51004385968075 |
| C | 1.22848331140055 | 5.44947341618205 | 5.76704133421068 |
| H | 0.81065363587868 | 6.32784780341170 | 6.23058310369161 |
| C | 0.79611688472507 | 4.11019035439661 | 5.99013403571390 |
| H | -0.00640313088853 | 3.80478927009453 | 6.64224980507606 |
| C | 4.45216150695059 | 2.34170200754538 | 10.02832832369590 |
| H | 4.25274283984252 | 1.33164108963717 | 9.70850903983316 |
| C | 5.64714416904823 | 3.07777482820783 | 9.76489692824417 |
| H | 6.50139844515961 | 2.71006691643216 | 9.22009935090971 |
| C | 5.48890760936431 | 4.37776296341983 | 10.30106588936757 |
| H | 6.21505292774579 | 5.17443049636353 | 10.27017369376578 |
| C | 4.18643459271917 | 4.45533186479609 | 10.86817878029119 |
| H | 3.75460815313380 | 5.32407451126398 | 11.33591404202351 |
| C | 3.55891856106431 | 3.18713403944356 | 10.72386502667682 |
| H | 2.56073637920672 | 2.93409874547992 | 11.04261138697357 |
| C | 5.75616295497006 | 2.32086903215325 | 5.48619891730230 |
| C | 6.20110853043764 | 1.06418258178588 | 5.02798447362029 |
| C | 7.05062180352537 | 0.95977284043872 | 3.93793309998354 |
| H | 7.37378957607513 | -0.02090486347219 | 3.60557826472606 |
| C | 7.49824058812656 | 2.09719676457063 | 3.26615828737174 |
| H | 8.16534130969836 | 2.01114546958261 | 2.41763597321852 |
| C | 7.07328113675798 | 3.34618729622681 | 3.71329614330260 |
| H | 7.41516465744050 | 4.24316611946213 | 3.20838144525412 |
| C | 6.21829516568956 | 3.46577412690191 | 4.79703246860418 |
| H | 3.37232781952688 | 10.32745126363304 | 12.03127578662337 |
| C | 1.84261667009637 | 9.14020999740895 | 11.07802260617651 |
| C | 2.60105654453533 | 7.39681940039880 | 9.55761200101565 |
| C | 3.92861441517736 | 7.79574535743584 | 9.82743462173933 |
| C | 1.56586572352881 | 8.10796944220606 | 10.19590964604075 |
| C | 4.19223982845427 | 8.83306508395213 | 10.70993030894623 |
| H | 5.22067392915952 | 9.12037906542328 | 10.90300220339325 |
| C | 3.15786327843265 | 9.51489537385152 | 11.34827592496567 |
| H | 5.85961720731629 | 0.18177884913401 | 5.55503605587212 |
| H | 5.89685579350454 | 4.43951426445493 | 5.14201668606350 |
| H | 1.02328635920896 | 9.66355316969143 | 11.55764362006154 |
| H | 4.73578434127267 | 7.27524274441527 | 9.32979971026307 |
| H | 0.54489903445383 | 7.81953478331738 | 9.97854429211181 |

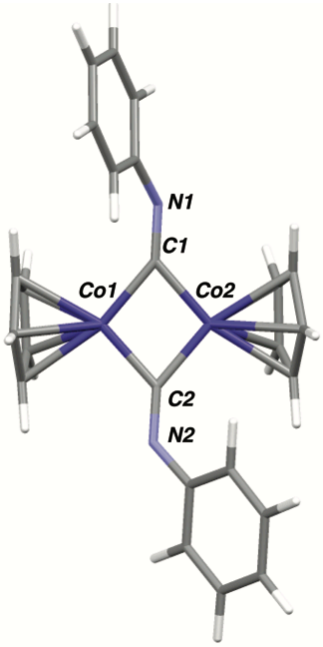


**Figure 4.34** Optimized molecular structure of $[(\mu\text{–CNPh})_2[CpCo]_2]^-$ [**2m**]$^-$.

## Input for geometry optimization of $[(\mu\text{–CNPh})_2[CpCo]_2]^{2-}$ [**2m**]$^{2-}$.

```
#UKS OPT of  phenyldianion

%pal nprocs 8 end

! UKS B3LYP/G ZORA def2-TZVP def2-TZVP/J Opt RIJCOSX VerySlowConv KDIIS XYZFile
%SCF
 MaxIter 1000

end

* xyz -2 1

 Co    3.209772   4.655301   6.689691
 Co    4.325481   4.251170   8.688136
 N     5.295928   2.563646   6.544591
 N     2.302497   6.407015   8.806833
 C     4.600574   3.464158   7.028681
 C     3.017379   5.522705   8.320035
 C     2.091684   3.677612   5.213188
 H     1.920409   2.605146   5.198855
 C     3.178391   4.361134   4.592156
 H     3.976980   3.900348   4.018574
 C     3.061087   5.754720   4.903836
```

| | | | |
|---|---|---|---|
| H | 3.754188 | 6.535680 | 4.604450 |
| C | 1.884039 | 5.933669 | 5.692055 |
| H | 1.541977 | 6.867766 | 6.126029 |
| C | 1.289759 | 4.651006 | 5.896998 |
| H | 0.404572 | 4.446110 | 6.491306 |
| C | 4.635642 | 2.730863 | 10.072345 |
| H | 4.235236 | 1.728279 | 9.953885 |
| C | 5.897352 | 3.194002 | 9.588237 |
| H | 6.608625 | 2.609954 | 9.012761 |
| C | 6.009808 | 4.582331 | 9.901015 |
| H | 6.838328 | 5.232003 | 9.633577 |
| C | 4.827198 | 4.973475 | 10.609616 |
| H | 4.601874 | 5.969200 | 10.977055 |
| C | 3.975670 | 3.833903 | 10.709936 |
| H | 2.987233 | 3.812772 | 11.159190 |
| C | 5.817600 | 2.110627 | 5.351078 |
| C | 5.708944 | 0.747390 | 5.008181 |
| C | 6.270524 | 0.273543 | 3.823910 |
| H | 6.168246 | -0.782914 | 3.569046 |
| C | 6.963121 | 1.135671 | 2.966878 |
| H | 7.405362 | 0.758196 | 2.044635 |
| C | 7.090622 | 2.485461 | 3.311571 |
| H | 7.637018 | 3.166655 | 2.656138 |
| C | 6.527536 | 2.975943 | 4.488827 |
| H | 2.063022 | 10.043716 | 12.638728 |
| C | 1.035771 | 8.437034 | 11.612179 |
| C | 2.264947 | 7.333574 | 9.827562 |
| C | 3.351796 | 8.204683 | 10.065778 |
| C | 1.098445 | 7.473976 | 10.607085 |
| C | 3.272922 | 9.166597 | 11.071640 |
| H | 4.121699 | 9.831694 | 11.243397 |
| C | 2.119813 | 9.287970 | 11.854434 |
| H | 5.176405 | 0.076876 | 5.683814 |
| H | 6.637728 | 4.024489 | 4.767769 |
| H | 0.127165 | 8.527045 | 12.210535 |
| H | 4.242750 | 8.117262 | 9.441902 |
| H | 0.252242 | 6.814738 | 10.409320 |

*

## S6.3.12 Optimized coordinates for $[(\mu\text{–}CNPh)_2[CpCo]_2]^{2-}$ $[\mathbf{2m}]^{2-}$.

| | | | |
|---|---|---|---|
| Co | 2.58021814250714 | 4.04991590011691 | 6.81317581516263 |
| Co | 3.62373666592899 | 3.75461637009819 | 8.92463046408026 |
| N | 5.25264523350439 | 2.84845623757890 | 6.72005967763966 |
| N | 2.55673955366713 | 6.46362581109543 | 8.38111260579553 |
| C | 4.24800141026378 | 3.45435364652984 | 7.23028641027628 |
| C | 2.92263356793872 | 5.25345747038812 | 8.14409249448050 |
| C | 1.40905441666033 | 2.59327363333736 | 5.63001857714138 |
| H | 1.53350851297912 | 1.52675497013579 | 5.74283703283484 |

| | | | |
|---|---|---|---|
| C | 2.19665836224683 | 3.44157087732391 | 4.80187826611099 |
| H | 2.99956989230634 | 3.12216836416327 | 4.15583311795003 |
| C | 1.76835463247728 | 4.78465944531474 | 5.00321469547459 |
| H | 2.16631188276334 | 5.66058090145122 | 4.51631324665555 |
| C | 0.72603357032699 | 4.75895787189179 | 5.97562664675902 |
| H | 0.23614020483594 | 5.62297428267650 | 6.39660413553110 |
| C | 0.50160144897757 | 3.41036562002147 | 6.35425224688009 |
| H | -0.18964000154894 | 3.07164181399955 | 7.11112190234866 |
| C | 3.53374762133560 | 1.93117203608224 | 10.16845309627203 |
| H | 3.23088436599754 | 0.97481112583977 | 9.77022473285105 |
| C | 4.84513017941969 | 2.47702744149513 | 10.12289627068089 |
| H | 5.70734608181738 | 2.00385104392369 | 9.67956826075050 |
| C | 4.80696560439258 | 3.77952979940035 | 10.69154750049893 |
| H | 5.64271461593080 | 4.44806030725991 | 10.82251972702533 |
| C | 3.45640465068361 | 4.04214923073900 | 11.06518315317587 |
| H | 3.08806081440364 | 4.96444784346069 | 11.48705764380824 |
| C | 2.67693275987463 | 2.89809642925136 | 10.75583613999719 |
| H | 1.61024843127892 | 2.80083457499987 | 10.89142151862319 |
| C | 5.98949702036303 | 3.00636384243676 | 5.60764613969826 |
| C | 6.61493426958702 | 1.88349281432200 | 4.99549401636885 |
| C | 7.47606984886781 | 2.02296057205079 | 3.92209117561592 |
| H | 7.92641904151344 | 1.13612497222409 | 3.48380722323237 |
| C | 7.76721096107955 | 3.28213920391062 | 3.38523189237373 |
| H | 8.45253151612744 | 3.39080280484876 | 2.55243938063668 |
| C | 7.15517709616964 | 4.39844400647803 | 3.96498364553595 |
| H | 7.36497704938505 | 5.38673862079826 | 3.56334833740460 |
| C | 6.27941818263341 | 4.27807314848636 | 5.03001740422711 |
| H | 4.66439187320656 | 10.42009496103194 | 11.19563265013086 |
| C | 2.86354372091727 | 9.53050099067713 | 10.38277576652243 |
| C | 3.11802523689554 | 7.41595229704322 | 9.16539069499718 |
| C | 4.50945726008911 | 7.48809670334057 | 9.45812512258322 |
| C | 2.31840971539204 | 8.47903447302425 | 9.66556709509728 |
| C | 5.04045179389315 | 8.55103073790417 | 10.16960196716857 |
| H | 6.10898311810559 | 8.57206103926039 | 10.36852203732995 |
| C | 4.23531429504294 | 9.58901420129113 | 10.64733970331942 |
| H | 6.39655277822694 | 0.90546027410296 | 5.40983566508581 |
| H | 5.80543016643654 | 5.14860849894424 | 5.46521517138421 |
| H | 2.21014135639241 | 10.31749797725770 | 10.75039375924089 |
| H | 5.14236886422492 | 6.68701491181893 | 9.09887322365690 |
| H | 1.25605321448123 | 8.44733390017266 | 9.44934054958550 |

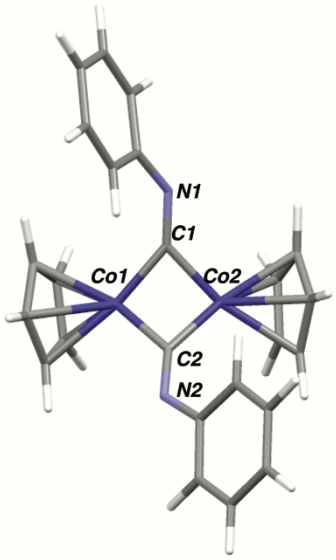


**Figure 4.35** Optimized molecular structure of $[(\mu\text{–CNPh})_2[CpCo]_2]^{2-}$ [**2m**]$^{2-}$.

## S6.3.13 Input for geometry optimization of $[(\mu\text{–CNPh})_2[CpNi]_2]$ (6m).

```
#UKS SP of  Cp2Ni2CNPh2_bridged

%pal nprocs 8 end

! UKS B3LYP/G ZORA def2-TZVP def2-TZVP/J OPT NormalPrint RIJCOSX NumFreq
VerySlowConv KDIIS XYZFile
%SCF
 MaxIter 1000

end
%output
Print[ P_Basis ] 2
Print[ P_MOs ] 1
end


* xyz 0 1
Ni      -4.253646000     10.639220000     18.414634000
Ni      -1.940160000     11.255390000     18.364477000
N       -3.709261000     13.035577000     16.894350000
N       -2.644408000      9.559271000     20.592398000
C       -3.416125000     12.115132000     17.574809000
C       -2.872408000     10.184839000     19.613220000
C       -5.766248000      9.930853000     17.018878000
H       -5.669928000      9.869896000     16.077503000
C       -6.207661000     11.063630000     17.745294000
```

| | | | |
|---|---|---|---|
| H | -6.447030000 | 11.899244000 | 17.362320000 |
| C | -6.234818000 | 10.758847000 | 19.124001000 |
| H | -6.518392000 | 11.327776000 | 19.828179000 |
| C | -5.755669000 | 9.430500000 | 19.245070000 |
| H | -5.627106000 | 8.960626000 | 20.060435000 |
| C | -5.499974000 | 8.919988000 | 17.947900000 |
| H | -5.199183000 | 8.041197000 | 17.742823000 |
| C | -0.260513000 | 11.083949000 | 16.989229000 |
| H | -0.306268000 | 10.804564000 | 16.082445000 |
| C | -0.429933000 | 12.409756000 | 17.475977000 |
| H | -0.619982000 | 13.171714000 | 16.939813000 |
| C | -0.264845000 | 12.412296000 | 18.871979000 |
| H | -0.294272000 | 13.169174000 | 19.445205000 |
| C | -0.045340000 | 11.068710000 | 19.257424000 |
| H | 0.063795000 | 10.756307000 | 20.149383000 |
| C | -0.017943000 | 10.266114000 | 18.098619000 |
| H | 0.138836000 | 9.331446000 | 18.073911000 |
| C | -4.034385000 | 14.152100000 | 16.146686000 |
| C | -3.778385000 | 15.427110000 | 16.690262000 |
| C | -4.102625000 | 16.544648000 | 15.926784000 |
| H | -3.933217000 | 17.413280000 | 16.272696000 |
| C | -4.671431000 | 16.407496000 | 14.666676000 |
| H | -4.879832000 | 17.179613000 | 14.152749000 |
| C | -4.929641000 | 15.147725000 | 14.162632000 |
| H | -5.340883000 | 15.068989000 | 13.310206000 |
| C | -4.604701000 | 13.984469000 | 14.866811000 |
| C | -2.604500000 | 8.765057000 | 21.715871000 |
| C | -1.714586000 | 7.670377000 | 21.713401000 |
| C | -1.723020000 | 6.839843000 | 22.835144000 |
| H | -1.148552000 | 6.082965000 | 22.857382000 |
| C | -2.544939000 | 7.096369000 | 23.909943000 |
| H | -2.543714000 | 6.509661000 | 24.656125000 |
| C | -3.368975000 | 8.196128000 | 23.907472000 |
| H | -3.913420000 | 8.366299000 | 24.666008000 |
| C | -3.424836000 | 9.067300000 | 22.822790000 |
| H | -4.067341459 | 9.935373607 | 22.828701723 |
| H | -1.054896571 | 7.482980503 | 20.879079473 |
| H | -3.342445978 | 15.533946018 | 17.672577242 |
| H | -4.781835592 | 13.003664665 | 14.450822789 |

*

### S6.3.14 Optimized coordinates for [(μ–CNPh)$_2$[CpNi]$_2$] (6m).

| | | | |
|---|---|---|---|
| Ni | -4.23802183780285 | 10.32268235757117 | 18.38004797432903 |
| Ni | -2.09951323009896 | 11.30248800649707 | 18.10484950708693 |
| N | -4.35462265114320 | 13.00812945292240 | 17.32411451255946 |
| N | -2.43285897575139 | 9.99617128306964 | 20.65792154051417 |
| C | -3.82885542007089 | 12.01442914717748 | 17.75517662728630 |
| C | -2.75789704388433 | 10.37754632389236 | 19.56469038483390 |

| | | | |
|---|---|---|---|
| C | -5.05232877663214 | 8.63930121346952 | 17.09788469134650 |
| H | -4.56821153497171 | 8.24183106296764 | 16.22094721064566 |
| C | -5.92077535851550 | 9.75673728269544 | 17.13924351947631 |
| H | -6.25140748532715 | 10.33496231401231 | 16.29138656952206 |
| C | -6.33239198784964 | 9.96528598384174 | 18.49593506717591 |
| H | -7.02405562716888 | 10.71669526073836 | 18.84001211111208 |
| C | -5.66655904647956 | 9.00932494763852 | 19.29227742450705 |
| H | -5.76258015863688 | 8.88243566073374 | 20.35856308054982 |
| C | -4.85259359207492 | 8.20707249324546 | 18.42568542755003 |
| H | -4.22019825010843 | 7.39231266479172 | 18.73948058914896 |
| C | -0.79052540995295 | 11.26441755530143 | 16.26138777559259 |
| H | -1.12575053612765 | 11.01856218942846 | 15.26653868498018 |
| C | -0.85821803819222 | 12.55812551982792 | 16.87138229750134 |
| H | -1.20909767874633 | 13.45908431160919 | 16.39522427757469 |
| C | -0.32256755634582 | 12.46465419360596 | 18.18104760971039 |
| H | -0.19136802729102 | 13.27394629442466 | 18.87986847264931 |
| C | -0.00139045056606 | 11.09740246631201 | 18.40277787983731 |
| H | 0.40434077728236 | 10.68441078849154 | 19.31243826506294 |
| C | -0.25487888017715 | 10.36998745869737 | 17.19828533745063 |
| H | -0.09567448607747 | 9.31353921522000 | 17.05339699659396 |
| C | -4.23271255928991 | 14.23117369784451 | 16.70178990609562 |
| C | -4.21732351242062 | 15.41341909790674 | 17.45126635555904 |
| C | -4.11350248728426 | 16.63755247939309 | 16.80609219958910 |
| H | -4.09354010436409 | 17.54631626296953 | 17.39414643474221 |
| C | -4.03727440688254 | 16.70378029568217 | 15.41817363674723 |
| H | -3.95776269992420 | 17.66159440319714 | 14.92109899305538 |
| C | -4.06576824764435 | 15.52855175705279 | 14.67382009294229 |
| H | -4.00601776357653 | 15.56981473735504 | 13.59322585459747 |
| C | -4.16845660202790 | 14.29711698744611 | 15.30371025480082 |
| C | -2.64299317492012 | 9.21728837266981 | 21.77029446522479 |
| C | -2.56467787162217 | 7.82044929288339 | 21.68355599954545 |
| C | -2.73030979650083 | 7.04604444706658 | 22.82259987360560 |
| H | -2.66736448651216 | 5.96758457773488 | 22.74511844656756 |
| C | -2.96900406930962 | 7.64339431354812 | 24.05648940412811 |
| H | -3.09301753560865 | 7.03484374156864 | 24.94227496705569 |
| C | -3.04603177677413 | 9.03053238144034 | 24.14067114398625 |
| H | -3.23445694558848 | 9.50648286011678 | 25.09467385496694 |
| C | -2.88097739672767 | 9.81883224277609 | 23.01212758020068 |
| H | -2.93407632394591 | 10.89758187646050 | 23.07401141990681 |
| H | -2.36536656865235 | 7.35998947900214 | 20.72542033931218 |
| H | -4.28331204697864 | 15.35694338007087 | 18.52965409001316 |
| H | -4.19469596073414 | 13.38058766063159 | 14.73031607976009 |

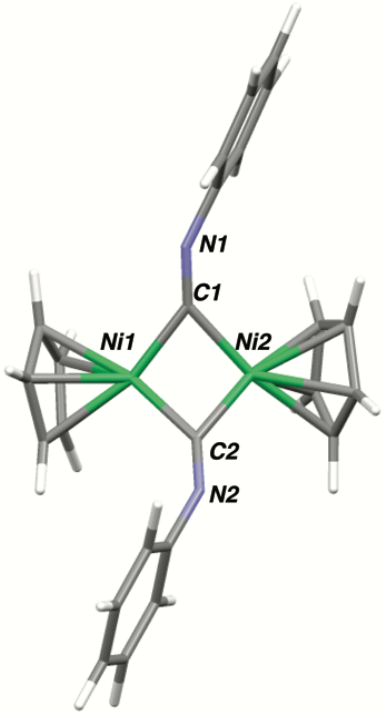


**Figure 4.36** Optimized molecular structure of $[(\mu^2\text{–}CN^{Ph})_2[CpNi]_2]$ (**6m**).

## Input for geometry optimization of $[CpNi(CNPh)]_2]$ (7m).

```
#UKS SP of  Cp2Ni2CNPh2_unbridged

%pal nprocs 8 end

! UKS B3LYP/G ZORA def2-TZVP def2-TZVP/J OPT NormalPrint RIJCOSX NumFreq
VerySlowConv KDIIS XYZFile
%SCF
 MaxIter 1000

end
%output
Print[ P_Basis ] 2
Print[ P_MOs ] 1
end

* xyz 0 1

Ni      8.964057000     5.207215000     7.666254000
N       7.953113000     6.797752000     9.916780000
C       8.022216000     7.614509000    11.036793000
C       9.242510000     7.653892000    11.768885000
```

| | | | |
|---|---|---|---|
| C | 6.911859000 | 8.383323000 | 11.418881000 |
| C | 9.776487000 | 3.996462000 | 6.165904000 |
| H | 9.305331000 | 3.823521000 | 5.384228000 |
| C | 9.314754000 | 8.556263000 | 12.824730000 |
| H | 10.106296000 | 8.614481000 | 13.311819000 |
| C | 8.262506000 | 9.359322000 | 13.174734000 |
| H | 8.350455000 | 9.963757000 | 13.874742000 |
| C | 7.070481000 | 9.271996000 | 12.483476000 |
| H | 6.359035000 | 9.816501000 | 12.731396000 |
| C | 8.304910000 | 6.195029000 | 8.968853000 |
| C | 10.505208000 | 3.866328000 | 8.300928000 |
| H | 10.627709000 | 3.585514000 | 9.178855000 |
| C | 9.727801000 | 3.217374000 | 7.350084000 |
| H | 9.262927000 | 2.421164000 | 7.466752000 |
| C | 11.078448000 | 5.023830000 | 7.720505000 |
| H | 11.632842000 | 5.633401000 | 8.152177000 |
| C | 10.663831000 | 5.085472000 | 6.372990000 |
| H | 10.921396000 | 5.719015000 | 5.742982000 |
| Ni | 6.741143000 | 5.207215000 | 6.917246000 |
| N | 7.752087000 | 6.797752000 | 4.666720000 |
| C | 7.682984000 | 7.614509000 | 3.546707000 |
| C | 6.462690000 | 7.653892000 | 2.814615000 |
| C | 8.793341000 | 8.383323000 | 3.164619000 |
| C | 5.928713000 | 3.996462000 | 8.417596000 |
| H | 6.399869000 | 3.823521000 | 9.199272000 |
| C | 6.390446000 | 8.556263000 | 1.758770000 |
| H | 5.598904000 | 8.614481000 | 1.271681000 |
| C | 7.442694000 | 9.359322000 | 1.408766000 |
| H | 7.354745000 | 9.963757000 | 0.708758000 |
| C | 8.634719000 | 9.271996000 | 2.100024000 |
| H | 9.346165000 | 9.816501000 | 1.852105000 |
| C | 7.400290000 | 6.195029000 | 5.614648000 |
| C | 5.199992000 | 3.866328000 | 6.282572000 |
| H | 5.077491000 | 3.585514000 | 5.404645000 |
| C | 5.977399000 | 3.217374000 | 7.233416000 |
| H | 6.442273000 | 2.421164000 | 7.116748000 |
| C | 4.626752000 | 5.023830000 | 6.862995000 |
| H | 4.072358000 | 5.633401000 | 6.431323000 |
| C | 5.041369000 | 5.085472000 | 8.210510000 |
| H | 4.783804000 | 5.719015000 | 8.840518000 |
| H | 5.631314954 | 7.012582939 | 3.067475081 |
| H | 9.739271774 | 8.290363193 | 3.677428365 |
| H | 10.073885046 | 7.012582939 | 11.516024919 |
| H | 5.965928226 | 8.290363193 | 10.906071635 |

*

**Optimized coordinates for [CpNi(CNPh)]$_2$] (7m).**

| | | | |
|---|---|---|---|
| Ni | 8.982342 | 4.718081 | 7.651888 |

| | | | |
|---|---|---|---|
| N | 8.184666 | 6.810392 | 9.521289 |
| C | 8.108852 | 7.906002 | 10.345899 |
| C | 9.282345 | 8.553815 | 10.747423 |
| C | 6.867706 | 8.372489 | 10.784234 |
| C | 9.724113 | 3.291376 | 6.268233 |
| H | 9.154478 | 2.951144 | 5.419211 |
| C | 9.205154 | 9.660798 | 11.578353 |
| H | 10.115053 | 10.159271 | 11.886907 |
| C | 7.971160 | 10.130968 | 12.014690 |
| H | 7.917047 | 10.996500 | 12.661761 |
| C | 6.806807 | 9.483364 | 11.613978 |
| H | 5.844312 | 9.846983 | 11.950128 |
| C | 8.464456 | 5.970216 | 8.744727 |
| C | 10.620447 | 3.406370 | 8.368546 |
| H | 10.845105 | 3.213043 | 9.405460 |
| C | 9.755780 | 2.662628 | 7.554464 |
| H | 9.184658 | 1.798917 | 7.852045 |
| C | 11.152243 | 4.486532 | 7.584657 |
| H | 11.851321 | 5.228575 | 7.937333 |
| C | 10.643106 | 4.377284 | 6.274131 |
| H | 10.863461 | 5.028688 | 5.444919 |
| Ni | 6.722611 | 4.719468 | 6.931633 |
| N | 7.518033 | 6.811677 | 5.060937 |
| C | 7.595023 | 7.907285 | 4.236450 |
| C | 6.422094 | 8.556292 | 3.835146 |
| C | 8.836539 | 8.372451 | 3.797788 |
| C | 5.982912 | 3.292605 | 8.316228 |
| H | 6.553455 | 2.952679 | 9.164746 |
| C | 6.500157 | 9.663133 | 3.004136 |
| H | 5.590690 | 10.162495 | 2.695756 |
| C | 7.734537 | 10.132014 | 2.567481 |
| H | 7.789414 | 10.997440 | 1.920326 |
| C | 8.898313 | 9.483262 | 2.967987 |
| H | 9.861081 | 9.845904 | 2.631552 |
| C | 7.239974 | 5.971477 | 5.838036 |
| C | 5.084468 | 3.406938 | 6.216815 |
| H | 4.858771 | 3.213355 | 5.180168 |
| C | 5.950274 | 2.663700 | 7.030091 |
| H | 6.521504 | 1.800239 | 6.731996 |
| C | 4.552783 | 4.486850 | 7.001152 |
| H | 3.852850 | 5.228382 | 6.649071 |
| C | 5.063256 | 4.377974 | 8.311169 |
| H | 4.843422 | 5.029345 | 9.140544 |
| H | 5.468999 | 8.184089 | 4.185331 |
| H | 9.733668 | 7.862021 | 4.120598 |
| H | 10.235169 | 8.180686 | 10.397483 |
| H | 5.970189 | 7.862937 | 10.461107 |

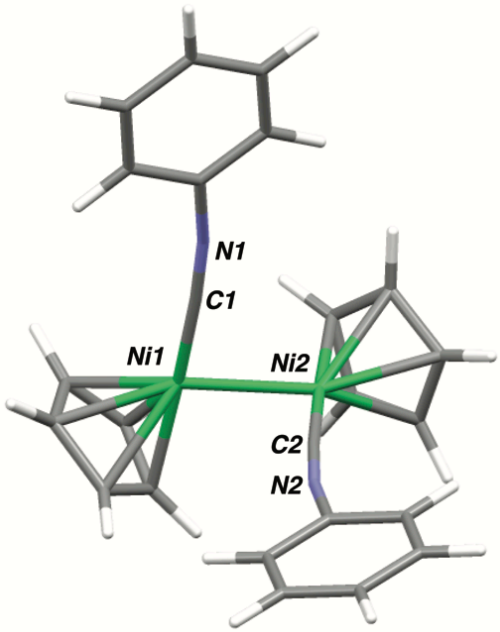


**Figure 4.37** Optimized molecular structure of $[CpNi(CNPh)]_2$] (**7m**).

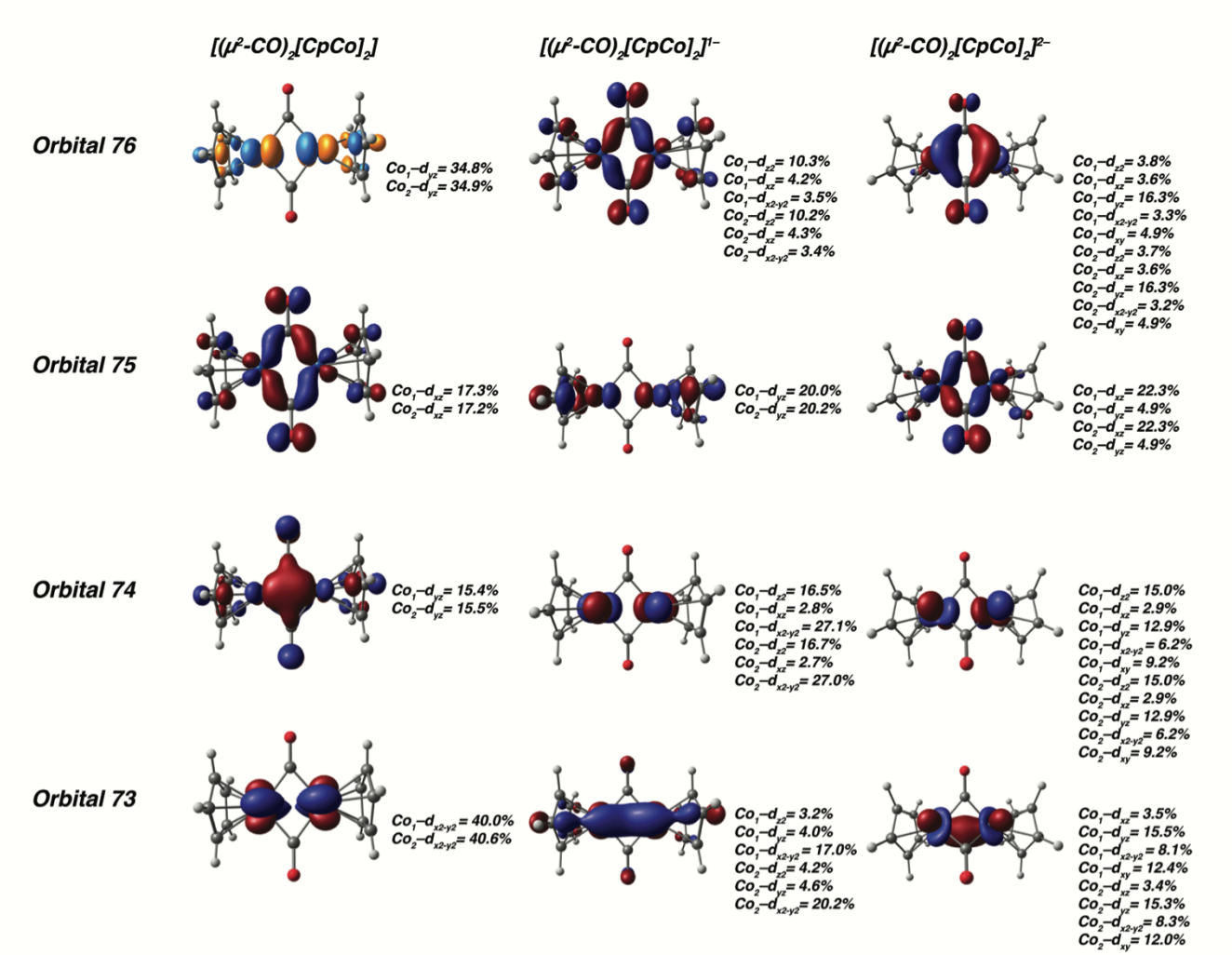


**Figure 4.38** $[(\mu\text{-CO})_2[\text{CpCo}]^n$ (n = 0, -1, -2) Bonding orbitals with percent d-orbital contribution: orbitals 76-73. **Note**: Orbital 76 of $[(\mu\text{-CO})_2[\text{CpCo}]^0$ is the lowest unoccupied molecular orbital (LUMO) included for reference.

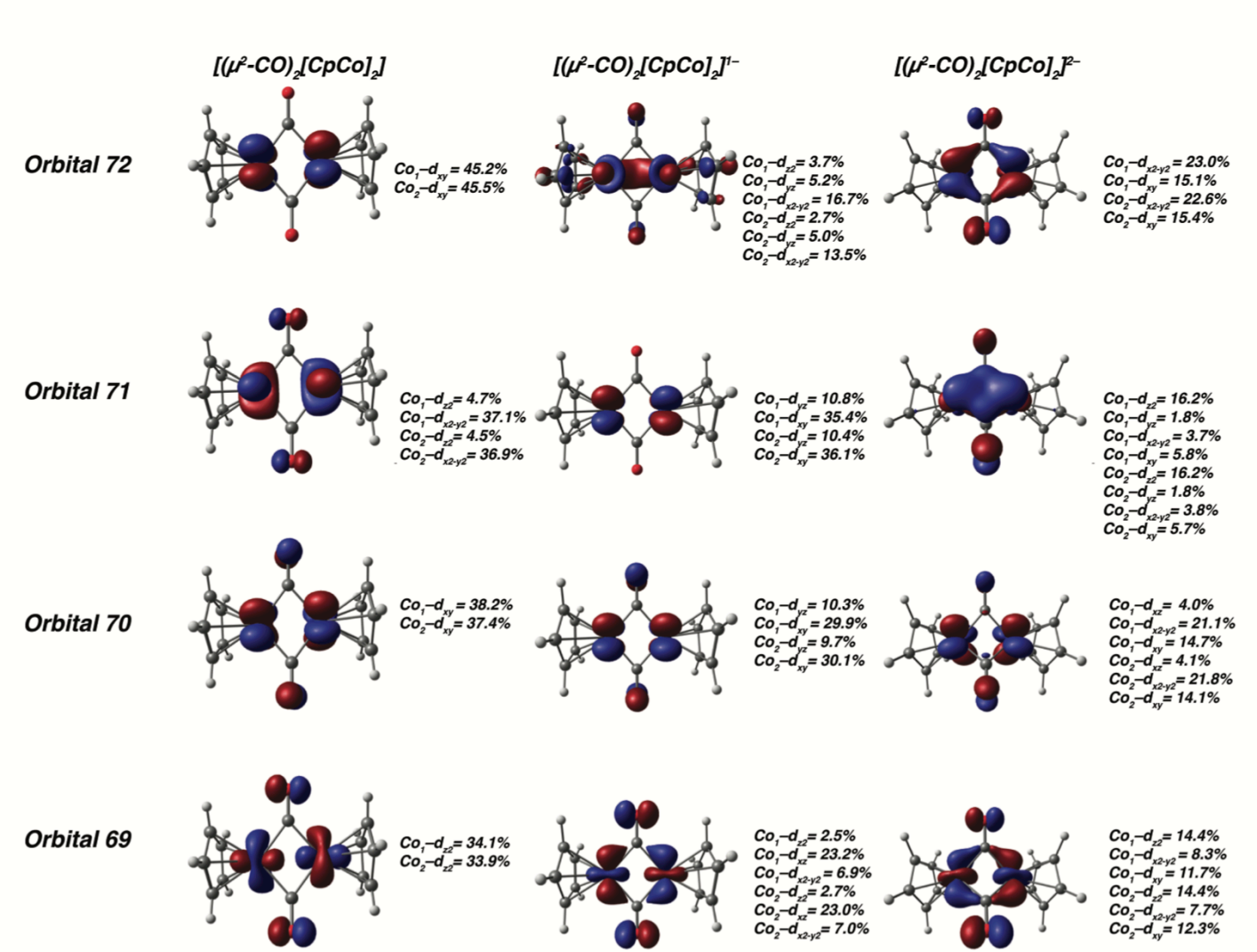


**Figure 4.39** $[(\mu\text{-CO})_2[\text{CpCo}]^n$ (n = 0, -1, -2) Bonding orbitals with percent d-orbital contribution: orbitals 72-69.

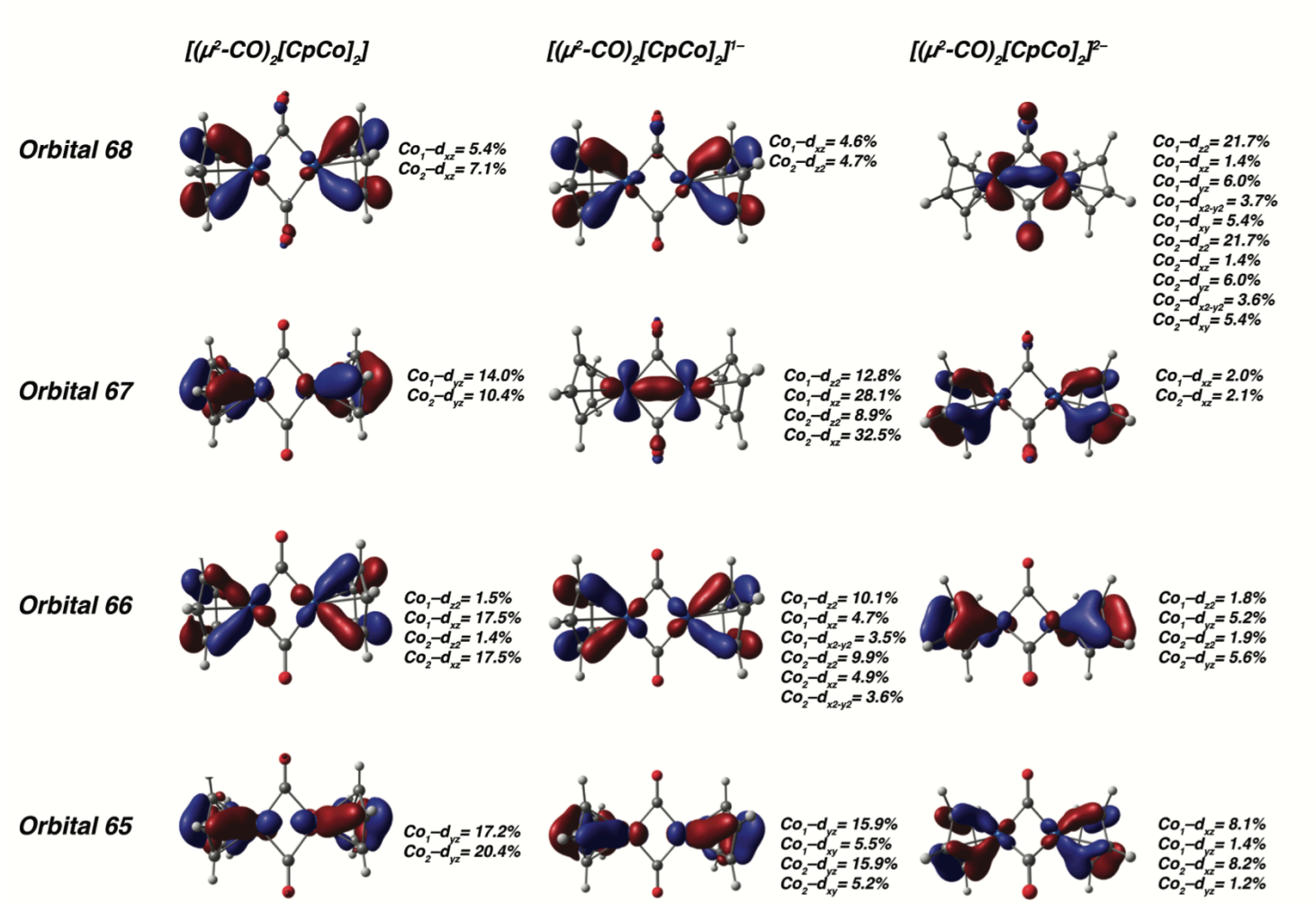


**Figure 4.40** $[(\mu\text{-CO})_2[\text{CpCo}]^n$ (n = 0, -1, -2) Bonding orbitals with percent d-orbital contribution: orbitals 68-65.

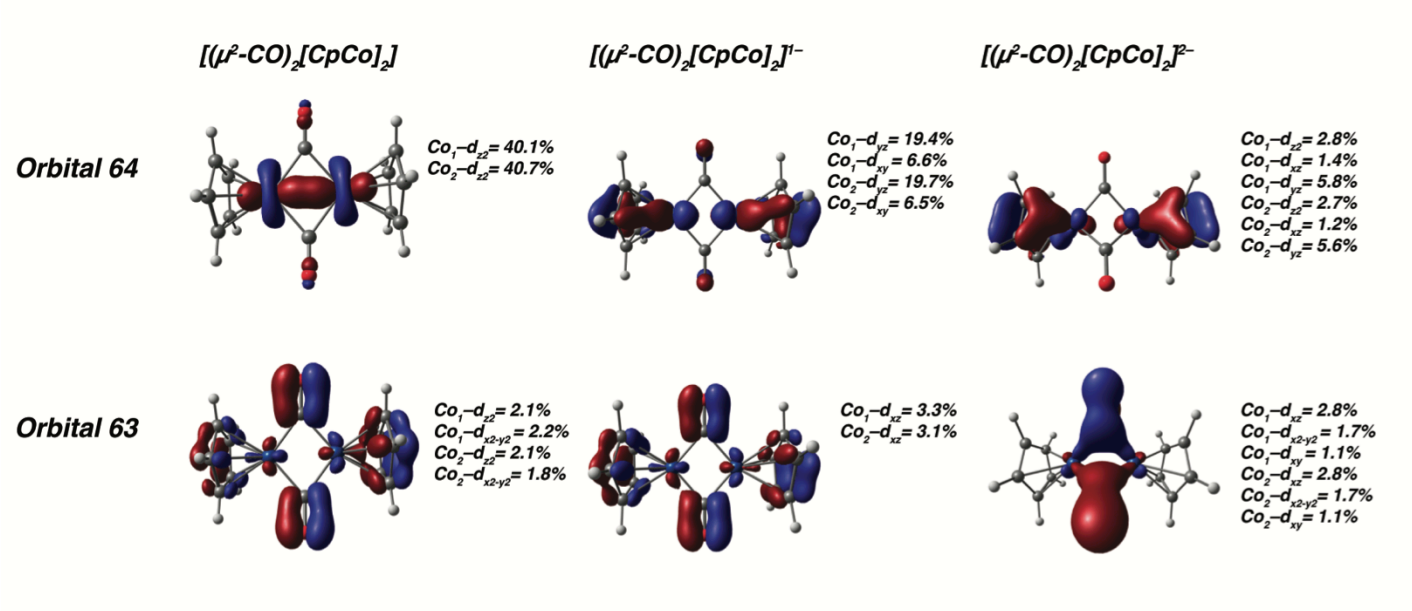


**Figure 4.41** $[(\mu\text{-CO})_2[\text{CpCo}]^n$ (n = 0, -1, -2) Bonding orbitals with percent d-orbital contribution: orbitals 64-63.

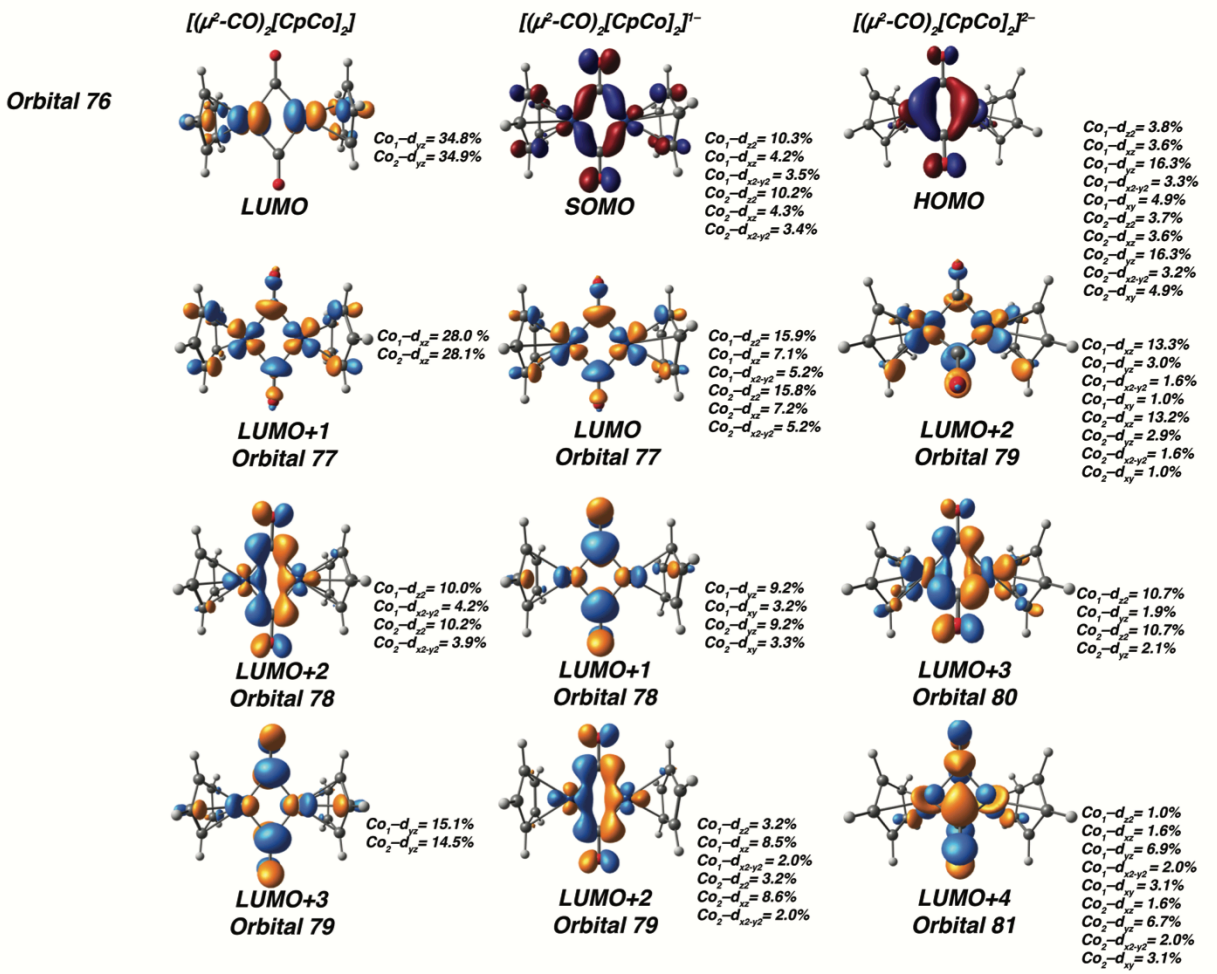


**Figure 4.42** [(μ-CO)$_2$[CpCo]$^n$ (n = 0, -1, -2) Unoccupied moleuclar orbitals with >5% d-orbital contribution. **Note**: Orbital 76 of [(μ-CO)$_2$[CpCo]$^{1/-2}$ are the SOMO (singly occupied molecular orbital) and HOMO (highest occupied molecular orbitals) for reference.

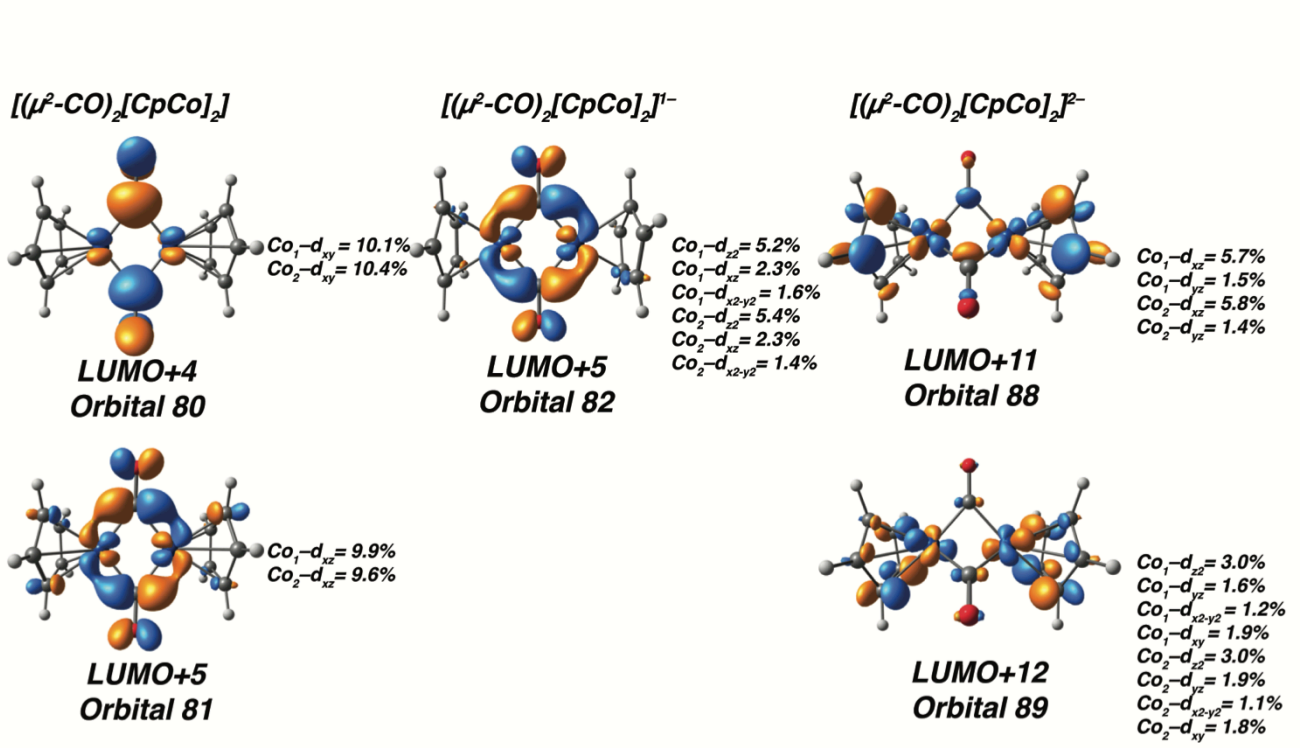


**Figure 4.43** [(μ-CO)$_2$[CpCo]$^n$ (n = 0, -1, -2) Unoccupied moleuclar orbitals with >5% d-orbital contribution.

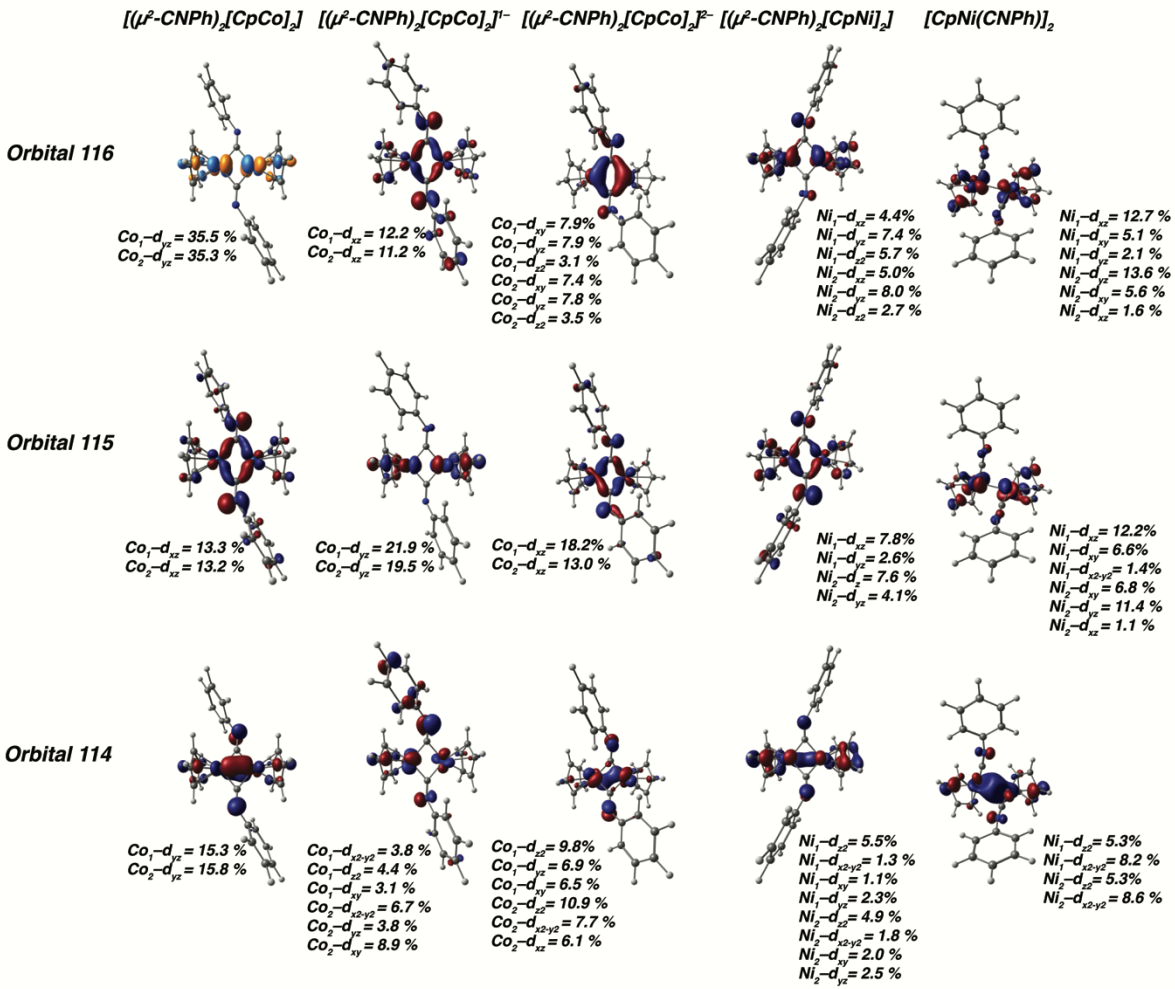


**Figure 4.44** $[(\mu\text{-CNPh})_2[CpCo]^n$ (n = 0, -1, -2), $[(\mu\text{-CNPh})_2[CpNi]$, and $[CpNi(CNPh)]_2$ bonding orbitals with percent d-orbital contribution: orbitals 116-114. **Note**: Orbital 116 of $[(\mu\text{-CNPh})_2[CpCo]^0$ is the lowest unoccupied molecular orbital (LUMO) for reference. All orbitals with <5% net d-contribution do not have contributions listed.

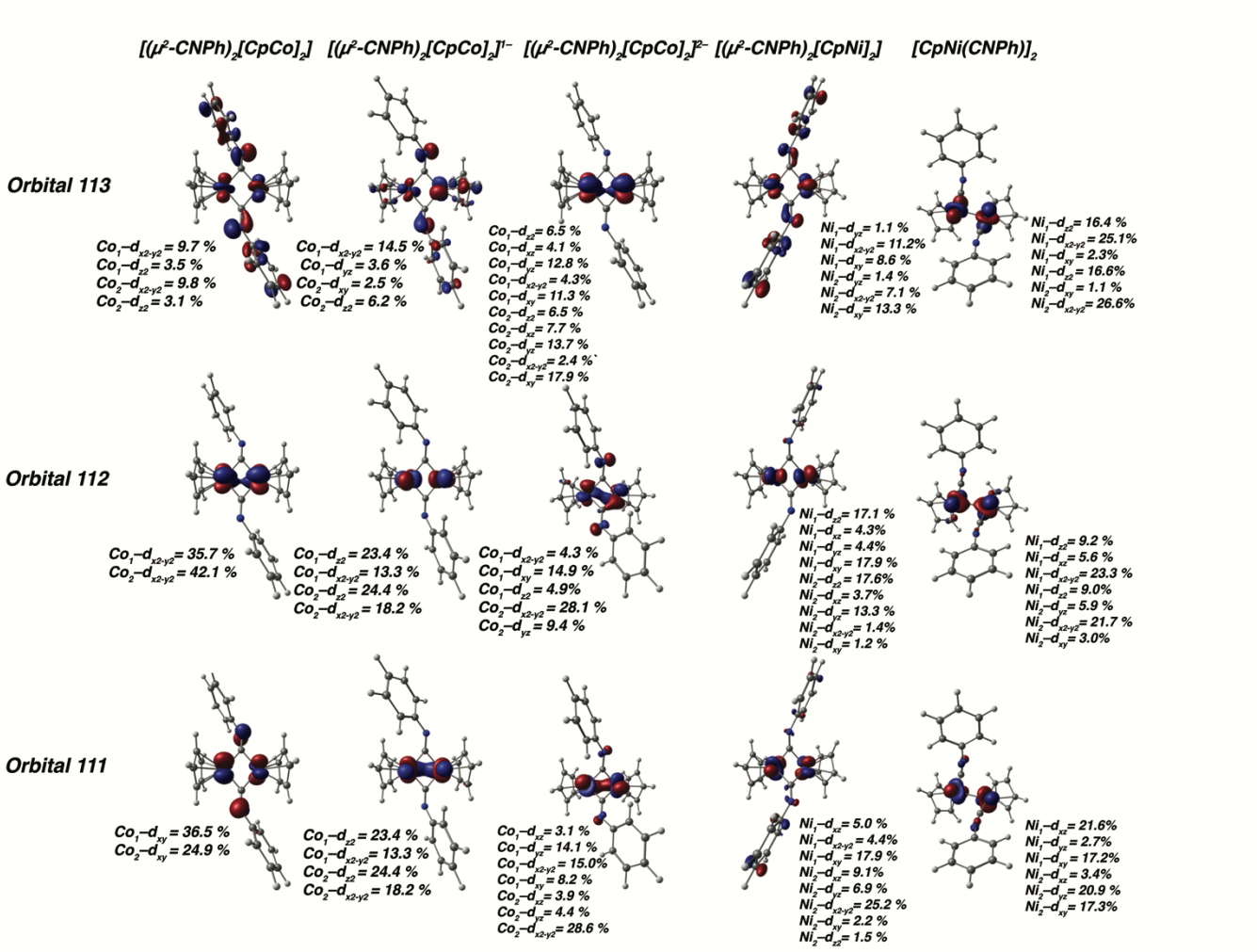


**Figure 4.45** [(μ-CNPh)$_2$[CpCo]$^n$ (n = 0, -1, -2), [(μ-CNPh)$_2$[CpNi], and [CpNi(CNPh)]$_2$ bonding orbitals with percent d-orbital contribution: orbitals 113-111. **Note:** All orbitals with <5% net d-contribution do not have contributions listed.

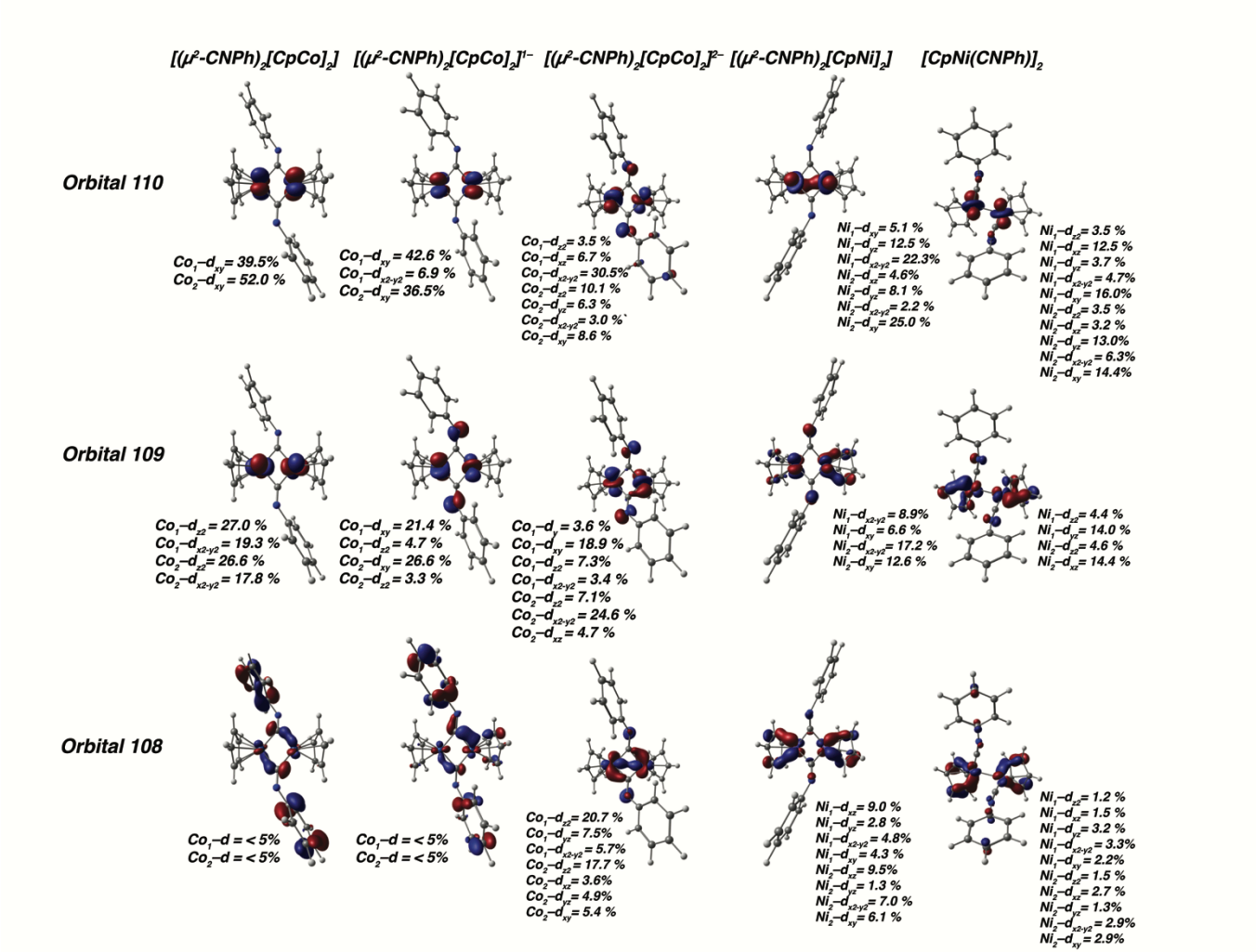


**Figure 4.46** [(μ-CNPh)$_2$[CpCo]$^n$ (n = 0, -1, -2), [(μ-CNPh)$_2$[CpNi], and [CpNi(CNPh)]$_2$ bonding orbitals with percent d-orbital contribution: orbitals 110-108. **Note:** All orbitals with <5% net d-contribution do not have contributions listed.

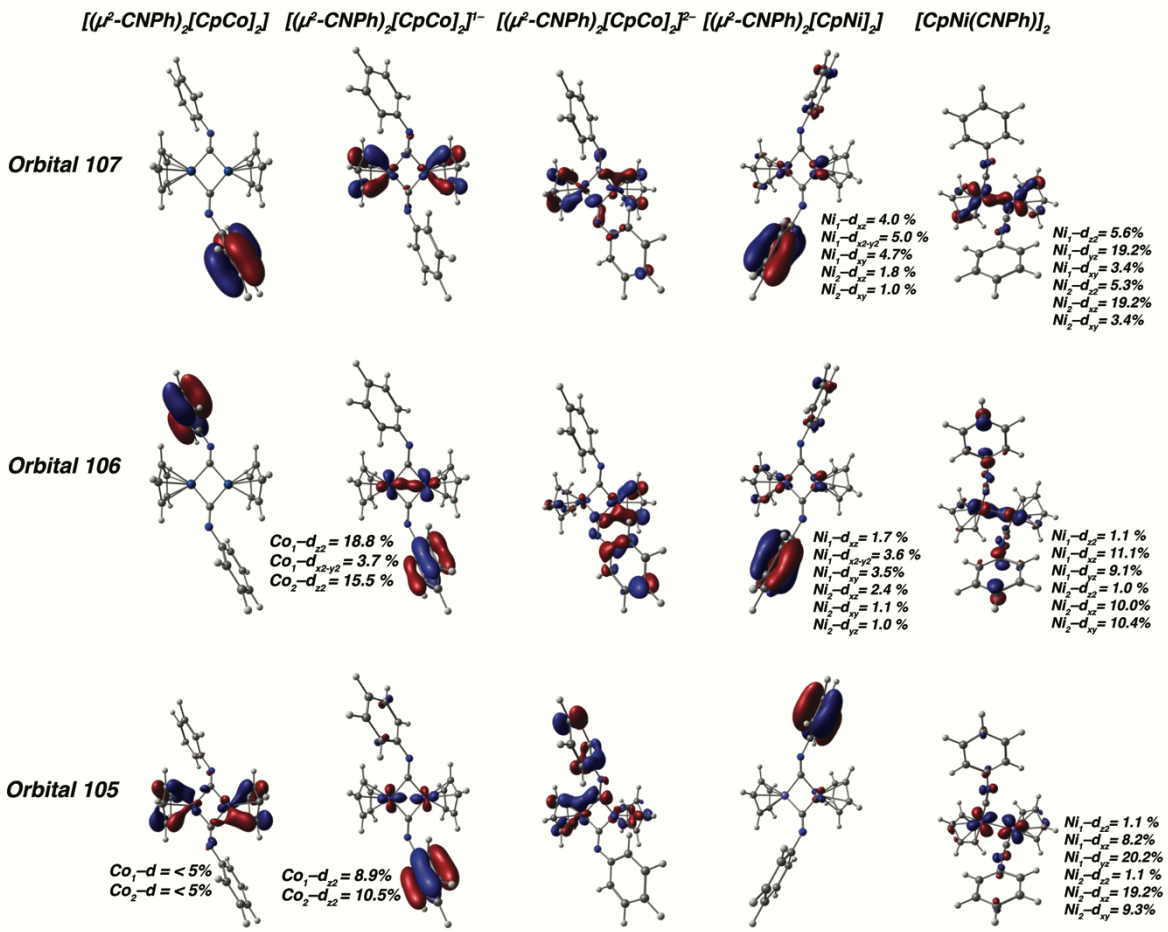


**Figure 4.47** [(μ-CNPh)$_2$[CpCo]$^n$ (n = 0, -1, -2), [(μ-CNPh)$_2$[CpNi], and [CpNi(CNPh)]$_2$ bonding orbitals with percent d-orbital contribution: orbitals 107-105. **Note:** All orbitals with <5% net d-contribution do not have contributions listed.

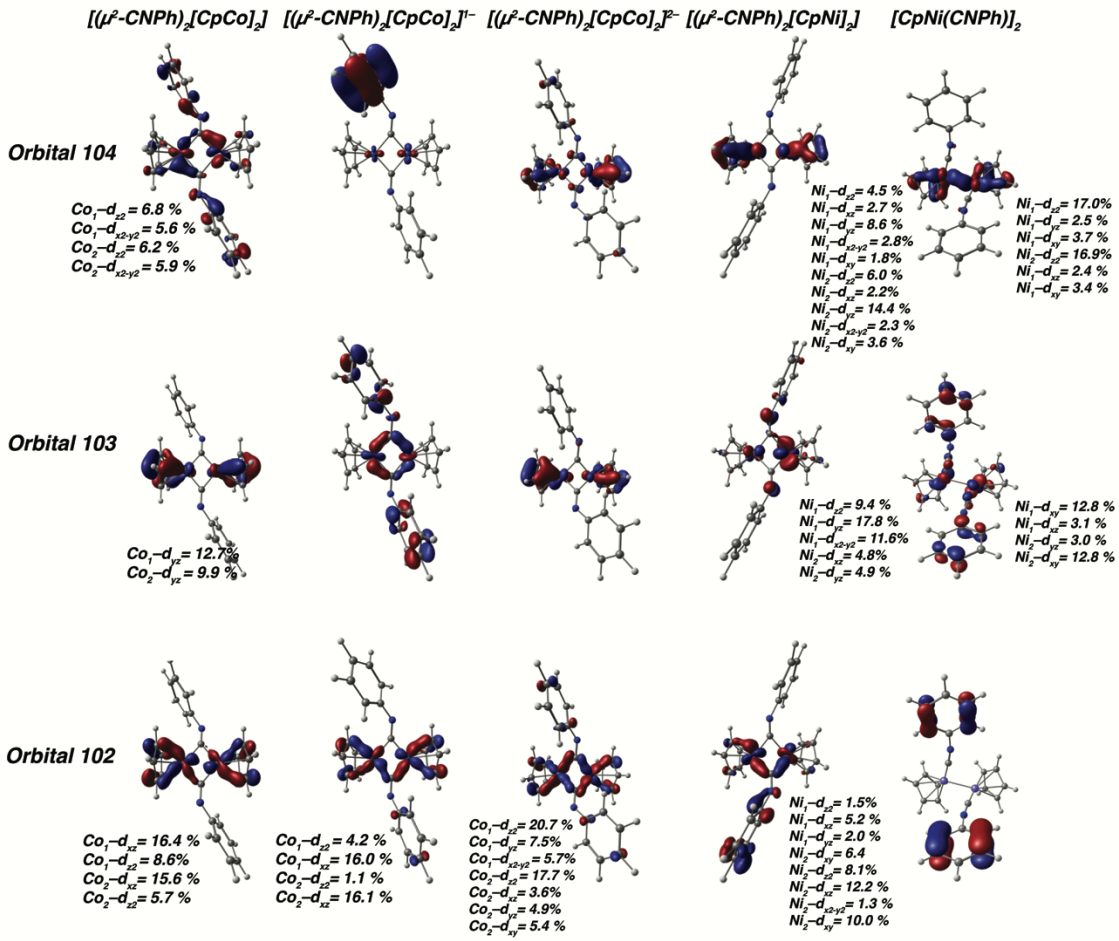


**Figure 4.48** [(μ-CNPh)$_2$[CpCo]$^n$ (n = 0, -1, -2), [(μ-CNPh)$_2$[CpNi], and [CpNi(CNPh)]$_2$ bonding orbitals with percent d-orbital contribution: orbitals 104-102. **Note:** All orbitals with <5% net d-contribution do not have contributions listed.

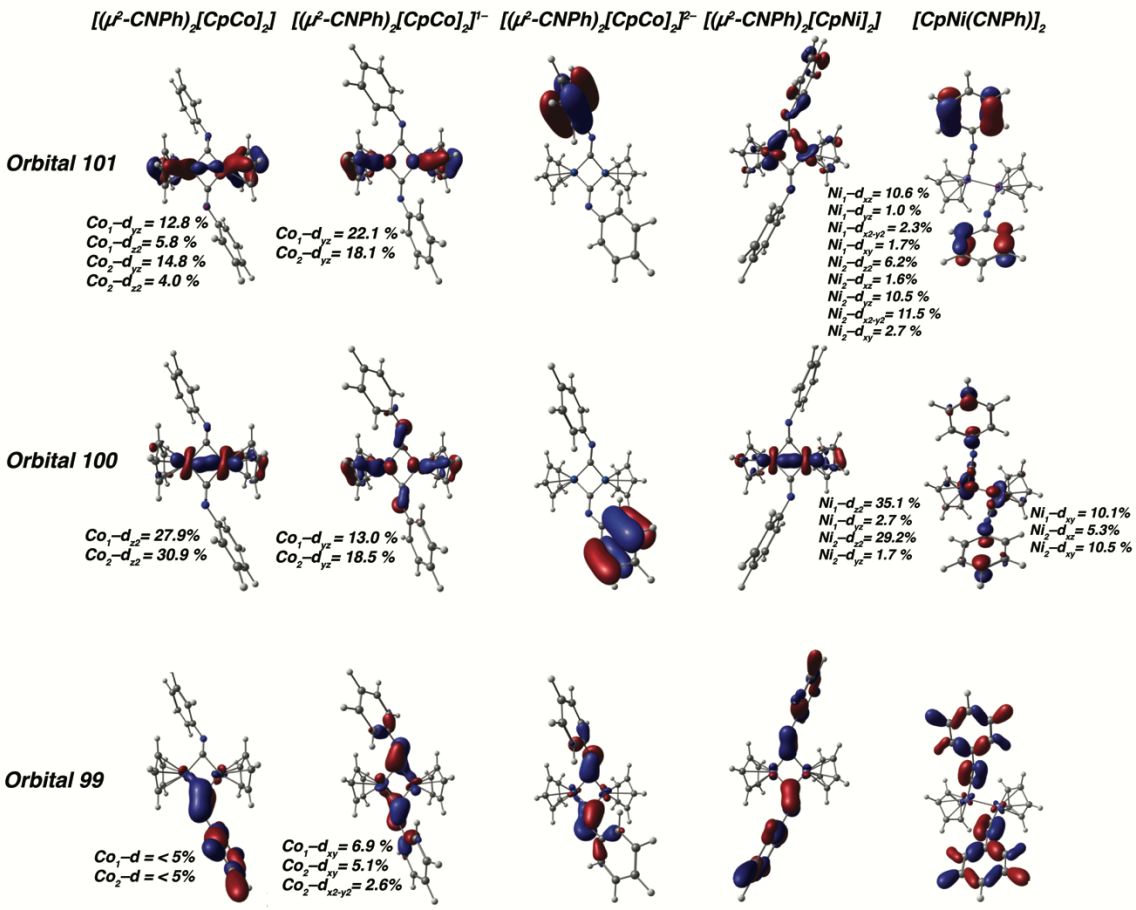


**Figure 4.49** [(μ-CNPh)$_2$[CpCo]$^n$ (n = 0, -1, -2), [(μ-CNPh)$_2$[CpNi], and [CpNi(CNPh)]$_2$ bonding orbitals with percent d-orbital contribution: orbitals 101-99. **Note:** All orbitals with <5% net d-contribution do not have contributions listed.

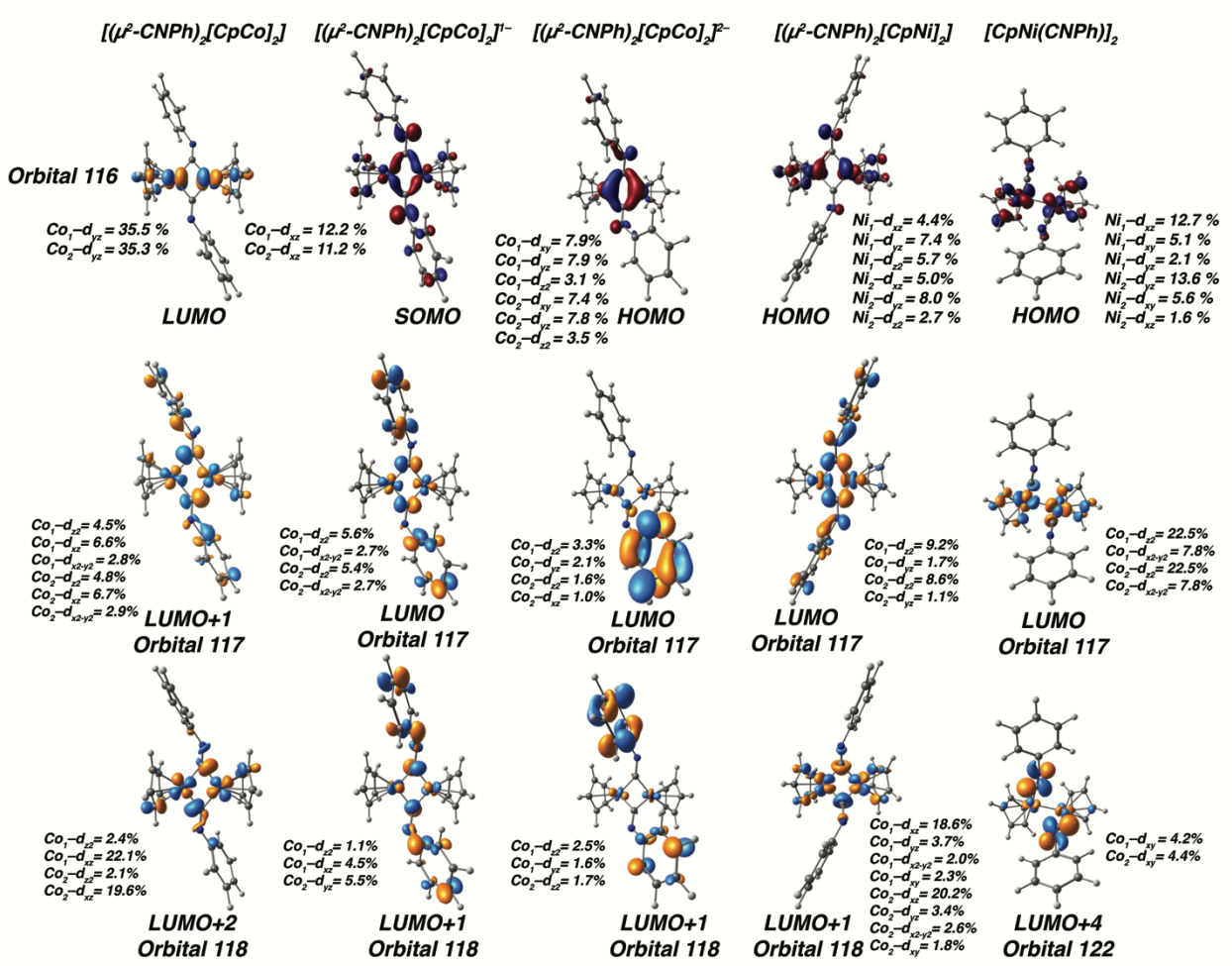


**Figure 4.50** $[(\mu\text{-CNPh})_2[CpCo]^n$ (n = 0, -1, -2), $[(\mu\text{-CNPh})_2[CpNi]$, and $[CpNi(CNPh)]_2$ unoccupied orbitals with percent d-orbital contribution. **Note**: Orbital 116 of $[(\mu^2\text{-CNPh})_2[CpCo]^{-1/-}2$, $[(\mu^2\text{-CNPh})_2[CpNi]$, and $[CpNi(\mu^2\text{-CNPh})]_2$ are the highest occupied molecular orbitals (HUMO's) for reference. Only unoccupied orbitals with >5% net d-contribution are listed.

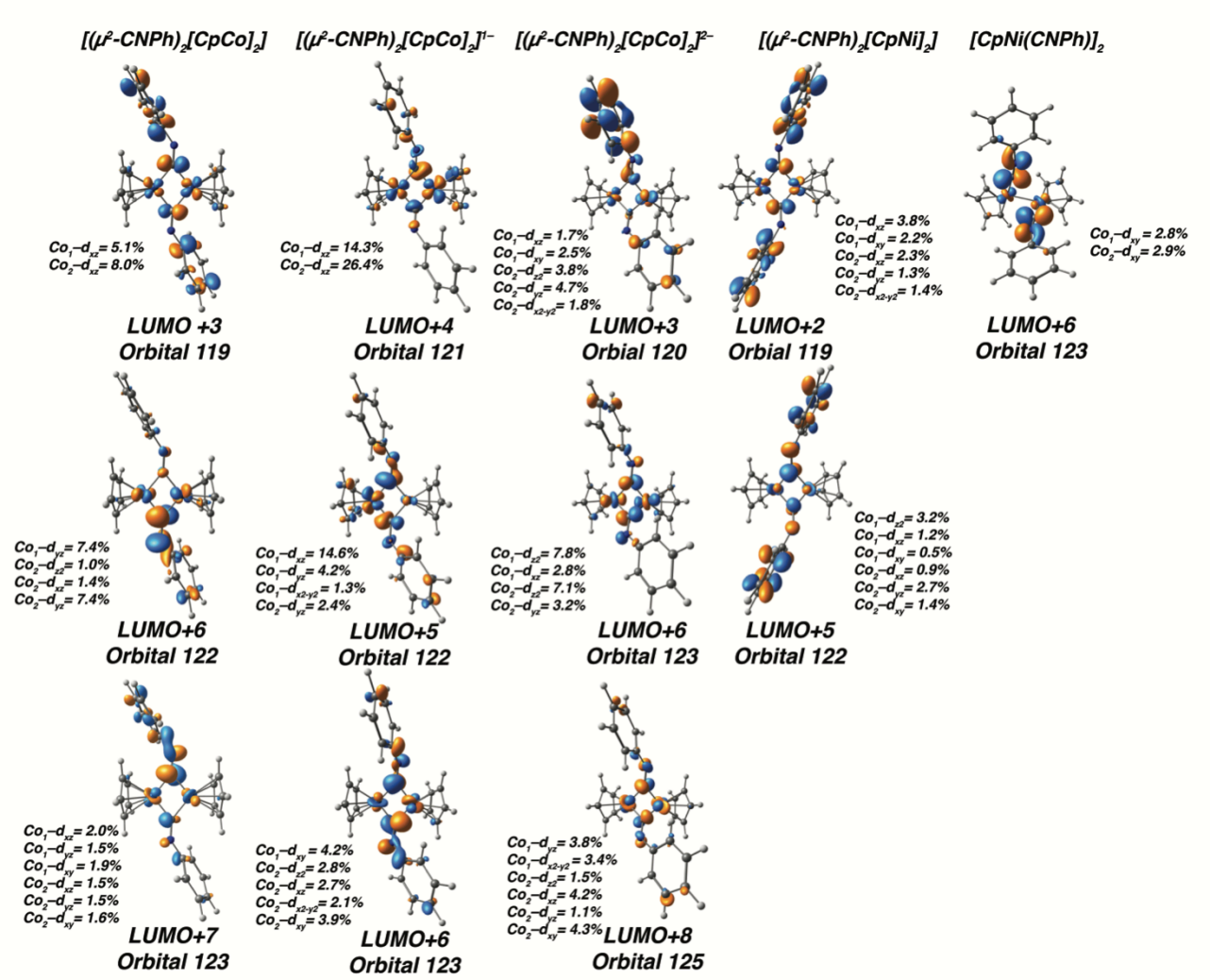


**Figure 4.51** [(μ-CNPh)$_2$[CpCo]$^n$ (n = 0, -1, -2), [(μ-CNPh)$_2$[CpNi], and [CpNi(CNPh)]$_2$ unoccupied orbitals with percent d-orbital contribution. Only unoccupied orbitals with >5% net d-contribution are listed.

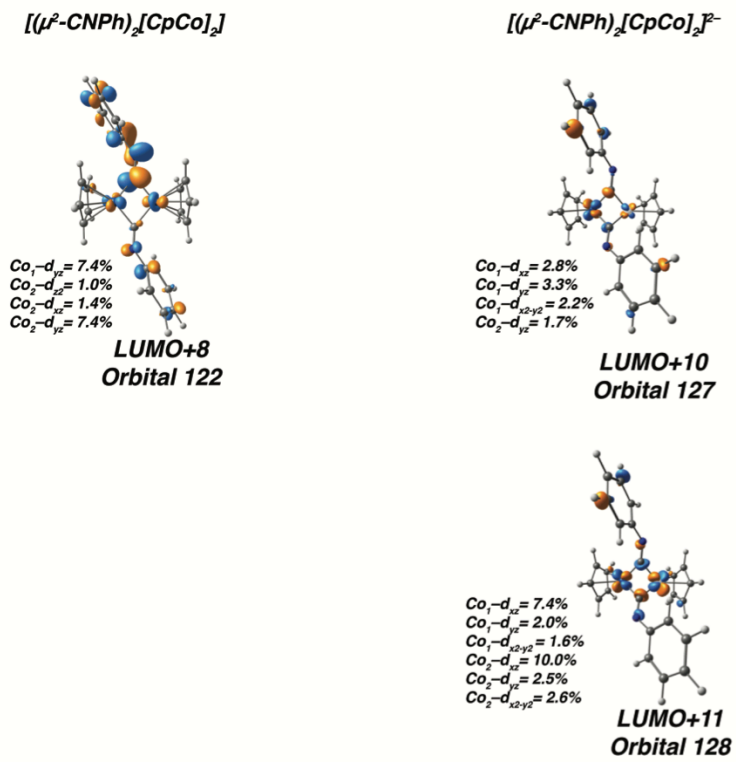


**Figure 4.52** [(μ-CNPh)$_2$[CpCo]$^n$ (n = 0, -2), unoccupied orbitals with percent d-orbital contribution. Only unoccupied orbitals with >5% net d-contribution are listed.

**4.10 Acknowledgments.**

Chapter 4 is currently in preperation as a manuscript by Mokhtarzadeh, C. C.; Carpenter A. E.; Spence, D. P.; Weidemann, N.; Agnew, D. W.; Melaimi, M.; Moore, C. E; Rheingold, A. L.; and Figueroa, J.S. The dissertation author is the primary author of this manuscript. Dr. Brandon R. Barnett, Kyle A. Mandla, Prof. Jeffery Rinehart are thanked for helpful discussions.

**4. 11 References.**

(1) Brunner, H. *J. Organomet. Chem.* **1968,** *12*, 517-522.

(2) Peter, K.; Vollhardt, C.; Bercaw, J. E.; Bergman, R. G., *J. Organomet. Chem.* **1975**, *97*, 283-297.

(3) Henda, C. S.; Schore, N. E.; Bergman, R. G. *J. Am. Chem. Soc.* **1976**, *98*, 255-256.

(4) Schore, N. E.; Ilenda, C. S.; Bergman, R. G. *J. Am. Chem. Soc.* **1976**, *98*, 256-258.

(5) Herrmann, W. A.; Bernal, I., *Angew. Chem. Int. Ed.* **1977**, *16*, 172-173.

(6) Lee, W. S.; Brintzinger, H. H., *J. Organomet. Chem.* **1977**, *127*, 87-92.

(7) Madach, T.; Fischer, K.; Vahrenkamp, H., *Chem. Ber.* **1980**, *113*, 3235-3244.

(8) Byers, L. R.; Dahl, L. F. *Inorg. Chem.* **1980**, *19*, 680-692.

(9) Bernal, I.; Korp, J. D.; Reisner, G. M.; Herrmann, W. A. *J. Organomet. Chem.* **1977**, *139*, 321-336.

(10) Ginsburg, R. E.; Cirjak, L. M.; Dahl, L. F. *J. Chem. Soc., Chem. Commun.* **1979**, 468-470.

(11) Pinhas, A. R.; Hoffmann, R *Inorg. Chem.* **1979**, *18*, 654-658.

(12) Schore, N. E. *J. Organomet. Chem.* **1979**, *173* (3), 301-316.

(13) Cirjak, L. M.; Ginsburg, R. E.; Dahl, L. F. *Inorg. Chem.* **1982**, *21*, 940-957.

(14) Dudeney, N.; Green, J. C.; Kirchner, O. N.; Smallwood, F. S. J. *J. Chem. Soc., Dalton Trans.* **1984**, 1883-1887.

(15) Connelly, N. G.; Geiger, W. E.; Lane, G. A. *J. Am. Chem. Soc.* **1986**, 108, 6219-6224.

(16) Schugart, K. A.; Fenske, R. F. *J. Am. Chem. Soc.* **1986**, *108*, 5100-5104.

(17) Schugart, K. A.; Fenske, R. F. *J. Am. Chem. Soc.* **1986**, *108,* 5094–5100.

(18) Pilloni, G.; Zecchin, S.; Casarin, M.; Granozzi, G. *Organometallics* **1987**, *6*, 597–606.

(19) Griewe, G. L.; Hall, M. B. *Organometallics* **1988**, *7*, 1923-1930.

(20) Winter, M. J. *Adv. Organomet. Chem.* **1989**, *29*, 101-162.

(21) Lichtenberger, D. L.; Copenhaver, A. S.; Hubbard, J. L *Polyhedron* **1990,** *9*, 1783-1797.

(22) Low, A. A.; Hall, M. B. *Inorg. Chem.* **1993**, *32*, 3880-3889.

(23) Xie, Y.; Schaefer, H. F.; King, R. B. *J. Am. Chem. Soc.* **2000**, *122*, 8746–8761.

(24) Wang, H.; Xie, Y.; King, R. B.; Schaefer, H. F. *J. Am. Chem. Soc.* **2005,** *127*, 11646-11651.

(25) Schore, N. E.; Ilenda, C. S.; Bergman, R. G. *J. Am. Chem. Soc.* **1977**, *99*, 1781–1787.

(26) Connelly, N. G.; Payne, J. D.; Geiger, W. E *J. Chem. Soc., Dalton Trans.* **1983**, 295-299.

(27) Enemark, J. H.; Feltham, R. D. *Coord. Chem. Rev.* **1974**, *13*, 339-406.

(28) Hayton, T. W.; Legzdins, P.; Sharp, W. B. *Chem. Rev.* **2002**, *102*, 935–992.

(29) Nguyen, T.; Sutton, A. D.; Brynda, M.; Fettinger, J. C.; Long, G. J.; Power, P. P. *Science* **2005,** *310*, 844-847.

(30) Wolf, R.; Ni, C.; Nguyen, T.; Brynda, M.; Long, G. J.; Sutton, A. D.; Fischer, R. C.; Fettinger, J. C.; Hellman, M.; Pu, L.; Power, P. P. *Inorg. Chem.* **2007,** *46*, 11277-11290.

(31) Kreisel, K. A.; Yap, G. P. A.; Dmitrenko, O.; Landis, C. R.; Theopold, K. H. *J. Am. Chem. Soc.* **2007,** *129*, 14162-14163.

(32) Nguyen, T.; Merrill, W. A.; Ni, C.; Lei, H.; Fettinger, J. C.; Ellis, B. D.; Long, G. J.; Brynda, M.; Power, P. P. *Angew. Chem. Int. Ed.* **2008**, *47*, 9115-9117.

(33) Hsu, C.-W.; Yu, J.-S. K.; Yen, C.-H.; Lee, G.-H.; Wang, Y.; Tsai, Y.-C. *Angew. Chem. Int. Ed.* **2008,** *120*, 10081-10084.

(34) Tsai, Y.-C.; Hsu, C.-W.; Yu, J.-S. K.; Lee, G.-H.; Wang, Y.; Kuo, T.-S. *Angew. Chem. Int. Ed.* **2008,** *47*, 7250-7253.

(35) Greenwood, B. P.; Rowe, G. T.; Chen, C.-H.; Foxman, B. M.; Thomas, C. M. *J. Am. Chem. Soc.* **2010,** *132*, 44-45.

(36) Wu, L.-C.; Hsu, C.-W.; Chuang, Y.-C.; Lee, G.-H.; Tsai, Y.-C.; Wang, Y. *J. Phys. Chem. A* **2011,** *115*, 12602-12615.

(37) Clouston, L. J.; Siedschlag, R. B.; Rudd, P. A.; Planas, N.; Hu, S.; Miller, A. D.; Gagliardi, L.; Lu, C. C. *J. Am. Chem. Soc.* **2013,** *135*, 13142-13148.

(38) Tamne, E. S.; Noor, A.; Qayyum, S.; Bauer, T.; Kempe, R. *Inorg. Chem.* **2013**, *52*, 329-336.

(39) Tereniak, S. J.; Carlson, R. K.; Clouston, L. J.; Young, V. G.; Bill, E.; Maurice, R.; Chen, Y.-S.; Kim, H. J.; Gagliardi, L.; Lu, C. C. *J. Am. Chem. Soc.* **2014**, *136*, 1842-1855.

(40) Krogman, J. P.; Gallagher, J. R.; Zhang, G.; Hock, A. S.; Miller, J. T.; Thomas, C. M., *Dalton Trans.* **2014**, *43*, 13852-13857.

(41) Noor, A.; Tamne, E. S.; Oelkers, B.; Bauer, T.; Demeshko, S.; Meyer, F.; Heinemann, F. W.; Kempe, R., *Inorg. Chem.* **2014**, *53*, 12283-12288.

(42) Clouston, L. J.; Bernales, V.; Cammarota, R. C.; Carlson, R. K.; Bill, E.; Gagliardi, L.; Lu, C. C., *Inorg. Chem.* **2015**, *54*, 11669-11679.

(43) Eisenhart, R. J.; Clouston, L. J.; Lu, C. C. *Acc. Chem. Res.* **2015**, *48*, 2885-2894.

(44) Falceto, A.; Theopold, K. H.; Alvarez, S. *Inorg. Chem.* **2015**, *54*, 10966-10977.

(45) Noor, A.; Schwarz, S.; Kempe, R. *Organometallics* **2015**, *34*, 2122-2125.

(46) Wu, B.; Wilding, M. J. T.; Kuppuswamy, S.; Bezpalko, M. W.; Foxman, B. M.; Thomas, C. M., *Inorg. Chem.* **2016**, *55*, 12137-12148.

(47) Green, J. C.; Green, M. L. H.; Parkin, G. *Chem. Commun.* **2012**, *48*, 11481-11503.

(48) Green, M. L. H.; Parkin, G. *Struct. Bond.* **2017**, 171, 79-139.

(49) Cotton, F. A.; Zingales, F. *J. Am. Chem. Soc.* **1961**, *83*, 351-355.

(50) Carpenter, A. E.; Mokhtarzadeh, C. C.; Ripatti, D. S.; Havrylyuk, I.; Kamezawa, R.; Moore, C. E.; Rheingold, A. L.; Figueroa, J. S. *Inorg. Chem.* **2015**, *54*, 2936-2944.

(51) Poveda, A.; Moyano, G. E.; Caipa, M. A. *J. Coord. Chem.* **2001**, *54*, 415-426.

(52) Fox, B. J.; Sun, Q. Y.; Dipasquale, A. G.; Fox, A. R.; Rheingold, A. L.; Figueroa, J. S., *Inorg. Chem.* **2008**, *47*, 9010-9020.

(53) Ditri, T.; Fox, B.; Moore, C.; Rheingold, A.; Figueroa, J. *Inorg. Chem.* **2009**, *48*, 8362-8375.

(54) Mokhtarzadeh, C. C.; Rheingold, A. L.; Figueroa, J. S. *Dalton Trans.* **2016**, *45*, 14561-14569.

(55) Koelle, U.; Fuss, B.; Belting, M.; Raabe, E. *Organometallics* **1986**, *5*, 980-987.

(56) Darensbourg, M. Y. *Prog. Inorg. Chem.* **1985**, *33*, 221-274.

(57) Macchioni, A. *Chem. Rev.* **2005**, *105*, 2039-2074.

(58) Margulieux, G. W.; Weidemann, N.; Lacy, D. C.; Moore, C. E.; Rheingold, A. L.; Figueroa, J. S. *J. Am. Chem. Soc* **2010**, *132* (14), 5033-5035.

(59) Mokhtarzadeh, C. C.; Margulieux, G. W.; Carpenter, A. E.; Weidemann, N.; Moore, C. E.; Rheingold, A. L.; Figueroa, J. S., *Inorg. Chem.* **2015**, *54*, 5579-5587.

(60) Carpenter, A. E.; Chan, C.; Rheingold, A. L.; Figueroa, J. S. *Organometallics* **2016,** *35*, 2319-2326.

(61) Barnett, B. R.; Rheingold, A. L.; Figueroa, J. S. *Angew. Chem. Int. Ed.* **2016**, *55*, 9253-9258.

(62) Barybin, M. V.; Brennessel, W. W.; Kucera, B. E.; Minyaev, M. E.; Sussman, V. J.; Young, V. G.; Ellis, J. E. *J. Am. Chem. Soc* **2007**, *129*, 1141-1150.

(63) Brennessel, W. W.; Ellis, J. E. *Angew. Chem. Int. Ed.* **2007**, *46*, 598-600.

(64) Carpenter, A. E.; Margulieux, G. W.; Millard, M. D.; Moore, C. E.; Weidemann, N.; Rheingold, A. L.; Figueroa, J. S. *Angew. Chem. Int. Ed.* **2012**, *51*, 9412-9416.

(65) Treichel, P. M.; Mueh, H. J.; Bursten, B. E. *J. Organomet. Chem.* **1976**, *110*, C49-C52.

(66) Treichel, P. M.; Mueh, H. J. *Inorg. Chem.* **1977**, *16* (5), 1167-1169.

(67) Barybin, M. V. *Coord. Chem. Rev.* **2010**, *254*, 1240-1252.

(68) Bertermann, R.; Braunschweig, H.; Constantinidis, P.; Dellermann, T.; Dewhurst, R. D.; Ewing, W. C.; Fischer, I.; Kramer, T.; Mies, J.; Phukan, A. K.; Vargas, A. *Angew. Chem. Int. Ed.* **2015**, *54*, 13090-13094.

(69) Cotton, F. A.; Cowley, A. H.; Feng, X. *J. Am. Chem. Soc.* **1998**, *120*, 1795-1799.

(70) Power, P. P. *Chem. Rev.* **1999**, *99*, 3463-3504.

(71) Robinson, G. H. *Acc. Chem. Res* **1999**, *32*, 773-782.

(72) Robinson, G. H. *Chem. Commun.* **2000**, 2175-2181.

(73) Darowicki, K.; Zieliński, A.; Ryl, J.; Slepski, P. *Electochimica Acta* **2013**, *87*, 930-939.

(74) Geiger, W. E.; Barrière, F. *Acc. Chem. Res.* **2010**, *43*, 1030-1039.

(75) The weakly coordinating anion $[BAr^F{}_4]^-$ was employed to preclude the formation of a contact ion pair with the $(\mu^2\text{-CNR})Co_2$ core of $[\mathbf{5}]^+$.

(76) Carpenter, A. E.; Wen, I.; Moore, C. E.; Rheingold, A. L.; Figueroa, J. S. *Chem. Eur. J.* **2013**, *19*, 10452-10457.

(77) Ditri, T. B.; Carpenter, A. E.; Ripatti, D. S.; Moore, C. E.; Rheingold, A. L.; Figueroa, J. S. *Inorg. Chem.* **2013**, *52*, 13216-13229.

(78) Adams, R. D.; Cotton, F. A.; Rusholme, G. A. *J. Coord. Chem.* **1972**, *1*, 275-283.

(79) Baik, M.-H.; Friesner, R. A.; Parkin, G., *Polyhedron* **2004**, *23*, 2879-2900.

(80) Smith, R. C.; Shah, S.; Urnezius, E.; Protasiewicz, J. D. *J. Am. Chem. Soc* **2003,** *125*, 40-41.

(81) Jarchow, O.; Schulz, H.; Nast, R. *Angew. Chem. Int. Ed.* **1970**, *9*, 71-71.

(82) Denninger, U.; Schneider, J. J.; Wilke, G.; Goddard, R.; Krüger, C. *Inorg. Chim. Acta* **1993**, *213*, 129-140.

(83) Mondal, K. C.; Samuel, P. P.; Roesky, H. W.; Carl, E.; Herbst-Irmer, R.; Stalk, D.; Schwederski, B.; Kaim, W.; Ungur, L.; Chitbotaru, L. F.; Hermann, M.; Frenking, G. *J. Am. Chem. Soc.* **2014**, *136*, 1770-1773.

(84) Notably, more recent computational studies at the DFT level concluded that a Co=Co double bond was present in the neutral bridging-carbonyl dimer $(\mu_2\text{-CO})_2[\text{CpCo}]_2$. However, this conclusion was based on 18-electron rule considerations and Co-Co bond lengths relative to the tricarbonyl species $(\mu_2\text{-CO})[\text{CpCo(CO)}]_2$, rather than an assessment of the molecular orbital manifold of the complex. See Ref. 24.

(85) Hofmann, P.; Padmanabhan, M. *Organometallics* **1983**, *2*, 1273-1284.

(86) Mayer, I. *Chem. Phys. Lett.* **1983**, *97*, 270-274.

(87) Mayer, I., *J. Comp. Chem.* **2007**, *28*, 204-221.

(88) Bridgeman, A. J.; Cavigliasso, G.; Ireland, L. R.; Rothery, J. *J. Chem. Soc., Dalton Trans.* **2001**, 2095-2108.

(89) Notably, the broad, low-field feature observed in the EPR spectrum of K[**2**] could be readily simulated by including a rotational correlation coefficient ($\tau$) of $1\text{x}10^{-8}$ s. We believe this slight anisotropy originates from the presence of the encumbering $\text{CNAr}^{\text{Mes2}}$ ligands, which slightly diminish diffusion limited tumbling. Similar effects on EPR spectra have been seen previously (See ref 91, 92).

(90) Stoll, S., Schweiger, A. *Biol. Magn. Reson.* **2007**, *27*, 299-321

(91) Earle, K. A., Budil, D. E., Freed, J. H. *J. Phys. Chem.* **1993**, *97*, 13289-13297.

(92) Pangborn, A. B.; Giardello, M. A.; Grubbs, R. H.; Rosen, R. K.; and Timmers, F. J. *Organometallics.* **1996**, *15*, 1518.

(93) Armarego, W. L. F.; Chai, C. L. L. *Purification of Laboratory Chemicals,* 5$^{\text{th}}$Ed.; Elsevier, 2003.

(94) Schwindt, M. A.; Lejon T.; Hegedus, L. S. *Organometallics*, **1990**, *9*, 2814.

(95) Heck, R. F. *Inorg. Chem.* **1965**, *4,* 855.

(96) Fulmer, G. R.; Miller, A. J. M.; Sherden, N. H.; Gottlieb, H. E.; Nudelman, A.; Stoltz, B. M.; Bercaw, J. E.; Goldberg, K. I. *Organometallics* **2010**, *178*, 42.

(97) Sheldrick, G. M. *Acta Crystallogr. A.*, **2008**, *64*, 112.

(98) Dolomanov, O. V.; Bourhis, L. J.; Gildea, R. J.; Howard, J. A. K.; Puschmann, H. *J. Appl. Cryst.* **2009**, *42*, 339.

(99) Neese, F. *ORCA-an Ab Inito, Density Functional Theory and Semiemperical SCF-MO Program Package, Version 3.0.0*. Max Planck Institute for Chemical Energy Conversion D-45470 Muelheim/Ruhr, Germany (2013).

(100) Becke, A. D. *J. Chem. Phys.* **1986**, *84*, 4524.

(101) Becke, A. D. *J. Chem. Phys.* **1993**, *98*, 5648.

(102) Neese, F. *Wiley Interdiscip. Rev.: Comput. Mol. Sci.* 2012, 2, 73.

(103) Lee, C. T.; Yang, W. T.; Parr. R. G. *Phys. Rev. B.* **1988**, *37*, 785.

(104) Pantazis, D. A.; Chen, X. Y.; Landis, C. R.; Neese F. *Chem. Theor. Comput.* **2008**, *4*, 908.

(105) Schaefer, A.; Horn, H.; Ahlrichs, R. *J. Chem. Phys.* **1992**, *97*, 2571.

(106) Eichkorn, K.; Treutler, O.; Ohm, H.; Haser, M.; Ahlrichs, R. *Chem. Phys. Lett.* **1995**, *240*, 283.

(107) Eichkorn, K.; Treutler, O.; Ohm, H.; Haser, M.; Ahlrichs, R. *Chem. Phys. Lett.* **1995**, *242*, 652.

(108) Eichkorn, K.; Treutler, O.; Ohm, H.; Haser, M.; Ahlrichs, R. *Theor. Chem. Acta* **1997**, *97*, 119.

(109) Weigend, F.; Ahlrichs, R. *Phys. Chem. Chem. Phys.* **2005**, *7*, 3297.

(110) Werner, H.-J.; Manby, F. R.; Knowles, P. J. *J. Chem. Phys.* **2003**, *118*, 8149.

(111) Van Lenthe, E.; Baerends, E. J.; Snijders, J. G. *J. Chem. Phys.* **1993**, *99*, 4597.

112) Van Lenthe, E.; Snijders, J. G.; Baerends, E. J. *J. Chem. Phys.* **1996**, *105*, 6505.

(113) ChemCraft. Zhurko, G. A.; Zhurko, D. A. 2014, www.chemcraftprog.com.

# *Chapter 5*

# *Targeting Isocyano Analogues to the CpCo(CO) Fragment: Dintrogen Binding, Aza-Büchner Ring Expansions and Small Molecule Activation.*

## 5.1 Introduction

Spin-triplet (S = 1) organometallic complexes exclusively possessing strong-field ligands are a rare, but fascinating, class of reactive species. Indeed, the most well-known, and arguably the most simple, representatives of this class include the unstable, coordinatively unsaturated molecules $Fe(CO)_4$[1-6] and CpCo(CO) (Cp = $\eta^5$-$C_5H_5$).[3,7-12] Despite featuring strong-field ligands, the S = 1 ground state of these $16e^-$ species is derived from a unique interplay of $d^n$ count, orbital symmetry and geometric structure. For $Fe(CO)_4$, Jahn-Teller instability of a $d^8$ configuration in a tetrahedral field results in a distortion to a "saw-horse" $C_{2v}$ geometry.[13,14] However, this saw-horse geometry renders the two highest-lying, non-degenerate Fe-based orbitals (*i.e.* $a^1(z^2)$ and $b_2(yz)$) close in energy, thereby resulting in a high-spin, S = 1 ground state.[13] Similarly, CpCo(CO) adopts a 'bent' ($C_s$), rather than linear, geometry with respect to the CO ligand and Cp-centroid to avoid populating a strongly Cp-Co anti-bonding orbital.[15] Accordingly, the bent geometry results in closely spaced, but non-degenerate a"(*xz*) and a"(*yz*) orbitals, each of which are singly occupied.[15] Both $Fe(CO)_4$ and CpCo(CO) have been established as unusually reactive species, with lifetimes in the picosecond regime.[3,6] However, both

have been shown to undergo important reaction chemistry, including alkane and $N_2$ binding, as well as E–H bond activation.[2,3,6]

In recent years, there have been a few reports of $FeL_4$ and CpCOL analogues to $Fe(CO)_4$ and CpCo(CO) with ligands that impart greater kinetic stability to the $S = 1$ Fe and Co centers. For example, Lavallo and Grubbs,[16] as well as Liang,[17] have reported four-coordinate, zero-valent iron bis-carbene/bis-olefin complexes that exhibit $S = 1$ ground states. These complexes exhibit distorted tetrahedral geometries consistent with the structure of $Fe(CO)_4$. However, they do not serve as precise electronic-structure mimics of $Fe(CO)_4$ due to the unidirectional $\pi$-acid properties of both singlet-carbene ligands and olefins,[18] despite the fact that they exhibit a rich and unique reaction chemistry. Likewise, Bradley has recently reported the isolable mono-(N-hetercyclic carbene) complex Cp*Co(IPr) (IPr = 1,3-bis(2,6-diisoprpylphenyl)imidazole-2-ylidene),[19] which does not possess two orthogonal $\pi$-backbonding interactions to the L ligand as is present in CpCo(CO). However, Cp*Co(IPr) displays a reaction profile quite similar to that of CpCo(CO).

Given our interest in isolating and studying precise electronic structure mimics[20-28] of the binary unsaturated metal carbonyls (*i.e.* $M(CO)_n$; $n \leq 5$) with encumbering *m*-terphenyl isocyanides,[29-32] we recently showed that an isocyanide analogue of $Fe(CO)_4$ could be generated and trapped with $N_2$.[28] This work utilized the dimesityl–substituted *m*-terphenyl isocyanide,[20,22,25] $CNAr^{Mes2}$ ($Ar^{Mes2}$ = 2,6-(2,4,6-$Me_3C_6H_2)_2C_6H_3$), which has been demonstrated to provide ready access to tetra-isocyanide transition metal complexes.[20] However, attempts to use $Fe(N_2)(CNAr^{Mes2})$ as a synthon for four-coordinate "$Fe(CNAr^{Mes2})_4$" resulted in intramolecular C–H activation of the flanking

mesityl groups. Moreover, previously in Chapter 5 of this dissertation we explored the reactivity of CoCoL fragments supported by the $CNAr^{Mes2}$ ligand, which were shown to undergo dimerization to afford the dimeric species $[(\mu^2\text{-}CNAr^{Mes2})_2[CpCo]_2]^n$ (N = 0, –1, –2) upon reduction of the diioded precursor $CpCoI_2(CNAr^{Mes2})$ with $KC_8$. Given this precedent we rationalized that the more encumbering *m*-terphenyl isocyanide $CNAr^{Dipp2}$ ($Ar^{Dipp2}$ = 2,6-(2,6-(*i*-Pr)$_2C_6H_3$)$C_6H_3$), which is known to stabilize two-coordinate transition metal complexes,[21,33-37] could provide access to an analogue or synthon of CpCo(CO) and mitigate ligand/ligand steric pressures that potentially lead to intramolecular degradation.[38] Accordingly, here we report the synthesis of the dintrogen complex $Cp^*Co(N_2)(CNAr^{Dipp2})$. It is shown that dinitrogen coordination is labile due to competition with the isocyanide π* manifold for π-backdonation which results in the intramoleuclar activation of the *m*-terphenyl ligand framework via aza-büchner ring expansion. To mitigate this deactivation process synthesis of the more sterically encumbering *m*-terphenyl isocyanide $CNAr^{Tripp2}$ ($Ar^{Tripp2}$ = 2,6-(2,4,6-(*i*-Pr)$_3C_6H_2$)$C_6H_3$) was undertaken.[32] Use of of $CNAr^{Tripp2}$ as a ligand ancillary provides access to $Cp^*Co(N_2)(CNAR^{Tripp2})$ which is resistant to intramolecular aza-büchner ring expansion. Furthermore, it is shown that the reactivity profile of both $Cp^*Co(N_2)(CNAr^{Dipp2})$ and $Cp^*Co(N_2)(CNAr^{Tripp2})$ both function as viable sources of "Cp*Co(CNR)" and display small-molecule activation chemistry that closely parallels that of CpCo(CO).

**5.2 Dimerization of *m*-Terphenyl Isocyanide Fragments of the Formula CpCoL.**

In an effort to most closely match the electronic environment present in CpCo(CO), we initially sought a simple CO for $CNAr^{Dipp2}$ substitution in the system. As

shown in Scheme 5.1, treatment of $CNAr^{Dipp2}$ with $CpCoI_2(CO)$ led readily to CO displacement and formation of the mono-isocyanide complex, $CpCoI_2(CNAr^{Dipp2})$ (**1**) (Figure 5.1). Reduction of complex **1** with 2.0 equivalents of $KC_8$ resulted in the generation of the diamagnetic, bridging-isocyanide dimer, $(\mu\text{-}CNAr^{Dipp2})_2[CpCo]_2$ (**2**), as determined by $^1H$ NMR spectroscopy and X-ray diffraction (Scheme 5.1, Figure 5.2). Dimer **2** is an isocyanide analogue of the well-investigated bridging carbonyl complex, $(\mu\text{-}CO)_2[CpCo]_2$,[39-45] which is known to form by dimerization of CpCo(CO) in solution.[7,10] Similarly, the formation of dimer **2** potentially suggests that the monomer $[CpCo(CNAr^{Dipp2})]$ is present as a fleeting intermediate in this reduction prior to dimerization. However, aliquots of the reduction mixture taken at various time points did not conclusively reveal the presence of an intermediate species. Furthermore, unobserved bridging-iodide dimers may be generated at intermediate stages of reduction und ultimately yield dimer **2** upon further addition of electrons (Chapter 4). Nevertheless, it was clear that the steric combination of an un-substituted Cp ligand and the $CNAr^{Dipp2}$ isocyanide was insufficient for the production of a persistently monomeric CpCo(L) species.

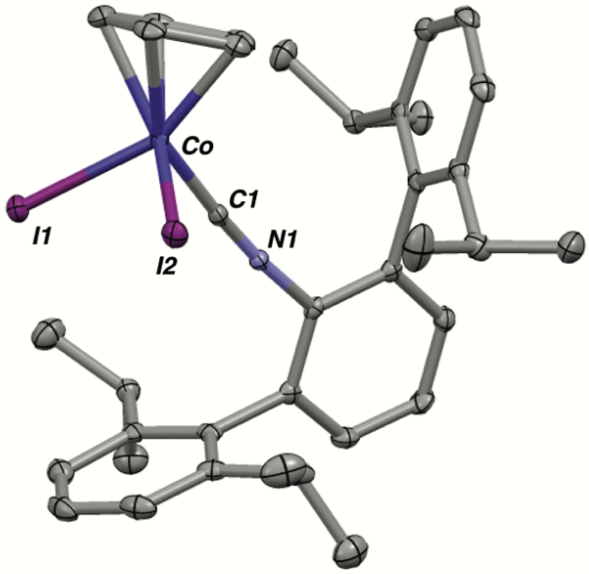


**Figure 5.1.** Molecular structure of $CpCoI_2CNAr^{Dipp2}$ **(1)**. Hydrogen atoms omitted for clarity. Selected Bond Distance (Å): Co-$I_1$ = 2.5716(3), Co-$I_2$ = 2.5786(3), Co-$C_1$ = 1.8232(19), $C_1$-$N_1$ = 1.159(2).

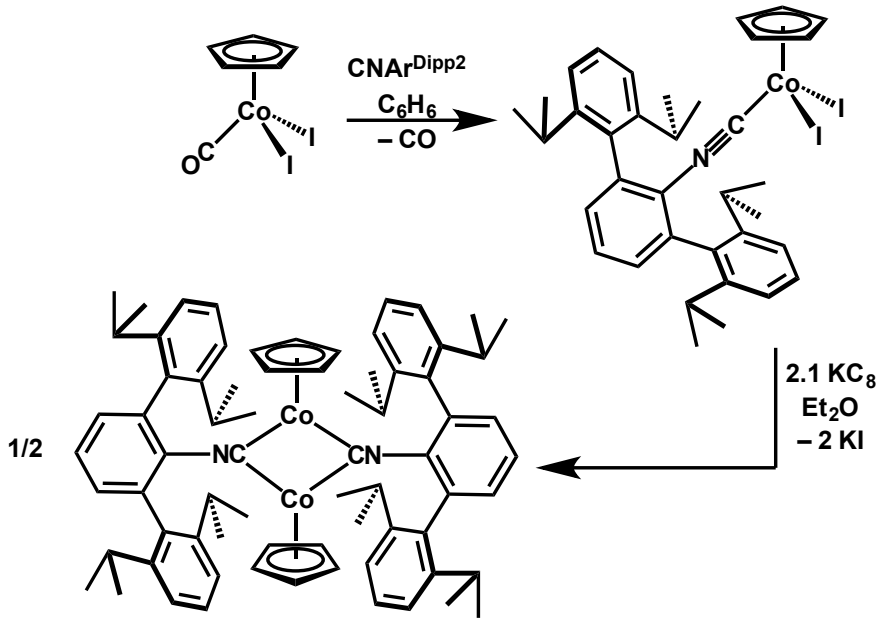


**Scheme 5.1.** Synthesis of complex **1** and subsequent reduction to complex **2.**

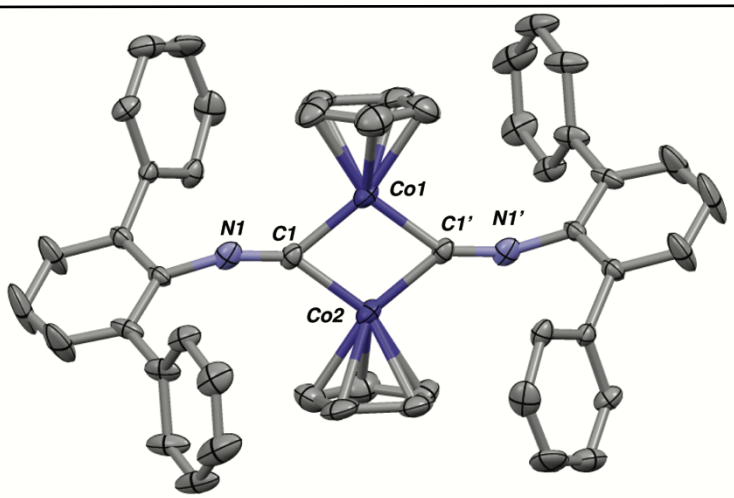


**Figure 5.2.** Molecular structure of (μ-$CNAr^{Dipp2}$)$_2$[CpCo]$_2$ (**2**). (μ-$CNAr^{Dipp2}$)$_2$[CpCo]$_2$ lies on a crystallographic mirror plane resulting in one half of ($\eta^5$-Cp)$_2$Co$_2$($\mu^2$-$CNAr^{Dipp2}$)$_2$ to be symmetry generated. Hydrogen atoms and flanking *i*-Pr groups omitted for clarity. Selected bond distances (Å): Co-Co = 2.321(1), Co-$C_1$ = 1.857(7), $C_1$-$N_1$ = 1.222(9). Selected bond angles (˚): $C_1$-$N_1$-$C_2$ = 157.6(7), $C_1$-$Co_1$-$C_1$-$Co_1$ = 180.0.

## 5.3. Synthesis Towards an Isolable Monomeric Cp*Co($N_2$)(CNR) Unit.

To inhibit dimerization, we followed the strategy set forth by Bradley and utilized the 1,2,3,4,5-pentamethylcyclopentadienyl group (*i.e.* $\eta^5$-$C_5Me_5$; Cp*).[19] Accordingly, synthesis of Cp*$CoI_2$($CNAr^{Mes2}$) (**3**) was accomplished in an analogous method to complex **1**, from CO ligand exchange from the isocyanide diiodide precursor, Cp*$CoI_2$(CO) in >95% yield. The solid-state structure of complex **3** is shown in Figure 5.3. Complex **3** adopts a three-legged piano stool coordination mode similar to complex **1**. Reduction of diiodide **3** with 2.1 equivalents of $KC_8$ in an $Et_2O$/DME mixture results in a color change from purple to red. The resulting solution indicates two different *m*-terphenyl environments as assayed by $^1$H NMR spectroscopy, and X-ray diffraction analysis from crystals grown from the reaction mixture were identified as (μ-$CNAr^{Mes2}$)$_2$[Cp*Co]$_2$ (**4**). Dimer **4** displays some structural differences from complex **2**, in that substitution of Cp for the more sterically encumbering Cp* results in a slight

degree of puckering of the $(\mu\text{-CNR})_2Co_2$ core when compared to dimer **2** featuring a torsion angle of 160.3(2)˚. Interestingly, the solid-state structure displays a "lock and key" type interaction between the Cp* units and the $Ar^{Mes2}$ units, providing evidence for the hindered rotation observed via $^1H$ NMR spectroscopy. Lastly dimer **4** also displays a significantly red-shifted ν(CN) band by solution FTIR at 1732 $cm^{-1}$ ($C_6D_6$). This indicates a significantly more electron rich core, and as we have previously shown the near identical electronic influence between $CNAr^{Mes2}$ and $CNAr^{Dipp232}$ complex **4** highlights the increased electron releasing capabilities of the Cp* ligands with respect to the less encumbering Cp unit.[46,47]

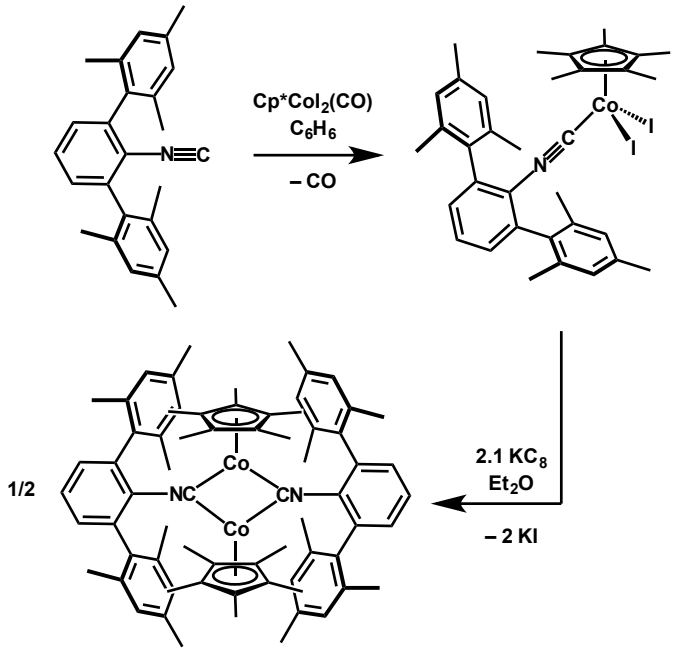


**Scheme 5.2** Synthesis of complex **1** and subsequent reduction to complex **2.**

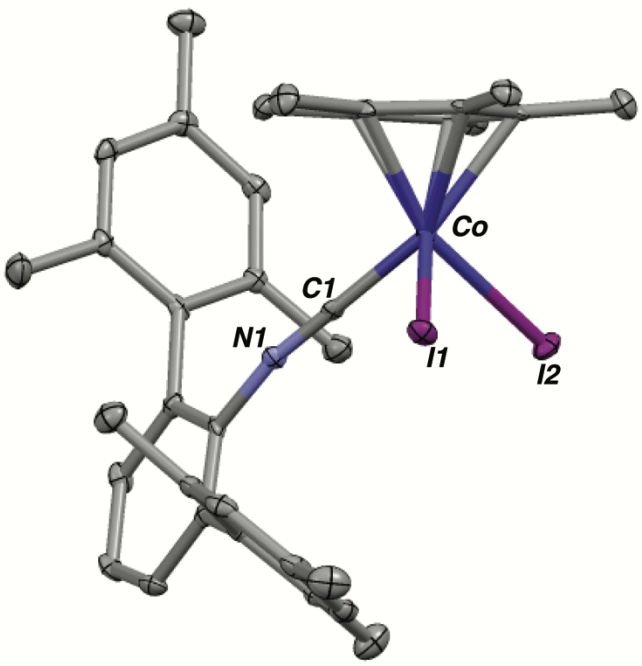


**Figure 5.3** Solid state molecular structure of $Cp^*CoI_2(CNAr^{Mes2})$ (**3**). Hydrogen atoms omitted for clarity. Selected bond distances (Å): Co-$C_1$ = 1.824(2), Co-$I_1$ = 2.5701(5), Co-$I_2$ = 2.5981(4), $C_1$-$N_1$ = 1.158(3). Selected bond angles (˚): $C_1$-$N_1$-$C_2$ = 169.6(2)˚.

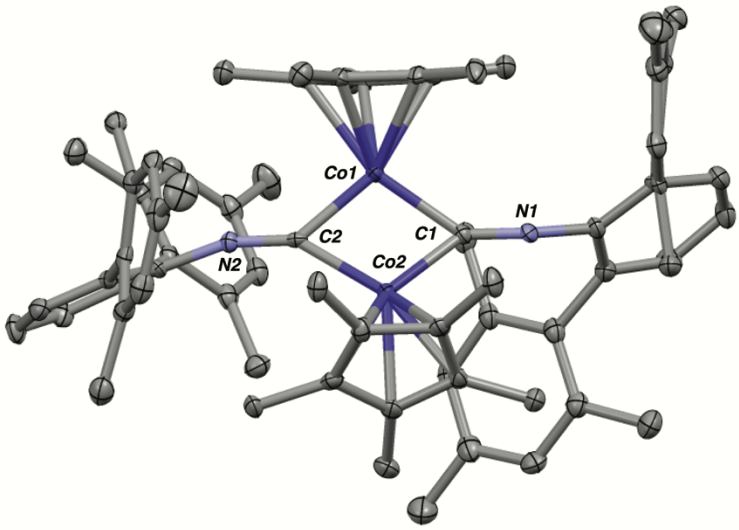


**Figure 5.4.** Molecular structure of $(\mu\text{-}CNAr^{Mes2})_2[Cp^*Co]_2$ (**4**). Hydrogen atoms and omitted for clarity. Selected bond distances (Å): $Co_1$-$Co_1$ = 2.3272(5), $Co_1$-$C_1$ = 1.906(3), $Co_1$-$C_2$ = 1.906(3), $Co_2$-$C_1$ = 1.929(3), $Co_2$-$C_2$ = 1.903(3), $C_1$-$N_1$ = 1.220(4), $C_2$-$N_2$ = 1.229(4). Selected bond angles (˚): $C_1$-$N_1$-$C_3$ = 158.0(2), $C_2$-$N_2$-$C_{27}$ = 157.6(3), $Co_1$-$C_1$-$C_2$-$Co_2$ = 160.3(2).

Analogous to the synthesis of complex **1** and **3**, treatment of $Cp^*CoI_2(CO)$ with an equivalent of $CNAr^{Dipp2}$ cleanly generated the diamagnetic mono-isocyanide complex, $Cp^*CoI_2(CNAr^{Dipp2})$ (**5**) as a purple crystalline solid in 85% isolated yield. Structural characterization of complex **5** (Figure 5.5) revealed a monomeric Co center and the classic three-legged piano stool coordination motif found for the previously described Co(III) cyclopentadienyl complexes. Most notably, treatment of **5** with 2.1 equivalents of $KC_8$ in a thawing $Et_2O$/DME mixture under an $N_2$ atmosphere produced the dark brown, diamagnetic dintrogen complex $Cp^*Co(N_2)(CNAr^{Dipp2})$ (**6**; Scheme 5.3) as determined by $^1H$ NMR spectroscopy (Figure 5.26) and X-ray diffraction (Figure 5.6). Remarkably, the Cambridge Structural Database contains nearly 3000 structures featuring a ($\eta^5$-$Cp^R$)Co unit,[91] but complex **6** is apparently the first structurally characterized dinitrogen adduct of this fragment. Indeed, the analogous carbonyl/$N_2$ complex, $CpCo(CO)(N_2)$, has been observed as a short-lived intermediate upon photo-induced CO dissociation of $CpCo(CO)_2$ in an $N_2$ atmosphere, and was proposed as an indicator for the formation of the $16e^-$ fragment CpCo(CO).[48] As shown in Figure 5.6, $Cp^*Co(N_2)(CNAr^{Dipp2})$ (**6**) adopts the familiar two-legged piano stool motif common to monovalent $Cp^RCoL_2$ complexes. The $Co–C_{iso}$ bond length of 1.766(2) Å in **4** is contracted from that in diiodide **5** ($d(Co–C_{iso})$ = 1.832(5) Å), which indicates a more $\pi$-basic Co center upon reduction. However, the FTIR spectrum of **6** in $C_6D_6$ solution features a relatively high-energy $\nu$(NN) band for the coordinated $N_2$ ligand (2110 $cm^{-1}$), Figure 5.28. We believe this spectroscopic feature likely arises from the presence of the strongly $\pi$-acidic isocyanide ligand, which very effectively completes with $N_2$ for $\pi$-symmetry electron density. To this end, it is also worthy of mention that Bradley's

Cp*Co(IPr) complex,[19] which features an NHC ligand lacking significant $\pi$-acid properties, has not been shown to bind $N_2$, despite being prepared under an $N_2$ atmosphere.

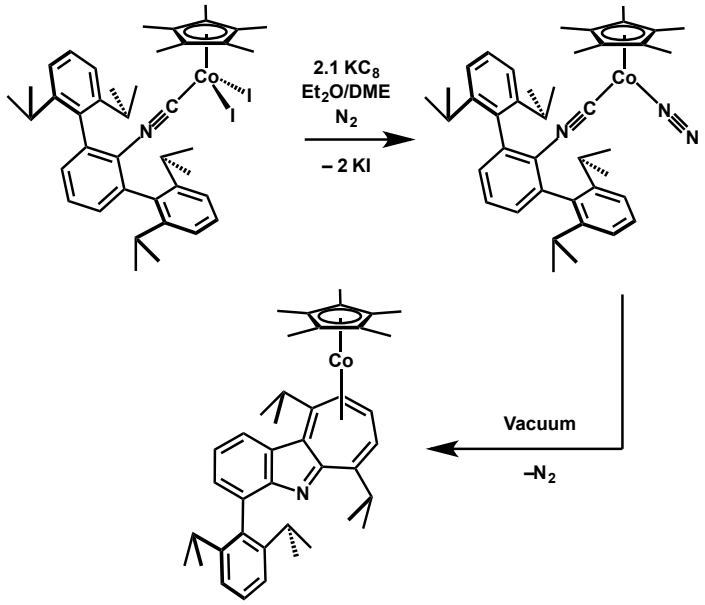


**Scheme 5.3** Synthesis of complex **6** and subsequent decomposition to complex **7**.

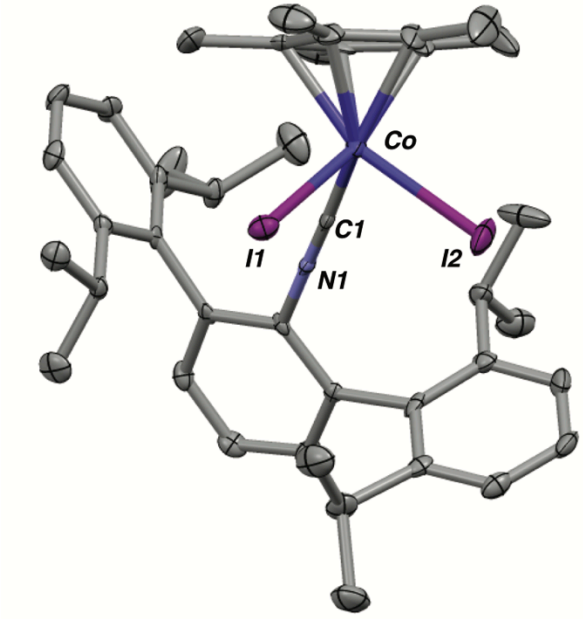


**Figure 5.5.** Molecular structure of Cp*CoI$_2$(CNAr$^{Dipp2}$) (**5**). Hydrogen atoms, and positionally disordered *i*-Pr methyl groups omitted for clarity. Selected bond distances (Å): Co-C$_1$ = 1.832(5), Co-I$_1$ = 2.5963(6), Co-I$_2$ = 2.5739(6), C$_1$-N$_1$ = 1.161(5).

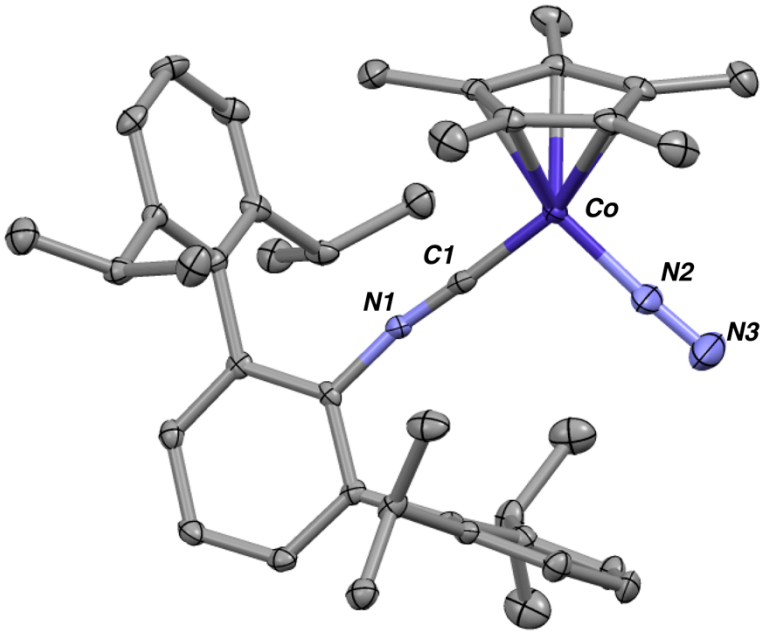


**Figure 5.6.** Molecular Structure of Cp*Co($N_2$)($CNAr^{Dipp2}$) (**6**). Hydrogen atoms omitted for clarity. Selected bond distances (Å): Co-$C_1$ = 1.766(2), $C_1$-$N_1$ = 1.179(3), Co-$N_2$ = 1.781(2), $N_2$-$N_3$ = 1.116(3). Selected bond angles (°): $C_1$-$N_1$-$C_2$ = 166.1(2), Co-$N_2$-$N_3$ = 177.1(2), $C_1$-Co-$N_2$ = 96.49(9).

## 5.4. Decomposition of Cp*Co($N_2$)($CNAr^{Dipp2}$) via aza-Büchner Ring Expansion.

While the dinitrogen complex Cp*Co($N_2$)($CNAr^{Dipp2}$) (**6**) can be isolated, its high-energy $\nu$(NN) band suggested that the coordinated $N_2$ ligand was potentially labile. Indeed, exposure of Cp*Co($N_2$)($CNAr^{Dipp2}$) (**6**) to successive freeze-pump-thaw cycles in $C_6D_6$ solution resulted in the clean formation of a single new product with a de-symmetrized $Ar^{Dipp2}$ environment and metal-coordinated olefinic resonances in its $^1$H NMR spectrum. Structural characterization of this new product revealed the $\eta^4$-coordinated 1-azabenz[*b*]azulene complex, Cp*Co($\eta^4$-1-azaben[*b*]azulene$^{Dipp2}$) (**7**; Scheme 5.3, Figure 5.7), in which $N_2$ removal from the Co center results in cyclization and ring expansion of the $CNAr^{Dipp2}$ isocyanide ligand. The formation of 1-azabenz[*b*]azulenes has been observed previously from photolysis of *ortho*-biaryl isocyanides[49] and is thought to proceed *via* carbenoid attack of a photochemically-

activated isocyanide $\alpha$-carbon on the *ipso-ortho* carbon bond of the isocyano-linked aryl ring and subsequent aza-Büchner ring expansion.[50, 92] Accordingly, the formation of **7** can be rationalized by the mechanistic sequence shown in Scheme 5.4 where dissociation of the $N_2$ ligand from complex **6** produces the target $16e^-$ intermediate [Cp*Co(CNAr$^{Dipp2}$)], which is trapped by intramolecular $\eta^2$-binding of a flanking Dipp ring of the CNAr$^{Dipp2}$ ligand. Such $\eta^2$-binding of a flanking ring would force a significant bending of the $C_{iso}$–N–$C_{ipso}$ angle of the CNAr$^{Dipp2}$ ligand and induce carbonic character at the $C_{iso}$ carbon due to disruption of N-to-$C_{iso}$ $\pi$-donation in the isocyano unit. Importantly, we have previously shown in Group 6 metal chemistry that flanking-ring binding of *m*-terphenyl isocyanides induces such $C_{iso}$–N–$C_{ipso}$ bending and results in significantly downfield $^{13}C\{^1H\}$ isocyano-carbon chemical shifts reflective of carbenic character.[31] We believe this precedent lends credence to the suggestion that *aza*-Büchner ring expansion can be initiated when sufficiently reactive, low-coordinate metal fragments generated in the presence of a coordinated *m*-terphenyl isocyanide. Notably both we and Arnold have previously reported the formation of 1-azabenz[*b*]azulenes from *m*-terphenyl isocyanides in reactions where coordinatively-unsaturated metal fragments were proposed as unobserved intermediates.[28,51] However, we believe the formation of complex **7** from simple $N_2$ dissociation from **6** represents a relatively straightforward and mechanistically minimalistic example where this transformation is operative.

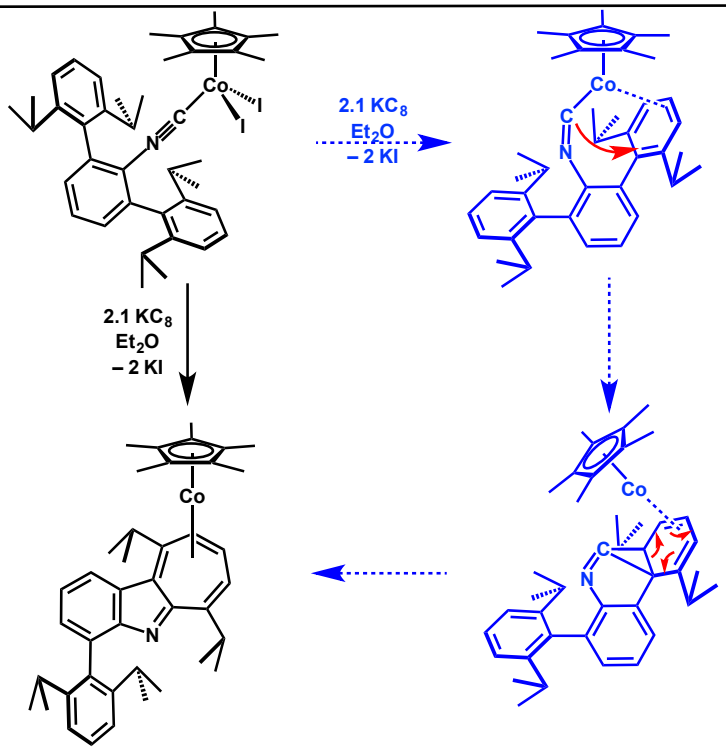


**Scheme 5.4** Mechanistic scheme depicting the aza-Büchner ring expansion of complex **6** to yield complex **7**.

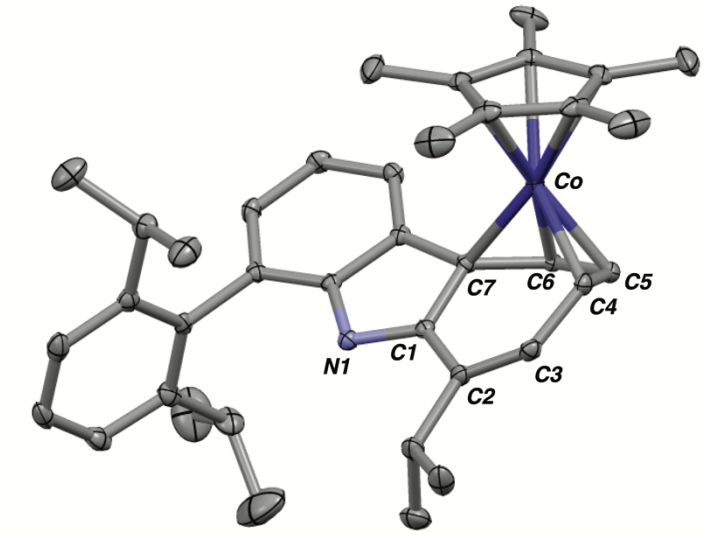


**Figure 5.7.** Molecular structure of Cp*Co(Azabenz[*b*]azulene$^{Dipp}$) (**7**). Hydrogen atoms and one *i*-Pr group at $C_6$ omitted for clarity. Selected bond distances (Å): $C_1$-$N_1$ = 1.3196(19), $C_1$-$C_2$ = 1.463(2), $C_3$-$C_4$ = 1.466(2), $C_4$-$C_5$ = 1.441(2), $C_5$-$C_6$ = 1.409(2), $C_6$-$C_7$ = 1.470(2), $C_1$-$C_7$ = , Co-$C_7$ = 2.0778(15), Co-$C_6$ = 2.0187(15), Co-$C_5$ = 1.9800(15), Co-$C_4$ = 2.0441(15). Selected bond angles (˚): $C_1$-$N_1$-$C_{19}$ = 106.60(12), $C_1$-$C_2$-$C_3$ = 119.73(13), $C_2$-$C_3$-$C_4$ = 127.71(14), $C_3$-$C_4$-$C_5$ = 124.77(14), $C_4$-$C_5$-$C_6$ = 120.02(13), $C_5$-$C_6$-$C_7$ = 117.07(13), $C_6$-$C_7$-$C_1$ = 126.20(13).

## 5.5. Reactivity of Cp*Co($N_2$)($CNAr^{Dipp2}$) Toward Unsaturated C–C, and E–E Bonds.

Whereas $N_2$ loss initiates an intramolecular ligand degradation process we probed whether Cp*Co($N_2$)($CNAr^{Dipp2}$) (**6**) itself could serve as a stabilized source of the [Cp*Co($CNAr^{Dipp2}$)] fragment in reactions with exogenous substrates. Gratifyingly, the $N_2$ ligand in Cp*Co($N_2$)($CNAr^{Dipp2}$) (**6**) can indeed be displaced by Lewis bases under ambient conditions. Accordingly, treatment of Cp*Co($N_2$)($CNAr^{Dipp2}$) (**6**) with and additional equivalent of $CNAr^{Dipp2}$ in a benzene solution at room temperature afforded the two-legged piano-stool, bis-isocyanide complex, Cp*Co($CNAr^{Dipp2}$)$_2$ (**8**; Scheme 5.5, Figure 5.8). Complex **8** gives rise to a strong $\nu$(CN) band in its IR spectrum at 1914 $cm^{-1}$, which is *ca*. 100 $cm^{-1}$ lower in energy than that found in **6** ($\nu$(CN) = 2010 $cm^{-1}$) and reflects the more strongly $\sigma$-donating nature of isocyanide ligands relative to coordinated $N_2$. In addition, Cp*Co($N_2$)($CNAr^{Dipp2}$) (**6**) reacts readily with diphenyl acetylene (PhCCPh) to produce the $\eta^2$-alkyne complex, Cp*Co($\eta^2$-*C,C*-PhCCPh)($CNAr^{Dipp2}$) (**9**), as determined by X-ray diffraction (Figure 5.9). Notably, treatment of **9** with additional equivalents of PhCCPh at room temperature does not lead to displacement of the $CNAr^{Dipp2}$ ligand or the production of substituted arene products characteristic of alkyne cyclotrimerization activity.[52] This observation indicates that the Co-isocyanide linkage in this system is markedly robust relative to the Co-carbonyl linkage in $CpCo(CO)_2$, which is a well-known [2+2+2] alkyne cyclotrimerization catalyst precursor.[52,53]

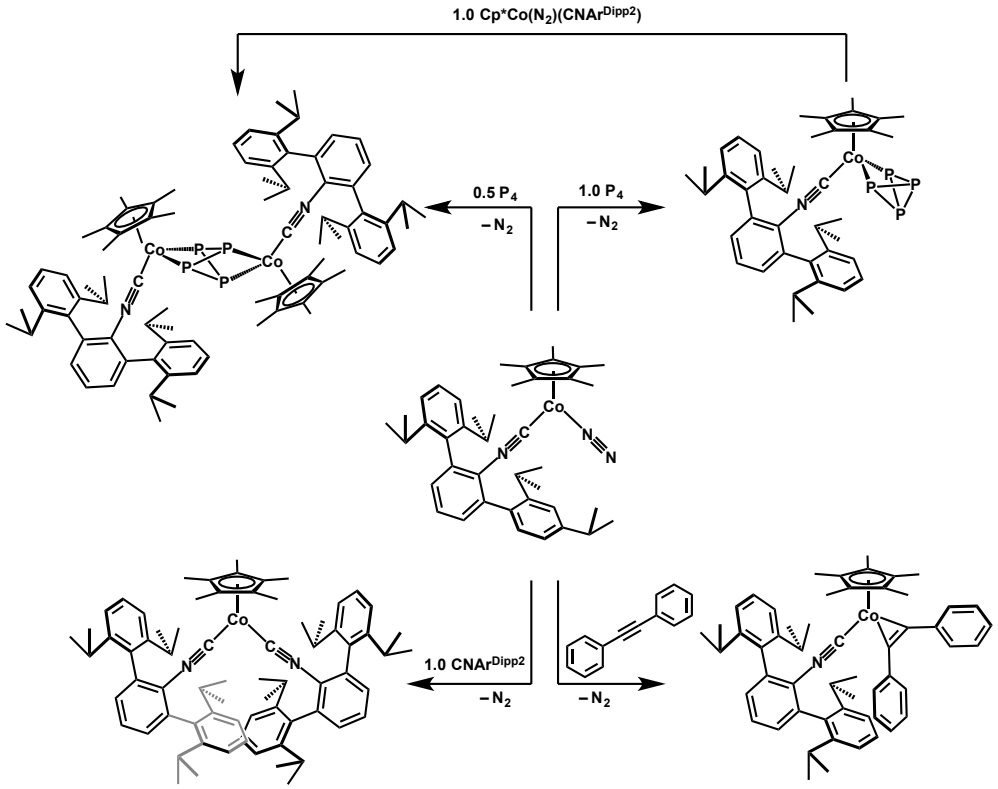


**Scheme 5.5**. Reactivity of complex **4** with $CNAr^{Dipp2}$, PhCCPh, and $P_4$.

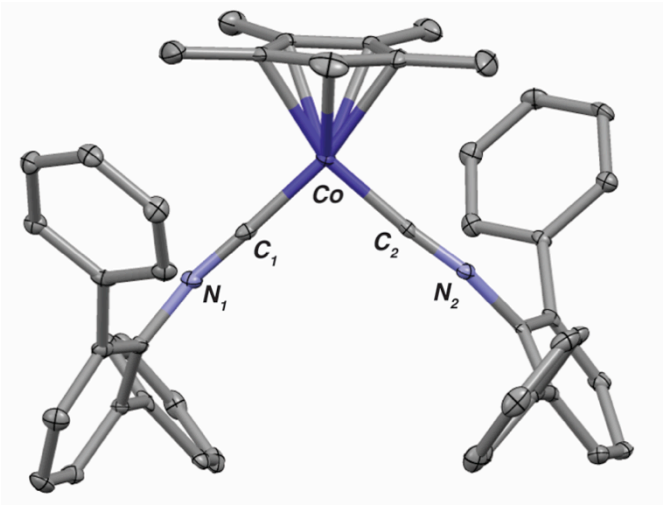


**Figure 5.8** Molecular structure of $Cp^*Co(CNAr^{Dipp2})_2$•($Et_2O$) (**8**)•($Et_2O$). Flanking *i*-Pr groups, Hydrogen atoms and one $Et_2O$ molecule of solvation omitted for clarity. Selected bond distances (Å): Co-$C_1$ = 1.766(13), Co-$C_2$ = 1.780(2), $C_1$-$N_1$ = 1.207(3), $C_2$-$N_2$ = 1.187(3). Selected bond angles (˚): $C_1$-$N_1$-$C_3$ = 153.4(2), $C_2$-$N_2$-$C_{33}$ = 163.3(2). $C_1$-Co-$C_2$ = 96.85(11).

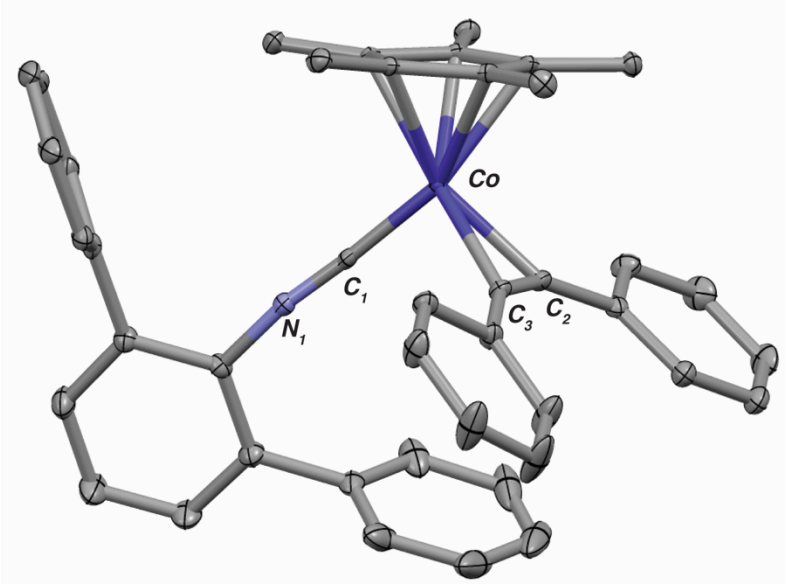


**Figure 5.9** Molecular structure of Cp*Co($\eta^2$-PhCCPh)($CNAr^{Dipp2}$) (**9**). Flanking *i*-Pr-Me groups and Hydrogen atoms omitted for clarity. Selected bond distances (Å): Co-$C_1$ = 1.782(2), Co-$C_2$ = 1.9668(19), Co-$C_3$ = 19819(19), $C_1$-$N_1$ = 1.176(3), $C_3$-$C_2$ = 1.269(3). Selected bond angles (˚): $C_1$-$N_1$-$C_4$ = 170.77(19), $C_3$-$C_2$-$C_{34}$ = 151.3(2), $C_2$-$C_3$-$C_{40}$ = 148.7(2).

In addition to simple $N_2$-for-Lewis base substitution reactions, Cp*Co($N_2$)($CNAr^{Dipp2}$) (**6**) can deliver a reactive fragment capable of activating the P–P bonds in white phosphorus ($P_4$). As shown in Scheme 5.5, treatment of **6** with an equivalent of white phosphorus in $C_6D_6$ solution affords the $P_4$-complex Cp*Co($\kappa^2$-$P_4$)($CNAr^{Dipp2}$) (**10**), as a red-orange solid after crystallization. Structural determination of complex **10** (Figure 5.10) revealed a butterfly $P_4$ unit with a 1,4-$\kappa^2$ coordination mode to the single cobalt center. The (P1)–P(4) distance in **10** of 2.600(3) Å is substantially elongated relative to the P–P single bond distance of 2.21 Å in $P_4$ and is indicative of P–P bond scission.[54-56] This product outcome mirrors the reaction between the bridging-carbonyl dimer, [Cp*Co(μ-CO)]$_2$ and $P_4$, which produces Cp*Co($\kappa^2$-$P_4$)(CO).[57] Notably, the latter reaction requires elevated temperatures to induce $P_4$ activation and, upon extended thermolysis in the presence of additional (μ-CO)$_2$[Cp*Co]$_2$, can be converted into the dimeric $\mu^2$-$\kappa^2$: $\kappa^2$-$P_4$ complex ($\mu^2$-$\kappa^2$: $\kappa^2$-$P_4$)[Cp*Co(CO)]$_2$, in which two edges of

the $P_4$ tetrahedron have been cleaved.[57] In a similar fashion, treatment of **10** with another equivalent of $Cp^*Co(N_2)(CNAr^{Dipp2})$ (**6**), or alternatively, treatment of $Cp^*Co(N_2)(CNAr^{Dipp2})$ (**6**) with 0.5 equivalents of $P_4$, generates the dinuclear complex $(\mu^2\text{-}\kappa^2\text{:}\ \kappa^2\text{-}P_4)[Cp^*Co(CNAr^{Dipp2})]_2$ (**11**) as a deep red/black crystalline solid (Scheme 4.4). Indeed, structural characterization of **11** (Figure 5.11) shows two Co centers with $\kappa^2$-$P_4$ units and P–P separations of 2.556(4) Å and 2.595(4) Å, which reflect complete P–P bond activation. Most significantly however, this $P_4$ double-activation sequence proceeds at room temperature, is stoichiometric in cobalt and releases only an innocuous $N_2$ molecule as a byproduct. Accordingly, while true electronic structure mimic of $S = 1$ CpCo(CO) is not accessible in this isocyanide system, the $N_2$ complex **6** can serve as a reliable surrogate in its reaction chemistry with small molecule substrates.

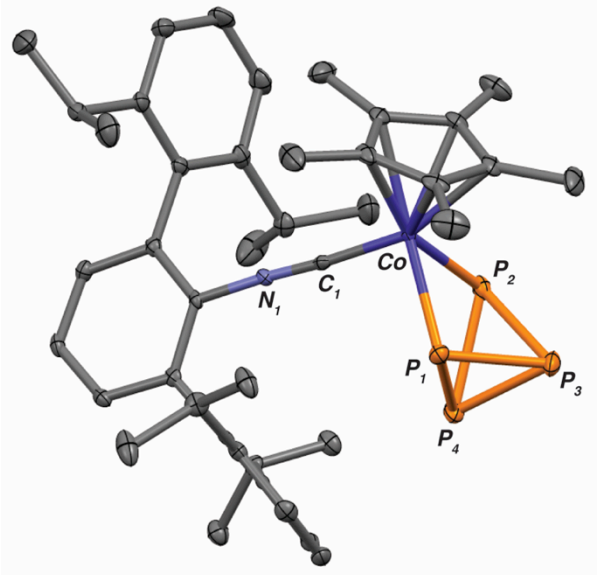


**Figure 5.10** Molecular structure of $Cp^*Co(\kappa^2\text{-}P_4)(CNAr^{Dipp2})$ (**10**). Hydrogen atoms omitted for clarity. Selected bond distances (Å): Co-$C_1$ = 1.7913(17), $C_1$-$N_1$ = 1.170(2), Co-$P_1$ = 2.2462(5), Co-$P_2$ = 2.2523(5), $P_1$-$P_2$ = 2.6065(8), $P_1$-$P_3$ = 2.2235(7), $P_1$-$P_4$ = 2.2096(7), $P_2$-$P_3$ = 2.2174(7), $P_2$-$P_4$ = 2.2201(7), $P_3$-$P_4$ = 2.1872(7). Selected bond angles (˚): $C_1$-$N_1$-$C_2$ = 175.24(16), $P_1$-Co-$P_2$ = 70.817(18), Co-$P_1$-$P_3$ = 99.74(2), Co-$P_2$-$P_3$ = 99.74(2), Co-$P_1$-$P_4$ = 101.49(2), Co-$P_2$-$P_4$ = 100.97(2), $P_2$-$P_3$-$P_1$ = 71.88(2), $P_2$-$P_4$-$P_1$ = 72.09(2).

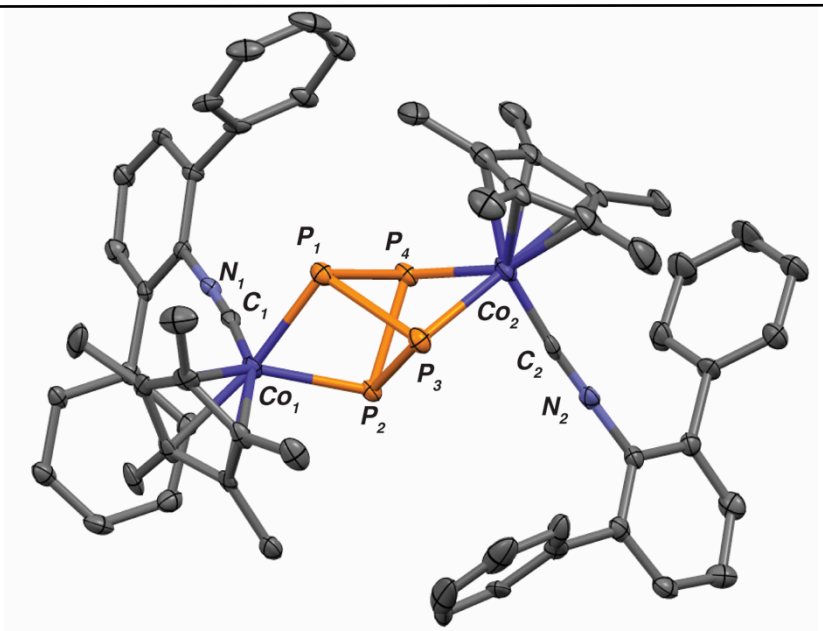


**Figure 5.11** Molecular structure of $[Cp^*Co(CNAr^{Dipp2})]_2(\mu^2{:}\kappa^2{;}\kappa^2\text{-}P_4)$ (**11**). Disordered Cp*, flanking *i*-Pr-Methyl groups, and Hydrogen atoms omitted for clarity. Selected bond distances (Å): $Co_1\text{-}C_1$ = 1.794(5), $C_1\text{-}N_1$ = 1.181(5), $Co_1\text{-}P_1$ = 2.2565(14), $Co_1\text{-}P_2$ = 2.2727(15), $Co_2\text{-}C_2$ = 1.765(6), $C_2\text{-}N_2$ = 1.193(6), $Co_2\text{-}P_3$ = 2.2614(13), $Co_2\text{-}P_4$ = 2.2635(15), $P_1\text{-}P_4$ = 2.2462(18), $P_1\text{-}P_3$ = 2.2581(19), $P_2\text{-}P_3$ = 2.2478(17), $P_2\text{-}P_4$ = 2.2207(17), $P_1\text{-}P_2$ = 2.5663(18), $P_3\text{-}P_4$ = 2.5951(18).

### 5.6 Developing Strategies to Circumvent Aza-Büchner Ring Expansion.

As discussed previously (Section 5.4) the activation of the $CNAr^{Dipp2}$ ligand framework from aza-Büchner ring expansion to form the corresponding coordianted aza-benz[*b*]azulene species (**7**) is proposed to occur from coordination of the flanking arene rings to the metal center. Due to our previous work with group 6 complexes,[31] which have additionally been shown, to under go $\eta^6$-arene tethering to sufficiently low-valent metals we sought to develop an *m*-terphenyl ligand scaffolds that could potentially resist arene coordination.[49] To combat this activation we reasoned that an increase in the steric profile of the *m*-terphenyl unit with respect to $CNAr^{Dipp2}$ could potentially discourage arene coordination. Accordingly we postulate that the *m*-terphenyl isocyanide $CNAr^{Tripp2}$ ($Ar^{Tripp2}$ = 2,6-(2,4,6-*i*$Pr_3$-$C_6H_2$)$C_6H_3$) would supply the desired steric profile and thus inhibit this decomposition pathway.[58-61]

## 5.7. Synthesis of $CNAr^{Tripp2}$.

The synthesis of $CNAr^{Tripp2}$ is depicted in Scheme 5.6. Condensation with excess formic acetic anhydride over 5 days at 60˚ C afforded the formamide $HC(O)NHAr^{Tripp2}$ (**11**). Similar to $CNAr^{Dipp2}$ a more electrophilic formylating agent (for less encumbered isocyanides condensation with formic acid (HC(O)OH) yields the corresponding formamide)[30] was required. Unlike the formylation conditions for $H_2NAr^{Dipp2}$, which proceeds smoothly at room temperature, formylation of $H_2NAr^{Tripp2}$ requires prolonged reaction times (*ca.* 5 days) and heating to drive the reaction to completion[32] as a result the of the increased steric profile on the $Ar^{Tripp2}$ unit when compared to the $Ar^{Dipp2}$ substituent. Subsequent dehydration with $OPCl_3$ under basic conditions provides the final isocyanide product $CNAr^{Tripp2}$ (**13**) in >94 % yield. The solid-state structure of $CNAr^{Tripp2}$ (**13**) was determined, Figure 5.12, and exhibits a $C_{iso}$–N bond distance of 1.143(3) Å approximately 0.01 Å contraction when compared to $CNAr^{Dipp2}$ ($C_{iso}$-N bond length = 1.1577(18) Å).[30] The formation of $CNAr^{Tripp2}$ was also verified by solid state and solution phase ($C_6D_6$) FTIR spectroscopy with an intense ν(CN) stretch at 2117 $cm^{-1}$. Interestingly the ν(CN) stretch of $CNAr^{Tripp2}$ is red-shifted by approximately 1 $cm^{-1}$ when compared to $CNAr^{Dipp230}$ suggesting that $CNAr^{Tripp2}$ is more electron releasing then other *m*-terphenyl isocyanides. To substantiate the increased electron richness of $CNAr^{Tripp2}$ with respect to other isocyanides its σ-donnor/π-acceptor propoerties were assayed via coordination to the $Cr(CO)_5$ fragment in a comparitive study done by our group,[32] and found to be the more electron releasing then both $CNAr^{Dipp2}$ and $CNAr^{Mes2}$ ($Ar^{Mes2}$ = 2,6-(2,4,6-$(Ch_3)_3C_6H_3)_2C_6H_3$).

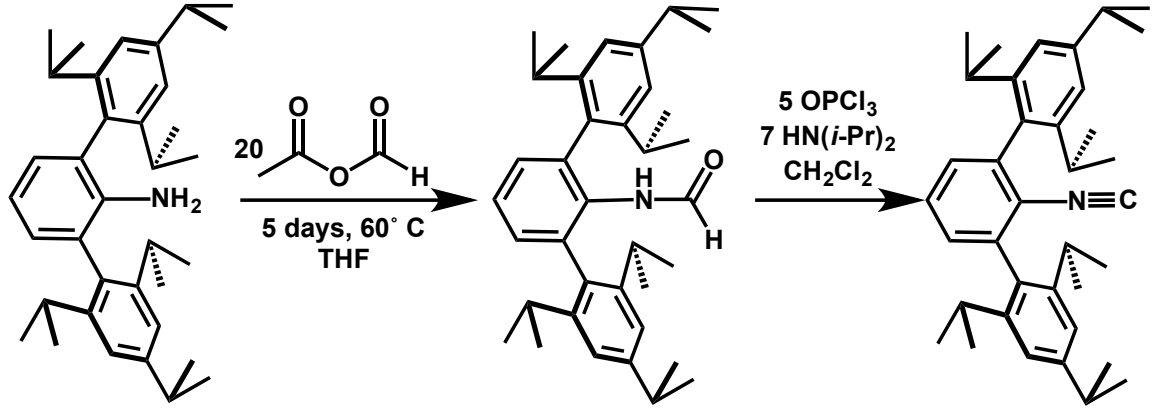


**Scheme 5.6.** Reaction scheme depicting the synthesis of $CNAr^{Tripp2}$ from the corresponding aniline $H_2NAr^{Tripp2}$.

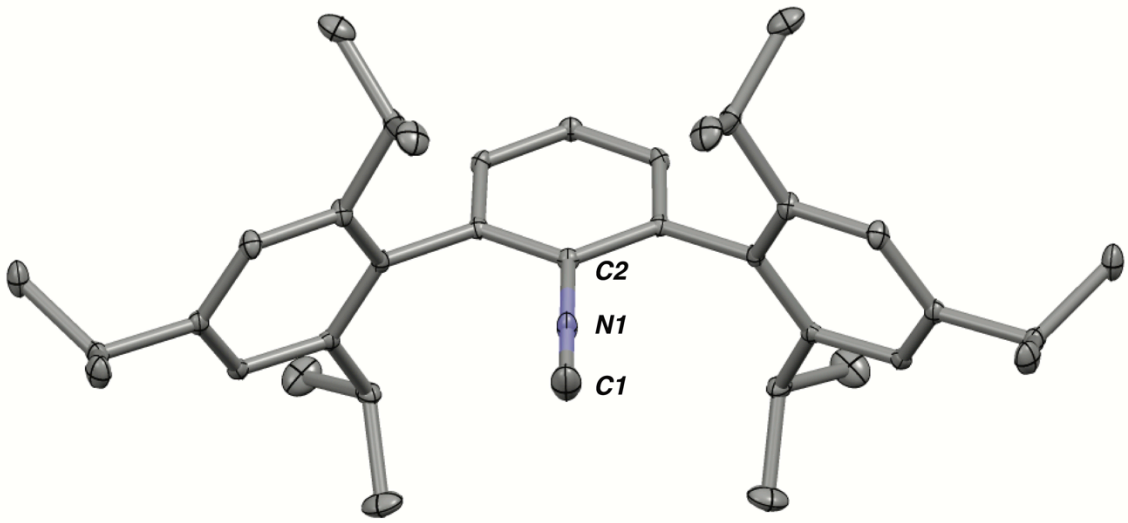


**Figure 5.12** Molecular structure of $CNAr^{Tripp2}$ (**13**). Selected bond distances (Å): $C_1$-$N_1$ = 1.143(3). Selected bond angles (˚): $C_1$-$N_1$-$C_2$ = 179.2(3).

## 5.8. Synthesis, Characterization and Stability Studies of $Cp^*Co(N_2)(CNAr^{Tripp2})$.

Similar to the synthesis of $Cp^*Co(N_2)(CNAr^{Dipp2})$ (**6**), addition of $CNAr^{Tripp2}$ (**12**) to $C_6H_6$ solutions of $Cp^*CoI_2(CO)$ at room temperature leads to the smooth formation of $Cp^*CoI_2(CNAr^{Tripp2})$, (**13**) via ejection of one equivalent of CO (Figure 5.13, Scheme 5.7). Subsequent reduction with two equivalents of $KC_8$ affords the dintrogen adduct $Cp^*Co(N_2)(CNAr^{Tripp2})$ (**14**) as dark orange/brown crystals, Scheme 5.7. The solid-state structure of (**14**) is shown in Figure 5.14, and exhibits gross structural similarities to

Cp*Co($N_2$)(CNAr$^{Tripp2}$). Dinitrogen adduct (**14**) exhibits a red-shifted isocyanide–*CN* stretch, ν(CN) = 2004, and 2037 $cm^{-1}$, when compared to the diiodide precursor (**13**) in addition to a ν(NN) = 2011$cm^{-1}$. Similar to Cp*Co($N_2$)(CNAr$^{Dipp2}$) (**6**) the high energy ν(NN) stretch reflects minimal M→π*(NN) back donation due to the inability of the coordinated $N_2$ to compete with the CNR π*-manifold for π-symmetry electron density, rendering it labile.[62] Similarly to complex (**6**), assessment of the lability of the $N_2$ ligand in Cp*Co($N_2$)(CNAr$^{Tripp2}$) (**14**) was accomplished by sequential freeze-pump-thaw (FPT) cycles (*ca.* 8). Unlike its less encumbered analogue, Cp*Co($N_2$)(CNAr$^{Dipp2}$) (**6**), which shows conversion to its aza-benz[*b*]azulene decomposition product (**7**),[62] dinitrogen (**14**) shows no indication of up field olefinic resonance characteristic of coordinated aza-benz[*b*]azulene upon sequential FPT cycles. However, upon removal of $N_2$ a color change to deep red is observed, and analysis via $^1$H NMR spectroscopy indicated partial conversion to a new Cp* containing product that exhibited a symmetric Ar$^{Tripp2}$ environment. Re-exposure of the reaction mixture to an $N_2$ atmosphere results in an immediate color change back to brown corresponding to the regeneration of Cp*Co($N_2$)(CNAr$^{Tripp2}$) (**15**) as the only *m*-terphenyl containing species as assayed by $^1$H NMR spectroscopy.

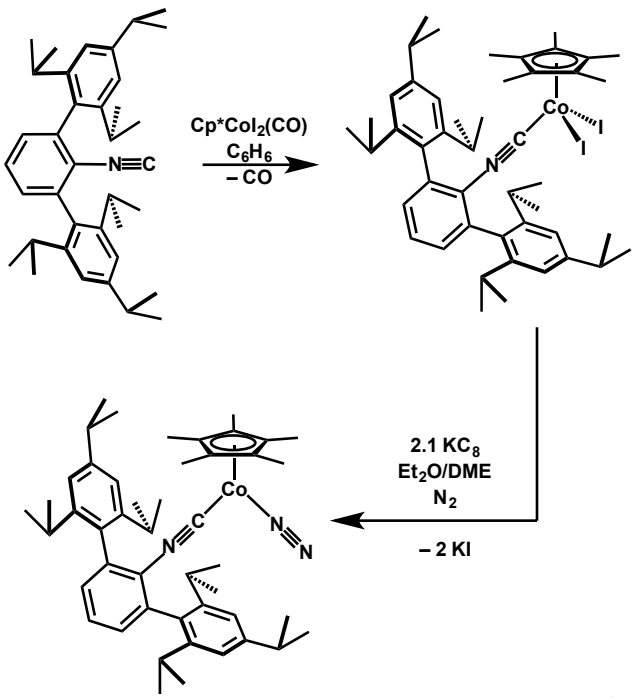


**Scheme 5.7.** Reaction scheme depicting the synthesis of $Cp^*CoI_2(CNAr^{Tripp2})$ (**13**) and subsequent reduction to $Cp^*Co(N_2)(CNAr^{Tripp2})$ (**14**).

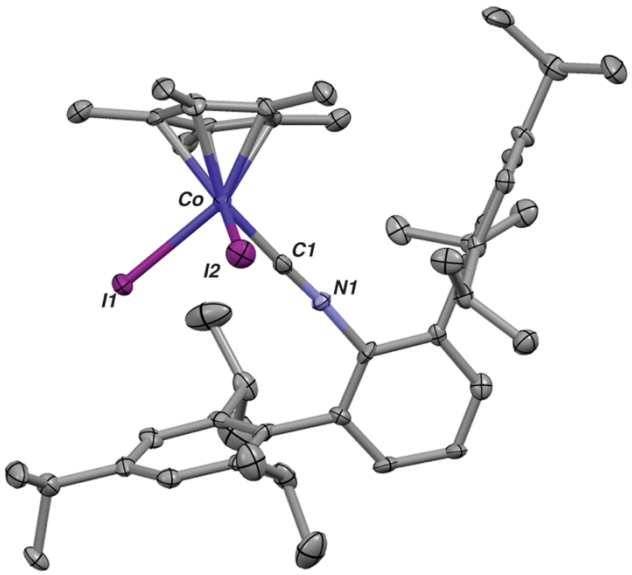


**Figure 5.13** Molecular structure of $Cp^*CoI_2CNAr^{Tripp2}$ **(14)**. Hydrogen atoms omitted for clarity. Selected bond distances (Å): Co-$I_1$ = 2.5682(18), Co-$I_2$ = 2.5944(14), Co-$C_1$ = 1.837(11), $C_1$-$N_1$ = 1.136(12). Selected bond angles (°): $C_1$-$N_1$-$C_2$ = 175.1(10).

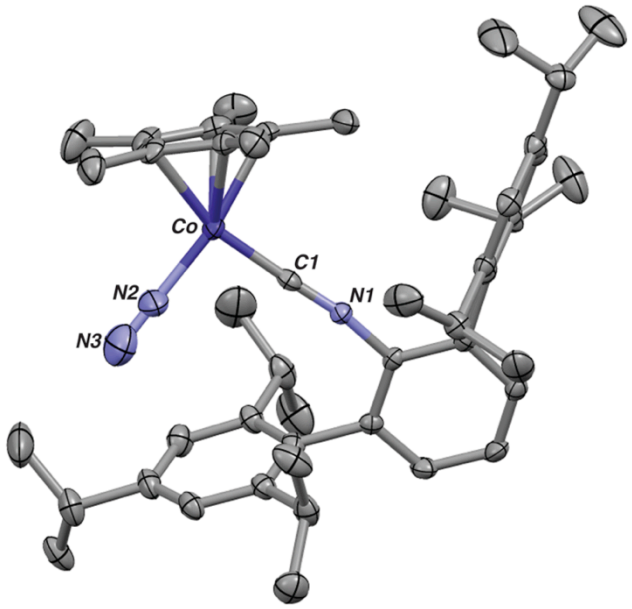


**Figure 5.14.** Molecular structure of Cp*Co($N_2$)CNAr$^{Tripp2}$ **(15)**. Hydrogen atoms omitted for clarity. Selected bond distances (Å): Co-$C_1$ = 1.770(3), $C_1$-$N_1$ = 1.173(4), Co-$N_2$ = 1.814(4), $N_2$-$N_3$ = 1.014(5). Selected bond angles (˚): $C_1$-$N_1$-$C_2$ = 167.7(3), Co-$N_2$-$N_3$ = 176.4(5), $C_1$-Co-$N_2$ = 95.50(14).

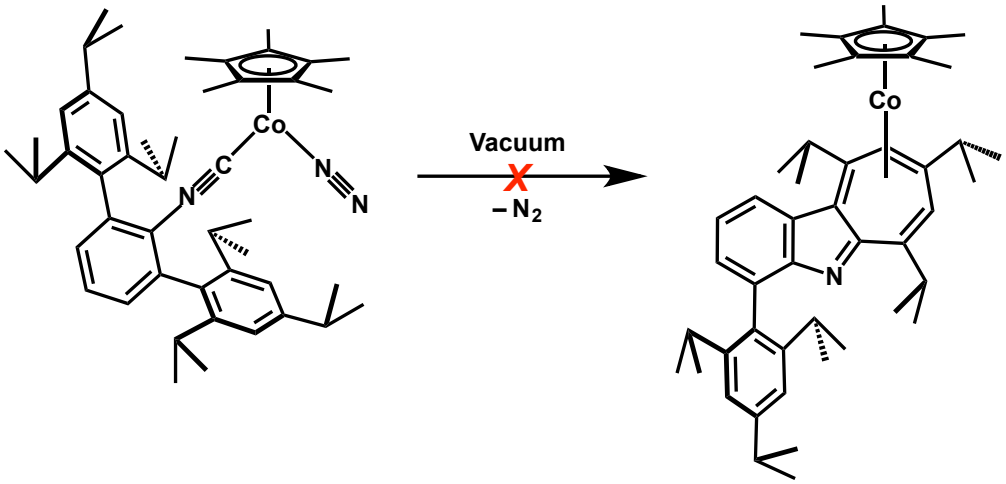


**Scheme 5.8.** Cp*Co($N_2$)(CNAr$^{Tripp2}$) (**14**) exhibits resistance to Aza-Büchner ring expansion.

In an effort to identify this new species which forms in the absences of an $N_2$ atmosphere, reductions to generate [Cp*Co(CNAr$^{Tripp2}$] under *rigorous* $N_2$ free conditions were undertaken. Reduction of Cp*$CoI_2$(CNAr$^{Tripp2}$) in $C_6H_6$ under an $Ar_{(g)}$ atmosphere provided deep red solutions, that exhibited the analogous $^1$H NMR spectroscopic signature previously observed upon degassing $C_6D_6$ solutions of Cp*Co($N_2$)(CNAr$^{Tripp2}$)

(**14**). Crystallization of the resulting reaction mixture from a saturated *n*-pentane solution spiked with $C_6H_6$ afforded the bridging benzene dimer [Cp*Co(CNAr$^{Tripp2}$)]$_2$($\mu^2$-$\eta^2$-(C,C)-$\eta^2$-(C,C)-$C_6H_6$) (**15**), Scheme 5.9. The solid state structure of benzene dimer (**15**) is shown in Figure 5.15, and depicts two Cp*Co(CNR) trans disposed coordinated in a 1,3-($\eta^2$,$\eta^2$) fashion to a single molecule of benzene. Inspection of the crystal structure displays an asymmetric $C_6H_6$ core with double bond localization at the points of coordination to Co. Moreover, each H-atom of the benzene ring was unambiguously located in the electron density map modeled with idealized $sp^2$ C–H distances (0.95 Å ± 0.02 Å) and set as riding without use of the HFIX command, and are shown to cant above and below the $C_6$–ring, Figure 5.16. This deformation of the coordinated benzene is suggestive of a substantial degree of π-donation in the coordinated arene resulting in a degree of dearomatization. Indeed this coordination mode featuring 1,3-($\eta^2$,$\eta^2$) coordination to benzene has been observed previously,[63,64] however this is the first example of a coordinated arene to Co through a 1,3-($\eta^2$,$\eta^2$) binding mode, and stands to highlight the propensity for Cp*CoL fragments to function as highly reactive and unstable organometallic fragments, such that there generation results in the coordination and activation of typically inert small molecule substrates. [6,65]

Importantly, isolation of benzene dimer (**15**) shows that increase in the steric profile of the *m*-terphenyl framework effectively disfavors intramolecular arene-metal interactions, and prevents intramolecular aza-Büchner ring expansion of the *m*-terphenyl unit. As noted previously coordination of benzene ($C_6H_6$) highlights the dichotomy of reactivity profiles between Cp*CoL fragments that posses unidirectional π*-manifolds[19] (*e.g.* Cp*CoIPr) and those that posses orthogonal π*-orbitals (*e.g.*

Cp*Co(CNR)/Cp*Co(CO)) such that the former display diminished reactivity toward weakly coordinating L-donor ligands, namely dinitrogen and benzene. This is presumably due to a small but non-negligible increase in the singlet-triplet gap for *N*-heterocyclic carbene complexes of the Cp*CoL fragment ( Cp*Co(iPr)) of >14 kcal mol$^{-1}$) rendering the S = 1 ground state comparatively lower in energy and more stable with respect to CpCo(CO), which has been shown to display a singlet-triplet gap ~ 11.2 kcal mol$^{-1}$.[66]

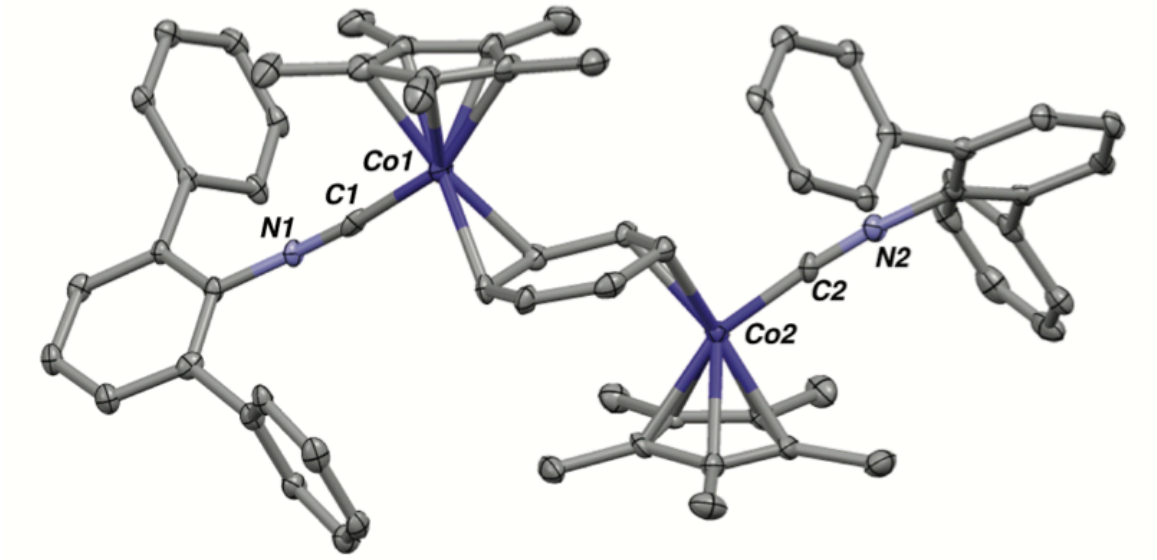


**Figure 5.15.** Molecular structure of [Cp*Co(CNAr$^{Tripp2}$)]$_2$($\mu^2$-$\eta^2$-(C,C)-$\eta^2$-(C,C)-$C_6H_6$) (**16**). Hydrogen atoms omitted for clarity. Selected bond distances depicted in Figure 5.16.

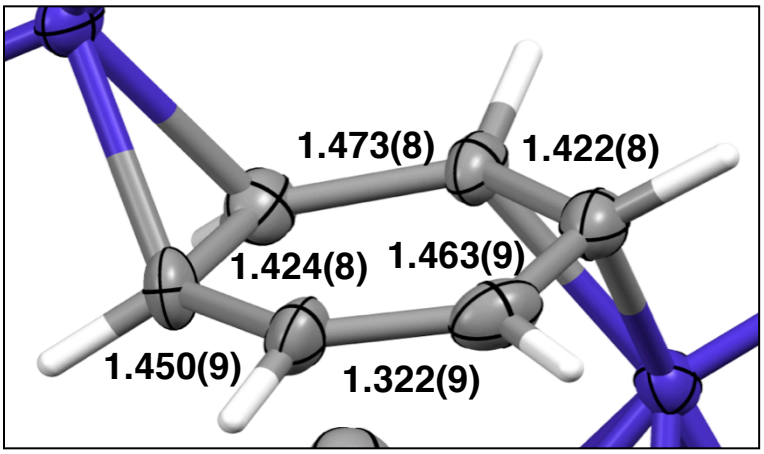


**Figure 5.16.** Zoom in of the bridging $C_6H_6$ unit in $[Cp^*Co(CNAr^{Tripp2})]_2(\mu^2\text{-}\eta^2\text{-}(C,C)\text{-}\eta^2\text{-}(C,C)\text{-}C_6H_6)$, (**3**). Hydrogen atoms located in the electron density map and are depicted as sticks.

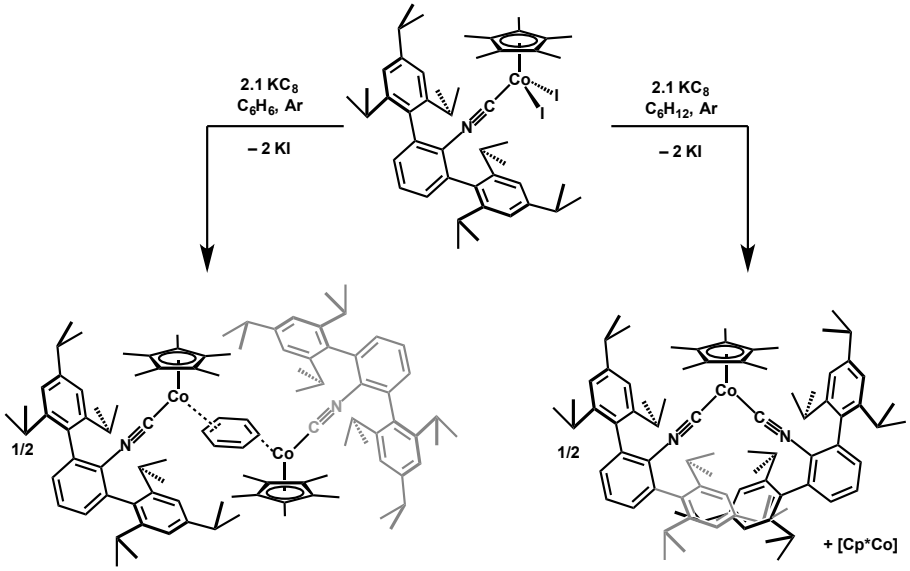


**Scheme 5.9.** Reaction scheme depicting recution products of $Cp^*CoI_2(CNAr^{Tripp2})$ (**13**) under an $Ar_{(g)}$ Atmosphere in $C_6H_6$ yielding $[Cp^*Co(CNAr^{Tripp2})]_2(\mu^2\text{-}\eta^2\text{-}(C,C)\text{-}\eta^2\text{-}(C,C)\text{-}C_6H_6)$ (**15**) and $C_6H_{12}$ yielding $Cp^*Co(CNAr^{Tripp2})_2$ (**16**).

Attempts to generate the $Cp^*Co(CNAr^{Tripp2})$ fragment in the absence of coordinating arene solvents was also attempted. Reduction under an $Ar_{(g)}$ atmosphere afforded the bis-isocyanide speces $Cp^*Co(CNAr^{Tripp2})_2$ (**16**) as the major isocyanide containing species. Complex (**16**) exhibits a diagnostic $^1H$ NMR spectrum displaying broadened $^1H$ resonances of the flanking *i*-Pr groups due to hindered rotation on the

NMR time scale. The $^{1}$H NMR spectrum was also authenticated via the addition of $CNAr^{Tripp2}$ to $Cp^{*}Co(N_2)(CNAr^{Tripp2})$ which exhibited the same broadened $^{1}$H chemical shifts. The solid state structure of complex (**16**) was unambiguously determined via X-ray diffraction and shows two coordinated isocyanide units with a substantial average bending in the CNC linkages (*ca.* 156.0(2)˚) of the isocyanide due to the tremendous steric pressure about Co, Figure 5.17. Moreover, $Cp^{*}Co(CNAr^{Tripp2})_2$ (**16**) displays a diagnostic ν(CN) stretch in the solution FTIR at (1915, 2002 $cm^{-1}$) consistent with local $C_{2v}$ site symmetry notwithstanding the large steric constraints. Despite the robustness of the Co–isocyanide linkage the redistribution of isocyanide ligands has been previously documented by us with the generation of unsaturated Ni species of the formulation $Ni(CNR)_3$.[20] Accordingly, this points to a decomposition pathway that in the absence of suitable L-donor ligands results in ligand redistribution to generate the electronically saturated [$Cp^{*}Co(CNAr^{Tripp2})$] fragment.

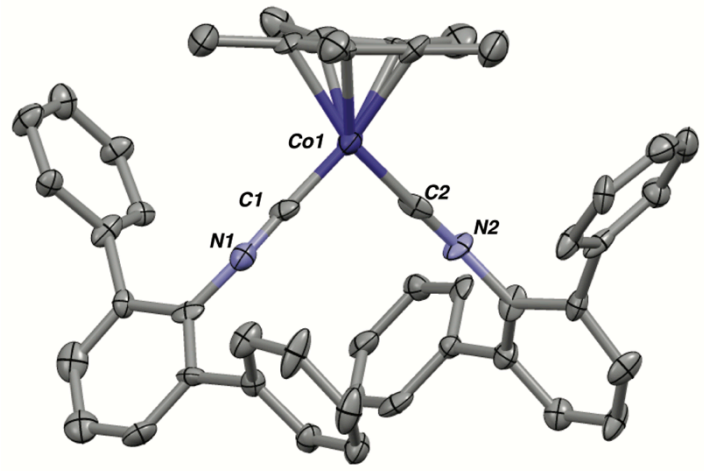


**Figure 5.17.** Molecular structure of $Cp^{*}Co(CNAr^{Tripp2})_2$ (**17**). Hydrogen atoms and flanking *i*-Pr groups omitted for clarity. Selected bond distances (Å): Co-$C_1$ = 1.760(7), Co-$C_2$ = 1.77(1), $C_1$-$N_1$ = 1.19(1), Co-$N_2$ = 1.19(1). Selected bond angles (˚): $C_1$-$N_1$-$C_3$ = 157.1(7), $C_2$-$N_1$-$C_{39}$ = 154.8(7), $C_1$-Co-$C_2$ = 96.2(3)˚.

Despite the inability to isolate an unsaturated [Cp*Co(CNR)] fragment the unusual coordination chemistry with unconventional L-donor ligands emphasizes the inherent reactivity of these fragments. From this reactivity profile we reasoned that Cp*Co($N_2$)($CNAr^{Tripp2}$) (**14**), like Cp*Co($N_2$)($CNar^{Tripp2}$) (**6**), should function as a more robust source of [Cp*Co(L)] capable of small molecule activation. To this end, the following sections will serve to display a preliminary reactivity survey and the effectiveness of Cp*Co($N_2$)($CNAr^{Tripp2}$) (**14**) as a platform for C-C coupling, oxidative addition, in addition to evidence for potential Co-E elemental multiple bonding.

**5.9. Reactivity of Cp*Co($N_2$)($CNAr^{Tripp2}$) Towards Unsaturated C–C Bonds.**

The reactivity of $CpCo(CO)_2$ has centered around its use as a pre-catalyst for the (2+2+2) cyclo-addition of alkynes to yield aromatic organic substrates.[67,68] This has been attributed to the ability of $CpCo(CO)_2$ to undergo CO ejection to yield [CpCo] [69,70] which is then capable of coordinating an equivalent of alkyne. Following the [CpCo] fragment enters the catalytic cycle shown in Scheme 5.10. Although the reactivity of Cp*Co($\eta^2$-*C,C*-PhCCPh)($CNAr^{Dipp2}$) (**8**) proved to only coordinate internal alkynes with no evidence of cyclotrimerization we postulated that the increased steric pressure of Cp*Co($N_2$)($CNAr^{Tripp2}$) (**14**) could potentially provide enough of a sterically crowed coordination sphere to force dissociation of isocyanide and provide access to cyclotrimerization reactivity. Treatment of Cp*Co($N_2$)($CNAr^{Tripp2}$) (**14**) with diphenyl acetylene proceeds smoothly to afford the $\eta^2$-bound alkyne species Cp*Co($\eta^2$-C,C-PhCCPh)($CNAr^{Tripp2}$), (**17**). The solid state structure is shown in Figure 5.18 and mimics the structural features observed for the Cp*Co($\eta^2$-C,C-PhCCPh)($CNAr^{Dipp2}$) (**9**), however, similarly to Cp*Co($\eta^2$-C,C-PhCCPh)($CNAr^{Dipp2}$) (**9**), addition of excess

equivalents of di-phenyl acetylene did not indicate any conversion to the corresponding hexa-phenyl benzene.

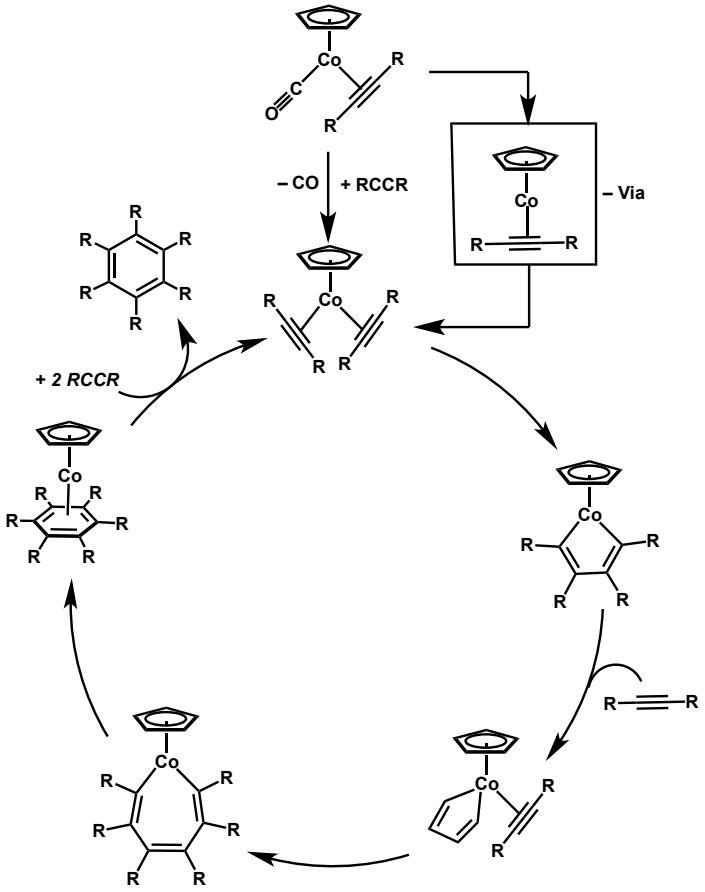


**Scheme 5.10** Synthetic scheme for the catalytic conversion of alkynes to arenes via [2+2+2] cycloaddition initiated by CpCo(CO)(alkyne).

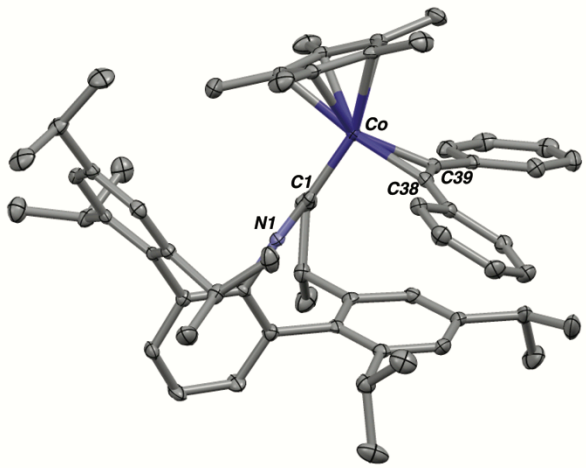


**Figure 5.18** Molecular structure of Cp*Co($\eta^2$-C,C-PhCCPh)(CNAr$^{Tripp2}$), (**18**). Hydrogen atoms omitted for clarity. Selected bond distances (Å): Co-$C_1$ = 1.787(2), $C_1$-$N_1$ = 1.181(2), Co-$C_{38}$ = 1.980(2), Co-$C_{39}$ =1.972(2), $C_{38}$-$C_{39}$ = 1.270(3). Selected bond angles (˚): $C_1$-$N_1$-$C_2$ = 176.5(2), $C_{39}$-$C_{38}$-$C_{40}$ = 148.2(2), $C_{38}$-$C_{39}$-$C_{46}$= 150.7(2).

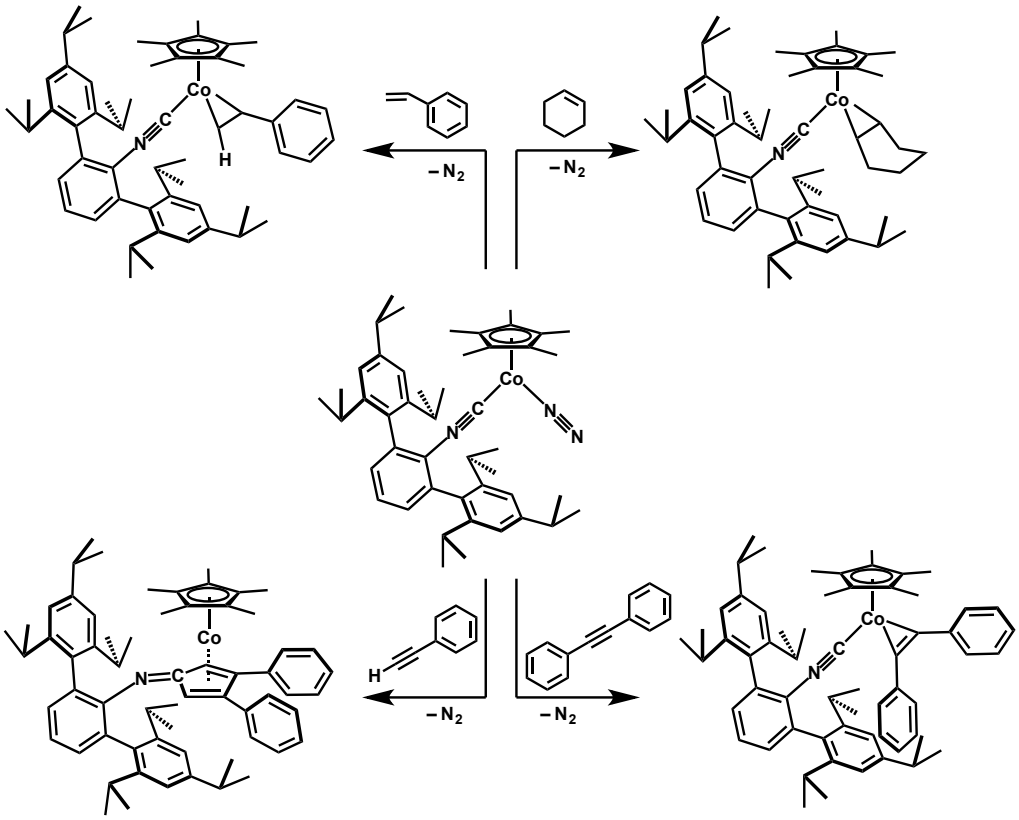


**Scheme 5.11** Reactivity profile of Cp*Co($N_2$)(CNAr$^{Tripp2}$) (**15**) with unsaturated C–C bonds.

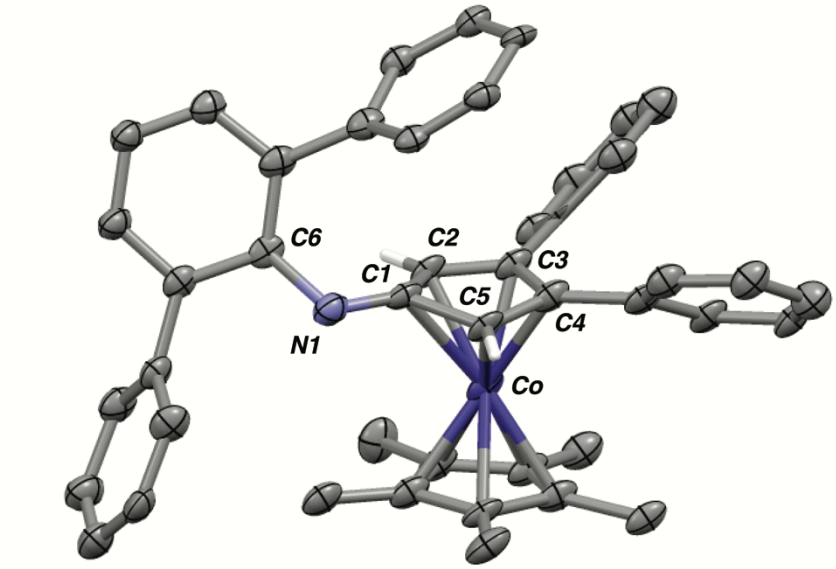


**Figure 5.19** Molecular structure of cyclopentadiene-exo-iminie[Cp*Co] (**19**) Hydrogen atoms and flanking *i*-Pr groups omitted for clarity. Selected bond distances (Å): Co-$C_1$ = 2.33(2), Co-$C_2$ = 2.03(2), Co-$C_3$ = 1.99(2), Co-$C_4$ = 2.02(2), Co-$C_5$ = 2.03(2), $C_1$-$N_1$ = 1.31(2), $C_6$-$N_1$ = 1.37(2), $C_1$-$C_2$ = 1.47(3), $C_2$-$C_3$ = 1.36(2), $C_3$-$C_4$ = 1.44(3), $C_4$-$C_5$ =1.39(3), $C_5$-$C_1$ = 1.47(2). Selected bond angles (˚): $C_1$-$N_1$-$C_6$ = 120(2), $C_1$-$C_2$-$C_5$-$C_4$ = 18(2).

Addition of terminal alkynes (*e.g* HCCPh) however does show interesting reactivity. Addition of two equivalents of HCCPh to Cp*Co($N_2$)($CNAr^{Tripp2}$) (**14**) shows rapid conversion to a new product that displays de-symmetrized $Ar^{Tripp2}$ resonances in addition to olefinic resonances at 3.46 ppm within the $^1$H NMR spectrum. Crystallization of the reaction mixture afforded the cyclopentadiene-exo-iminie complex (**19**), Figure 5.19. Complex (**18**) displays a near planar cycopentadienyl ligand with additional interaction of the envelope carbon bond to the imine. Bond lengths of the ring are shown in Table 6.1 and display double bond localization at the C2-C3 and C4-C5 position. Formation of complex (**18**) can be rationalized via an analogous mechanism depicted in Scheme 5.10 and can be envisioned as an overall (2+2+1) cycloaddition. Initial displacement of $N_2$ by alkyne and subsequent displacement of isocyanide leads to the

oxidative coupling of two HCCPh units. Subsequent reintroduction of isocyanide and coupling yields the final imine fragment bound to Co yielding complex (**19**). [71-73]

Attempts to extend this reactivity towards alkenes (*e.g.* Cyclohexene, Styrene) to generate the corresponding carbo-cyclic-imine complexes was also attempted, however reactivity with both terminal and internal olefins yielded the corresponding Cp*Co(alkene)(CNR) adducts as the major Co containing species. The solid state structure of Cp*Co($\eta^2$-*C,C*-$C_6H_{10}$)($CNAr^{Tripp2}$) (**20**), and Cp*Co($\eta^2$-*C,C*-$CH_2CHPh$)($CNAr^{Tripp2}$) (**21**) are shown in Figure 5.20 and 5.21 respectively.

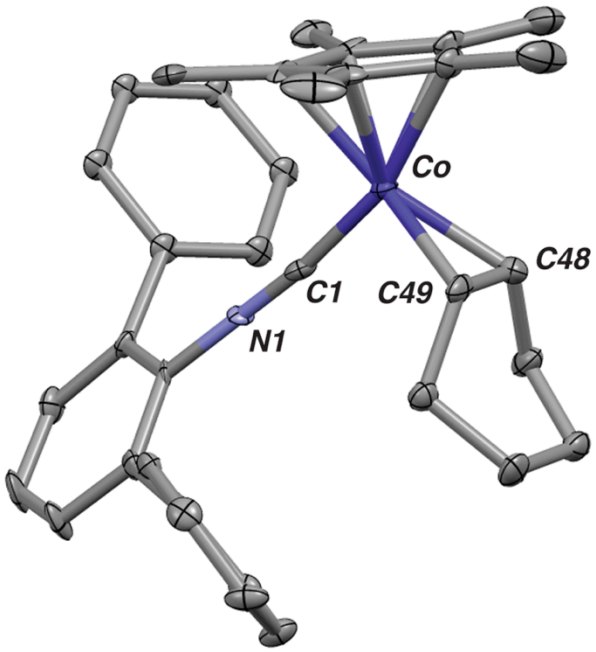


**Figure 5.20** Molecular structure of Cp*Co($\eta^2$-*C,C*-$C_6H_{10}$)$CNAr^{Tripp2}$ (**20**). Hydrogen atoms and positional disorder omitted for clarity. Selected bond distances (Å): $O_1$-$C_1$ = 1.172(4), $C_1$-$N_1$ = 1.1334(3. Selected bond angles (˚): $C_1$-$N_1$-$C_2$ = 146.27(16), $O_1$-$C_1$-$N_1$ = 174.0(3).

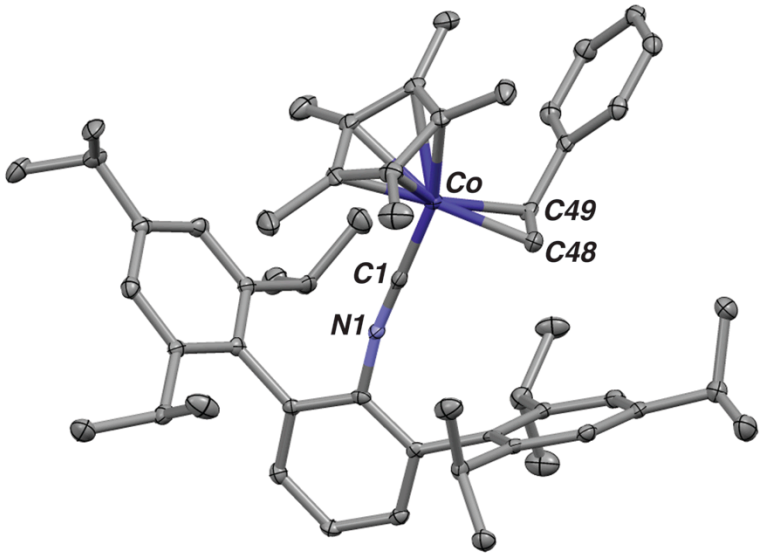


**Figure 5.21** Molecular structure of Cp*Co($\eta^2$-*C,C*-$CH_2CHPh$)$CNAr^{Tripp2}$ (**21**). Hydrogen atoms and positional disorder omitted for clarity. Selected bond distances (Å): $O_1$-$C_1$ = 1.172(4), $C_1$-$N_1$ = 1.1334(3). Selected bond angles (˚): $C_1$-$N_1$-$C_2$ = 146.27(16), $O_1$-$C_1$-$N_1$ = 174.0(3).

## 5.10 Probing Oxidative Addition of $H_2$ and Silanes with Cp*Co($N_2$)($CNAr^{Tripp2}$).

Due to ability of Cp*Co($N_2$)($CNAr^{Dipp2}$) (**6**) to activate elemental $P_4$ via facile P–P bond sission at room temperature, we thought to probe the ability of Cp*Co($N_2$)($CNAr^{Tripp2}$) (**14**) to participate in oxidative addition of more challenging substrates (*i.e.* H–$SiR_3$ and $H_2$). For comparison to the carbonyl congener, it has been shown via ultrafast solution FTIR experiments that CpCo(CO) has the ability to activate silane Si–H bonds,[6] however structural elucidation of these types of species remain extremely rare for the the CpCoL framework with the only example from Brookhart and co-workers, Cp*Co($H)_2$($SiPh_2Et.)_2$.[74] Accordingly, we thought to explore the reactivity of Cp*Co($N_2$)($CNAr^{Tripp2}$) (**14**) toward trialkyl-silanes. Addition of $HSiEt_3$ to Cp*Co($N_2$)($CNAr^{Tripp2}$) (**14**) at room temperature in benzene solutions proceeds smoothly with a faint color change from dark brown/orange to dark yellow/orange. Analysis of the crude reaction mixture via $^1$H NMR spectroscopy indicated broadened $Ar^{Tripp2}$ *i*-Pr

resonances in addition to an upfield shifted resonance at 15 ppm ($C_6D_6$) corresponding to hydride formation. Crystals of the reaction mixture afforded complex (**22)** which confirmed the presence of a $–SiEt_3$ fragment bound to cobalt, in addition to a hydride ligand found in the electron density map. The Si–H separation is *ca.* 1.82(3) Å is suggestive that formal Si–H bond sission to generate the oxidative addition produce, Co(III) silyl hydride. Silyl hydride (**22**) is thermally stable and was shown to be persistent in solution as assayed by ROESY and NOESY 2D NMR spectroscopy. Gratifyingly the increased nucleophilicty at Co engendered by the increased σ-donation provided by an isocyanide ligand field allows for facile activation of Si–H bonds, in a similar manor to the reactivity of $Cp^*Co(N_2)(CNAr^{Dipp2})$ which promoted facile P–P bond scission upon treatment of white phosphorous. Attempts to use complex (**22**) as a catalyst for the hydrosilaytion of olefins however was unsuccessful with no apparent reactivity with cyclohexene over days at elevated temperatures.

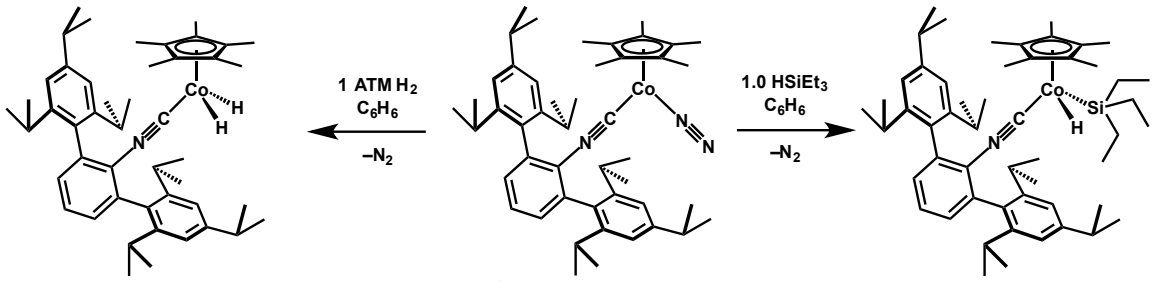


**Scheme 5.11** Reactivty of $Cp^*Co(N_2)(CNAr^{Tripp2})$ with $HSiEt_3$ and $H_2$.

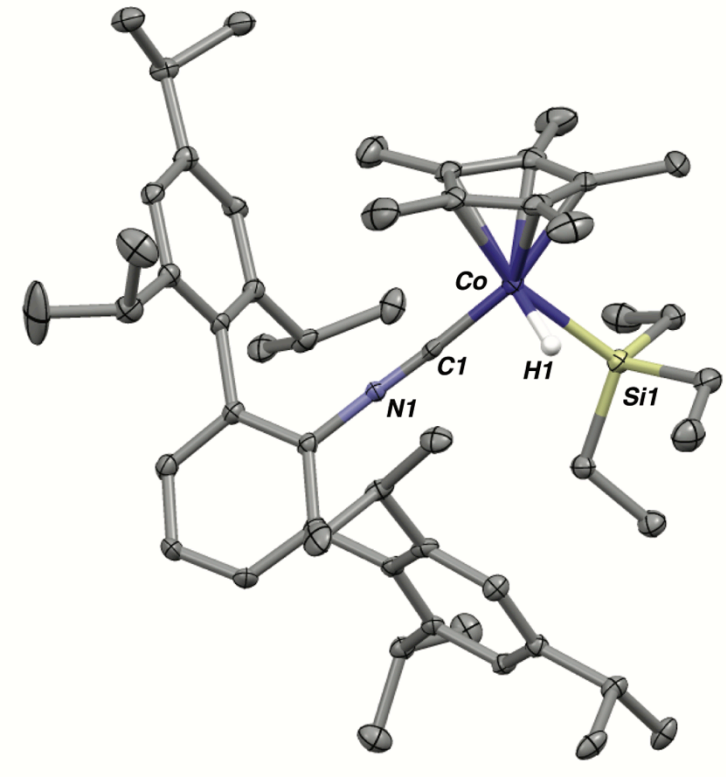


**Figure 5.22** Molecular structure of Cp*Co(H)($SiEt_3$)($CNAr^{Tripp2}$) (**22**). Hydrogen atoms and positional disorder omitted for clarity. Selected bond distances (Å): Co-Si = 2.286(1), Co-$C_1$ = 1.779(3), Co-$H_1$ = 1.31(3), Si-$H_1$ = 1.82(3), $C_1$-$N_1$ = 1.174(5). Selected bond angles (˚): $C_1$-$N_1$-$C_2$ = 172.4(3).

To further probe the competency of Cp*Co($N_2$)($CNAr^{Tripp2}$) towards oxidative addition we turned to $H_2$ as its activation still presents a worthwhile endeavor for a number of catalytically relevant transformations.[75,76] Addition of an atmosphere of $H_{2(g)}$ to a resealable J-Young's NMR tube containing Cp*Co($N_2$)($CNAr^{Tripp2}$) (**14**) results in a color change from dark orange/brown to deep yellow. Analysis of the crude $^1$H NMR indicated formation of a new species with symmetric $Ar^{Tripp2}$ resonances and an up-field shifted singlet at –15 ppm. Attempts to structurally authenticate this species under an atmosphere of $N_2$ have been precluded and have only afforded Complex (**14**) as assayed by $^1$H NMR spectroscopy of the crystalline material, suggesting that the activation of $H_2$ is reversible under an $N_2$ atmosphere. Further attempts to promote crystallization under

$Ar_{(g)}$ and $H_{2(g)}$ atmospheres have also been unsuccessful. Analysis of the reaction mixture via solution FTIR spectroscopy ($C_6D_6$) immediately after addition of $H_2$ indicate a blue shifted isocyanide ν(CN) stretch at 2071 $cm^{-1}$ in addition to the absence of coordinated dinitrogen at 2110 $cm^{-1}$. The subsequent blue shift in the solution FTIR spectrum of the reaction mixture is suggestive of formal oxidation of the Co center form (I) to (III). Based on the reactivity profile presented *vida supra* we tentatively propose that this new species as the dihydride complex $Cp^*Co(H)_2(CNAr^{Tripp2})$ (**23**). Attempts to elucidate the molecular structure of this species are on going within our laboratory.

### 5.11 Reactivity of $Cp^*Co(N_2)(CNAr^{Tripp2})$ with Organo-Azides.

Additionally attempts at generating coordination complexes that display unusual electronic structures and bonding schemes. To this end $Cp^*Co^*(N_2)(CNAr^{Tripp2})$ was used as a source of [Cp*Co(CNR)] as means of stabilizing M–E multiple bonding. Treatment of $N_3Ar^{Mes2}$ ($Ar^{Mes2}$ = 2,6-(2,4,6-$Me_3C_6H_3)_2C_6H_3$) at room temperature in $Et_2O$ solutions results in a color change to dark brown. Crystallization of the reaction mixture afforded the $\kappa^1$-azide species $Cp^*Co(\kappa^1\text{-}N_3Ar^{Mes2})(CNAr^{Tripp2})$ (**24**) (Figure 5.24, Scheme 5.13). Complex (**24**) exhibits a high energy ν($N_3$) stretch at 2003 $cm^{-1}$ in the solution FTIR spectrum ($C_6D_6$), and a diamagnetic $^1H$ NMR signature.

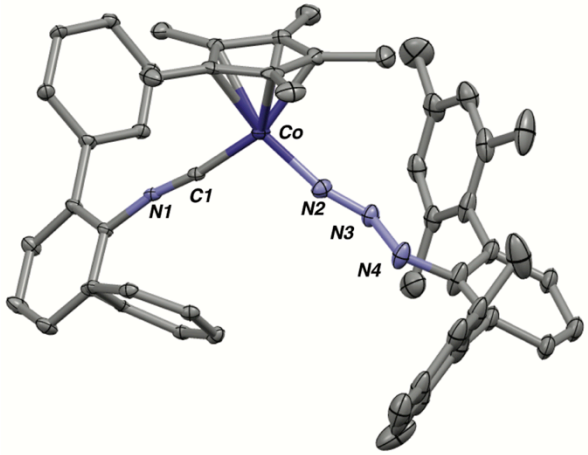


**Figure 5.23** Solid state molecular structure of Cp*Co($\kappa^1$-$N_3Ar^{Mes2}$)($CNAr^{Tripp2}$) (**24**). Hydrogen atoms and disordered mesityl ring omitted for clarity. . Selected bond distances (Å): Co-$C_1$ = 1.811(3), $C_1$-$N_1$ = 1.170(4), Co-$N_2$ = 1.786(3), $N_2$-$N_3$ = 1.184(4), $N_3$-$N_4$ = 1.324(4). Selected bond angles (˚): $C_1$-$N_1$-$C_2$ = 168.9(3), $N_2$-$N_3$-$N_4$ = 135.1(3).

Analysis of the solid-state structure indicates a significant degree of steric pressure about Co, with a bent azide–$N_3$ unit at 135.1(3) ˚. Due to the activation of the azide unit in (**24**) it followed that it could potentially provide access to species that exhibit Co–N multiple bonding upon extrusion of $N_2$. However photolysis of (**24**) and heating indicate robust thermal and photo-stability. Moreover, prolonged exposer to UV light for 12 hours at room temperature indicated no reactivity or decomposition of azide (**24**). We believe the stability of complex (**24**) stems from the encumbering $Ar^{Mes2}$ group which provides large amounts of kinetic stabilization to the $N_3$–unit. In an effort to facilitate extrusion of $N_2$ we turned to the less encumbering adamantyl azide $N_3$–Ad which has been shown to provide access to transition metal imido and amanyl species.[86,87] Treatment of Cp*Co($N_2$)($CNAr^{Tripp2}$) with $N_3$–Ad at low temperature (*ca.* –78 ˚C) resulted in an immediate color change to dark brown with concomitant effervescence. Examination of the reaction mixture by $^1$H NMR spectroscopy indicated a new paramagnetic species in addition to no indication of an azide ν($N_3$) resonance by

solution phases FTIR ($C_6H_6$). Crystallization of the resulting mixture afforded the amido dimer (**25**).

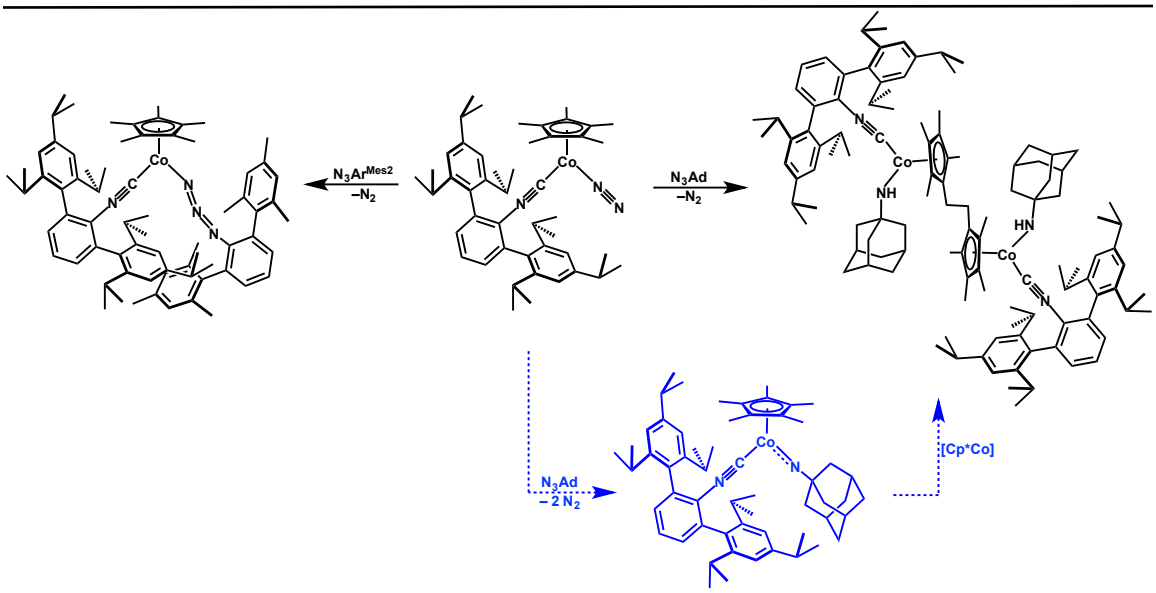


**Scheme 5.12** Reactivty of Cp*Co($N_2$)($CNAr^{Tripp2}$) (**15**) with organo-azide substrates.

Accordingly, a mechanism for the formation of amido dimer (**25**) can be envisioned in that initial coordination of azide to Co is immediately followed by extrusion of $N_2$ to produce a Cp*M=NR(CNR) unit. Multiply bound nitrogen ligands to Co are rare,[77-80] they have been observed, however due to the inherent reactivity observed for M=NR fragment when bound to late transition metals which have shown open shell reactivity pathways activation of the surrounding ligand environment is common. Accordingly, for the generation of dimer (**25**) a radical H-atom abstraction pathway from the Cp* ligand can be rationalized, which is then subsequently followed by radical recombination of the Cp* ligands[81] to yield amido-dimer **27**. This reactivity profile is unique such that the development of systems that can participate in M=E (M = metals to the right of group 8, E = O, N, S, P) are of high interest for group transfer reactivity.

Moreover, due to the unusual electronic structure for M=E multiple bonding when M is a late first row transition metals (*e.g.* Co[82-83], Ni[84]), complexes featuring M=NR linkages have been shown to display interesting and broad reactivity profiles and could provide new in-roads to small molecule activation. Work is on going to further understand these species, and M=E multiple bonding.

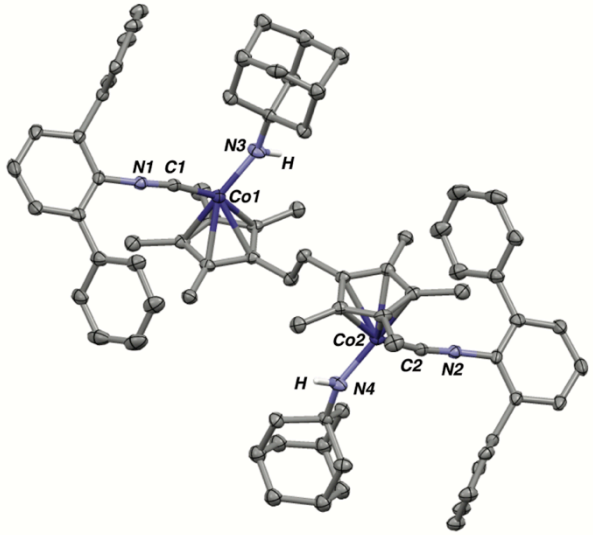


**Figure 5.24** Solid state molecular structure of $[Cp^*Co(N(H)Ad)(CNAr^{Tripp2})]_2$ (**25**). Hydrogen atoms and disordered adamantane groups omitted for clarity. Note $[Cp^*Co(N(H)Ad)(CNAr^{Tripp2})]_2$ lies on a a screw access and ½ of the molecule is symmetry generated resulting in bond lengths and angles presented being equivalent. Selected bond distances (Å): Co-$C_1$ = 1.788(6), $C_1$-$N_1$ = 1.189(7), Co-$N_2$ = 1.823(5). Selected bond angles (˚): $C_1$-$N_1$-$C_2$ = 170.9(5), Co-$N_2$-$C_{38}$ = 141.3(4).

## 5.12 Concluding Remarks.

Encumbering *m*-terphenyl isocyanides are an attractive ancillary ligand choice for the construction of a stable analogue of the $S = 1$ organometallic CpCo(CO). This work demonstrates that the isocyanide ligand $CNAr^{Dipp2}$, and $CNAr^{Tripp2}$ in conjunction with the Cp* group, can provide monomeric $[Cp^RCo(CNR)]$ fragments that begin to mimic the chemistry established for prototypical CpCo(CO). Specifically, the dinitrogen complex

$Cp^*Co(N_2)(CNAr^{Dipp2})$ (**6**), and $Cp^*Co(N_2)(CNAr^{Tripp2})$ (**15**) have been isolated and shown to possess a significantly labile $N_2$ ligand. Accordingly, simple dissociation of $N_2$ from $Cp^*Co(N_2)(CNAr^{Dripp2})$ (**4**) results in an aza-Büchner ring expansion of the $CNAr^{Dipp2}$ ligand where the $16e^-$ species $[Cp^*Co(CNAr^{Dipp2})]$ is a reasonable intermediate. While direct observation of $[Cp^*Co^*(CNAr^{Dipp2})]$ has not been achieved, the dinitrogen complex's $Cp^*Co(N_2)(CNAr^{Dipp2})$ (**6**) serves as synthon for the reactive entity [Cp*CoL] upon introduction of small-molecules substrates. A highlight of this reaction chemistry is the mild single and double activation of white phosphorous ($P_4$) by $[Cp^*Co(CNAr^{Dipp2})]$ fragment.

It is also shown that the use of the more sterically encumbering *m*-terphenyl isocyanide $CNAr^{Tripp2}$ that intramolecular aza-Büchner ring expansion can be prevented by discouraging arene coordination to Co due to the increased steric profle ot the $Ar^{Tripp2}$ unit. Additionally due to the stability of the $[Cp^*Co(CNAr^{Tripp2})]$ fragment in the absence of $N_2$ as a ligand, additional bond-activation reactions are accessible, notably the mild activation of H–Si, and H–H. $Cp^*Co(N_2)(CNAr^{Tripp2})$ (**15**) also serves as an attractive platform for the coordination of small molecules and understanding unusual electronic structure profiles. This is shown with the reactivity between $Cp^*Co(N_2)(CNAr^{Tripp2})$ and NO to yield the first example of an $\eta^2$–NO adduct bound to a transition metal, and the ability of $Cp^*Co(N_2)(CNAr^{Tripp2})$ to react with organo-azides.

## 5.13 Synthetic Procedures and Characterization Data.

**General Considerations:** All manipulations were carried out under an atmosphere of dry dinitrogen or Argon using standard schlenk, and glove box techniques.

Solvents were dried and degassed according to standard procedures.[85] Unless otherwise stated all materials were obtained from commercial vendors and used as received or purified by standard procedures.[86] Benzene-$d_6$, and cylcohexane-$d_{12}$ were dried with Na/K and Benzophenone followed by distillation and stored on 4 Å molecular sieves for 3 days prior to use. Celite 405 (Fischer Scientific) was dried under vacuum for 24 hours at a temperature greater then 250° C and stored inside the glove box prior to use. $KC_8$ was prepared according to published procedures.[87] The *m*-terphenyl isocyanide $CNAr^{Dipp2}$,[30] $CpCoI_2CO$,[88] and $Cp^*CoI_2(CO)$[89] were prepared according to literature procedures.

Solution $^1H$, $^{13}C\{^1H\}$, and $^{31}P$ NMR spectra were recorded on a Varian Mercury 400 spectrometer, a Bruker Advance 300, a Varian XSENS-500, and a Joel ECA 500 spectrometers. $^1H$, and $^{13}C$ chemical shifts are reported in ppm relative to $SiMe_4$ ($^1H$ and $^{13}C$ $\delta$ = 0.0 ppm) with reference to residual $C_6D_5H$ or solvent references of 7.16 ppm (1H) and 128.06 ppm ($^{13}C$) for benzene–$d_6$ and 1.38 ppm (1H) and 26.43 ppm (13C) for cyclohexane-$d_{12}$.[62] $^{31}P$ NMR chemical shifts were referenced externally to 85% $H_3PO_4$ ($\delta$ = 0 ppm). $^{29}Si$ NMR chemical shifts were referenced externally to TMS in $CDCl_3$ ($\delta$ = 0 ppm). FTIR spectra were recorded on a Thermo-Nicolet iS10 FTIR spectrometer. Samples were prepared either as KBr pellets, or a $C_6D_6$, solution injected into a Thermo Fischer solution cell equipped with KBr of $CaF_2$ windows. For solution FTIR spectra, solvent peaks were digitally subtracted from all spectra by comparisons with an authentic spectrum obtained immediately prior to that of the sample. The following abbreviations were used for the intensities and characteristic of important IR absorption bands: vs = very strong, s = strong, m = medium, w = weak, vw = very weak, b = broad, vb = very

broad, sh = shoulder. Combustion analyses were performed by Midwest Microlab LLC, Indianapolis, IN. High-resolution mass spectrometry (HRMS) was conducting in the UCSD Chemistry and Biochemistry Molecular MS facility using an Agilent 6230 ESI-TOFMS running in positive or negative ion mode as necessary.

**Synthesis of $CpCoI_2CNAr^{Dipp2}$ (1):** To a stiring $C_6H_6$ solution (10 mL) of $CpCoI_2CO$ (0.192 g, 0.472 mmol, 1 equiv) $CNAr^{Dipp2}$ (0.200 g, 0.472 mmol, 1 equiv.) was added as a solid all at once. Upon addition there was immediate effervescence indicating the loss of CO. The mixture was allowed to react for 4 hours at room temperature, there after $C_6H_6$ was removed via lyophilization. The resulting purple solid was slurried in *n*-Pentane (15 mL) and filtered over a medium porosity glass sintered frit to yield $CpCoI_2CNAr^{Dipp2}$ as a dark purple solid, 0.250 g, 0.312 mmol, 66% yield. Analytically pure crystals were grown from a $CH_2Cl_2$ solution layered with *n*-Hexane at room temperature over 1 week. $^1$H NMR (499.8 MHz, $C_6D_6$, 20 ˚C): δ = 7.2 (t, 2H, 8 Hz), 7.1 (d, 4H, 4Hz), 7.0 (d, 2H, 8Hz), 6.9 (t, 1H, 8Hz), 4.4 (s, 5H, Cp-*H*), 2.7 (septet, 4H, 7Hz), 1.4 (d, 12H, 7Hz), 1.1 (d, 12H, 7Hz) ppm. $^{13}C\{^1H\}$ NMR (125.8 MHz, $C_6D_6$, 20 ˚C): δ = 130.2 (*C*NR), 146.9, 140, 134.6, 129.9, 128.9, 123.6, 127.7, 123.6, 86.8, 31.5, 25.0, 24.6 ppm. FTIR ($C_6D_6$; KBr Window; 20 ˚C): $\nu_{CN}$ = 2160 (s), also 2962 (m), 2927 (w), 2869 (w), 1594 (w), 1579 (w), 1471 (w), 1464 (w), 1417 (w), 1385 (w), 1364 (w), 1252 (w), 1057 (w), 836 (w), 757 (m) $cm^{-1}$. Anal. Calcd. For $C_{32}H_{42}NCoI_2$: C, 53.93; H, 5.28; N, 1.75. Found: C, 54.02; H, 5.35; N, 1.79.

**Isolation of $Cp_2Co_2(CNAr^{Dipp2})_2$ (2):** To a thawing $Et_2O$/DME solution (2:1, 9 mL) of $CpCoI_2CNAr^{Dipp2}$ (0.201 g, 0.273 mmol, 1 equiv) $KC_8$ (0.0780 g, 0.574 mmol, 2.1 equiv) was added all at once. The reaction mixture was allowed to stir for *ca*. 10 minutes at -40˚C after thawing, where after a color change from purple to dark red was observed. Upon completion the reaction mixture was filtered over Celite packed on fiberglass (2 cm) to remove $C_8$ and KI followed by removal of all volatiles *in vacuo.* Upon concentration to a solid the resulting red residue was taken up in *n*-Pentane (2 mL) and allowed to stir for 10 minutes at room temperature followed by evaporation to a solid to desolvate any residual KI. This procedure was repeated an additional two times. Following concentration to a solid the red solid was taken up in $C_6H_6$ and filtered over Celite packed on fiberglass followed by lyophilization to a solid. Analysis via $^1$H NMR indicated a mixture of complex **3** and complex **2** in an approximate ratio of 90:10. Crystallization of the mixture from a saturated $Et_2O$ solution at -40˚ C afforded two types of crystals. The first, which made up a majority of the crystalline material, was complex **3** as red orange plates. The second were dark green blocks that were manually separated and subject to X-ray diffraction analysis yielding $Cp_2Co_2(CNAr^{Dipp2})_2$, **(2),** <2 mg, <0.00183 mmol <5%. $^1$H NMR (500 MHz, $C_6D_6$, 20 ˚C): δ = 7.50 (d, 4H, 8 Hz, *m*-Ph), 7.11 (multip., 10H, *m*-Dipp/*p*-Ph), 7.00 (t, 4H, 8 Hz, *p*-Dipp), 3.56 (s, 10H, Cp-*H*), 3.48 (sept. 8H, 7 Hz, C*H*$(CH_3)_2$, 1.20 (d, 24H, 7 Hz, CH(C*H*$_3)_2$, 1.06 (d, 24H, 7 Hz, CH(C*H*$_3)_2$ ppm. $^{13}$C{$^1$H} NMR (125.8 MHz, $C_6D_6$, 20 ˚C): δ = 148.5, 148.1, 141.9, 138.6, 134.1, 133.4, 123.5, 123.0, 83.8 (Cp-*C*), 30.7 *C*H$(CH_3)_2$, 26.4 CH(*C*H$_3)_2$, 23.8 CH(*C*H$_3)_2$ ppm. Prolonged scanning did not reveal the isocyanide-*C* resonance. FTIR ($C_6D_6$; KBr Window; 20 ˚C): $\nu_{CN}$ = 1820 (s), also 2961 (m), 2930 (w), 2901 (w), 2866 (w), 1573 (w),

1396 (m), 1385 (w), 1115 (w), 760 (m), 747 (w), 685 (w) $cm^{-1}$. Suitable combustion analysis was not obtained.

**Synthesis of $Cp^*CoI_2CNAr^{Mes2}$ (3):** To a stiring $C_6H_6$ solution (10 mL) of $Cp^*CoI_2CO$ (0.314 g, 0.659 mmol, 1 equiv) $CNAr^{Mes2}$ (0.224 g, 0.659 mmol, 1 equiv.) was added as a solid all at once. Upon addition there was immediate effervescence indicating the loss of CO. The mixture was allowed to react for 4 hours at room temperature, there after $C_6H_6$ was removed via lyophilization. The resulting purple solid was slurried in *n*-Pentane (15 mL) and filtered over a medium porosity glass sintered frit to yield $Cp^*CoI_2CNAr^{Mes2}$ as a dark purple solid, 0.492 g, 0.625 mmol, 95% yield. Analytically pure crystals were grown from a $CH_2Cl_2$ solution layered with *n*-Hexane at room temperature over 1 week. $^1H$ NMR (500 MHz, $C_6D_6$, 20 ˚C): δ = 6.97 (s, 4H, *m*-Mes), 6.90 (t, 1H, 8Hz, *p*-Ph), 6.78 (d, 2H, 8 Hz, *m*-Ph), 2.29 (s, 6H, *p*-C*H*$_3$), 2.17 (s, 12H, *o*-C*H*$_3$), 1.57 (s, 15H, Cp*–C*H*$_3$). $^{13}C\{^1H\}$ NMR (125.8 MHz, $C_6D_6$, 20 ˚C): δ = 158.0 (*C*NR), 140.4, 138.0, 136.0, 134.4, 129.8, 129.6, 129.5, 127.7, 96.4, 21.3, 21.0, 11.0. FTIR ($C_6D_6$; KBr Window; 20 ˚C): $\nu_{CN}$ = 2147 (s), also 2960 (w), 2917 (w), 2851 (w), 1582 (m), 1488(w), 1468 (w), 1430 (w), 1415 (w), 1376 (w), 1020 (w), 851 (w), 757 (w) Anal. Calcd. For $C_{35}H_{40}NCoI_2$: C, 53.36; H, 5.12; N, 1.78. Found: C, 53.23; H, 4.98; N, 1.70.

**Synthesis of $(\mu\text{-}CNAr^{Mes2})_2[CpCo]_2$ (4):** To a solution of $Cp^*CoI_2(CNAr^{Mes2})$ (0.102 g, 0.131 mmol, 1 equiv) in a 2:1 solution $Et_2O$/DME (4 mL) was added $KC_8$ (0.041 g, 0.302 mmol, 2.3 equiv) all at once. The reaction mixture was allowed to stir for a *ca.* 10 mins where upon a color change from purple to red was observed. The resulting mixture

was filtered over Celite packed on fiberglass (2 m) to remove KI. The solution was then concentrated to a solid where it was taken up in *n*-pentane (2 mL) stirred and concentrated to a solid. This step was repeated two additional times to desolvate any remaining KI. Following the red solid was taken up in $C_6H_6$ (3 mL) and filtered over Celite packed on fiberglass (2 cm) to remove any remaining KI. The solid was then lyophilized to yield a fluffy dark red powder. The powder was then recrystallized from a saturated *n*-pentane/$Et_2O$ solution (1 mL) over 1 week to afford dark red analytically pure crystals of $(\mu\text{-CNAr}^{Mes2})_2[CpCo]_2$, 0.045 g, 0.0421 mmole, 33%. $^1$H NMR (500 MHz, $C_6D_6$, 20 ˚C): δ = 7.20 (dd, 2H, 6Hz, *m*-Ph), 7.03 (dd, 2H, 6Hz, *m*-Ph), 6.89 (s, 4H, *m*-Mes), 6.87 (t, 2H, 8Hz, *p*-Ph), 6.72 (s, 4H, *m*-Mes), 2.69 (s, 12H, *o*-C*H*$_3$), 2.18 (s, 6H, *p*-C*H*$_3$), 2.10 (s, 6H, *p*-C*H*$_3$), 1.96 (s, 12H, *o*-C*H*$_3$), 1.06 (s, 30H, Cp*–C*H*$_3$). $^{13}$C{$^1$H} NMR (125.8 MHz, $C_6D_6$, 20 ˚C): δ = 231.5 (*C*NR), 139.3, 138.6, 138.2, 138.1, 137.7, 136.8, 135.7, 132.5, 132.4, 132.3, 129.4, 129.0, 128.5, 127.7, 121.4, 91.2, 30.3, 23.6, 22.3, 21.0, 20.9, 9.5 ppm. FTIR ($C_6D_6$; KBr Window; 20 ˚C): $\nu_{CN}$ = 1732 (s), 1787 (w, sh) also, 2917 (w), 2854 (w), 1609 (w), 1571 (m), 1382 (m), 1190 (w), 1030( (w), 850 (w), 749 (w), 741 (w), 640 (w), 626 (w), 562 (w). Suitable combustion analysis was not obtained.

**Synthesis of Cp*CoI$_2$CNAr$^{Dipp2}$ (5):** To a $C_6H_6$ solution (60 mL) of Cp*CoI$_2$CO (0.923 g, 1.94 mmol, 1 equiv) was added CNAr$^{Dipp2}$ (0.821 g, 1.94 mmol, 1 equiv) all at once. Upon addition there was an immediate effervescence indicating CO loss. The mixture was allowed to stir for *ca.* 4 hours where upon all volatiles were removed *in vacuo.* There after the resulting purple solid was taken up in *n*-Pentane and filtered over a medium

glass sintered frit to yield Cp*$CoI_2CNAr^{Dipp2}$ as a purple solid, 1.43 g, 1.64 mmol, 85 % yield. X-ray Diffraction/Analytically pure crystals were grown from a $CH_2Cl_2$ solution layered with *n*-Hexane (1:6) over one week. $^1$H NMR (499.8 MHz, $C_6D_6$, 20 ˚C): δ = 7.37 (t, 2H, 8 Hz, *p*-Dipp), 7.26 (d, 4H, 8Hz, *m*-Dipp), 6.96 (d, 2H, 7Hz, *m*-ph), 6.83 (t, 1 H, 8 Hz, *p*-Ph) 2.80 (sept, 4H, C*H*$(CH_3)_2$), 1.60 (s, 15H, *H*-Cp*), 1.53 (d,12H, 7 Hz, CH(C*H*$_3)_2$), 1.06 (d, 12H, 7 Hz, CH(C*H*$_3)_2$) ppm. $^{13}$C{$^1$H} NMR (125.8 MHz, $C_6D_6$, 20 ˚C): δ = 157.0 (*C*NR), 146.9, 139.5, 135.4, 131.6, 129.8, 128.4, 127.7, 123.9, 31.3, 25.3, 24.5, 11.3. FTIR ($C_6D_6$; KBr Window; 20 ˚C): $\nu_{CN}$ = 2128 (s), 2091 (sh), also 3063 (w), 2962 (w), 2926 (m), 2908 (w), 2868 (w), 1594 (w), 1579 (w), 1464 (w), 1433 (w), 1413 (w), 1383 (w), 1375 (w), 1363 (w), 1252 (w), 1180 (w), 1072 (w), 1057 (w), 1019 (w), 793 (w), 757 (m), 681 (w) $cm^{-1}$. Anal. Calcd. For $C_{41}H_{52}NI_2Co$: C, 56.48; H, 6.02; N, 1.61. Found: C, 56.46; H, 6.09; N, 1.72.

**Synthesis of Cp*Co($N_2$)$CNAr^{Dipp2}$ (6):** To a thawing $Et_2O$/DME solution (2:1, 9 mL) of Cp*$CoI_2CNAr^{Dipp2}$ (0.321 g, 0.369 mmol, 1 equiv) $KC_8$ (0.105 g, 0.774 mmol, 2.1 equiv) was added all at once. The reaction mixture was allowed to stir for *ca*. 20 minutes where upon a color change from purple to yellow/brown was observed. Upon completion the reaction mixture was filtered over a medium porosity glass sintered frit packed with Celite to remove $C_8$ and KI followed by removal of all volatiles *in vacuo.* Upon concentration to a solid the resulting brown residue was taken up in *n*-Pentane (20 mL) and allowed to stir for 10 minutes at room temperature followed by evaporation to a solid to desolvate any residual KI. This procedure was repeated an additional two times. Following concentration to a solid the brown solid was taken up in $C_6H_6$ and filtered over

Celite packed on fiberglass followed by lyophilization to a solid. The resulting solid was then recrystallize from $Et_2O$ (1 mL) with 2 drops of $C_6H_6$ over 36 hours to yield $Cp^*Co(N_2)CNAr^{Dipp2}$ as dark brown plates 0.165 g, 0.255 mmol, 69% yield. $^1H$ NMR (499.8 MHz, $C_6D_6$, 20 ˚C): δ = 7.32 (t, 2H, 8 Hz, *o*-Dipp), 7.22 (d, 4H, 8 Hz, *m*-Dipp), 6.94 (d, 2H, 8Hz, *m*-Ph), 6.89 (t, 1H, 8 Hz, *o*-Ph), 2.90 (sept, 4H, 7 Hz, C*H*$(CH_3)_2$), 1.45 (d, 12H, 7Hz, CH(C*H*$_3)_2$), 1.42 (s, 15H, Cp*-*H*), 1.16 (d, 12H, 7Hz, CH(C*H*$_3)_2$) ppm. $^{13}C\{^1H\}$ NMR (125.8 MHz, $C_6D_6$, 20 ˚C): δ = 180.2 (*C*NR), 146.9, 136.4, 136.2, 130.9, 129.8, 129.2, 124.1, 123.3, 92.7, 31.3, 24.5, 24.3, 10.1 ppm. FTIR ($C_6D_6$; KBr Window; 20 ˚C): $\nu_{CN}$ = 2010 (s), 2040 (m), $\nu_{NN}$ = 2110 (m), also 3065 (w), 2959 (m), 2923 (w), 2904 (w), 2865 (w), 1580 (w), 1471 (w), 1463 (w), 1413 (w), 1380 (w), 1366 (w), 1177 (w), 1055 (w), 1027 (w), 936 (w), 791 (w), 758 (w), 639 (w), 578 (w) $cm^{-1}$. Anal. Calcd. For $C_{41}H_{51}N_3Co$: C, 76.37; H, 7.97; N, 6.52. Found: C, 76.34; H, 8.18; N, 6.45.

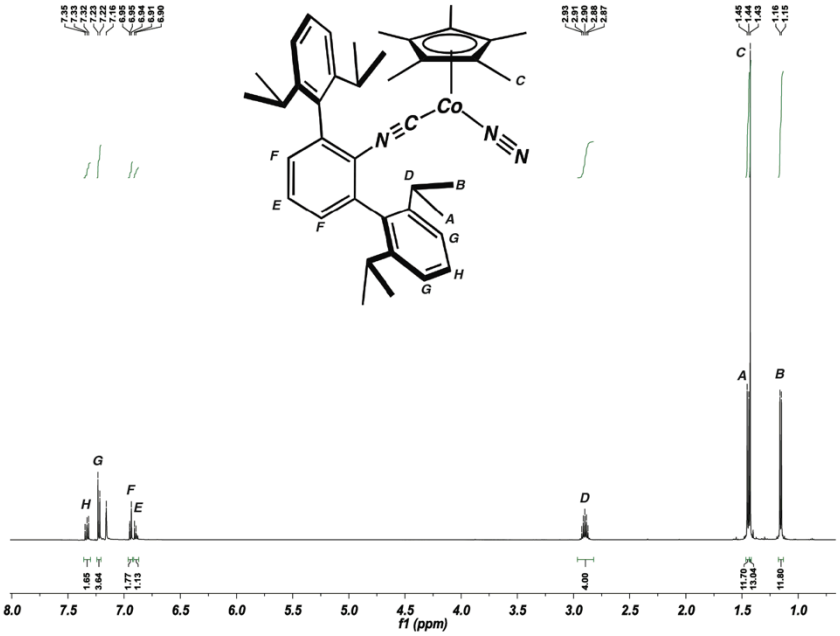


**Figure 5.26.** $^1H$ NMR Spectrum of $Cp^*Co(N_2)(CNAr^{Dipp2})$ (**4**) ($C_6D_6$, 500.1 MHz, 20 ˚C).

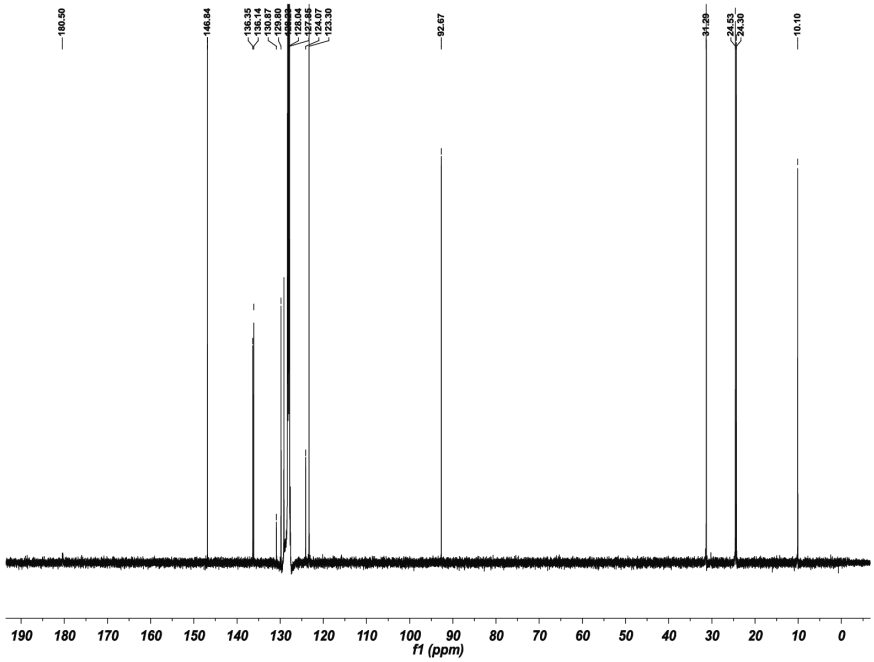


**8**

**Figure 5.27.** $^{13}C\{^{1}H\}$ NMR spectrum of $Cp^*Co(N_2)(CNAr^{Dipp2})$ (**4**) ($C_6D_6$, 128.1 MHz, 20 ˚C).

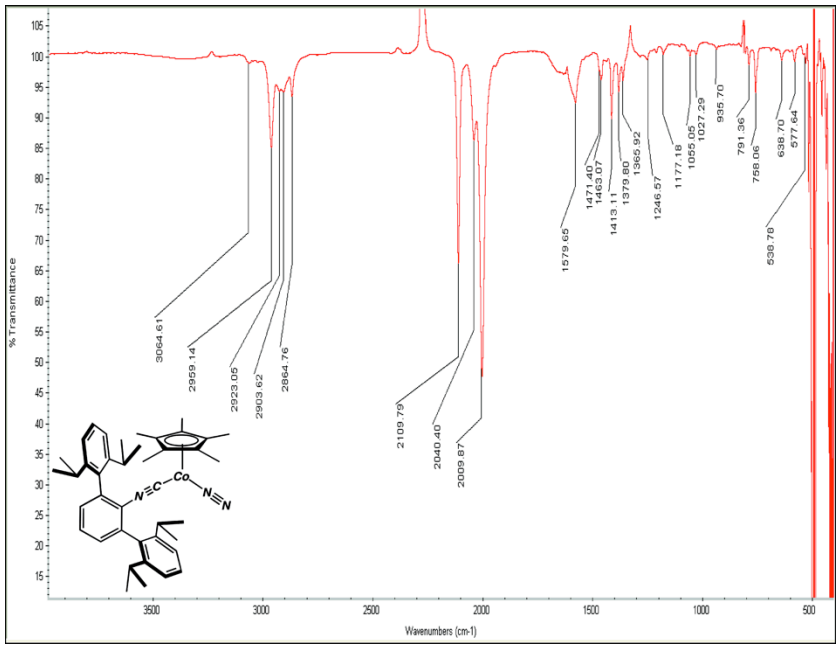


**Figure 5.28.** Baseline-corrected, solution-state transmittance FTIR Spectrum ($C_6D_6$) of ($\eta^5$-$Cp^*$)$Co(N_2)(CNAr^{Dipp2})$ (**5**). Solvent background ($C_6D_6$) for subtraction was obtained immediately prior to experiment.

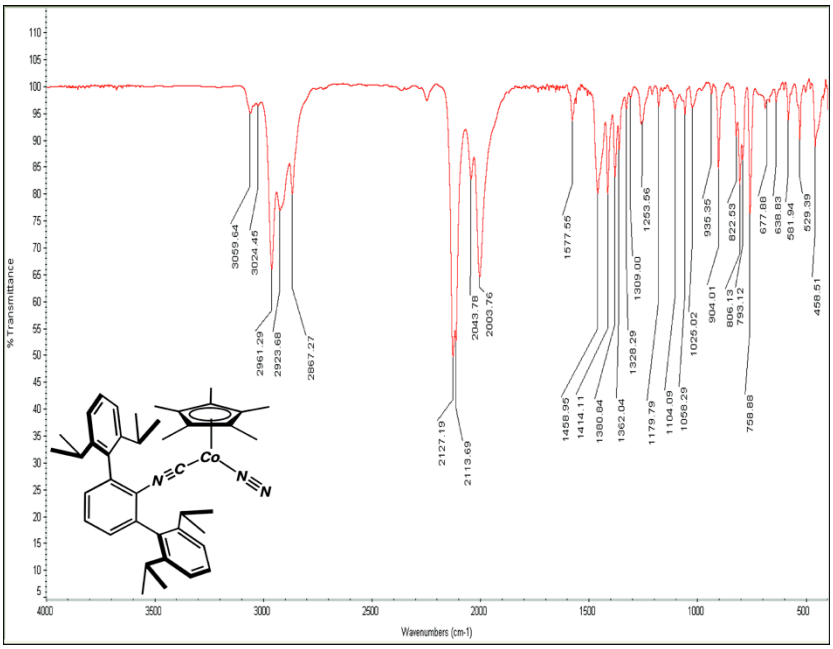


**Figure 5.29.** Baseline–corrected, solid-state transmittance FTIR Spectrum (KBr) of crystalline ($\eta^5$-Cp*)Co($N_2$)($CNAr^{Dipp2}$) (**5**).

**Synthesis of Cp*Co(Azabenz[*b*]azulene$^{Dipp}$) (7):** Cp*Co($N_2$)$CNAr^{Dipp2}$ (0.022 g, 0.034 mmol, 1 equiv) was dissolved in $C_6D_6$ (1 mL) and transferred to a J-Young resalable NMR tube. The resulting brown solution as subject to a series of Freeze Pump Thaw (FPT) cycles to degass and remove $N_2$ (approx. 8 times) until there was no indication of Cp* Co($N_2$)$CNAr^{Dipp2}$ by $^1$H NMR. The resulting solution was then pumped back into the glove box and all volatiles were removed *in vacuo* and the resulting brown sold was recrystallized from $Et_2O$ to yield Cp*Co(Azabenz[*b*]azulene$^{Dipp}$) as analytically pure crystals, 0.014 g, 0.023 mmol, 66% yield. $^1$H NMR (499.8 MHz, $C_6D_6$, 20 ˚C): δ = 7.34 (mult. 3H, *m/p*-Ph), 7.19 (d, 2H, 7 Hz, *m*-Dipp), 7.12 (t, 1H, 8 Hz, *p*-Dipp), 5.64 (d, 1H, 8 Hz, , *m*-Azabenz[*b*]azulene$^{Dipp}$ -*H*), 5.12 (d, 1H, 8 Hz, *m*-Azabenz[*b*]azulene$^{Dipp}$ -*H*), 3.68 (sept, 1H, 7 Hz, C*H*($CH_3$)$_2$), 3.13 (sept, 2H, 7 Hz, C*H*($CH_3$)$_2$), 2.96 (sept, 1H, 7 Hz, C*H*($CH_3$)$_2$), 2.02 (t, 1H, 8 Hz, , *p*-Azabenz[*b*]azulene$^{Dipp}$ -*H*), 1.71 (d, 3H, 7 Hz,

CH(C$H_3$)$_2$), 1.47 (d, 3H, 8 Hz, CH(C$H_3$)$_2$), 1.33 (d, 3H, 7 Hz, CH(C$H_3$)$_2$), 1.23 (s, 15H, Cp*-*H*), 1.17 (d, 3H, 7 Hz, CH(C$H_3$)$_2$), 1.14 (t, 6H, 7 Hz, CH(C$H_3$)$_2$), 0.99 (d, 3H, 7Hz, CH(C$H_3$)$_2$), 0.86 (d, 3H, 7 Hz, CH(C$H_3$)$_2$) ppm. $^{13}C\{^1H\}$ NMR (125.8 MHz, $C_6D_6$, 20 ˚C): δ = 177.2 (*C*N), 155.4, 147.9, 147.3, 140.6, 140.1, 138.4, 134.5, 133.6, 127.6, 127.4, 122.7, 122.6, 121.2, 110.9, 90.6, 81.3, 58.9, 51.5, 31.2, 31.1, 30.9, 29.0, 26.0, 24.9, 24.6, 24.3, 23.3, 22.9, 22.8, 22.7, 9.4. FTIR ($C_6D_6$; KBr Window; 20 ˚C): $\nu_{CN}$ = 1471 (m), also 2962 (s), 2925 (m), 2906 (m), 2867 (m), 1446 (m), 1397 (s), 1381 (m), 1360 (m), 1288 (w), 1251 (m), 1229 (m), 1104 (w), 1064 (m), 1029 (m), 937 (w), 912 (w), 883 (w), 852 (w), 768 (m), 758 (m), 716 (w), 659 (m), 657 (w) $cm^{-1}$. Anal. Calcd. For $C_{41}H_{52}NCo$: C, 79.70; H, 8.49; N, 2.27. Found: C, 77.89; H, 8.40; N, 2.62.

**Synthesis Cp*Co(CNAr$^{Dipp2}$)$_2$ (8):** To a stirring solution of Cp*Co($N_2$)CNAr$^{Dipp2}$ (0.021 g, 0.033 mmol, 1equiv) in $C_6H_6$ (1 mL) CNAr$^{Dipp2}$ (0.014 g, 0.033 mmol, 1 equiv) was added as a solution in 1 mL of $C_6H_6$. Upon addition a color change from brown to red was observed where after the mixture was allowed to stir for 30 minutes. The resulting red solution was concentrated to a solid and recrystallized from $Et_2O$ with a *ca.* 2 drops of $C_6H_6$ at -40˚C over 2 days to yield Cp*Co(CNAr$^{Dipp2}$)$_2$ as red needles 0.013 g, 0.013 mmol 38 % yield. $^1H$ NMR (499.8 MHz, $C_6D_6$, 20 ˚C): δ = 7.33 (t, 2H, 8 Hz, *p*-Dipp), 7.21 (d, 4H, 8 Hz, *m*-Dipp), 6.85 (d, 2H, 8 Hz, *m*-Ph), 6.75 (t, 1H, 7 Hz, *p*-Ph), 2.79 (bs, 4H, C*H*(CH$_3$)$_2$), 1.32 (s, 15H, Cp*-*H*), 1.10 (bs, 48H, CH(C$H_3$)$_2$) ppm. $^{13}C\{^1H\}$ NMR (125.8 MHz, $C_6D_6$, 20 ˚C): δ = 187.2 (*C*NR), 147.4, 137.8, 137.5, 132.0, 131.5, 128.8, 124.3, 123.7, 93.5, 31.1, 25.3, 23.5, 10.7. FTIR ($C_6D_6$; KBr Window; 20 ˚C): $\nu_{CN}$ = 1914 (s), 2002 (m), 2035 (w), also 3061 (w), 2963 (m), 2926 (w), 2904 (w), 2867 (w), 1577

(w), 1463 (w), 1412 (m), 1382 (w), 1362 (w), 1252 (w), 1056 (w), 791 (w), 761 (m), 754 (w), 680 (w), 668 (w), 640 (w), 580 (w) $cm^{-1}$. Anal. Calcd. For $C_{72}H_{89}CoN_2$: C, 82.88; H, 8.79; N, 2.68. Found: C, 81.67; H, 8.64; N, 3.12.

**Synthesis of Cp*Co($\eta^2$-PhCCPh)($CNAr^{Dipp2}$) (9):** To a benzene solution (1 mL) of Cp*Co($N_2$)$CNAr^{Dipp2}$ (0.039 g, 0.0600 mmol, 1 equiv) a benzene solution (1 mL) of Diphenylacetylene ( 0.011 g, 0.0600 mmol 1 equiv) was added all at once. Upon addition a color change from brown to red was observed. All volatiles were removed via lyophilization. Analytically pure red crystals were obtained from a saturated solution $TMS_2O/Et_2O$ (2:1; 1.5 mL) at -40˚C over 12 hours, 0.034g, 0.043 mmol, 71%. $^1$H NMR (499.8 MHz, $C_6D_6$, 20 ˚C): δ = 7.93 (d, 4H, 8 Hz, *o*-Ph-acetylene), 7.34 (t, 4H, 8 Hz, *m*-Ph-acetylene), 7.18 (d, 2H, 8 Hz, *m*-Ph), 6.99 (s, 6H, *m/p*-Dipp), 6.81 (multi., 3H, *p*-Ph-acetylene/*p*-Dipp), 2.66 (sept., 4H, 8 Hz, C*H*$(CH_3)_2$), 1.44 (s, 15H, Cp*-*H*), 1.29 (d, 12H, 7Hz, CH(C*H*$_3)_2$), 1.03 (d, 12H, CH(C*H*$_3)_2$) ppm. $^{13}$C{$^1$H} NMR (125.8 MHz, $C_6D_6$, 20 ˚C): δ = 172.5 (*C*NR), 146.1, 137.4, 136.0, 132.8, 132.1, 130.4, 130.0, 128.9, 125.6, 124.5, 123.2, 93.7, 93.0, 31.2, 24.6, 24.1, 10.4, 2.08. FTIR ($C_6D_6$; KBr Window; 20 ˚C): $\nu_{CN}$ = 2039 (s), 2011 (s), 2086 (w), also 3072 (w), 3057 (w), 3023 (w), 3008 (w), 2961 (m), 2927 (w), 2906 (w), 2868 (m), $\nu_{CC}$ = 1832 (m), 1591 (w), 1484 (w), 1464 (w), 1439 (w), 1413 (m), 1382 (w), 1363 (w), 1070 (w), 1058 (w), 1027 (w), 756 (m), 692 (m), 569 (w) $cm^{-1}$. Anal. Calcd. For $C_{53}H_{62}NCo$: C, 82.76; H, 8.72; N, 1.64. Found: C, 82.31; H, 8.56; N, 1.71.

**Synthesis of Cp*Co($\kappa^2$-$P_4$)($CNAr^{Dipp2}$) (10):** To a benzene-$d_6$ solution (0.75 mL) of Cp*Co($N_2$)$CNAr^{Dipp2}$ (0.030 g, 0.0466 mmol, 1 equiv) a benzene-$d_6$ solution (0.75 mL) of $P_4$ ( 0.0087 g, 0.0699 mmol 1.5 equiv) was added all at once and allowed to react for 1 hour, whereupon completion of the reaction was judged by $^1$H NMR. Thereafter the reaction mixture was concentrated to a solid and recrystallized from a saturated $Et_2O/C_6H_6$ (5:1; 2 mL) at -40˚ C over 24 hours to yield Cp*Co($\kappa^2$-$P_4$)($CNAr^{Dipp2}$) as orange yellow crystals 0.031 g, 0.042 mmol, 89%. $^1$H NMR (499.8 MHz, $C_6D_6$, 20 ˚C): δ = 7.29 (mult., 6H, *m/p*-H Dipp), 6.97 (d, 2H, 10 Hz, *m*-Ph), 2.91 (sept, 4H, 9 Hz, C*H*($CH_3$)$_2$), 1.47 (d, 12H, 8Hz, CH(C*H*$_3$)$_2$), 1.35 (s, 15H, Cp*-*H*), 1.11 (d, 12H, 9 Hz, CH(C*H*$_3$)$_2$) ppm. $^{13}$C{$^1$H} NMR (125.8 MHz, $C_6D_6$, 20 ˚C): δ = 168.1 (*C*NR), 146.8, 138.3, 136.2, 131.3, 129.7, 127.6 126.1, 124.5, 96.9, 31.2, 25.0, 24.1, 9.0 ppm. $^{31}$P {$^1$H} NMR (202.7 MHz, C6D6, 20 ˚C): δ = -229.2 (t, 1P, 258 Hz), -326.4 (q, 2P, -254 Hz), -365.9 (q, 1P, -256 Hz) ppm. FTIR ($C_6D_6$; KBr Window; 20 ˚C): $\nu_{CN}$ = 2060 (s), 2013 (w), also 2968 (m), 2926 (w), 2907 (w), 2869 (w), 1464 (w), 1412 (w), 1383 (w), 1362 (w), 760 (m) cm$^{-1}$. Anal. Calcd. For $C_{41}H_{52}NCoP_4$: C, 66.30; H, 7.19; N, 1.89. Found: C, 61.52; H, 6.94; N, 1.90.

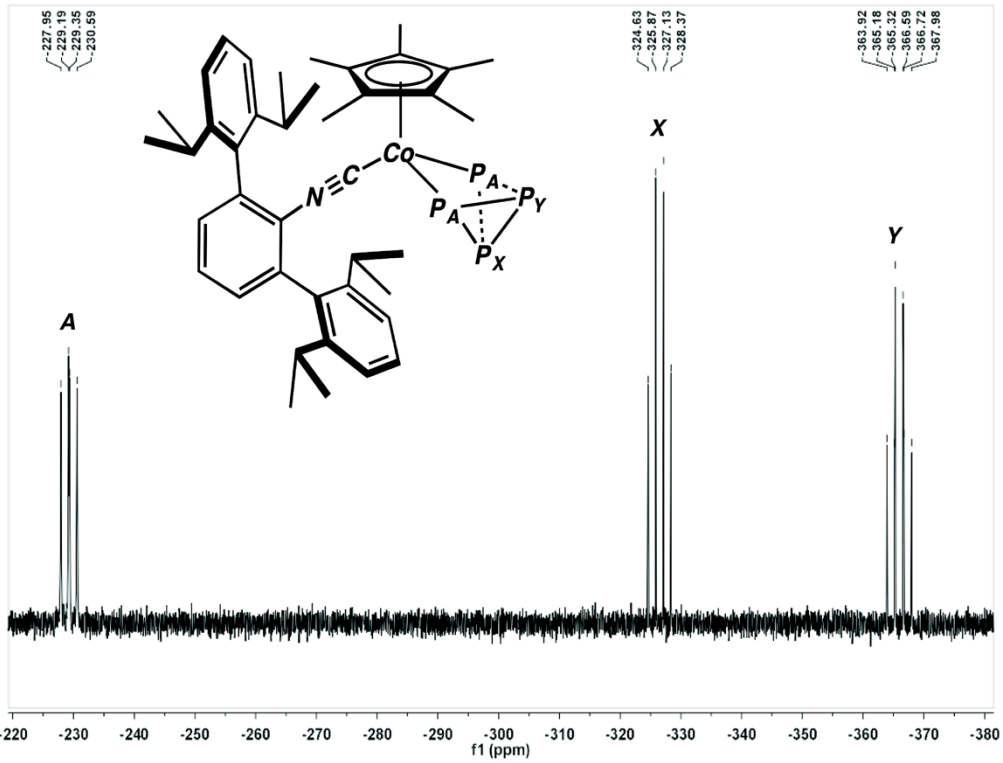


**Figure 5.30.** $^{31}P\{^{1}H\}$ spectrum of ($\eta^5$-Cp*)Co($\kappa^2$-$P_4$)($CNAr^{Dipp2}$) (**9**) ($C_6D_6$, 300 MHz) displaying an $A_2XY$ spin system.

**Synthesis of [Cp*Co ($CNAr^{Dipp2}$)]$_2$($\mu^2$-$\kappa^2$;$\kappa^2$-$P_4$) (11):** To a benzene-$d_6$ solution (0.75 mL) of Cp*Co($N_2$)$CNAr^{Dipp2}$ (0.042 g, 0.064 mmol, 1 equiv) a benzene-$d_6$ solution (0.75 mL) of $P_4$ ( 0.004 g, 0.032 mmol, 0.5 equiv) was added all at once and allowed to react for 1 hour, whereupon completion of the reaction was judged by $^{1}H$ NMR. Thereafter the reaction mixture was concentrated to a solid and recrystallized from a saturated $Et_2O/C_6H_6$ (5:1; 2 mL) at -40˚ C over 24 hours to yield Cp*Co($CNAr^{Dipp2}$)($\mu^2$-$\kappa^2$;$\kappa^2$-$P_4$) as dark black/red crystals 0.027 g, 0.020 mmol, 60%. $^{1}H$ NMR (300 MHz, $C_6D_6$, 20 ˚C): δ = 7.36 (mult., 6H, *m/p*-H Dipp), 7.00 (d, 2H, 7 Hz, *m*-Ph), 6.89 (t, 1H, 7Hz, *p*-Ph), 3.05 (sept, 2H, 7 Hz, C*H*($CH_3$)$_2$), 2.83 (sept., 2H, 7 Hz, C*H*($CH_3$)$_2$), 1.63 (d, 6H, 6Hz, CH(C*H*$_3$)$_2$), 1.53 (s, 15H, Cp*-*H*), 1.43 (d, 6H, 7 Hz, CH(C*H*$_3$)$_2$), 1.21 (d, 6H, 6 Hz, CH(C*H*$_3$)$_2$), 1.10 (d, 6H, 6 Hz, CH(C*H*$_3$)$_2$) ppm. $^{13}C\{^{1}H\}$ NMR (125.8 MHz, $C_6D_6$, 20

˚C): δ = 170.3 (*C*NR), 147.1, 146.9, 138.1, 136.6, 132.0, 130.2, 129.5, 124.9, 124.4, 123.4, 97.1, 31.2, 25.7, 25.2, 24.7, 24.2, 9.9 ppm. $^{31}P\{^{1}H\}$ NMR (202.7 MHz, C6D6, 20 ˚C): δ = -125.9 (multi., 2P, $J^1$ = -149 Hz, $J^2$ = -32 Hz, $J^3$ = 0), -166.3 (q, 2P, $J^1$ = -149 Hz, $J^2$ = -32 Hz, $J^3$ = 0 Hz) ppm. FTIR ($C_6D_6$; KBr Window; 20 ˚C): $\nu_{CN}$ = 2033 (s), 2005 (m), also 2962 (m), 2925 (w), 2903 (w), 2867 (w), 1577 (w), 1464 (w), 1410 (w), 1381 (w), 1362 (w), 760 (m) $cm^{-1}$. Anal. Calcd. For $C_{82}H_{104}N_2Co_2P_4$: C, 72.34; H, 7.85; N, 2.06. Found: C, 71.20; H, 6.94; N, 2.01.

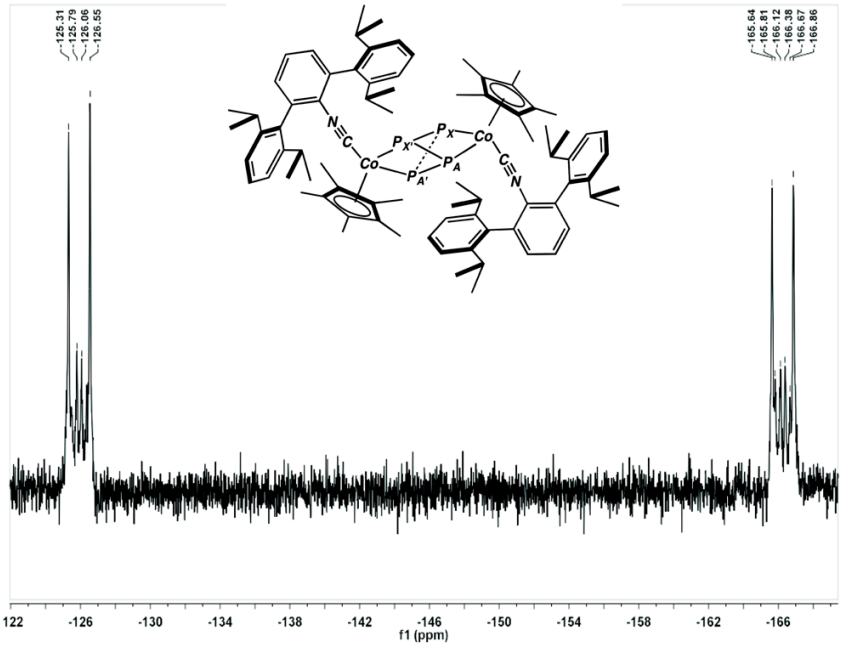


**Figure 5.31.** $^{31}P\{^{1}H\}$ spectrum of $[(\eta^5\text{-Cp*})Co(CNAr^{Dipp2})]_2(\mu^2{:}\kappa^2{;}\kappa^2\text{-}P_4)$ (**10**) ($C_6D_6$, 300 MHz) displaying an AA'XX' spin system.

**Synthesis[32] of $HC(O)NHAr^{Tripp2}$ (12):** Acetic anhydride ($Ac_2O$; 17.7 g, 0.0173 mol, 20 equiv) was cooled to 0 ˚C under an $N_2$ atmosphere and formic acid (7.96 g, 0.173 mol, 20 equiv) was added dropwise, via syringe, over 20 min. The mixture was stirred at 0 ˚C for 20 min and then heated to 50 ˚C for 5 h. The mixture, no containing formylacetic anhydride,(Citation) was then cooled to room temperature and added, via cannula, to a

THF solution of $H_2NAr^{Tripp2}$ (4.30g, 8.65 mmol, 100 mL) over the course of 1 h. The reaction mixture was then heated to 60 ˚C for 5 days. Thereafter, the reaction mixture was allowed to cool to room temperature and the volatile components removed via rotary evaporation. The crude residue was then washed with $H_2O$ (3 X 100 mL) to remove residual acetic acid. The resulting solid was then dissolved in $Et_2O$ (200 mL), dried over $Na_2SO_4$, and filtered. All volatile materials were then removed by rotary evaporation, and the resulting solid was suspended in EtOH (100 mL) and cooled to 0 ˚C. The mixture was then filtered to provide $HC(O)NHAr^{Tripp2}$as a colorless solid, which was dried *in vacuo*. Yield 3.55 g, 6.76 mmol, 78.2 %. H NMR (400.1 MHz, CDCl3, 20 °C): δ = 7.66 (d, 1H, J = 11 Hz, HC(O)NH), 7.22 (t, 1H, p-Ph), 7.17 (d, 2H, J = 7 Hz, m-Ph), 7.087 (s, 4H, m-Tripp), 6.7 (br d, 1H, J = 11 Hz, HC(O)NH), 2.93 (septet, 2H, J = 7 Hz, p-(CH(CH3)2)), 2.61 (septet, 4H, J = 7 Hz, p- (CH(CH3)2)), 2.22 (br s, 2H, NH2), 1.30 (d, 12 H, J = 7 Hz, (CH(CH3)2)), 1.12 (d, 12H, J = 7 Hz, (CH(CH3)2), 1.10 (d, 12H, J = 7 Hz, (CH(CH3)2) ppm. 13C{1 H}NMR (125.7 MHz, CDCl3, 20 °C): δ = 162.8 (HC(O)N), 149.5, 146.4, 133.8, 132.4, 131.6, 131.0, 124.4, 121.9, 34.4 ((CH(CH3)2), 30.8 ((CH(CH3)2), 25.0 ((CH(CH3)2), 24.2 ((CH(CH3)2), 23.4 ((CH(CH3)2) ppm. FTIR (KBr window, CDCl3): νNH = 3352 (w) cm−1 , νCO = 1677 (s) cm−1 , also 2964 (m), 2929 (w), 2870 (w), 1606 (w), 1461 (w), 1448 (w), 1410 (w), 1364 (w), 1318 (w), 1278 (w), 1070 (w) cm−1 . HRMS (ESI pos. ion; NCMe): m/z Calcd, 548.3863; m/z Found, 548.3864 [M]+.

**Synthesis[32] of $CNAr^{Tripp2}$ (13):** $HC(O)NHAr^{TRIPP2}$ ( 3.55 g, 0.00638 moles, 1 equiv) was charged into a 500 mL schlenk flask already containing dry $CH_2Cl_2$ and a stir bar under a

$N_2$ atmosphere. Diisopropoyl amine (4.52 g, 0.04463 moles, 7 equivs) was added via syringe. The resulting mixture was cooled to 0°C where upon $POCl_3$ (4.89 g, 0.0319 moles, 5 equivs) was added drop wise via syringe over 20 mins. The resulting mixture was allowed to warm to room temperature and react for 12 hours. Following 200 mL's of a 1.5 M $Na_2CO_3$ solution was added to quench any remaining $POCl_3$. The resulting organic layer was separated from the aqueous layer. The aqueous layer was back extracted with 3 X 100 mL $CH_2Cl_2$. All organics were combined and dried over $MgSO_4$ and separated via vacuum filtration. All volatiles were removed via rotary evaporation. The resulting off white solid was slurried in 100 mL of thawing MeCN and filtered followed by 2 X 50 mL washes with MeCN. The resulting white solid was dried via rotary evaporation to yield $CNAr^{Tripp2}$ (3.07 g, 95%). $^1$HNMR (400.1 MHz, $C_6D_6$, 20°C): δ = 7.25 (S, 4H, *m*-Tripp), 7.02 (d, 2H, 7Hz, *m*-Ph), 6.94 (t, 1H, 7Hz, *p*-Ph), 2.86 (septet, 2H, 7Hz, *p*-methylene Tripp), 2.78 (septet, 4H, 7Hz, *o*-methylene Tripp), 1.37 (d, 12H, 7Hz, Tripp isopropyl methyl), 1.24 (d, 12H, 7Hz, Tripp isopropyl methyl), 1.18 (d, 12H, 7Hz, Tripp Isopropyl methyl). $^{13}$CNMR (125.7 MHz, $CDCl_3$, 20°C) δ = 171.7, 149.7, 146.7, 139.7, 132.9, 129.9, 128.5, 127.8, 121.4, 34.8, 31.6, 24.7, 24.4, 24.3. FTIR ($C_6D_6$; KBr Window; 20 ˚C): ($C_6D_6$): 2961 (m), 2930 (w), 2870 (w), 2118 (s/m), 1464 (w), 1383 (w), 1363 (w), 1104 (w), 879 (w), 760 (w). HRMS (ESI-APCI-TOF, pos. ion; MeCN) *m/z* calcd for $[C_{37}H_{50}NH]^+$: 508.3938. Found for $[C_{37}H_{50}NOH]^+$: 508.3941, δ = 0.6.

**Synthesis of $Cp^*CoI_2CNAr^{Dipp2}$ (14):** To a $C_6H_6$ solution (60 mL) of $Cp^*CoI_2CO$ (1.55 g, 3.26 mmol, 1 equiv) was added $CNAr^{Tripp2}$ (1.89 g, 3.32 mmol, 1.02 equiv) all at once. Upon addition there was an immediate effervescence indicative of CO loss. The mixture was allowed to stir for *ca.* 4 hours where upon all volatiles were removed *in vacuo.* There

after, the resulting purple solid was taken up in *n*-Pentane and filtered over a medium glass sintered frit to yield $Cp^*CoI_2CNAr^{Tripp2}$ as a purple solid, 3.05 g, 3.19 mmol, 98% yield. X-ray Diffraction/Analytically pure crystals were grown from a $CH_2Cl_2$ solution layered with *n*-Hexane (1:6) over one week. $^1H$ NMR (400.1 MHz, $C_6D_6$, 20 ˚C): δ = 7.26 (s, 4H, *m*-Trip), 7.02 (d, 2H, 8Hz, *m*-Ph), 6.84 (t, 1H, 8Hz, *p*-ph), 2.91 (sept, 2H, 7Hz, C*H*$(CH_3)_2$), 2.85 (sept, 4H, 7Hz, C*H*$(CH_3)_2$), 1.60 (s, 15H, *H*-Cp*), 1.57 (d, 12H, 7 Hz, CH(C*H*$_3)_2$), 1.37 (d, 12H, 7 Hz, CH(C*H*$_3)_2$), 1.12 (d, 12H, 7 Hz, CH(C*H*$_3)_2$) ppm. $^{13}C\{^1H\}$ NMR (125.7 MHz, $C_6D_6$, 20 ˚C): δ = 158.9 (*C*NR), 149.7, 146.8, 139.7, 133.2, 131.7, 122.0, 127.7, 96.5, 35.1, 31.4, 25.4, 24.7, 24.5, 11.4. FTIR ($C_6D_6$; KBr Window; 20 ˚C): $\nu_{CN}$ = 2130 (s), also 2960 (m), 2927 (w), 2905 (w), 2868 (w), 1605 (w), 1566 (w), 1464 (w), 1430 (w), 1412 (w), 1382 (w), 1363 (w), 1204 (w), 1071 (w), 1054 (w), 1020 (w), 941 (w), 877 (w), 759 (w), 681 (w) $cm^{-1}$. Anal. Calcd. For $C_{47}H_{64}NI_2Co$: C, 59.04; H, 6.75; N, 1.47. Found: C, 59.17; H, 6.80; N, 1.47.

**Synthesis of $Cp^*Co(N_2)CNAr^{Tripp2}$ (15):** To a thawing $Et_2O$/DME solution (2:1, 9 mL) of $Cp^*CoI_2CNAr^{Dipp2}$ (0.627 g, 0.656 mmol, 1 equiv) $KC_8$ (0.189 g, 1.40 mmol, 2.1 equiv) was added all at once. The reaction mixture was allowed to stir for *ca*. 20 minutes where upon a color change from purple to yellow/brown was observed. Upon completion the reaction mixture was filtered over a medium porosity glass sintered frit packed with Celite to remove $C_8$ and KI followed by removal of all volatiles *in vacuo.* Upon concentration to a solid the resulting brown residue was taken up in *n*-Pentane (20 mL) and allowed to stir for 10 minutes at room temperature followed by evaporation to a solid to desolvate any residual KI. This procedure was repeated an additional two times.

Following concentration to a solid the brown solid was taken up in $C_6H_6$ and filtered over Celite packed on fiberglass followed by lyophilization to a solid. The resulting solid was then recrystallize from $Et_2O$ (1 mL) with 2 drops of $C_6H_6$ over 36 hours to yield $Cp^*Co(N_2)CNAr^{Tripp2}$ as dark brown plates 0.298 g, 0.408 mmol, 62 % yield. $^1H$ NMR (499.8 MHz, $C_6D_6$, 20 ˚C): δ = 7.23 (s, 4H, *m*-Tripp), 6.99 (d, 2H, 7 Hz, *m*-Ph), 6.94 (d, 2H, 8Hz, *m*-Ph), 6.90 (t, 1H, 7 Hz, *o*-Ph), 2.95 (sept, 4H, 8 Hz, C*H*$(CH_3)_2$), 2.89 (sept, 2H, 7 Hz, C*H*$(CH_3)_2$), 1.49 (d, 12H, 7Hz, CH(C*H*$_3)_2$), 1.44 (s, 15H, Cp*-*H*), 1.32 (d, 12H, 7Hz, CH(C*H*$_3)_2$), 1.22 (d, 12H, 7Hz, CH(C*H*$_3)_2$) ppm. $^{13}C\{^1H\}$ NMR (125.8 MHz, $C_6D_6$, 20 ˚C): δ = 179.7 (*C*NR), 148.9, 146.8, 136.5, 134.2, 131.2, 130.0, 124.2, 121.3, 92.6, 34.9, 31.4, 24.6, 24.4, 24.3, 10.2 ppm. FTIR ($C_6D_6$; KBr Window; 20 ˚C): $\nu_{CN}$ = 2004 (s), 2037 (m), $\nu_{NN}$ = 2111 (m), also 2961 (m), 2929 (w), 2905 (w), 2868 (w), 1573 (w), 1463 (w), 1412 (m), 1381 (w), 1362 (w), 1105 (w), 1070 (w), 1028 (w), 941 (w), 878 (w), 745 (w) $cm^{-1}$. Anal. Calcd. For $C_{47}H_{64}N_3Co$: C, 73.34; H, 8.34; N, 5.77. Found: C, 77.57; H, 8.49; N, 5.55.

**Synthesis of $[Cp^*Co(CNAr^{Tripp2})]_2(\mu^2\text{-}\eta^2\text{-}(C,C)\text{-}\eta^2\text{-}(C,C)\text{-}C_6H_6)$ (16):** *Due to the extreme sensitivity to $N_{2\,(g)}$ and the subsequent formation of $Cp^*Co(N_2)(CNAr^{Tripp2})$ all reduction were conducted under an $Ar_{(g)}$ atmosphere, and all solvents were rigorously degassed and stored on combination of activated 3 and 4 Å mol sieves stored under an $Ar_{(g)}$ atmosphere for 3 days prior to use.* A 20 mL scintillation vial was charged with $Cp^*CoI_2(CNAr^{Tripp2})$ and dissolved in $C_6H_6$, (0.096 g, 0.102 mmol, 1.0 equiv.). Separately a pipet with a glass-wool filter as a plug was charged with $KC_8$ (0.029 g, 0.214 mmol, 2.2 equiv). Following the $C_6H_6$ solution of $Cp^*CoI_2(CNAr^{Tripp2})$ was filtered over

$KC_8$ at a rate of 1 drop/5 sec to yield a deep red solution. The resulting solution was then lyophilized to a fluffy burgundy powder, 0.070 g, 0.047 mmol, 93%. X-ray diffraction quality crystals were grown from *n*-pentane (0.5 mL) and spiked with 2 drops of $C_6H_6$ at –40 ˚C for 1 week. Transfer of the crystals to the X-ray diffactometer was accomplished by suspending the crystals in Trilene oil under $Ar_{(g)}$ and kept at –78 ˚C upon removal from the glove box. Selection of crystals was done rapidly under atmospheric conditions and transferred to the goniometer head and cooled to 100 K under a $N_2$ stream. Sufficiently low temperature renders displacement of coordinate $C_6H_6$ by $N_2$ slow where upon data collections were implemented. . $^1$H NMR (500 MHz, $C_6D_6$, 20 ˚C): δ = 7.20 (s, 8H, *m*-Tripp), 7.12 (d, 3H, 7 Hz, $C_6H_6$), 7.02 (mult., 4H, $C_6H_6$), 6.94 (d, 4H, 7Hz, *m*-Ph), 6.85 (t, 2H, 7Hz, *p*-Ph), 2.87 (Sept., 12H, 7Hz, C*H*$(CH_3)_2$), 1.50 (d, 24H, 6Hz, CH(C*H*$_3)_2$), 1.38 (s, 30H, Cp*–*H*), 1.30 ((d, 24H, 6Hz, CH(C*H*$_3)_2$), 1.17 ((d, 24H, 6Hz, CH(C*H*$_3)_2$) ppm. $^{13}$C{$^1$H} NMR (125.8 MHz, $C_6D_6$, 20 ˚C): δ = 173.5 (*C*NR), 152.5, 149.3, 146.8, 136.8, 134.4, 131.0, 130.7, 129.3, 125.7, 123.9, 121.6, 91.2, 35.0, 31.3, 25.0, 24.5, 24.1, 9.8 ppm. FTIR ($C_6D_6$; KBr Window; 20 ˚C): $\nu_{CN}$ = 2033 (m, sh), 2000 (s), 1917 (w), also 2961 (s), 2930 (m), 2903 (m) 2868 (m), 1605 (w), 1572 9w), 1463 (w), 1425 (w), 1411 (m), 1382 9w), 1362 (w), 1127 (w), 1107 (w), 1027 (w), 972 (w) $cm^{-1}$. Due to the extreme $N_2$ sensitivity suitable combustion analysis was not obtained.

**Synthesis of Cp*Co(CNAr$^{Tripp2}$)$_2$ (17):** A 20 mL scintillation vial was charged with Cp*Co($N_2$)(CNAr$^{Tripp2}$) (0.022 g, 0.032 mmol, 1 equiv) and dissolved in $C_6H_6$ (1 mL). Separately a second scintillation vial was charged with CNAr$^{Tripp2}$ (0.016g, 0.032 mmol, 1 equiv) and dissolved in $C_6H_6$ and added to the solution of Cp*Co($N_2$)(CNAr$^{Tripp2}$) in

$C_6H_6$. Immediately upon addition effervescence was observed in addition to a color change from dark brown to dark red. Lyophilization of $C_6H_6$ under reduced pressure afforded analytically pure samples of Cp*Co($CNAr^{Tripp2}$)$_2$ as a fluffy red powder, 0.033 g, 0.027 mmol, 87 %. X-ray diffraction quality crystals can be grown from saturated *n*-pentane solutions spiked with $C_6H_6$ over the course of 1 week at –40 ˚C. $^1$H NMR (500 MHz, $C_6D_6$, 20 ˚C): δ 7.26 (broad singlet. 8 H, *m*-Tripp), 6.83 (broad doublet. 4H, *m*-Ph), 6.70 (t, 2H, 7Hz, *p*-Ph), 3.14 (broad Sept. 2H, C*H*($CH_3$)$_2$), 3.07 (broad Sept. 2H, C*H*($CH_3$)$_2$), 2.97 (broad Sept. 2H, C*H*($CH_3$)$_2$), 2.87 (broad Sept. 4H, C*H*($CH_3$)$_2$), 2.37 ((broad Sept. 2H, C*H*($CH_3$)$_2$), 1.53 (broad singlet. 6 H, CH(C*H*$_3$)$_2$), 1.44 (broad singlet. 12 H, CH(C*H*$_3$)$_2$), 1.36 (s. 15H, Cp*–*H*), 1.34 (broad singlet. 12 H, CH(C*H*$_3$)$_2$), 1.30 (broad singlet. 18 H, CH(C*H*$_3$)$_2$), 1.12 (broad singlet. 6 H, CH(C*H*$_3$)$_2$), 1.03 (broad singlet. 6 H, CH(C*H*$_3$)$_2$), 0.99 (broad singlet. 12 H, CH(C*H*$_3$)$_2$). $^{13}$C{$^1$H} NMR (125.8 MHz, $C_6D_6$, 20 ˚C): δ = 187.1 (*C*NR), 148.5, 148.2, 148.1, 147.3, 147.2, 146.6, 139.6, 136.1, 135.7, 135.4, 132.3, 131.9, 131.4, 124.4, 122.6, 121.8, 121.1, 93.4, 34.9, 31.8, 30.8, 30.6, 26.5, 25.5, 25.4, 25.3, 24.9, 24.8, 24.4, 24.3, 24.1, 23.8, 20.7, 10.9 ppm. FTIR ($C_6D_6$; KBr Window; 20 ˚C): $\nu_{CN}$ = 1916 (s), 2001 (s), 2031 (sh), also 2962 (s), 2926 (m), 2905 (m), 2868 (m), 1570 (m), 1461 (m), 1444 (w), 1428 (w), 1411 (m), 1382 (m), 1361 (m), 1240 (w), 1203 (w), 1194 (w), 1172 (w), 1104 (w), 1070 (w), 10523 (w0, 1030 (w), 942 9w), 878 (m), 756 (m), 644 (w) cm$^{-1}$. Suitable combustion analysis was not obtained.

**Synthesis of Cp*Co($\eta^2$-C,C-PhCCPh)($CNAr^{Tripp2}$) (18):** To a solution of Cp*Co($N_2$)($CNAr^{Tripp2}$) (0.052 g, 0.0706 mmol, 1 equiv.) in $C_6D_6$ (1 mL) was added

PhCCPh (0.013 g, 0.0706 mmol, 1 equiv.) as a solution in $C_6D_6$. Upon addition a color change from brown to red-orange was observed, and analysis via $^1$H NMR spectroscopy concluded the complete consumption of Cp*Co($N_2$)($CNAr^{Tripp2}$). Concentration of the solution and crystallization of the resultant red solid from a saturated $Et_2O$/*n*-pentane solution (1 mL; 1:10) afforded analytically pure X-ray diffraction quality red-orange crystals of Cp*Co($\eta^2$-CC, PhCCPh)($CNAr^{Tripp2}$), 0.033g, 0.028 mmol, 53 %. $^1$H NMR (499.8 MHz, $C_6D_6$, 20 ˚C): δ = 7.87 (d, 4 H, 8 Hz), 7.30 (t, 4H, 8 Hz), 7.14 (t, 2 H, 8 Hz), 7.07 (s, 4 H, *m*-Trip), 6.82 (d, 2H, 8 Hz, *m*-Ph), 6.75 (t, 1 H, 8 Hz, *p*-Ph), 2.74 (sept., 6H, 7 Hz, C*H*($CH_3$)$_2$), 1.40 (s, 15H, Cp*-*H*), 1.34 (d, 12H, 8Hz, CH(C*H*$_3$)$_2$), 1.25 (d, 12H, 8Hz, CH(C*H*$_3$)$_2$), 1.10 (d, 12H, 8Hz CH(C*H*$_3$)$_2$) ppm. $^{13}$C{$^1$H} NMR (125.8 MHz, $C_6D_6$, 20 ˚C): δ = 172.5 (*C*NR), 148.7, 146.5, 138.0, 134.4, 132.6, 132.5, 132.2, 131.1, 130.6, 128.9, 128.8, 128.6, 127.9, 125.7, 124.7, 121.6, 93.8, 93.0, 34.4, 31.5, 24.9 24.4, 24.3, 10.6 ppm. FTIR ($C_6D_6$; KBr Window; 20 ˚C): $\nu_{CN}$ = 2032 (s), 2008 (m), 2961 (m), 2927 (w), 2906 (w), 2867 (w), 1836 (C≡C, w), 1591 (w), 1485 (w), 1464 (w), 1440 (w), 1412 (w), 1382 (w), 1363 (w), 56 (m), 692 (w), 569 (w) cm$^{-1}$. Suitable combustion analysis was not obtained.

**Synthesis of Cp*Co($\eta^5$-3,4-(Ph)$_2$-1-($NAr^{Tripp2}$)$C_5H_2$) (19):** To a solution of Cp*Co($N_2$)($CNAr^{Tripp2}$) (0.052 g, 0.0706 mmol, 1 equiv.) in $C_6D_6$ (1 mL) was added PhCCPh (0.013 g, 0.0706 mmol, 1 equiv.) as a solution in $C_6D_6$. Upon addition a color change from brown to red-orange was observed, and analysis via $^1$H NMR spectroscopy concluded the complete consumption of Cp*Co($N_2$)($CNAr^{Tripp2}$). Concentration of the solution and crystallization of the resultant red solid from a saturated $Et_2O$/*n*-pentane

solution (1 mL; 1:10) afforded analytically pure X-ray diffraction quality red-orange crystals of Cp*Co($\eta^2$-CC, PhCCPh)($CNAr^{Tripp2}$), 0.033g, 0.028 mmol, 53 %. $^1$H NMR (499.8 MHz, $C_6D_6$, 20 ˚C): δ = 7.30 (broad doublet, 2H, 6Hz, *m*-Ph), 7.17 (broad singlet, 6 H, *m*-Tripp/$C_6H_5$), 7.07 (multp., 6 H, $C_6H_5$), 6.97 (t, 2H, 10 Hz, $C_6H_5$), 6.90 (t, 1 H, 10 Hz, *p*-Ph), 3.46 (s, 2H, $C_5$–*H),* 3.4 (broad sept., 4H, C*H*$(CH_3)_2$), 2.85 (broad sept., 2H, C*H*$(CH_3)_2$), 1.23 (broad peak, 36H, CH(C*H*$_3)_2$), 1.15 (s, 15H, Cp*-*H*), ppm. $^{13}$C{$^1$H} NMR (125.8 MHz, $C_6D_6$, 20 ˚C): δ = 173.4 (*C*NR), 150.8, 147.3, 146.6, 145.2, 139.1, 135.0, 132.1, 130.1, 127.3, 120.9, 117.5, 91.2, 89.9, 65.1, 34.7, 30.8, 30.3, 26.5, 24.5, 23.5, 10.2, 8.9 ppm. FTIR ($C_6D_6$; KBr Window; 20 ˚C): $\nu_{CN}$ = 1545 (s), also 3057 (w), 3037 (w), 2960 (s), 2925 (w), 2866 (w), 1585 (w), 1506 (w), 1485 (w), 1460 (w), 1424 (w), 1397 (w), 1382 (w), 1361 (w), 1240 (m), 1100 (w), 1081 (w), 1070 (w), 1027 (w), 959 (w), 940 (w), 917 (w), 875 (w), 766 (m), 699 (m), 680 (w) cm$^{-1}$. Suitable combustion analysis was not obtainted.

**Synthesis of Cp*Co($\eta^2$-*C,C*-$C_6H_{10}$)($CNAr^{Tripp2}$) (20):** To a solution of Cp*Co($N_2$)$CNAr^{Tripp2}$ (0.039 g, 0.054 mmol, 1 equivs) in 1 mL of $C_6D_6$ a solution of $C_6H_{10}$ (0.0055 mL, 0.054 mmol, 1 equivs) in 0.5 mL of $C_6D_6$ was added in one portion. Upon addition an immediate color change from brown to red/orange was observed. Analysis via $^1$H NMR indicated complete conversion to a new diamagnetic product. The resulting solution was concentrated to a solid under reduced pressure and recrystallized from a saturated solution of $TMS_2O$/*n*-pentane (1:5; 1.5 mL) at -40 ˚C over 1 week to afford analytically pure black crystals of Cp*Co($\eta^2$-*C,C*-$C_6H_{10}$)$CNAr^{Tripp2}$ 0.017 g, 0.022 mmol, 39.5 % yield. $^1$H NMR (499.8 MHz, $C_6D_6$, 20 ˚C): 7.23 (s, 4H, 8 Hz, *m*-Tripp),

6.97 (d, 2H, 8Hz *m*-Ph), 6.81 (t, 1H, 7 Hz, *p*-Ph), 5.70 (s, 2H, cyclohexene), 2.94 (overlapped sept., 6H, C*H*$(CH_3)_2$), 2.24 (broad mult., 2H, cyclohexene), 2.00 (broad mult. 2H, cyclohexene), 1.90 (broad mult., 2H, cyclohexene), 1.50 (d, 12H, 7Hz, CH(C*H*$_3)_2$), 1.46 (s, 15H, Cp-*Me*), 1.34 (d, 12H, 7Hz, CH(C*H*$_3)_2$), 1.31 (overlapped broad mult., 2H, cyclohexene), 1.14 (d, 12H, 7Hz, CH(C*H*$_3)_2$) ppm. $^{13}C\{^1H\}$ NMR (125.8 MHz, $C_6D_6$, 20 ˚C): δ = 175.0 (*C*NR), 148.8, 147.1, 137.0, 134.9, 132.2, 130.6, 130.0, 123.8, 121.9, 92.7, 53.7, 35.0, 31.1, 30.3, 29.6, 25.7, 25.5, 24.3, 23.8, 23.7, 23.0, 9.6 ppm. FTIR ($C_6D_6$; KBr Window; 20 ˚C): $\nu_{CN}$ = 1990 (s), 2035 (sh) also 2961 (s), 2928 (m), 2906 (m), 2868 (m), 2109 (w), 2091 (w), 1465 (w), 1411 (w), 1382 (w), 1363 (w), 1252 (w), 1240 (w), 1196 (w), 1104 (w), 1070 (w), 879 (w), 756 (w) $cm^{-1}$. Anal. Calcd. For $C_{53}H_{74}NCo$: C, 81.19; H, 9.51; N, 1.79. Found: C, 78.70; H, 9.35; N, 1.78.

**Synthesis of Cp*Co($\eta^2$-*C,C*-$CH_2CHPh$)($CNAr^{Tripp2}$) (21):** To a solution of Cp*Co($N_2$)$CNAr^{Tripp2}$ (0.040 g, 0.056 mmol, 1 equivs) in 1 mL of $C_6D_6$ a solution of Styrene (0.0064 mL, 0.056 mmol, 1 equivs) in 0.5 mL of $C_6D_6$ was added in one portion. Upon addition an immediate color change from brown to red/orange was observed. Analysis via $^1H$ NMR indicated complete conversion to a new diamagnetic product. The resulting solution was concentrated to a solid under reduced pressure and recrystallized from a saturated solution of $TMS_2O$ (1.0 mL) at -40 ˚C over 1 week to afford analytically pure black crystals of Cp*Co($\eta^2$-*C,C*-$C_6H_{10}$)$CNAr^{Tripp2}$ 0.021 g, 0.027 mmol, 47 % yield. $^1H$ NMR (499.8 MHz, $C_6D_6$, 20 ˚C): 7.22-7.26 (mult., 8H, *m*-Tripp/*m/p*-styrene), 6.98 (t, 1H, 9Hz, *p*-styrene), 6.95 (d, 2H, 8Hz, m-*Ph*), 6.85 (t, 1H, 8 Hz, *p*-Ph), 2.86 (mult., 6H, C*H*$(CH_3)_2$), 1.74, (dd, 1H, 8Hz, 4Hz, $CH_2CHPh$), 1.85 (d, 2H, 12Hz, $CH_2$CHPh) 1.54 (d,

6H, 7Hz CH(C$H_3$)$_2$), 1.47 (d, 6H, 7Hz, , CH(C$H_3$)$_2$), 1.29 (d, 6H, 7Hz, CH(C$H_3$)$_2$), 1.26 (s (overlapped with Cp*–H), 6H, CH(C$H_3$)$_2$), 1.25 (broad singlet, 15H, CH(C$H_3$)$_2$), 1.18 (d, 12H, 7Hz, CH(C$H_3$)$_2$). $^{13}C\{^1H\}$ NMR (125.8 MHz, $C_6D_6$, 20 ˚C): δ = 175.6 (*C*NR), 149.3, 147.6, 146.7, 146.6, 137.3, 134.1, 130.7, 130.5, 124.6, 123.2, 121.8, 121.5, 92.9, 50.2, 35.0, 31.3, 25.0, 24.7, 24.6, 24.3, 24.2, 24.1, 9.8 ppm. FTIR ($C_6D_6$; KBr Window; 20 ˚C): $\nu_{CN}$ = 2039 (s), 2012 (s) also 2961 (m), 2927 (w), 2904 (w), 2868 (w), 1606 (w), 1595 (w), 1574 (w), 1495 (w), 1461 (w), 1412 (w), 1381 (w), 1363 (w), 1253 (w), 1229 (w), 1104 (w), 1069 (w), 1052 (w), 943 (w), 877 (w), 847 (w), 755 (w), 742 (w), 697 (w), 643 (w) $cm^{-1}$. Anal. Calcd. For $C_{54}H_{72}NCo$: C, 81.68; H, 9.00; N, 1.74. Found: C, 81.68; H, 9.50; N, 1.06.

**Generation and Detection of Cp*Co(H)$_2$(CNAr$^{Tripp2}$) (22):** Cp*Co(N$_2$)(CNAr$^{Tirpp2}$) (0.030 g, 0.042 mmol, 1equivs) was dissolved in $C_6D_6$ (1 mL) and transferred to a resealable J-Young's NMR tube. The sample was the brought out of the glove box and connected to the schlenk line where the solution was subject to 1 FPT cycle (*ca.* 0.02 mTorr). Upon thawing the reaction mixture was placed under an atmosphere of $H_{2\,(g)}$ where upon a color change to deep yellow was observed. Analysis via $^1$H NMR spectroscopy indicated complete consumption of Cp*Co(N$_2$)(CNAr$^{Tripp2}$) and the observation of a new species that exhibited a symmetric *m*-tephenyl environment. Isolation of this material as a solid, in a pure state has not been accomplished, however, spectroscopic characterization of what we tentatively assign as Cp*Co(H)$_2$(CNAr$^{Tripp2}$) is presented. $^1$H NMR (399.9 MHz, $C_6D_6$, 20 ˚C): δ = 7.24 (s, 4H, *m*-Tripp), 7.03 (d, 2H, 7Hz, *m*-Ph), 6.91 (t, 1H, 8HZ, *p*-Ph), 2.92 (sept. 2H, 7HZ, C*H*(CH$_3$)$_2$), 2.79 (sept. 4H,

7Hz, C*H*($CH_3$)$_2$), 1.68 (s, 15H, Cp*–*H*), 1.43 (d, 12H, 7Hz, CH(C*H*$_3$)$_2$), 1.36 (d, 12H, 7Hz, CH(C*H*$_3$)$_2$), 1.19 (d, 12H, 7Hz, CH(C*H*$_3$)$_2$) ppm. $^{13}C\{^1H\}$ NMR (125.8 MHz, $C_6D_6$, 20 ˚C): δ = 177.4 (*C*NR), 149.0, 146.9, 138.0, 133.7, 131.3, 129.5, 125.4, 121.1, 93.4, 35.1, 31.3, 24.9, 24.5, 24.2, 11.3 ppm. FTIR ($C_6D_6$; KBr Window; 20 ˚C): $\nu_{CN}$ = 2071 (s), 2032 (s, sh), also 2960 (s), 2926 (m), 2905 (m), 2868 (m), 1934 (w), 1901 (w), 1606 (w), 1574 (w), 1462 (m), 1416 (m), 1382 (m), 1363 (m), 1104 (w), 1071 (w), 1054 (w), 1032 (w), 943 (w), 877 (w), 756 (w), 746 (w), 680 (w), 646 (w). Suitable combustion analysis was not obtained.

**Synthesis of Cp*Co(H)(SiEt$_3$)(CNAr$^{Tripp2}$) (23):** Cp*Co($N_2$)(CNAr$^{Tirpp2}$) (0.028 g, 0.039 mmol, 1equivs) was dissolved in $C_6D_6$ where upon $HSiEt_3$ (6.2 μL, 0.039 mmol, 1 equiv) was added neat via microsyringe. Upon addition a color change from dark brown to deep yellow was observed in addition to a noticeable amount of effervescence indicating liberation of $N_2$. Analysis via $^1H$ NMR spectroscopy indicated complete consumptions of Cp*Co($N_2$)(CNAr$^{Tirpp2}$). Lyophilization of the resulting solution to constant mass afforded Cp*Co(H)(SiEt$_3$)(CNAr$^{Tirpp2}$) as a fluffy yellow powder 0.030 g, 0.037 mmol, 95%. X-Ray diffraction quality crystals were grown from a saturated $Et_2O$ solution (ca. 0.75 mL) over 3 days at –40 ˚C. $^1H$ NMR (399.9 MHz, $C_6D_6$, 20 ˚C): 7.24 (s, 4H, *m*-Tripp), 7.01 (d, 2H, 7Hz, *m*-Ph), 6.85 (t, 1H, 7Hz, *p*-Ph), 2.93 (overlapped sept. 6H, C*H*($CH_3$)$_2$), 1.58 (s, 15H, Cp*–*H*), 1.35 (d, 12H, 8Hz, , CH(C*H*$_3$)$_2$), 1.12 (br. s., 12H, CH(C*H*$_3$)$_2$), 1.06 (t, 12H, 8Hz, CH(C*H*$_3$)$_2$), 0.98 (t, 6H, 8Hz, C*H*$_2$CH$_3$), 0.55 (quart. Of d., 9H, 4Hz, $CH_2$C*H*$_3$), -16.03 (s, 1H, Co–*H*) ppm. $^{13}C\{^1H\}$ NMR (125.8 MHz, $C_6D_6$, 20 ˚C): δ = 178.3 (*C*NR), 148.9, 146.9, 137.3, 134.8, 132.2, 124.4, 121.9, 121.4, 93.8, 34.9,

31.4, 26.0, 25.4, 24.6, 23.4, 10.9, 10.2, 10.0, 9.9 ppm ppm. $^{29}Si\{^{1}H\}$(99.3 MHz, $C_6D_6$, 20 ˚C): δ = 41.5 (sext., 11Hz) ppm FTIR ($C_6D_6$; KBr Window; 20 ˚C): $\nu_{CN}$ = 2031 (s), 2004 (s), also 2960 (s), 2927 (s), 2868 (s), 1605 (w), 1567 (w), 1463 (m), 1408 (m), 1382 (m), 1363 (w), 1104 (w), 1070 (w), 1004 (w), 943 (w), 877 (w), 756 (w), 713 (w), 683 (w), 572 (w) $cm^{-1}$. Anal. Calcd. For $C_{53}H_{80}NSiCo$: C, 72.57; H, 9.19; N, 1.60. Suitable combustion analysis was not obtained.

**Isolation of Cp*Co($N_3Ar^{Mes2}$)($CNAr^{Tripp2}$) (24):** A 20 mL scintillation vial was charged with Cp*Co($N_2$)($CNAr^{Tripp2}$) (0.057 g, 0.077 mmol, 1 equiv) and dissolved in $Et_2O$ (2 mL). Following $N_3Ar^{Mes2}$ (0.028 g, 0.077 mmol, 1 equiv) was added as a solution in $Et_2O$ 2 mL all at once. Upon addition immediate effervescence was observed and attributed to the release of coordinated $N_2$. The reaction mixture was allowed to stir at room temperature for *ca.* 20 min, where upon it was concentrated to approx. 0.75 mL and placed in the freezer at –40 ˚C. After two weeks deep brown X-ray diffraction quality crystals had deposited with in the mixture. Removal of the mother liquor and drying *in vacuo* afforded Cp*Co($\kappa^1$-$N_3Ar^{Mes2}$)($CNAr^{Tripp2}$) as dark brown crystals, 0.026 g, 0.312 mmol, 31 %. Isolation of Cp*Co($\kappa^1$-$N_3Ar^{Mes2}$)($CNAr^{Tripp2}$) has only been limited to mixtures containing Cp*Co($N_2$)($CNAr^{Tripp2}$), and due to this suitable combustion analysis has not been obtained.

**Isolation of [Cp*Co(N(H)Ad)($CNAr^{Tripp2}$)]$_2$ (25):** A 20 mL scintillation vial was charged with Cp*Co($N_2$)($CNAr^{Tripp2}$) (0.043 g, 0.059 mmol, 1 equiv) and dissolved in $Et_2O$ (2 mL) at which point the mixture was placed in the cold well and frozen. Upon

thawing an equally cold solution of $N_3Ad$ (0.011 g, 0.059 mmol, 1 equiv) was added dropwise over 1 min. Upon addition immediate effervescence was observed and attributed to the release of coordinated $N_2$. The reaction mixture rapidly transferred to the freezer and stored at –40 ˚C. Storage for two weeks deposited dark orange X-ray diffraction quality crystals. Removal of the mother liquor and drying *in vacuo* afforded $[Cp^*Co(N(H)Ad)(CNAr^{Tripp2})]_2$ as dark brown crystals, 0.016 g, 0.009 mmol, 31 %.

## 5.14 Details of Crystallographic Structure Determinations.

**General Information.** Single crystal X-ray structure determinations were carried out at low temperature on Bruker Kappa diffractometers equipped with a Mo sealed tube or rotating anode or Cu rotating anode radiation source and a Bruker APEX-II, APEX-I, or Proteum Pt135 detector. All structures were solved via direct methods with SHELXS[90] and refined by full-matrix least squares procedures using SHELXL[90] within the Olex2 small-molecule solution, refinement and analysis software package.[91] Crystallographic data collection and refinement information are listed in Table 5.3-5.10.

The following molecules contained positionally disordered components that were modeled and refined anisotropically. They are listed along with their respective disordered components:

$(\mu^2\text{-}CNAr^{Mes2})_2[CpCo]_2$ (**4**): Exhibits twinning. TwinAbs was used for absorption correction and geration of HKL4 files which were used in refinement.

$(\eta^5\text{-}Cp^*)CoI_2(CNAr^{Dipp2})$ (**5**): Two site positional disorder *i*-Pr Methyl groups on flanking DIPP rings.

($\eta^5$-Cp*)Co($CNAr^{Dipp2}$)$_2$•($Et_2O$); (**8**): Two site positional disorder in one $Et_2O$ molecule of solvation.

($\eta^5$-Cp*)Co($\eta^2$-PhCCPh)($CNAr^{Dipp2}$) (**9**): Two site positional disorder *i*-Pr Methyl groups on flanking DIPP rings. ($\eta^5$-Cp*)Co($\eta^2$-PhCCPh)($CNAr^{Dipp2}$) contains one $TMS_2O$ molecule of solvation that was severely disordered. The Platon routine SQUEEZE was used to account for this disordered molecule as a diffuse contribution to the overall scattering pattern without specific atom positions.

[($\eta^5$-Cp*)Co($CNAr^{Dipp2}$)]$_2$($\mu^2$:$\kappa^2$;$\kappa^2$-$P_4$) (**10**): Two site positional disorder *i*-Pr Methyl groups. Two site rotational and translational disorder in one Cp* ring that was modeled using the AFIX 106 command to generate an idealized Cp* ring that is set to approximately 30% occupancy. [($\eta^5$-Cp*)Co($CNAr^{Dipp2}$)]$_2$($\mu^2$:$\kappa^2$;$\kappa^2$-$P_4$) also contains severe compositional solvent disorder. The Platon routine SQUEEZE was used to account for these disordered molecules as a diffuse contribution to the overall scattering pattern without specific atom positions.

[Cp*Co($CNAr^{Tripp2}$)]$_2$($\mu^2$-$\eta^2$-(C,C)-$\eta^2$-(C,C)-$C_6H_6$) (**16**): Two site positional disorder *i*-Pr Methyl groups. The Platon routine SQUEEZE was used to account for these disordered $C_6H_6$ of solvation as a diffuse contribution to the overall scattering pattern without specific atom positions.

$Cp^*Co(CNAr^{Tripp2})_2$ (**17**): Exhibited twinning. Accordingly absorption corrections were conducting using the routine TWINABS to generate appropriate HKL4 and HKL5 files. Refinement was done using HKL5 with a BASF5 treatment to account for overlap of twinning. Additionally the RIGU command to restrain the Arene C atoms within flanking Tripp2 rings. The Platon routine SQUEEZE was used to account for these disordered molecules of solvation as a diffuse contribution to the overall scattering pattern without specific atom positions.

Cp*Co(exo-cyclopentadienyl-imine) (**19)**: Is twined. Absorance corrections were done utilizing TwinAbs. And a global RIGU restraint was utilized.

$Cp^*Co(\eta^2\text{-}C,C\text{-}C_6H_{10})CNAr^{Tripp2}$ (**20**) displays positional disorder in one of th 2,4,6-triisoprpylphenyl rings. Each ring was modeled at 50% occupancy and linked with the FVAR command and then subjected to the EADP command. The Cp* ring displays two site positional disorder which was modeled and refined with the AFIX command n = 10 to generate and idealized Cp* bond metrics. Each ring was modeled and anisotropically refined.

$Cp^*Co(H)(SiEt_3)(CNAr^{Tripp2})$ (**23**): Displays two site posional disorder of iPr group which was modeled and refined anisotropically.

$Cp^*Co(N_3Ar^{Mes2})(CNAr^{Tripp2})$ (**24**): Displays translation disorder of the central ring in the $Ar^{Mes2}$ unit which was modeled and refined anisotropically.

[Cp*Co(N(H)Ad)($CNAr^{Tripp2}$)]$_2$ (**25**): Displays two site positional disorder of iPr groups and adamantly groups. Both were modeled and refined anisotropically. The EADP command was used to give both adamantyl units the same anisotropic displacement parameters.

**Table 5.1** Crystallographic data collection and refinement information.

| Name | $(\eta^5\text{-Cp})CoI_2CNAr^{Dipp2}$ (**1**) | $(\eta^5\text{-Cp})_2Co_2(\mu^2\text{-}CNAr^{Dipp2})_2\bullet(Et_2O)$; (**2**$\bullet Et_2O$) | $Cp^*CoI_2(CNAr^{Mes2})$ (**3**) |
|---|---|---|---|
| Formula | $C_{36}H_{42}CoI_2N$ | $C_{72}H_{84}Co_2N_2$ | $C_{35}H_{40}CoI_2N$ |
| Crystal System | Monoclinic | Monoclinic | Monoclinic |
| Space Group | $P2_1/c$ | C2/c | $P2_1/C$ |
| *a*, Å | 11.2236(3) | 29.1006(17) | 14.7734(6) |
| *b*, Å | 18.3864(4) | 10.4530(7) | 12.5075(5) |
| *c*, Å | 17.5003(4) | 21.8596(13) | 17.6414(7) |
| α, deg | 90 | 90 | 90 |
| β, deg | 108.6110(10) | 102.775(4) | 98.647(2) |
| γ, deg | 90 | 90 | 90 |
| V, $Å^3$ | 3422.54(14) | 6484.8(7) | 3222.7(2) |
| *Z* | 4 | 4 | 4 |
| Radiation (λ, Å) | Mo-$K_\alpha$, 0.71073 | Cu-$K_\alpha$, 1.54178 | Mo-$K_\alpha$, 0.71073 |
| ρ (calcd.), $g/cm^3$ | 1.555 | 1.122 | 1.623 |
| μ (Mo Ka), $mm^{-1}$ | 2.329 | 4.298 | 2.472 |
| Temp, K | 100 | 100 | 100 |
| θ max, deg | 25.378 | 50.431 | 25.461 |
| data/parameters | 6278/369 | 3378/351 | 5907/363 |
| $R_1$ | 0.0183 | 0.0776 | 0.0201 |
| $wR_2$ | 0.0453 | 0.1991 | 0.0432 |
| GOF | 1.036 | 1.063 | 1.042 |

**Table 5.2** Crystallographic data collection and refinement information.

| Name | $[(\mu^2\text{-}CNAr^{Mes2})_2[Cp^*Co]_2 \bullet (Et_2O)_2$ (**4**) | $(\eta^5\text{-}Cp^*)CoI_2(CNAr^{Dipp2})$ (**5**) | $(\eta^5\text{-}Cp^*)Co(N_2)(CNAr^{Dipp2})$ (**6**) |
|---|---|---|---|
| Formula | $C_{78}H_{97}Co_2N_2O_2$ | $C_{41}H_{52}CoI_2N$ | $C_{41}H_{52}CoN_3$ |
| Crystal System | Triclinic | Monoclinic | Monoclinic |
| Space Group | *P–1* | $P2_1/n$ | $P2_1/c$ |
| *a*, Å | 12.4887(8) | 10.1747(2) | 18.1976(8) |
| *b*, Å | 13.9778(9) | 21.3662(5) | 10.5931(5) |
| *c*, Å | 20.3577(12) | 17.6111(4) | 18.9124(8) |
| α, deg | 99.356(3) | 90 | 90 |
| β, deg | 106.168(3) | 96.1823(13) | 92.5640(19) |
| γ, deg | 90.506(3) | 90 | 90 |
| V, $Å^3$ | 3363.3(4) | 3806.29(15) | 3642.1(13) |
| *Z* | 2 | 4 | 4 |
| Radiation (λ, Å) | Mo-$K_\alpha$, 0.71073 | Mo-$K_\alpha$, 0.71073 | Mo-$K_\alpha$, 0.71073 |
| ρ (calcd.), $g/cm^3$ | 1.198 | 1.521 | 1.178 |
| μ (Mo Ka), $mm^{-1}$ | 0.540 | 2.101 | 0.502 |
| Temp, K | 100 | 100 | 100 |
| θ max, deg | 25.027 | 25.501 | 26.027 |
| data/parameters | 11851/783 | 7028/428 | 7156/419 |
| $R_1$ | 0.0481 | 0.0392 | 0.0408 |
| $wR_2$ | 0.1168 | 0.0672 | 0.0772 |
| GOF | 1.084 | 1.054 | 1.022 |

**Table 5.3** Crystallographic data collection and refinement information.

| Name | ($\eta^5$-Cp*)Co (Azabenz[*b*]azulene$^{Dipp}$) (**7**) | ($\eta^5$-Cp*)Co($CNAr^{Dipp2}$)$_2$ •($Et_2O$); (**8**• $Et_2O$) | ($\eta^5$-Cp*)Co($\eta^2$-PhCCPh)($CNAr^{Dipp2}$) (**9**) |
|---|---|---|---|
| Formula | $C_{41}H_{53}CoN$ | $C_{74}H_{92.5}CoN_2O_{0.5}$ | $C_{55}H_{62}CoN$ |
| Crystal System | Monoclinic | Monoclinic | Monoclinic |
| Space Group | $P2_1/c$ | $P2_1/c$ | C2/c |
| *a*, Å | 12.3600(4) | 21.222(3) | 39.4977(15) |
| *b*, Å | 14.5680(4) | 14.0788(17) | 10.7818(4) |
| *c*, Å | 19.8481(6) | 21.829(3) | 25.7877(9) |
| α, deg | 90 | 90 | 90 |
| β, deg | 97.9218(15) | 96.131(7) | 110.826(3) |
| γ, deg | 90 | 90 | 90 |
| V, Å$^3$ | 3539.75(18) | 6484.6(14) | 10624.3(7) |
| *Z* | 4 | 4 | 8 |
| Radiation (λ, Å) | Mo-$K_\alpha$, 0.71073 | Mo-$K_\alpha$, 0.71073 | Mo-$K_\alpha$, 0.71073 |
| ρ (calcd.), g/cm$^3$ | 1.161 | 1.143 | 1.030 |
| μ (Mo Ka), mm$^{-1}$ | 0.512 | 0.310 | 0.366 |
| Temp, K | 100 | 100 | 100 |
| θ max, deg | 28.310 | 25.384 | 26.029 |
| data/parameters | 8774/401 | 11827/731 | 10126/554 |
| $R_1$ | 0.0369 | 0.0513 | 0.0427 |
| $wR_2$ | 0.0813 | 0.1247 | 0.1019 |
| GOF | 1.013 | 1.039 | 1.031 |

**Table 5.4** Crystallographic data collection and refinement information.

| Name | $(\eta^5\text{-Cp*})Co(\kappa^2\text{-P}_4)(CNAr^{Dipp2})$ (**10**) | $[(\eta^5\text{-Cp*})Co(CNAr^{Dipp2})]_2(\mu^2{:}\kappa^2{;}\kappa^2\text{-P}_4)$ (**11**) | $CNAr^{Tripp2}$ (**13**) |
|---|---|---|---|
| Formula | $C_{41}H_{52}CoNP_4$ | $C_{82}H_{104}Co_2N_2P_4$ | $C_{37}H_{49}N$ |
| Crystal System | Triclinic | Triclinic | Orthorhombic |
| Space Group | *P-1* | *P-1* | *Pbcm* |
| *a*, Å | 10.5024(5) | 12.0968(7) | 10.9087(13) |
| *b*, Å | 11.2267(5) | 12.4201(7) | 12.0442(14) |
| *c*, Å | 17.5316(7) | 29.0162(18) | 25.283(3) |
| α, deg | 91.4990(10) | 94.200(3) | 90 |
| β, deg | 90.424(2) | 93.812(2) | 90 |
| γ, deg | 110.691(2) | 108.525(2) | 90 |
| V, $Å^3$ | 1932.81(15) | 4103.9(4) | 3321.8(7) |
| *Z* | 2 | 2 | 4 |
| Radiation (λ, Å) | Mo-$K_\alpha$, 0.71073 | Mo-$K_\alpha$, 0.71073 | Mo-$K_\alpha$, 0.71073 |
| ρ (calcd.), $g/cm^3$ | 1.274 | 1.100 | 1.015 |
| μ (Mo Ka), $mm^{-1}$ | 0.639 | 0.522 | 0.057 |
| Temp, K | 100 | 100 | 100 |
| θ max, deg | 25.364 | 26.338 | 25.331 |
| data/parameters | 7084/437 | 14930/890 | 3111/184 |
| $R_1$ | 0.0284 | 0.0677 | 0.0454 |
| $wR_2$ | 0.0670 | 0.1526 | 0.1143 |
| GOF | 1.020 | 1.004 | 1.043 |

**Table 5.5** Crystallographic data collection and refinement information.

| Name | ($\eta^5$-Cp*)$CoI_2CNAr^{Tripp2}$ (**14**) | ($\eta^5$-Cp*)$Co(N_2)$ $CNAr^{Tripp2}$ (**15**) | $[Cp^*Co(CNAr^{Tripp2})]_2(\mu^2$-$\eta^2$-(C,C)-$\eta^2$-(C,C)-$C_6H_6)$ (**16**) |
|---|---|---|---|
| Formula | $C_{47}H_{64}CoI_2N$ | $C_{47}H_{64}CoN_3$ | $C_{106}H_{140}Co_2N_2$ |
| Crystal System | Orthorhombic | Orthorhombic | Triclinic |
| Space Group | *Pca2₁* | *Pbca* | *P–1* |
| *a*, Å | 23.0483(13) | 17.4002(4) | 12.7861(9) |
| *b*, Å | 14.0290(9) | 20.7307(5) | 15.0182(10) |
| *c*, Å | 27.3737(18) | 23.4789(6) | 28.266(2) |
| α, deg | 90 | 90 | 100.809(5) |
| β, deg | 90 | 90 | 97.786(5) |
| γ, deg | 90 | 90 | 103.390(4) |
| V, $Å^3$ | 8851.1(10) | 8469.3(4) | 5094.8(6) |
| *Z* | 8 | 8 | 2 |
| Radiation (λ, Å) | $MoK_\alpha$ (λ = 0.71073) | $MoK_\alpha$ (λ = 0.71073) | $MoK_\alpha$ (λ = 0.71073) |
| ρ (calcd.), $g/cm^3$ | 1.434 | 1.145 | 1.017 |
| μ (Mo Ka), $mm^{-1}$ | 1.814 | 0.439 | 0.368 |
| Temp, K | 100.0 | 100.0 | 100 |
| θ max, deg | 25.381 | 25.762 | 23.533 |
| data/parameters | 15163/929 | 8045/477 | 15098/1053 |
| $R_1$ | 0.0567 | 0.0878 | 0.0543 |
| $wR_2$ | 0.0897 | 0.1613 | 0.1099 |
| GOF | 1.034 | 1.082 | 0.979 |

**Table 5.6** Crystallographic data collection and refinement information.

| Name | $Cp^*Co(CNAr^{Tripp2})_2$ (**17**) | $Cp^*Co(\eta^2\text{-C,C-PhCCPh})(CNAr^{Tripp2})$ (**18**) | $Cp^*Co(2,3\text{-}Ph_2\text{-}1\text{-}NAr^{Tripp2}\text{-}C_5H_2)$ (**19**) |
|---|---|---|---|
| Formula | $C_{84}H_{113}CoN_2$ | $C_{63.5}H_{78.5}CoN$ | $C_{63}H_{76}CoN$ |
| Crystal System | Triclinic | Triclinic | Triclinic |
| Space Group | *P–1* | *P–1* | *P–1* |
| *a*, Å | 13.3401(9) | 10.6203(7) | 11.8419(10) |
| *b*, Å | 17.3969(13) | 13.5543(7) | 16.7868(15) |
| *c*, Å | 19.4948(15) | 19.0697(13) | 28.048(2) |
| α, deg | 108.013(3) | 89.688(2) | 102.510(7) |
| β, deg | 100.833(3) | 77.748(2) | 99.108(6) |
| γ, deg | 90.980(3) | 79.641(2) | 90.235(7) |
| V, $Å^3$ | 4212.1(5) | 2637.3(3) | 5370.2(8) |
| *Z* | 2 | 2 | 2 |
| Radiation (λ, Å) | $MoK_\alpha$ (λ = 0.71073) | $MoK_\alpha$ (λ = 0.71073) | $CuK_\alpha$ (λ = 1.54178) |
| ρ (calcd.), $g/cm^3$ | 0.954 | 1.152 | 1.121 |
| μ (Mo Ka), $mm^{-1}$ | 0.241 | 0.365 | 2.777 |
| Temp, K | 100 | 100 | 100 |
| θ max, deg | 23.289 | 25.350 | 49.751 |
| data/parameters | 22557/802 | 9651/619 | 10818/1205 |
| $R_1$ | 0.0844 | 0.0349 | 0.1703 |
| $wR_2$ | 0.1919 | 0.0770 | 0.4287 |
| GOF | 1.033 | 1.038 | 1.075 |

**Table 5.7** Crystallographic data collection and refinement information.

| Name | ($\eta^5$-Cp*)Co ($\eta^2$-*C,C*-$C_6H_{10}$)CNAr$^{Tripp2}$) (**20**) | ($\eta^5$-Cp*)Co($\eta^2$-*C,C*-$CH_2CHPh$)CNAr$^{Tripp2}$ (**21**) | Cp*Co(H)($SiEt_3$) ($CNAr^{Tripp2}$) (**22**) |
|---|---|---|---|
| Formula | $C_{53}H_{74}CoN$ | $C_{55}H_{72}CoN$ | $C_{53}H_{80}CoNSi$ |
| Crystal System | Monoclinic | Monoclinic | Orthorhombic |
| Space Group | $P2_1/n$ | $C2$ | $Pna2_1$ |
| *a*, Å | 17.8319(19) | 16.9664(8) | 18.2845(4) |
| *b*, Å | 13.874(2) | 18.9180(9) | 17.0303(5) |
| *c*, Å | 19.914(3) | 14.5574(6) | 15.2821(4) |
| α, deg | 90 | 90 | 90 |
| β, deg | 105.982(6) | 90.497(2) | 90 |
| γ, deg | 90 | 90 | 90 |
| V, Å$^3$ | 4737.7(11) | 4672.3(4) | 4758.7(2) |
| *Z* | 4 | 4 | 4 |
| Radiation (λ, Å) | $MoK_\alpha$ (λ = 0.71073) | $MoK_\alpha$ (λ = 0.71073) | $MoK_\alpha$ (λ = 0.71073) |
| ρ (calcd.), g/cm$^3$ | 1.099 | 1.146 | 1.142 |
| μ (Mo Ka), mm$^{-1}$ | 0.396 | 0.403 | 0.420 |
| Temp, K | 100 | 100 | 100 |
| θ max, deg | 25.012 | 25.498 | 25.378 |
| data/parameters | 8321/524 | 8635/531 | 8513/533 |
| $R_1$ | 0.01454 | 0.0346 | 0.0402 |
| $wR_2$ | 0.3041 | 0.0701 | 0.0902 |
| GOF | 1.365 | 1.028 | 1.037 |

**Table 5.8** Crystallographic data collection and refinement information.

| Name | $Cp^*Co(\kappa^1\text{-}N_3Ar^{Mes2})(CNAr^{Tripp2})$ (**24**) | $[Cp^*Co(N(H)Ad)(CNAr^{Tripp2})]_2$ (**25**) |
|---|---|---|
| Formula | $C_{71}H_{89}CoN_4$ | $C_{120}H_{164}Co_2N_4$ |
| Crystal System | Triclinic | Monoclinic |
| Space Group | *P–1* | $P2_1/c$ |
| *a*, Å | 13.7270(3) | 21.4458(4) |
| *b*, Å | 14.6320(4) | 23.5522(5) |
| *c*, Å | 17.0079(5) | 11.1264(2) |
| α, deg | 80.849(2) | 90 |
| β, deg | 78.223(2) | 98.1690(10) |
| γ, deg | 74.354(2) | 90 |
| V, $Å^3$ | 3200.62(15) | 5562.87(19) |
| *Z* | 2 | 2 |
| Radiation (λ, Å) | $CuK_\alpha$ (λ = 1.54178) | $CuK_\alpha$ (λ = 1.54178) |
| ρ (calcd.), $g/cm^3$ | 1.097 | 1.063 |
| μ (Mo/Cu Ka), $mm^{-1}$ | 2.408 | 2.674 |
| Temp, K | 100 | 100 |
| θ max, deg | 58.928 | 50.645 |
| data/parameters | 9182/680 | 5850/591 |
| $R_1$ | 0.0638 | 0.0756 |
| $wR_2$ | 0.1438 | 0.2904 |
| GOF | 1.060 | 1.108 |

## 5.15 Acknowledgements

Chapter 5 is adapted in part from Mokhtarzadeh, C. C.; Rheingold, A. L.; Figueroa, J. S. *Dalton Tras.* **2016**, *In Press.* Copyright 2016 The Royal Society of Chemistry. The dissertation author is the first author on this publication. The synthesis

of $CNAr^{Tripp2}$ is adapted in part from Carpenter, A. E.; Mokhtarzdeh, C. C.; Ripatti, D. S.; Havrylyuk, I.; Kamezawa, R.; Moore, C. E.; Rheingold, A. L.; and Figueroa, J. S. *Inorg. Chem.* **2105**, *54*, 2936-2944. Copyright 2015, American Chemical Society. The dissertation author is the second author of this pubilication. Permission to include published material in this dissertation has been obtained from all coauthors. Additional unpublished results are reported here in, and are to currently in preparation as manuscript by Mokhtarzadeh, C. C., Moore, C. E., Gimbecky, M., Rheingold, A. L., Figueroa, J. S. The dissertation author is the primary author of this manuscript.

## 5.16 References


(1) Poliakoff, M.; Turner, J. J. *J. Chem. Soc., Dalton Trans.* **1973**, No. 13, 1351.

(2) Poliakoff, M.; Weitz, E. *Acc. Chem. Res.* **1987**, *20* (11), 408.

(3) Snee, P. T.; Payne, C. K.; Kotz, K. T.; Yang, H.; Harris, C. B. *J. Am. Chem. Soc.* **2001**, *123* (10), 2255.

(4) Poliakoff, M.; Turner, J. J. *Angew. Chem. Int. Ed.* **2001**, *40* (15), 2809.

(5) Ihee, H.; Cao, J.; Zewail, A. H. *Angew. Chem. Int. Ed.* **2001**, *40* (8), 1532.

(6) Lomont, J. P.; Nguyen, S. C.; Harris, C. B. *Acc. Chem. Res.* **2014**, *47* (5), 1634.

(7) Peter, K.; Vollhardt, C.; Bercaw, J. E.; Bergman, R. G. *J. Organ. Chem.* **1975**, *97* (2), 283.

(8) Vollhardt, K. P. C.; Bercaw, J. E.; Bergman, R. G. *J. Am. Chem. Soc.* **1974**, *96* (15), 4998.

(9) Lee, W. S.; Brintzinger, H. H. *J. Organomet. Chem.* **1977**.

(10) Lee, W.-S.; Brintzinger, H. H. *J. Organomet. Chem.* **1977**, *127* (1), 93.

(11) Bengali, A. A.; Bergman, R. G.; Moore, C. B. *J. Am. Chem. Soc.* **1995**, *117* (13), 3879.

(12) Siegbahn, P. E. M. *J. Am. Chem. Soc.* **1996**, *118* (6), 1487.

(13) Elian, M.; Hoffmann, R. *Inorg Chem* **1975**, *14* (5), 1058.

(14) Burdett, J. K. *Inorg Chem* **1975**, *14* (2), 375.

(15) Hofmann, P.; Padmanabhan, M. *Organometallics* **1983**, *2* (10), 1273.

(16) Lavallo, V.; El-Batta, A.; Bertrand, G.; Grubbs, R. H. *Angew. Chem. Int. Ed.* **2010**, *50* (1), 268.

(17) Zhang, H.; Ouyang, Z.; Liu, Y.; Zhang, Q.; Wang, L.; Deng, L. *Angew. Chem. Int. Ed.* **2014**, *53* (32), 8432.

(18) Back, O.; Henry-Ellinger, M.; Martin, C. D.; Martin, D.; Bertrand, G. *Angew. Chem. Int. Ed.* **2013**, *52* (10), 2939.

(19) Andjaba, J. M.; Tye, J. W.; Yu, P.; Pappas, I.; Bradley, C. A. *Chem. Commun. (Camb.)* **2016**, *52* (12), 2469.

(20) Fox, B. J.; Millard, M. D.; DiPasquale, A. G.; Rheingold, A. L.; Figueroa, J. S. *Angew. Chem. Int. Ed. Engl.* **2009**, *48* (19), 3473.

(21) Labios, L. A.; Millard, M. D.; Rheingold, A. L.; Figueroa, J. S. *J. Am. Chem. Soc.* **2009**, *131* (32), 11318.

(22) Margulieux, G. W.; Weidemann, N.; Lacy, D. C.; Moore, C. E.; Rheingold, A. L.; Figueroa, J. S. *J. Am. Chem. Soc.* **2010**, *132* (14), 5033.

(23) Emerich, B. M.; Moore, C. E.; Fox, B. J.; Rheingold, A. L.; Figueroa, J. S. *Organometallics* **2011**, *30* (9), 2598.

(24) Stewart, M. A.; Moore, C. E.; Ditri, T. B.; Labios, L. A.; Rheingold, A. L.; Figueroa, J. S. *Chem. Commun.* **2011**, *47* (1), 406.

(25) Carpenter, A. E.; Margulieux, G. W.; Millard, M. D.; Moore, C. E.; Weidemann, N.; Rheingold, A. L.; Figueroa, J. S. *Angew. Chem. Int. Ed. Engl.* **2012**, *51* (37), 9412.

(26) Carpenter, A. E.; Wen, I.; Moore, C. E.; Rheingold, A. L.; Figueroa, J. S. *Chemistry* **2013**, *19* (32), 10452.

(27) Agnew, D. W.; Moore, C. E.; Rheingold, A. L.; Figueroa, J. S. *Angew. Chem. Int. Ed.* **2015**, *54* (43), 12673.

(28) Mokhtarzadeh, C. C.; Margulieux, G. W.; Carpenter, A. E.; Weidemann, N.; Moore, C. E.; Rheingold, A. L.; Figueroa, J. S. *Inorg Chem* **2015**, *54* (11), 5579.

(29) Fox, B. J.; Sun, Q. Y.; DiPasquale, A. G.; Fox, A. R.; Rheingold, A. L.; Figueroa, J. S. *Inorg Chem* **2008**, *47* (19), 9010.

(30) Ditri, T. B.; Fox, B. J.; Moore, C. E.; Rheingold, A. L.; Figueroa, J. S. *Inorg Chem* **2009**, *48* (17), 8362.

(31) Ditri, T. B.; Carpenter, A. E.; Ripatti, D. S.; Moore, C. E.; Rheingold, A. L.; Figueroa, J. S. *Inorg Chem* **2013**, *52* (22), 13216.

(32) Carpenter, A. E.; Mokhtarzadeh, C. C.; Ripatti, D. S.; Havrylyuk, I.; Kamezawa, R.; Moore, C. E.; Rheingold, A. L.; Figueroa, J. S. *Inorg Chem* **2015**, *54* (6), 2936.

(33) Tomson, N. C.; Labios, L. A.; Weyhermüller, T.; Figueroa, J. S.; Wieghardt, K. *Inorg Chem* **2011**, *50* (12), 5763.

(34) Barnett, B. R.; Moore, C. E.; Rheingold, A. L.; Figueroa, J. S. *J. Am. Chem. Soc.* **2014**, *136* (29), 10262.

(35) Carpenter, A. E.; McNeece, A. J.; Barnett, B. R.; Estrada, A. L.; Mokhtarzadeh, C. C.; Moore, C. E.; Rheingold, A. L.; Perrin, C. L.; Figueroa, J. S. *J. Am. Chem. Soc.* **2014**, *136* (44), 15481.

(36) Barnett, B. R.; Labios, L. A.; Moore, C. E.; England, J.; Rheingold, A. L.; Wieghardt, K.; Figueroa, J. S. *Inorg Chem* **2015**, *54* (14), 7110.

(37) Barnett, B. R.; Moore, C. E.; Chandrasekaran, P.; Sproules, S.; Rheingold, A. L.; DeBeer, S.; Figueroa, J. S. *Chem. Sci.* **2015**, *6* (12), 7169.

(38) Shah, S.; Simpson, M. C.; Smith, R. C.; Protasiewicz, J. D. *J. Am. Chem. Soc.* **2001**, *123* (28), 6925.

(39) Wang, H.; Xie, Y.; King, R. B.; Schaefer, H. F. *J. Am. Chem. Soc.* **2005**, *127* (33), 11646.

(40) Cirjak, L. M.; Ginsburg, R. E.; Dahl, L. F. *Inorg Chem* **1982**, *21* (3), 940.

(41) Pinhas, A. R.; Hoffmann, R. *Inorg Chem* **1979**, *18* (3), 654.

(42) Schore, N. E.; Ilenda, C. S.; Bergman, R. G. *J. Am. Chem. Soc.* **1976**, *98* (1), 256.

(43) Henda, C. S.; Schore, N. E.; Bergman, R. G. *J. Am. Chem. Soc.* **1976**, *98* (1), 255.

(44) Schore, N. E.; Ilenda, C. S.; Bergman, R. G. *J. Am. Chem. Soc.* **1977**, *99*, 1781.

(45) Schugart, K. A.; Fenske, R. F. *J. Am. Chem. Soc.* **1986**, *108*, 5100-5104.

(46) Zachmanoglou, C. E.; Docrat, A.; Bridgewater, B. M.; Parkin, G.; Brandow, C. G.; Bercaw, J. E.; Jardine, C. N.; Lyall, M.; Green, J. C.; Keister, J. B. *J. Am. Chem. Soc.* **2002**, *124* (32), 9525.

(47) Möhring, P. C.; Coville, N. J. *J. Organomet. Chem.* **1994**, *479* (1-2), 1.

(48) Wasserman, E. P.; Bergman, R. G.; Moore, C. B. *J. Am. Chem. Soc.* **1988**, *110* (18), 6076.

(49) Boyer, J. H.; De Jong, J. *J. Am. Chem. Soc.* **1969**, *91* (21), 5929.

(50) Buchner, E.; Curtius, T. *Ber. Dtsch. Chem. Ges.* **1885**, *18* (2), 2377.

(51) Chomitz, W. A.; Sutton, A. D.; Krinsky, J. L.; Arnold, J. *Organometallics* **2009**, *28* (12), 3338.

(52) Schore, N. E. *Chem. Rev.* **1988**, *88* (7), 1081.

(53) Vollhardt, K. P. C. *Acc. Chem. Res.* **1977**, *10* (1), 1.

(54) Caporali, M.; Gonsalvi, L.; Rossin, A.; Peruzzini, M. *Chem. Rev.* **2010**.

(55) Cossairt, B. M.; Piro, N. A.; Cummins, C. C. *Chem. Rev.* **2010**, *110* (7), 4164.

(56) Scheer, M.; Balázs, G.; Seitz, A. *Chem. Rev.* **2010**, *110* (7), 4236.

(57) Scherer, O. J.; Swarowsky, M.; Wolmershaeuser, G. *Organometallics* **1989**, *8* (3), 841.

(58) Rivard, E.; Power, P. P. *Inorg Chem* **2007**, *46* (24), 10047.

(59) Robinson, G. H. *Chem. Commun.* **1999**, 2157.

(60) Stanciu, C.; Richards, A. F.; Fettinger, J. C.; Brynda, M.; Power, P. P. *J. Organomet. Chem.* **2006**, *691* (11), 2540.

(61) Wolf, R.; Ni, C.; Nguyen, T.; Brynda, M.; Long, G. J.; Sutton, A. D.; Fischer, R. C.; Fettinger, J. C.; Hellman, M.; Pu, L.; Power, P. P. *Inorg Chem* **2007**, *46* (26), 11277.

(62) Mokhtarzadeh, C. C.; Rheingold, A. L.; Figueroa, J. S. *Dalton Trans.* **2016**.

(63) van der Heijden, H.; Orpen, A. G.; Pasman, P. *J. Chem. Soc., Chem. Commun.* **1985**, No. 22, 1576.

(64) Bach, I.; Pörschke, K.-R.; Goddard, R.; Kopiske, C.; Krüger, C.; Rufińska, A.; Seevogel, K. *Organometallics* **1996**, *15* (23), 4959.

(65) Lomont, J. P.; Nguyen, S. C.; Schlegel, J. P.; Zoerb, M. C.; Hill, A. D.; Harris, C. B. *J. Am. Chem. Soc.* **2012**, *134* (6), 3120.

(66) Poli, R. *Chem. Rev.* **1996**, *96*, 2135.

(67) Lautens, M.; Klute, W.; Tam, W. *Chem. Rev.* **1996**.

(68) Heller, B.; Hapke, M. *Chem Soc Rev* **2007**, *36* (7), 1085.

(69) Field, L. D.; Ward, A. J.; Turner, P. *Aust. J. Chem.* **1999**, *52* (11), 1085.

(70) Diercks, R.; Eaton, B. E.; Gürtzgen, S. *J. Am. Chem. Soc* **1998**, *120*, 8247.

(71) Schaefer, C.; Werz, D. B.; Staeb, S. H.; Gleiter, R.; Rominger, F. *Organometallics* **2005**, *24*, 2106.

(72) Park, J. H.; Chang, K.-M.; Chung, Y. K. *Coord. Chem. Rev.* **2009**, *253* (21-22), 2461.

(73) Rolf Gleiter, A.; Daniel B Werz. *Organometallics* **2005**.

(74) Brookhart, M.; Grant, B.; Lenges, C.; Prosenc, M.; White, P. *Angew. Chem. Int. Ed. Engl.* **2000**, *39* (9), 1676.

(75) Crabtree, R. H. *Chem. Rev.* **2016**, DOI: 10.10.1021/acs/chemrev/6b0037.

(76) Kubas, G. J. *Chem. Rev.* **2007**, *107*, 4152.

(77) Hennessy, E. T.; Liu, R. Y.; Iovan, D. A.; Duncan, R. A.; Betley, T. A. *Chem. Science* **2014**, *5* (4), 1526.

(78) King, E. R.; Betley, T. A. *Inorg Chem* **2009**, *48* (6), 2361.

(79) Shay, D. T.; Yap, G. P. A.; Zakharov, L. N.; Rheingold, A. L.; Theopold, K. H. *Angew. Chem. Int. Ed.* **2005**, *44* (10), 1508.

(80) King, E. R.; Sazama, G. T.; Betley, T. A. *J. Am. Chem. Soc.* **2012**, *134* (43), 17858.

(81) Hu, X.; Meyer, K. *J. Am. Chem. Soc.* **2004**, *126* (50), 16322.

(82) Zhang, L.; Liu, Y.; Deng, L. *J. Am. Chem. Soc.* **2014**, *136* (44), 15525.

(83) Bitterwolf, T. E. *Coordination Chemistry Reviews* **2000**, *206-207*, 419.

(84) Laskowski, C. A.; Miller, A.; Hillhouse, G. L. *Journal of the ...* **2010**.

(85) Pangborn, A. P.; Giardello, M. A.; Grubbs, R. H.; Rosen, R. K.; Timmers, F. J. *Organometallics.* **1996**, *15*, 1518.

(87) Armarego, W. L. F.; Chai, C. L. L. *Purification of Laboratory Chemicals,* 5thEd.; Elsevier, 2003.

(86) Sun, B.; Yoshino, T.; Matsunaga, S.; Kanai, M. *Adv. Synth. Catal.* **2014**, *356*, 1491-1495.

(87) Heck, R. F. *Inorg. Chem.* **1965**, *4,* 855-857.

(88) Dürr, S.; Ertler, D.; Radius, U. *Inorg. Chem*, **2012**, *51*, 3904-3909.

(89) Schwindt, M. A.; Lejon, T.; Hegedus, L. S. *Organometallics*, **1990**, *9*, 2814.

(90) Sheldrick, G. M. *Acta Crystallogr. A.*, **2008**, *64*, 112.

(91) Dolomanov, O. V.; Bourhis, L. J.; Gildea, R. J.; Howard, J. A. K.; Puschmann, H. *J. Appl. Cryst.* **2009**, *42*, 339.

(92) Cambridge, Strucural Database (CSD), version 5.36 (Nov. 2014).

(93) Li, J. *Name Reactions for Carbocyclic Ring Formations*, John Wiley & Sons, Inc., New York, **2010**, p. 423.

# *Chapter 6*

# *The Crystal Structure, Spectroscopic Characterization, and Decomposition of an $\eta^2$-(N,N) Bound Nitrous Oxide Complex.*

## 6.1. Introduction

Nitrous Oxide ($N_2O$) is now recognized as the third most abundant greenhouse gas (approx. 300 ppb) behind $CO_2$ (~400 ppm) and $CH_4$ (1800 ppb) resultant of its increased production from anthropogenic sources.[1-3] The increases in atmospheric $N_2O$ have proven difficult for the global nitrification and de-nitrification mechanisms to balance,[1,4] subsequently leading to deleterious effects on the atmospheric ozone concentrations.[5,6] Accordingly, nitrous oxide capture, subsequent activation and use as a potentially "green" oxidant with inorganic and organometallic systems are still prominent areas of study. However, despite the attractiveness of $N_2O$ as an oxidant its use is somewhat hampered due to the large thermodynamic stability. Break down of $N_2O$ into its constituents, $N_2$ and $O_2$, is not operable in the absence of catalysts until elevated temperatures (~400 ˚C) (*7*), and this thermodynamic stability is only exasperated by an energy of activation of ~59 kcals/mol.[8] Nevertheless, the thermodynamic oxidizing power of $N_2O$ in the presence of many transition metal based systems has been documented.[7,9,10] Activation of $N_2O$ generally proceeds via extrusion of $N_{2(g)}$ and invokes the formation of reactive metal–oxo species that go on to function as potent oxidants. Conversely, functionalization by direct insertion into M–C or M–H bonds has also been

documented,[11-17] in addition, to one case where N-N bond-sission was operative to deliver nitric oxide (NO) and transition metal nitrides.[18,19]

Despite the use of nitrous oxide as an oxidant under thermodynamic conditions, the kinetic activation of $N_2O$ remains difficult. On account of its low diploe (0.161 D) and its poor σ-donnor/π-acceptor qualities,[9,20,21] the binding and subsequent functionalization of $N_2O$ by transition metal complexes remains a significant challenge in organometallic chemistry. To date the coordination of an unsupported nitrous oxide ligand to transition metal centers is sparse. Armor and Taube first to reported the preparation of $[Ru(NH_3)_5(N_2O)]^+$, however, the thermal instability of $[Ru(NH_3)_5(N_2O)]^+$ precluded its isolation in the solid state,[22] but was later shown computationally to favor a $\kappa^1$–(N)–bound coordination mode of the $N_2O$ ligand.[23,24] To our knowledge there are only two other discrete examples of transition metal nitrous oxide adducts.[25,26] The most recent from Chang and co-workers in 2011, $(tpa^{Mes})V(N_2O)$ ($tpa^{Mes}$ = Tri-mesityl-tris(pyrrolylmethyl)amine), is the only structurally authenticated transition metal $N_2O$ complex which features an $\kappa^1$–*N* coordination mode resultant of $N_2O$ coordination to a lewis-acidic vanadium center via $\sigma$–donation into the V $d_z^2$ orbital and only weak $\pi$–backdonation from the degenerate V $d_{xz}$ and and $d_{yz}$ orbitals to the $N_2O$ $\pi^*$ manifold.[26]

Our group has previously shown the success in utilizing sterically encumbering *m*-terphenyl isocyanides (CNR) as ligand platforms for the generation of reactive transition metal species capable of a number of novel reactivity patterns.[27-30] Herein we report the use of the dinitrogen stabilized Cp*Co(CNR) fragment $Cp^*Co^*(N_2)(CNAr^{Tripp2})$ (**1**) ($Ar^{Tripp2}$ = 2,6-Bis-(2,4,6- triisopropylphenyl)phenyl) as a platform for the generation of the fist $\eta^2$-(*N,N*) bound nitrous oxide transition metal

complex upon direct complexation of $N_2O_{(g)}$. In addition to the solid-state structure determination, we present spectroscopic and computational evidence for an $\eta^2$-(*N-N)* coordination mode for the nitrous oxide ligand. $\eta^2$-(*N-N)* coordination is feasible through σ-donation from $N_2O$ in to the LUMO of the Cp*CoL fragment, while tandemly employing the electron rich Co center to engage in π-bonding into the $N_2O$ π* manifold. Insight into the mechanism of $N_2O$ activation is presented via two competing yet spectrocopically distinct pathways: oxygen atom transfer to the isocyanide ligand to afford organic isocyanate, and H-atom abstraction to afford the hydroxide complex Cp*Co(OH)($CNAr^{Tripp2}$), and 1,2,3,4-tetramethylcyclopentadienylfulvene.

### 6.2. Attempted Oxygen-Atom-Transfer to Phosphines.

Previously we reported the generation of Cp*Co($N_2$)($CNAr^{Dipp2}$) (2,6-(2,6-(*i*-Pr)$_2C_6H_3)_2C_6H_3$ however it was unstable to $N_2$ release resulting in decomposition of the ligand framework. We reasoned the incorporation of the more encumbering *m*-terphenyl substituent –$Ar^{Tripp2}$ (2,6-(2,4,6-(*i*-Pr)$_3C_6H_3)_2C_6H_3$) would provide added stability.[32] Under analogues conditions to our previous report smooth conversion to Cp*Co($N_2$)($CNAr^{Tripp2}$) (**1**) was achieved via $KC_8$ reduction of the diiodide precursor Cp*Co$I_2$($CNAr^{Tripp2}$).[31] With Cp*Co($N_2$)($CNAr^{Tripp2}$) (**1**) in hand, and having access to a stable precursor capable of delivering an equivalent of Cp*Co($CNAr^{Tripp2}$) for small molecule activation, we targeted the activation of $N_2O_{(g)}$ in an effort to access facile OAT. Addition of $N_2O$ at room temperature followed by addition of one equivalent of tri-phenyl phosphine ($PPh_3$) only afforded the corresponding phosphine oxide, O=$PPh_3$, in low conversions, < 35%, as assayed via $^{31}P\{^1H\}$ NMR. Analysis of the crude reaction

mixture found that the other major constituents of the reaction mixture consisted of $OCNAr^{Tripp2}$ (**2**), and $Cp^*Co(PPh_3)(CNAr^{Tripp2})$ (**3**) as assayed by $^1H$ NMR spectroscopy. In attempt to deduce whether nitrous oxide activation was occurring in the absence of phosphine,[33] addition of $N_2O$ to a room temperature $C_6D_6$ solution of $Cp^*Co(N_2)(CNAr^{Tripp2})$ (**1**), showed quick conversion (*ca.* 15 mins) to afford primarily the organic isocyanate $OCNAr^{Tripp2}$ (**2**) as assayed by $^1H$ NMR spectroscopy and solution FTIR ($C_6H_6$) with the observation of a strong blue shifted stretch at 2242 $cm^{-1}$ corresponding to the *ν*(OCN) stretching mode.

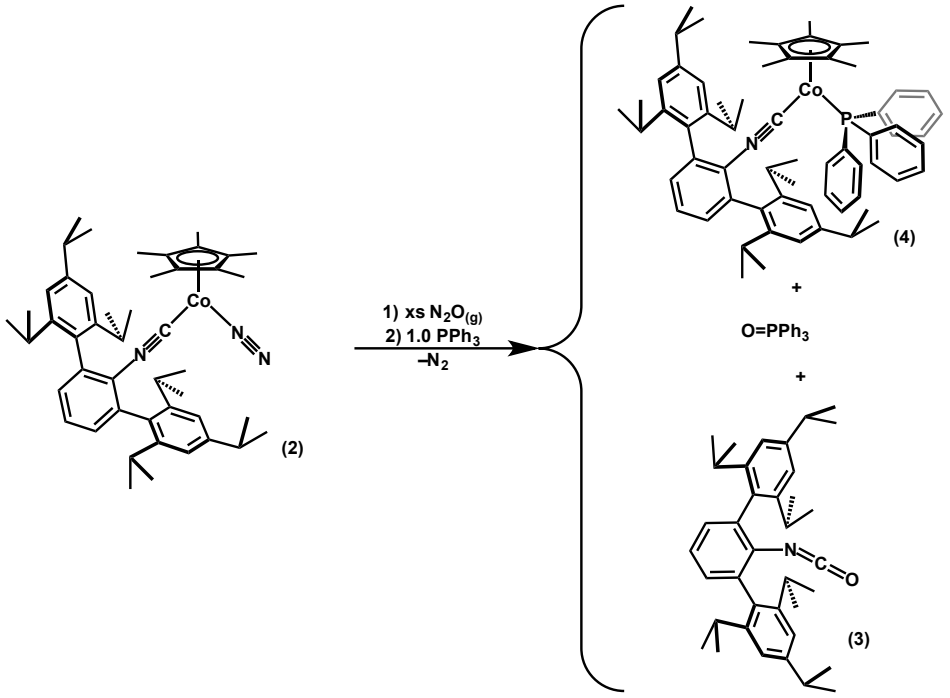


**Scheme 6.1.** Reaction scheme depicing the product distribution from the attempted OAT from $N_2O$ to $PPh_3$ mediated by $Cp^*Co(N_2)(CNAr^{Tripp2})$.

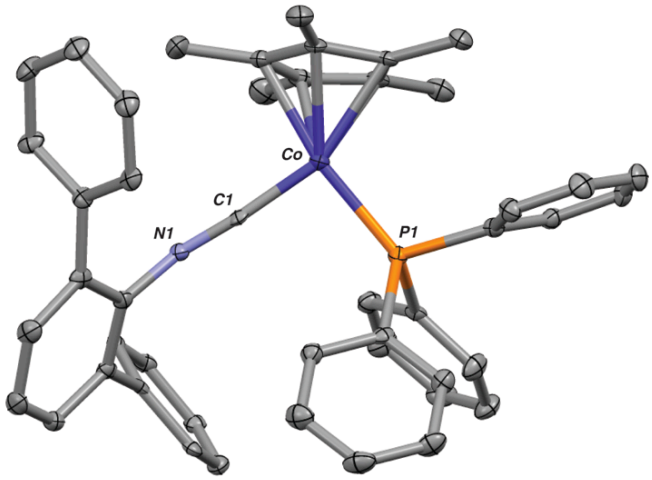


**Figure 6.1.** Molecular structure of Cp*Co(PPh$_3$)CNAr$^{Tripp2}$ (**3**). Hydrogen atoms and flanking *i*-Pr groups omitted for clarity. Selected bond distances (Å): $Co_1$-$P_1$ = 2.1472(10), $Co_1$-$C_1$ = 1.738(4), $C_1$-$N_1$ = 1.204(4). Selected bond angles (˚): $C_1$-$N_1$-$C_2$ = 151.5(3).

## 6.3. Reactivity of Cp*Co(N$_2$)(CNAr$^{Tripp2}$) with N$_2$O.

Placement of a Tol-$d^8$ solution of Cp*Co(N$_2$)(CNAr$^{Tripp2}$) (**1**) under an N$_2$O atmosphere at -78 ˚C using a J-Young's resalable NMR tube, followed by rapid injection into a pre-cooled NMR spectrometer, indicated slow conversion to a new diamagnetic product that features shifted *i*-Pr septets with respect to complex **1** upon warming to -25 ˚C, Figure 6.2-5. Addition of N$_2$O to Cp*Co(N$_2$)(CNAr$^{Tripp2}$) (**1**) in Et$_2$O at –78˚C followed by warming to –25 ˚C and crystallization at –40 ˚C under an $N_{2(g)}$ atmosphere afforded yellow/orange X-ray diffraction quality crystals that were determined to be Cp*Co(N$_2$O)(CNAr$^{Tripp2}$) (**4**), Scheme 6.2., Figure 6.6.A. Complex **4** crystalizes in the orthorhombic space group *Pbca*, and displays an intact Cp*Co(CNR) fragment engaging in $\eta^2$-coordination to an N$_2$O unit. The solid-state structure exhibits positional disorder of the terminal E-atom which models most accurately as two O-atoms each at ½ occupancy.

Attempts to model the electron density with dinitrogen as a compositional component proved to inaccurately model the electron density about Co. The bond distances of coordinated $N_2O$ are shown in Figure 6.8.B. Comparison to free $N_2O$ to the $N_2O$ unit coordinated in complex **4** displays substantially elongated N–N, and N–O bonds suggestive that the electron rich Cp*Co(CNR) fragments participates in a substantial degree of $\pi$-donation into the $N_2O$ $\pi^*$ system. Comparison of the two coordinated E-atoms displays a significantly shorter bond length, 1.212(7) Å, when compared to the coordinated $\eta^2$-(*N,O*) linkage in the *o*-tolyl-nitrosobenzene complex Cp*Co($\eta^2$-*N,O*-*o*-$CH_3$-$C_6H_4$NO)$CNAr^{Tripp2}$ (**5,** Figure 6.7) at 1.371(3) Å, which provides a comparison to $\eta^2$–(*N-O*) single bond distance in coordinated nitroxide linkages.[27,34] However, due to the difficulty of distinguishing small atom constituents (*i.e.* O and N) via X-ray diffraction definitive assessment of the coordination mode is not entirely possible based on purely crystallographic characterization.

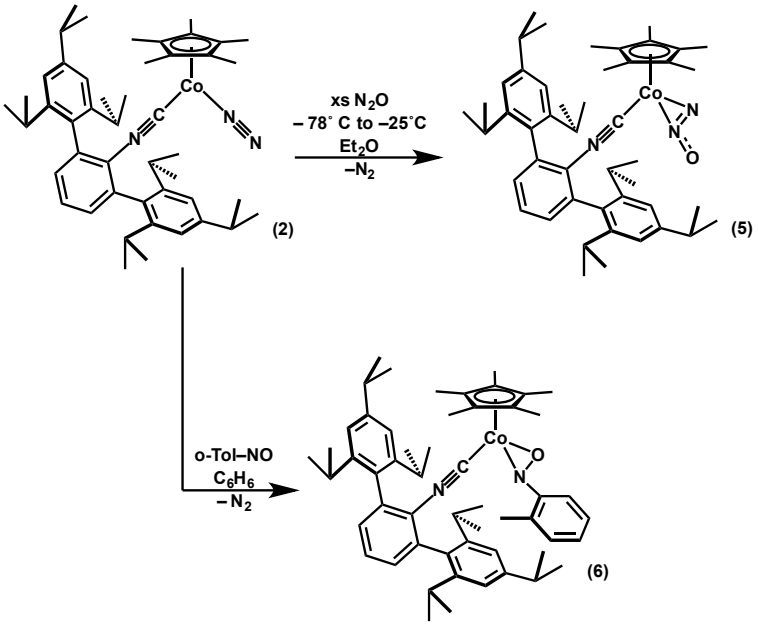


**Scheme 6.2.** Reaction scheme for the synthesis of Cp*Co($\eta^2$-*N,N*-$N_2O$)($CNAr^{Tripp2}$) (**5**), and Cp*Co($\eta^2$-*N,O*-*o*-$CH_3$-$C_6H_4$NO)$CNAr^{Tripp2}$ (**6**).

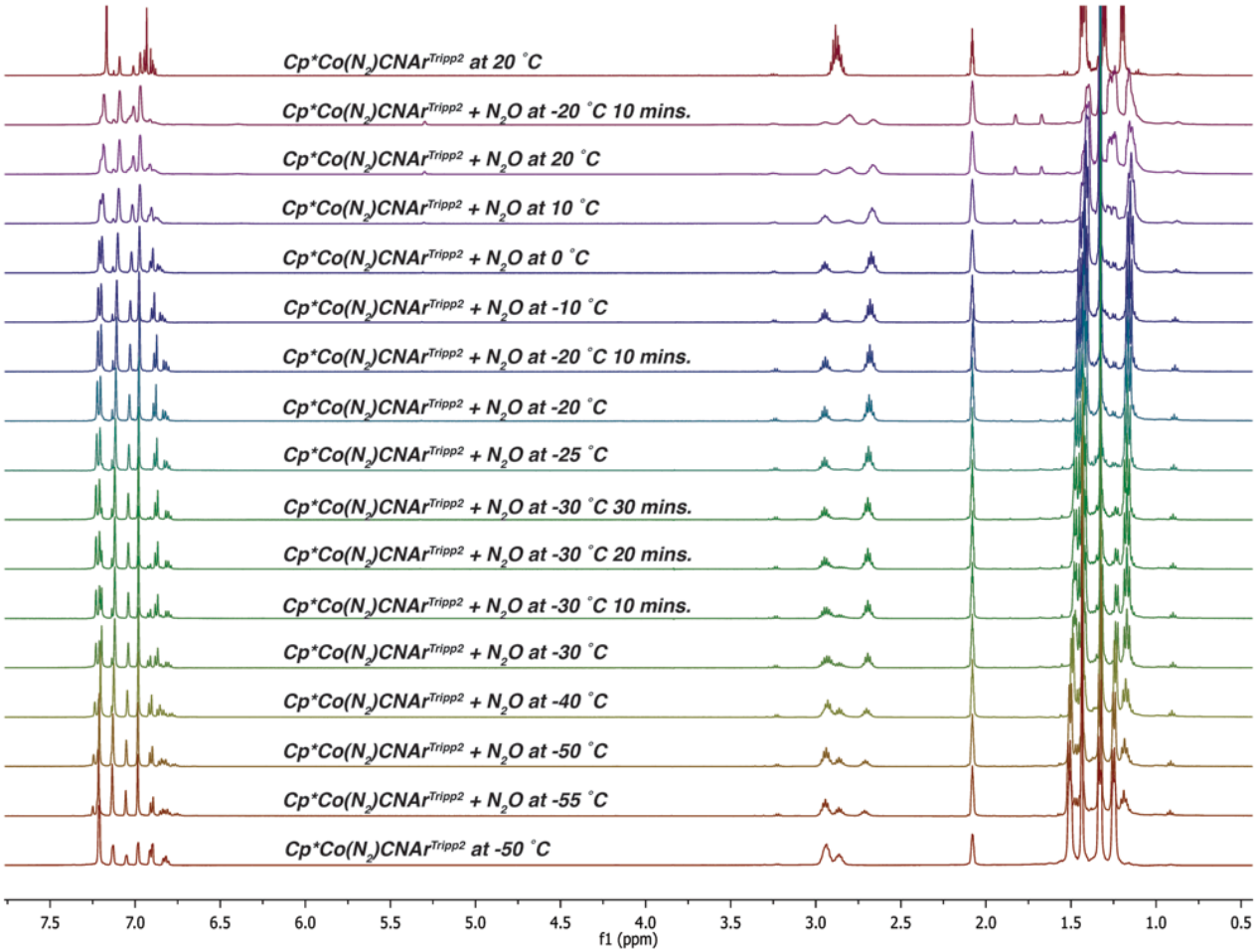


**Figure 6.2** Full variable temperature $^{1}$H NMR (499.8 MHz, Tol-$d^8$) of the generation of Cp*Co($\eta^2$-*N,N*-$N_2O$)CNAr$^{Tripp2}$. Note the top, and bottom spectrum depicts the starting material (Cp*Co($N_2$)CNAr$^{Tripp2}$) in Tol-$d^8$ at 20 ˚C, and -55 ˚C respectfully.

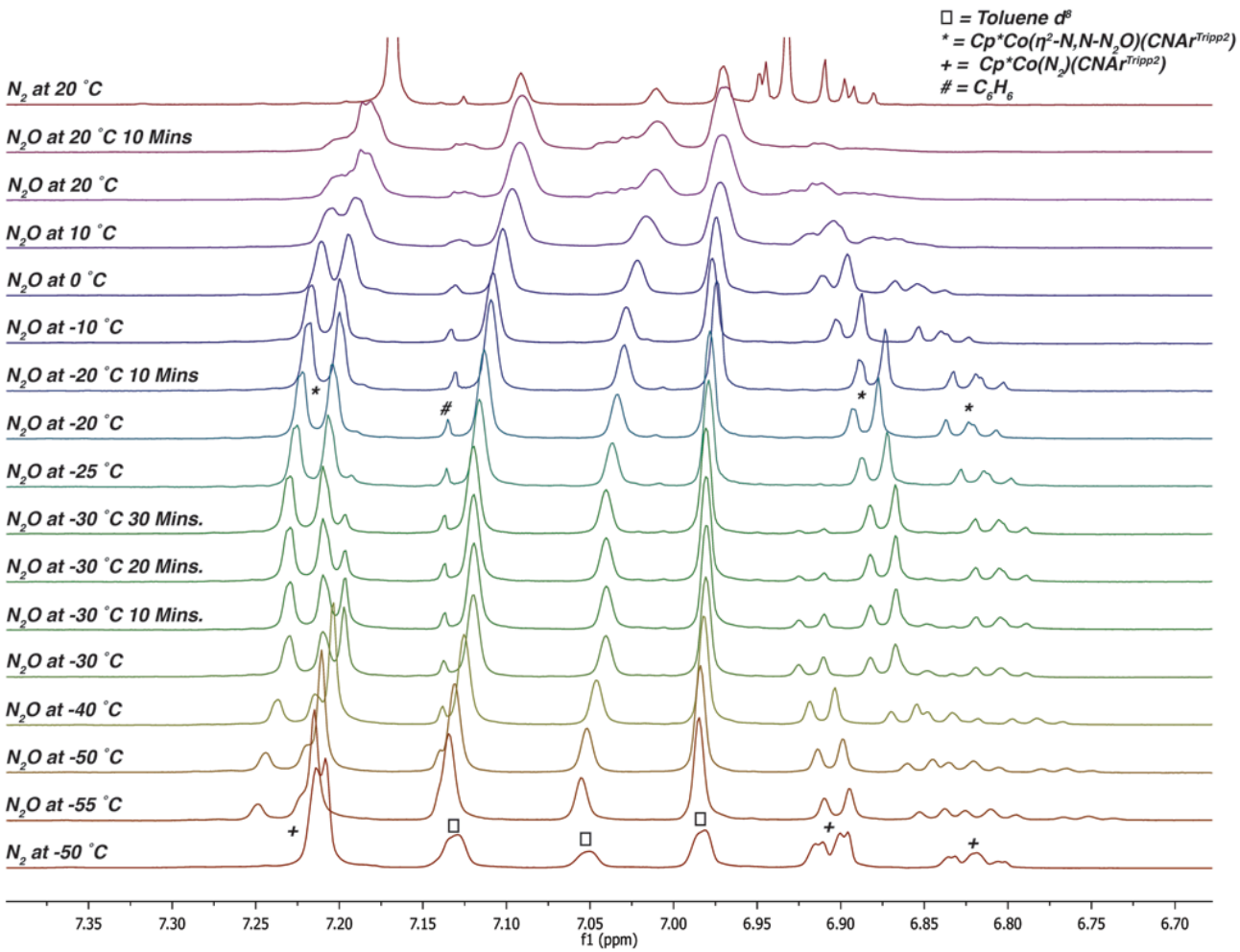


**Figure 6.3** Zoomed in variable temperature $^{1}$H NMR (499.8 MHz, Tol-$d^{8}$) of the generation of Cp*Co($\eta^{2}$-*N,N*-$N_2O$)CNAr$^{Tripp2}$ focused at the aromatic region. Note the top, and bottom spectrum depicts the starting material (Cp*Co($N_2$)CNAr$^{Tripp2}$) in at 20 ˚C, and -55 ˚C respectfully.

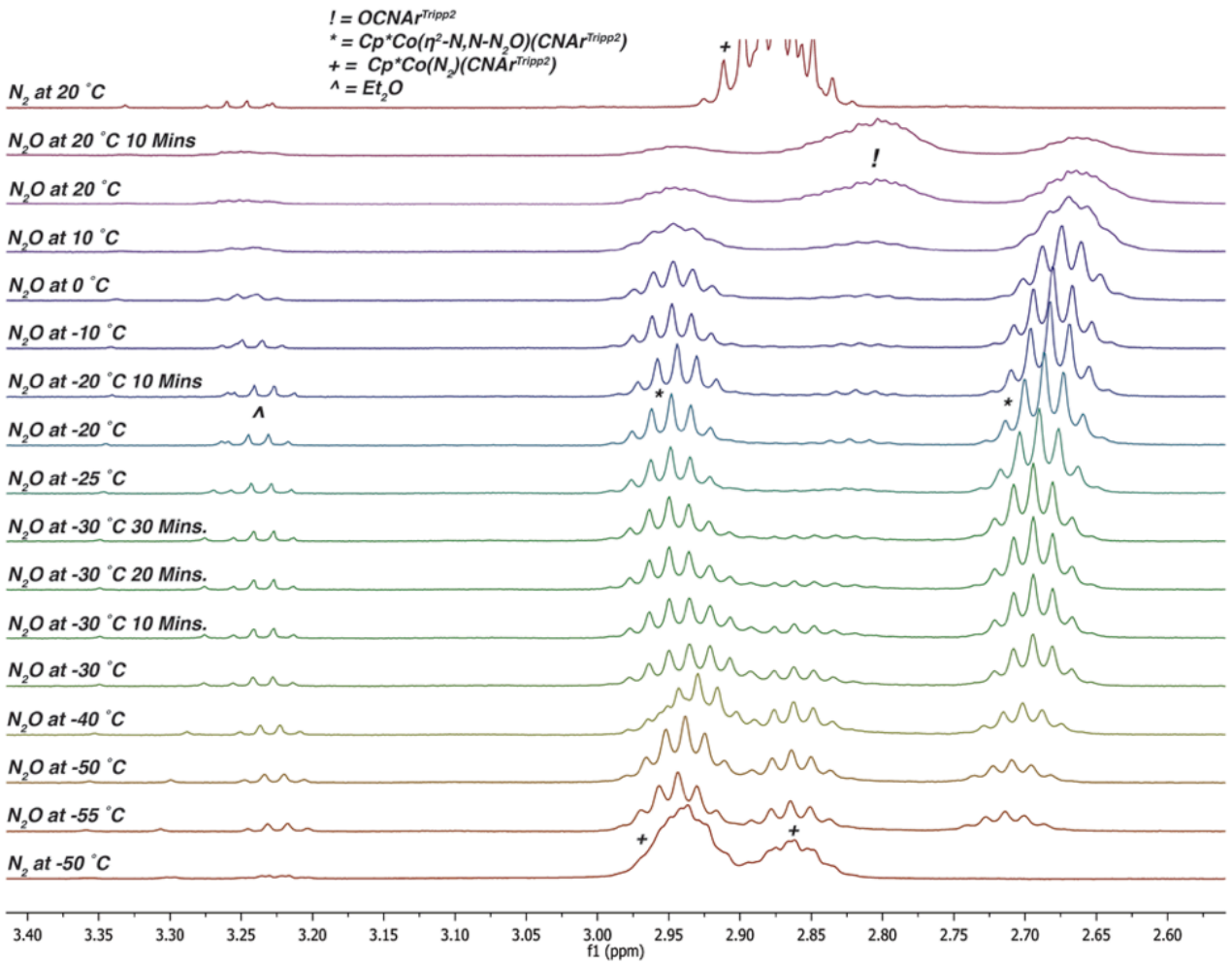


**Figure 6.4** Zoomed in variable temperature $^{1}$H NMR (499.8 MHz, Tol-$d^8$) of the generation of Cp*Co($\eta^2$-*N,N*-$N_2O$)CNAr$^{Tripp2}$ focused at the isopropyl methylene proton region ($CH(CH_3)_2$). Note the top, and bottom spectrum depicts the starting material (Cp*Co($N_2$)CNAr$^{Tripp2}$) in Tol-$d^8$ at 20 ˚C, and -55 ˚C respectfully. At ~10 ˚C the observation of a new septet at 2.80 ppm with is attributed to OCNAr$^{Tripp2}$.

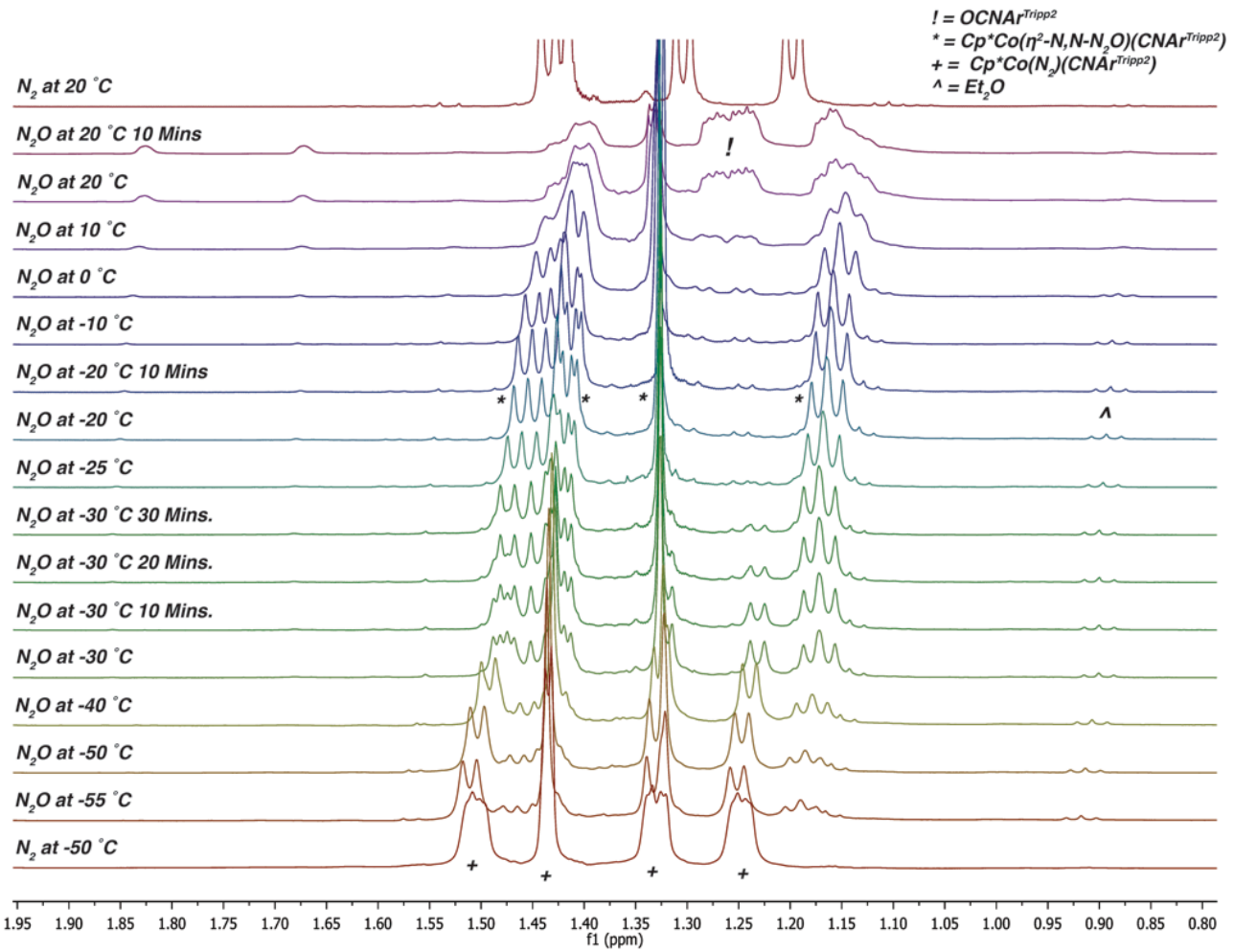


**Figure 6.5** Zoomed in variable temperature $^{1}$H NMR (499.8 MHz, Tol-$d^{8}$) spectrum of the generation of Cp*Co($\eta^{2}$-*N,N*-$N_2O$)CNAr$^{Tripp2}$ focused at the aliphatic proton region (CH(C$H_3$)$_2$). Note the top, and bottom spectrum depicts the starting material (Cp*Co($N_2$)CNAr$^{Tripp2}$) at 20 ˚C, and -55 ˚C respectfully.

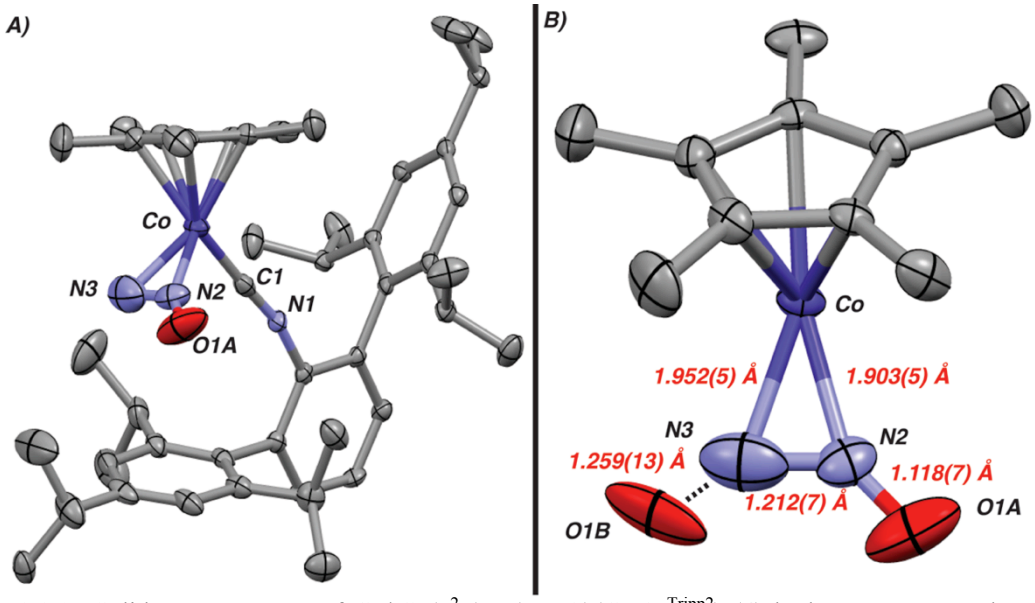


**Fig. 6.6 A)** Solid state structure of Cp*Co($\eta^2$-(*N,N*)-$N_2O$)($CNAr^{Tripp2}$) (**4**) hydrogen atoms and positional disorder of $N_2O$ omitted for clarity. **B)** Zoom in on $N_2O$ coordination to Cp*Co showing positional disorder of the oxygen atoms in $N_2O$. O1A and O1B are split and linked by the FVAR command, and modeled at 66.4% and 33.6 % respectively. No restraints or constraints have been used in the modeling of positional disorder found in the $N_2O$ unit. Hydrogen atoms and coordinated $CNAr^{Tripp2}$ have been removed for clarity.

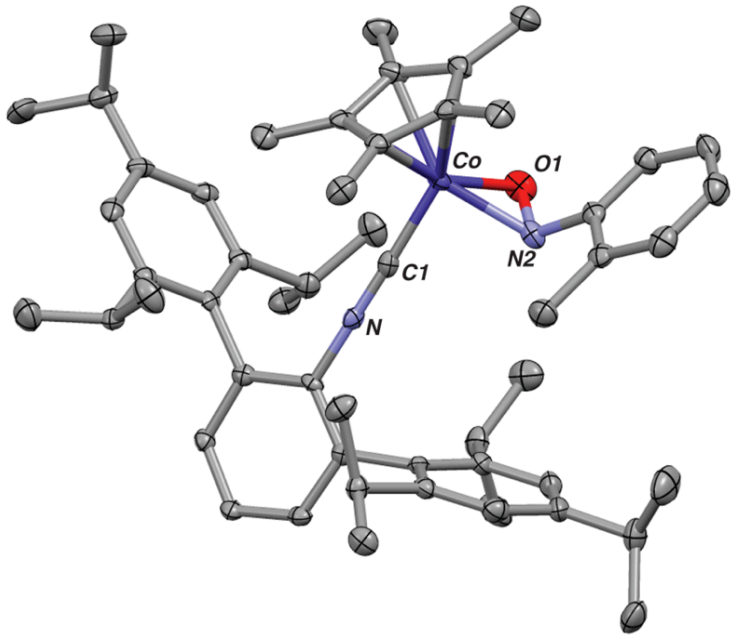


**Figure 6.7** Molecular structure of Cp*Co($\eta^2$-*N,O-o*-$CH_3$-$C_6H_4NO$)$CNAr^{Tripp2}$ (**5**). Hydrogen atoms and one molecule of $TMS_2O$ of solvation omitted for clarity. Selected bond distances (Å): Co-$C_1$ = 1.818(3), $C_1$-$N_1$ = 1.179(4), Co-$N_2$ = 1.945(3), Co-$O_1$ = 1.908(2), $N_2$-$O_1$ = 1.371(3). Selected bond angles (°): $C_1$-$N_1$-$C_2$ = 179.0(3), $O_1$-$N_2$-$C_{48}$ = 124.1(2).

To resolve the ambiguity between possible $\eta^2$-(*N,N*) and $\eta^2$-(*N,O*) coordination modes an $^{15}N$ NMR and in-situ FTIR analysis of the product using $^{15}N$ $N_2O$ were undertaken. Solution FTIR measurements for complex **4** are shown in Figure 6.8-11. Use of either $^{14}N$ or $^{15}N$ $N_2O$ display a strong band at 2095 $cm^{-1}$ which we assign to the *v*(CN) stretch of the isocyanide. This assignment is corroborated using $^{15}N_2O$ where no blue shift is observed for the peak at 2095 $cm^{-1}$. Moreover, upon isotopic labeling with $^{15}N_2O$, the bands related to the various stretching and bending vibrations of $N_2O$ can be discerned. Importantly vibrational frequency calculations of geometry optimized structures (B3LYP, (def2-TZ2P)/(def2-TZVP/J)) of both $\eta^2$-(*N,N),* $\eta^2$-(*N,O*) Cp*Co($N_2O$)(CNXyly) show good correlation with $\eta^2$-*N,N* coordination mode, Figure 6.8. It is critical to note that the major band found in the simulated IR spectrum for $\eta^2$–(*N,O*) Cp*Co($N_2O$)(CNXyly) results from an admixture of both C–N and N–N stretching modes associated with CNXyly and $N_2O$ respectively, and that resonance would be subject to a red-shift upon $^{15}N$ enrichment, which is not observed. Moreover, generation of **$^{15}N_2O$-4** followed by analysis via $^{15}N\{^1H\}$ NMR shows two $^{15}N$ doublets at -49 ppm and -198 ppm associated with the O-$^{15}N$, and $^{15}N$-$^{15}N$ resonances respectively, that feature $^{15}N$ coupling of 17 Hz respectively, Figure 6.12. These resonances display a substantial shift from free $N_2O_{(g)}$ observed at –138, and –222 ppm. These data coupled with the $\eta^2$-(*N,N)* isomer lying a calculated 10.3 kcals lower in energy then the $\eta^2$-(*N,O)* isomer present a compelling argument that the structural assignments are consistent with $\eta^2$-(*N,N)* coordination to Co (structural comparisons between experimental and computed bond metrics are tabulated in Table 6.1).

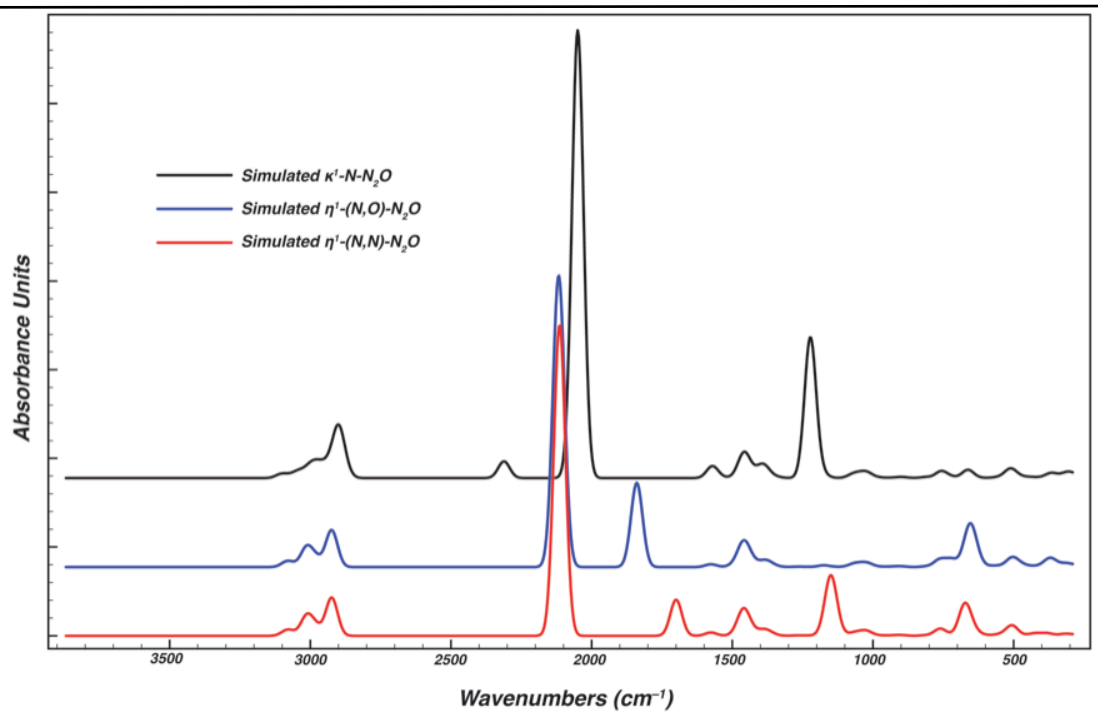


**Figure 6.8** Simulated absorbance FTIR spectrums of Cp*Co($\kappa^1$-*N*-$N_2O$)($CNAr^{Tripp2}$) (black), Cp*Co($\eta^2$-*N,N*-$N_2O$)($CNAr^{Tripp2}$) (red), and Cp*Co($\eta^2$-*N,O*-$N_2O$)($CNAr^{Tripp2}$) (blue). All IR spectrums have been scaled by 0.9671.[35]

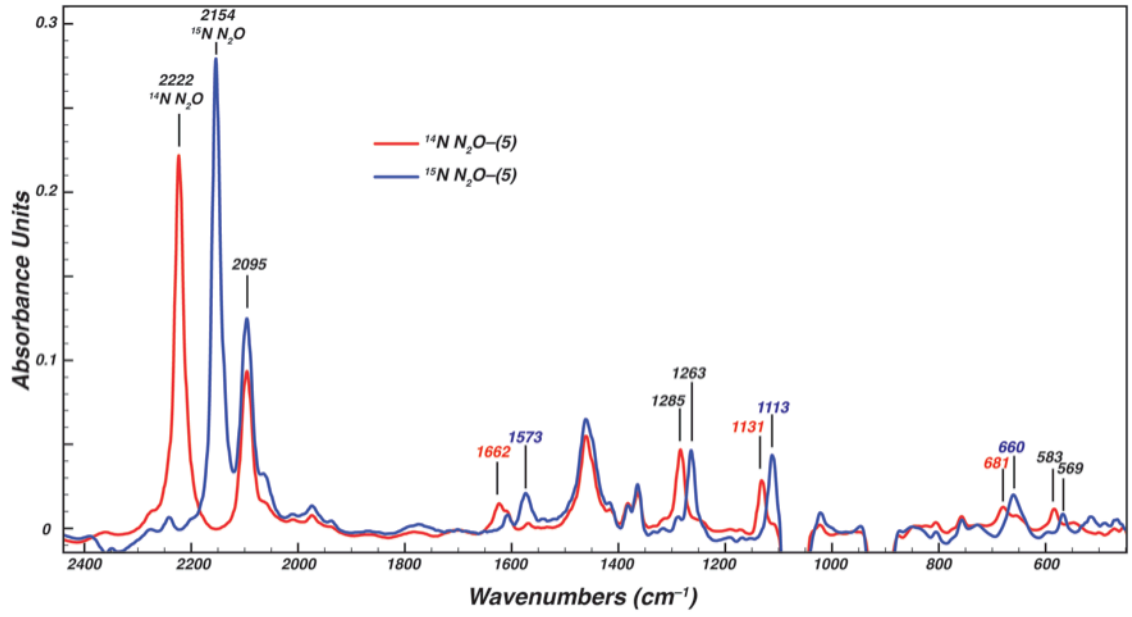


**Figure 6.9** Full baseline corrected absorbance FTIR spectrum in THF upon immediately warming to room temperature of Cp*Co($\eta^2$-($^{14}N,^{14}N$)-$N_2O$)$CNAr^{Tripp2}$ (Red) and Cp*Co($\eta^2$-($^{15}N,^{15}N$)-$N_2O$)$CNAr^{Tripp2}$ (Blue) denoting isotope sensitive vibrations and bends of the $N_2O$ ligand. Peaks denoted in black correspond to uncoordinated $N_2O$ gas.

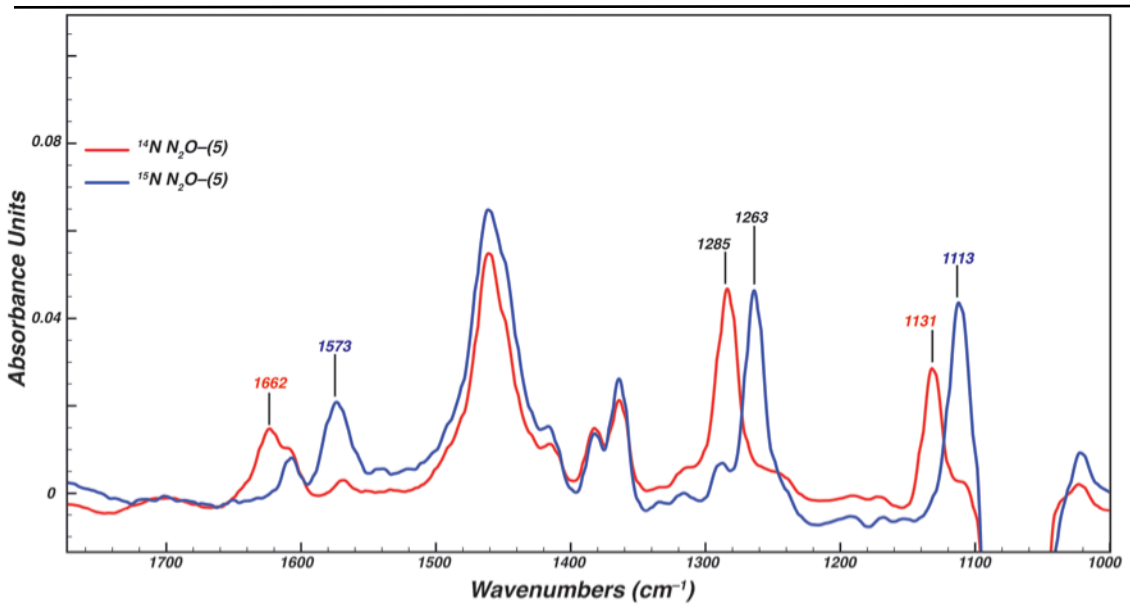


**Figure 6.10** Zoomed in baseline corrected absorbance FTIR spectrum in THF immediately warming to room temperature of Cp*Co($\eta^2$-($^{14}N,^{14}N$)-$N_2O$)CNAr$^{Tripp2}$ (Red) and Cp*Co($\eta^2$-($^{15}N,^{15}N$)_-$N_2O$)CNAr$^{Tripp2}$ (Blue) denoting isotope sensitive vibrations and bends of the $N_2O$ ligand. . Peaks denoted in black correspond to uncoordinated $N_2O$ gas.

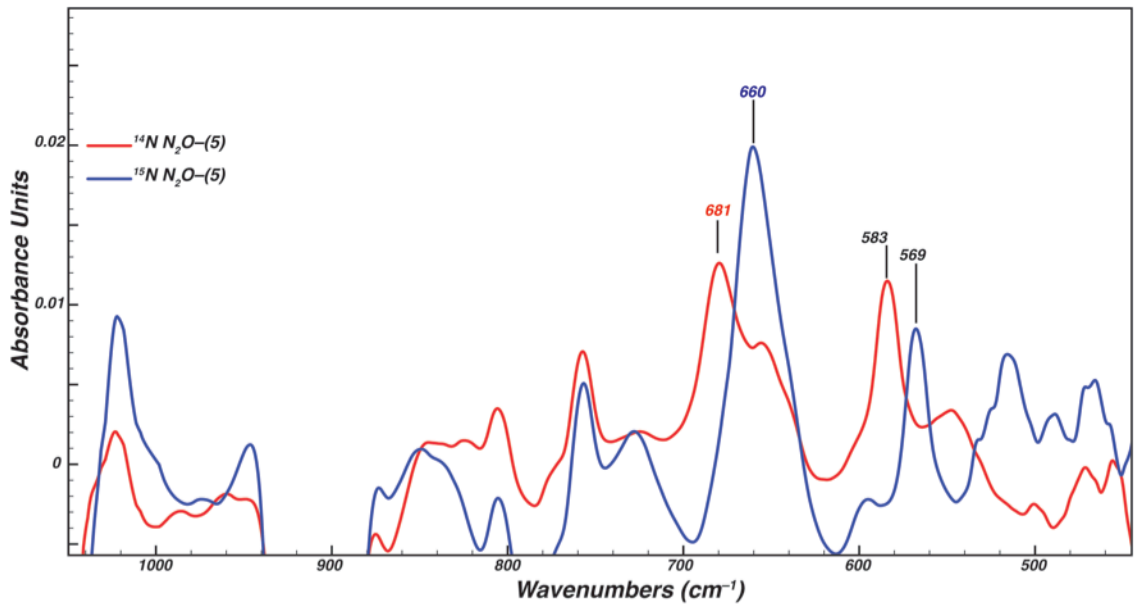


**Figure 6.11** Zoomed in baseline corrected absorbance FTIR spectrum in THF immediately warming to room temperature of Cp*Co($\eta^2$-($^{14}N,^{14}N$)-$N_2O$)CNAr$^{Tripp2}$ (Red) and Cp*Co($\eta^2$-($^{15}N,^{15}N$)-$N_2O$)CNAr$^{Tripp2}$ (Blue) denoting isotope sensitive vibrations and bends of the $N_2O$. Peaks denoted in black correspond to uncoordinated $N_2O$ gas.

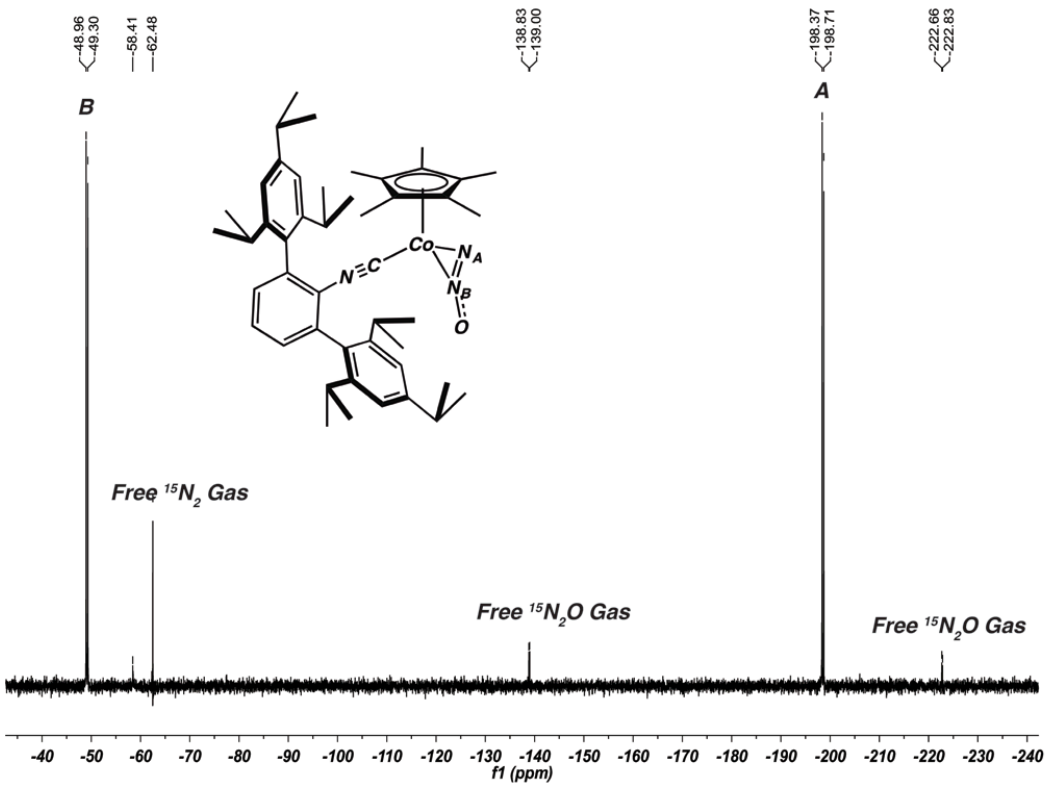


**Figure 6.12** $^{15}N\{^{1}H\}$ NMR spectrum (Tol-$d^8$, 50.7 MHz, -20 ˚C) of Cp*Co($\eta^2$-*N,N*-$^{15}N_2O$)CNAr$^{Tripp2}$ referenced to $CH_3NO$.

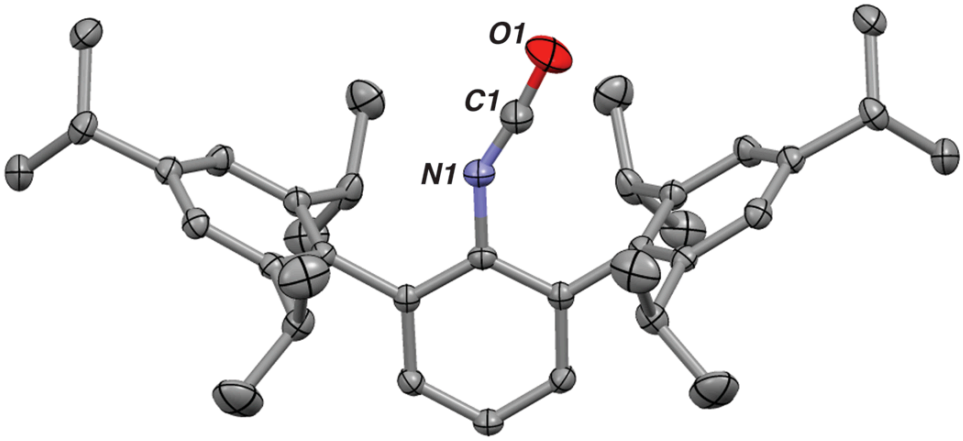


**Figure 6.13** Molecular structure of OCNAr$^{Tripp2}$ (**2**). Hydrogen atoms and positional disorder omitted for clarity. Selected bond distances (Å): $O_1$-$C_1$ = 1.172(4), $C_1$-$N_1$ = 1.1334(3. Selected bond angles (˚): $C_1$-$N_1$-$C_2$ = 146.27(16), $O_1$-$C_1$-$N_1$ = 174.0(3).

**Table 6.1** Comparison of experimental and computed structural features and vibrational energies of $(\eta^5\text{-Cp*})Co(\eta^2\text{-}N,N\text{-}N_2O)(CNAr^{Tripp2})$ (**5**), computed ($\eta^2$-*N,N*), computed ($\eta^2$-*N,O*) coordination modes and free $N_2O$.

| | **Complex 5: $\eta^2$–(N,N)** | Calculated $\eta^2$–(N,N) | Calculated $\eta^2$–(N,O) | $N_2O$ (exp.) | $N_2O$ (calc.) |
|---|---|---|---|---|---|
| $d$(Co–$E_1$) (Å) | 1.904(5) (Co–N2) | 1.983 | 1.9504 | – | – |
| $d$(Co–$E_2$) (A)° | 1.952(5) (Co–N3) | 1.8902 | 1.8973 | – | – |
| $d$($E_1$–$E_2$) (Å) | 1.212(8) (N2–N3)) | 1.1989 | 1.3581 | 1.128 (NN) | 1.121 |
| $d$($E_2$–$E_3$) (Å) | 1.12(1) (N2–O1A)/ 1.26(1) (N3–O1B) | 1.2347 | 1.1553 | 1.184 (NO) | 1.1831 |
| ∠($E_1$–$E_2$–$E_3$) (°) | 135.2(6) (O1A–N2–N3)/ 146.5(8) (O1B–N3–N2) | 142.56 | 139.15 | 180 | 179.98 |
| $\nu_1$ ($cm^{-1}$) | 1662 (1573)[b] | 1701 | 1840 | 2276 (2206)[b,c] | 2277 (2206)[b,c] |
| $\nu_2$ ($cm^{-1}$) | 1131 (1113)[b] | 1149 | 757 | 1300 (1280)[b,c] | 1299 (1280)[b,c] |
| $\nu_3$ ($cm^{-1}$) | 681 (660)[b] | 676 | 654 | 597 (579)[b,c] | 597 (579)[b,c] |

[a] All computed vibrational energies have been scaled by a factor of 0.9671.[8] [b] Values represent $^{15}N_2O$ vibrational frequencies. [c] Values are taken from Begun, G. M. and Fletcher, W. H. *j. Chem. Phys.* **1958**, *28,* 414-418.

**6.4. Decomposition of Cp*Co($\eta^2$-*N,N*-$N_2O$)($CNAr^{Tripp2}$).**

Warming of Cp*Co($\eta^2$-*N,N*-$N_2O$)($CNAr^{Tripp2}$) (**4**) to room temperature again affords the organic isocyanate $OCNAr^{Tripp2}$ (**2**), Figure 6.13, as the major diamagnetic *m*-terphenyl containing product as assayed by variable temperature $^1H$ NMR (Figure 6.14-17), and solution FTIR spectroscopy of the resultant reaction mixture. In an attempt to detect intermediate species the decomposition of Cp*Co($\eta^2$-(*N,N*)-$N_2O$)($CNAr^{Tripp2}$) (**4**) was monitored by in-situ FTIR (THF) spectroscopy, Figure 6.18. Additions of $N_2O$ at low temperature (*ca.* –25 ˚C) indicated clean conversion to complex **4** denoted by the isocyanide *v*(CN) stretch observed at 2095 $cm^{-1}$, Figure 6.19. Remarkably, in contrast to previously observed transition metal nitrous oxide species which are only stable under an $N_2O$ atmosphere,[22,25,26] Cp*Co($\eta^2$-*N,N*-$N_2O$)($CNAr^{Tripp2}$) (**4**) shows relatively robust stability at low temperatures in the absence of an $N_2O$ atmosphere. Cp*Co($\eta^2$-*N,N*-$N_2O$)($CNAr^{Tripp2}$) (**4**) is persistent in solution at low temperature (–25 ˚C) in the absence of an $N_2O_{(g)}$ atmosphere, from sparging with $Ar_{(g)}$, sparging with $N_{2(g)}$, and placement under brief vacuum with only minimal liberation of $N_2O_{(g)}$, Figure 6.19. Warming to room temperature indicated a new isocyanide *v*(CN) resonance at 2065 $cm^{-1}$ (THF) as a major byproduct of decomposition, Figure 6.19. FTIR spectroscopy on crystals grown from the resultant reaction mixture manifested the same isocyanide *v*(CN) resonance at 2065 $cm^{-1}$ (THF), which were unambiguously identified by X-ray diffraction as the hydroxide complex, Cp*Co(OH)($CNAr^{Tripp2}$) (**6**), Figure 6.20.

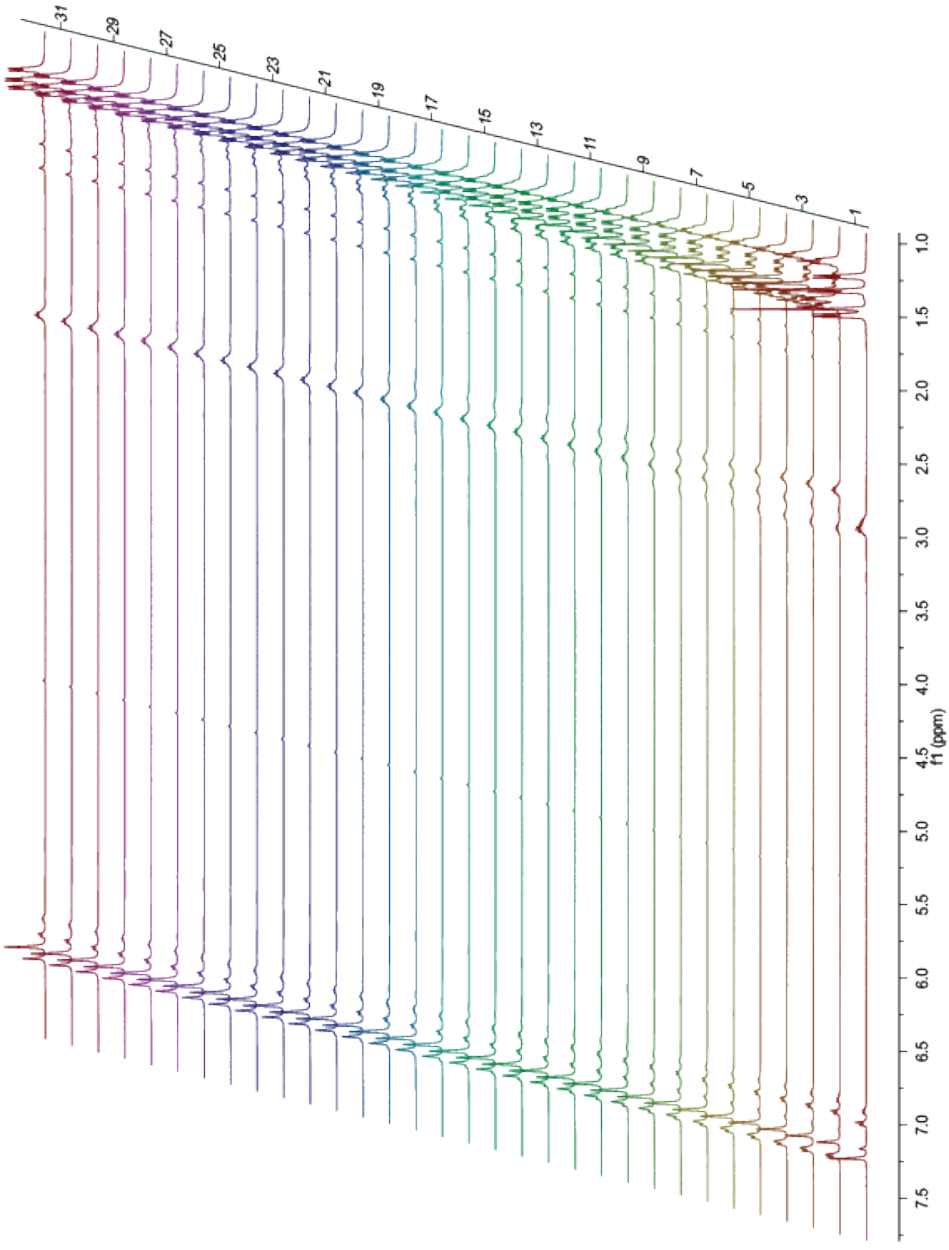


**Figure 6.14** Full $^{1}$H NMR (399.9 MHz, $C_6D_6$) of the generation of Cp*Co($\eta^2$-*N*,*N*-$N_2$O)CNAr$^{Tripp2}$ and subsequent decomposition. The bottom spectrum depicts the starting material (Cp*Co($N_2$)CNAr$^{Tripp2}$) in $C_6D_6$ at 22 ˚C.

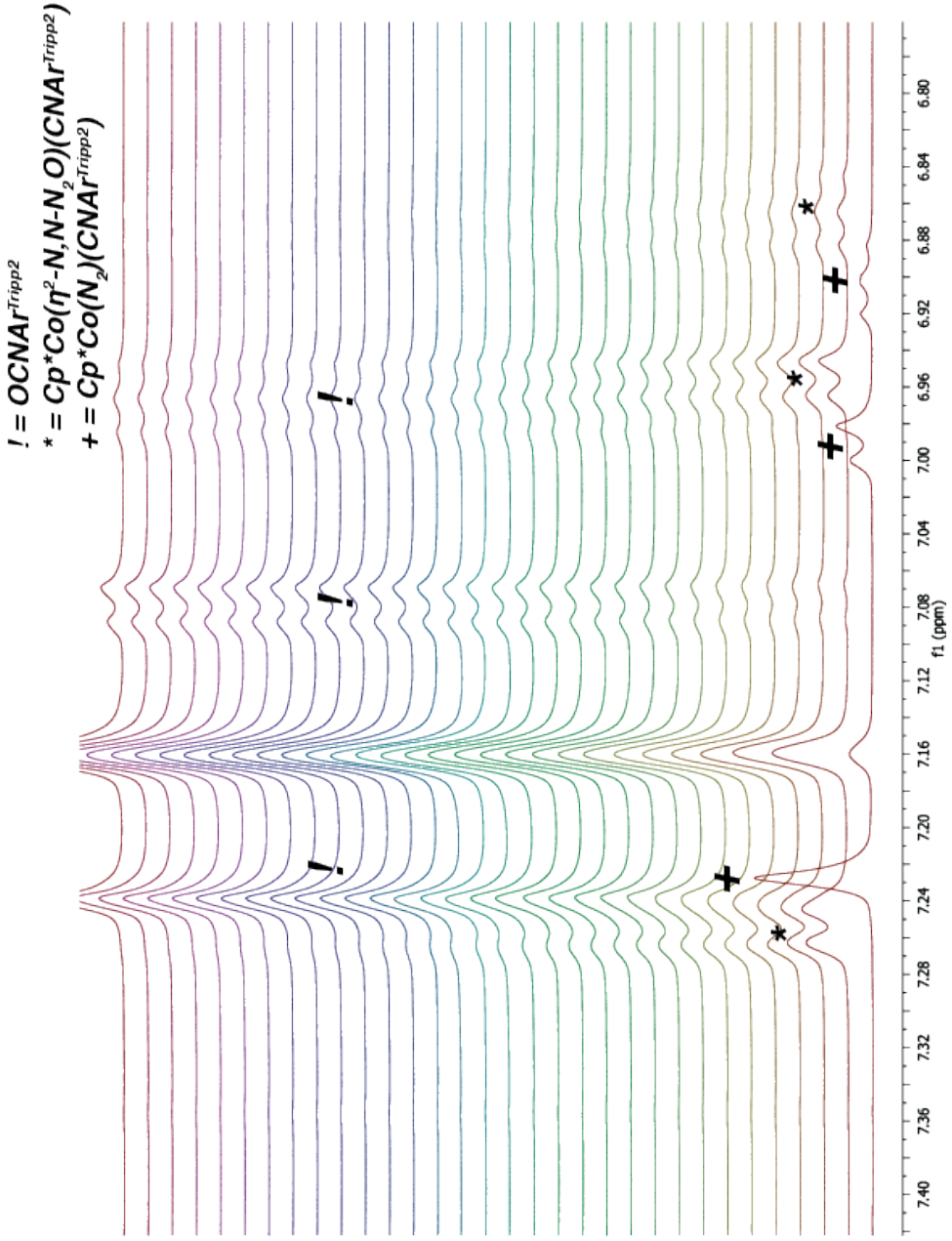


**Figure 6.15** Zoomed in room temperature $^{1}$H NMR (399.9 MHz, $C_6D_6$) of the generation of Cp*Co($\eta^2$-*N*,*N*-$N_2$O)CNAr$^{Tripp2}$ and subsequent decomposition to OCNAr$^{Tripp2}$ focused at the aromatic region. Note the bottom spectrum depicts the starting material (Cp*Co($N_2$)CNAr$^{Tripp2}$) in at 22 °C.

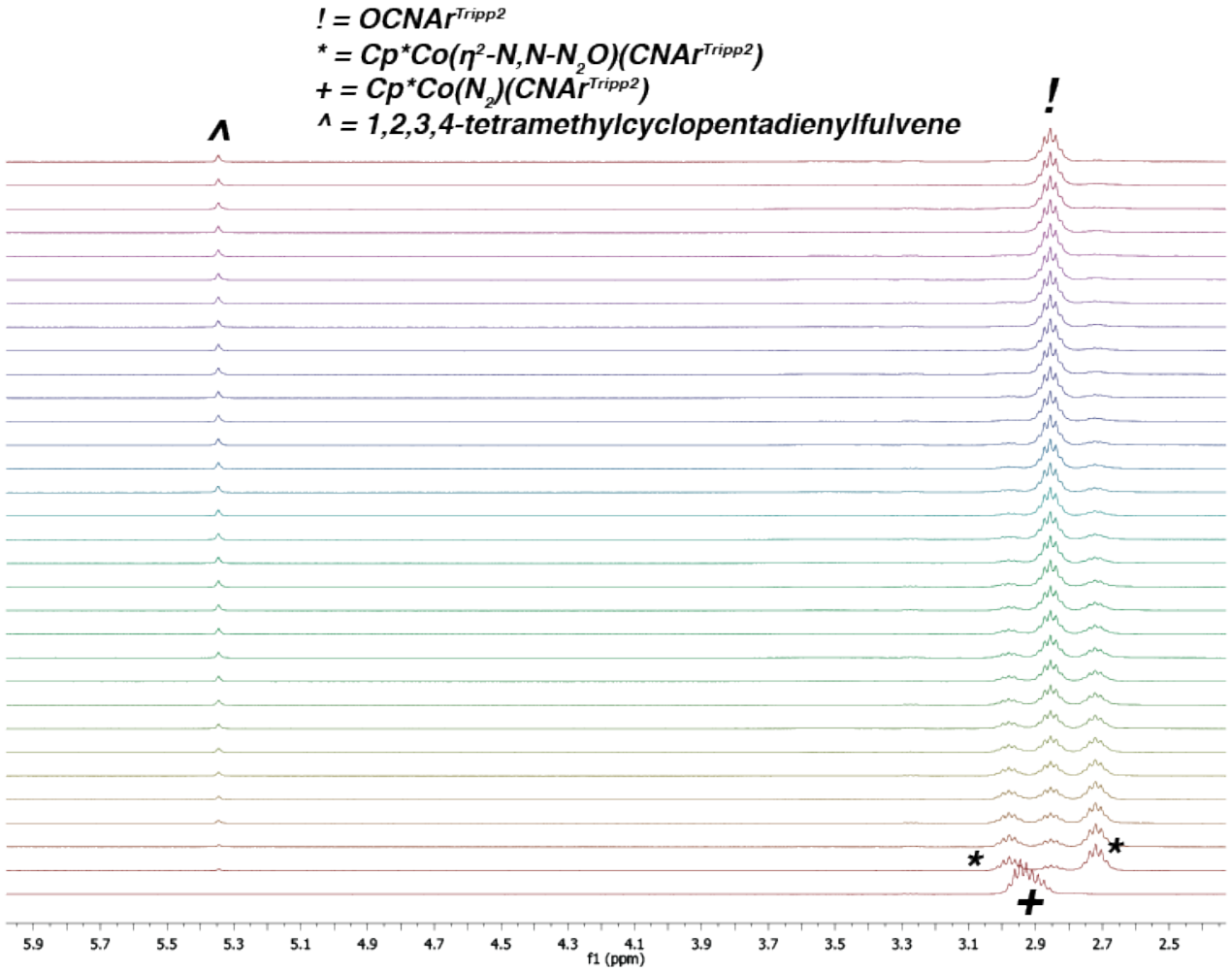


**Figure 6.16** Zoomed in room temperature $^{1}$H NMR (399.9 MHz, $C_6D_6$) of the generation of Cp*Co($\eta^2$-*N,N*-$N_2O$)CNAr$^{Tripp2}$ and subsequent decomposition to OCNAr$^{Tripp2}$ focused at 2.0-5.9 ppm. Note the bottom spectrum depicts the starting material (Cp*Co($N_2$)CNAr$^{Tripp2}$) in at 22 ˚C. The singlet at 5.31 ppm indicates formation of 1,2,3,4-tetramenthylcyclopentadienylfulvene.[36]

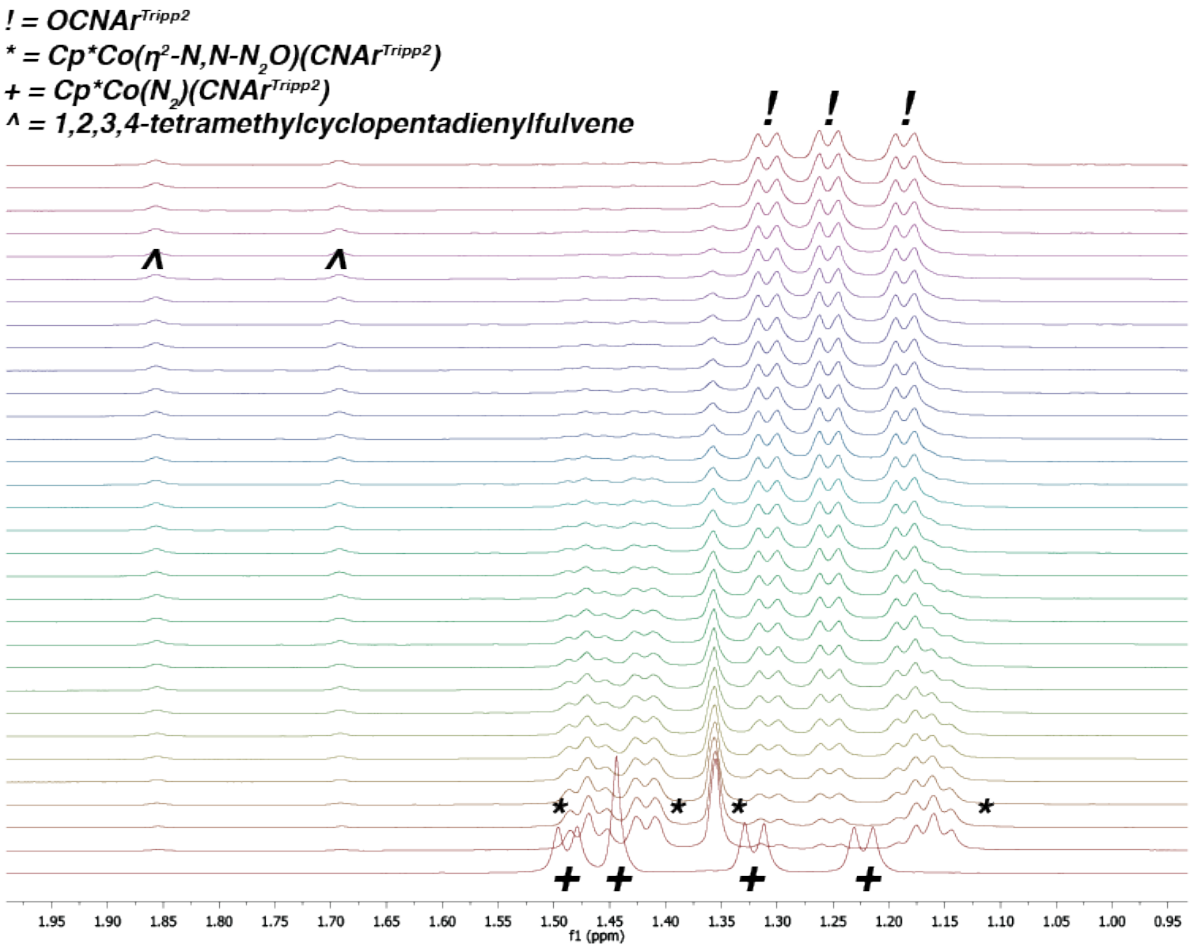


**Figure 6.17** Zoomed in room temperature $^{1}$H NMR (399.9 MHz, $C_6D_6$) of the generation of Cp*Co($\eta^2$-*N,N*-$N_2O$)CNAr$^{Tripp2}$ and subsequent decomposition to OCNAr$^{Tripp2}$ focused at 0.95-1.95 ppm. Note the bottom spectrum depicts the starting material (Cp*Co($N_2$)CNAr$^{Tripp2}$) in at 22 ˚C. The singlet at 1.70 and 1.85 ppm indicates formation of 1,2,3,4-tetramenthylcyclopentadienylfulvene.[36]

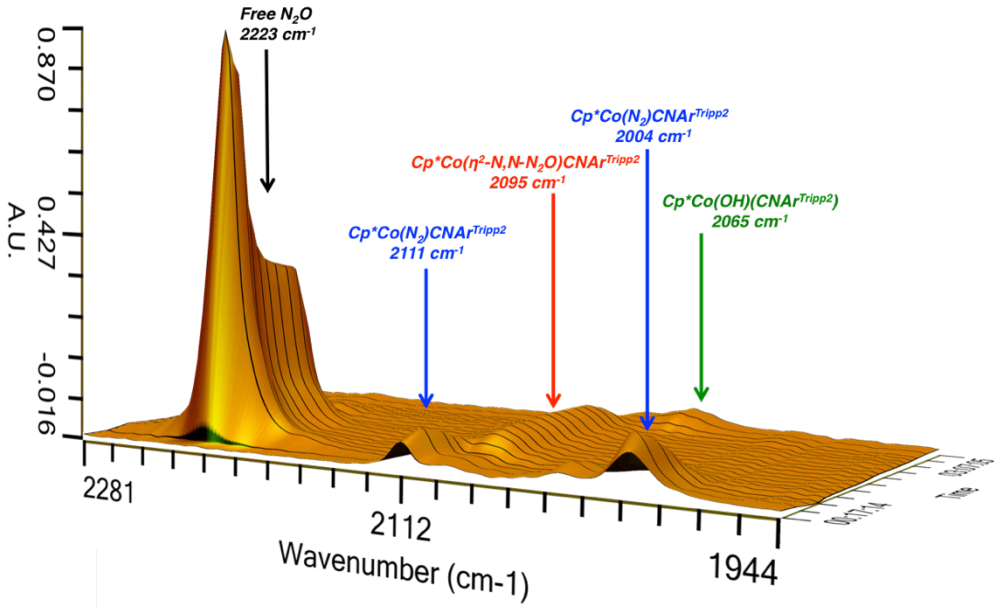


**Figure 6.18** React-IR FTIR spectrum v. Time (THF, -25 ˚C - 22 ˚C) depicting the *in situ* formation of Cp*Co($\eta^2$-*N,N*-$N_2O$)CNAr$^{Tripp2}$ and subsequent decomposition to Cp*Co(OH)(CNAr$^{Tripp2}$) upon sparging with $Ar_{(g)}$ and warming to room temperature.

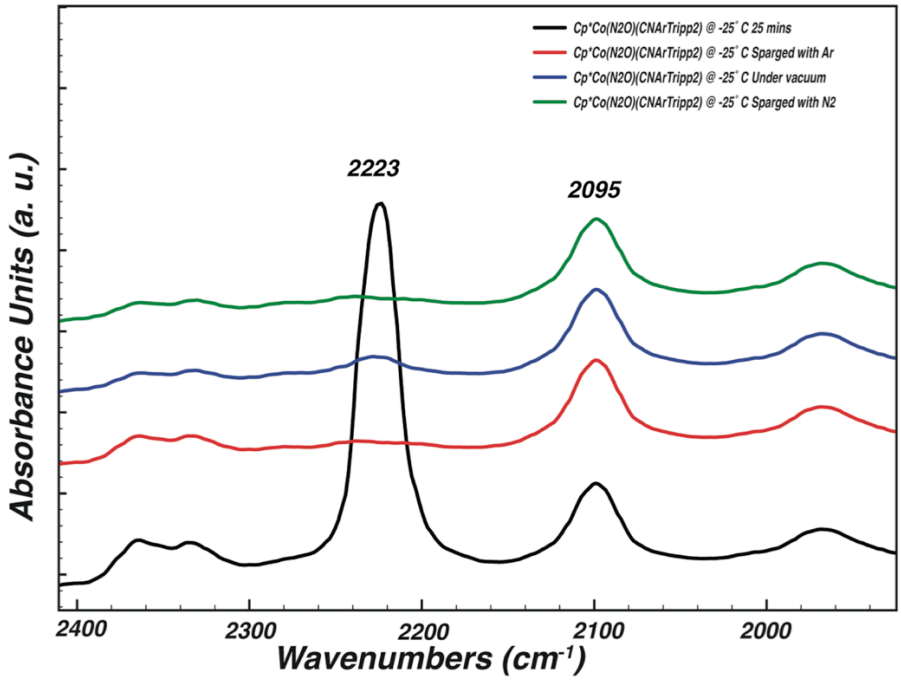


**Figure 6.19** *In situ* solution FTIR (THF -25 ˚C) depicting the generation of Cp*Co($\eta^2$-*N,N*-$N_2O$)CNAr$^{Tripp2}$ (black), and the stability under an $Ar_{(g)}$ atmosphere (Red), post exposure to vacuum (Blue), and exposure to a $N_{2(g)}$ atmosphere.

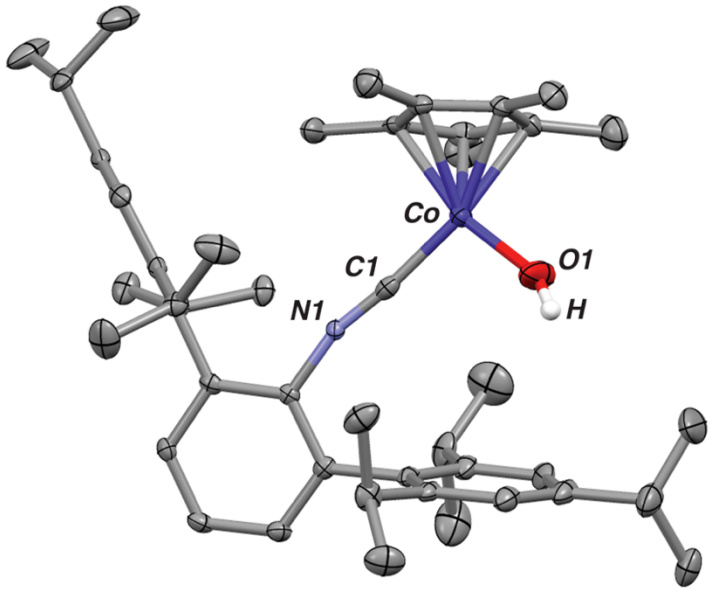


**Figure 6.20** Molecular structure of Cp*Co(OH)(CNAr$^{Tripp2}$) (**6**). Hydrogen atoms and positional disorder omitted for clarity. Selected bond distances (Å): $O_1$-$C_1$ = 1.172(4), $C_1$-$N_1$ = 1.1334(3. Selected bond angles (˚): $C_1$-$N_1$-$C_2$ = 146.27(16), $O_1$-$C_1$-$N_1$ = 174.0(3).

Decomposition of Cp*Co($\eta^2$-*N,N*-$N_2O$)(CNAr$^{Tripp2}$) (**4**) poses an interesting opportunity to investigate the mechanistic pathway that affords OCNAr$^{Tripp2}$ (**2**), and Cp*Co(OH)(CNAr$^{Tripp2}$) (**7**). Analysis of the product distribution by FTIR spectroscopy from reactions done in $C_6D_6$, $C_6H_6$, THF, THF-$d^8$, Toluene, Tol-$d^8$, and *n*-hexane indicate that formation of OCNAr$^{Tripp2}$ (**2**) to be the predominant byproduct of decomposition of (**4**). Moreover, analyses of the resultant absorbance concentration distributions via FTIR spectroscopy suggest that a percent composition of the decomposition mixture, OCNAr$^{Tripp2}$ (**2**) and Cp*Co(OH)(CNAr$^{Tripp2}$ (**6**), which maintains constant despite solvent choice. Additionally analysis via $^{15}N\{^1H\}$ NMR spectroscopy with $^{15}N_2O$ indicated formation of $^{15}N_{2(g)}$ at –62 ppm[42] suggesting extrusion of $N_{2(g)}$ from the isotopically enriched $^{15}N_2O$ upon activation, Figure 6.12. In attempt to pinpoint the origin of hydrogen affording Cp*Co(OH)(CNAr$^{Tripp2}$) (**6**). $^1H$ NMR spectroscopy was used to assess the decomposition mixture in the aforementioned solvents and in all cases

formation of 1,2,3,4-tetramethylcylopentadienylfulvene was observed as a byproduct of decomposition. Figure 6.14-17 show a representative distribution of NMR active species from the decomposition of Cp*Co($\eta^2$-*N,N*-$N_2O$)($CNAr^{Tripp2}$) (**4**) at room-temperature over the course of 1 hour including 1,2,3,4-tetramenthylcyclopentadienylfulvene.[37] The activation of Cp* ligands via radical H–atom abstraction has been observed form early transition metal and lanthanide species, to generate 1,2,3,4-tetramethylcyclopentadienylfulvene, suggesting that this could be a possible mechanism of activation.[38,39] Generation of Cp*Co($\eta^2$-*N,N*-$N_2O$)($CNAr^{Tripp2}$) (**4**) followed by addition of 9,10-dihydroanthracene (DAH) as an H• source did not indicate conversion to anthracene as assayed by $^1$H NMR spectroscopy, however, significant fulvene formation was still observed.

We hypothesize that decomposition of Cp*Co($\eta^2$-*N,N*-$N_2O$)($CNAr^{Tripp2}$) (**4**) could potentially proceeds through two distinct mechanistic pathways Scheme 6.3. The first could potentially be direct insertion of $N_2O$ in the coordinated isocyanide followed by $N_2$ extrusion, pathway 1 (Scheme 6.3), however this does not account for the observation of Cp*Co(OH)($CNAr^{Tripp2}$) and 1,2,3,4,-tetramethylcyclopentadienylfulvene. The second potential mechanism could involve the liberation of $N_2$ to afford a fleeting Co-oxyl. The resulting Co-oxyl could then have two potential modes of reactivity: pathway 2A (Scheme 6.3) results in oxygen atom insertion into coordinated isocyanide to afford $OCNAr^{Tripp2}$. Additionally generation of a fleeting Co-oxyl could lead to intermolecular H-atom abstraction from a second equivalent of [Cp*Co] providing Cp*Co(OH)($CNAr^{Tripp2}$) (**7**), 1,2,3,4-tetramenthylcyclopentadienylfulvene, and some unidentified residual [Co] species (Pathway 2B, Scheme 6.3). Rational for this could be

that intramoleculer O-atom transfer occurs fast to generate isocyanate and H–atom abstraction is slow as a result from being an intermolecular process (no intramolecular HAT is observed), thus favoring isocyante formation versus hydroxide as the major byproduct.

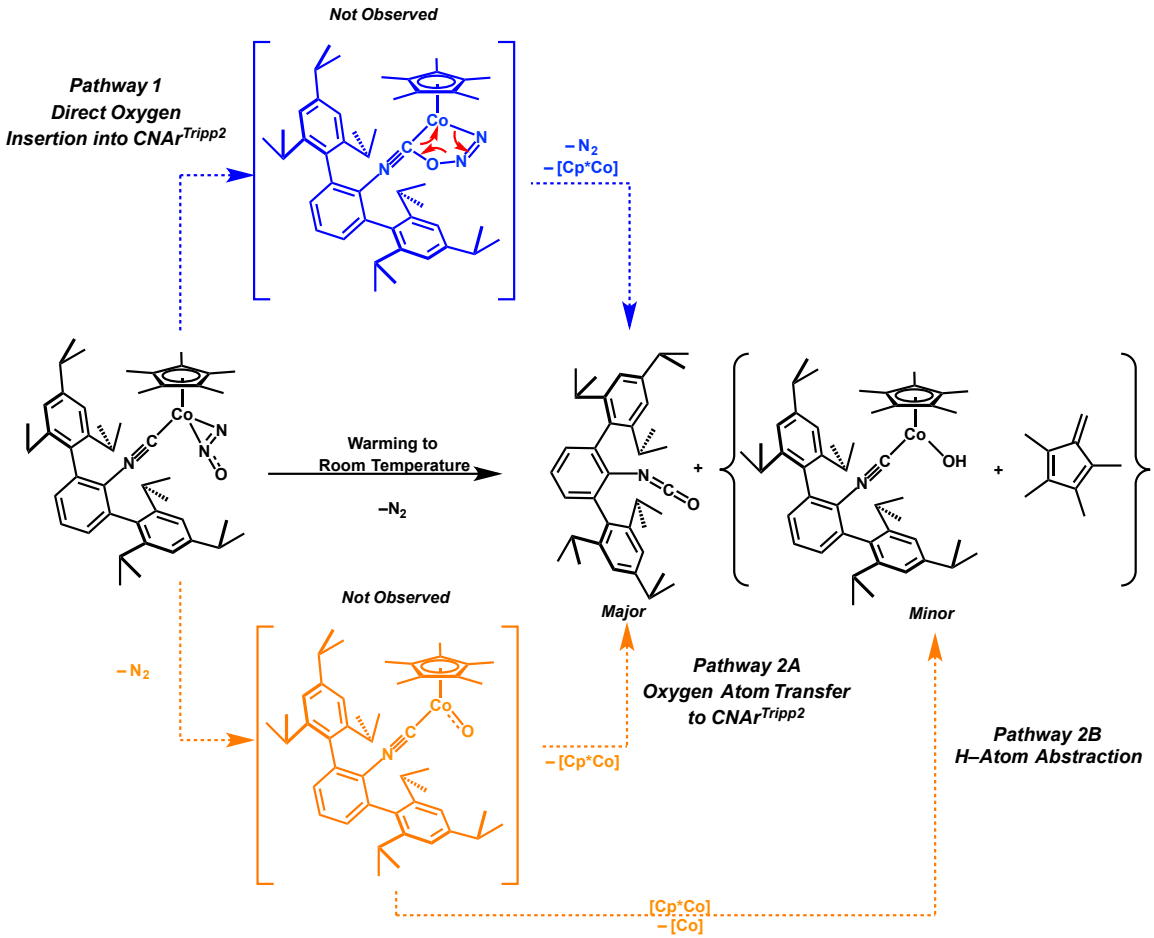


**Scheme 6.3** Possible decomposition pathways for Cp*Co($\eta^2$-*N,N*-$N_2O$)($CNAr^{Tripp2}$) (**5**) to afford $OCNAr^{Tripp2}$ (**5**), Cp*Co(OH)($CNAr^{Tripp2}$) (**7**), and 1,2,3,4-tetramethylcyclopentadienylfulvene (detected by $^1$H NMR Spectroscopy).

## 7.5. Concluding Remarks.

In conclusion, Cp*Co($N_2$)($CNAr^{Tripp2}$) (**1**) presents a unique platform to explore the coordination and activation of $N_2O$. Accordingly this electron rich platform functions as an effective means for the stabilization of a $\eta^2$-(*N,N*) transition metal $N_2O$ adduct,

Cp*Co($\eta^2$-*N,N*-$N_2O$)$CNAr^{Tripp2}$ (**4**), that is stabilized via π-donation to the π* manifold located on $N_2O$. The use of DFT in conjunction with solution spectroscopy featuring $^{15}N$ isotopic labeling studies provides good evidence for $\eta^2$-(*N,N)* coordination versus $\eta^2$-(*N,O)* coordination of $N_2O$. Complex **4** is shown to decompose to afford the organic isocyante $OCNAr^{Tripp2}$ (**3**), Cp*Co(OH)($CNAr^{Tripp2}$) (**6**), and 1,2,3,4-tetramethycyclopentadienylfulvene. We favor a decomposition mechanism that progresses through a fleeting Co-oxo species which displays both OAT reactivity in addition to the capability to perform H-atom abstraction of the Cp*–*Me* group. A more in-depth understanding of the mechanisms of oxygen atom transfer and decomposition of Cp*Co($\eta^2$-*N,N*-$N_2O$)$CNAr^{Tripp2}$ (**4**) are on going in our laboratory.

**7.6 Synthetic Procedures and Characterization Data.**

**General Considerations:** All manipulations were carried out under an atmosphere of dry dinitrogen or Argon using standard schlenk, and glove box techniques. Solvents were dried and degassed according to standard procedures.[40] Unless otherwise stated all materials were obtained from commercial vendors and used as received or purified by standard procedures.[41] Benzene-$d_6$ and Toluene-$d_8$ were dried with Na/K and Benzophenone followed by distillation and stored on 4 Å molecular sieves for 3 days prior to use. Celite 405 (Fischer Scientific) was dried under vacuum for 24 hours at a temperature greater then 250° C and stored inside the glove box prior to use. $^{15}N_2O$ (99.2%) was purchased from ICON Stable Isotopes and used as received. $KC_8$ was prepared according to published procedures.[42] The *m*-terphenyl isocyanide $CNAr^{Tripp2}$,[43]

and $Cp^*CoI_2(CO)$[44] were prepared according to literature procedures. For the synthesis and characterization of $Cp^*Co(N_2)(CNAr^{Tripp2})$ the reader is referred to Chapter 6.3.

Solution $^1H$, $^{13}C\{^1H\}$, and $^{15}N$ NMR spectra were recorded on a Varian Mercury 400 spectrometer, a Bruker Advance 300 spectrometer, a Varian XSENS-500 spectrometer, and a Joel ECA 500 spectrometer. $^1H$, and $^{13}C$ chemical shifts are reported in ppm relative to $SiMe_4$ ($^1H$ and $^{13}C$ $\delta$ = 0.0 ppm) with reference to residual solvent references of 7.16 ppm ($^1H$) and 128.06 ppm ($^{13}C$) for benzene–$d_6$[5], and 2.08 ppm ($^1H$), and 20.4 ppm ($^{13}C$) for cyclohexane-$d^{12}$. $^{15}N$ chemical shifts were externally referenced to $(^{15}NH_4)_2SO_4$ and calibrated to $CH_3{}^{15}NO$ (0 ppm).[45] $^{31}P$ chemical shifts were externally referenced to 85% $H_3PO_4$. FTIR spectra were recorded on a Thermo-Nicolet iS10 FTIR spectrometer. Samples were prepared either as KBr pellets, or a $C_6D_6$, solution injected into a Thermo Fischer solution cell equipped with KBr windows. For solution FTIR spectra, solvent peaks were digitally subtracted from all spectra by comparisons with an authentic spectrum obtained immediately prior to that of the sample. *In situ* FTIR measurements were recorded with a Metler Toledo ReactIR 45M utilizing a SiComp tipped probe. *In situ* FTIR spectra, solvent peaks were digitally subtracted from all spectra by comparisons with an authentic spectrum obtained immediately prior to that of the sample. *In situ* FTIR spectra were prepared as solutions with a concentration of 0.05 M or higher to maximize signal to noise. The following abbreviations were used for the intensities and characteristic of important IR absorption bands: vs = very strong, s = strong, m = medium, w = weak, vw = very weak, b = broad, vb = very broad, sh = shoulder. Combustion analyses were performed by Midwest Microlab LLC, Indianapolis, IN

**$^1$H NMR Spectroscopy Cp*Co($N_2$)CNAr$^{Tripp2}$ (1) in Tol-$d_8$:** $^1$H NMR (400.1 MHz, Tol-$d_8$, 20 ˚C): 7.17 (s, 4H, *m*-Tripp), 6.93 (multip, 3H, *m/p*-Ph), 2.88 (multip, 6H, C*H*($CH_3$)$_2$), 1.44 (d, 12H, 7Hz, CH(C*H*$_3$)$_2$), 1.41 (s, 15H, Cp*-*H*), 1.30 (d, 12H, 7Hz, CH(C*H*$_3$)$_2$), 1.20 (d, 12H, 7Hz, CH(C*H*$_3$)$_2$).

**Independent Synthesis OCNAr$^{Tripp2}$ (2):** The isocyanate (OCNR) was prepared according to a modified literature procedure.[46] Under an intert atmosphere a $CH_2Cl_2$ solution (4 mL) containing DMSO (27 μL, 0.388 mmoles, 1.1 equiv) was added CNAr$^{Tripp2}$ (0.200 g, 0.352, 1 equiv) as a solid. The reaction mixture was then cooled to -60˚ C and allowed to equilibrate for 10 minutes where upon Trifluroaceticanhydride (0.004 g, 0.018 mmoles, 5 mol %) was added all at once. The reaction was then allowed to warm to room temperature and react for 2 hours where upon a color change from colorless to yellow was observed. The resulting reaction mixture was then concentrated to a solid using rotary evaporation and then passed through a plug of Silica and eluted with a 3% EtOAc/Hexanes solution, which was then concentrated to a solid to afford OCNAr$^{Tripp2}$ as a white solid 0.180 g, 0.344 mmoles, 89%. $^1$H NMR (499.9 MHz, Tol-$d_8$, -20 ˚C): 7.22 (s, 2H, *m*-Tripp), 7.20 (s, 2H *m*-Tripp), 6.88 (d, 2H, 7 Hz, *m*-Ph), 6.82 (t, 1H, 7 Hz, *p*-Ph), 2.94 (sept., 2H, 7 Hz, C*H*($CH_3$)$_2$), 2.70 (sept., 4H, 7 Hz, C*H*($CH_3$)$_2$), 1.46 (d, 6H, 7Hz, CH(C*H*$_3$)$_2$), 1.43 (d, 6H, 7Hz, CH(C*H*$_3$)$_2$), 1.41 (dd, 12H, 5Hz, 3Hz, CH(C*H*$_3$)$_2$) 1.32 (s, 15H, Cp*-*H*), 1.16 (t, 12H, 7Hz, CH(C*H*$_3$)$_2$). $^{13}$C{$^1$H} NMR (125.8 MHz, $C_6D_6$, -20 ˚C): δ = 149.8, 147.3, 137.2, 134.3, 133.6, 130.0, 127.1, 125.3 (O=*C*=N), 121.4, 34.9, 31.3, 24.7, 24.3, 24.1 ppm. FTIR ($C_6H_6$; KBr Window; 20 ˚C): $\nu_{OCN}$ = 2278

(m), 2242 (s), also 2963 (m), 2929 (w), 2869 (w), 1605 (w), 1566 (w), 1433 (w), 1384 (w), 1364 (w), 1073 (w), 879 (w), 860 (w), 803 (w), 758 (w), 522 (w) $cm^{-1}$. HRMS (ESI-APCI-TOF, pos. ion; MeCN) *m/z* calcd for $[C_{37}H_{50}NOH]^+$: 534.3887. Found for $[C_{37}H_{50}NOH]^+$: 524.3883, δ = -0.8.

**$^1$H NMR Spectroscopy of OCNAr$^{Tripp2}$ (2) in Tol-$d_8$:** $^1$H NMR (499.9 MHz, Tol-$d_8$, 20 ˚C): 7.19 (s, 4H, *m*-Tripp), 7.03 (d, 2H, 8Hz, *m*-Ph), 6.96 (t, 1H, 8 Hz, *p*-Ph), 2.80 (sept., 6H, 7 Hz, C*H*$(CH_3)_2$), 1.28 (d, 12H, 7Hz, CH(C*H*$_3)_2$), 1.25 (d, 12H, 7Hz, CH(C*H*$_3)_2$), 1.17 (d, 12H, 7Hz, CH(C*H*$_3)_2$). $^{13}$C{$^1$H} NMR (125.8 MHz, Tol-$d_8$, 20 ˚C): δ = 149.6, 147.2, 137.2, 134.3, 133.6, 130.0, 127.0 (O=*C*=N), 121.3, 121.2, 34.9, 31.3, 24.6, 24.3, 24.1 ppm.

**Solution FTIR Spectroscopy of OCNAr$^{Tripp2}$ (2) in Toluene:** FTIR (Toluene; KBr Window; 20 ˚C): $\nu_{OCN}$ = 2276 (m), 2241 (s), also 1394 (w), 1385 (w), 1363 (w), 1239 (w), 942 (w), 878 (w), 802 (w), 653 $cm^{-1}$.

**Solution FTIR Spectroscopy OCNAr$^{Tripp2}$ (2) in THF:** FTIR (THF; KBr Window; 20 ˚C): $\nu_{OCN}$ = 2276 (m), 2242 (s), also 1607 (w), 1569 (w), 758 (w) $cm^{-1}$.

**S1.5: Independent Synthesis of Cp*Co(PPh$_3$)(CNAr$^{Tripp2}$) (3):** To a solution of Cp*Co($N_2$)CNAr$^{Tripp2}$ (0.041 g, 0.056 mmoles, 1 equivs) in 1 mL of $C_6D_6$ a solution of $PPh_3$ (0.015 g, 0.056 mmoles, 1 equivs) in 0.5 mL of $C_6D_6$ was added in one portion. Upon addition an immediate color change from brown to purple/black was observed.

Analysis via $^{1}$H NMR indicated complete conversion to a new diamagnetic product. The resulting solution was concentrated to a solid under reduced pressure and recrystallized from a super-saturated solution of *n*-pentane and $Et_2O$ (1:5; 2 mL) at -40 ˚C over 1 week to afford analytically pure black crystals of $Cp^*Co(PPh_3)CNAr^{Tripp2}$ 0.028 g, 0.029 mmoles, 53 % yield. $^{1}$H NMR (499.8 MHz, $C_6D_6$, 20 ˚C): 7.66 (t, 6H, 8 Hz, P-*Ph*), 7.16 (s, 4H, *m*-Tripp), 7.04 (d, 2H, 8 Hz, *m*-Ph), 7.00 (m, 8H, P-*Ph*), 6.83 (t, 1H, 8 Hz, *p*-Ph), 2.95 (sept., 6H, 7 Hz, C*H*$(CH_3)_2$), 1.40 (d, 12H, 7Hz CH(C*H*$_3)_2$), 1.37 (s, 15H, Cp-*Me*), 1.31 (d, 12H, 7Hz, CH(C*H*$_3)_2$), 1.14 (d, 12H, 7Hz, CH(C*H*$_3)_2$), 1.09 (broad singlet, 15H, CH(C*H*$_3)_2$). $^{13}$C{$^{1}$H} NMR (125.8 MHz, $C_6D_6$, 20 ˚C): δ = 192.1 (*C*NR, d, $^{13}$C-$^{31}$P coupling = 34.6 Hz), 148.0, 147.0, 138.5, 138.2, 137.0, 135.9, 134.5, 134.4, 134.3, 134.1, 133.9, 131.9, 128.9, 128.8, 127.5, 127.4, 123.1, 121.3, 92.4, 34.7, 31.2, 26.1, 24.4, 23.1, 10.8 ppm. $^{31}$P{$^{1}$H} NMR (121.4 MHz, $C_6D_6$, 20 ˚C): δ = 66.7 ppm. FTIR ($C_6D_6$; KBr Window; 20 ˚C): $\nu_{CN}$ = 1919 (s), also 3054 (w), 2961 (s), 2928 (m), 2904 (m), 2867 (m), 2118 (w), 2091 (w), 1605 (w), 1570 (w), 1481 (w), 1461 (w), 1434 (w), 1407 (w), 1381 (w), 1362 (w), 1203 (w), 1086 (w), 1069 (w), 1027 (w), 1000 (w), 943 (w), 877 (w), 757 (w), 746 (w), 722 (w), 690 (m) cm$^{-1}$. Anal. Calcd. For $C_{63}H_{82}NPCo$: C, 80.22; H, 8.76; N, 1.48. Found: C, 80.55; H, 8.67; N, 1.50.

**Synthesis of $Cp^*Co(\eta^2$-*N*,*N*-$N_2O)(CNAr^{Tripp2})$ (4):** In a typical reaction $Cp^*Co(N_2)(CNAr^{Tripp2})$ (0.049 g, 0.067 mmoles, 1 equiv) was dissolved in $Et_2O$ (~1 mL) and transferred to a 25 mL re-sealable ampule in a $N_{2(g)}$ filled glove box, and then brought out of the glove box and connected to the schlenk line. There after the solution was subject to one freeze pump thaw cycle (FPT) and then cooled to -78 ˚C and allowed

to equilibrate for 10 mins. The mixture was then placed under an atmosphere of $N_2O_{(g)}$ and allowed to warm to -25 ˚C and react for 20 mins. The reaction mixture was then cooled back to -78 ˚C and rapidly transferred back into a $N_{2\ (g)}$ filled glove box and placed in the freezer at -40 ˚C. Storage at -40 ˚C for 24 hours afforded yellow crystals that were suitable for X-ray diffraction, 0.020 g, 0.027 mmoles, 40 % yield. $^1$H NMR (499.9 MHz, Tol-$d_8$, -20 ˚C): 7.22 (s, 2H, *m*-Tripp), 7.20 (s, 2H *m*-Tripp), 6.88 (d, 2H, 7 Hz, *m*-Ph), 6.82 (t, 1H, 7 Hz, *p*-Ph), 2.94 (sept., 2H, 7 Hz, C*H*$(CH_3)_2$), 2.70 (sept., 4H, 7 Hz, C*H*$(CH_3)_2$), 1.46 (d, 6H, 7Hz, CH(C*H*$_3)_2$), 1.43 (d, 6H, 7Hz, CH(C*H*$_3)_2$), 1.41 (dd, 12H, 5Hz, 3Hz, CH(C*H*$_3)_2$) 1.32 (s, 15H, Cp*-*H*), 1.16 (t, 12H, 7Hz, CH(C*H*$_3)_2$). $^{13}$C{$^1$H} NMR (125.8 MHz, Tol-$d_8$, -20 ˚C): δ = 166.4 (*C*NR), 149.5, 146.0, 145.9, 146.8, 138.8, 132.4, 129.8, 127.1, 121.6, 121.5, 94.9, 35.1, 31.4, 31.3, 24.8, 24.4, 24.5, 24.1, 9.2 ppm. $^{15}$N{$^1$H} NMR (50.7 MHz, Tol-$d_8$, –20 ˚C): –49.13 (d, 17Hz), –198.37 (d, 17Hz). (Due to the thermal sensitivity and its propensity to decompose at temperatures greater than 0 ˚C elemental analysis was not obtained. IR spectroscopy is presented below in Section 2.

**Synthesis of Cp*Co($\eta^2$-*N,O*-*o*-$CH_3$-$C_6H_4$NO)($CNAr^{Tripp2}$) (5):** To a solution of Cp*Co($N_2$)$CNAr^{Tripp2}$ (0.052 g, 0.071 mmoles, 1 equivs) in 1 mL of $C_6D_6$ a solution of *o*-Tol-Nitroso-benzene (0.009 g, 0.071 mmoles, 1 equivs) in 0.5 mL of $C_6D_6$ was added in one portion. Upon addition an immediate color change from brown to forest green was observed. Analysis via $^1$H NMR indicated complete conversion to a new diamagnetic product. The resulting solution was concentrated to a solid under reduced pressure and recrystallized from a saturated solution of *n*-pentane and $TMS_2O$ (1:5; 2 mL) at -40 ˚C

over 1 week to afford analytically pure forest green crystals of Cp*Co($\eta^2$- *N,O*-$C_7H_7NO$)$CNAr^{Tripp2}$•$TMS_2O$ 0.031 g, 0.033 mmoles, 45 % yield. $^1$H NMR (499.8 MHz, $C_6D_6$, 20 ˚C): 7.24 (bd, 1H, 10 Hz, *m*-Tol), 7.22 (s, 4H, *m*-Tripp), 7.10 (d, 1H, 7Hz, *m*-Tol), 7.03 (t, 1H, 6Hz, *m*-Tol), 6.98 (t, 1H, 8 Hz, *p*-Tol), 6.90 (d, 2H, 8Hz, *m*-Tripp), 6.81 (t, 1H, 8 Hz, *p*-Tripp), 2.88 (sept., 2H, 7 Hz, C*H*$(CH_3)_2$), 2.79 (sept., 4H, 7 Hz, C*H*$(CH_3)_2$), 2.12 (s, 3H, *Me*-Tol), 1.49 (bd, 12H, 6Hz, CH(C*H*$_3)_2$), 1.31 (d, 12H, 7Hz, CH(C*H*$_3)_2$), 1.15 (d, 12H, 7Hz, CH(C*H*$_3)_2$), 1.13 (s, 15H, Cp*-*H)*. $^{13}$C{$^1$H} NMR (125.8 MHz, $C_6D_6$, 20 ˚C): δ = 166.3 (*C*NR), 162.5, 149.3, 146.9, 139.1, 133.3, 131.0, 130.8, 130.0, 129.1, 127.0, 121.6, 126.4, 121.6, 121.5, 115.1, 93.8, 34.9, 31.5, 24.8, 24.4, 24.2, 19.6, 9.4 ppm. FTIR ($C_6D_6$; KBr Window; 20 ˚C): $\nu_{CN}$ = 2099 (s), also 2961 (m), 2927 (w), 2906 (w), 2869 (w), 1587 (w), 1464 (w), 1414 (w), 1382 (w), 1363 (w), 1254 (w), 1201 (w), 1108 (w), 1071 (w), 1053(w), 1029 (w), 940 (w), 879 (w), 756 (w), 719 (w) $cm^{-1}$. Anal. Calcd. For $C_{54}H_{71}N_2OCo$: C, 78.79; H, 8.70; N, 3.41. Found: C, 77.23; H, 8.37; N, 3.41.

**Independent Synthesis of Cp*Co(OH)($CNAr^{Tripp2}$) (6):** To a solution of Cp*Co($N_2$)($CNAr^{Tripp2}$) (0.053 g, 0.0721 mmoles, 1 equiv.) in 2 mL of THF a solution of Cp*$CoI_2$($CNAr^{Tripp2}$) (0.068 g, 0.0721 mmoles, 1 equiv.) in 1 mL of THF was added dropwise over the course of 1 min. An instant color change to deep orange was observed and solution FTIR analysis of the reaction mixture displayed a prominent isocyanide shift at 2089 $cm^{-1}$ (THF) intermediate in intensity to both starting materials and indication of the *in situ* formation of Cp*CoI($CNAr^{Tripp2}$). There after a THF solution containing NaOH (0.009 g, 0.216 mmoles, 3 equiv.) and 18-crown-6 (0.036 g, 0.144 mmols, 2

equiv.) were added and the solution was allowed to stir at room temperature for 24 hours. After 24 hours a color change from deep orange to dark red was observed. The solution was concentrated to an oil and then slurried in *n*-pentane (4 mL) and evaporated to a solid to desolvate any remaining NaOH/NaI/18-crown-6. This was repeated two additional times. There after the resultant solid was taken up in *n*-pentane and filtered over Celite packed on fiberglass (2 cm) and concentrated to *ca.* 1 mL and placed in the freezer for recrystallization at –40 ˚C for X days to afford analytically pure red crystals of Cp*Co(OH)(CNAr$^{Tripp2}$), 0.040 g, 0.056 mmoles, 39 %. Analysis via $^{1}$H NMR indicated paramagnetically shifted resonances. $^{1}$H NMR analysis indicated that Cp*Co(OH)(CNAr$^{Tripp2}$) does not have any distinguishable NMR features. Evans method magnetic moment determination based on an average of 5 measurements: 1.72 $\mu_B$ consistent with a spin ½ system. FTIR ($C_6D_6$; KBr Window; 20 ˚C): $\nu_{CN}$ = 2059 (s), 2013 (w, sh), $\nu_{OH}$ =3607 also 2959 (s), 2925 (w), 2869 (w), 2850 (w), 1604 (w), 1569 (w), 1413 (w), 1382 (w), 1363 (w), 1106 (w), 1071 (w), 990 (w), 940 (w), 879 (w), 757 (w), 596 (w) cm$^{-1}$. Anal. Calcd. For $C_{47}H_{65}NOCo$: C, 78.52; H, 9.11; N, 1.95. Found: C, 78.41; H, 8.99; N, 1.85.

**Solution FTIR spectroscopy of Cp*Co(OH)(CNAr$^{Tripp2}$) (6) in THF**: FTIR (THF; KBr Window; 20 ˚C): $\nu_{CN}$ = 2061 (s), 2014 (w, sh), $\nu_{OH}$ =3608 also 1605 (w), 1570 (w), 1412 (w), 1384 (w)cm$^{-1}$.

## 7.7 Results of Computational Studies.

**Computational Details.** Density Functional Theory (DFT) calculations were carried out on Cp*Co($\eta^2$-*N,N*-$N_2O$)$CN^{Xylyl}$, and Cp*Co($\eta^2$-*N,O*-$N_2O$)$CNAr^{Xylyl}$ which are truncated models of the structurally characterized complex Cp*Co($\eta^2$-*N,N*-$N_2O$)$CNAr^{Tripp2}$. Calculations were carried out using the ORCA program package.[47] Geometry optimizations and single-point calculations were performed using the B3LYP hybrid density functional.[48,49] The all-electron Ahlrichs triple-zeta basis sets def2-TZVP (standard)[50] and def2-TZVP/J (auxiliary)[51] were used in all calculations. The resolution of identity (RI) approximation was employed.[52] Relativistic effects were included by use of the zerothorder regular approximation (ZORA).[53-56] Crystallographic atomic coordinates were used as input for geometry optimizations where appropriate. Simulated frequency calculations were conducted on geometry optimized coordinates and calibrated according to literature values.[35] Viewing of optimized structures and rendering of molecular orbitals was performed using the program Chemcraft.[57] After each geometry optimization, the optimized coordinates were reorientated so as to make the Cp* ring coplanar with the Cartesian *xy* plane. These coordinates were then used to run a single point calculation to deconvolute orbital contributions. This research was supported in part by the W. M. Keck Foundation through computing resources at the W. M. Keck Laboratory for Intergrated Biology II.

### Input for the geometry optimization of Cp*Co($\eta^2$-*N,N*-$N_2O$)$CN^{Xylyl}$

```
#UKS OPT of  NNboundnew
#
#
%pal nprocs 8 end
```

```
! UKS B3LYP/G ZORA def2-TZVP def2-TZVP/J RIJCOSX OPT NormalPrint NumFreq VerySlowConv KDIIS XYZFile
%SCF
 MaxIter 1000
end

%output
Print[ P_Basis ] 2
Print[ P_MOs ] 1
end

* xyz 0 1
Co       2.522787000     6.282059000    16.508058000
N        4.012889000     8.203695000    14.804084000
C        5.454382000     9.010970000    13.057836000
C        6.181366000    10.080905000    12.529217000
H        6.656189000     9.968527000    11.714102000
C        6.217709000    11.297450000    13.176375000
H        6.741334000    12.004501000    12.818072000
C        5.499455000    11.500765000    14.343210000
H        5.547036000    12.341777000    14.782445000
C        4.740308000     9.246227000    14.234942000
C        3.335159000     4.641406000    15.573633000
C        1.907919000     4.595783000    15.438846000
C        1.357027000     4.582308000    16.744576000
C        4.711822000    10.492796000    14.878574000
N        1.292423000     7.532094000    17.223565000
C        3.420322000     7.472604000    15.500287000
C        3.658196000     4.581813000    16.961112000
C        2.436491000     4.557877000    17.682479000
C        4.310592000     4.658925000    14.439596000
H        3.883507000     5.046612000    13.647334000
H        4.597128000     3.743029000    14.241034000
H        5.090123000     5.198587000    14.687553000
C        1.134764000     4.496158000    14.160265000
H        0.343212000     5.071683000    14.211458000
H        0.854954000     3.567612000    14.019222000
H        1.700169000     4.783993000    13.413337000
C       -0.104816000     4.586951000    17.085487000
H       -0.248467000     5.111508000    17.900720000
H       -0.409192000     3.666886000    17.231175000
H       -0.611174000     4.985491000    16.347150000
C        5.044981000     4.512604000    17.525026000
H        5.648437000     5.055299000    16.975725000
H        5.351570000     3.581789000    17.525003000
H        5.041810000     4.855472000    18.443087000
C        2.288920000     4.522261000    19.181635000
H        3.085456000     4.913208000    19.597666000
H        2.188025000     3.593592000    19.477960000
H        1.497298000     5.036790000    19.444275000
N        2.183948000     7.453187000    18.033895000
O        2.546447000     7.629243000    19.260910000
```

| | | | |
|---|---|---|---|
| C | 5.441107391 | 7.632085912 | 12.372195819 |
| H | 6.458323018 | 7.270845347 | 12.182759616 |
| H | 4.934948381 | 6.883170520 | 12.991902472 |
| H | 4.919732247 | 7.670419597 | 11.408968350 |
| C | 3.842379156 | 10.731470525 | 16.127054522 |
| H | 2.778716929 | 10.784512646 | 15.868370057 |
| H | 3.964335769 | 9.924447856 | 16.858456286 |
| H | 4.108256776 | 11.670976557 | 16.624795597 |

*

**Optimized coordinates for Cp*Co($\eta^2$-*N*,*N*-$N_2O$)$CN^{Xylyl}$**

| | | | |
|---|---|---|---|
| Co | 2.75385717567891 | 6.25345542620474 | 16.65362209505800 |
| N | 3.86718087544374 | 8.31075267694419 | 14.81686625318813 |
| C | 4.95901020677372 | 9.13709585908256 | 12.84859585584350 |
| C | 5.62727263838873 | 10.18646247752662 | 12.22671007122375 |
| H | 5.97955725022588 | 10.05783505987336 | 11.21097472578802 |
| C | 5.85166125194878 | 11.38533372288050 | 12.89076393198200 |
| H | 6.37145354792188 | 12.19122236834784 | 12.38894582542306 |
| C | 5.41784985505556 | 11.55032791324047 | 14.19959142880295 |
| H | 5.60657485130232 | 12.48302984694041 | 14.71567869348690 |
| C | 4.52476240009549 | 9.33523506783267 | 14.16895659315047 |
| C | 3.55310328616478 | 4.51716103002380 | 15.80171761762116 |
| C | 2.15643473817311 | 4.63901629536567 | 15.40366339419241 |
| C | 1.37373721019919 | 4.60958576669608 | 16.57624521708293 |
| C | 4.74660231383903 | 10.53332668332384 | 14.87092954121488 |
| N | 1.81044384428247 | 7.57600201308644 | 17.79074548763877 |
| C | 3.39620634820438 | 7.48755839715877 | 15.50201904064009 |
| C | 3.60351127250658 | 4.38722859618250 | 17.21589458210562 |
| C | 2.26010201848334 | 4.49599826819064 | 17.69952854778717 |
| C | 4.71371092067055 | 4.41223534847081 | 14.85978903528713 |
| H | 4.55096573881593 | 4.99994174403049 | 13.95661427119259 |
| H | 4.87268270405492 | 3.37545368682995 | 14.54741034976110 |
| H | 5.63691998400353 | 4.76218500843569 | 15.32081980083778 |
| C | 1.64773294808728 | 4.67648941838975 | 13.99504578122569 |
| H | 0.76475643530089 | 5.30726582114245 | 13.89807847074737 |
| H | 1.37360068834208 | 3.67314713122677 | 13.65343479490903 |
| H | 2.40081932476167 | 5.05800864396198 | 13.30579069206731 |
| C | -0.11334720661066 | 4.71891389340410 | 16.67660195039733 |
| H | -0.40628498107825 | 5.43187887962655 | 17.44755190146424 |
| H | -0.55796965600573 | 3.75369195927251 | 16.93924681511817 |
| H | -0.55691568687141 | 5.04804193068062 | 15.73783818636715 |
| C | 4.83025358947815 | 4.20395581751693 | 18.05520153510962 |
| H | 5.71992244149898 | 4.56372561865928 | 17.53936345837577 |
| H | 4.99130447114437 | 3.14911862939251 | 18.29943172846189 |
| H | 4.75744380750262 | 4.75362492252598 | 18.99288635950773 |
| C | 1.81271901503091 | 4.42404479716982 | 19.12556630569835 |
| H | 2.63449743694076 | 4.60851469910310 | 19.81552586438648 |
| H | 1.39798088610389 | 3.43660412763618 | 19.35248208547864 |
| H | 1.03455411613236 | 5.15877011719562 | 19.33387920733234 |
| N | 2.95028008414304 | 7.41994251198672 | 18.12789508374516 |
| O | 3.77919874718109 | 7.77207176488915 | 18.97250691963682 |
| C | 4.72048722088379 | 7.83038342239899 | 12.14473686159737 |

| | | | |
|---|---|---|---|
| H | 5.19525181193965 | 7.00313793096574 | 12.67666207481016 |
| H | 3.65527507102456 | 7.59710738670772 | 12.07756735129844 |
| H | 5.12836714900420 | 7.85884105518818 | 11.13565834519866 |
| C | 4.28367064604168 | 10.69467951776681 | 16.29096953893580 |
| H | 3.19643274508497 | 10.61517979126445 | 16.37236139068610 |
| H | 4.70019124604933 | 9.92324856905313 | 16.94160826726398 |
| H | 4.58448288365696 | 11.66553434620682 | 16.68145538987200 |

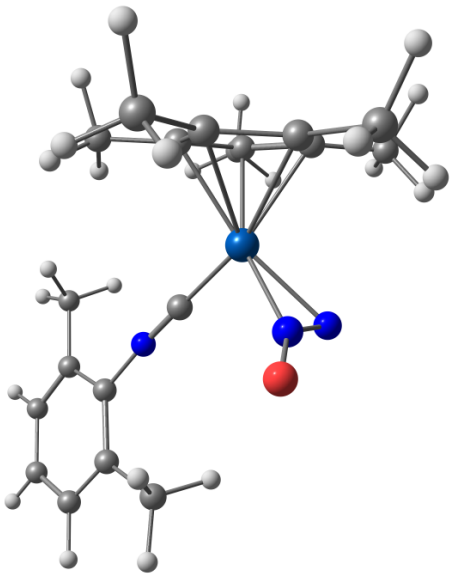

**Figure 6.21** Geometry optimized structure of Cp*Co($\eta^2$-*N,N*-$N_2O$)$CN^{Xylyl}$.

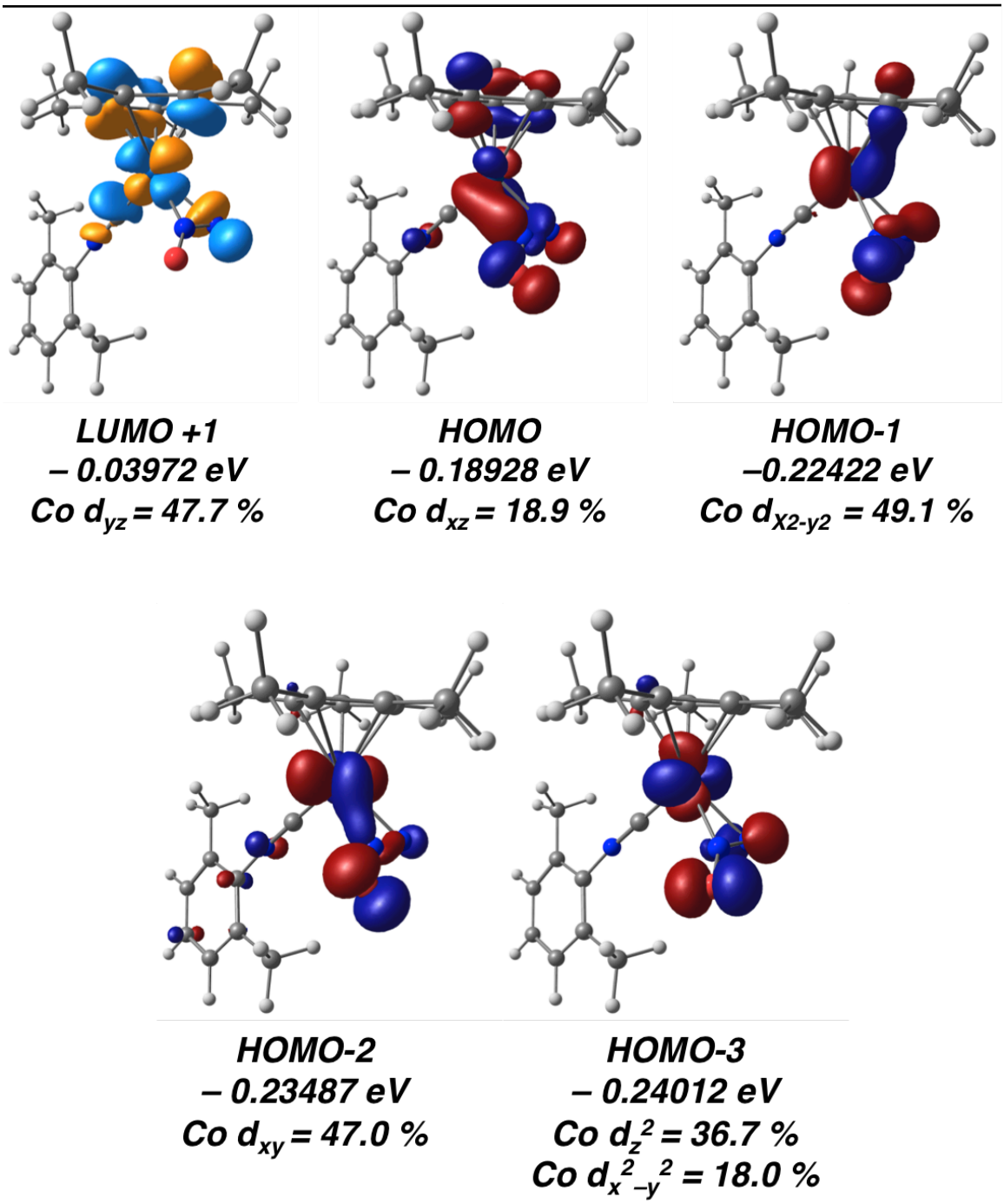


**Figure 6.22** Primary orbital interactions composed of Co-d orbital character.

**Input for the geometry optimization of Cp*Co($\eta^2$-*N,O*-$N_2O$)$CN^{Xylyl}$**

```
#UKS OPT of  NOboundnew
#
#
%pal nprocs 8 end
! UKS B3LYP/G ZORA def2-TZVP def2-TZVP/J RIJCOSX OPT NormalPrint NumFreq
VerySlowConv KDIIS XYZFile
%SCF
 MaxIter 1000
end

%output
Print[ P_Basis ] 2
Print[ P_MOs ] 1
end

* xyz 0 1
Co       2.522787000     6.282059000    16.508058000
N        4.012889000     8.203695000    14.804084000
C        5.454382000     9.010970000    13.057836000
C        6.181366000    10.080905000    12.529217000
H        6.656189000     9.968527000    11.714102000
C        6.217709000    11.297450000    13.176375000
H        6.741334000    12.004501000    12.818072000
C        5.499455000    11.500765000    14.34321000
H        5.547036000    12.341777000    14.782445000
C        4.740308000     9.246227000    14.234942000
C        3.335159000     4.641406000    15.573633000
C        1.907919000     4.595783000    15.438846000
C        1.357027000     4.582308000    16.744576000
C        4.711822000    10.492796000    14.878574000
O        1.292423000     7.532094000    17.223565000
C        3.420322000     7.472604000    15.500287000
C        3.658196000     4.581813000    16.961112000
C        2.436491000     4.557877000    17.682479000
C        4.310592000     4.658925000    14.439596000
H        3.883507000     5.046612000    13.647334000
H        4.597128000     3.743029000    14.241034000
H        5.090123000     5.198587000    14.687553000
C        1.134764000     4.496158000    14.160265000
H        0.343212000     5.071683000    14.211458000
H        0.854954000     3.567612000    14.019222000
H        1.700169000     4.783993000    13.413337000
C       -0.104816000     4.586951000    17.085487000
H       -0.248467000     5.111508000    17.900720000
H       -0.409192000     3.666886000    17.231175000
H       -0.611174000     4.985491000    16.347150000
C        5.044981000     4.512604000    17.525026000
H        5.648437000     5.055299000    16.975725000
H        5.351570000     3.581789000    17.52500300
H        5.041810000     4.855472000    18.443087000
```

| | | | |
|---|---|---|---|
| C | 2.288920000 | 4.522261000 | 19.181635000 |
| H | 3.085456000 | 4.913208000 | 19.597666000 |
| H | 2.188025000 | 3.593592000 | 19.477960000 |
| H | 1.497298000 | 5.036790000 | 19.444275000 |
| N | 2.183948000 | 7.453187000 | 18.033895000 |
| N | 2.546447000 | 7.629243000 | 19.260910000 |
| C | 5.441107391 | 7.632085912 | 12.372195819 |
| H | 6.458323018 | 7.270845347 | 12.182759616 |
| H | 4.934948381 | 6.883170520 | 12.991902472 |
| H | 4.919732247 | 7.670419597 | 11.408968350 |
| C | 3.842379156 | 10.731470525 | 16.127054522 |
| H | 2.778716929 | 10.784512646 | 15.868370057 |
| H | 3.964335769 | 9.924447856 | 16.858456286 |
| H | 4.108256776 | 11.670976557 | 16.624795597 |

*

## Optimized coordinates for Cp*Co($\eta^2$-*N,O*-$N_2O$)$CN^{Xylyl}$

| | | | |
|---|---|---|---|
| Co | 2.43298752156827 | 6.27253493729352 | 16.34871936075815 |
| N | 4.21581036779841 | 8.31191222414303 | 15.12173849142928 |
| C | 5.28828700005819 | 9.09783625783507 | 13.12597514291217 |
| C | 5.93870457219561 | 10.13810395401634 | 12.47086397095829 |
| H | 6.25943304010150 | 9.99587097234851 | 11.44642225596565 |
| C | 6.17435916923247 | 11.34861260220309 | 13.10938658576841 |
| H | 6.67458566296514 | 12.14902022561924 | 12.57949104732347 |
| C | 5.77113820770168 | 11.53555696169786 | 14.42471236732826 |
| H | 5.96231111072499 | 12.48041526860878 | 14.91695090819787 |
| C | 4.88565192933795 | 9.31731434418659 | 14.45352525706715 |
| C | 3.30810029799447 | 4.51492372590003 | 15.52104036087226 |
| C | 1.90535178082627 | 4.40425525673063 | 15.39784423977463 |
| C | 1.35014799068854 | 4.49777786507533 | 16.72337140609714 |
| C | 5.11981919499705 | 10.52668170298598 | 15.12760207732245 |
| O | 0.93451491679107 | 7.52085354810462 | 16.32921086235113 |
| C | 3.55923449746783 | 7.50560588183389 | 15.65603617753225 |
| C | 3.63125238001617 | 4.65914268670847 | 16.93180968029616 |
| C | 2.41848843945832 | 4.57377432465569 | 17.66551994970178 |
| C | 4.31489749017731 | 4.42644463405217 | 14.41637733718743 |
| H | 3.88596208487651 | 4.71557410395901 | 13.45758821896018 |
| H | 4.69175822487454 | 3.40394388597980 | 14.31444779649356 |
| H | 5.17572552711587 | 5.06764056789781 | 14.60510600431111 |
| C | 1.12070210712171 | 4.24760337301900 | 14.13154279364071 |
| H | 0.21366706456370 | 4.85232249299644 | 14.14672735827941 |
| H | 0.81545513646582 | 3.20810142877014 | 13.97388311579115 |
| H | 1.70313723403934 | 4.55470874842204 | 13.26319501421438 |
| C | -0.10270857173399 | 4.44236851530868 | 17.07746862441151 |
| H | -0.34040038867341 | 5.12463037663008 | 17.89326283685624 |
| H | -0.38488437856511 | 3.43404282903499 | 17.39669345953092 |
| H | -0.73193807384818 | 4.71425581828656 | 16.23161225974419 |
| C | 5.00815135591256 | 4.70616218792452 | 17.52223200727728 |
| H | 5.74263934000749 | 5.06577218729970 | 16.80186179260032 |
| H | 5.32986768504931 | 3.71073984898631 | 17.84580304557192 |
| H | 5.05226195561222 | 5.36252054544693 | 18.39101409252838 |
| C | 2.27493049104609 | 4.63543566647917 | 19.15244821354195 |

| | | | |
|---|---|---|---|
| H | 2.12779067672012 | 5.66081278854685 | 19.50761103839861 |
| H | 3.16113545855077 | 4.23523202496883 | 19.64647185774061 |
| H | 1.41839729916369 | 4.04769834057638 | 19.48501065567674 |
| N | 1.58369519537132 | 7.49809164333804 | 17.52194431513804 |
| N | 1.48859488110637 | 7.95773576692670 | 18.57764799057866 |
| C | 5.01595128356909 | 7.78943170449839 | 12.43979766388619 |
| H | 5.50099478822769 | 6.96019108551509 | 12.95697468161474 |
| H | 3.94686176590234 | 7.56595173365059 | 12.41687016372422 |
| H | 5.38443665353528 | 7.81070162210898 | 11.41532675595300 |
| C | 4.67164490704178 | 10.71280023065066 | 16.54898295344704 |
| H | 3.58656157961499 | 10.62421820355691 | 16.64348682020284 |
| H | 5.10387023492749 | 9.95453568088165 | 17.20478709769774 |
| H | 4.96896857930303 | 11.69250518433723 | 16.91903261234718 |

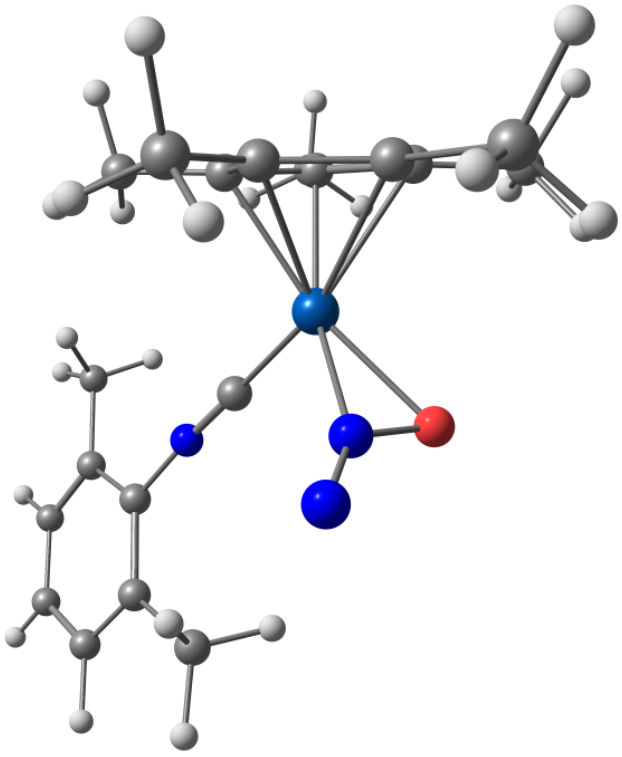

**Figure 6.23** Geometry optimized structure of Cp*Co($\eta^2$-*N,O*-$N_2O$)$CN^{Xylyl}$.

## 6.9 Details of Crystallographic Structure Determinations.

**General Information.** Single crystal X-ray structure determinations were carried out at low temperature on Bruker Kappa diffractometers equipped with a Mo sealed tube or rotating anode or Cu rotating anode radiation source and a Bruker APEX-II, APEX-I, or

Proteum Pt135 detector. All structures were solved via direct methods with SHELXS[58] and refined by full-matrix least squares procedures using SHELXL[58] within the Olex2 small-molecule solution, refinement and analysis software package.[59] Crystallographic data collection and refinement information are listed in Table 6.2.

**Information on Crystallographic Disorder:** The following molecules contain positionally disordered components that were modeled and refined anisotropically. They are listed along with their respective disordered components.

$OCNAr^{Tripp2}$ (**3**) displays twosite positional disorder in the OCN unit due to the crystallographic mirror in which it resides on. Each fragment was modeled at 50% and linked with the FVAR command and anisotropically refined.

($\eta^5$-Cp*)Co($\eta^2$-*N,N*-$N_2O$)($CNAr^{Tripp2}$) (**4**) displays two site positional disorder in the $N_2O$ unit in which the oxygen is disordered over two positions. Each oxygen atom was spilt and linked with the FVAR command such that O1A and O1B are ate 66.4% and 33.6% occupancy and anisotropically refined. It is important to note that no constraints or restraints were used in the modeling of $N_2O$ positional disorder such that the most accurate crystallographic model has displays the large degree of thermal movement within the crystal lattice.

Cp*Co($\eta^2$-*N,O-o*-$CH_3$-$C_6H_4NO$)($CNAr^{Tripp2}$)•($TMS_2O$) (**5**•($TMS_2O$)): Eight molecules of $TMS_2O$ per unit cell.

**Table 6.2** Crystallographic Determination and Refinement Data.

| Name | $OCNAr^{Tripp2}$ (**2**) | $(\eta^5\text{-Cp*})Co(PPh_3)(CNAr^{Tripp2})$ (**3**) | $(\eta^5\text{-Cp*})Co(\eta^2\text{-}N,N\text{-}N_2O)(CNAr^{Tripp2})$ (**4**) |
|---|---|---|---|
| Formula | $C_{37}H_{49}NO$ | $C_{65}H_{79}CoNP$ | $C_{47}H_{64}CoN_3O$ |
| Crystal System | Orthorhombic | Monoclinic | Orthorhomnic |
| Space Group | Pbcm | $P2_1/C$ | Pbca |
| $a$, Å | 10.9033(9) | 13.5984(11) | 17.4228(7) |
| $b$, Å | 12.0359(11) | 17.6290(12) | 20.6348(9) |
| $c$, Å | 25.140(2) | 23.0085(18) | 23.4337(11) |
| α, deg | 90 | 90 | 90 |
| β, deg | 90 | 90.367(5) | 90 |
| γ, deg | 90 | 90 | 90 |
| V, $Å^3$ | 3299.2(5) | 5515.6(7) | 8392.4(6) |
| $Z$ | 4 | 4 | 8 |
| Radiation (λ, Å) | $MoK_\alpha$ (λ = 0.71073) | $MoK_\alpha$ (λ = 0.71073) | $MoK_\alpha$ (λ = 0.71073) |
| ρ (calcd.), $g/cm^3$ | 1.054 | 1.161 | 1.181 |
| μ (Mo Ka), $mm^{-1}$ | 0.062 | 0.380 | 0.446 |
| Temp, K | 100.0 | 100 | 100.0 |
| θ max, deg | 50.852 | 50.654 | 50.744 |
| data/parameters | 3120/196 | 10028/630 | 7687/496 |
| $R_1$ | 0.0572 | 0.1271 | 0.0743 |
| $wR_2$ | 0.1223 | 0.1287 | 0.1637 |
| GOF | 1.040 | 1.00 | 1.062 |

**Table 6.3** Crystallographic Determination and Refinement Data.

| Name | ($\eta^5$-Cp*)Co($\eta^2$-*N,O*-*o*-$CH_3C_6H_4NO$)($CNAr^{Tripp2}$)•$TMS_2O$ (**5**) | ($\eta^5$-Cp*)Co(OH)($CNAr^{Tripp2}$) (**6**) |
|---|---|---|
| Formula | $C_{60}H_{89}CoN_2O_2Si_2$ | $C_{47}H_{65}CoNO$ |
| Crystal System | Orthorhombic | Orthorhombic |
| Space Group | Pbca | Pbca |
| *a*, Å | 18.4221(6) | 17.3101(7) |
| *b*, Å | 17.1331(4) | 20.4836(8) |
| *c*, Å | 36.3469(10) | 23.4544(11) |
| α, deg | 90 | 90 |
| β, deg | 90 | 90 |
| γ, deg | 90 | 90 |
| V, Å$^3$ | 11472.1(6) | 8316.3(6) |
| *Z* | 8 | 8 |
| Radiation (λ, Å) | $CuK_\alpha$ (λ = 1.54178) | $MoK_\alpha$ (λ = 0.71073) |
| ρ (calcd.), g/cm$^3$ | 1.141 | 1.148 |
| μ (Mo/Cu Ka), mm$^{-1}$ | 3.0051 | 0.447 |
| Temp, K | 100.0 | 100 |
| θ max, deg | 59.007 | 50.8 |
| data/parameters | 8238/628 | 7611/472 |
| $R_1$ | 0.0879 | 0.0593 |
| $wR_2$ | 0.1047 | 0.1408 |
| GOF | 1.022 | 1.022 |

**6.9 Acknowledgements.**

Chapter 6 is currently in preparation as a manuscript by Mokhtarzadeh, C. C., Moore, C. E., Gimbecky, M., Rheingold, A. L., Figueroa, J. S. The dissertation author is the primary author of this manuscript. Prof. Adah Almutairi, and Dr. Amy Moore are thanked for generous access to their *in-situ* React-IR spectrometer. Dr. Anthony Mrse is thanked for assistance with hetero-nuclear NMR experiments.

**6.10 References.**

(1) Kanter, D.; Mauzerall, D. L.; Ravishankara, A. R.; Daniel, J. S.; Portmann, R. W.; Grabiel, P. M.; Moomaw, W. R.; Galloway, J. N. *PNAS* **2013**, *110* (12), 4451.

(2) Kramlich, J. C.; Linak, W. P. *Progress in Energy and Combustion Science* **1994**, *20* (2), 149.

(3) Blasing, T. J. July 2009.

(4) Wüst, A.; Schneider, L.; Pomowski, A.; Zumft, W. G.; Kroneck, P. M. H.; Einsle, O. *Biological Chemistry 393* (10).

(5) Ravishankara, A. R.; Daniel, J. S.; Portmann, R. W. *Science* **2009**, *326* (5949), 123.

(6) Prasad, S. S. *Geophys. Res. Lett.* **1998**, *25* (12), 2173.

(7) Leont'ev, A. V.; Fomicheva, O. A.; Proskurnina, M. V.; Zefirov, N. S. *Russ. Chem. Rev.* **2007**, *70* (2), 91.

(8) Okabe, H. *Photochemistry of small molecules*; 1978.

(9) Tolman, W. B. *Angew. Chem. Int. Ed.* **2010**, *49* (6), 1018.

(10) Severin, K. *Chem Soc Rev* **2015**, *44* (17), 6375.

(11) Vaughan, G. A.; Sofield, C. D.; Hillhouse, G. L.; Rheingold, A. L. *J. Am. Chem. Soc.* **1989**, *111* (14), 5491.

(12) Vaughan, G. A.; Hillhouse, G. L.; Rheingold, A. L. *J. Am. Chem. Soc.* **1990**, *112* (22), 7994.

(13) Whited, M. T.; Grubbs, R. H. *J. Am. Chem. Soc.* **2008**, *130* (49), 16476.

(14) Bottomley, F.; Lin, I. J. B.; Mukaida, M. *J. Am. Chem. Soc.* **1980**, *102* (16), 5238.

(15) Bottomley, F.; Brintzinger, H. H. *J. Chem. Soc., Chem. Commun.* **1978**, No. 6, 234.

(16) Vaughan, G. A.; Rupert, P. B.; Hillhouse, G. L. *J. Am. Chem. Soc.* **1987**, *109* (18), 5538.

(17) Harrold, N. D.; Waterman, R.; Hillhouse, G. L.; Cundari, T. R. *J. Am. Chem. Soc.* **2009**, *131* (36), 12872.

(18) Laplaza, C. E.; Odom, A. L.; Davis, W. M.; Cummins, C. C.; Protasiewicz, J. D. *Journal of the ...* **2002**.

(19) Cherry, J.-P. F.; Johnson, A. R.; Baraldo, L. M.; Tsai, Y.-C.; Cummins, C. C.; Kryatov, S. V.; Rybak-Akimova, E. V.; Capps, K. B.; Hoff, C. D.; Haar, C. M.; Nolan, S. P. *J. Am. Chem. Soc.* **2001**, *123* (30), 7271.

(20) Hutchings, G. J.; Comninos, H.; Copperthwaite, R. G.; van Rensburg, L. J.; Hunter, R.; Themistocleous, T. *Journal of the Chemical Society, Faraday Transactions 1: Physical Chemistry in Condensed Phases* **1989**, *85* (3), 633.

(21) Heyden, A.; Peters, B.; Bell, A. T.; Keil, F. J. *J. Phys. Chem. B* **2005**, *109* (5), 1857.

(22) Armor, J. N.; Taube, H. *J. Am. Chem. Soc.* **1969**, *91* (24), 6874.

(23) Paulat, F.; Kuschel, T.; Näther, C.; Praneeth, V. K. K.; Sander, O.; Lehnert, N. *Inorg Chem* **2004**, *43* (22), 6979.

(24) Tuan, D. F. T.; Hoffmann, R. *Inorg Chem* **1985**, *24* (6), 871.

(25) Pamplin, C. B.; Ma, E. S. F.; Safari, N.; Rettig, S. J.; James, B. R. *J. Am. Chem. Soc.* **2001**, *123* (35), 8596.

(26) Piro, N. A.; Lichterman, M. F.; Harman, W. H.; Chang, C. J. *J. Am. Chem. Soc.* **2011**, *133* (7), 2108.

(27) Labios, L. A.; Millard, M. D.; Rheingold, A. L.; Figueroa, J. S. *J. Am. Chem. Soc.* **2009**, *131* (32), 11318.

(28) Fox, B. J.; Millard, M. D.; DiPasquale, A. G.; Rheingold, A. L.; Figueroa, J. S. *Angew. Chem. Int. Ed. Engl.* **2009**, *48* (19), 3473.

(29) Barnett, B. R.; Moore, C. E.; Rheingold, A. L.; Figueroa, J. S. *J. Am. Chem. Soc.* **2014**, *136* (29), 10262.

(30) Agnew, D. W.; Moore, C. E.; Rheingold, A. L.; Figueroa, J. S. *Angew. Chem. Int. Ed.* **2015**, *54* (43), 12673.

(31) Mokhtarzadeh, C. C.; Rheingold, A. L.; Figueroa, J. S. *Dalton Trans.* **2016**.

(32) Schiemenz, B.; Power, P. P. *Angew. Chem. Int. Ed. Engl.* **1996**, *35* (18), 2150.

(33) Neu, R. C.; Otten, E.; Stephan, D. W. *Angew. Chem. Int. Ed.* **2009**, *48* (51), 9709.

(34) Barnett, B. R.; Labios, L. A.; Moore, C. E.; England, J.; Rheingold, A. L.; Wieghardt, K.; Figueroa, J. S. *Inorg Chem* **2015**, *54* (14), 7110.

(35) M. K. Kesharwani, B. Brauer, J. M. L. Martin. *J. Phys Chem. A.* **2015**, *119*, 1701.

(36) Döring,S.; Erker, G. *Synthesis*, **2001**, *1*, 43-45.

(37) Döring, S.; Erker, G. *Synthesis* **2001**, *2001* (01), 0043.

(38) Booij, M.; Meetsma, A.; Teuben, J. H. *Organometallics* **1991**, *10* (9), 3246.

(39) Luinstra, G. A.; Teuben, J. H. *Organometallics* **1992**, *11* (5), 1793.

(40) Pangborn, A. P.; Giardello, M. A.; Grubbs, R. H.; Rosen, R. K.; Timmers, F. J. *Organometallics.* **1996**, *15*, 1518.

(41) Armarego, W. L. F.; Chai, C. L. L. *Purification of Laboratory Chemicals,* 5$^{th}$Ed.; Elsevier, 2003.

(42) Schwindt, M. A.; Lejon, T.; Hegedus, L. S. *Organometallics*, **1990**, *9*, 2814.

(43) Carpenter, A. E.; Mokhtarzadeh, C. C.; Ripatti, D. S.; Havrylyuk, I.; Kamezawa, R.; Moore, C. E.; Rheingold, A. L.; Figueroa, J. S. *Inorg. Chem.* **2015**, *54*, 2936.

(44) Sun, B.; Yoshino, T.; Matsunaga, S.; Kanai, M. *Adv. Synth. Catal.*, **2014**, *356*, 1491.

(45) Bertani, P.; Raya, J.; Bechinger, B. *Solid State Nuc. Mag. Res.* **2014**, *61-62*, 15.

(46) Le, H. V.; Ganem. B. *Org. Lett.* **2011**, *13*, 2584-2585.

(47) Neese, F. *Wiley Interdiscip. Rev.: Comput. Mol. Sci.* 2012, 2, 73.

(48) Becke, A. D. *J. Chem. Phys.* **1986**, *84*, 4524.

(49) Becke, A. D. *J. Chem. Phys.* **1993**, *98*, 5648.

(50) Lee, C. T.; Yang, W. T.; Parr, R. G. *Phys. Rev. B.* **1988**, *37*, 785

(51) Schaefer, A.; Horn, H.; Ahlrichs, R. *J. Chem. Phys.* **1992**, *97*, 2571.

(52) Weigend, F.; Ahlrichs, R. *Phys. Chem. Chem. Phys.* **2005**, *7*, 3297.

(53) Werner, H.J.; Manby, F. R.; Knowles, P. J. *J. Chem. Phys.* **2003**, *118*, 8149.

(54) van Lenthe, E.; Baerends, E. J.; Snijders, J. G. *J. Chem. Phys.* **1993**, *99*, 4597.

(55) van Lenthe, E.; Snijders, J. G.; Baerends, E. J. *J. Chem. Phys.* **1996**, *105*, 6505.

(56) Pantazis, D. A.; Chen, X. Y.; Landis, C. L.; Neese, F. *J. Chem. Theory Comput.* **2008**, *4*, 908.

(57) ChemCraft. Zhurko, G. A.; Zhurko, D. A. 2014, www.chemcraftprog.com

(58) Sheldrick, G. M. *Acta Crystallogr. A.*, **2008**, *64*, 112.

(59) Dolomanov, O. V.; Bourhis, L. J.; Gildea, R. J.; Howard, J. A. K.; Puschmann, H. *J. Appl. Cryst.* **2009**, *42*, 339.

# *Chapter 7*

# *Synthesis, Reactivity, and Electronic Structure Analysis of an m–Terphenyl Isocyanide Derived Cobalt–Carbyne.*

## 7.1 Introduction.

Transition metal systems that feature metal-carbon multiple bonding (*i.e*. bond orders >1) have received untiring intrigue from the organometallic community as result of their use in a number of industrially relevant and stoichiometric chemical transformations.[1-10] Of particular interest are systems that feature metal-carbon triple bonds due to their ability to facilitate alkyne metathesis.[1,3,11] Based on the specific transition metal platform varying reactivity patterns are available to carbyne complexes stemming from the differing electronic structures and $d^n$ count, specifically, high-spin Schrock-alkylidynes vs. low spin Fischer-Carbynes.[12-16] Accordingly, carbyne complexes of the late transition metals are primarily limited to Os[17-20] and Ru[20-22] and carbyne complexes featuring first row transition metals (*e.g* Fe[23-25], Co, Ni) are exceedingly rare or unknown. Of particular interest are complexes featuring group IX metals (*e.g*. Co, Rh, Ir) which to date are limited to Rh[26] and Ir.[27-29] Extension of M–C multiple bonding to Co has remained under developed since 2002 with work from Erker,[30] and has only recently seen a resurgence with the generation of Co-carbene complexes (M-C bond order = 2) from the labs of Baker,[31] Thomas,[32] and Groysman.[33] Surprisingly the actualization of a terminal cabyne ligand bound to Co is completely absent from the literature.

The dearth of Co-carbnye species make them attractive synthetic targets not only for electronic structure purposes but as potential platforms for the activation of small molecules and unsaturated C-C bonds.

Traditionally, late transition metal carbyne species adopt an electronic structure consistent with that of classical Fischer-carbynes, resultant from an electron rich metal center donating into the π*-mainfold of a π-acidic ligand.[12-16] Due to the propensity to engage in Metal→Ligand π-back bonding from electron rich metal centers isocyanides (C≡NR)[34-37] are attractive ligand architectures for the purpose of generating Fischer-type carbynes. Indeed the electrophilic functionalization of the isocyano–*N* atom has been realized and provided access to amiocarbyne ligand motifs of the early to mid transition block, [38-49] in addition to Fe reported in Chapter 3 of this dissertation.

Previously our groups has shown the effectiveness of sterically encumbering *m*-terphenyl isocyanides as ligand scaffolds for the generation of highly reduced metallates.[50-55] Herein we report the isolation of $K_2$[Cp*Co≡CNAr$^{Tripp2}$] (Ar$^{Tripp2}$ = 2,6-(2,4,6-(*i*-Pr)$_3$C$_6$H$_3$)C$_6$H$_3$). $K_2$[Cp* Co≡CNAr$^{Tripp2}$], which functions as a rare example of a terminal *m*-terphenyl isocyanide derived Co-iminocarbyne. Due to the geometric flexibility of the Cp*CoL framework, in addition to the isocyanide π*-manifold which exhibits appropriate orbital energetics,[56] the CNAr$^{Tripp2}$ can engage the Co *d*(xz) and *d*(yz) orbitals in two orthogonal π-bonding interactions to produce a net 3-fold bonding interaction between Co and the carbon atom of the isocyanide unit. This "extreme" form of π-backdonation emphasizes the versatility of *m*-terphenyl isocyanides as competent π-acids, a quality generally overlooked due to their attenuated π-acceptor/σ-donor ratio when compared to other cylindrically symmetric π-acidic ligands (*e.g.* CO, NO). [56,57]

Additionally, based on the reactivity profile of $K_2[Cp^*Co{\equiv}CNAr^{Tripp2}]$ with oxidants and electrophilic substrates (*e.g.* $H^+$, $Me_3Si^+$) coupled with Density Functional calculations, a molecular orbital analysis on the electronic structure of $K_2[Cp^*Co{\equiv}CNAr^{Tripp2}]$ is presented. It is found that the reactivity of $K_2[Cp^*Co{\equiv}CNAr^{Tripp2}]$ is facilitated by a metal based HOMO rendering the Co center extremely nucleophilic, and a functional form of $[Cp^*Co(CNR)]^{2-}$.

**7.2 Synthesis and Characterization of $K_2[Cp^*Co{\equiv}CNAr^{Tripp2}]$.**

Dissolution of $Cp^*CoI_2CNAr^{Tripp2}$ **(1)** in benzene ($C_6H_6$) and filtration over $KC_8$ (10 equivs) afforded a new diamagnetic species that featured a single $Ar^{Tripp2}$ environment as assayed by $^1H$ NMR spectroscopy(Scheme 7.1, Figure 7.11). Additionally, analysis of the resulting mixture exhibited an extremely red-shifted ν(CN) stretching frequency in the solution FTIR at 1509 $cm^{-1}$ ($C_6D_6$) suggestive of complete annihilation of C-N triple bond character ($CNAr^{Tripp2}$ ν(CN) = 2122 $cm^{-1}$ ($C_6D_6$)) of the isocyanide ligand. The isocyanide parentage of this low energy vibration was corroborated via $^{13}C$ isotopic enrichment of the $^{13}CNAr^{Tripp2}$ ligand, which displays a strong red-shifted resonance at 1490 $cm^{-1}$ diagnostic of the C–N bond Figure 7.10. Crystallization of the resultant reaction mixtures from a saturated *n*-pentane/$Et_2O$ solution (10:1; 1 mL) yielded the diethyl ether solvated dianion $K_2(Et_2O)_2[Cp^*Co{\equiv}CNAr^{Tripp2}]$, $K_2(Et_2O)_3$[**2**], as deep brown/black crystals suitable for X-ray diffraction, Figure 7.1.

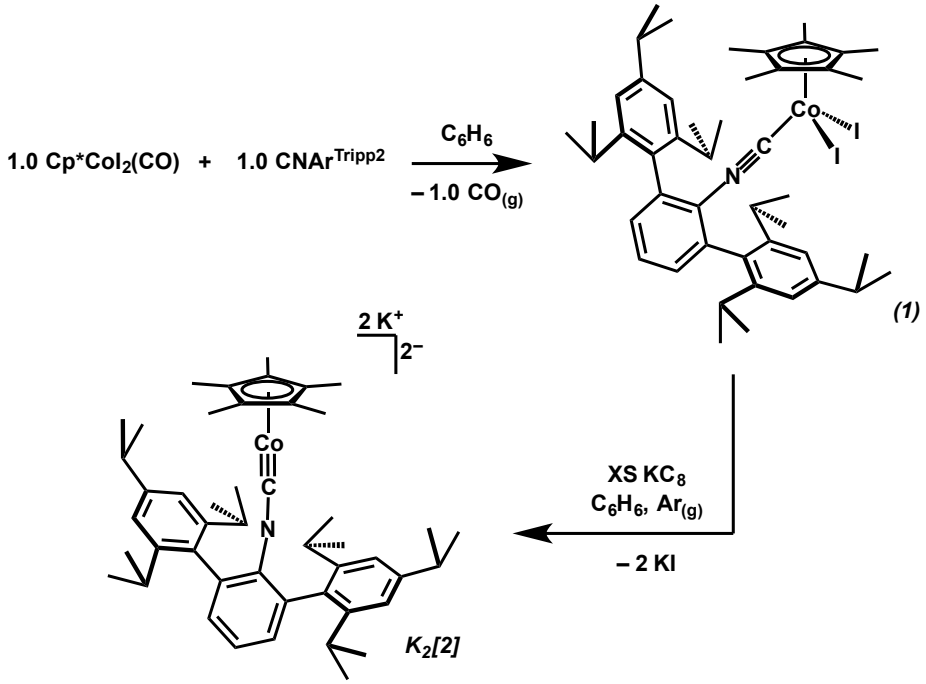


**Scheme 7.1** Synthetic scheme for the generation of (1) through CO for $CNAr^{Tripp2}$ ligand substitution and $K_2$[2] through reduction of (1) with excess $KC_8$.

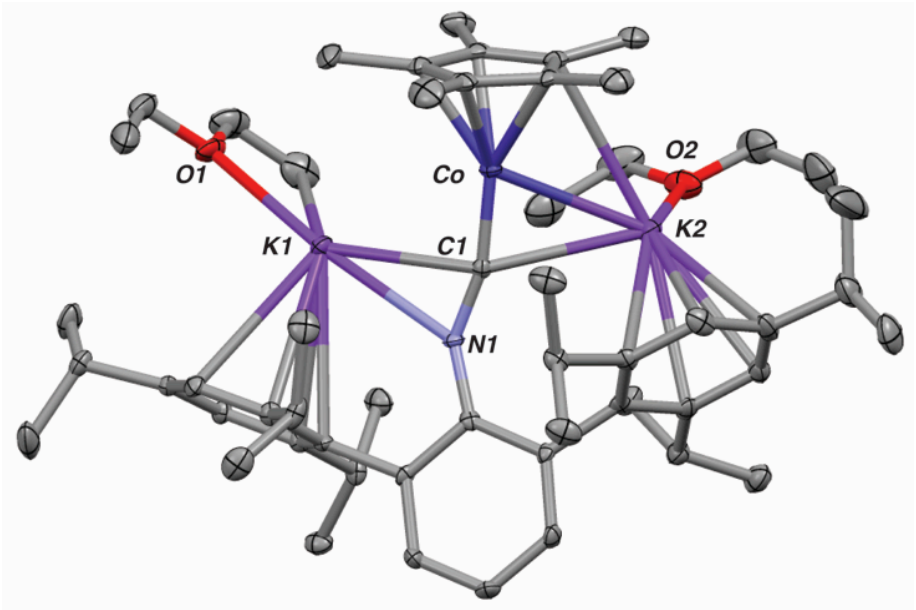


**Figure 7.1** Solid state structure of Molecular structure $K_2(Et_2O)_3$[Cp*Co≡$CNAr^{Tripp2}$], $K_2(Et_2O)_3$[**2**]. Hydrogen atoms and one $Et_2O$ molecule of solvation omitted for clarity.

Analysis of the solid state structure of $K_2(Et_2O)_3[Cp^*Co{\equiv}CNAr^{Tripp2}]$, $K_2(Et_2O)_3$[**2**] displays a Cp*Co unit supported by a single *m*-terphenyl isocyanide ligand. Further inspection of the solid-state structure reveals an extremely contracted Co-$C_{iso}$ distance of 1.670(3) Å, which when compared to recent examples of Co-based carbenes[30-33] displays a significant amount of contraction within the M–C linkage which can be rationalized as an increase in bond order (B.O.) between Co-C to three. Additionally, the angle at which the CNR unit coordinates to Co with respect to the "trans" ligand (*e.g.* the centroid of the Cp* ring) is 175.0(5)˚. This near-linear "trans" configuration in $K_2(Et_2O)_3$[**2**] is reminiscent of traditional transition metal complex's featuring a terminal amino-carbyne ligands which exhibit analogous linear coordination modes with respect to trans ligands.[58,59] $K_2$[**2**] also exhibits a rather elongated $C_1$-$N_1$ bond length at 1.307(3) Å consistent with a substantial degree of M→(CN) π*-back donation. Interestingly, further analysis of the *m*-terphenyl unit indicates an elongation of the $C_{ipso}$-$C_{ortho}$ bond lengths within the central ring of the *m*–terphenyl to 1.416(3), and 1.420(7) Å, with a concomitant contraction in the N–$C_{ipso}$ bond length to 1.372(3) Å, Figure 7.2. These structural deformities potentially point to a degree of dearomitization of the central ring within the *m*-terphenyl unit. Presumably this dearomitization we believe is due to accumulation of excess electron density in order to stabilize the extra charge equivalents localized on Co. Accordingly, a secondary description of the resultant ligand framework is shown in Scheme 7.2, where a resonance structure resulting in an anionic *m*–terphenyl unit can be rationalized.[40]

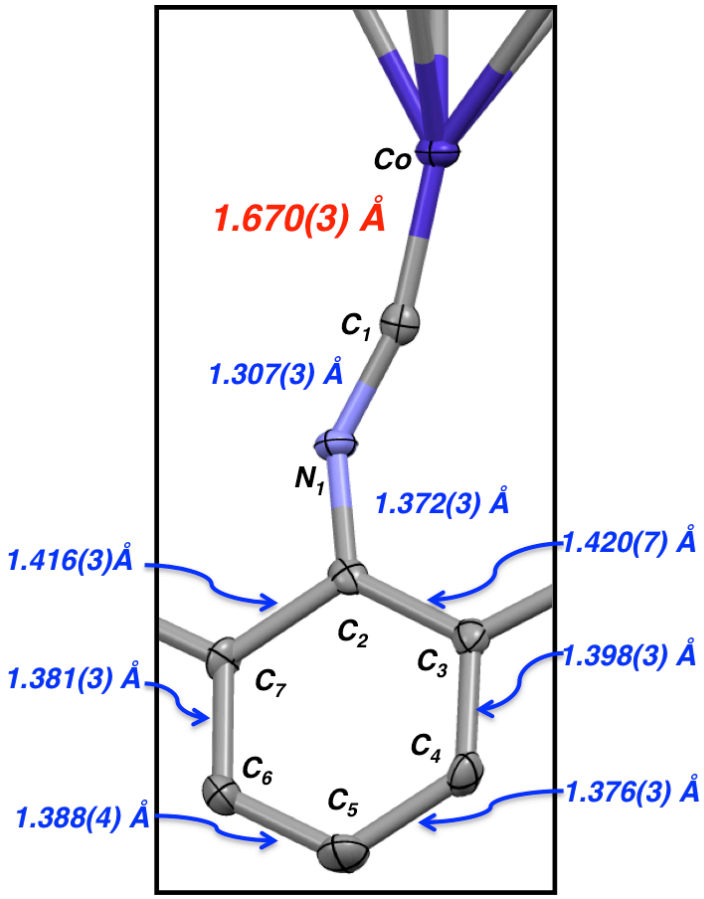


**Figure 7.2** Zoom in of the carbyne-Fe linkage and central ring of the *m*-terphenyl unit depicting relative bond lengths.

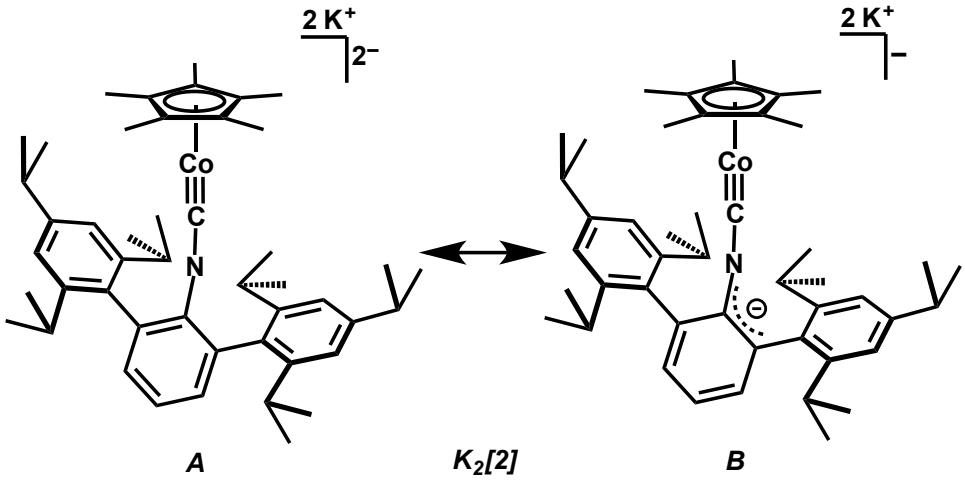


**Scheme 7.2** Resonance structures for $K_2$[2] depicting delocalization of electron density onto the *m*-terphenyl unit.

Furthermore, $K_2$[**2**] exits as a tight ion-pair displaying close cartion-π interactions between the alkali cations and the flanking rings of the *m*-terphenyl substituent and the CN–π*-manifold. Attempts to disrupt this interaction with the use of cation sequestration agents such as 18-crown-6, di-benzo-18-crown-6, 2,2,2-cryptand in addition to cation exchange with traditionally non-coordinating cations such as $PPN^+$ (Bis-(triphenylphosphine)iminium, $[Ph_3P{=}N{=}PPh_3]^+$) have proven unsuccessful, only affording intractable mixtures. Previously our group[50-53] and others[60-62] have shown the importance of cation-π interactions in the generation of highly reduced *m*-terphenyl containing species, such that disruption of these non-covalent interactions have deleterious effects on the stability of the overall molecular structure of the anionic species.[52,55]

### 7.3 Probing the Oxidation Chemistry of $K_2$[Cp*Co≡CNAr$^{Tripp2}$].

Due to the unusual solid state structure of $K_2$[**2**] we thought to probe Co-C interaction to determine if multiple bonding was persistent in the of a less electron releasing Co center upon oxidation. Treatment of $K_2(Et_2O)_3$[**2**] with one equivalent of Fc(OTf) (Fc = $Cp_2Fe$; OTf = $[CF_3SO_3]^-$) led only to partial oxidation and observation of the dinitrogen species Cp*Co($N_2$)(CNAr$^{Tripp2}$) (**3**) (Ch. 6 of this Dissertation). Complete oxidization of $K_2$[**2**] to Cp*Co($N_2$)(CNAr$^{Tripp2}$) (**3**) can be achieved via addition of a second equivalent of FcOTf. Cp*Co($N_2$)(CNAr$^{Tripp2}$) (**3**) displays a blue shifted ν(CN) stretch at 2004 $cm^{-1}$ in addition to a high energy ν(NN) stretch at 2110 $cm^{-1}$. Due to the high energy ν(NN) stretch we believe that coordination of $N_2$ is weak due to competition for π-backdonation with the CNR π*-manifold, rendering $N_2$ potentially labile,[63] and thus

potentially delivering an equivalent of Cp*Co(CNR). Comproportionation of $K_2$[**2**] and Cp*Co($N_2$)($CNAr^{Tripp2}$) (**3**) in THF–$d^8$ and analysis via $^1$H NMR spectroscopy (Figrue 7.13) indicated paramagnetically shifted $^1$H resonances indicative of a new species, that additionally exhibits an intermediate ν(CN) stretch at 1669 $cm^{-1}$ (*n*-pentane) with respect to both $K_2$[**2**] and (**3**). Although structural authentication of this species has been precluded, based on solution $^1$H NMR and FTIR spectroscopy we tentatively assign this species as the radical anion K[Cp*Co($CNAr^{Tripp2}$)], K[**4**]. Unfortunately additional analysis via room-temperature, low-temperature and solid-state EPR have also proven inconclusive in observing localization of the lone electron due to broadened and poorly resolved resonances that make it difficult to distinguish Co-hyperfine coupling ($I$ =7/2).

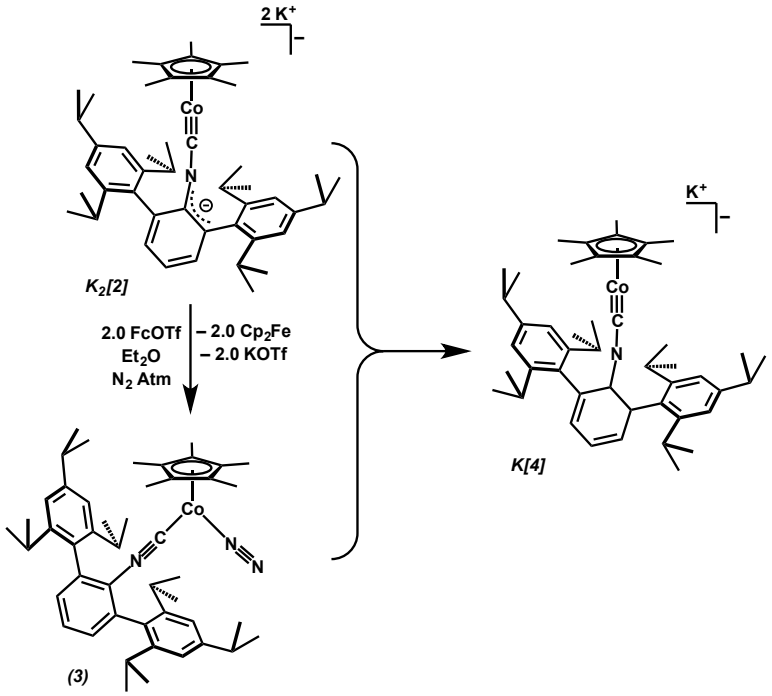


**Scheme 7.3** Reaction Scheme depicting the oxidation of $K_2$[2] to (3) under a dinitrogen atmosphere and the comproportionation of $K_2$[2] and (3) to afford the radical anion K[4].

## 7.4 Attempts at Electrophilic Functionalization of the Activated Isocyano-Unit in $K_2$[Cp*Co≡CNAr$^{Tripp2}$].

Treatment of $K_2$[**2**] with TMSCCH results in the smooth conversion to a new diamagnetic product that exhibits a singlet in the $^1$H NMR spectrum at –14.7 ppm ($C_6D_6$) consistent with the formation of a metal-hydride. Indeed, recrystallization of the reaction mixture affords the anionic mono-hydrido species K($Et_2O$)[Cp*Co(H)(CNAr$^{Tripp2}$)], K[**5**], as dark brown analytically pure crystals, Figure 7.3. Interstingly K[**5**] is the first mononuclear hydride of the formula CpCo(H)L. Analysis of the electron density map allowed for identification of the hydride–H and as such K[**5**] adopts a two legged piano stool coordination mode typical of mono-valent Cp$^R$Co species. Additionally, K[**5**] displays a blue shifted ν(CN) stretch at 1709 cm$^{-1}$ consistent with diminished Co→π*(CN) backdonation with respect to $K_2$[**2**]. The diminished Co→π*(CN) π-backdonation is also manifested in the solid state structure of K[**5**] with a slight elongation of the Co-$C_1$ bond length of 1.698(5) Å, an increase of *ca.* 1.3% compared to $K_2$[**2**]. K[**5**], also displays a downfield $^{13}$C resonance at 207.5 ppm for the isocyanide–*C* consistent with other reduced isocyano-metallates.[34,35,50-52,55,64] Surprisingly, the down field $^{13}$C shift of the isocyanide carbon is in stark contrast to its dianionic precursor $K_2$[**2**] which displays an up field $^{13}$C resonance for the carbyne carbon at 180 ppm, Figure 7.12. We believe this shift stems from the formal Co-C multiple bonding. K[**5**] displays a "classical" isocyanide coordination in that interactions with Co are ascribed to π-backdonation resulting in re-hybridization of the coordinated isocyanide from *sp* to *sp*$^2$ resulting in a deshielded isocyanide–*C* providing a downfield shifted $^{13}$C resonance.[35] However unlike K[**3**], $K_2$[**2**] can be rationalized to engage in two formal π-bonding

interactions between Co and the "isocyanide" carbon via deposition of electron density into both orthogonal π*-orbitals of the CN. This in turn maintains a formal *sp* hybridization of the "isocyanide" carbon due to the cylindrical π-bonds to Co, thus maintaining the cylindrically symmetric bonding mode about carbon which results in an up-field shifted $^{13}$C resonance. This is notable within in the context of aminocarbyne ligands which typically exhibit downfield $^{13}$C-resonances.[65] Moreover, this highlights an unusual extreme in isocyanide coordination that points to the versatility of the isocyanide ligands as π-acidic ligands for the stabilization of reduced transition metal systems.

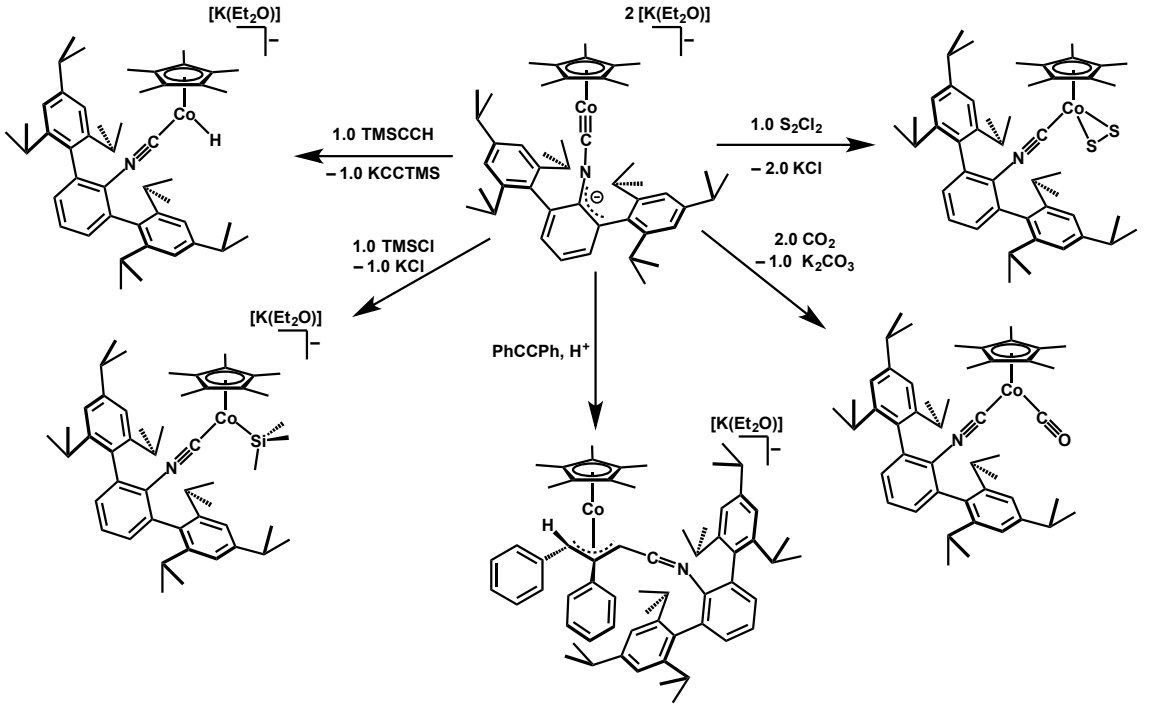


**Scheme 7.4** Reactivity pinwheel for $K_2$[Cp*Co≡CNAr$^{Tripp2}$], $K_2$[2], with various electrophiles.

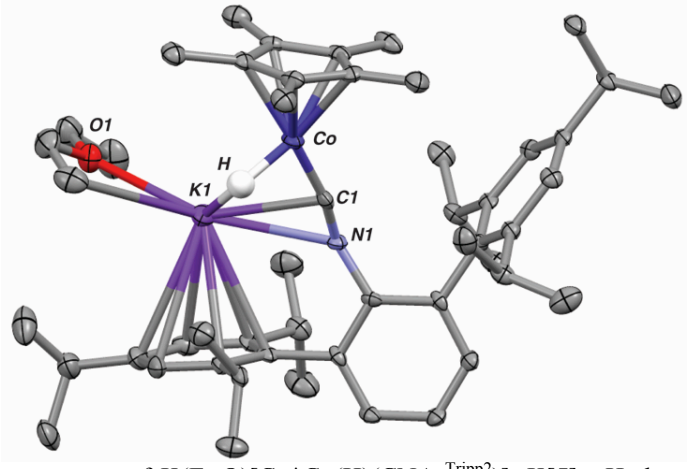


**Figure 7.3** Solid state structure of $K(Et_2O)[Cp^*Co(H)(CNAr^{Tripp2})]$, K[**5**]. Hydrogen atoms omitted for clarity.

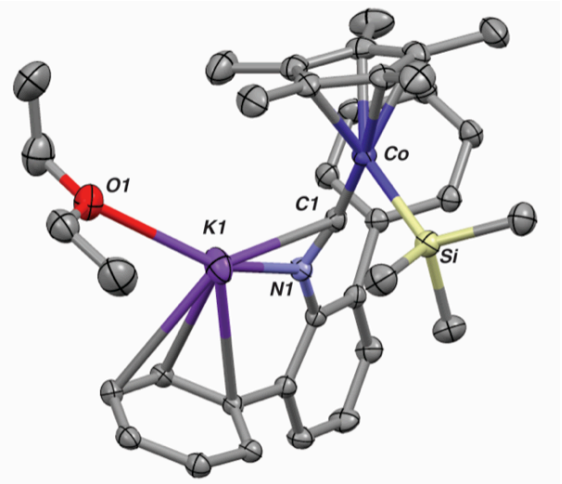


**Figure 7.4** Solid state structure of $K(Et_2O)[Cp^*Co(TMS)(CNAr^{Tripp2})]$, $K(Et_2O)$[**6**]. Hydrogen atoms and flanking *i*-Pr groups omitted for clarity.

**Table 7.1** Comparative structural paramaters for $K_2(Et_2O)_2$[**2**], $K(Et_2O)$[**5**], $K(Et_2O)$[**6**] depicting the variation in the isocyanide–Co linkage.

| | $K_2(Et_2O)_2$[**2**] | $K(Et_2O)$[**5**] | $K(Et_2O)$[**6**] |
|---|---|---|---|
| Co-$C_1$ (Å) | 1.670(3) | 1.699(4) | 1.687(1) |
| $C_1$-$N_1$ (Å) | 1.307(3) | 1.244(5) | 1.252(2) |
| $Cp_{centroid}$-$C_1$-$N_1$ (˚) | 174.88 | 146.31 | 142.80 |
| $C_1$-$N_1$-$C_2$ (˚) | 138.1(2) | 134.8(4) | 134.2(1) |

To further probe the point nucleophilic character in $K_2$[**2**] we sought the activation of Si-X bonds. Accordingly, treatment of a benzene solution of $K_2$[**2**] with TMSCl shows complete conversion to the mono-silayted species $K(Et_2O)$[Cp*Co(TMS)($CNAr^{Tripp2}$)], K[**6**], over two hours at room temperature. The molecular structure was unambiguously determined by X-ray diffraction, Figure 7.4. K[**6**] adopts a two legged piano stool coordination mode similar to K[**5**], and exhibits an elongated Co-C bond length of 1.687(1) Å similar to K[**5**] and is is a *ca.* 0.7 % longer the $K_2$[**2**]. Moreover, the spectroscopic features of K[**6**] also mimic K[**5**], with a ν(CN) stretch of 1707 $cm^{-1}$, and a downfield shifted $^{13}C$ NMR resonance of 209.3 ppm. This reactivity profile points to an interesting counterpoint of reduced isocyano-metallates. Typically isocyanide coordination to electron rich metal centers induces distortion of the CNC linkage (*e.g.* bending and subsequent re-hybridzation of the isocyanide unit)[35,52] activating the isocyanide toward electrophilic[45] functionalization with incoming substrates. However, despite the gross topological features of $K_2$[**2**] pointing to an extreme degree of activation of the isocyanide unit, functionalization of the isocyano–*N* is precluded. This lack of activation points to two interesting points: the first is that the *m*-terphenyl unit provides a steric profile significant enough to discourage further functionalization of the isocyano–*N*. The second is that the reactivity of $K_2$[**2**] is disjoint to previous examples of transition metal complexes featuring isocyanide derived carbyne ligands to the point that $K_2$[**2**] chemically functions as a potent metal based nucleophile akin to group 6, and 8 homoleptic carbonyl metallates specifically to its isoelectronic valence analogue $Na_2$[Fe($CNAr^{Mes2}$)].[52]

Further assessment of this metal-based nucleophilicty is seen with the activation main-group species. Treatment of $K_2$[**2**] with $S_8$ results in the formation of the Co(III) species Cp*Co($\eta^2$–$S_2$)($CNAr^{Tripp2}$) (**7**), as determined by X-ray diffraction, Figure 7.5. Complex **5** is a rare example of a $\eta^2$–$S_2$ disulfide ligand bound to a group 9 metal, and can be further described as a "heavy" analogue to transition metal peroxide complexes.[66] Disulfide **5** adopts a formally three legged piano-stool configuration common of trivalent Cp*Co species, with an S–S bond length of 2.05(1) Å. As a formal oxidation to Co(III) occurs, the resultant spectroscopic features are also observed resulting in a blue shifted ν(CN) stretch of 2117 $cm^{-1}$ and an up field shifted $^{13}C$ resonance at 164.6 ppm consistent with diminished Co→π*(CN).

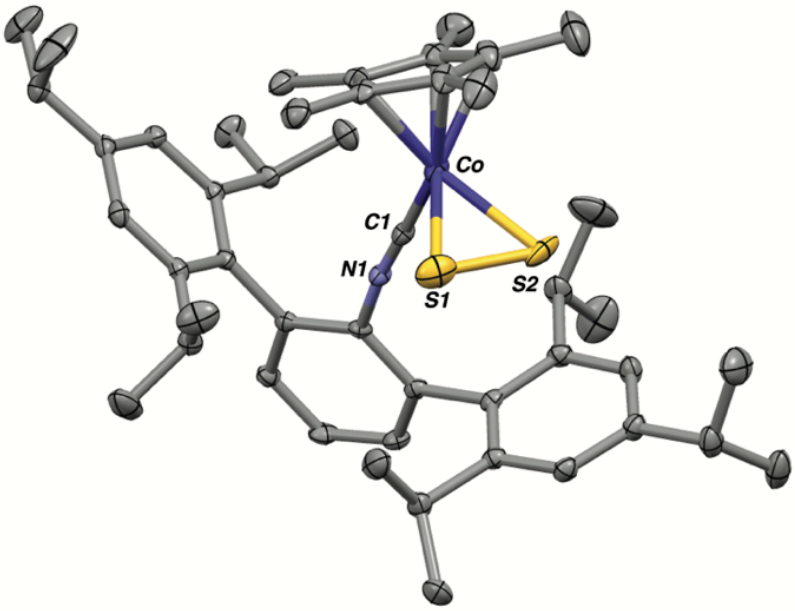


**Figure 7.5** Solid state molecular structure of Cp*Co($\eta^2$–$S_2$)($CNAr^{Tripp2}$) (**7**). Hydrogen atoms and disorderd $S_2$ and $S_4$ components omitted for clarity.

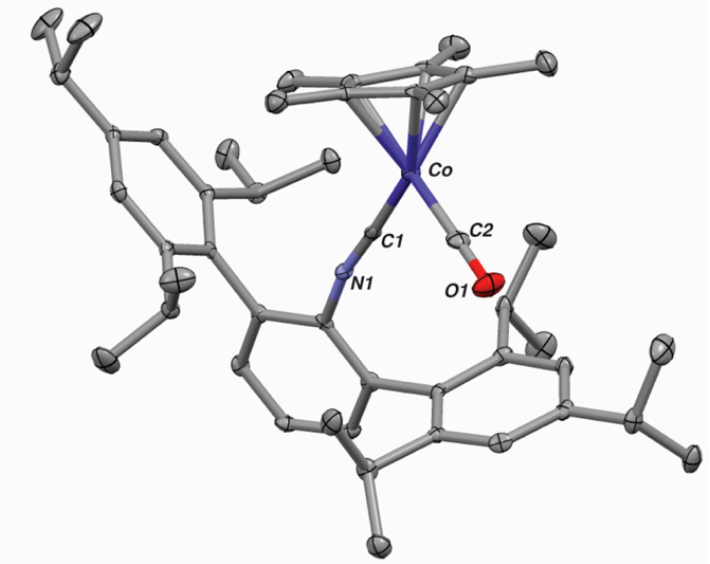


**Figure 7.6** Solid state structure of Cp*Co(CO)(CNAr$^{Tripp2}$), (**8**). Hydrogen atoms omitted for clarity.

To draw further comparison to highly reduced isocyano metallates that exhibit potent metal based nucleophilicty, the reactivity of $K_2$[**2**] toward $CO_2$ activation was undertaken. As noted previously $K_2$[**2**] can be reasoned to be an isoelectronic valence mimic of the group 8 dianionic metallates $[M(CO)_4]^{2-}$ (M = Fe, Ru, Os) similar to the relationship between $Fe(CO)_4$ and CpCo(CO),[67-69] which show an aptitude to facilitate the reductive disproportionation of $CO_2$ to CO and $CO_3^{2-}$.[70,71,76,79] Indeed treatment of $K_2$[**2**] with an atmosphere of $CO_2$ results in an immediate color change from dark brown to deep red with the formation of Cp*Co(CO)(CNAr$^{Tripp2}$), (**8**) as determined by X-ray diffraction. Complex **8** is isostructural with the dinitrogen adduct **3** (Chapter 6), and adopts a two legged piano stool coordination mode. Coordinated CO was verified with an intense ν(CO) stretch in the FTIR at 1934 $cm^{-1}$, in addition to displaying a downfield shifted $^{13}C$ resonance at 209.2 ppm corresponding to coordinated CO. In an effort to verify the formation of $CO_3^{2-}$ and show that reduction of $CO_2$ proceeded via a reductive

disproportionation mechanism, $K_2$[**2**] was treated with $^{13}CO_2$. Removal of solvents and dissolution in alkaline $D_2O$ followed by analysis via $^{13}C\{^1H\}$ NMR spectroscopy indicated the production of $^{13}C$ carbonate at 168 ppm.[72] Accordingly, we assert that activation of $CO_2$ occurs through a reductive disproportionation mechanism depicted in Scheme 7.5. [71,73-75] Initial nucleophilic attack by $K_2$[**2**] at the $CO_2$–*C* to generate an insipient $\kappa^1$–*C*-metalo-carboxylate, followed by rapid interception with a second equivalent of $CO_2$ and subsequent O-atom transfer to afford complex **8**, and an equivalent of $K_2CO_3$. Importantly this reactivity profile with electrophilic hetero-allene substrates further emphasizes the metal-based nucleophilicty of $K_2$[**2**] consistent with the formulation of a highly reduced isocyano-metallate with substantial nucleopholicity at Co.

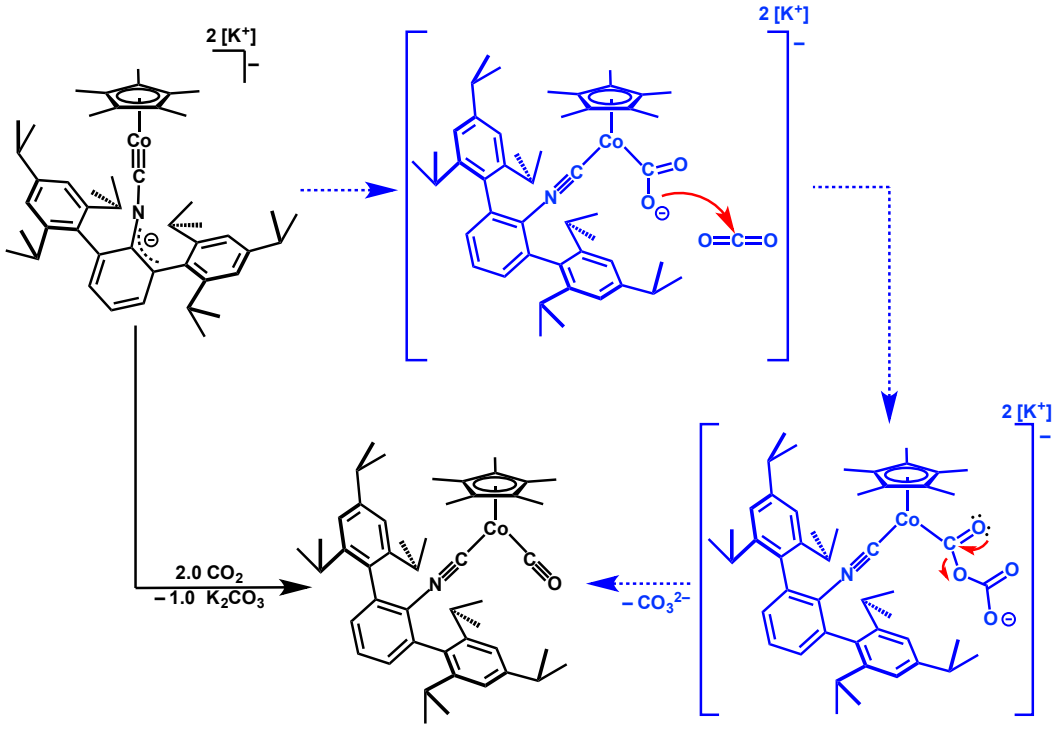


**Scheme 7.5** Reaction scheme depicting the reductive disproportionation of $CO_2$ to $CO_3^{2-}$ and CO to yield complex **8.**

In an effort to access "classical" aminocarbyne C-C bond forming reactivity[43,48,76,77] we targeted the activation of internal alkynes. Accordingly, treatment of $K_2$[**2**] with diphenyl acetylene results in the rapid color change from brown to black and then to brown over the course of 1 hour. Crystallization of the resultant reaction mixture afforded the anionic allyl species K[**9**] as the diethylether solvate, Figure 7.7. Generation of complex K[**9**] features a rather unusual cyclic core can shows formal insertion of the Carbyne-*C* carbon into the acetylene C-C bond followed by subsequent protonation. Monitoring the reaction mixture via $^1$H NMR spectroscopy at various time points revealed the presence of multiple species which over the course of 1 hour convert to yield allyl-K[**9**]. Multiple attempts to isolate these intermediates have been unsuccessful and have only afforded K[**9**] as the major Co-containing species upon work up. Attempts to pinpoint the origin of the subsequent $H^+$ source are on going. Reactions done in benzene-$d^6$ give analogous vinylic-proton resonances as assayed by $^1$H NMR spectroscopy when compared to reactions done in protio-benzene, suggestive that subsequent protonation of the fleeting dianionic intermediate is not a result of solvent activation.

Accordingly, treatment of $K_2$[**2**] with sub-stoichiometric amounts of diphenylacetylene (*ca.* 0.5 equivs) and analysis via $^1$H NMR spectroscopy indicate the immediate formation of a 2:1 mixture of allyl K[**9**], and an unidentified Cp* containing species with complete consumption of $K_2$[**2**]. Monitoring of the reaction over the course of 2 hours via $^1$H NMR spectroscopy, resulted in the consumption of the unidentified Cp* containing species and smooth conversion to K[**9**]. In an effort to target what can be rationalized as a doubly reduced alkyne adduct as a preliminary reduction intermediate

upon addition of PhCCPh to $K_2$[**2**], we sought to explore the reduction chemistry of Cp*Co(CNAr$^{Tripp2}$)($\eta^2$-C,C-PhCCPh) (**10**, Ch 6). Treatment of **10** with 2.0 equivalents $KC_8$ results in an immediate color change from red-orange to black. Analysis of the crude reaction mixture via $^1$H NMR spectroscopy indicated formation of a paramagnetic species as the primary constituent of the reaction mixture in addition to small amounts of K[**9**]. Efforts to intercept this species and structurally authenticate it have been precluded and are ongoing within our laboratory.

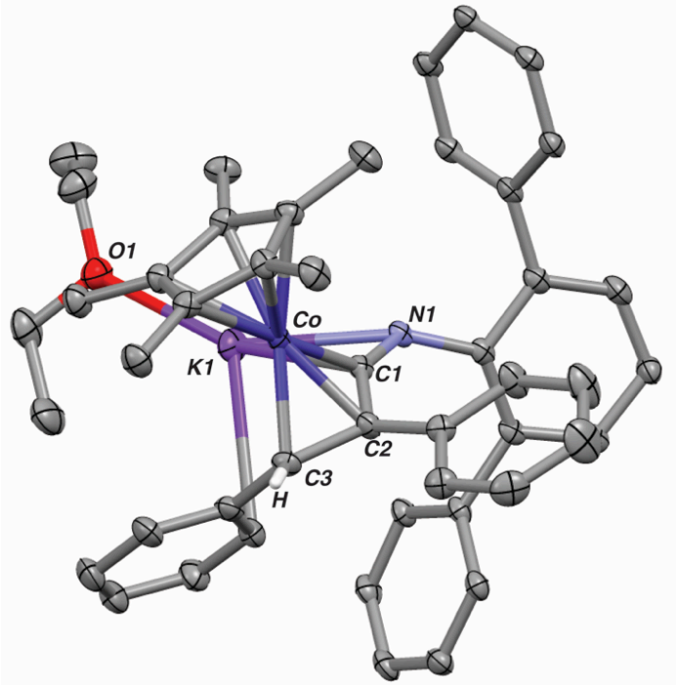


**Figure 7.7** Solid state structure of Alyl Complex K[**7**]. Hydrogen atoms and *i*-Pr groups omitted for clarty.

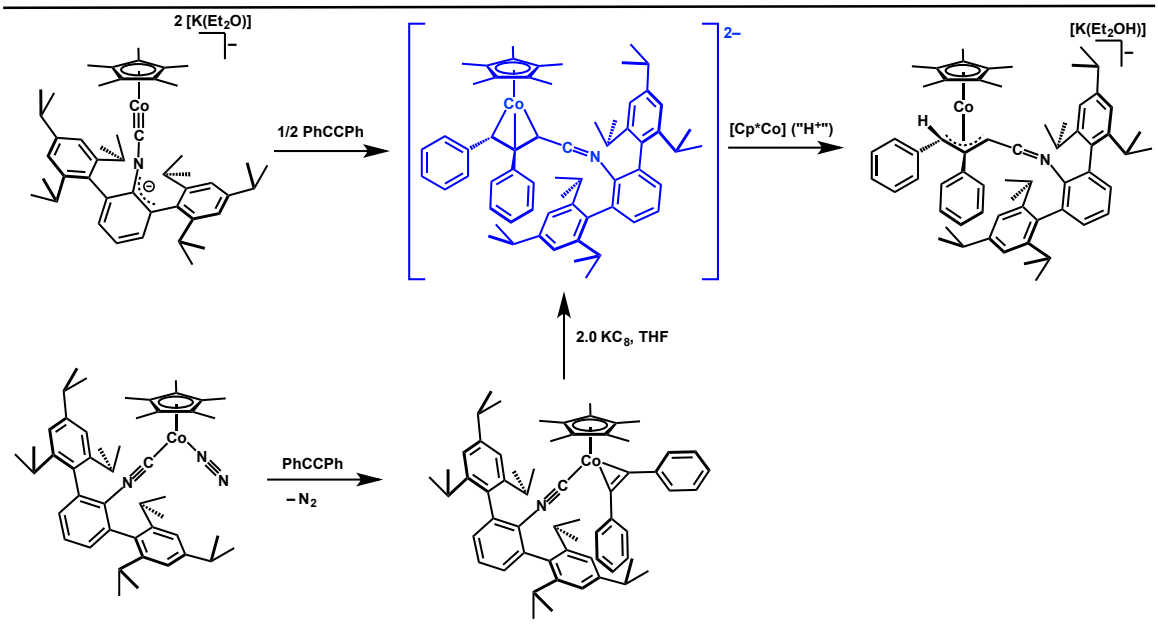


**Scheme 7.6** Reaction scheme depicting the formation of allyl K[**9**].

## 7.5 Electronic Structure Analysis of $K_2$[Cp*Co(CNAr$^{Tripp2}$)].

In the interest of developing an understanding of the electronic structure of $K_2$[**2**] a computational investigation was undertaken. Geometry optimizations of the truncated model complex [Cp*Co≡CNXyly]$^{2-}$ (xylyl = 2,6-dimethylphenyl) were conducted and indicate good correlation between experimental and computed bond metrics, Table 8.2. Computations done with both BP86 and B3LYP functionals indicate a three fold bonding interaction between Co and the isocyanide carbon by virtue of π-backdonation into the isocyanide π*-manifold. Interestingly however, analysis of the orbital configuration for [Cp*Co≡CNXyly]$^{2-}$ suggest that orbital energy ordering is functional dependent (*e.g.* BP86 v. B3LYP). A computed ordering of metal-based *d*–orbital for both functionals is shown in Figure 7.8. Use of the hybrid functional B3LYP places the Co-isocyanide π-bonding orbitals *d*(xz)/(yz) high in energy as HOMO/-1 and the non bonding metal

*d*(xy)/($x^2$-$y^2$) lower in energy (HOMO-2/-3). Reducing the percentage of Hartree-Fock,[78] with the use of the pure functional BP86 reflects a switch in relative orbital energy orderings resulting in a lowering of the π-bonding orbitals *d*(xz)/(yz) (HOMO-2/-3) below the filled metal non-bonding orbitals *d*(xy)/($x^2$-$y^2$) (HOMO/-1).

**Table 7.2** Experimental and geometry optimized bond distances (Å) and angles (˚) for $K_2(Et_2O)_2$[Cp*Co($CNAr^{Tripp2}$)], $K_2(Et_2O)$[**2**], and $[Cp*Co(CNXylyl)]^{2-}$ utilizing both B3LYP and BP86 functional.

| | $K_2(Et_2O)_2$[Cp*Co($CNAr^{Tripp2}$)] $K_2(Et_2O)$[**2**] | $[Cp*Co(CNXylyl)]^{2-}$ BP86 | $[Cp*Co(CNXylyl)]^{2-}$ B3LYP |
|---|---|---|---|
| Co-$C_1$ (Å) | 1.670(3) | 1.67030 | 1.64441 |
| $C_1$-$N_1$ (Å) | 1.307(3) | 1.29143 | 1.29481 |
| $N_1$-$C_2$ (Å) | 1.372(3) | 1.34796 | 1.33596 |
| $C_2$-$C_3$ (Å) | 1.424(4) | 1.45173 | 1.44778 |
| $C_2$-$C_7$ (Å) | 1.416(3) | 1.44925 | 1.44601 |
| Co-$C_1$-$N_1$ (˚) | 164.3(2) | 171.56 | 171.77 |
| $C_1$-$N_1$-$C_2$ (˚) | 138.1(2) | 138.95 | 138.08 |

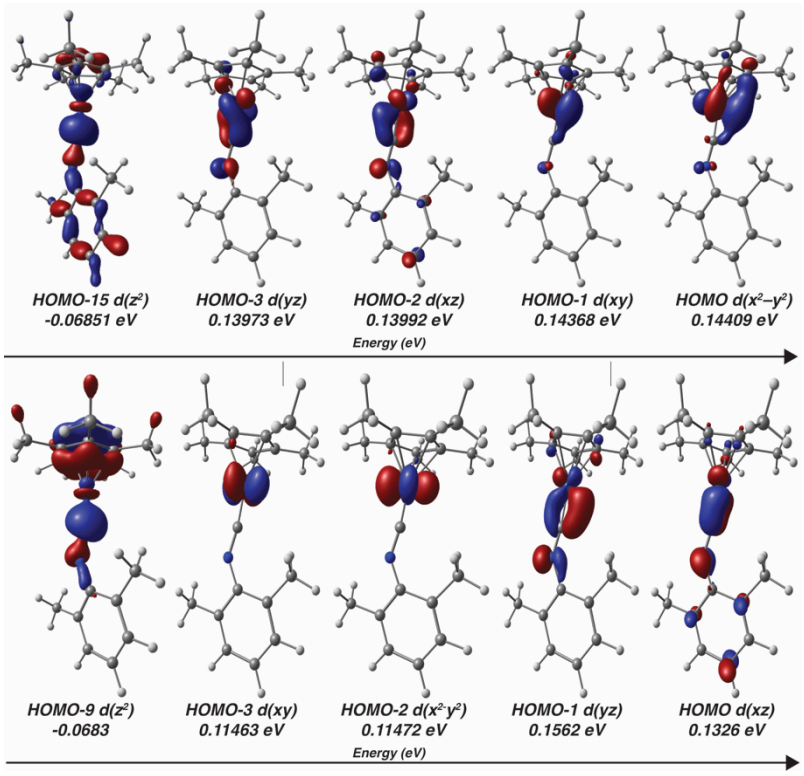


**Figure 7.8** Calculated metal based orbitals for the truncated model complex [Cp*Co≡CNXyly]$^-$, BP86 Def2-TZVP/J (Top), and B3LYP Def2-TZVP/J (Bottom) depicting orbitals of metal-$3^d$ paraentage.

Although direct interrogation of the HOMO of $K_2$[**2**] from the oxidation to K[**4**] has been precluded due to a lack of structural and well resolved EPR data qualitative molecular orbital diagram can be derived based on computational analysis and experimental reactivty, Figure 7.9. Accordingly the isocyanide carbon engages in a σ-interaction with the Co $dz^2$ orbital in addition to two π-bonds with the *d*(xz)/(yz) orbitals by virture of extreme π-backdonation.[12,15,16] That leaves the Co *d*(xy)/($x^2$-$y^2$) as non-bonding and the two highest occupied molecular orbitals. This arrangement is takes advantage of favorable interactions between Co *d*(xz)/(yz) and the isocyanide π*-manifold lowering the resulting molecular orbitals with respect to the *d*(xy)/($x^2$-$y^2$). Further more, this electronic strucutre analysis accounts for the reactivity profile with $K_2$[**2**] with electrophilic stubstrates and explains why electrophilic functionalization of the isocyanide–*N* is not observed. Moreover, this substantiates the characterization of $K_2$[**2**] as a unique isocyanide derived carbyne that functions as a potent metal-based nucleophile and a masked source of $[Cp^*Co(CNR)]^{2-}$ .

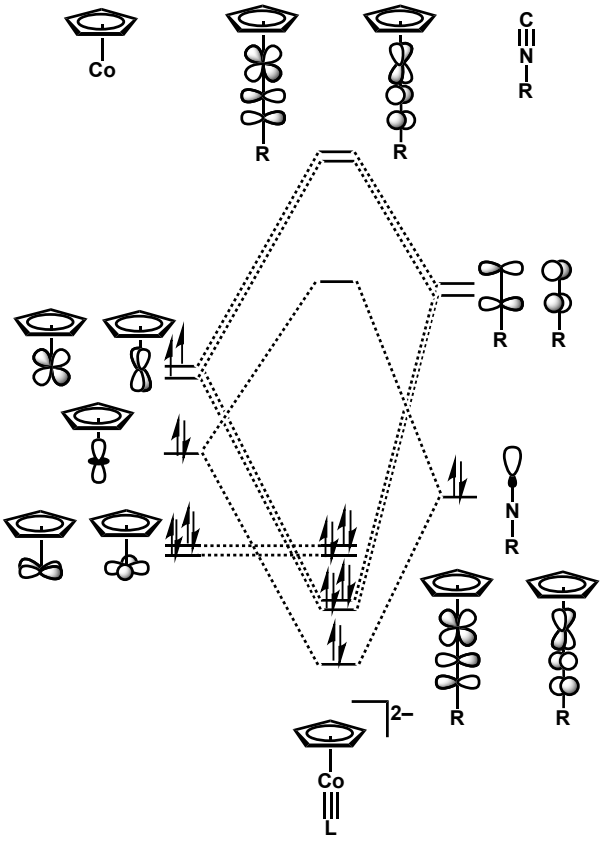


**Figure 7.9** Qualitative molecular orbital diagram for $K_2[Cp^*Co{\equiv}CNAr^{Tripp2}]$, $K_2$[**2**] depicting frontier orbital interactions between coordinated isocyanide and 3d orbital manifold on Co.

## 7.6 Concluding Remarks.

Here in reported is the isolation of the first example of a Co-carbyne derived from an *m*-terphenyl isocyanide. Due to the extreme degree of Co→π*(CN) donation, a formal shift from π-backdonation to π-bonding is observed consistent with a 3-fold bonding interaction between Co and C. Indeed, the formal Co-C triple bond is observed computationally, and depicted with a qualitative MO argument such that the Co-*C* π-bonds are Co (xz) and (*yz*) and CNR π* in parentage. Additionally this bonding interaction results in Co–C π-bonds lowering in energy with respect to the Co non-

bonding orbitals (*xy*) and ($x^2$-$y^2$) yielding a highly reduced Co-based nucleophile. The electronic structure analysis of $K_2$[**2**] was explored chemically and is reflected with the one electron oxidation via comproportionation with the dintrogen species Cp*Co*($N_2$)($CNAr^{Tripp2}$) (**3**) yield a paramagnetic species with an intermediate isocyanide ν(CN) stretch in the FTIR which we tentatively assign to the radical anion K[**2**]. Further more, the metal-based nucleophilicty is further corroborated with the reactivity profile observed with electrophiles culminating in the reductive disproportionation of $CO_2$ to yield **6** and inorganic $CO_3^{2-}$, analogous to the isoelectronic group 8 carbonyl metallates which function are potent metal-based nucleophiles. Finally, activation of internal alkynes leads to novel C-C bond forming reactivity resulting in the isolation of metal-alyl K[**9**]. Mechanistic investigation to describe the pathway of C-C bond formation for K[**9]** are ongoing in our laboratory.

**7.7 Synthetic Procedures and Characterization Data.**

**General Considerations:** All manipulations were carried out under an atmosphere of dry dinitrogen or Argon using standard schlenk, and glove box techniques. Solvents were dried and degassed according to standard procedures.[80] Unless otherwise stated all materials were obtained from commercial vendors and used as received or purified by standard procedures.[81] Benzene-$d_6$, Tetrahydrofuran-$d_8$, were dried with Na/K and Benzophenone followed by distillation and stored on 4 Å molecular sieves for 3 days prior to use. Celite 405 (Fischer Scientific) was dried under vacuum for 24 hours at a temperature greater then 250° C and stored inside the glove box prior to use. $KC_8$ was

prepared according to published procedures.[82] The *m*-terphenyl ioscyanide $CNAr^{Tripp2}$,[57] and $Cp^*CoI_2(CO)$[83] were prepared according to literature procedures.

Solution $^1H$, $^{13}C\{^1H\}$ spectra were recorded on a Varian Mercury 400 spectrometer, a Bruker Advance 300, a Varian XSENS-500, and a Joel ECA 500 spectrometers. $^1H$, and $^{13}C$ chemical shifts are reported in ppm relative to $SiMe_4$ ($^1H$ and $^{13}C$ $\delta$ = 0.0 ppm) with reference to residual $C_6D_5H$ or solvent references of 7.16 ppm (1H) and 128.06 ppm ($^{13}C$) for benzene–$d_6$[84], and THF-$d_8$[84]. FTIR spectra were recorded on a Thermo-Nicolet iS10 FTIR spectrometer. Samples were prepared either as KBr pellets, or a $C_6D_6$, solution injected into a Thermo Fischer solution cell equipped with KBr, or $CaF_2$ windows. For solution FTIR spectra, solvent peaks were digitally subtracted from all spectra by comparisons with an authentic spectrum obtained immediately prior to that of the sample. The following abbreviations were used for the intensities and characteristic of important IR absorption bands: vs = very strong, s = strong, m = medium, w = weak, vw = very weak, b = broad, vb = very broad, sh = shoulder. Combustion analyses were performed by Midwest Microlab LLC, Indianapolis, IN.

**Synthesis of $Cp^*CoI_2CNAr^{Tripp2}$ (1):** To a $C_6H_6$ solution (60 mL) of $Cp^*CoI_2CO$ (1.55 g, 3.26 mmoles, 1 equiv) was added $CNAr^{Tripp2}$ (1.89 g, 3.32 mmoles, 1.02 equiv) all at once. Upon addition there was an immediate effervescence indicative of CO loss. The mixture was allowed to stir for *ca.* 4 hours where upon all volatiles were removed *in vacuo*. There after, the resulting purple solid was taken up in *n*-Pentane and filtered over a medium glass sintered frit to yield $Cp^*CoI_2CNAr^{Tripp2}$ as a purple solid, 3.05 g, 3.19

mmoles, 98% yield. X-ray Diffraction/Analytically pure crystals were grown from a $CH_2Cl_2$ solution layered with *n*-Hexane (1:6) over one week. $^1$H NMR (400.1 MHz, $C_6D_6$, 20 ˚C): δ = 7.26 (s, 4H, *m*-Trip), 7.02 (d, 2H, 8Hz, *m*-Ph), 6.84 (t, 1H, 8Hz, *p*-ph), 2.91 (sept, 2H, 7Hz, C*H*$(CH_3)_2$), 2.85 (sept, 4H, 7Hz, C*H*$(CH_3)_2$), 1.60 (s, 15H, *H*-Cp*), 1.57 (d, 12H, 7 Hz, CH(C*H*$_3)_2$), 1.37 (d, 12H, 7 Hz, CH(C*H*$_3)_2$), 1.12 (d, 12H, 7 Hz, CH(C*H*$_3)_2$) ppm. $^{13}$C{$^1$H} NMR (125.7 MHz, $C_6D_6$, 20 ˚C): δ = 158.9 (*C*NR), 149.7, 146.8, 139.7, 133.2, 131.7, 122.0, 127.7, 96.5, 35.1, 31.4, 25.4, 24.7, 24.5, 11.4. FTIR ($C_6D_6$; KBr Window; 20 ˚C): $\nu_{CN}$ = 2130 (s), also 2960 (m), 2927 (w), 2905 (w), 2868 (w), 1605 (w), 1566 (w), 1464 (w), 1430 (w), 1412 (w), 1382 (w), 1363 (w), 1204 (w), 1071 (w), 1054 (w), 1020 (w), 941 (w), 877 (w), 759 (w), 681 (w) cm$^{-1}$. Anal. Calcd. For $C_{47}H_{64}NI_2Co$: C, 59.04; H, 6.75; N, 1.47. Found: C, 59.17; H, 6.80; N, 1.47.

**Synthesis of H$^{13}$C(O)NHAr$^{Tripp2}$**: A schlenk tube was charged with neat acetic anhydride (1.27 g, 0.0124 moles, 2.05 equiv) was cooled to 0 °C under an $N_2$ atmosphere and $^{13}$C formic acid (0.58 g, 0.0124 moles, 2.05 equiv) was added via syringe over 5 min. The resulting colorless solution was gently refluxed for 3 h, allowed to cool to room temperature, and added via cannula to a THF solution of $NH_2Ar^{TRIPP2}$ (3 g, 0.00603 mol, 1 equiv, 100 mL) over the course of 1 hour. The reaction mixture was then heated to 60$^o$C for 4 days. Upon completion the reaction mixture was cooled to room temperature and all volatiles were removed via rotary evaporation. To remove residual acetic acid the solid was slurried in $H_2O$ (100 mL) and filtered over a medium porosity glass sintered frit and subsequently washed 3 X 100 mL with $H_2O$. The resulting solid was dissolved in $Et_2O$ and dried with anhydrous $Na_2SO_4$ followed by vacuum filtration and subsequent

rotary evaporation. The resulting solid was then suspended in EtOH (100 mL) and triturated for 30 mins where upon it was cooled to 0°C precipitated out of solution and isolated via vacuum filtration. Subsequent drying via rotary evaporation yielded $HC(O)NHAr^{TRIPP2}$ as a white solid (2.28 g, 65 %). For characterization the reader is referenced to Chapter 6. Verification of $^{13}C$ incorporation was verified with a prominent $^{13}C$ resonance in the $^{13}C\{^{1}H\}$ spectrum that matched the resonance presented in Chapter 6.

**Synthesis of $^{13}CNAr^{Tripp2}$** $H^{13}C(O)NHAr^{TRIPP2}$ ( 2.28 g, 4.34 mmoles, 1 equiv) was charged into a 100 mL schlenk flask already containing dry $CH_2Cl_2$ (75 mL) and a stir bar under a $N_2$ atmosphere. Diisopropoyl amine (3.06 g, 30.3 mmoles, 7 equivs) was added via syringe. The resulting mixture was cooled to 0°C where upon $POCl_3$ (3.32 g, 21.7 mmoles, 5 equivs) was added drop wise via syringe over 20 mins. The resulting mixture was allowed to warm to room temperature and react for 5 days at 60˚C. Following 50 mL's of a 1.5 M $Na_2CO_3$ solution was added to quench any remaining $POCl_3$. The resulting organic layer was separated from the aqueous layer. The aqueous layer was back extracted with 3 X 100 mL $CH_2Cl_2$. All organics were combined and dried over $MgSO_4$ and separated via vacuum filtration. All volatiles were removed via rotary evaporation. The resulting off white solid was slurried in 100 mL of thawing MeCN and filtered followed by 2 X 50 mL washes with MeCN. The resulting white solid was dried via rotary evaporation to yield $CNAr^{Tripp2}$ (1.98 g, 3.91 mmol, 90%). $^{1}H$ NMR spectroscopy confirmed the purity with an analogus spectroscopic features

described in Chapter 6. Verification of $^{13}C$ incorporation was accomplished by $^{13}\{^{1}H\}$ NMR spectroscopy and matched the $^{13}C$ resonance of the *C*NR described in Chapter 6.

**Synthesis of Cp*CoI$_2$($^{13}$CNArTripp2):** Preparation of Cp*CoI$_2$($^{13}$CNAr$^{Tripp2}$) was prepared in an analogous fashion to Cp*CoI$_2$(CNAr$^{Tripp2}$): 0.331 g, 0.696, mmoles, 1.0 equivs of Cp*CoI$_2$(CO), 0.353 g, 0.696 mmoles, 1 equivs of $^{13}$CNAr$^{Tripp2}$; Yield = 598 g, 0.626 mmoles, 90 % yield.

**Synthesis of K$_2$[(Cp*Co(CNAr$^{Tripp2}$)] from the reduction of ($\eta^5$-Cp*)CoI$_2$CNAr$^{Tripp2}$:** In an Argon filled glove box Cp*CoI$_2$CNAr$^{Tripp2}$ (0.202 g, 0.215 mmoles, 1 equiv) was dissolved in $C_6H_6$ (1.5 mL). Separately $KC_8$ (0.290 g, 2.15 mmoles, 10 equiv) was split into two fractions and packed in a glass pipett atop a fiberglass filter pad. The benzene solution of Cp*CoI$_2$CNAr$^{Tripp2}$ was filtered over the previously prepared $KC_8$ filters sequentially at a rate of 3 drops/second to afford a dark red-brown solution. The resultant solution was then filtered over Celite packed on fiberglass (2 cm) to remove any adventitious KI. The solution was then frozen in the freezer at -40 ˚C and lyophilized under reduced pressure to afford K$_2$[Cp*CoCNAr$^{Tripp2}$] as an analytically pure dark brown fluffy solid 0.147 g, 0.188 mmoles, 88 %. X-ray diffraction quality crystals were grown from a saturated $Et_2O$/*n*-pentane solution (1 mL, 1:10) over 1 week at -40˚C. $^{1}H$ NMR (400.0 MHz, $C_6D_6$, 20 ˚C): δ = 6.99 (s, 4H, *m*-Tripp), 6.81 (s, 3H, *m/p*-Ph), 3.36 (sept. 4H, 7Hz, C*H*(CH$_3$)$_2$), 2.625 (sept. 2H, 7Hz, C*H*(CH$_3$)$_2$), 2.25 (s, 15H, Cp*-*H*), 1.53 (d, 12H, 7Hz CH(C*H$_3$*)$_2$), 1.53 (d, 12H, 7Hz, CH(C*H$_3$*)$_2$), 1.10 (d, 12H, 7Hz, CH(C*H$_3$*)$_2$) ppm. $^{13}C\{^{1}H\}$ NMR (125.8 MHz, $C_6D_6$, 20 ˚C): δ = 181.3 (*C*NR), 149.6, 146.7, 143.0,

142.7, 131.4, 130.4, 119.9, 111.9, 79.2, 34.5, 30.9, 24.7, 24.5, 24.2, 14.6 ppm. FTIR ($C_6D_6$; KBr Window; 20 ˚C): $\nu_{CN}$ = 1510(s), also 2960 (s), 2927 (sh), 2897 (m), 2871 (m), 2708 (w), 1566 (w), 1411 (w), 1377 (m), 1068 (w), 1025 (w), 995 (w), 947 (w), 882 (w), 749 (w) $cm^{-1}$. Due to the extreme air sensitivity of multiple attempts at acquiring elemental analysis resulted in substantial deviation from predicted values. Anal. Calcd. For $C_{47}H_{64}NCoK_2$: C, 72.36; H, 8.27; N, 1.80. Found: C, 67.67; H, 8.21; N, 2.20.

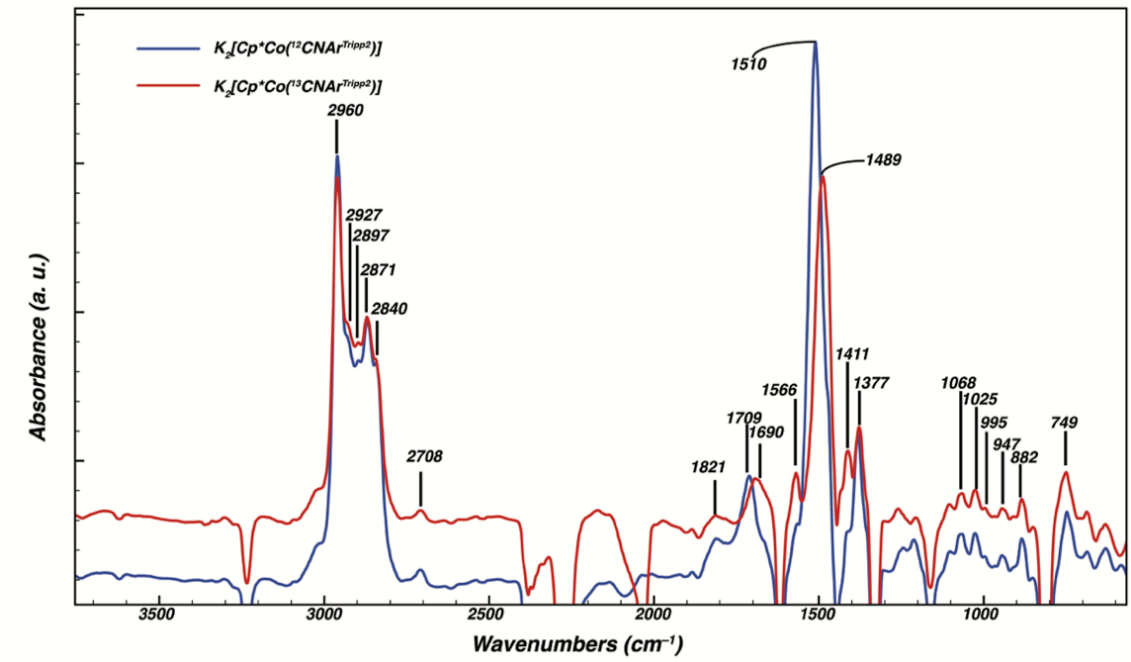


**Figure 7.10** Full baseline corrected room temperature absorbance FTIR spectrum in $C_6D_6$ of $K_2[Cp^*Co(^{12}CNAr^{Tripp2})]$ (blue) and $K_2[Cp^*Co(^{13}CNAr^{Tripp2})]$ (Red) denoting isotope sensitive vibrations of the $CNAr^{Tripp2}$ ligand.

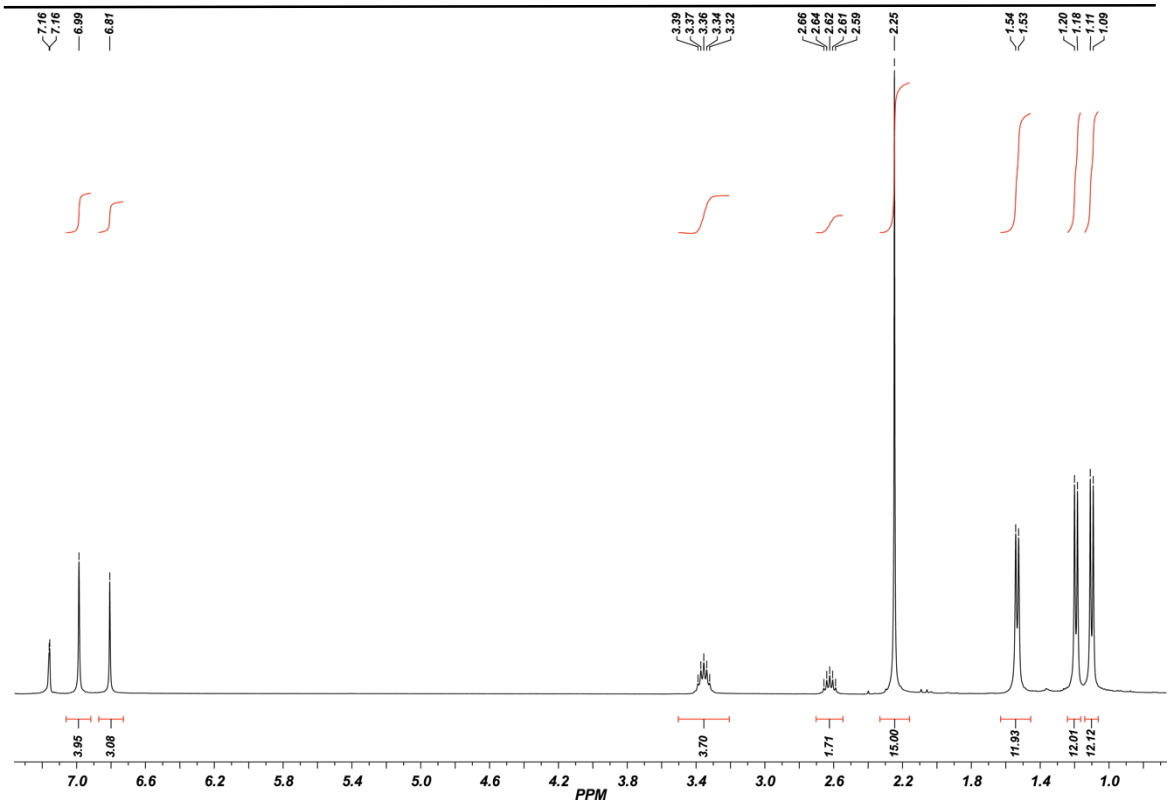


**Figure 7.11** Room temperature $^{1}$H NMR spectrum (399.9 MHz, $C_6D_6$) of $K_2$[Cp*Co(CNAr$^{Tripp2}$)]. $K_2$[**2**].

### $^{13}$C{$^{1}$H} NMR Spectrum of $K_2$[Cp*Co(CNAr$^{Tripp2}$)], $K_2$[2].

$^{13}$C NMR chemical shits of carbyne carbon resonances on highly reduced metal species can be challenging to detect due to coupling to $^{59}$Co ($I$ = 7/2, 100%). This coupling often induces rapid relaxation and large amounts of line broadening. Attempts at locating the carbyne $^{13}$C resonances using $K_2$[Cp*Co($^{12}$CNAr$^{Tripp2}$)] were unsuccessful. However, it was possible to locate the carbyne carbon $^{13}$C resonance utilizing isotopically enriched $^{13}$CNAr$^{Tripp2}$, and a 500 MHz Varian Xsens spectrometer equipped with a high sensitivity cryoprobe. The carbyne resonance is centered at 181.0 ppm ($C_6D_6$) with a half-peak line width of 2,485 Hz (Figure 7.12).

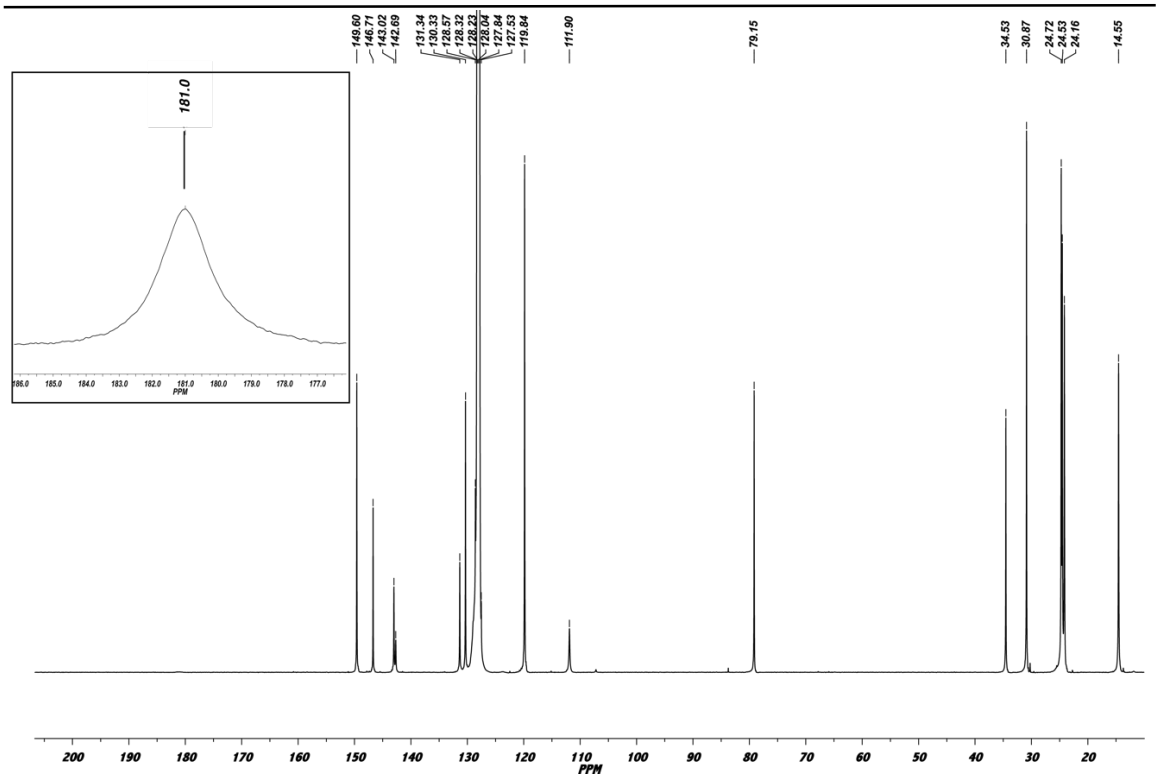


**Figure 7.12** Room temperature $^{13}C\{^{1}H\}$ NMR spectrum (125.7 MHz, $C_6D_6$) of $K_2$[Cp*Co(CNAr$^{Tripp2}$)]. $K_2$[**2**]. Inset depicts the carbyne-$^{13}C$ resonance from $^{13}C$ enriched $K_2$[Cp*Co($^{13}$CNAr$^{Tripp2}$).

**Synthesis of Cp*Co(N$_2$)(CNAr$^{Tripp2}$), (3), from the oxidation of K$_2$[Cp*CoCNAr$^{Tripp2}$], K$_2$[2], with FcOTf:** To a solution of $K_2$[Cp*CoCNAr$^{Tripp2}$] (0.0265 g, 0.0340 mmoles, 1.0 equivs) in THF (1 mL) was added FcOTf (0.0228g, 0.0679 mmole, 2.0 equivs) in a 2 mL of THF mixture under an atmosphere of dintrogen. The reaction mixture was manually swirled for 20 mins where a color change from deep red-brown to orange-brown was observed. The reaction mixture was then concentrated to a solid and slurried in *n*-pentane and followed by concentration to a solid to desolvate KOTf. After the reaction mixture was taken up in *n*-pentane (2 mL) and filtered over Celite packed on fiberglass (2 cm) to remove KOTf. After evaporation to dryness the reaction was judged complete by anaylsis of the crude solid via $^{1}H$ NMR spectroscopy

which indicted clean/quantative conversion to Cp*Co($N_2$)($CNAr^{Tripp2}$), isolated yield; 0.0197 g, 0.0271 mmole, 80%. Spectroscopic characterization can be found in **Chapter 5.6**.

**Synthesis of K[Cp*Co($CNAr^{Tripp2}$)], K[4], via comproportionation of $K_2$[Cp*Co($CNAr^{Tripp2}$)] and Cp*Co($N_2$)($CNAr^{Tripp2}$):** To a THF-$d^8$ solution of $K_2$[Cp*Co($CNAr^{Tripp2}$)] (0.055 g, 0.0706 mmol, 1.0 equivs, 0.5 mL) was added Co*Co($N_2$)($CNAr^{Tripp2}$) in THF-$d^8$ (0.0515 g, 0.0706 mmoles, 1 equivs, 0.5 mL). The resulting mixture was then transferred to a resalable J-Young's nmr tube where it was analyzed by proton NMR and displayed paramagnetically shifted resonances. The resulting solution was then transferred back into the glove box where it was concentrated to a solid to yield K[Cp*Co($CNAr^{Tripp2}$) as a dark red solid, 0.0800 g, 0.108 mmol, 77%. Analytically pure X-ray diffraction crystals were grown from a saturated solution of *n*-pentane (1 mL) spiked with 5 drops of THF, and placed in the freezer at –40 ˚C for 1 week to afford K[Cp*Co($CNAr^{Tripp2}$) as dark brown diffraction quality crystals. The $^1$H NMR spectrum of K[Cp*Co($CNAr^{Tripp2}$) (399.9 MHz, THF-$d^8$, 20 ˚C) exhibits paramagnetically shifted resonances: δ = 35.10 (broad singlet), 12.44 (broad singlet), 11.49 (broad singlet), 7.62 (broad singlet), 5.64 (broad singlet), 1.84 (broad singlet), -1.45 (broad singlet), -3.82 (broad singlet), -5.52 (broad singlet) ppm. Due to residual THF solvent peaks the aliphatic C-H resonances for K[Cp*Co($CNAr^{Tripp2}$) are not reported: FTIR ($C_6D_6$; KBr Window; 20 ˚C): $\nu_{CN}$ = 1694 (s), 1683 (s), 1669 (s) also 1606 (w), 1570 (s), 1477(w), 1463 (w), 1424 (sh), 1405 (s), 1379 (m), 1363 (w), 1338

(w), 1317 (w), 777 (w), 753 (w)cm$^{-1}$. Anal. Calcd. For $C_{47}H_{64}NCoK$: C, 76.18; H, 8.70; N, 1.89. Suitable combustion analysis was not obtained.

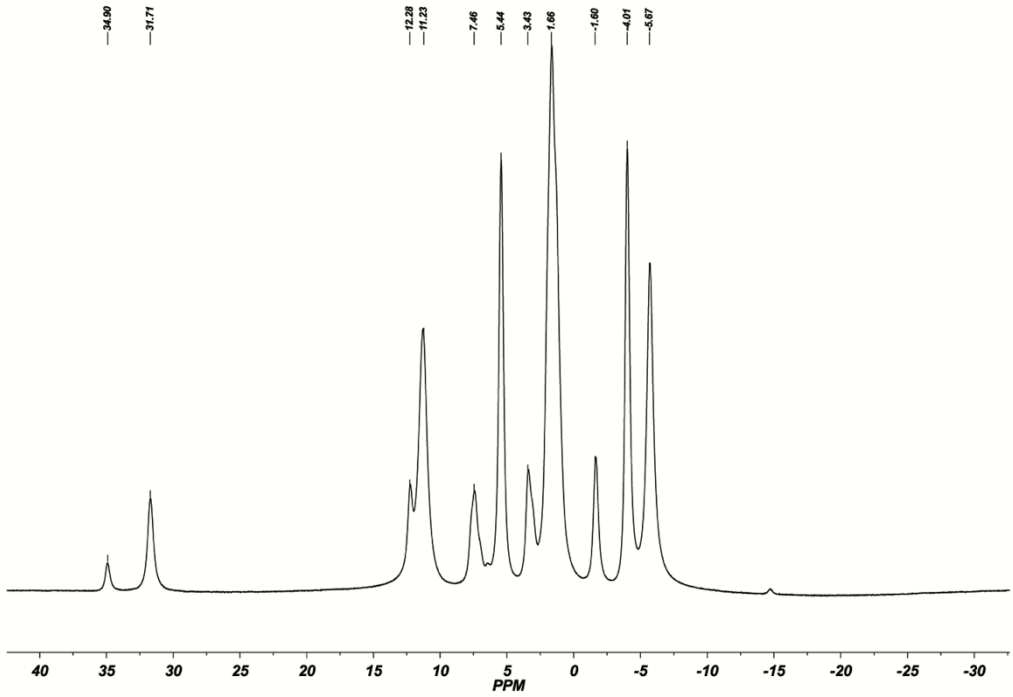


**Figure 7.13** Room temperature $^1$H NMR spectrum (399.9 MHz, THF-$d^8$) of K[Cp*Co(CNAr$^{Tripp2}$)]. K[**4**].

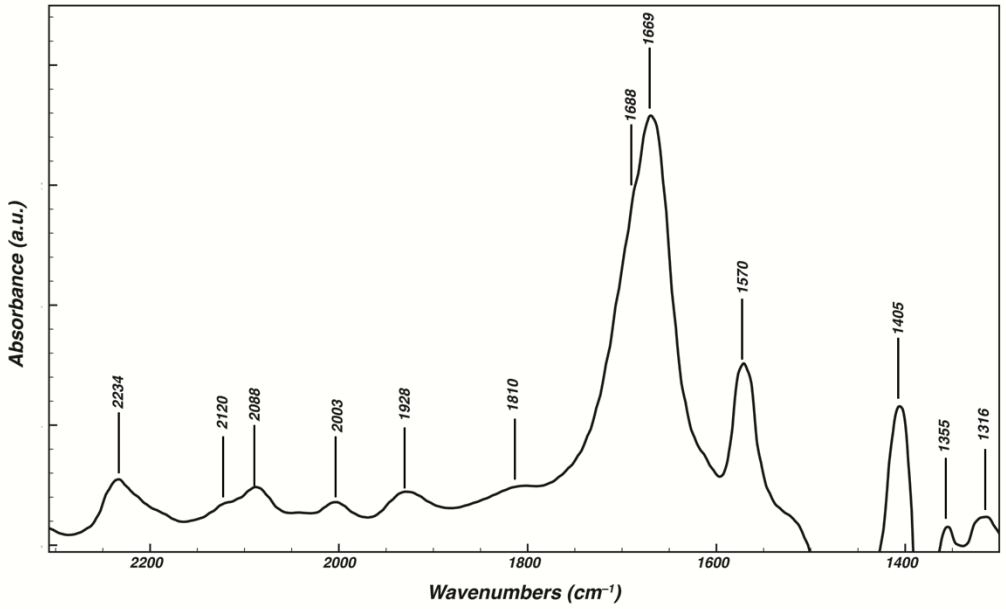


**Figure 7.14** Room temperature solution FTIR of K[Cp*Co(CNAr$^{Tripp2}$)], K[**4**] in *n*-pentane. The resonance at 1669 cm$^{-1}$ is diagnositic of radical anion K[**4**]

**Synthesis of K[Cp*Co(H)CNAr$^{Tripp2}$], K[5]:** To a solution of $K_2$[Cp*Co(CNAr$^{Tripp2}$)] (0.105 g, 0.135 mmoles, 1 equiv.) in $C_6H_6$ was added TMSCCH (19.75 μL, 0.135 mmoles, 1 equiv) in $C_6H_6$ (1 mL). The resulting mixture was then manually swirled for 10 mins. Thereafter the reaction mixture was filtered over Celite packed on fiberglass (2 cm) to remove KCCTMS yielding a dark brown solution that was then lyophilized to a solid. Recrystallization of the resultant solid from *n*-pentane spiked with 5 drops of $Et_2O$ (1 mL total) and storage at –40 ˚C for 4 days afforded dark brown analytically pure crystals suitable for X-ray diffraction, 0.052 g, 0.0695 mmoles, 51 %yield. $^1$H NMR (400.0 MHz, $C_6D_6$, 20 ˚C): δ = 7.13 (s, 4H, *m*-Tripp), 6.85 (mult. 3H, *m/p*-Ph), 3.04 (sept. 4H, 7Hz, C*H*$(CH_3)_2$), 2.77 (sept. 2H, 7Hz, C*H*$(CH_3)_2$), 2.05 (s, 15H, Cp*-*H*), 1.49 (d, 12H, 7Hz, CH(C*H*$_3)_2$), two of the Tripp *i*-Pr groups overlap to yield a triplet at 1.20 (t, 24H, 7Hz, CH(C*H*$_3)_2$), -14.65 (s, 1H, Co-*H*) ppm. $^{13}$C{$^1$H} NMR (125.8 MHz, $C_6D_6$, 20 ˚C): δ = 207.5 (*C*NR), 147.8, 147.6, 138.6, 137.2, 133.6, 130.1, 120.8, 119.8, 87.6, 34.6, 31.1, 24.6, 24.4, 24.1, 13.1 ppm. FTIR ($C_6D_6$; KBr Window; 20 ˚C): $\nu_{CN}$ = 1710 (s), 1805 (m), $\nu_{CoH}$ = 2069 also 3049 (w), 2961 (s), 2928 (m), 2893 (m), 2867 (m), 2806 (w), 1572 (m), 1462 (m), 1408 (m), 1378 (w), 1362 (w), 1207 (w), 1119 (m), 1071 (w) 1029 (w), 940 (w), 923 (w), 877 (w), 756 (w), 710 (w) cm$^{-1}$. Anal. Calcd. For $C_{49}H_{65}NCoK$: C, 76.07; H, 8.83; N, 1.89. Found: C, 75.76; H, 9.27; N, 2.19.

**S1.9. Preparation of K[Cp*Co(SiMe$_3$)CNAr$^{Tripp2}$], K[6]:** To a $C_6H_6$ solution of $K_2$[Cp*Co(CNAr$^{Tripp2}$)] (0.051 g, 0.056 mmoles, 1 equiv., 2 mL) was added TMSCl (8.3 μL, 0.0056 mmoles, 1 equiv) via micro-syringe. The resulting mixture was then allowed to react for 3 hours where after it was filtered over Celite packed on fiberglass (2 cm) to

remove KCl yielding a dark brown solution that was then lyophilized to a fluffy powder. Recrystallization of the resultant solid from *n*-pentane spiked with 5 drops of $Et_2O$ (1 mL total) and storage at –40 ˚C over 1 day afforded dark brown analytically pure crystals suitable for X-ray diffraction, 0.027 g, 0.033 mmoles, 51 %yield. $^1$H NMR (499.8 MHz, $C_6D_6$, 20 ˚C): δ = 6.96 (d, 2H, 8Hz, *m*-Ph), 6.83(t, 1H, 7Hz, *p*-Ph), The proton resonance corresponding to the *m*-Tripp–*H* protons are overlapped with the residual solvent peak, 3.24 (overlapped sept., 2H, *p*-C*H*$(CH_3)_2$, 2.90-2.77(two overlapped spet., 4H, *o*-C*H*$(CH_3)_2$), 1.76 (s, 15H, Cp*–*H*), 1.53 (broad singlet, 6H, CH(C*H*$_3)_2$), 1.44 broad singlet, 6H, CH(C*H*$_3)_2$, 1.23 (d, 12H, 7Hz, CH(C*H*$_3)_2$), 1.11(broad singlet, 12H), 0.39 (s, 9H, TMS–*H)* ppm. $^{13}$C{$^1$H} NMR (125.8 MHz, $C_6D_6$, 20 ˚C): δ = 209.3 (*C*NR), 148.4, 148.2, 148, 139.0, 138.0, 134.7, 131.7, 121.3, 121.1, 120.8, 89.1, 34.8, 31.2, 31.1, 26.6, 25.9, 24.8, 24.5, 24.4, 23.9, 12.3, 9.5 ppm. FTIR ($C_6D_6$; KBr Window; 20 ˚C): $\nu_{CN}$ = 1707 (s), 1685 (m, sh), 1671 (m, sh) also 2960 (s), 2927 (m), 2891 (m), 2867 (m), 1570 (m), 1462 (m), 1405 (m), 1381 (m), 1362 (w), 1248 (w), 1236 (w), 1223 (w), 1104 (w), 1070 (w), 1053 (w), 1028 (w), 940 (w), 878 (w), 830 (m), 760 (w), 651 (w), 641 (w), 597 (w), 532 (w) cm$^{-1}$. Anal. Calcd. For $C_{50}H_{73}NSiKCo$: C, 73.75; H, 9.04; N1.72. . Found: C, 65.03; H, 7.79; N, 1.25.

**S1.10. Preparation of Cp*Co(η$^2$-S$_2$)CNAr$^{Tripp2}$, (7):** To a solution of $K_2$[Cp*Co(CNAr$^{Tripp2}$)] (0.060 g, 0.0767 mmol, 1.0 equiv) in $C_6H_6$ (1 mL) was added $S_8$ (0.020 g, 0.0767 mmole, 1.0 equiv) in $C_6H_6$ where upon an immediate color change from a homogenous deep brown to a cloudy deep red was observed. The reaction mixture was then allowed to react for 30 mins., where it was then filtered over Celite packed on

fiberglass (2 cm), and concentrated to a solid. Recrystaliztion of the resulting solid from a saturated *n*-pentane/$Et_2O$ solution (1 mL; 3:1) over 2 days at –40 ˚C to afford deep red crystals of Cp*Co($\eta^2$-$S_2$)($CNAr^{Tripp2}$), 0.015 g, 0.0196 mmol, 26%. $^1$H NMR (499.8 MHz, $C_6D_6$, 20 ˚C): δ = 7.25 (s, 4H, *m*-Tripp), 6.95 (d, 2H, 7Hz, *p*-Ph), 6.84 (t, 1H, 8Hz, *p*-Ph), 2.96 (sept., 2H, 7Hz, , C*H*($CH_3$)$_2$), 2.70 (sept., 4H, 7Hz, C*H*($CH_3$)$_2$), 1.44 (d, 12H, 5Hz, CH(C*H*$_3$)$_2$), 1.42 (d, 12H, 5Hz, CH(C*H*$_3$)$_2$), 1.38 (s, 15H, Cp*-*H*), 1.15 (d, 12H, 5Hz, CH(C*H*$_3$)$_2$) ppm. $^{13}$C{$^1$H} NMR (125.8 MHz, $C_6D_6$, 20 ˚C): δ = 164.6 (*C*NR), 149.6, 146.7, 139.3, 132.8, 130.6, 127.6, 127.2, 121.6, 95.0, 35.1, 31.3, 25.0, 24.7, 24.3, 10.0 ppm. FTIR ($C_6D_6$; KBr Window; 20 ˚C): $\nu_{CN}$ = 2117 (s), 2068 (w) also 2961 (m), 2926 (w), 2868 (w), 2851 (w), 1464 (w), 1430 (w), 1415 (w), 1382 (w), 1363 (w), 1105 (w), 1071 (w), 1054 (w), 1027 (w), 940 (w), 878 (w), 758 (w) $cm^{-1}$. Anal. Calcd. For $C_{47}H_{64}NCoS_2$: C, 73.69; H, 8.42; N, 1.83. Found: C, 71.47; H, 8.21; N, 2.88.

**Synthesis of Cp*Co(CO)($CNAr^{Tripp2}$), (8), from the reduction of $CO_2$ with $K_2$[Cp*Co($CNAr^{Tripp2}$)]:** $K_2$[Cp*Co($CNAr^{Tripp2}$)], $K_2$[**2**], (0.020 g, 0.0256 mmol., 1 equiv) was dissolved in $C_6D_6$ (1 mL) and transferred to a resalable J-Young NMR tube. The J-Yong NMR tube was then connected to the schlenk line where it was subject two 2 freeze-pump-thaw cycles (*ca.* 0.012 torr). Thereafter, the solution was exposed to 1 ATM of $CO_{2(g)}$. Upon addition of $CO_2$ and immediate color change from dark brown to red was observed in addition to the precipitation of a solid. Analysis of the reaction mixture by $^1$H NMR indicated complete conversion to Cp*Co(CO)($CNAr^{Tripp2}$). The resultant mixture was transferred to the glove box where it was filtered over Celite packed on fiberglass (2 cm) to remove $K_2CO_3$. All volatiles were removed to afford

Cp*Co(CO)(CNAr$^{Tripp2}$) as a red fluffy powder judged pure by $^{1}$H NMR spectroscopy, 0.017 g, .00233 mmol., 91 %. Analytically pure X-ray diffraction quality crystals were grown from a saturated $Et_2O$/*n*-Pentane mixture (1:3, 1 mL). $^{1}$H NMR (499.8 MHz, $C_6D_6$, 20 ˚C): δ = 7.25(s, 4H, *m*-Tripp), 6.99 (d, 2H, 8Hz, *m*-Ph), 6.90 (t, 1H, 8Hz, *p*-Ph), 2.85 (overlapped Sept., 6H, C*H*$(CH_3)_2$), 1.55 (s, 15H, Cp*–*H*), (d, 12H, 7Hz, CH(C*H*$_3)_2$), 1.35 (d, 12H, 7Hz, CH(C*H*$_3)_2$), 1.21 (d, 12H, 7Hz, CH(C*H*$_3)_2$) ppm. $^{13}$C{$^{1}$H} NMR (125.8 MHz, $C_6D_6$, 20 ˚C): δ = 209.2 (*C*O), 176.8 (*C*NR), 149.1, 146.8, 137.4, 133.9, 131.0, 130.1, 124.9, 121.4, 94.3, 35.0, 31.4, 24.7, 24.4, 24.3, 10.7 ppm. FTIR ($C_6D_6$; KBr Window; 20 ˚C): $\nu_{CN}$ = 2065 (s), 2027 (m, sh), $\nu_{CO}$ = 1934 (s) also 2961 (m), 2928 (w), 2904 (w), 2868 (m), 1574 (w), 1414 (m), 1382 (m), 1363 (w), 1118 (m), 1100 (w), 754 (w) cm$^{-1}$. Anal. Calcd. For $C_{48}H_{64}CoNO$: C, 78.98; H, 8.84; N, 1.92. Suitable combustion analysis was not obtained.

**Detecting $CO_3^{2-}$ formation:** In order to mechanistically probe the reduction of $CO_2$ the use of $^{13}CO_2$ was utilized to verify $CO_3^{2-}$. Addition of excess $^{13}CO_2$ was achieved via addition to a J-Young's resalable NMR tube containing degassed $K_2$[Cp*Co(CNAr$^{Tripp2}$)], (0.020 g, 0.256 mmol, 1 equiv). Following addition the reaction mixture was concentrated to a solid and the resulting solid slurried in basic $D_2O$ (*ca.* 0.5 M KOH) and spiked with THF for reference. The sample was then analyzed via $^{13}$C{$^{1}$H} NMR spectroscopy using a 500 MHz Varian NMR spectrometer with a X-sense high sensitivity cryoprobe.

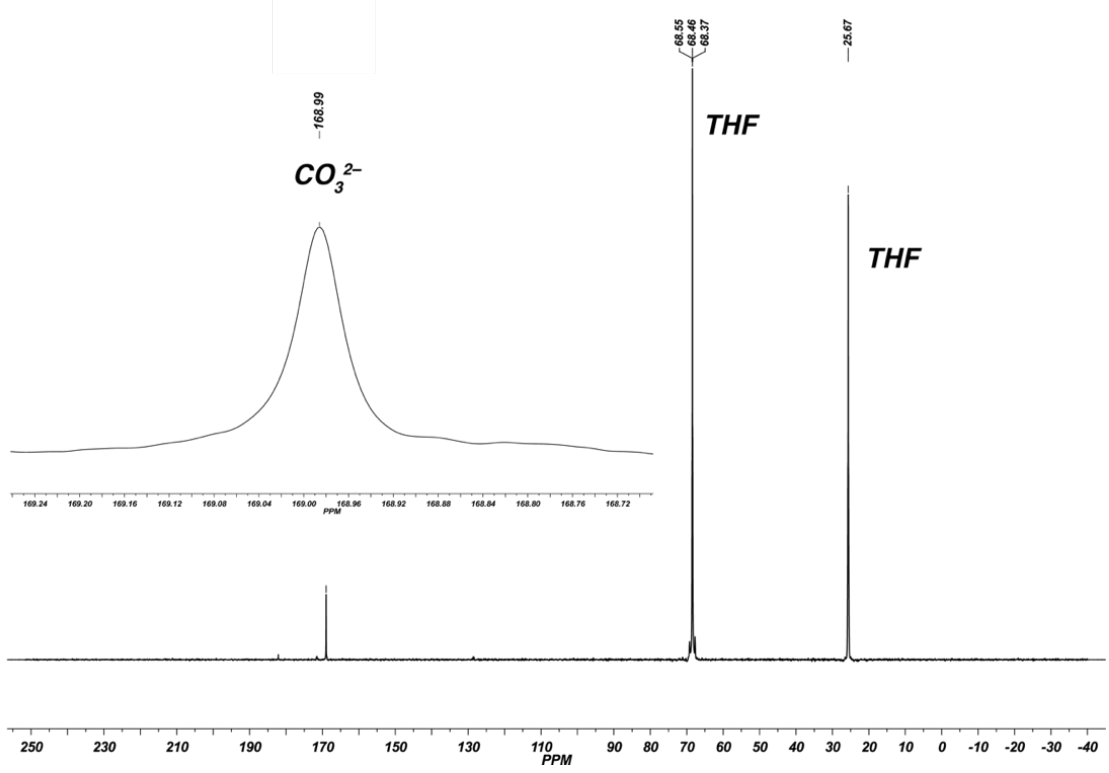


**Figure 7.15** Room temperature $^{13}C\{^{1}H\}$ NMR spectrum (125.7 MHz, $C_6D_6$) of the crude reaction mixture from the reaction of $K_2$[**2**] with $^{13}CO_2$ in order to verify $CO_3^{2-}$ formation. Inset depicts the carbon-$^{13}C$ resonance from $^{13}CO_3^{2-}$.

**Preparation of K[Cp*Co(PhCC(H)(Ph)(CNAr$^{Tripp2}$))], K[9]:** To a $C_6H_6$ solution (1 mL) of $K_2$[Cp*Co(CNAr$^{Tripp2}$)] ( 0.101 g, 0.129 mmol, 1 equiv) was added a $C_6H_6$ solution (1 mL) of PhCCPh (0.023 g, 0.129 mmol, 1 equiv) at room temperature. The reaction mixture immediately tuned black followed by deep red-brown over the course of 5 mins. The resulting mixture was allowed to react for 1 hour. The reaction mixture was concentrated to a solid to afford crude K[Cp*Co(PhCC(H)(Ph)(CNAr$^{Tripp2}$))], K[**9**]. Fractional recrystallization (2x) from a saturated *n*-pentane/$Et_2O$ solution (1.5 mL, 1:5) over 1 week afforded analytical pure X-ray diffraction quality crystals of K[Cp*Co(PhCC(H)(Ph)(CNAr$^{Tripp2}$))], 0.020 g, 0.0217 mmol, 17%. $^{1}H$ NMR (499.8 MHz, $C_6D_6$, 20 ˚C): δ = 7.39 (d, 4H, 8Hz), 7.11 (t, 4H, 8Hz), 7.01 (t, 2H, 7Hz), 6.90 (t,

2H, 8Hz), 6.64 (t, 2H, 8Hz), 6.58 (t, 1H, 7Hz), 6.00 (d, 2H, 5Hz), 4.16 (s, 1H), 3.83 (broad Sept., 1H), 3.73 (broad Sept., 1H), 3.01 (broad Sept., 2H), 2.82 (broad Sept., 2H), 1.30 (s, 15H, Cp*–*H*), 1.13 (t, 9H, 7Hz), the remaining aliphatic *i*-Pr resonances are effected by hindered rotation and exhibit sever broadening: 1.53 (6H), 1.40 (9H), 1.21 (9H), 1.03 (3H), 0.94 (3H) ppm. $^{13}C\{^{1}H\}$ NMR (125.8 MHz, $C_6D_6$, 20 ˚C): δ = The *C*=N resonance could not be located even with extended scans, 209.8, 152.8, 149.4, 149.1, 147.8, 147.4, 146.5, 144.8, 142.5, 139.7, 135.2, 134.3, 132.4, 131.9, 125.3, 123.6, 123.1, 122.8, 121.4, 120.1, 119.8, 117.8, 86.6, 43.7, 42.7, 35.0, 34.9, 34.5, 31.1, 30.3, 29.9, 28.1, 26.6, 25.8, 25.5, 25.2, 24.7, 24.4, 24.0, 23.1, 22.8, 14.3, 11.2, 9.8 ppm. FTIR ($C_6D_6$; KBr Window; 20 ˚C): $\nu_{CN}$ = 1546(s), also 3052 (w), 3018 (w), 2961 (s), 2928 (s), 2903 (s), 2866 (s), 1597 (m), 1586 (s), 1491 (m), 1483 (m), 1469 (w), 1440 (w), 1381 (m), 1361 (w), 1247 (w), 1187 (w), 1119 (w), 1083 (w), 1069 (w), 1026 (w), 1003 (w), 987 (w), 942 (w), 876 (w), 722 (w), 763 (w), 747 (w), 739 (w), 699 (w) $cm^{-1}$. Anal. Calcd. For $C_{61}H_{75}NCoK$: C, 79.61; H, 8.21; N, 1.52. Found: C, 78.33; H, 8.27; N, 1.43.

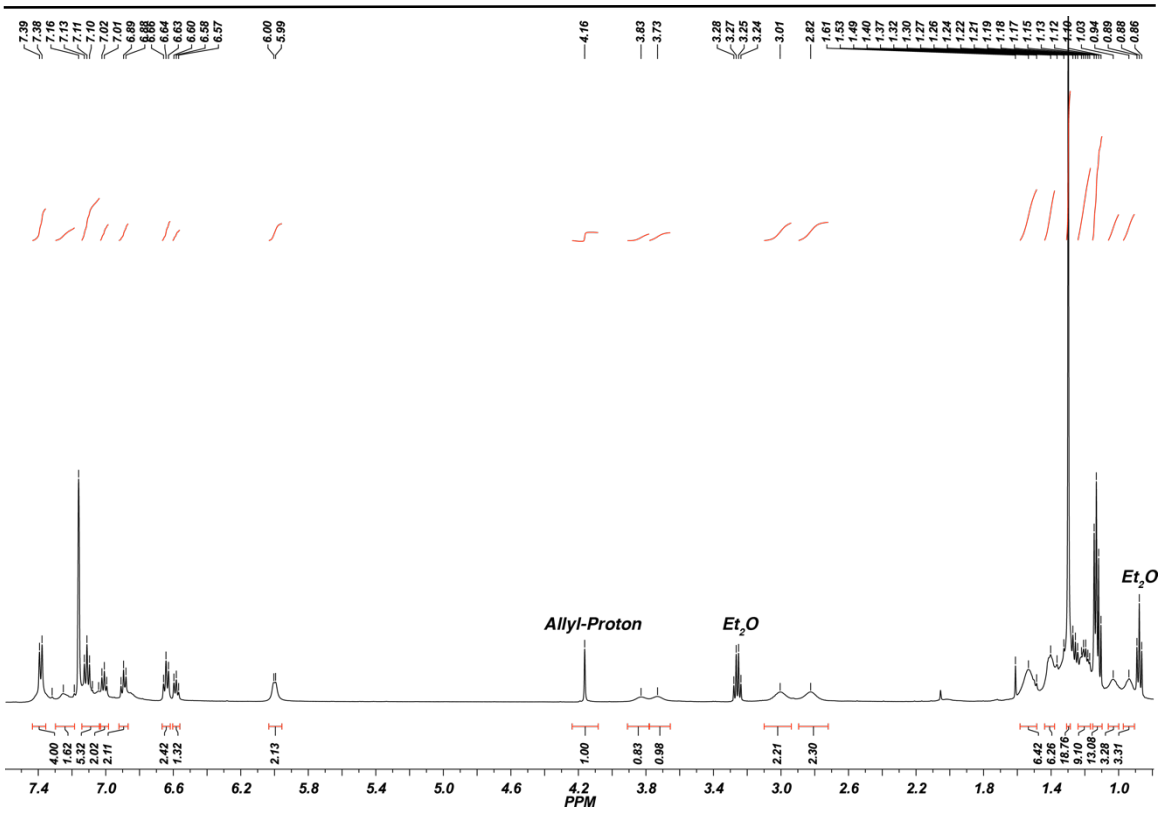


**Figure 7.16** Room temperature $^{1}$H NMR spectrum (399.9 MHz, $C_6D_6$) of crystalline K[Cp*Co(PhCC(H)(Ph)(CNAr$^{Tripp2}$))]. K[**9**].

### 7.8 Results of Computational Studies.

**Computational Details:** Density Functional Theory (DFT) calculations were carried out on [Cp*Co(CN$^{Xylyl}$)]$^{2-}$,which is a truncated model of the structurally characterized complex $K_2$[Cp*Co(CNAr$^{Tripp2}$)] were preformed with the ORCA computational suite 3.0.0.[85] Geometry optimizations and single-point calculations were performed using the pure functional BP86 and B3LYP hybrid density functional.[86-88] The all-electron Ahlrichs triple-zeta basis sets def2-TZVP (standard)[89-91] and def2-TZVP/J (auxiliary)[92-94] were used in all calculations. The resolution of identity (RI) approximation was employed.[95] Relativistic effects were included by use of the zerothorder regular approximation (ZORA).[94-98] Crystallographic atomic coordinates were used as input for geometry

optimizations where appropriate. Viewing of optimized structures and rendering of molecular orbitals was performed using the program Chemcraft.[99] After each geometry optimization, the optimized coordinates were reorientated so as to make the Co-C bond along the z axis. These coordinates were then used to run a single point calculation to deconvolute orbital contributions. This research was supported in part by the W. M. Keck Foundation through computing resources at the W. M. Keck Laboratory for Intergrated Biology II.

**Input for the geometry optimization of $[Cp^*Co(CN^{Xylyl})]^{2-}$ Utilizing BP86.**

```
#RKS OPT cpstarcodianion BP86

%pal nprocs 8 end

! RKS OPT BP86 ZORA def2-TZVP def2-TZVP/J RIJCOSX NormalPrint SlowConv XYZFile
%SCF
 MaxIter 1000

end

%output
Print[ P_Basis ] 2
Print[ P_MOs ] 1
end


* xyz -2 1

 Co  21.74314911437590     7.60659664065561    15.27967147478942
  C  24.58809656631372     9.16687697493453    14.91641822594166
  H  22.51352855246454     4.16687361739482    14.92802877598485
  N  19.45152020267139     8.65680172305128    13.78277706832823
  H  23.06152143594024    10.27419649786733    17.13052586557558
  H  15.61215099865043     6.12704009143484    13.64775383982930
  C  23.10868206293846     8.14765455184307    16.81127885493983
  C  22.62324645648210     4.50598467219550    15.96132338912577
  H  25.64384501994403     9.18785977997816    15.24582704600017
  H  21.69010074192298     4.25778654688335    16.47382244006597
  C  16.14390362662906     7.02873551389579    13.34630786456042
  C  18.24719884769921    10.57276375527281    12.18532542720867
  C  22.90942817738892     5.97521979541071    16.02658662116391
  C  23.79485157822653     8.06875952095669    15.55651546393845
```

| | | | |
|---|---|---|---|
| C | 21.84537097856755 | 6.46643830367769 | 18.35856995804400 |
| C | 17.44403294200391 | 7.19327490394210 | 13.79693895857517 |
| C | 18.19599963711817 | 8.37320948501560 | 13.42496843380646 |
| C | 15.49098039637476 | 7.96446753356331 | 12.53341703830586 |
| H | 14.47426047797402 | 7.80162012810315 | 12.19376951069687 |
| C | 18.07270691348658 | 6.14632546167494 | 14.67556664417647 |
| C | 16.20586847145530 | 9.11132566909278 | 12.16930530166415 |
| H | 15.73116185660944 | 9.86338251004670 | 11.54018465720140 |
| C | 17.50608270069438 | 9.33032947220583 | 12.58897688357976 |
| C | 23.66564956143499 | 6.72704046833149 | 15.06910753920550 |
| C | 22.56237242999871 | 6.85397234888648 | 17.10131015687940 |
| H | 23.41780371868379 | 3.88854748594356 | 16.42105916973490 |
| H | 23.69561826318657 | 5.37181437795478 | 13.39900296035594 |
| H | 21.26879813116162 | 7.30308342677826 | 18.76182523437993 |
| H | 22.52996140383431 | 6.13017533358565 | 19.16026819062857 |
| H | 21.13816769030208 | 5.65306691918382 | 18.17748166687073 |
| C | 20.40449361379464 | 8.11105159781731 | 14.46873123141820 |
| C | 23.05076163582612 | 9.34618994212000 | 17.70811564346625 |
| H | 24.16184251437278 | 10.14765605172699 | 15.14367816573301 |
| C | 24.29714005831303 | 6.17873027604582 | 13.82530570181396 |
| H | 25.31104713357870 | 5.77248755405143 | 13.99803145156989 |
| H | 24.59319745519233 | 9.07074954059788 | 13.82714221768200 |
| H | 24.38701955377729 | 6.94812686692324 | 13.05377574559858 |
| H | 19.16378953487210 | 10.32938312927252 | 11.63723059053679 |
| H | 18.58231915796987 | 11.13736648887504 | 13.06203833672348 |
| H | 17.61731133840721 | 11.21829081356636 | 11.56214915969325 |
| H | 18.97761017160460 | 5.72840205508183 | 14.22928941726509 |
| H | 17.36030727286452 | 5.33601969642560 | 14.87203652947633 |
| H | 18.41267894909002 | 6.56435932035134 | 15.62527647611695 |
| H | 23.89576604557215 | 9.39658700564728 | 18.42064191150084 |
| H | 22.13217863023089 | 9.35530454173664 | 18.30128476984804 |

*

**Optimized coordinates for $[Cp^*Co(CN^{Xylyl})]^{2-}$ Utilizing BP86.**

| | | | |
|---|---|---|---|
| Co | 21.77607955475089 | 7.58543716346963 | 15.30457801233881 |
| C | 24.57917412482066 | 9.17612770426820 | 14.89365137674752 |
| H | 22.51199723363062 | 4.14383162469961 | 14.93927893087559 |
| N | 19.46253371101268 | 8.63321418232148 | 13.79635694575168 |
| H | 23.05106811607606 | 10.29953613167344 | 17.11502440877932 |
| H | 15.59565149583132 | 6.10652226203046 | 13.62098225492788 |
| C | 23.09976591763278 | 8.16345277615062 | 16.80974087745829 |
| C | 22.62692752964687 | 4.49296636379843 | 15.97838983564613 |
| H | 25.64718285862120 | 9.20238556235457 | 15.21720448082705 |
| H | 21.68993417414087 | 4.24054733112541 | 16.50138207617715 |
| C | 16.13302216772653 | 7.01921030789991 | 13.32908202917356 |
| C | 18.26555238407999 | 10.58389807610553 | 12.21493766282481 |
| C | 22.90170257653648 | 5.96625969032259 | 16.03098406477247 |
| C | 23.78774676691997 | 8.07955963331499 | 15.54176483686377 |
| C | 21.84568384147172 | 6.47523676422188 | 18.37731182187097 |
| C | 17.44018185434100 | 7.17686627846737 | 13.78581225495356 |
| C | 18.19471206452336 | 8.36381540697865 | 13.42616209341320 |
| C | 15.48340686735929 | 7.97312660358842 | 12.52044153761175 |
| H | 14.45755652658253 | 7.81874206132480 | 12.17669541648292 |

| | | | |
|---|---|---|---|
| C | 18.07629931087397 | 6.12377124373333 | 14.65355794056423 |
| C | 16.20526227529412 | 9.12938198174761 | 12.17076432746871 |
| H | 15.73246049771521 | 9.89846639895576 | 11.54503432001122 |
| C | 17.51325334463885 | 9.33902312743021 | 12.59857203298414 |
| C | 23.65932520744280 | 6.72233464654550 | 15.05806975539566 |
| C | 22.55385298796848 | 6.85772852660174 | 17.11192250925865 |
| H | 23.43340733337885 | 3.87441662160646 | 16.44132921930201 |
| H | 23.68175877413252 | 5.35135143220105 | 13.39166915158350 |
| H | 21.26225686443662 | 7.31957781979611 | 18.77984173758928 |
| H | 22.53906983477921 | 6.14496698386713 | 19.18810870894772 |
| H | 21.13532777192997 | 5.65075477949991 | 18.20359103187893 |
| C | 20.41348870167549 | 8.09011696199892 | 14.48084163679056 |
| C | 23.04173036160655 | 9.36674251540999 | 17.70248018238550 |
| H | 24.14927080729589 | 10.16530294906202 | 15.12170983783755 |
| C | 24.28942429742892 | 6.16797021527958 | 13.81441588493508 |
| H | 25.31458334403832 | 5.76030768015243 | 13.98261534496237 |
| H | 24.57681705011753 | 9.07561018054415 | 13.79540828932674 |
| H | 24.37410302529549 | 6.94050960973744 | 13.03236537662036 |
| H | 19.18728035807949 | 10.34059199450554 | 11.65830169302496 |
| H | 18.61047408018460 | 11.13252945927951 | 13.10831330274872 |
| H | 17.63635387850166 | 11.25069791066967 | 11.59922102371364 |
| H | 18.99558226073758 | 5.71998681961771 | 14.20146373129488 |
| H | 17.36684692394454 | 5.29812547210073 | 14.84198381826335 |
| H | 18.41843224232141 | 6.53804725118953 | 15.61447273850012 |
| H | 23.89240665607761 | 9.42536626969794 | 18.42340683926104 |
| H | 22.11457406439949 | 9.37751361465395 | 18.29940065785462 |

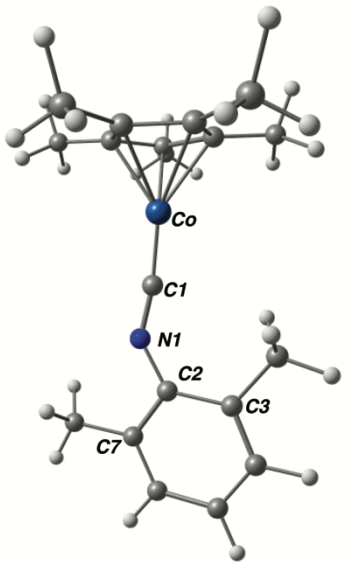


**Figure 7.17** Geomoetry optimized structure of $[Cp^*Co(CNXylyl)]^{2-}$ utilizing BP86 def2TZVP/J. Selected bond lengths (Å): Co-$C_1$ = 1.6703, $C_1$-$N_1$= 1.29143, $N_1$-$C_2$ = 1.33796, $C_2$-$C_3$ = 1.45173, $C_2$-$C_7$ = 1.44925. Selected bond angles (˚): Co-$C_1$-$N_1$ = 171.57, $C_1$-$N_1$-$C_2$ = 138.95.

## Input for the geometry optimization of $[Cp^*Co(CN^{Xylyl})]^{2-}$ Utilizing B3LYP.

```
#RKS OPT of cpstarcodianion B3LYP

%pal nprocs 16 end
! RKS OPT B3LYP/G ZORA def2-TZVP def2-TZVP/J RIJCOSX NormalPrint SlowConv XYZFile
%SCF

MaxIter 1000
end

%output
Print[ P_Basis ] 2
Print[ P_MOs ] 1
end

* xyz -2 1

Co     21.62933697      7.58554764     15.54406151
C      24.30447412      9.27678709     14.76638685
H      22.73069989      4.19647051     15.12625411
N      19.20511895      8.64690355     14.23573028
H      23.14084646     10.16478104     17.30981209
H      15.54234022      6.25694304     13.13265169
C      23.16496973      8.16158214     16.86035029
C      22.76525728      4.51521933     16.05213300
H      25.30196085      9.52474914     15.09795140
H      21.93110177      4.27724656     16.50991845
C      16.06736438      7.04086975     13.00939509
C      18.45678473     10.48096436     12.34818458
C      22.93341033      6.00691040     16.06135575
C      23.63887890      8.13005519     15.49443932
C      22.34680659      6.37441908     18.53941840
C      17.23276832      7.18432612     13.75583103
C      18.04779521      8.33838211     13.57534492
C      15.63494593      7.99079191     12.09557957
H      14.82880653      7.87230315     11.60756202
C      17.55998710      6.05636951     14.68188396
C      16.42190086      9.12421321     11.91578599
H      16.14829896      9.79214226     11.29609774
C      17.60216371      9.28987507     12.62566209
C      23.50092772      6.80391382     15.00750144
C      22.72907918      6.85998155     17.18580884
H      23.52310728      4.09912546     16.51267133
H      23.69539380      5.38068137     13.54633121
H      22.50168005      7.02029474     19.27331673
H      22.67564957      5.46735943     18.76601429
H      21.38966794      6.12642363     18.97391105
C      20.16479957      8.01100878     14.86239647
C      23.25129243      9.32868275     17.80801754
```

| | | | |
|---|---|---|---|
| H | 23.71824259 | 10.17989927 | 14.68200093 |
| C | 23.98112299 | 6.31082874 | 13.67235899 |
| H | 24.95810709 | 6.36083086 | 13.63797014 |
| H | 24.46288241 | 9.00393859 | 13.73349745 |
| H | 23.79945461 | 6.64398857 | 12.66122046 |
| H | 19.44514798 | 10.45373119 | 12.78269171 |
| H | 17.99950959 | 11.43759890 | 12.55348877 |
| H | 18.66299353 | 10.53733572 | 11.28955329 |
| H | 18.52201036 | 5.59122459 | 14.52519495 |
| H | 16.80110397 | 5.29300458 | 14.77003372 |
| H | 17.63874866 | 6.43098229 | 15.69176607 |
| H | 24.20495232 | 9.50574306 | 18.28297277 |
| H | 22.46163059 | 9.42749834 | 18.53813373 |

*

**Optimized coordinates for $[Cp^*Co(CN^{Xylyl})]^{2-}$ Utilizing B3LYP.**

| | | | |
|---|---|---|---|
| Co | 21.74314911437590 | 7.60659664065561 | 15.27967147478942 |
| C | 24.58809656631372 | 9.16687697493453 | 14.91641822594166 |
| H | 22.51352855246454 | 4.16687361739482 | 14.92802877598485 |
| N | 19.45152020267139 | 8.65680172305128 | 13.78277706832823 |
| H | 23.06152143594024 | 10.27419649786733 | 17.13052586557558 |
| H | 15.61215099865043 | 6.12704009143484 | 13.64775383982930 |
| C | 23.10868206293846 | 8.14765455184307 | 16.81127885493983 |
| C | 22.62324645648210 | 4.50598467219550 | 15.96132338912577 |
| H | 25.64384501994403 | 9.18785977997816 | 15.24582704600017 |
| H | 21.69010074192298 | 4.25778654688335 | 16.47382244006597 |
| C | 16.14390362662906 | 7.02873551389579 | 13.34630786456042 |
| C | 18.24719884769921 | 10.57276375527281 | 12.18532542720867 |
| C | 22.90942817738892 | 5.97521979541071 | 16.02658662116391 |
| C | 23.79485157822653 | 8.06875952095669 | 15.55651546393845 |
| C | 21.84537097856755 | 6.46643830367769 | 18.35856995804400 |
| C | 17.44403294200391 | 7.19327490394210 | 13.79693895857517 |
| C | 18.19599963711817 | 8.37320948501560 | 13.42496843380646 |
| C | 15.49098039637476 | 7.96446753356331 | 12.53341703830586 |
| H | 14.47426047797402 | 7.80162012810315 | 12.19376951069687 |
| C | 18.07270691348658 | 6.14632546167494 | 14.67556664417647 |
| C | 16.20586847145530 | 9.11132566909278 | 12.16930530166415 |
| H | 15.73116185660944 | 9.86338251004670 | 11.54018465720140 |
| C | 17.50608270069438 | 9.33032947220583 | 12.58897688357976 |
| C | 23.66564956143499 | 6.72704046833149 | 15.06910753920550 |
| C | 22.56237242999871 | 6.85397234888648 | 17.10131015687940 |
| H | 23.41780371868379 | 3.88854748594356 | 16.42105916973490 |
| H | 23.69561826318657 | 5.37181437795478 | 13.39900296035594 |
| H | 21.26879813116162 | 7.30308342677826 | 18.76182523437993 |
| H | 22.52996140383431 | 6.13017533358565 | 19.16026819062857 |
| H | 21.13816769030208 | 5.65306691918382 | 18.17748166687073 |
| C | 20.40449361379464 | 8.11105159781731 | 14.46873123141820 |
| C | 23.05076163582612 | 9.34618994212000 | 17.70811564346625 |
| H | 24.16184251437278 | 10.14765605172699 | 15.14367816573301 |
| C | 24.29714005831303 | 6.17873027604582 | 13.82530570181396 |
| H | 25.31104713357870 | 5.77248755405143 | 13.99803145156989 |
| H | 24.59319745519233 | 9.07074954059788 | 13.82714221768200 |

| | | | |
|---|---|---|---|
| H | 24.38701955377729 | 6.94812686692324 | 13.05377574559858 |
| H | 19.16378953487210 | 10.32938312927252 | 11.63723059053679 |
| H | 18.58231915796987 | 11.13736648887504 | 13.06203833672348 |
| H | 17.61731133840721 | 11.21829081356636 | 11.56214915969325 |
| H | 18.97761017160460 | 5.72840205508183 | 14.22928941726509 |
| H | 17.36030727286452 | 5.33601969642560 | 14.87203652947633 |
| H | 18.41267894909002 | 6.56435932035134 | 15.62527647611695 |
| H | 23.89576604557215 | 9.39658700564728 | 18.42064191150084 |
| H | 22.13217863023089 | 9.35530454173664 | 18.30128476984804 |

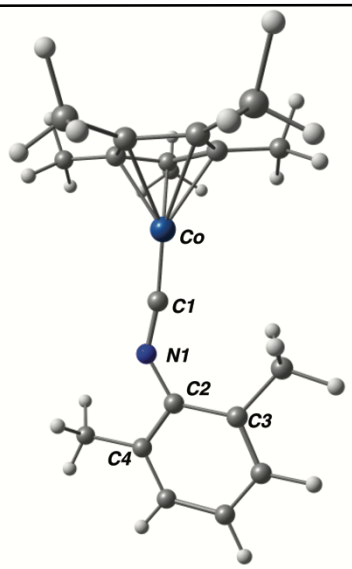


**Figure 7.18** Geomoetry optimized structure of $[Cp^*Co(CNXylyl)]^{2-}$ utilizing B3LYP/G def2TZVP/J. Selected bond lengths (Å): Co-$C_1$ = 1.64441, $C_1$-$N_1$= 1.29481, $N_1$-$C_2$ = 1.33596, $C_2$-$C_3$ = 1.44778, $C_2$-$C_7$ = 1.44601. Selected bond angles (˚): Co-$C_1$-$N_1$ = 171.77, $C_1$-$N_1$-$C_2$ = 138.08.

## 7.9 Information on Crystallographic Structure Determinations.

**General Information.** Single crystal X-ray structure determinations were carried out at low temperature on Bruker Kappa diffractometers equipped with a Mo sealed tube or rotating anode or Cu rotating anode radiation source and a Bruker APEX-II, APEX-I, or Proteum Pt135 detector. All structures were solved via direct methods with SHELXS[100] and refined by full-matrix least squares procedures using SHELXL[100] within the Olex2

small-molecule solution, refinement and analysis software package.[101] Crystallographic data collection and refinement information are listed in Table 7.3-4.

The following molecules contained positionally disordered components that were modeled and refined anisotropically. They are listed along with their respective disordered components:

**$K_2(Et_2O)[Cp^*Co(CNAr^{Tripp2})$, $K_2$[2]:** contains one non-coordinating solvation molecule of $Et_2O$ that is positionally disordered. The Platon routine SQUEEZE was used to account for this disordered molecule as a diffuse contribution to the overall scattering pattern without specific atom positions.

**$K[Cp^*Co(PhCC(H)(Ph)(CNAr^{Tripp2}))]$, K[9]:** contains one non-coordinating solvation molecule of $Et_2O$ that is positionally disordered. The Platon routine SQUEEZE was used to account for this disordered molecule as a diffuse contribution to the overall scattering pattern without specific atom positions.

**$Cp^*Co(\eta^2\text{-}S_2)CNAr^{Tripp2}$, (7):** The $S_2$ fragments exhibits positional disorder over two postions. Additionally complex **7** contains 8% compositional disorder with $Cp^*Co(\kappa^2\text{-}S,S\text{-}S_4)CNAr^{Tripp2}$. Both Fragments share a coordinated sulfur atom that was linked via the EXYZ command, and refined anisotropically.

**Table 7.3.** Crystallographic data collection and refinement information.

| Name | $K_2(Et_2O)_2$ [(Cp*Co(CNAr$^{Tripp2}$)] $K_2(Et_2O)_2$[**2**] | $K(Et_2O)$ [Cp*Co(H)(CNAr$^{Tripp2}$)], K[**5**] | $K(Et_2O)$ [Cp*Co($SiMe_3$)(CNAr$^{Tripp2}$)] •($C_5H_{14}$), K[**6**] |
|---|---|---|---|
| Formula | $C_{55}H_{83}CoK_2NO_2$ | $C_{55}H_{75}CoKNO$ | $C_{59}H_{86}CoKNOSi$ |
| Crystal System | Monoclinic | Monoclinic | Triclinic |
| Space Group | *C2/c* | *P2$_1$/c* | *P–1* |
| *a*, Å | 46.323(2) | 11.1895(6) | 12.4898(4) |
| *b*, Å | 12.1188(5) | 42.067(3) | 12.5227(4) |
| *c*, Å | 24.6506(10) | 10.8206(6) | 20.6102(6) |
| α, deg | 90 | 90 | 93.0540(10) |
| β, deg | 121.309(2) | 108.693(3) | 104.8680(10) |
| γ, deg | 90 | 90 | 110.9260(10) |
| V, Å$^3$ | 11823.2(9) | 4824.7(5) | 2872.39(16) |
| *Z* | 8 | 4 | 2 |
| Radiation (λ, Å) | Mo-Kα, 0.71073 | Mo-Kα, 0.71073 | Mo-Kα, 0.71073 |
| ρ (calcd.), g/cm$^3$ | 1.042 | 1.124 | 1.100 |
| μ (Mo Ka), mm$^{-1}$ | 0.465 | 0.476 | 0.429 |
| Temp, K | 100 | 100 | 100 |
| θ max, deg | 25.347 | 24.406 | 27.943 |
| data/parameters | 10751/619 | 7905/519 | 12771/635 |
| $R_1$ | 0.0489 | 0.0592 | 0.0382 |
| $wR_2$ | 0.0999 | 0.1083 | 0.1018 |
| GOF | 1.022 | 0.985 | 1.026 |

**Table 7.4.** Crystallographic data collection and refinement information.

| Name | Cp*Co($\eta^2$-$S_2$)($CNAr^{Tripp2}$) (**7**) | Cp*Co(CO)($CNAr^{Tripp2}$) (**8**) | K($Et_2O$)[Cp*Co($\eta^3$-PhCC(H)(Ph)($CNAr^{Tripp2}$))], K(Et2O)[**9**] |
|---|---|---|---|
| Formula | $C_{47}H_{64.02}CoNS_{2.15}$ | $C_{48}H_{64}CoNO$ | $C_{65}H_{85}CoKNO$ |
| Crystal System | Orthorhombic | Orthorhombic | Triclinic |
| Space Group | *Pbca* | *Pbca* | *P–1* |
| *a*, Å | 17.3289(4) | 17.3291(8) | 11.4478(6) |
| *b*, Å | 21.0424(4) | 20.7344(11) | 12.1071(7) |
| *c*, Å | 23.5283(5) | 23.3175(11) | 21.3849(12) |
| α, deg | 90 | 90 | 82.679(3) |
| β, deg | 90 | 90 | 86.994(3) |
| γ, deg | 90 | 90 | 81.566(3) |
| V, $Å^3$ | 8579.4(3) | 8387.2(7) | 2906.3(3) |
| *Z* | 8 | 8 | 2 |
| Radiation (λ, Å) | Cu-Kα, 1.54178 | Mo-Kα, 0.71073 | Mo-Kα, 0.71073 |
| ρ (calcd.), $g/cm^3$ | 1.193 | 1.157 | 1.136 |
| μ (Mo Ka), $mm^{-1}$ | 4.337 | 0.444 | 0.407 |
| Temp, K | 100 | 100 | 100 |
| θ max, deg | 68.378 | 25.041 | 28.446 |
| data/parameters | 7856/535 | 7414/477 | 14496/645 |
| $R_1$ | 0.0475 | 0.0376 | 0.0904 |
| $wR_2$ | 0.1230 | 0.0909 | 0.2228 |
| GOF | 1.031 | 1.024 | 1.021 |

**7.10 Acknowledgements.**

Chapter 7 is currently in preperation as a manuscript by Mokhtarzadeh, C. C.; Moore, C. E; Rheingold, A. L.; and Figueroa, J.S. The dissertation author is the primary author of this manuscript. Dr. Brandon R. Barnett, Douglas W. Agnew, Kyle A. Mandla are thanked for helpful discussions.

**7.11 References.**

(1) Doyle, M. P. *Acc. Chem. Res.* **1986**, *19*, 348.

(2) Harvey, D. F.; Sigano, D. M. *Chem. Rev.* **1996**, *96*, 271.

(3) Schrock, R. R. *Acc. Chem. Res.* **1986**, *19*, 342.

(4) Herndon, J. W. *Coord. Chem. Rev.* **2012**, *256*, 1281.

(5) Herndon, J. W. *Coord. Chem. Rev.* **2000**, *209*, 387.

(6) Herndon, J. W. *Coord. Chem. Rev.* **2007**, *251*, 1158.

(7) Herndon, J. W. *Coord. Chem. Rev.* **2009**, *253*, 86.

(8) Herndon, J. W. *Coord. Chem. Rev.* **2013**, *257*, 2899.

(10) Herndon, J. W. *Coord. Chem. Rev.* **2016**, *317*, 1.

(11) Schrock, R. R. *J. Chem. Soc., Dalton Trans.* **2001**, 2541.

(12) Frenking, G.; Fröhlich, N. *Chem. Rev.* **2000**, *100*, 717.

(13) Kostic, N.; Fenske, R. *J. Am. Chem. Soc.* **1981**, *103*, 4677.

(14) Kostic, N. M.; Fenske, R. F. *Organometallics* **1982**, *1*, 489.

(15) Vyboishchikov, S. F.; Frenking, G. *Chem. Eur. J.* **1998**, *4*, 1428.

(16) Vyboishchikov, S. F.; Frenking, G. *Chem. Eur. J.* **1998**, *4*, 1439.

(17) Bolaño, T.; Esteruelas, M. A.; Oñate, E. *J. Organomet. Chem.* **2011**, *696* (25), 3911.

(18) Jia, G. *Coord. Chem. Rev.* **2007**, *251*, 2167.

(19) Esteruelas, M. A.; López, A. M *Organometallics* **2005**, *24*, 3584.

(20) Gallop, M. A.; Roper, W. R. Advances in Organometallic Chemistry; Elsevier, 1986; Vol. 25, 121–198.

(21) Takemoto, S.; Matsuzaka, H. *Coord. Chem. Rev.* **2012**, *256*, 574.

(22) Rigaut, S.; Touchard, D.; Dixneuf, P. H. *Coord. Chem. Rev.* **2004**, *248*, 1585.

(23) Harrold, N. D.; Waterman, R.; Hillhouse, G. L.; Cundari, T. R. *J. Am. Chem. Soc.* **2009**, *131*, 12872.

(24) Lee, Y.; Peters, J. C. *J. Am. Chem. Soc.* **2011**, *133*, 4438.

(25) Fischer, E. O.; Schneider, J.; Neugebauer, D. *Angew. Chem. Int. Ed. Engl.* **1984**, *23*, 820.

(26) Rappert, T.; Nuernberg, O.; Mahr, N.; Wolf, J.; Werner, H. *Organometallics* **1992**, *11*, 4156.

(27) Höhn, A.; Werner, H. *Angew. Chem. Int. Ed. Engl.* **1986**, *25*, 737.

(28) Höhn, A.; Werner, H. *J. Organomet. Chem.* **1990**, *382*, 255.

(29) Luecke, H. F.; Bergman, R. G. *J. Am. Chem. Soc.* **1998**, *120*, 11008.

(30) Erker, G.; Lecht, R.; Petersen, J. L.; Boennemann, H. *Organometallics* **2002**, *6*, 1962.

(31) Harrison, D. J.; Lee, G. M.; Leclerc, M. C.; Korobkov, I.; Baker, R. T. *J. Am. Chem. Soc.* **2013**, *135*, 18296.

(32) Marquard, S. L.; Bezpalko, M. W.; Foxman, B. M.; Thomas, C. M. *J. Am. Chem. Soc.* **2013**, *135*, 6018.

(33) Bellow, J. A.; Stoian, S. A.; van Tol, J.; Ozarowski, A.; Lord, R. L.; Groysman, S. *J. Am. Chem. Soc.* **2016**, *138*, 5531.

(34) Brennessel, W. W.; Ellis, J. E. *Angew. Chem. Int. Ed. Engl.* **2007**, *46*, 598.

(35) Barybin, M. V.; Brennessel, W. W.; Kucera, B. E.; Minyaev, M. E.; Sussman, V. J.; Young, V. G.; Ellis, J. E. *J. Am. Chem. Soc.* **2007**, *129*, 1141.

(36) Leach, P. A.; Geib, S. J.; Corella, J. A.; Warnock, G. F.; Cooper, N. J. *J. Am. Chem. Soc.* **1994**, *116*, 8566.

(37) Barybin, M. V.; Young, V. G.; Ellis, J. E. *J. Am. Chem. Soc.* **1998**, *120*, 429.

(38) Henderson, R. A.; Pombeiro, A.; Richards, R. L. *J. Chem. Soc.* **1995**, 1193.

(39) Fischer, H.; Motsch, A.; Schubert, ,U.; Neugebauer, D. *Angew. Chem. Int. Ed. Engl.* **1981**, *20*, 463.

(40) Pombeiro, A.; da Silva, M.; Michelin, R. A. *Coord. Chem. Rev.* **2001**, *218*, 43.

(41) Michelin, R. A.; Pombeiro, A.; da Silva, M. *Coord. Chem.Rev.* **2001**, *218,* 43.

(42) Filippou, A. C.; Grünleitner, W.; Fischer, E. O. *J. Organomet. Chem.* **1991**, *411*, C21.

(43) da Silva, J. J. R. F.; Pellinghelli, M. A.; Pombeiro, A. J. L.; Richards, R. L.; Tiripicchio, A.; Wang, Y. *J. Organomt. Chem.* **1993**, *454*, C8.

(44) Chatt, J.; Pombeiro, A. J. L.; Richards, R. L.; Royston, G. H. D.; Muir, K. W.; Walker, R. *J. Chem. Soc., Chem. Commun.* **1975**, 708.

(45) Pombeiro, A. J. L. *Polyhedron* **1989**, *8* (13-14), 1595.

(46) Protasiewicz, J. D.; Masschelein, A.; Lippard, S. J. *J. Am. Chem. Soc.* **1993**, *115* (2), 808.

(47) Pombeiro, A. J. L.; Richards, R. L. *Coord. Chem. Rev.***1990**, *104* (1), 13.

(48) Warner, S.; Lippard, S. J. *Organometallics* **1989**, *8* (1), 228.

(49) Filippou, A. C.; Wagner, C.; Fishcer, E. O.; Völkl, C. *J. Organomet. Chem.* **1992**, *438,* C15-C22.

(50) Margulieux, G. W.; Weidemann, N.; Lacy, D. C.; Moore, C. E.; Rheingold, A. L.; Figueroa, J. S. *J. Am. Chem. Soc.* **2010**, *132* (14), 5033.

(51) Stewart, M. A.; Moore, C. E.; Ditri, T. B.; Labios, L. A.; Rheingold, A. L.; Figueroa, J. S. *Chem. Commun.* **2011**, *47* (1), 406.

(52) Mokhtarzadeh, C. C.; Margulieux, G. W.; Carpenter, A. E.; Weidemann, N.; Moore, C. E.; Rheingold, A. L.; Figueroa, J. S. *Inorg Chem* **2015**, *54* (11), 5579.

(53) Barnett, B. R.; Rheingold, A. L.; Figueroa, J. S. *Angew. Chem. Int. Ed.* **2016**, *55*

(32), 9253.

(54) Carpenter, A. E.; Chan, C.; Rheingold, A. L.; Figueroa, J. S. *Organometallics* **2016**, *35* (14), 2319.

(55) Carpenter, A. E.; Margulieux, G. W.; Millard, M. D.; Moore, C. E.; Weidemann, N.; Rheingold, A. L.; Figueroa, J. S. *Angew. Chem. Int. Ed. Engl.* **2012**, *51* (37), 9412.

(56) Cotton, F. A.; Zingales, F. *J. Am. Chem. Soc.* **1961**, *83* (2), 351.

(57) Carpenter, A. E.; Mokhtarzadeh, C. C.; Ripatti, D. S.; Havrylyuk, I.; Kamezawa, R.; Moore, C. E.; Rheingold, A. L.; Figueroa, J. S. *Inorg Chem* **2015**, *54* (6), 2936.

(58) Seino, H.; Nonokawa, D.; Nakamura, G.; Mizobe, M.; Hidai, M. *Organometallics* **2000**, *19*, 2002.

(59) da Silva, M. F. C. G.; Lemos, M. A. N. D. A.; da Silva, J. J. R. F.; Pombeiro, A. J. L.; Pellinghelli, M. A.; Tiripicchio, A. *J. Chem. Soc., Dalton Trans.* **2000**, 373.

(60) Robinson, G. H. *Chem. Commun.* **2000**, 2175.

(61) Su, J.; Li, X.-W.; Crittendon, R. C.; Robinson, G. H. *J. Am. Chem. Soc.* **1997**, *119*, 5471.

(62) Hino, S.; Olmstead, M. M.; Fettinger, J. C.; Power, P. P. *J. Organomet. Chem.* **2005**, *690*, 1638.

(63) Mokhtarzadeh, C. C.; Rheingold, A. L.; Figueroa, J. S. *Dalton Trans.* **2016**, *45*, 14561.

(64) Ellis, J. E. *Organometallics* **2003**, *22* (17), 3322.

(65) Pombeiro, A. J. L.; Hughes, D. L.; Pickett, C. J.; Richards, R. L. *J. Chem. Soc., Chem. Commun.* **1986**, 246.

(66) Chen, P.; Fujisawa, K.; Helton, M. E.; Karlin, K. D.; Solomon, E. I. *J. Am. Chem. Soc.* **2003**, *125*, 6394.

(67) Lomont, J. P.; Nguyen, S. C.; Harris, C. B. *Acc. Chem. Res.* **2014**, *47*, 1634.

(68) Hofmann, P.; Padmanabhan, M. *Organometallics* **1983**, *2*, 1273.

(69) Snee, P. T.; Payne, C. K.; Kotz, K. T.; Yang, H.; Harris, C. B. *J. Am. Chem. Soc.*

**2001**, *123*, 2255.

(70) Lee, G. R.; Cooper, N. J. *Organometallics* **1989**, *8*, 1538.

(71) Lee, G. R.; Maher, J. M.; Cooper, N. J. *J. Am. Chem. Soc.* **1987**, *109*, 2956.

(72) Gottlieb, H. E.; Kotlyar, V.; Nudelman, A. *J. Org. Chem.* **1997**, *62*, 7512.

(73) Fan, T.; Chen, X.; Lin, Z. *Chem. Commun.* **2012**, *48*, 10808.

(74) Gibson, D. H. *Chem. Rev.* **1996**, 2063.

(75) Alvarez, R.; Atwood, J. L.; Carmona, E.; Perez, P. J. *Inorg. Chem.* **1991**, *30*, 1493.

(76) Carnahan, E. M.; Lippard, S. J. *J. Am. Chem. Soc.* **1992**, *114*, 4166.

(77) Filippou, A. C.; Grünleitner, W. *Zeitschrift für Naturforschung B* **1991**, *46*, 216.

(78) Fouqueau, A.; Casida, M. E.; Daku, L. M. L.; Hauser, A.; Neese, F. *J Chem Phys* **2005**, *122*, 044110.

(79) The reductive disproportionation of $CO_2$ with $Na_2[Fe(CNAr^{Mes2})_4]$ is detatiled in Chapter 3 of this Disertation.

(80) Pangborn, A. B.; Giardello, M. A.; Grubbs, R. H.; Rosen, R. K.; Timmers, F. J. *Organometallics*, **1996**, *15*, 1518.

(81) Armarego, W. L. F.; Chai, C. L. L. *Purification of Laboratory Chemicals,* Elsevier, 5th edn., **2003**.

(82) Schwindt, M. A.; Lejon, T.; Hegedus, L. S. *Organometallics,* **1990**, *9*, 2814.

(83) Heck, R. F. *Inorg. Chem.* **1965**, *4,* 855.

(84) Fulmer, G. R.; Miller, A. J. M.; Sherden, N. H.; Gottlieb, H. E.; Nudelman, A.; Stoltz, B. M.; Bercaw, J. E.; Goldberg, K. I. *Organometallics*, **2010**, *29*, 2176.

(85) Neese, F. *ORCA-an Ab Inito, Density Functional Theory and Semiemperical SCF-MO Program Package, Version 3.0.0*. Max Planck Institute for Chemical Energy Conversion D-45470 Muelheim/Ruhr, Germany (2013).

(86) Becke, A. D. *J. Chem. Phys.* **1986**, *84*, 4524.

(87) Becke, A. D. *J. Chem. Phys.* **1993**, *98*, 5648.

(88) Neese, F. *Wiley Interdiscip. Rev.: Comput. Mol. Sci.* 2012, 2, 73.

(89) Lee, C. T.; Yang, W. T.; Parr. R. G. *Phys. Rev. B.* **1988**, *37*, 785.

(90) Pantazis, D. A.; Chen, X. Y.; Landis, C. R.; Neese F. *Chem. Theor. Comput.* **2008**, *4*, 908.

(91) Schaefer, A.; Horn, H.; Ahlrichs, R. *J. Chem. Phys.* **1992**, *97*, 2571.

(92) Weigend, F.; Ahlrichs, R. *Phys. Chem. Chem. Phys.* **2005**, *7*, 3297.

(93) Werner, H.-J.; Manby, F. R.; Knowles, P. J. *J. Chem. Phys.* **2003**, *118*, 8149.

(94) Van Lenthe, E.; Baerends, E. J.; Snijders, J. G. *J. Chem. Phys.* **1993**, *99*, 4597.

(95) Van Lenthe, E.; Snijders, J. G.; Baerends, E. J. *J. Chem. Phys.* **1996**, *105*, 6505.

(96) Eichkorn, K.; Treutler, O.; Ohm, H.; Haser, M.; Ahlrichs, R. *Chem. Phys. Lett.* **1995**, *240*, 283.

(97) Eichkorn, K.; Treutler, O.; Ohm, H.; Haser, M.; Ahlrichs, R. *Chem. Phys. Lett.* **1995**, *242*, 652.

(98) Eichkorn, K.; Treutler, O.; Ohm, H.; Haser, M.; Ahlrichs, R. *Theor. Chem. Acta* **1997**, *97*, 119.

(99) ChemCraft. Zhurko, G. A.; Zhurko, D. A. 2014, www.chemcraftprog.com

(100) Sheldrick, G. *Acta. Crystallogr., Sect. A: Fundam. Crystallog.* **2008**, *64*, 112.

(101) Dolomanov, O.V.; Bourhis, L. J.; Gildea, R. J.; Howard, J. A. K.; Puschmann, H. *J. Appl. Crystallogr.* **2009**, *42*, 339.